

INTRODUCTION TO **LENS DESIGN**

With Practical ZEMAX® Examples

Joseph M. Geary

*Center for Applied Optics
University of Alabama in Huntsville*

Published by



P.O. Box 35025 • Richmond, Virginia 23235 • USA (804) 320-7016
www.willbell.com

Published by Willmann-Bell, Inc.
P.O. Box 35025, Richmond, Virginia 23235

Copyright © 2002 by Joseph M. Geary
All Rights Reserved

Reproduction or translation of any part of this work beyond that permitted by Sections 107 or 108 of the United States Copyright Act without written permission of the copyright owner is unlawful. Requests for permission or further information should be sent to the Permissions Department, Willmann-Bell, Inc., P.O. Box 35025, Richmond, VA 23235.

Printed in the United States of America
First Printing: September, 2002

Library of Congress Cataloging in Publication Data

Geary, Joseph M.

Introduction to lens design: with practical ZEMAX examples / Joseph M. Geary
p. m.
Includes bibliographical references and index.
ISBN 0-943396-75-1
1. Lenses—Design and construction. 2. Lenses—Design and construction—Data processing. 3. ZEMAX. I. Title

QC385.2.D47 G43 202
681'.423—dc21

2002026274

The following trademarks are acknowledged here and elsewhere in this book:
CODE V by Optical Research Associates, LensVIEW by Optical Data Solutions,
OSLO by Sinclair Optics and ZEMAX by Focus Software

Table of Contents

Preface	xiii
Chapter 1 Agenda	1
1.1 Introduction	1
1.1.1 Why Lens Design?	1
1.1.2 Type of Course	1
1.1.3 Acquired Skills	1
1.2 Setting the Stage	3
1.2.1 A Comparison	3
1.2.2 Aberration and Imagery	3
1.2.3 Lens Size and FOV	4
1.2.4 Specifications	5
1.3 Homework	8
Chapter 2 ZEMAX	11
2.1 Introduction to ZEMAX	11
2.2 Data Entry	11
2.2.1 Inserting a Prescription in the Lens Data Editor	11
2.2.2 Dialog Boxes	12
2.3 Layout	13
2.4 First Order Properties	17
2.5 Analysis	17
2.6 Keeping Track of Designs	17
2.7 ZEMAX Glass Catalog	18
2.8 Odds and Ends	19
2.8.1 More on f -number	19
2.8.2 Ray Selection	20
Chapter 3 Conventions and Aspheres	21
3.1 Introduction	21
3.2 Sign Conventions	21
3.3 Shape Factor	21
3.4 Surface Sag	22
3.5 Aspheric Surfaces	23
3.6 Departure From Sphere	27
3.7 Homework	28
3.7.1 Singlet	29

Chapter 4 Paraxial World	33
4.1 Introduction	33
4.2 Paraxial Ray Trace Equations	33
4.3 Gaussian Lens Formula.....	34
4.4 What Lenses Look Like in the PRTE World.....	35
4.5 Determination of Surface Power.....	36
4.6 Other Important Power Expressions	37
4.6.1 Single Reflecting Surface.....	37
4.6.2 Two-Element System	37
4.6.3 Thin Lens	39
4.7 Principal Plane Locations in a Two-Element System	40
4.8 Magnification	41
4.9 Homework	42
Chapter 5 Stops and Pupils	43
5.1 Introduction	43
5.2 Stop and Pupils	43
5.3 Marginal and Chief Rays.....	46
5.4 Locating Buried Stop Entrance and Exit Pupils Using PRTE.....	46
5.5 Pupil Size and <i>F</i> -Number	47
5.6 The Lagrange Invariant	48
5.7 Homework.....	49
Chapter 6 Glass, and the Landscape Lens	51
6.1 Introduction	51
6.2 Glass Properties.....	51
6.2.1 Refractive Index	51
6.2.2 Dispersion.....	51
6.2.3 How Can We Quantify the Dispersive Property of Glasses?.	52
6.2.4 Glass Chart	54
6.2.5 Melt Data	55
6.2.6 Partial Dispersion	55
6.2.7 Practical Considerations	58
6.3 Stop Shifting and Aberration Control	58
6.4 Wollaston Rear Landscape Lens	61
6.5 Historical Note: William Wollaston	62
6.6 Homework.....	62
Chapter 7 Aberrations in General.....	65
7.1 Introduction	65
7.2 Diagnostic Plots.....	65
7.2.1 The Ray Fan Plot	65
7.2.2 The Spot Diagram.....	67
7.3 Ray Description of Aberrations.....	68
7.3.1 Defocus.....	68
7.3.2 Spherical Aberration.....	68

7.3.3 Coma.....	71
7.3.4 Astigmatism	73
7.3.5 Field Curvature and Distortion.....	75
7.4 Wavefront Aberrations	77
7.4.1 Description of Wavefront.....	77
7.4.2 Interaction Of Wavefronts With Optical Systems	78
7.4.3 Wavefront Description	79
7.4.4 Wavefronts and Diffraction	82
7.5 Connection Between Image Plane and Exit Pupil Aberrations.....	82
7.6 Abbe Sine Condition	83
Chapter 8 Solves and Merit Function	85
8.1 Introduction	85
8.2 The M-solve.....	85
8.3 The F-solve	86
8.4 Rings and Arms.....	87
8.5 The Merit Function	88
8.6 RMS Spot Size	90
8.7 RMS Spot Plots	93
Chapter 9 Splitting a Lens	95
9.1 Introduction	95
9.2 Lens Splitting.....	95
9.2.1 Single Element	95
9.2.2 Double Element	95
9.2.3 Triple Element	96
9.3 Micro-lithography and Lens Splitting	98
9.4 Fizeau Interferometry	98
9.5 Homework.....	101
Chapter 10 Spherical Aberration.....	103
10.1 Introduction	103
10.2 Heuristic Approach to W_{ijk}	104
10.3 Example: W_{040} via Paraxial Ray Trace	107
10.4 Thin Lens Form For W_{040}	109
10.5 Example: W_{040} via Thin Lens Calculation	110
10.6 Off-Axis Aberration Coefficients	110
10.7 Derivation W_{040}	110
10.8 Homework.....	116
Chapter 11 Lens Bending and Aberration Balancing.....	117
11.1 Introduction	117
11.2 The Thin Lens Form	117
11.3 Thin Lens Bending	119
11.4 Focus Shift.....	120
11.5 Difference Between W_{020} and W_d	121

11.6 Aberration Balancing: Spherical Aberration and Defocus	123
11.7 Basis For Equation	124
11.8 Connection Between W_{040} and SA3	125
11.9 Example With Spherical Aberration:	128
11.10 Derivation of Thin Lens Form	128
11.11 Homework	134
Chapter 12 Symmetry and the Perisopic Lens.....	135
12.1 Introduction	135
12.2 Determining Starting Radii	136
12.3 Setting Up the Pre-Design In ZEMAX	137
12.4 Object At Infinity	139
12.5 Field Flattening	140
12.6 Comparison With Rear Landscape Lens.....	141
12.7 Breaking Symmetry.....	143
12.8 Historical Note: Carl Steinheil	143
12.9 Homework.....	145
Chapter 13 Coma and Astigmatism	147
13.1 Introduction	147
13.2 Transverse Spherical Aberration: SA3	148
13.3 ZEMAX Off-Axis Aberration Calculations	150
13.3.1 Coma (W_{131}) via Seidel Contributions	151
13.3.2 Coma (W_{131}) via Thin Lens Formulation	152
13.3.3 Astigmatism (W_{222}) via Seidel Contributions	152
13.3.4 Astigmatism (W_{222}) via Thin Lens Formulation.....	153
13.4 Coma and Lens Bending	154
13.5 Coma and Astigmatism vs. F-Number and Field	154
13.6 Homework.....	156
Chapter 14 Field Curvature and Field Flattener.....	157
14.1 Introduction	157
14.2 Petzval Curvature	157
14.3 The Petzval Wavefront Aberration	159
14.4 The Petzval Aberration Coefficient and Petzval Sum.....	159
14.5 Sample Calculation	160
14.6 Petzval Radius.....	161
14.7 Basic Theory of the Field Flattener.....	163
14.8 Homework.....	165
Chapter 15 Distortion.....	167
15.1 Introduction	167
15.2 Wavefront Tilt	167
15.3 Distortion.....	169
15.4 Example.....	171
15.5 Discussion	173

Chapter 16 Axial Color and Achromats.....	175
16.1 Introduction	175
16.2 Primary Axial Color	175
16.3 Derivation of C_L	177
16.4 The Wavefront Color Aberration W_{ax}	178
16.5 The Achromat	180
16.5.1 Constraints	180
16.5.2 Achromat Powers	181
16.5.3 Achromat Example.....	181
16.6 Homework.....	182
Chapter 17 Bending Achromats	185
17.1 Introduction	185
17.2 Achromats in ZEMAX	185
17.3 Achromat Bending and Seidel Spherical Aberration	187
17.4 Higher Order Spherical	189
17.5 Spherochromatism.....	190
17.6 Achromat Bending and Coma and Astigmatism.....	191
17.7 The Aplanat.....	192
17.8 Lateral Color	193
17.9 Homework.....	194
Chapter 18 Secondary Color	195
18.1 Introduction	195
18.2 Partial Dispersion	195
18.3 Achromat Secondary Spectrum.....	198
18.4 ZEMAX Corrected Achromat.....	202
18.5 When Is Secondary Spectrum Worrisome?.....	202
18.6 Flat Field Achromat.....	205
18.7 Homework.....	205
Chapter 19 Large Air-Spaced Achromat and French Landscape Lens .	207
19.1 Introduction	207
19.2 Separated Thin Lens Achromat	207
19.2.1 Dispersion Constraint Modification	207
19.2.2 Determining Component Powers	208
19.2.3 One-Glass Achromat	211
19.3 The Apochromatic Constraint	212
19.3.1 Partial Primary Axial Color	213
19.3.2 Partial Primary Color Applied to Doublets and Triplets ..	214
19.4 Color Correction vs. Spot Size	216
19.5 The Chevalier Lens	217
19.6 Homework.....	218
Chapter 20 Mid-Term Exam	221
20.1 Introduction	221

20.2 The Microscope	221
20.3 Design Overview and Helpful Hints	223
20.3.1 Part I: Thin Lens Pre-Design	223
20.3.2 Part II: ZEMAX Design Optimization	224
20.4 Mid-Term Exam	225
20.5 Where Do We Go From Here	226
Chapter 21 Apochromat.....	229
21.1 Introduction	229
21.2 Apochromatic Constraints.....	229
21.3 Apochromatic Power Solution	230
21.4 Calculation Example	232
21.5 ZEMAX Optimization.....	234
Chapter 22 Eyepiece Design.....	239
22.1 Introduction	239
22.2 First Order Layout of Eyepiece.....	239
22.3 Insertion into ZEMAX	241
22.4 Field Lens	242
22.5 The Ramsden and Kellner Eyepieces	245
22.6 The Ramsden Eyepiece and Eye Model	245
22.7 Ramsden Design Example Using ZEMAX.....	246
Chapter 23 Field Lens and Windows	249
23.1 Introduction	249
23.2 Field Lenses in Relay Systems	249
23.3 Windows	251
23.4 Aberrations Introduced by Perfect Windows	253
23.4.1 Focus Shift	253
23.4.2 Spherical Aberration.....	255
23.4.3 Simple Formulas for Window Seidel Coefficients.....	257
23.5 Tilted Window in ZEMAX.....	258
23.6 Effect on Axial Color	259
23.7 Homework.....	259
Chapter 24 Mirrors and Corrector Plates	261
24.1 Introduction	261
24.2 The Parabolic Mirror.....	261
24.3 Aberration Content Comparison	263
24.4 Aspheric Correction of Lens	263
24.5 Corrector Plate for Spherical Mirrors	264
24.5.1 Qualitative Description.....	264
24.5.2 Quantitative Description.....	264
24.5.3 Schmidt Plate in ZEMAX.....	266
24.6 Spectral Effects	267
24.7 Applications.....	268

24.8 Historical Note: Bernhard Schmidt	270
24.9 Homework	270
Chapter 25 Symmetric Achromat and Vignetting	271
25.1 Introduction	271
25.2 Basic Design Approach	271
25.3 Application of Design Approach	271
25.4 Area Weighted RMS	277
25.5 Breaking Symmetry	277
25.6 Vignetting	280
25.7 Relative Illumination	282
25.8 The Rapid Rectilinear	283
25.9 Historical Note: John Henry Dallmeyer	283
25.10 Homework	284
Chapter 26 Telescopes	287
26.1 Introduction	287
26.2 Telescope Types	287
26.2.1 Newtonian Form	287
26.2.2 Cassegrain Form	287
26.2.3 Gregorian Form	289
26.2.4 Schmidt Telescope	289
26.2.5 Complementary Apheres in Telescopes	290
26.3 Designing a Cassegrain	290
26.3.1 Secondary Mirror and First Order Properties of System	290
26.3.2 Conic Constant Design	292
26.4 Cassegrain in ZEMAX	294
26.5 Other Design Considerations	296
26.5.1 Effect of Central Obscuration	296
26.5.2 Stray Light and Baffles	298
26.6 Historical Note: G.W. Ritchey and H.J. Chrétien	298
26.7 Homework	299
Chapter 27 Relating Defocus, Astigmatism, and Field Curvature	301
27.1 Introduction	301
27.2 Wavefront Description of Aberrations in Cartesian Coordinates	301
27.3 Wavefront Gradients in Cartesian Form	302
27.4 Defocus, Astigmatism, and Petzval Curvature in Pupil	303
27.5 Making the Connection to Image Space	305
27.5.1 Image Focus Locations Along Chief Ray	305
27.5.2 Example	306
27.5.3 Separation Between Tangential and Sagittal Foci	307
27.5.4 Image Sizes at Respective Focal Planes	309
27.6 Checking Out the Image Predictions in ZEMAX	310
27.7 Basis for the Use of $\cos U'$	312
27.8 Homework	314

Chapter 28 Celor Lens.....	315
28.1 Introduction	315
28.2 Generalized Power.....	315
28.3 Celor Lens Constraints	316
28.4 Derivation of Celor Equation	317
28.5 Celor Rear Half Lens Powers	318
28.6 Celor ZEMAX Design Procedure	321
28.7 Historical Note: Emil von Hoegh	326
28.8 Homework.....	327
Chapter 29 Coddington's Equations	329
29.1 Introduction	329
29.2 Coddington	329
29.3 Oblique Power.....	330
29.4 Coddington's Equations.....	331
29.5 Thin Lens Example	332
29.6 Thin Lens Expression for $\Delta l'$	333
29.7 Coddington's Equations and Mirrors	334
29.8 Comparison of $\Delta l'$ and δ_{TS} for Mirrors	335
29.9 Field Curvature Plot in ZEMAX.....	335
29.10 Toric Surfaces.....	336
29.11 Aberration Generator	338
29.12 Homework	340
Chapter 30 Triplet Lens and Image Compactness.....	343
30.1 Introduction	343
30.2 Philosophy Behind Triplet Lens Design	343
30.3 Outline of Triplet Design	344
30.4 Historical Note: H. Dennis Taylor.....	345
30.5 An Important Triplet Variant.....	346
30.6 Image Quality I	346
30.6.1 Average Volume Over Unit Circle.....	346
30.6.2 Image Compactness	347
30.6.3 Calculation Example.....	348
30.6.4 Numerical Example	349
30.6.5 ZEMAX Example.....	349
30.7 Axial Location of σ_C	350
30.8 Lateral Color Revisited	350
30.9 Homework.....	353
Chapter 31 Strehl Ratio	355
31.1 Introduction	355
31.2 Image Quality II	355
31.2.1 Strehl Ratio.....	355
31.2.2 Wavefront Variance	357
31.2.3 Calculation Example.....	358

31.2.4 Numerical Example	360
31.2.5 Axial Location of σ	360
31.2.6 Wavefront Variance in ZEMAX	361
31.3 Minimum Blur in ZEMAX	362
31.4 Wavefront Variance for Asymmetric Aberrations	363
31.5 Homework	364
Chapter 32 Axial Intensity and Depth of Focus.....	365
32.1 Introduction	365
32.2 Image Quality III.....	365
32.2.1 Axial Intensity	365
32.2.2 Diffractive Depth of Focus.....	370
32.2.3 Geometric Depth of Focus	371
32.2.4 Resolution	373
32.2.4.1 Star Sources	373
32.2.4.2 Broad Sources	374
32.2.5 Rayleigh Rules	375
32.3 Strehl in ZEMAX	375
Chapter 33 Petzval Lens.....	377
33.1 Introduction	377
33.2 Paraxial Thin Lens Petzval Design	377
33.3 Outline of Petzval Design Procedure on ZEMAX	380
33.4 Historical Note: Joseph M. Petzval	381
33.5 Image Quality IV.....	382
33.6 Homework	387
Chapter 34 MTF: Image Quality V.....	389
34.1 Introduction	389
34.2 What is Modulation?.....	389
34.3 Convolution and Fourier Transform	390
34.4 The Optical Transfer Function	392
34.5 MTF in ZEMAX	396
34.6 MTF and Symmetry	396
Chapter 35 Null Lens Design.....	399
35.1 Introduction	399
35.2 Spherical Aberration Generated by a Parabolic Mirror.....	399
35.3 Test Configuration For Concave Mirrors	400
35.4 Purpose Of Null Lens in Testing Parabolic Mirrors	401
35.5 Derivation of Surface Normals for Parabolic Mirror	402
35.6 The Offner Null Lens	405
35.6.1 Predesign.....	406
35.6.2 Generator Power	406
35.6.3 Power of Tuning Lens	408
35.7 Null Lens in ZEMAX	408

Chapter 36 Final Exam	413
36.1 Introduction.....	413
36.2 First Order Telephoto	413
36.2.1 Focal Length of Positive Component.....	413
36.2.2 Focal Length of Negative Component	415
36.2.3 Example	416
36.2.4 Preparation For ZEMAX Telephoto Optimization.....	416
36.3 Telephoto in ZEMAX	417
36.4 Final Exam.....	418
Chapter 37 The Attic	421
37.1 Introduction.....	421
37.2 Paraxial Lenses	421
37.3 Tilting a Flat Mirror.....	422
37.4 Right Angle Prism.....	423
37.5 Lens Alignment.....	424
37.5.1 Lens Decentration.....	424
37.5.2 Lens Tilt	425
37.6 Off-Axis Parabola	425
37.7 Aberrations Induced by Decentration	426
37.8 Zernike Polynomials.....	430
Chapter 38 Fini	433
38.1 Introduction.....	433
38.2 What Has Been Accomplished	433
38.3 Tolerancing	436
38.4 Things Not Covered	440
38.5 Optical Design Codes	442
Appendix A Bibliography.....	443
Appendix B Answers to Manual Calculation Assignments.....	445
Appendix C Final Prescriptions for ZEMAX Design Assignments	447
Appendix D Glossary	453
Appendix E Description of ZEMAX Merit Function Operands Utilized in this Book	457
Index.....	459

Preface

This book evolved from an introductory course in lens design sponsored by the Center for Applied Optics for use in the Optical Science & Engineering doctoral program at the University of Alabama in Huntsville. At the inception of this course, I searched for a lens design textbook and found, to my surprise and dismay, that there really were none! Although there were several good books about lens design (see the booklist in Appendix A), these tended to be either monographs or compilations of different designs. None were written with students (or instructors) in mind. Hopefully this book is a step in the pedagogical direction. As I began preparing lectures it also seemed obvious that no modern lens design course could be given without thoroughly integrating one of the commercially available lens design codes into the syllabus. For a variety of reasons (including user friendliness and cost effectiveness) ZEMAX was selected.

This is not a textbook in the traditional sense. It is a formalized embodiment of lectures with assigned homework and exams. The course is designed around a 14-week semester (MWF) with enough material to fill 38 lectures of 55 minutes each. The material is at the first-year graduate level, and is intended as a first course in lens design. It is also structured to be hands-on and engineering oriented. A solid footing in undergraduate geometrical optics (Appendix A) is the only prerequisite. Math requirements are modest: algebra, trig, geometry, and calculus. Although this course is about lens design, I believe its scope is more general in that it can provide optical engineers with important tools and skills that will be useful in their professional careers.

Though written in lecture format and suitable for classroom use, the book is primarily designed for self-study. As such it can be used on three distinct levels. Obviously, the full benefit will be had by those having access to ZEMAX (and the accompanying manual). However, I believe enough information is provided (particularly with the help of Appendices C and E) to allow readers using alternate codes (such as Code-V, SYNOPSIS, and Super OSLO) to work the examples and assignments in a beneficial manner. Finally, for readers who do not have any major code readily available, a great deal can still be learned about design and analysis in conjunction with working the manual calculation problems and by doing the thin lens pre-designs preceding code work.

With a few exceptions, the backbone of the course is the photographic lens, and we follow an almost historic development. There are ten photographic lens design problems from the simple Wollaston landscape lens to the more complex achromatic telephoto. Along the way we visit such things as the Rapid Rectilinear and Cooke Triplet. The design principles covered in the course include: lens bend-

xiv *Preface*

ing, stop shift, symmetry, element splitting, color correction, aberration balancing, field flattening, aspherics, as well as the proper use and construction of the merit function. Though ZEMAX is an integral part of the course, its use will not be blind. Manual thin lens pre-design calculations provide the starting prescriptions for every ZEMAX homework. Paraxial ray tracing, element power computations, and aberration calculations are utilized throughout the course. Consequently, all designs are firmly anchored by theory.

Of equal importance to the design principles covered in the course are the analytical tools used to determine the quality of the design. ZEMAX and its sister codes are built upon a strong tradition of optical analysis, and will provide the user with a rich variety of numbers and plots (such as axial color and ray fan plots, spot diagrams, and MTF). This course will provide the student with a thorough understanding of where these numbers come from and what the plots mean. This understanding is supported by 26 assignments evenly split between “pencil and paper” calculations and ZEMAX code work. The course is structured so that students start using ZEMAX in the very first week, and every week thereafter. This affects the arrangement of material because roughly every third lecture focuses on a specific lens design and provides background for the ZEMAX assignment.

I would like to dedicate this book to Professors Roland Shack and Bob Shannon who were my mentors at the Optical Sciences Center. I also want to include Prof. Rudolph Kingslake in this dedication. All three have provided inspiration for this work, and I thank each for the things I’ve learned from them.

My thanks to Dr. John Dimmock, Director of both the Center for Applied Optics and the Optical Sciences and Engineering program, for his generous support in developing the lens design course upon which this book is based. I also owe a debt of gratitude to all the reviewers of the manuscript. In alphabetical order they are: Dr. Richard Buchroeder, Dr. Qian Gong (Swales Aerospace), Dr. John Loomis (University of Dayton Research Institute), Dr. Malcolm MacFarlane (Goodrich), Mr. Ken Pitalo (University of Alabama in Huntsville), Dr. Pat Reardon (University of Alabama in Huntsville), Dr. Babak Saif (Space Telescope Institute), Dr. José Sasian (University of Arizona), Dr. Lynn Seppala (Lawrence Livermore National Laboratory), Dr. Bob Shannon (University of Arizona), Dr. Greg Smith, Dr. Phil Stahl (Marshall Space Flight Center), Dr. Harold Suiter, Dr. Bill Swantner (BSC Optics), and Dr. Mary Turner (Focus Software Inc.). The constructive criticism provided by these professionals has greatly improved the quality of this work. Finally, I want to thank my daughter, Jennifer, for the fine art work she contributed to this book.

Note on ZEMAX: ZEMAX SE versions 6.0 – 7.2 have been used in the development of this book and in the instruction of this course. I have found that different versions can give slightly different numbers for variables in the lens data editor and for operand values in the merit function editor at the end of an optimization run. The differences tend to be of no significance. I provide many design examples using ZEMAX optimization where specific numerical values are pointed out or tabulated. For those using other versions of ZEMAX, please do not be

Section : xv

surprised if your post-optimization numbers do not agree precisely with mine.
They should, however, be reasonably close.

Instructor Note: I found the use of a computer projector absolutely indispensable in teaching this course. I strongly encourage any instructor to employ a computer projector not only for homework reviews but also for live demonstrations of ZEMAX features, and for illustrating design principles.

Joseph M. Geary
Center for Applied Optics
University of Alabama in Huntsville
October 15, 2002

Chapter 1

Agenda

1.1 Introduction

1.1.1 Why Lens Design?

Lens design used to be a skill reserved for a few professionals. They employed company proprietary optical design and analysis software which was resident on large and expensive mainframes. Today, with readily available commercial design software and powerful personal (and portable) computers, lens design tools are accessible to the general optical engineering community. Consequently, some rudimentary skill in lens design is now expected by a wide range of employers who utilize optics in their products. Lens design is, therefore, a strong component of a well-rounded education in optics, and a skill valued by industries employing optical engineers.

1.1.2 Type of Course

This is an introductory lens design course at the first-year graduate level. It is a nuts and bolts, hands-on oriented course. A good working knowledge of geometric optics (as may be found in such texts as Hecht and Zajac's *Optics* or Jenkins and White's *Fundamentals of Optics*) is presumed. Photographic lenses will form the backbone of the course. We will follow an historic progression (which also has correspondence from simpler to more complex systems). The code used is Focus Software's ZEMAX® and the student must have access to a PC running ZEMAX. The math level required is not taxing: algebra, trigonometry, geometry (plane and analytic), and some calculus. A book list of references is provided in Appendix A.

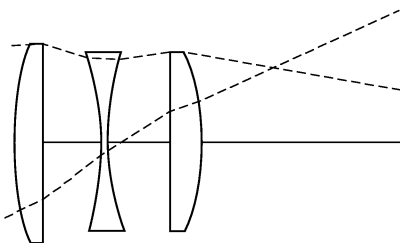
1.1.3 Acquired Skills

This course will provide you with three basic skills: manual, design code, and design philosophy. The manual skills will include first and third order hand calculations and thin lens pre-designs. (Analysis skills are illustrated in Figure 1.1). The code skills will include prescription entry, variable selection, merit function construction and optimization, and design analysis. The design philosophy includes understanding specifications, selecting a starting point, and developing a plan of attack.

2 Chapter 1 Agenda

GIVEN

1. Curvatures
2. Thickness
3. Indices
4. Stop size and location
5. Field Angle



USING

1. Paraxial ray trace equations
2. Seidel aberration formulas

FIND

First order

- Effective and back focal lengths
- F-number
- Image location
- Image size
- Location of principal planes
- Separation between vertex and principal plane
- Entrance pupil size and location
- Exit pupil size and location
- Lagrange invariant
- Axial and lateral color

Third order

- Spherical aberration
- Location and size of minimum blur
- Coma
- Astigmatism
- Location and size of medial focus
- Petzval curvature
- Distortion
- Wavefront variance
- Strehl ratio
- Required conic constant

Fig. 1.1 Summary of manual skills to be acquired.

Section 1.2: Setting the Stage 3

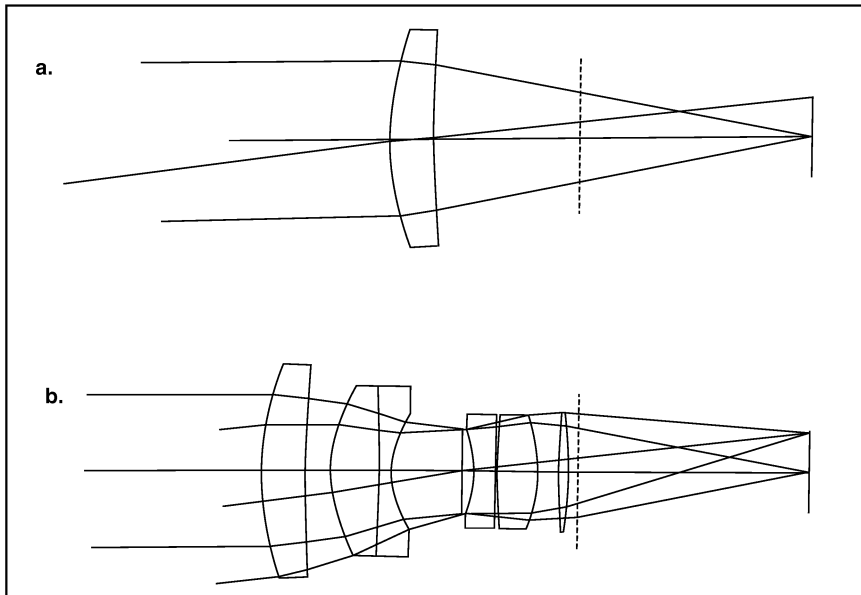


Fig. 1.2 Two lenses that give the same image size but with quite different quality.

1.2 Setting the Stage

1.2.1 A Comparison

Consider the two optical systems in Figure 1.2. Both are viewing the same distant object. Both have the same focal length (so the image is the same size). System *a* is simple, while system *b* is complex. If both systems yield the same image size, why not use the simpler system? Why does system *b* have extra lenses? Aside from image size, we assume that you want good, crisp, uniformly bright images across the entire field-of-view (FOV) over a flat recording format. System *b* will give that. System *a* will not. The latter's images will be of poor quality because there is inadequate correction for:

1. color
2. spherical aberration
3. off-axis aberrations
4. field curvature

The extra lenses in *b* are made from different kinds of glass to correct for color. The glass curvatures and thicknesses, and the air-spaces between them, help correct aberrations over the FOV. The result will be high-quality imagery over a flat recording surface (whether that be film or a CCD).

1.2.2 Aberration and Imagery

Figure 1.3a shows a resolution target being imaged by a “perfect” optical system.

4 Chapter 1 Agenda

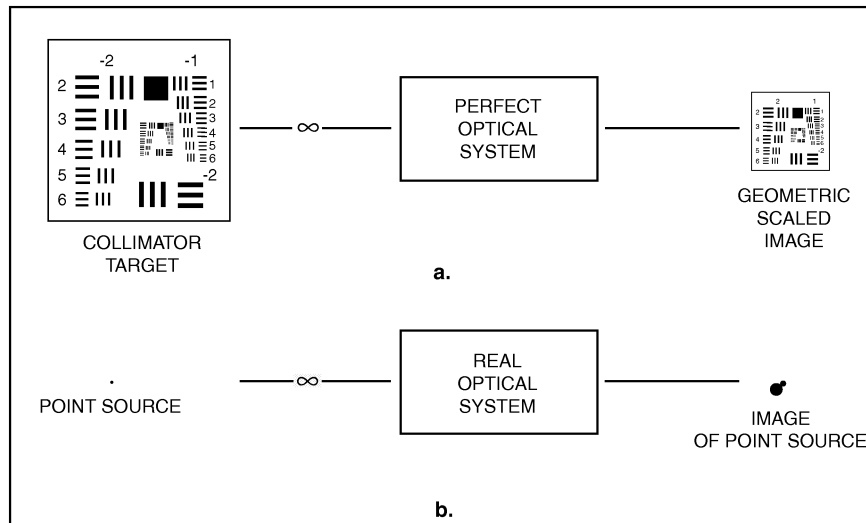


Fig. 1.3 A resolution target perfectly imaged (a); a poorly imaged point source (b).

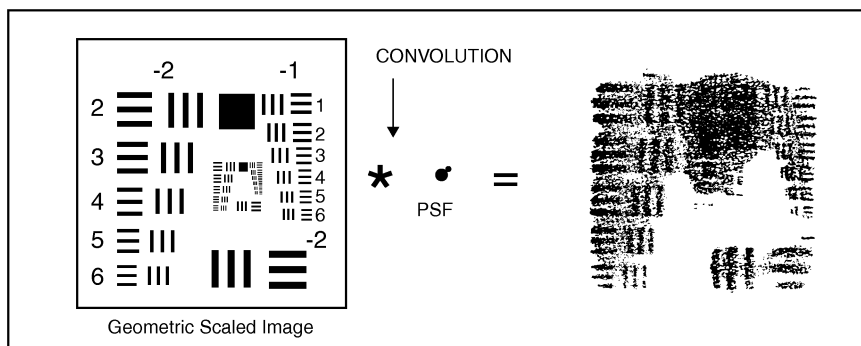


Fig. 1.4 Degradation of the resolution target image due to convolution with blob point image.

The image is simply a scaled version of the object. In Figure 1.3b we have a point source being imaged by an imperfect optical system. The resulting image is a fuzzy blob instead of a point. If we now combine the two so that we image the resolution target with the imperfect system, the image is of poor quality, as illustrated in Figure 1.4. What has happened is that we have essentially replaced every *image point* in Figure 1.3a with the *blob image* in Figure 1.3b.

1.2.3 Lens Size and FOV

Fundamentally, aberrated point images that degrade image quality are caused by the nonlinear behavior of Snell's Law. Aberrations arise when the angle of incidence of a ray with the normal of an optical surface starts getting large. This can happen in two ways for a given radius of curvature. For a ray parallel to the optical

Section 1.2: Setting the Stage 5

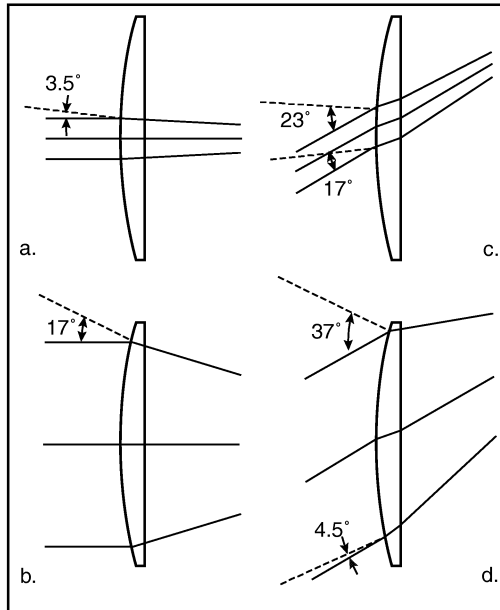


Fig. 1.5 Angle of incidence change with ray height and field angle.

axis, as per Figure 1.5*a* and *b*, the angle of incidence increases as the ray height increases (from 3.5° in Figure 1.5*a* to 17° in Figure 1.5*b*). If the ray strikes at the same height but from a different field angle, the angle of incidence can increase (as shown for the upper ray from 3.5° in Figure 1.5*a* to 23° in Figure 1.5*c*). When both conditions happen at the same time, the angle of incidence is even larger (from 3.5° in Figure 1.5*a* to 37° in Figure 1.5*d*). For the lower ray in *c* and *d*, the angle of incidence decreases. But now there is an asymmetry between upper and lower rays, which is indicative of off-axis aberrations.

As a system f-number decreases and field angles (and spectral bandwidth) increase, the complexity of optical systems (required to maintain good image quality) also increases. Figure 1.6 shows a qualitative plot of optical system types as a function of f-number (*x*-axis) and field angle (*y*-axis). For a $\frac{1}{4}^\circ$ field at *f*/10, a simple parabolic mirror would suffice. However, for a field of 20° at *f*/2, a six-element double-Gauss lens might be employed.

1.2.4 Specifications

Before any design can commence, the designer must have a clear understanding of the customer's requirements. This is not as straightforward as it seems. There are times when the customer is not sure of the requirements. This may lead to unexpected specification changes after much design work has already been done. In this case, the designer must take an active role in helping the customer solidify the requirements. At the other extreme is over-specification. Here the customer has placed unrealistic constraints on the design. For example, tolerances may be

6 Chapter 1 Agenda

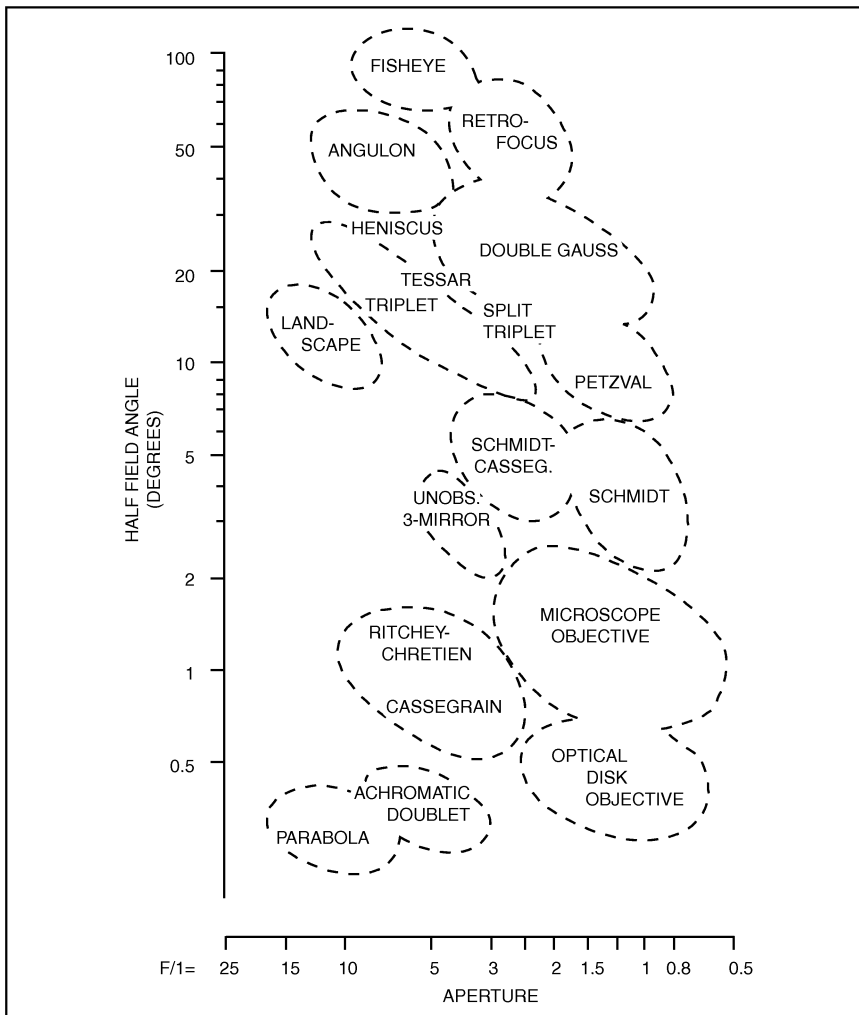


Fig. 1.6 Map showing the design types which are commonly used for various combinations of aperture and field of view. (From W. Smith, Modern Lens Design (McGraw-Hill, 1992). Reprinted with permission of the McGraw-Hill Companies.)

beyond current fabrication or metrology capabilities. Here again the designer must interact with the customer to arrive at realistic specifications.

Field coverage depends on the format size and effective focal length (EFL) of the optics. For example, the format size may be fixed by the use of 35 mm film, or an 8×6 mm CCD chip. The customer will say how much of the outside world or scene is to fit on the given format. This defines a certain FOV or field angle which then dictates an EFL.

Section 1.2: Setting the Stage 7

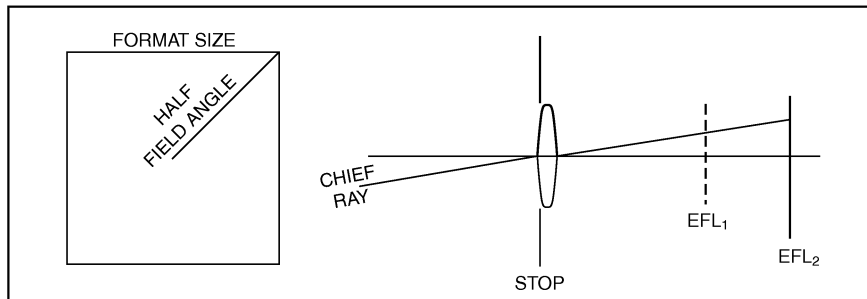


Fig. 1.7 Dependence of EFL on format size and field coverage.

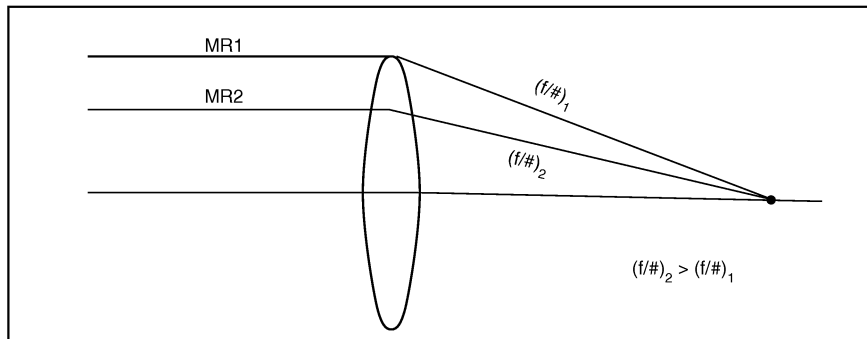


Fig. 1.8 A lower f-number means bigger diameter optics.

Figure 1.7 shows, for a given scene or angular coverage, the EFL needed for two different format sizes. The half-field angle is taken at the corner of the format.

The sensor employed will operate over a certain irradiance range. This will help define the f-number range of the objective. For example, on a cloudy day the f-number will be smaller than that used on a sunny day. Figure 1.8 shows how the usable diameter of a singlet is related to the f-number.

The next important specification is resolution. For a given scene, how much detail do we wish to see? Resolution is usually given as line pairs per millimeter. For example, a 100 lp/mm will present more of a design challenge than 50 lp/mm. We also have to distinguish between aerial resolution (i.e., the amount of detail in the image formed by the objective in air) and system resolution (which folds in the limitations imposed by the sensor). For example, black and white Tri-X film has poorer resolution than Pan-X because the silver halide grain sizes are bigger in the former.

Resolution may be specified as an average over the entire format, or specific targets may be given at certain field points. The design task becomes harder as the field angle increases, the f-number decreases, and resolution requirement increases.

8 Chapter 1 Agenda

Detectors have sensitivity over certain color ranges, hence the next important specification concerns spectral bandwidth and location. Monochromatic designs or designs where color does not matter are generally easier than polychromatic designs. As the bandwidth of a polychromatic design increases, the design task gets harder. Designs can also become more difficult if the location of the bandwidth lies outside the visible spectrum. Here there are fewer choices of materials for color correction.

The above mentioned design specifications are those of primary interest. However, there are several other constraints on designs. There may be volume, packaging, and/or weight constraints. There are constraints imposed by the thermal environment in which the optics will function. There may be constraints imposed by atmospheric or oceanic pressures. There may be constraints on glass choice imposed by humidity (or salinity) in the operational environment.

Finally, there are fabrication, alignment, metrology, and cost constraints. It is preferable to design refractive systems with spherical surfaces rather than aspheric surfaces. The latter are harder to make and test, and thus cost more. You do not want to design a system whose tolerances are so tight that it cannot be made. Again, tighter tolerances increase fabrication, assembly, and metrology costs. If possible, you want to avoid systems that will be difficult to align; e.g., off-axis systems are harder to align than on-axis systems. They are also harder to test. You usually will have to find a compromise between what the customer wants and what he can afford.

1.3 Homework

With the information provided in Figure 1.9, find:

- a. the effective focal length (EFL),
- b. the lens power ϕ ,
- c. surface curvatures C_1 and C_2 (assume equiconvex),
- d. radius of curvatures R_1 and R_2 ,
- e. format size (assume square), and
- f. Airy disk diameter.

Note: The lens can be considered as a thin lens.

Section 1.3: Homework 9

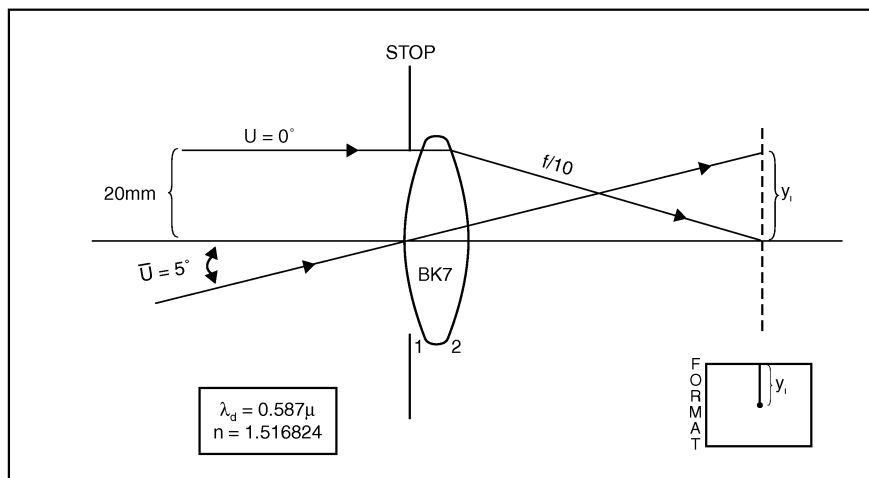


Fig. 1.9 Illustration for Homework.

10 *Chapter 1 Agenda*

Chapter 2

ZEMAX

2.1 Introduction to ZEMAX

The optical design and analysis code ZEMAX® from Focus Software will be used as the main workhorse throughout this course. This user-friendly software is both powerful and cost effective. In addition, the code is one used extensively in today's workplace. There are other major codes you will encounter in your professional career such as Code-V®, Synopsis®, and SuperOslo®. However, it is important for the student to become adept in at least one major program. This chapter will provide a general introduction and basic orientation to ZEMAX. More detailed information can be found in the ZEMAX manual.

2.2 Data Entry

Before you can begin your design and analysis work, you need to enter an initial prescription into the code. There are four areas requiring input of basic information about the lens, aperture, field, and wavelength. As an example, we will enter a biconvex lens.

2.2.1 Inserting a Prescription in the Lens Data Editor

The main ZEMAX screen (Figure 2.1) shows a toolbar at the top with File, Editor, System, etc. Below that is a row of buttons designated as Upd, Gen, Fie, Wav, etc. Beneath that is the Lens Data Editor (LDE).

Under Surface Type is a column on the extreme left with OBJ, STO, and IMA. With the mouse, move the arrow to the box just to the right of STO and click. The box (Standard) will be highlighted. (You can also do this using the arrow keys.) Now press the Insert key. You have just added a surface designated as 1. Go to Standard next to the IMA row, click, and then press Insert twice. You have now added two more surfaces designated as 3 and 4.

To the right of the Surface Type row are columns labeled Comment, Radius, Thickness, Glass, Semi-Diameter and Conic. Under the Radius column, move the cursor to Surface 3 and enter 100. Drop down to Surface 4 and enter -100.

Under the thickness column, move the cursor to Surface 1 and enter 25. Drop down to Surface 3 and enter 10. Drop down to Surface 4 and double click on the box to the immediate right of the data entry line. A submenu will appear. On the

12 Chapter 2 ZEMAX

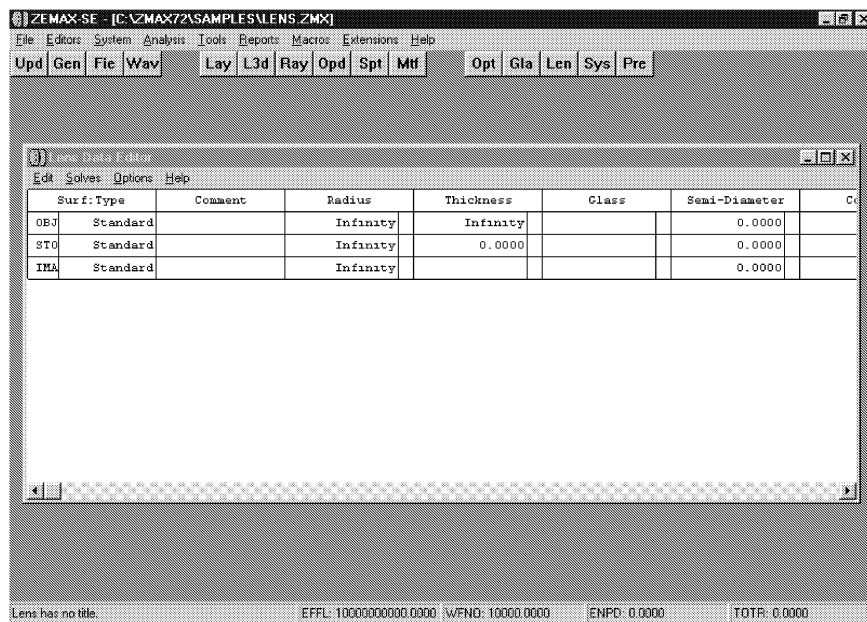


Fig. 2.1 Main ZEMAX menu as it initially appears.

line labeled **Solve Type**, click on the arrow. Several options will appear. Select Marginal Ray Height. (On the height and pupil zone lines the number 0 should also appear.) Click on OK to exit this submenu. The letter M will appear in the little box. This solve will automatically locate the paraxial back focal length since the object is at infinity.

Go to the **Glass** column. Drop down to **Surface 3** and insert **BK7**.

Go to the **Semi-Diameter** column. Drop down to **Surface 3** and enter **25**. Do the same on **Surface 4**. (Note that the letter U appears in the narrow column on the right. This indicates a user-defined quantity.) The semi-diameter specified here defines the actual size of the lens and how it is drawn. It does *not* define the system aperture. This will be done in the dialog boxes.

This completes the information needed in the Lens Data Editor.

2.2.2 Dialog Boxes

Click on the **Gen** button. A submenu will appear. This is where the *system* aperture size is defined, glass catalogs are selected, and units are chosen. Click the arrow on the line **Aper Type**. Another submenu will appear. Click on **Entrance Pupil Diameter**. On the line **Aper Value** insert **40**. This defines the system aperture. Note that the default units are millimeters. Leave this as it is.

Had we not specified lens size in the LDE, all surface aperture sizes would be automatically defined by the EPD just inserted. Also note that the default glass

Section 2.3: Layout 13

SURFACE DATA SUMMARY:

Surf	Type	Comment	Radius	Thickness	Glass	Diameter	Conic
OBJ	STANDARD		Infinity	Infinity		0	0
1	STANDARD		Infinity	25		48.81635	0
STO	STANDARD		Infinity	0		40	0
3	STANDARD		100	10	BK7	50	0
4	STANDARD		-100	95.0681		50	0
IMG	STANDARD		Infinity			43.61104	0

Fig. 2.2 Hard copy prescription of biconvex lens.

catalog is Schott. Click on OK to exit this submenu.

Click on the Fie button. A new submenu appears through which field angles are selected. The zero field (on-axis) is already activated. Click on the little box on the extreme left to activate fields 2 and 3. Under the Y-Field column, move the cursor to field 2 and click. Enter 7.07. Go to field 3, click, and enter 10. We have active field angles now at 0°, 7.07°, and 10°. Click OK.

Click on the Wav button. A new submenu will appear. One wavelength is already activated, but this is not the one we want. Move the cursor to row 1 under wavelength, click on the box, and enter 0.486. Activate two more wavelengths by clicking on the little boxes to the extreme left. Under wavelength, click on row 2 and enter 0.587. For row 3 enter 0.656. You have just inserted the three classic wavelengths (in microns)¹ used to define the visible spectrum. They are also designated as the F, d and C lines. In the column marked Primary, click on the button on row 2. This designates the reference wavelength that will be used in the calculation of all first and third order properties.

It may seem confusing at first, but with a little practice it will become second nature. The Lens Data Editor should look like that shown in Figure 2.2. (To get a hard copy of the prescription click on the Pre button → Settings → surface data → OK → Print.)

2.3 Layout

To see what the system looks like, click on the Lay button. The diagram is shown in Figure 2.3. To obtain the scale for this diagram click on Settings. In the Scale Factor box insert 1. Click on OK. The drawing reappears with a scale bar illustrated below it. Note that the Settings box allows you to choose the number of rays and also what fields and wavelengths to display. Explore these to gain a better understanding of these options.

Our object is at infinity, so we have collimated light coming in at the three selected field angles. But we are only seeing 25 mm of collimated space in front of the lens. The stop lies in the plane of the vertex of the first lens surface. The stop diameter (40 mm) is smaller than the 50 mm diameter of the lens. Recall that the semi-diameter column in the LDE designates how big the surfaces are drawn on the

¹ SI units use micrometer.

14 Chapter 2 ZEMAX

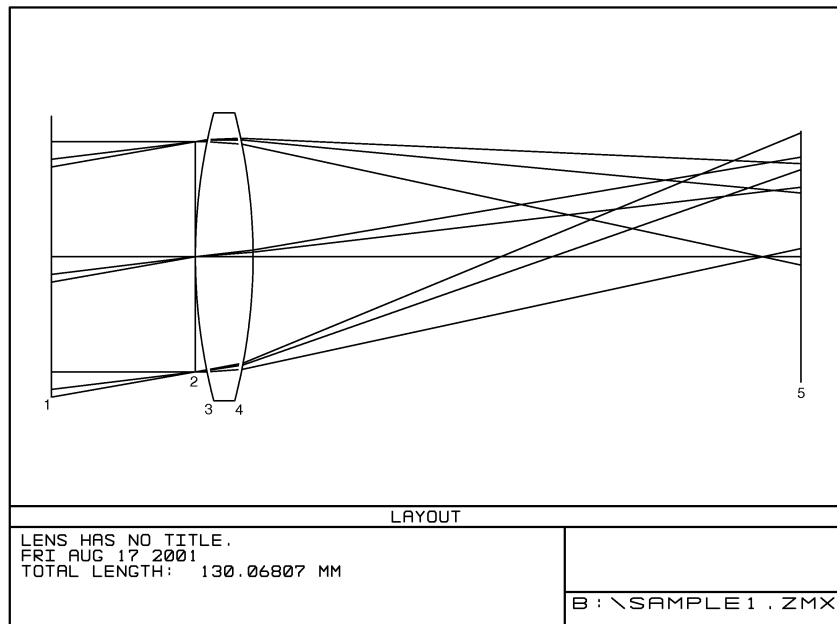


Fig. 2.3 Layout of example prescription of a biconvex lens.

GENERAL LENS DATA:

```

Surfaces      :          5
Stop          :          2
System Aperture : Entrance Pupil Diameter = 40
Ray aiming    : Off
Apodization   : Uniform, factor = 0.00000E+000
Eff. Focal Len. :      98.42156 (in air)
Eff. Focal Len. :      98.42156 (in image space)
Back Focal Len. :     95.06807
Total Track   :     130.0681
Image Space F/# :    2.460539
Para. Wrkng F/# :    2.460539
Working F/#   :    2.361136
Image Space N.A.: 0.203207
Obj. Space N.A. : 2e-009
Stop Radius   :      20
Parax. Ima. Hgt.:      0
Parax. Mag.    :      0
Entr. Pup. Dia. :      40
Entr. Pup. Pos. :      25
Exit Pupil Dia. :    41.41099
Exit Pupil Pos. : -101.8934
Field Type    : Angle in degrees
Maximum Field :      10
Primary Wave   :      0.587
Lens Units    : Millimeters
Angular Mag.  :      0

```

Fig. 2.4 List of system level first-order properties.

Section 2.3: Layout 15

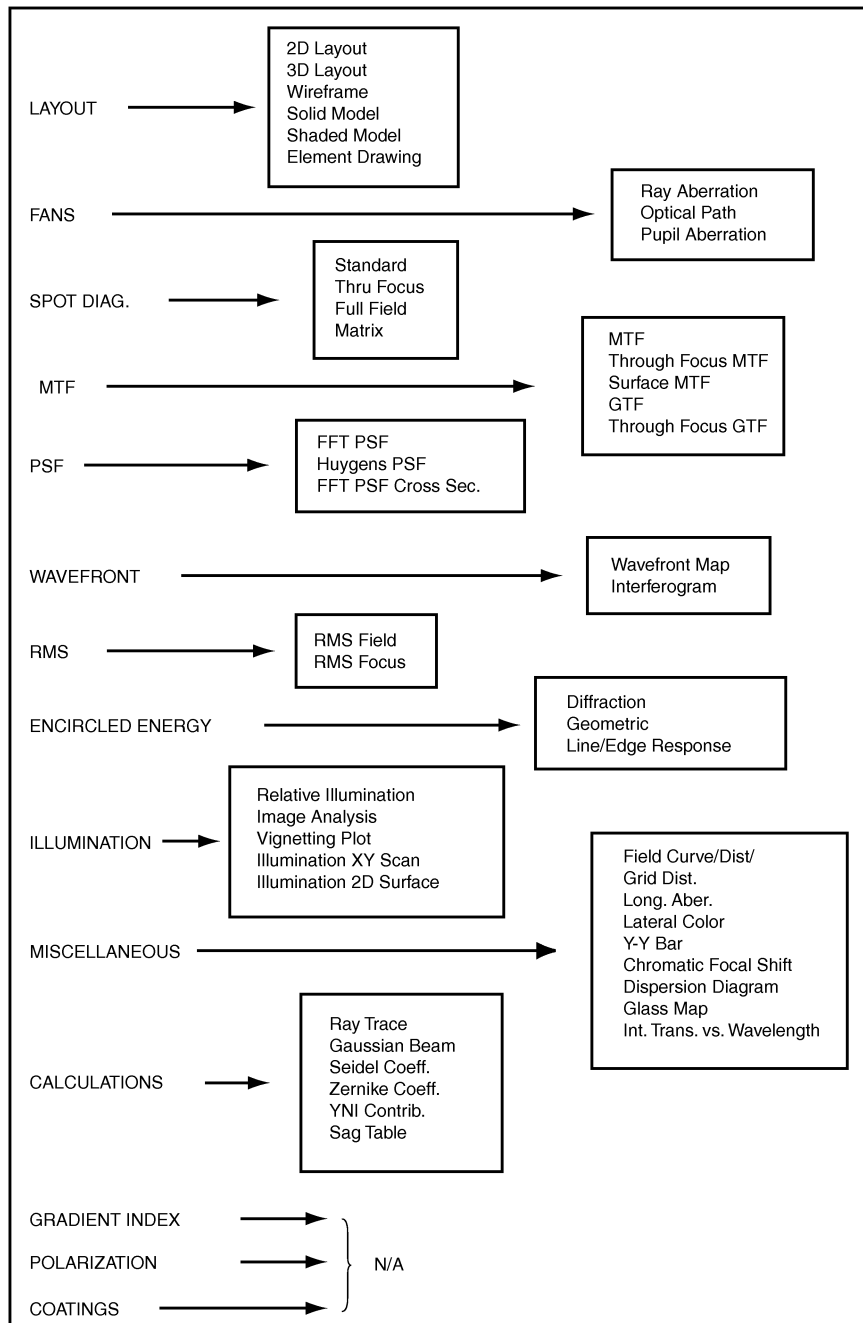


Fig. 2.5 List of analysis options in ZEMAX.

16 Chapter 2 ZEMAX

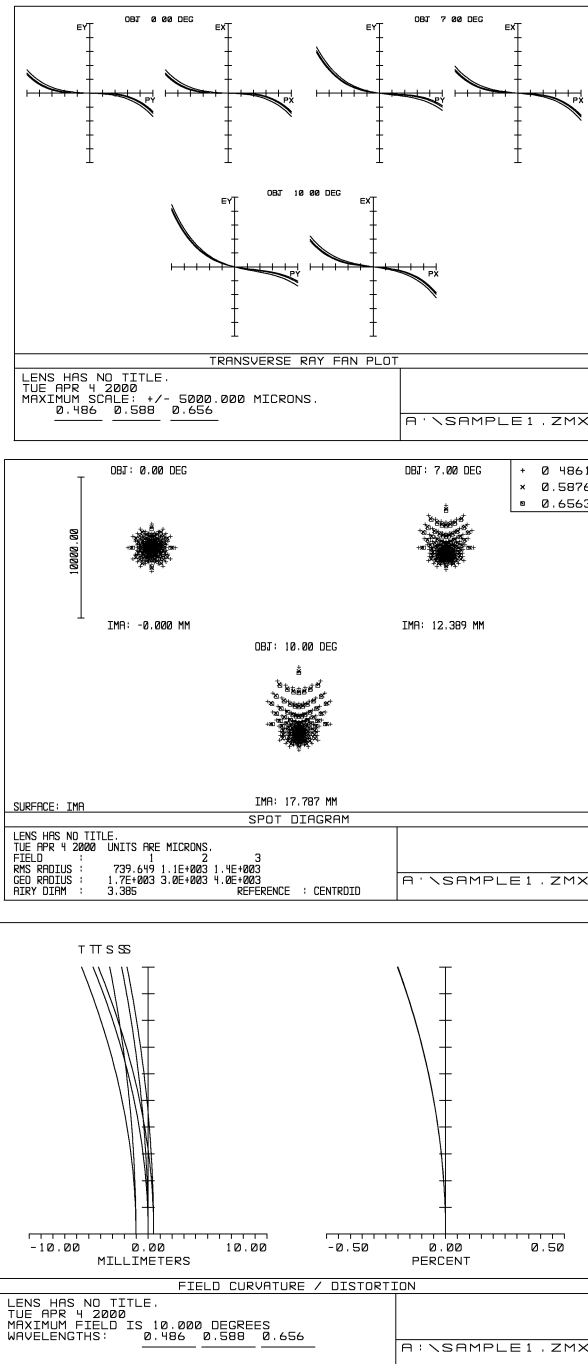


Fig. 2.6 Illustration of several plot options.

Section 2.4: First Order Properties 17

layout and nothing more. The image plane designated in the plot is where the paraxial marginal ray height is zero (defined by the M-solve). The back focal length is found in the LDE in the thickness column on Surface 4 and is 95.068 mm.

2.4 First Order Properties

We are left with the question, “What is the effective focal length (EFL) and f-number of the system?” To find out what these are as well as other first order properties, click on the **Sys** button. This will bring up a chart with all the system information listed as shown in Figure 2.4. We see that the EFL is 98.42 mm. The total track = 130.07 mm and is the sum of thicknesses as measured from the first surface to the image plane. Note that there are three f-numbers listed. The first, image space f-number, is $f/2.46$ or EFL divided by EPD (object at infinity). The others will be discussed in Section 2.8.

2.5 Analysis

At the main menu, clicking on **Analysis** provides the user with options for calculations, plots and graphs that cover nearly every aspect of design analysis. What is available is summarized in Figure 2.5.

For example, to find ray trace information, click on **Calculations**. Another menu box will appear to the right. Click on **Ray Trace**. Information on the marginal ray for both the real and paraxial rays is then displayed. Ray selection can be made by clicking on **Settings**. You can choose the object point’s field location (H) and the ray pierce location in the entrance pupil (ρ). Both are given in normalized coordinates; i.e., they have values between 0 and 1. The more frequently used analysis plot options can be accessed either through **Analysis** or by using the buttons **Ray**, **Opd**, **Spt**, and **Mtf**. As an example, Figure 2.6 shows ray fan, spot diagram, and field curvature and distortion plots.

2.6 Keeping Track of Designs

In the heat of doing battle with aberrations, many different things are tried to optimize a design. It is very easy to lose track of how you got to a certain point. Therefore, documentation of each step of your design process is extremely important. This documentation should include not only what variables were manipulated and what merit function structure was used, but also the step-by-step file names. For this course, all design homework will be handed in on a 3.5" floppy disk. The following character file name protocol will be used:

- the first four characters will be letters which will identify the type of system with which we are working;
- the fifth character will be a number (1–9) which will either identify separate designs within the same type or different optimization approaches for the same design problem;

18 Chapter 2 ZEMAX

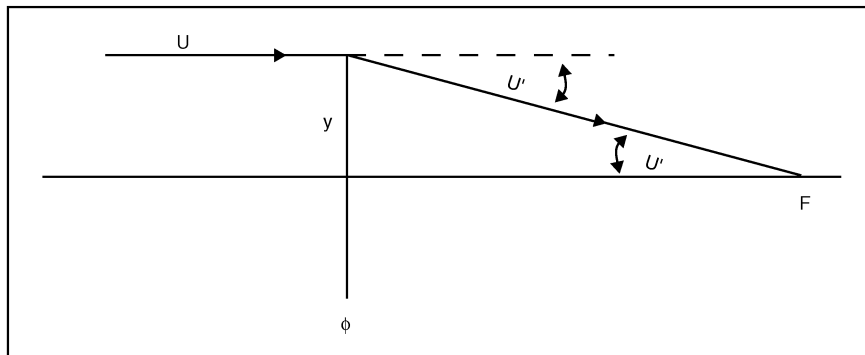


Fig. 2.7 How *f*-number is related to image space U' .

- the sixth character will always be the letter **o** which stands for the optimization path;
- the next character(s) will be a number which designates a particular step in the optimization path;
- the last character will be either the letter **b** or **a**, indicating the condition of the design *before* and *after* the optimization step.

For example, TRIP2o4b indicates a second triplet design at the fourth step of the optimization process just prior to the new optimization run. It is also recommended that each design problem be kept in a separately named folder. For example, the folder containing TRIP2o4b would be called “Triplet.”

The naming protocol also serves another important and practical function. It allows the instructor to keep his sanity. It is much easier to grade homework when every student follows the same protocol. When homework is handed in on disk, a script should accompany it. The script should describe what is being done at each optimization step. An example of scripting will be found in your second homework assignment (in Chapter 3). All subsequent ZEMAX assignments should be scripted in a similar manner.

2.7 ZEMAX Glass Catalog

When you insert data under the parameter heading **Glass** in the LDE you will usually do so using a designation supplied by the manufacturer, e.g., Schott, Ohara, or Corning. ZEMAX has a library of glass designations in folders identified by the company name. Different folders are accessed by ZEMAX *only* when the manufacturer is identified in the **Gen** menu. There is also a folder which contains commonly used IR transmissive materials such as zinc selenide. Finally, there is a miscellaneous folder that is a mixed bag of different materials including air, water, and plastics.

Glass in ZEMAX is *not* stored as a refractive index versus wavelength look-up table. Rather, glass is stored as a polynomial function; it is the first six coeffi-

Section 2.8: Odds and Ends 19

ients of this polynomial that are stored. If you click on the **Gla** button, the glass catalog menu will appear. The coefficients for any particular glass are represented by the numbers just to the right of the A0–A5 alpha-numerics. ZEMAX uses these coefficients to calculate the refractive index at any selected wavelength within the valid domain of the polynomial. Of course these coefficients are based on a polynomial fit to *measured* data over a certain spectral range.

The ZEMAX glass catalog provides explicit index data only for “*d*” light ($\lambda = 587$ nm). If you want to find out what the indices are for the wavelengths you have selected, you must click on **Pre** → **Settings** → **Index Data** → **OK**.

2.8 Odds and Ends

2.8.1 More on f-number

We saw that there are three distinct f-numbers shown in ZEMAX’s General Lens Data list. The traditional f-number is given by the “image space f-number.” What about the other two? Consider a ray parallel to the optical axis incident on a thin singlet at a height y as shown in Figure 2.7.

$$\text{image space f-number: } f/\# = \frac{\text{EFL}}{\text{EPD}} \quad (2.1)$$

$$f/\# = \frac{\text{EFL}}{2y} \quad (2.2)$$

$$f/\# = \frac{1}{2y/\text{EFL}} \quad (2.3)$$

$$\text{paraxial working } f/\# = \frac{1}{2 \tan U'} \quad (2.4)$$

Here we see that f-number is related to the bend angle on the ray coming to a focus in image space. We’ll call this the “paraxial working f-number.” It will be the same as the “image space f-number” *only* when the object is at infinity. If the object is at some finite distance, then the bend angle U' will be different resulting in a different *effective* f-number.

The last f-number ZEMAX uses is called the “working f-number.” It is defined as:

$$\text{working } f/\# = \frac{1}{2 \sin U'} . \quad (2.5)$$

This f-number applies to real aberrated systems where U' departs from its ideal unaberrated path.

We will talk more about paraxial and real rays in Chapter 4.

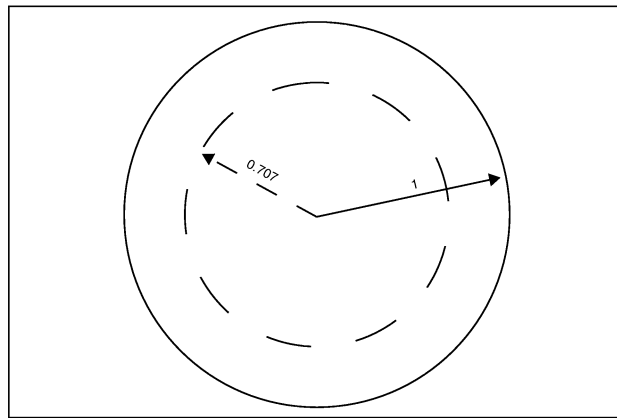


Fig. 2.8 Zone selection for rays either in object field or in pupil.

2.8.2 Ray Selection

Consider a unit circle as shown in Figure 2.8. Its area is 3.1416 units. What is the subradius that will enclose *half* this value?

$$\text{subradius} = \sqrt{\frac{3.1416}{2\pi}} = 0.7071 \quad (2.6)$$

The subradius 0.7071 divides the unit circle into two regions (an inner circle and an outer annulus) having the *same* area. There are two traditional applications of this in lens design and in ZEMAX. The first is in selecting where in a circular object field rays emanate; the second, where in the circular entrance pupil rays are incident. When we use the *default* merit function in ZEMAX to set up the ray ensemble for tracing through the system for optimization, you'll see that use is made of this subradius. Back in Section 2.2.2 we selected fields of 0°, 7.07°, and 10°. The middle value was not an arbitrary selection; it was 0.707 times the maximum field angle.

Chapter 3

Conventions and Aspheres

3.1 Introduction

In the last chapter you gained some familiarity with ZEMAX. In this chapter you will start using it. The problem assignment in Section 3.6 will walk you through an extensive exercise set involving the singlet from the first homework. Part of that exercise will involve bending the lens, while maintaining power, to minimize spherical aberration. You will also be using an aspheric surface to drive the spherical aberration to zero. Much of this chapter provides background material for this ZEMAX exercise.

3.2 Sign Conventions

The prescription information fed into ZEMAX and the data for manual calculations will follow a specific sign convention. Figure 3.1 will serve as a guide and reminder of those conventions. Radius of curvature, R , and curvature, C [$= 1/R$], are positive if the center of curvature lies to the right of the surface vertex; negative if the center is to the left of the vertex. Shown in the figure are the front and rear principal planes. The former lies to the right of the first surface vertex and the separation (δ) is positive; the latter (δ') is negative. The effective focal length, f' , (measured from the rear principle plane) is positive. The front focal length, f , is negative. The object distance (l), measured from the front principal plane, is negative. The image distance (l'), measured from the rear principal plane, is positive. A ray angle is positive if it has an upward slope; negative if downward.

3.3 Shape Factor

Figure 3.2 shows five lenses, all of which have the same focal length or power. The shape of the lens is defined by the shape factor, X . It is defined as:

$$X = \frac{(C_1 + C_2)}{(C_1 - C_2)} \quad (3.1)$$

An equi-biconvex lens has a zero shape factor. A plano-convex lens has a -1 shape factor while a convex-plano lens is $+1$. In the exercise, the lens shape will be

22 Chapter 3 Conventions and Aspheres

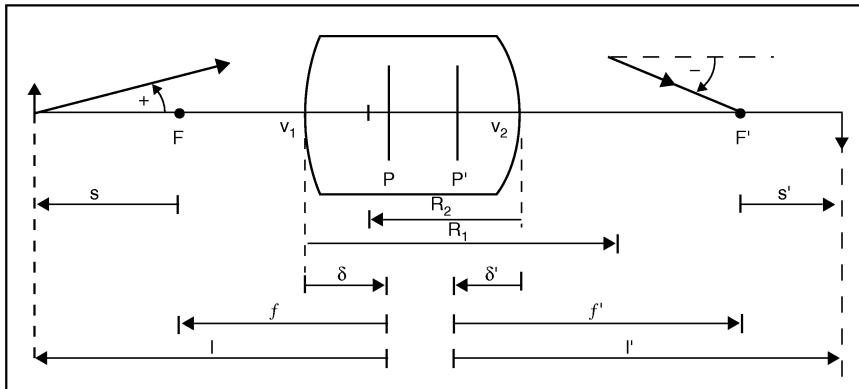


Fig. 3.1 Sign conventions as used in this book.

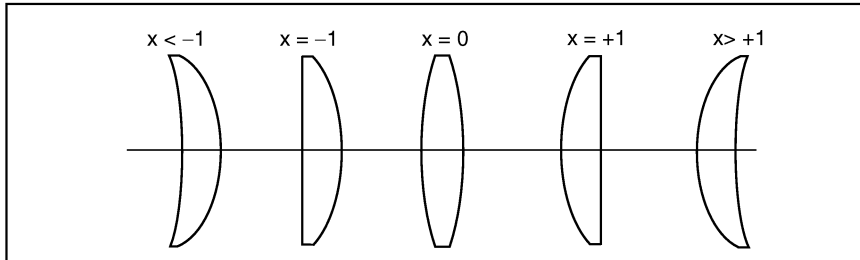


Fig. 3.2 Lenses have identical power but different shapes.

changed, and the amount of spherical aberration in image space will also change. Also note that the principal planes will shift position relative to the lens for different bendings.

3.4 Surface Sag

An important property of an optical surface is surface sag, which is illustrated in Figure 3.3. In optical shops, the radii of curvatures specified in your design will be verified by measuring their sags (using a device called a spherometer). Sag will also show up in our discussion on aspheric surfaces.

The exact definition of sag is:

$$\text{sag} = R - \sqrt{R^2 - y^2} \quad (3.2)$$

A convenient approximation is now derived. Rewriting Eq. 3.2:

$$\text{sag} = R - R \left[1 - \left(\frac{y}{R} \right)^2 \right]^{\frac{1}{2}} \quad (3.3)$$

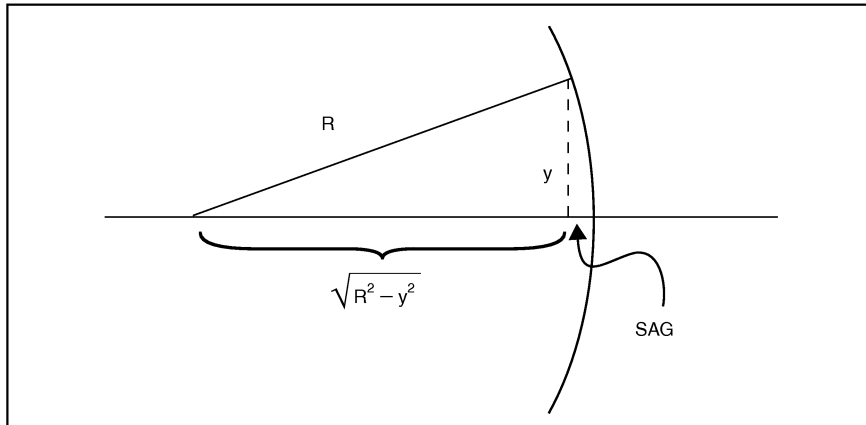


Fig. 3.3 Illustration of surface sag.

After taking a binomial expansion and keeping the first two terms:

$$\text{sag} \cong R - R \left[1 - \frac{y^2}{2R^2} \right] \quad (3.4)$$

$$\text{sag} \cong R - R + \frac{y^2}{2R} \quad (3.5)$$

$$\text{sag} \cong \frac{y^2}{2R} \quad (3.5)$$

Equation 3.5 is the parabolic approximation of the sag of a sphere.

3.5 Aspheric Surfaces

All of the optical surfaces we have dealt with thus far have been either flat or spherical. We must now enter the realm of aspherics. Such optics play a very important role in optical systems. For example, almost all reflective astronomical telescopes have at least one aspheric component, either on the primary or secondary. In most cases both components are aspheric. Closer to earth, the Kodak disc camera uses injection-molded glass elements, some of which are aspheric. The primary reason for using aspheric components is to eliminate spherical aberration (especially when there is a constraint on the number of optical surfaces and indices allowed). However, most designers still prefer to use spherical rather than aspherical surfaces. The reason has more to do with fabrication issues than anything else. Aspherics are much harder to make and measure. More time and skill are required of the optician and metrologist, thereby driving up costs. Consequently, the use of

24 Chapter 3 Conventions and Aspheres

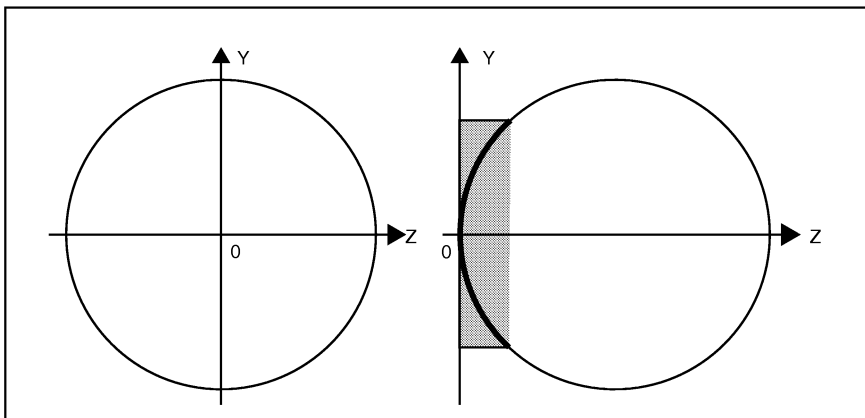


Fig. 3.4 Unshifted and shifted circles.

aspherics is limited to cases where (a) there is no other way, or (b) a trade-off study has shown it to be cost effective in the long run. Finally, it should be noted that the use of an aspheric does not change any of the first order design characteristics (cardinal points). All paraxial data remains the same.

The modification made to an optical surface designating it as aspheric is the presence of the conic constant. We will begin by deriving the standard form employed in geometrical optics. Consider the diagrams in Figure 3.4.

On the left we have a circle concentric with the origin of the coordinate system. The equation describing the circle is:

$$z^2 + y^2 = R^2 \quad (3.6)$$

Now we translate the coordinate system as shown on the right. The origin of the coordinate system is now coincident with the vertex of the optical surface. The equation for this translated circle is given by:

$$z^2 - 2zR + y^2 = 0 \quad (3.7)$$

The region of the surface we are interested in is the darkened arc passing through the vertex.

The equation describing a conic asphere is given by:

$$Pz^2 - 2zR + y^2 = 0 \quad (3.8)$$

where $P = 1 + K$, and $K = -e^2$, and e is the numerical eccentricity. (Note that $e^2 = (a^2 - b^2)/a^2$, where a is the semimajor, and b the semiminor axis of the conic respectively.) The conic constant is identified with P by some authors (Kingslake), and K by others (Malacara). One must be careful to ascertain which author is using which constant. This text uses K as does ZEMAX.

We now use the quadratic equation to solve Equation 3.8 for z (where

Section 3.5: Aspheric Surfaces 25

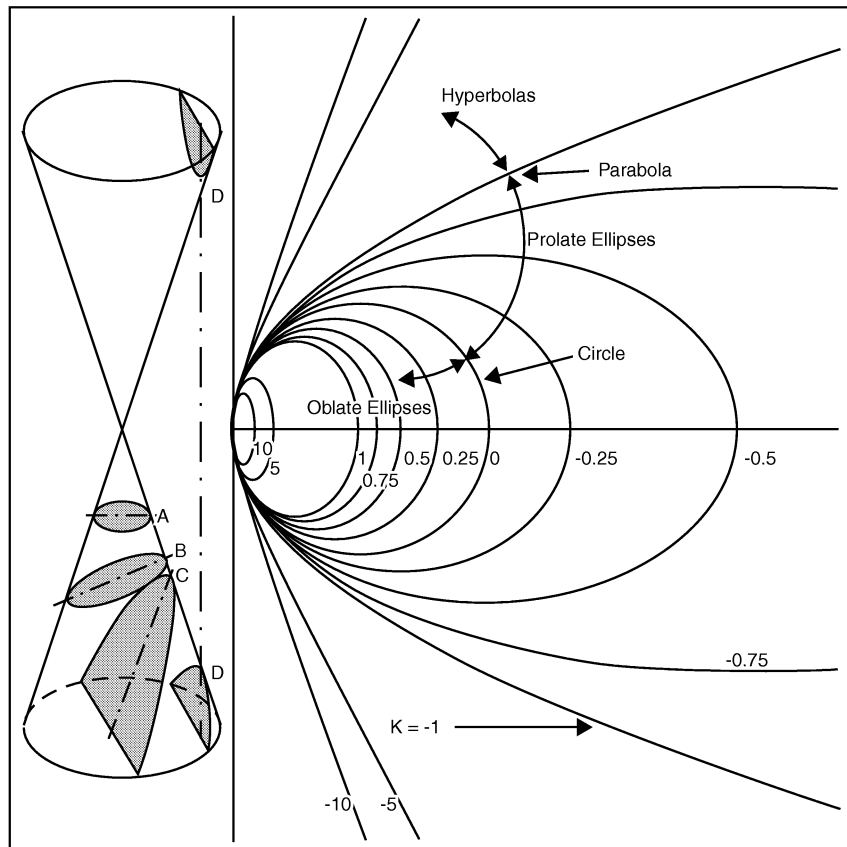


Fig. 3.5 Various conic constants. Reprinted with permission from Rutten and van Venrooij, Telescope Optics (Willmann-Bell, 1988).

$$a = P; b = -2R; c = y^2.$$

$$z = \frac{[2R \pm \sqrt{4R^2 - 4Py^2}]}{2P} \quad (3.9)$$

$$z = \frac{R \pm \sqrt{R^2 - Py^2}}{P}$$

Now select z_- (which makes $z \rightarrow 0$ when $y \rightarrow 0$).

$$z_- = \frac{R - R \sqrt{1 - P \left(\frac{y}{R} \right)^2}}{P}$$

26 Chapter 3 Conventions and Aspheres

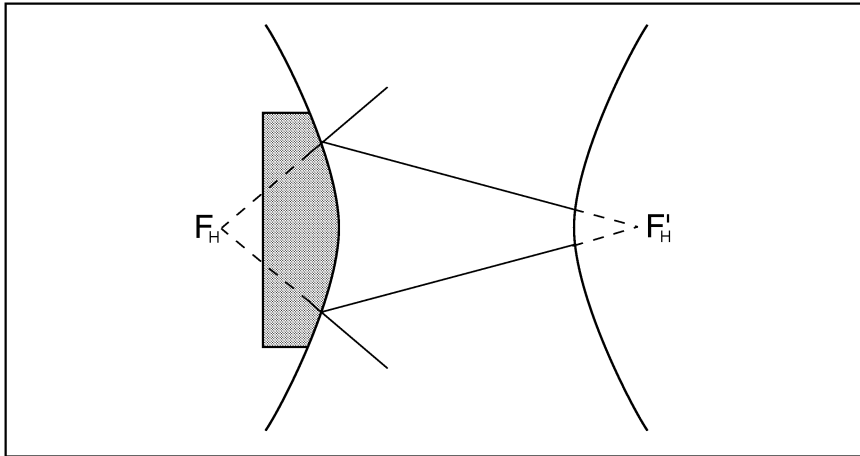


Fig. 3.6 Ray behavior with hyperbolic surfaces.

Table 3.1
Conic constant associated with different surface types.

Surface Type	Conic constant (K)	$P = 1 + K$
Circle	0	1
Parabola	-1	0
Hyperbola	< -1	< 0
Prolate Ellipse	$-1 < K < 0$	$0 < P < 1$
Oblate Ellipse	> 0	> 1

$$z_- = \left(\frac{R}{P} \right) \left[1 - \sqrt{1 - P \left(\frac{y}{R} \right)^2} \right] \quad (3.10)$$

Using the binomial expansion on the square root, and letting z_A replace z_- :

$$z_A \sim \left(\frac{R}{P} \right) \left\{ 1 - \left[1 - \left(\frac{P}{2} \right) \left(\frac{y}{R} \right)^2 - \left(\frac{P^2}{8} \right) \left(\frac{y}{R} \right)^4 - \left(\frac{P^3}{16} \right) \left(\frac{y}{R} \right)^6 - \text{etc.} \right] \right\} \quad (3.11)$$

$$z_A \sim \frac{y^2}{2R} + \left(\frac{P}{8} \right) \left(\frac{y^4}{R^3} \right) + \left(\frac{P^2}{16} \right) \left(\frac{y^6}{R^5} \right) + \left(\frac{5P^3}{128} \right) \left(\frac{y^8}{R^7} \right) + \text{etc.} \quad (3.12)$$

Note that the first term is simply the approximate sag of a spherical surface (as per Equation 3.5). The higher order terms represent the aspherical departure. The particular aspheric associated with various values of the conic constant are shown in Figure 3.5 and tabulated in Table 3.1.

The image of very distant source (e.g., a star) contains spherical aberration

Section 3.6: Departure From Sphere 27

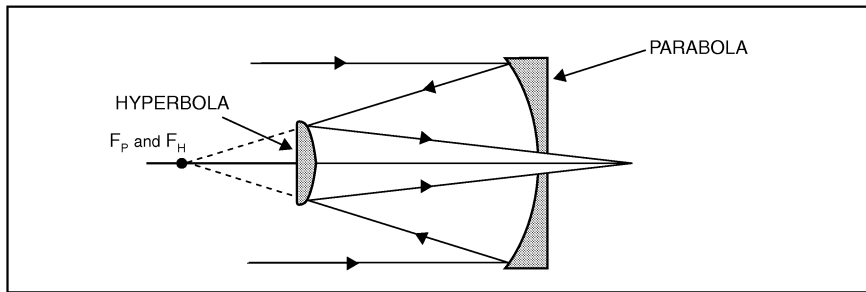


Fig. 3.7 Cassegrain telescope.

when its light is reflected from a spherical mirror. This reduces the detail in the image. A parabolic mirror, on the other hand, introduces no spherical aberration. Imagery is sharper. In the classical Cassegrain telescope, the primary mirror is parabolic. The secondary mirror is also aspheric and hyperbolic. A hyperbola has two foci. As illustrated in Figure 3.6, a ray directed toward the focus behind a hyperbolic reflector will be redirected toward the primed focus. In the Cassegrain telescope configuration, the parabolic focus coincides with the hyperbolic focus F_H as shown in Figure 3.7.

3.6 Departure From Sphere

As a designer you must have a good feel for the manufacturability and metrology of your optics. It may be the best diffraction-limited design ever—but if it can not be built what's the point. Also, it may prove difficult, or impossible, to align and test. Meeting spec is not the only criteria of a good design. Consequently, when aspherics are employed, be mindful of the fabrication and testing issues that arise, as well as the added costs and increased delivery times such surfaces usually entail.

When discussing an aspheric design with people in the optics shop, be prepared to provide information on how far the aspheric surface departs from a spherical surface at full aperture (or marginal ray height). This is illustrated in Figure 3.8.

The mathematical description of a spherical surface, Equation 3.7, can be recast into an expansion as was done for the aspheric surface in Equation 3.12. (The form can be quickly obtained by setting $P = 1$ in Equation 3.12.)

$$z_s \sim \frac{y^2}{2R} + \frac{1}{8} \left(\frac{y^4}{R^3} \right) + \frac{1}{16} \left(\frac{y^6}{R^5} \right) + \frac{5}{128} \left(\frac{y^8}{R^7} \right) + \text{etc.} \quad (3.13)$$

Of interest is the difference between Equation 3.13 and Equation 3.12 which, is the departure from sphere:

28 Chapter 3 Conventions and Aspheres

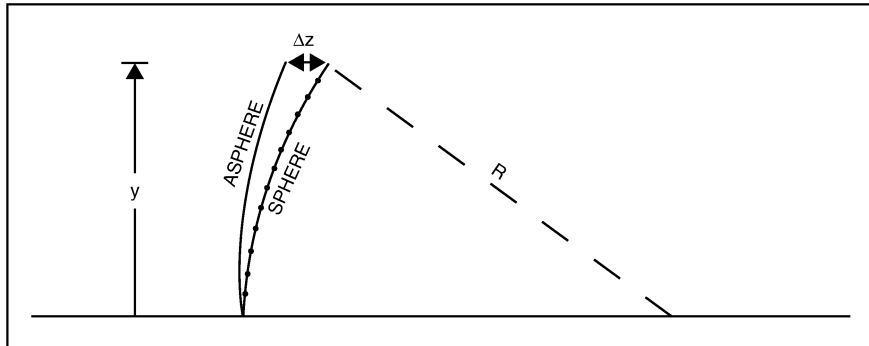


Fig. 3.8 Departure from sphere.

$$\Delta z = z_A - z_s \quad (3.14)$$

$$\Delta z \sim \left(\frac{1}{8}\right)(P-1)\left(\frac{y^4}{R^3}\right) + \left(\frac{1}{16}\right)(P^2-1)\left(\frac{y^6}{R^5}\right) + \left(\frac{5}{128}\right)(P^3-1)\left(\frac{y^8}{R^7}\right) + \text{etc.} \quad (3.15)$$

As an example, let's find Δz for a 31.25 cm focal length $f/1.25$ parabola. This means that the parameter values used in Equation 3.15 are: $P = 0$; $y = 12.5$ cm; $R = 62.5$ cm. Calculating the first two terms in Equation 3.15:

$$\Delta z = -0.0125 - 0.00025$$

$$\Delta z = -0.01275 \text{ cm} = -127.5 \text{ microns} = -201\lambda \text{ (for } \lambda = 0.6328\text{)}$$

This is a significant departure from sphere and means that a null lens (Chapter 35) would have to be designed to test this parabola interferometrically at its center of curvature.

3.7 Homework

This exercise consists of 11 parts. Its purpose is to give you some initial experience in the use of ZEMAX as a design and analysis tool. You will also start learning how to select variables and build a merit function for optimization. You will start by entering the lens used in the Homework for Chapter 1 and the radii calculated there. Use the same wavelength and dimensional unit (namely mm). Also, use the M-solve on the thickness after the second lens surface. Surface No.1 will be the first glass surface of the lens. (So initially you will have lines OBJ, STO [which is surf no.1], 2, and IMA.) The merit function editor (MFE) is accessed by clicking on Editors → Merit Function. Get in the habit of inserting all the Seidel operands as a means of keeping track of their values. (While on the first operand row, hit Insert several times for more rows to appear.) Whether operands are used in the optimization will be determined by the number under the weight column (keep moving cursor to right until you see the Weight, Value, and % Contribution

Section 3.7: Homework 29

Table 3.2
Initial MFE

Operand	Target	Weight
EFFL	400	0
SPHA	0	0
COMA	0	0
ASTI	0	0
DIST	0	0
PETC	0	0
BLNK		

column headings). Initially your MFE should look like Table 3.2.

Currently, all operands in the above table are turned off. The EFL and Seidels will be computed for wavelength 1 (the only one we're using). Insert 1 under the wavelength column for all operands.

3.7.1 Singlet

1. Load the lens from Homework for Chapter 1. That was a thin lens computation. Now use a real thickness: 4 mm. Field angles are: 0° , 3.5° , 5° , and $\lambda = 0.587$. Units are mm. Put M-solve on thickness of the second glass surface.

SING1o1b

Note: EFL and f-number are not quite the paraxial values. This is due to the insertion of real thickness.

2. Use f-number solve on R_2 to tweak back to paraxial.

Double click (DC) on R_2

Select f-number

Insert 10

SING1o1a

Check out spherical aberration: look at the ray fan plot; spot diagram; Seidel value.

3. Bend lens to reduce spherical. Remove F-solve on R_2 . (DC on R_2 , select variable). Make R_1 variable.

	Oper	T	W
Go to MFE:	EFFL	400	1
	SPHA	0	1

SING1o2b → OPT → SING1o2a

Note: SPHA has dropped from 1.716 to 1.09λ !

30 Chapter 3 Conventions and Aspheres

4. Go back to SING1o1a. Remove F-solve on R_2 . Variables on R_1 and R_2 .

	Oper	T	W
Go to MFE:	EFFL	400	1
	COMA	0	1

SING1o3b → OPT → SING1o3a

Note: coma has dropped from -4.88λ to 0.

5. Go back to SING1o1a. Remove F-solve on R_2 . Variables on R_1 and R_2 .

	Oper	T	W
Go to MFE:	EFFL	400	1
	ASTI	0	1

SING1o4b → OPT → SING1o4a

Note: ASTI has dropped from 6.40λ to 0 λ

SPHA increased to 325λ

COMA increased to -68λ

Look at layout—this lens is unusable.

6. Go back to SING1o2b. Remove variables on R_1 and R_2 . Place variable on *conic constant* of surf no. 2.

SING1o5b → OPT → SING1o5a

Note: SPHA is 0 without affecting coma or astigmatism.

7. Go back to SING1o2b. Set field to zero (this is important.). Go to MFE. Set weight on SPHA to 0. Go to the BLNK surface below all the other operands. Set cursor on BLNK. Go to:

Tools → Default Merit Function → RMS/Spot Radius/Centroid → OK

TRAC will now show up in MFE.

SING1o6b → OPT → SING1o6a

Note: SPHA $1.716 \rightarrow 1.09\lambda$!

8. Start with SING1o6a. Remove variables on radii. Insert surf no.3. This will be a dummy surface. Put a variable on its thickness. Change semi-diam on surf no. 3 and IMA to 2.

SING1o7b → OPT → SING1o7a

What this does is SHIFT our dummy plane to find the “BEST RMS FOCUS” location. This should be about -0.682 . Use Zoom on Layout

Section 3.7: Homework 31

to look at image region more closely.

- 9.** Start with SING1o7a. Restore 3.5° and 5° fields. Put variables on R_1 and R_2 . Go to MFE:

Tools → Default Merit Function → OK

This adds more TRAC terms to account for off-axis field points. Now we want to find the best RMS spot size compromise over *entire* field.

SING1o8b → OPT → SING1o8a

The shift should be about – 2.7.

- 10.** Start with SING1o8a. Add lens thickness as a variable.

SING1o9b → OPT → SING1o9a

Note that the lens is thicker. Astigmatism is considerably improved. Spherical and coma have gone up a bit.

- 11.** Such a thick lens is impractical. If lens thickness is to be used as a variable, we must put constraints on it. The operands used for this are:

MNCG minimum center glass thickness

MXCG maximum center glass thickness

Go back to SING1o9b. Insert two lines between PETC and the first TRAC line in the MFE.

	Surf no.	Surf no.	T	W
MNCG	1	2	3.0	1
MXCG	1	2	10.0	1

SING1o10b → OPT → SING1o10a

Spherical is better. So is coma. Not much happened to astigmatism.

32 *Chapter 3 Conventions and Aspheres*

Chapter 4

Paraxial World

4.1 Introduction

When you call up a ray trace in ZEMAX via Analysis → Calculations → Ray Trace you obtain surface height and angle data for a single ray selected via Settings. You will see two tables of data. The upper table is for the real ray; the lower, for the paraxial ray. In this chapter we will concentrate on where the numbers in the paraxial table come from, and answer the question: What is a paraxial ray?

In this book, most designs will be preceded by a thin lens pre-design. This will be done using manual first-order calculations. The basis for such calculations are the paraxial ray trace equations (PRTE). Real ray tracing is best left to the computer, but paraxial ray tracing is relatively easy. Though an approximation, it is nonetheless quite powerful. The EFL, BFL, f-number, magnification, principal plane locations, pupil locations, and image location can all be found using PRTE. Further, the paraxial ray heights and angles found on optical surfaces will also be used to calculate the Seidel aberrations.

4.2 Paraxial Ray Trace Equations

The PRTE are a pair of linear equations:

$$\text{PRTE1: } n\bar{u}' = n\bar{u} - y\phi \quad (4.1)$$

$$\text{PRTE2: } y_{j+1} = y_j + \bar{u}' \quad (4.2)$$

where $\bar{u} = \tan U$ and $\bar{u}' = \tan U'$, and ϕ is the optical power.

The first equation bends the ray (and will be derived in Section 4.5). The second equation provides the transfer height at the following optical surface (or plane of interest). Figures 4.1 and 4.2 illustrate the meaning of each equation.

As an example, we trace the ray from an axial object located 25 units from an optical element having $\phi = 0.05$ (with units of inverse length), and incident on that surface at a height of 5 units (as illustrated in Figure 4.3).

We first use Equation 4.2 to find the incidence angle on the optical surface.

$$5 = 0 + \bar{u} \cdot 25$$

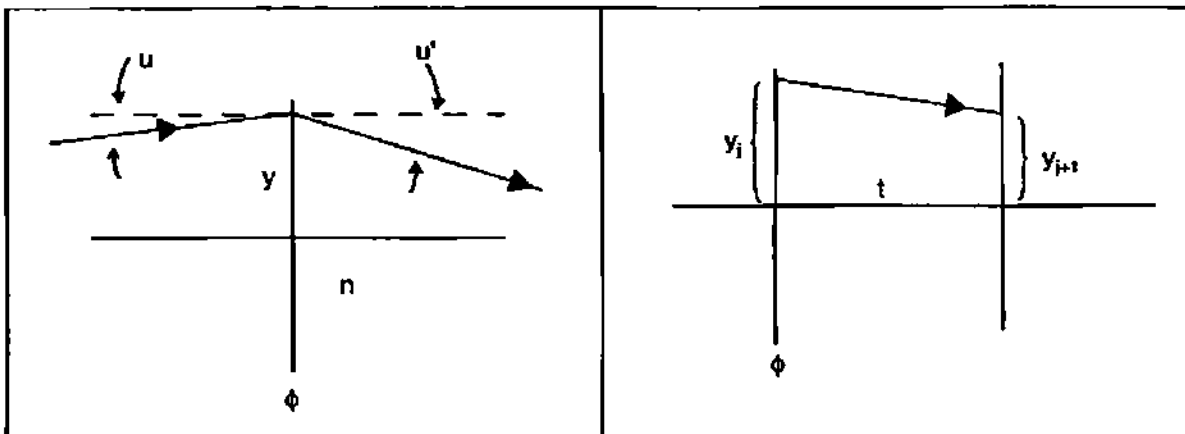


Fig. 4.1 Ray bending at a powered surface.

Fig. 4.2 Ray transfer to next optical surface.

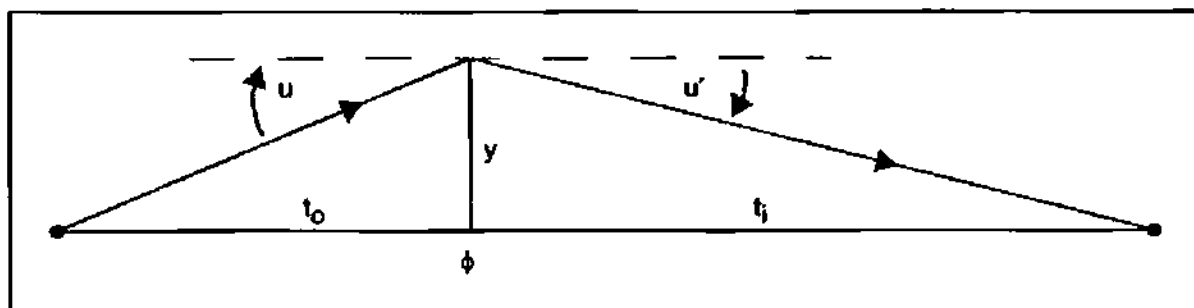


Fig. 4.3 Example of PRTE (thin lens).

$$u = \frac{1}{5}$$

We next use Equation 4.1 to find the amount of bending performed by the element. (Note in this example we have assumed that $n' = n = 1$. This is valid if ϕ is the power of a thin lens in air.)

$$u' = \frac{1}{5} - (0.05)5$$

$$\therefore u' = -0.05$$

Finally, we again employ Equation 4.2 to find the real image axial location.

$$0 = 5 + (-0.05)t_i ;$$

$$\therefore t_i = 100$$

Please note that any ray launched from the object to any height on the optical element would yield the same image distance, t_i . This is illustrated in Figure 4.4.

4.3 Gaussian Lens Formula

We will now derive a formula which relates the object and image conjugates. This is a basic formula learned in high school physics.

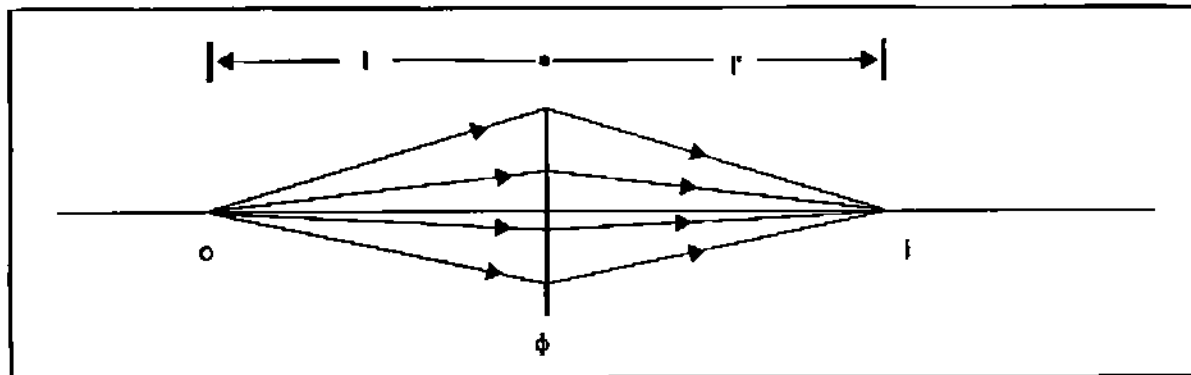


Fig. 4.4 All paraxial rays yield the same image distance.

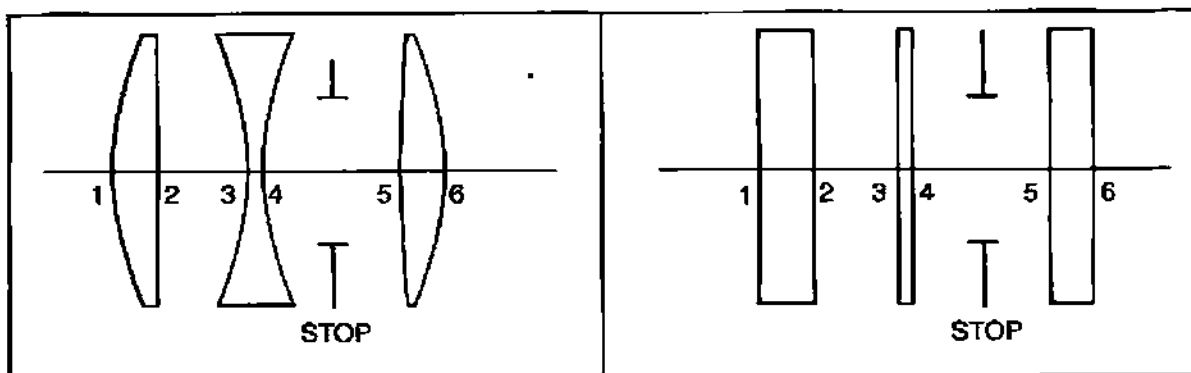


Fig. 4.5 Real triplet.

Fig. 4.6 PRTE triplet.

Rewrite Equation 4.1 as:

$$nu - n'u' = y \cdot \phi$$

Referring to Figure 4.4 once again, note that $u = -y/l$ (since u is positive, y is positive and l negative) and $u' = -y/l'$ (since u' is negative, y and l' are positive). (Refer to sign conventions in Figure 3.1 on page 22.)

Insert into the first equation:

$$-\frac{ny}{l} + \frac{n'y}{l'} = y \cdot \phi .$$

Divide through by y :

$$-\frac{n}{l} + \frac{n'}{l'} = \phi . \quad (4.3)$$

This is the Gaussian formula for a thin lens derived via the PRTE. Note that l in Figure 4.4 is (according to the convention in Figure 3.1) negative.

4.4 What Lenses Look Like in the PRTE World

Figure 4.5 shows a lens system known as a Cooke triplet. You will design one of these lenses later on. However, in the PRTE world the triplet has the look shown

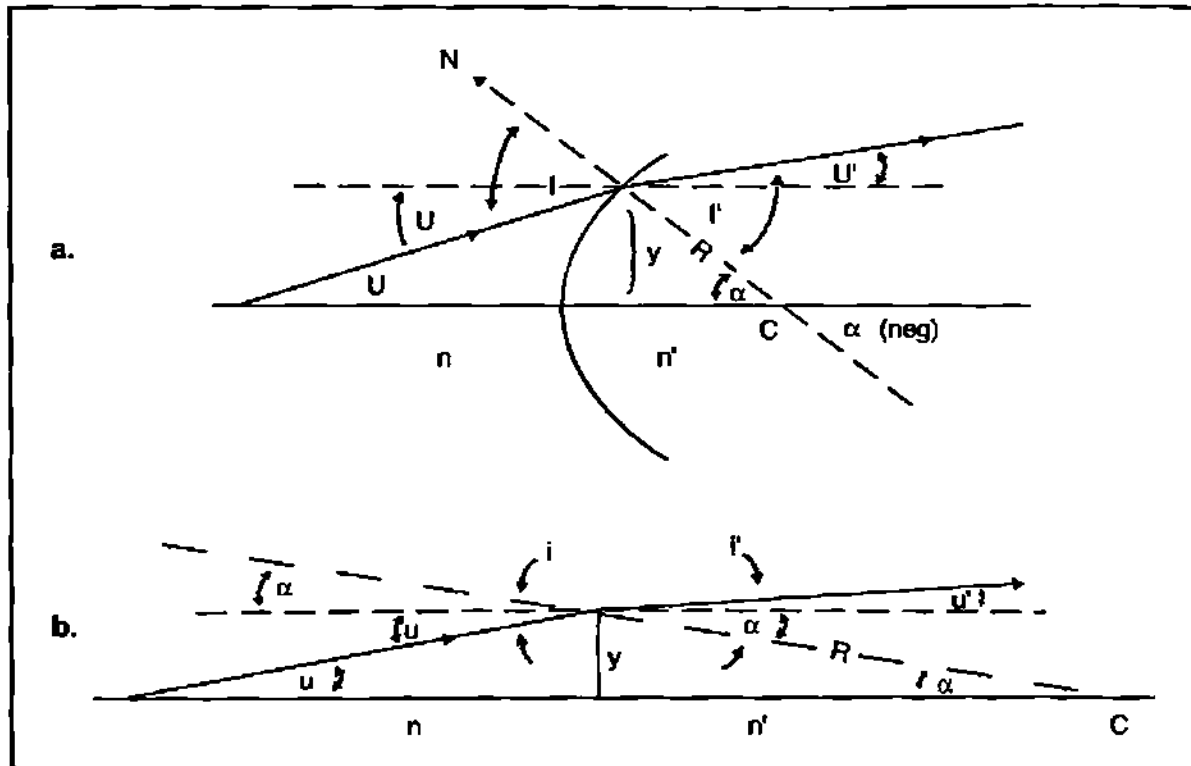


Fig. 4.7 Real ray trace at an optical surface: a. significant y height; b. paraxial y height.

in Figure 4.6. All dimensions are the same. This includes lens diameters, axial thicknesses, and axial separations. The curved surfaces are replaced with flat surfaces. But these surfaces have power. They can bend rays. The power of a surface is given by:

$$\Phi = (n' - n)C \quad (4.4)$$

where n' is the index to the right of the surface, n is the index to the left, C is the curvature ($1/R$).

All the first order properties of a real lens system can be determined using the surrogate paraxial system and the PRTE.

4.5 Determination of Surface Power

Consider the optical refractive surface in Figure 4.7a. We show a ray hitting the surface at a height y and bending. At the ray-surface intersection point, we also show the normal to the surface, and a dashed line parallel to the optical axis. Ray angles (U and U') and incident and refracted angles (I and I') are also shown. Now imagine sliding the intersection point downward so it is close to the optical axis. If we blow up the scale, we get the picture shown in Figure 4.7b. Using this latter picture and some math we can come up with Equation 4.4.

We start by obtaining an expression for α . From Figure 4.7b we see that:

$$\alpha = -\frac{y}{R} = -yC \quad (4.5)$$

Next we relate the incident and refracted angles to alpha and the ray angles:

$$\left\{ \begin{array}{l} i = -\alpha + u \\ i' = -\alpha + u' \end{array} \right\} \quad (4.6)$$

Next we write an expression for Snell's Law for small angles:

$$ni = n'i' \quad (4.7)$$

Now substitute Equations 4.6 into Equation 4.7 and rearrange:

$$\begin{aligned} n(u - \alpha) &= n'(u' - \alpha) \\ nu' &= nu - n\alpha + n\alpha \\ nu' &= nu + (n' - n)\alpha \end{aligned} \quad (4.8)$$

Now substitute in Equation 4.5:

$$nu' = nu - y[(n' - n)C] \quad (4.9)$$

This is the bending PRTE where $[(n' - n)C] = \phi$, the power of a single refracting surface.

4.6 Other Important Power Expressions

4.6.1 Single Reflecting Surface

We obtain the power of a curved mirror by setting $n' = -n$, in Equation 4.4.

$$\phi = -2nC \quad (4.10)$$

In air:

$$\phi = -2C \quad (4.11)$$

4.6.2 Two-Element System

Consider the paraxial ray trace of the two-element system shown in Figure 4.8.

We begin by using PRTE1 to find the ray bending introduced by the first element:

$$nu'_1 = 0 - y_1\phi_1$$

$$u'_1 = -\frac{y_1\phi_1}{n} = u_2 \quad (4.12)$$

Then we determine the ray height on the second surface using PRTE2:

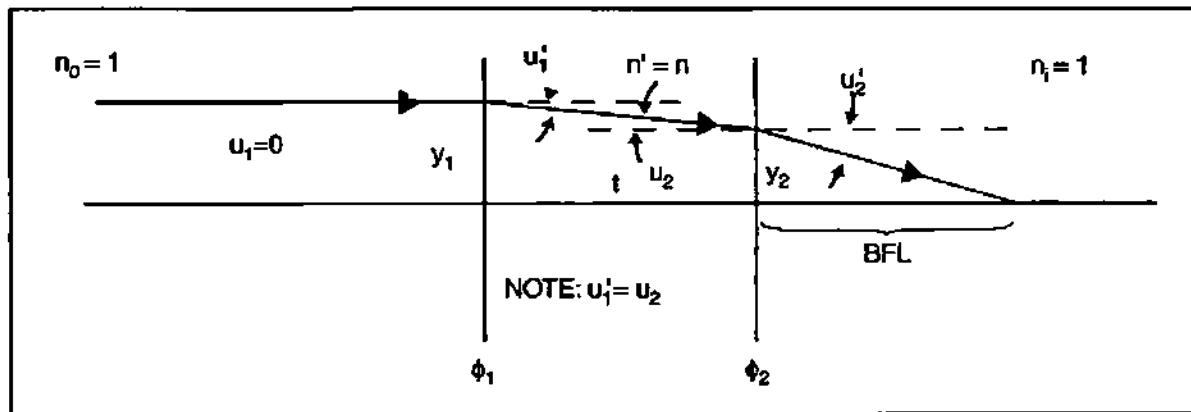


Fig. 4.8 PRTE on two-element system.

$$y_2 = y_1 + u_1' t \quad (4.13)$$

Going back to PRTE1, we calculate the ray bending due to the second element:

$$u_2' = nu_2 - y_2\phi_2 \quad (4.14)$$

Substitute Equation 4.13 into Equation 4.14:

$$u_2' = nu_2 - [y_1 + u_1' t]\phi_2 \quad (4.15)$$

And substitute Equation 4.12 into Equation 4.15:

$$\begin{aligned} u_2' &= n\left(\frac{-y_1\phi_1}{n}\right) - \left[y_1 + \left(\frac{-y_1\phi_1}{n}\right)t\right]\phi_2 \\ u_2' &= -y_1\phi_1 - y_1\phi_2 + y_1\left(\frac{t}{n}\right)\phi_1\phi_2 \\ u_2' &= -y_1\left[\phi_1 + \phi_2 - \left(\frac{t}{n}\right)\phi_1\phi_2\right] \end{aligned} \quad (4.16)$$

In Figure 4.9 we *backtrack* the ray emerging from the last element so that it crosses the continuation of the incident ray on the first surface. This locates the rear principal plane. The axial separation from this plane to the image point is the effective focal length (EFL).

$$u_2' = \frac{-y_1}{\text{EFL}} \quad (4.17)$$

Equating Equation 4.16 and Equation 4.17 and canceling out y_1 :

$$\frac{1}{\text{EFL}} = \left[\phi_1 + \phi_2 - \left(\frac{t}{n}\right)\phi_1\phi_2\right] = \phi \quad (4.18)$$

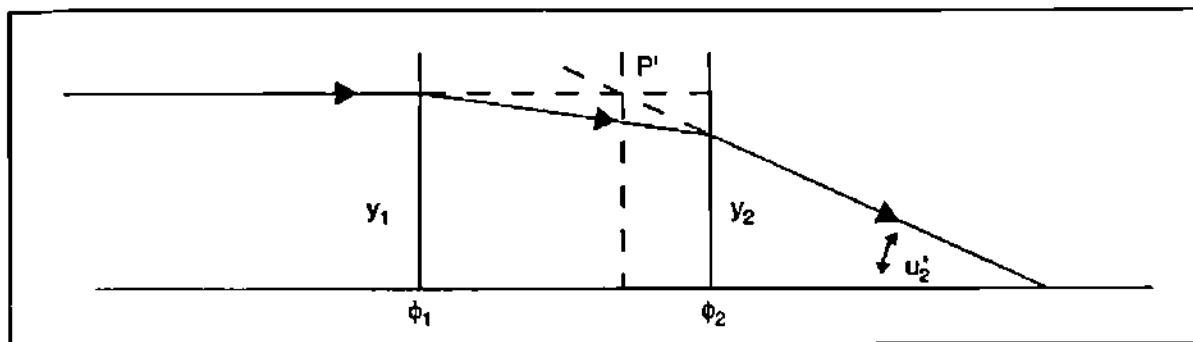


Fig. 4.9 EFL of two-element paraxial system.

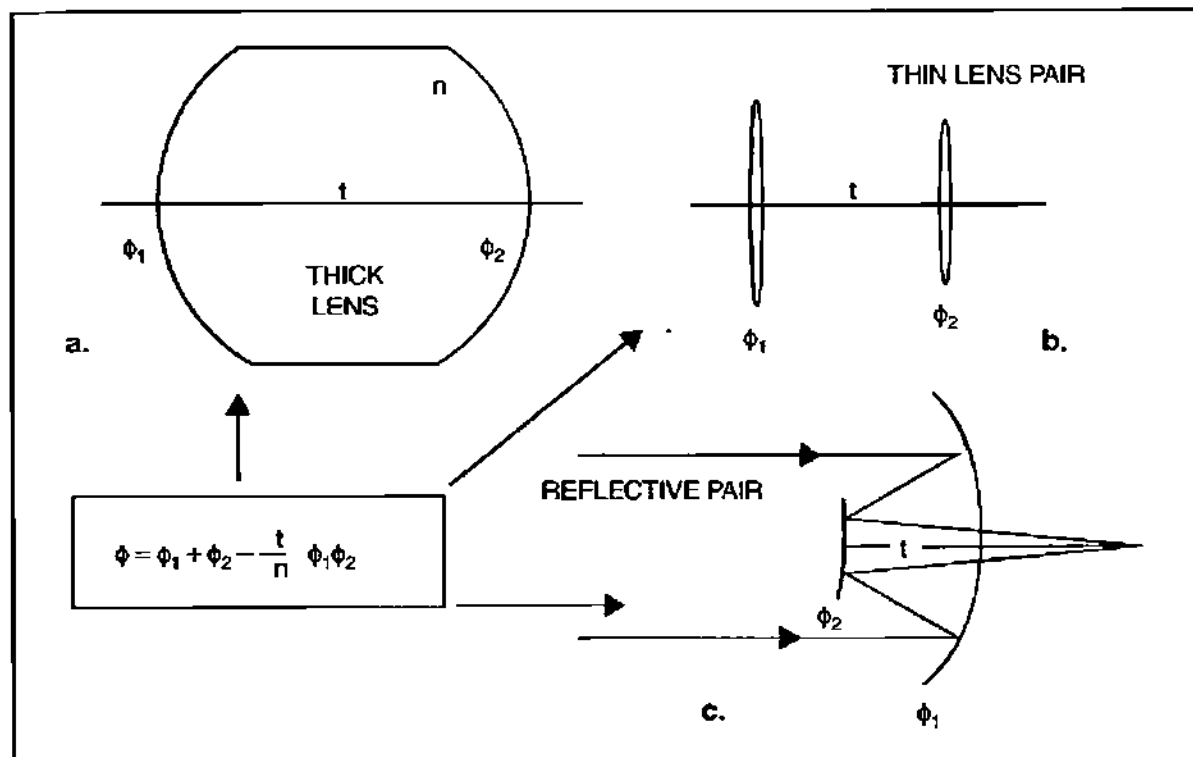


Fig. 4.10 Several physical embodiments of two-element systems.

Thus, ϕ is the system power of the two element optical system.

Equation 4.18 has a wide range of system applications as is illustrated in Figure 4.10. It can be used to determine the power of a thick lens and a separated two-lens or two-mirror system.

4.6.3 Thin Lens

For a thin lens, the thickness in Equation 4.18 is set to zero. The power becomes:

$$\phi = \phi_1 + \phi_2 \quad (4.19)$$

Now substitute in the power of single refracting surfaces (from Equation 4.4) for ϕ_1 and ϕ_2 :

$$\phi = (n' - n)C_1 + (n - n')C_2 \quad (4.20)$$

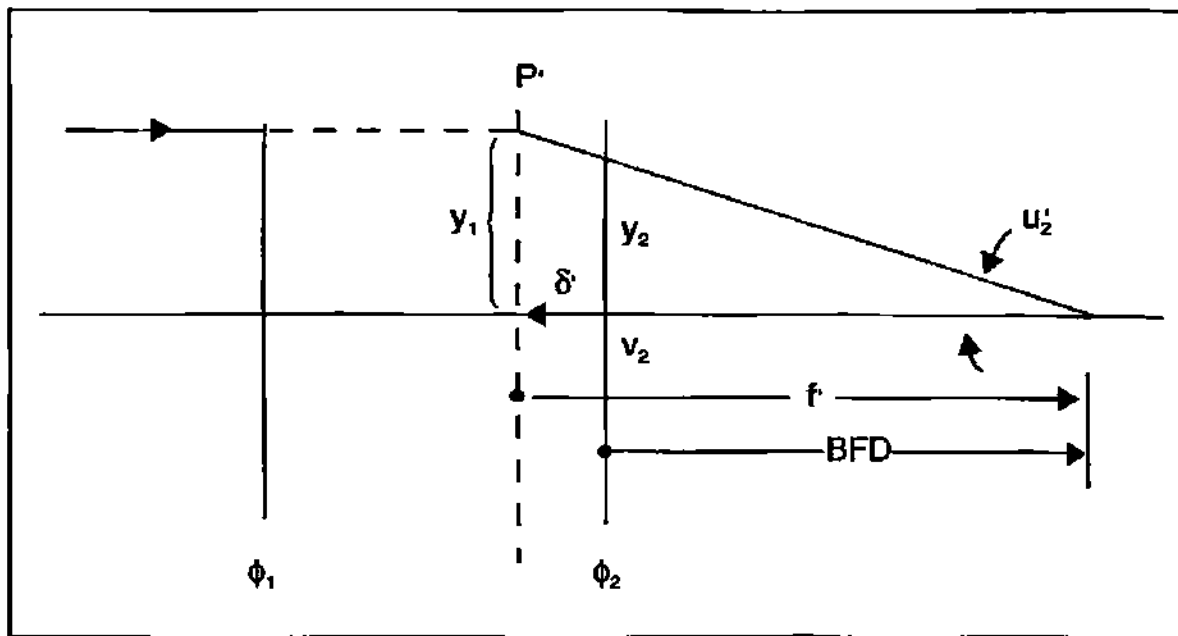


Fig. 4.11 Separation between rear principal plane and vertex.

Rearrange:

$$\begin{aligned}\phi &= n'(C_1 - C_2) - n(C_1 - C_2) \\ \phi &= (n' - n)(C_1 - C_2)\end{aligned}\quad (4.21)$$

If the lens is in air:

$$\phi = (n - 1)(C_1 - C_2) \quad (4.22)$$

Equation 4.22 is the famous “Lens Maker’s Equation.”

4.7 Principal Plane Locations in a Two-Element System

In Figure 4.9 we showed you how to find the rear principal plane of a two-element paraxial lens by backtracking, and that the axial separation between this plane and the focal point gave the EFL (or $f' = 1/\phi$). We now give the derivation of a handy formula which provides the axial separation between the rear principal plane and the vertex of the second element. Please refer to Figure 4.11.

First we relate two ratios:

$$\frac{y_2}{f' + \delta'} = \frac{y_1}{f'} . \quad (4.23)$$

Cross-multiply and solve for δ' :

$$\delta' = \left(\frac{y_2}{v_1} - 1 \right) f' . \quad (4.24)$$

Substitute PRTE2 for y_2 :

$$\delta' = \left[\frac{(y_1 + tu_2)}{y_1} - 1 \right] f'. \quad (4.25)$$

Substitute PRTE1 for u_2 :

$$\delta' = \left[1 - \left(\frac{t}{y_1} \right) \left(\frac{-y_1 \phi_1}{n} \right) - 1 \right] f'. \quad (4.26)$$

We arrive at:

$$\delta' = -\left(\frac{t}{n} \right) \left(\frac{\phi_1}{\phi} \right). \quad (4.27)$$

Note also that:

$$\delta' = -(EFL - BFD) \quad (4.28)$$

where BFD is the back focal distance.

There is a complementary expression which provides the separation between the first element vertex and the front focal point:

$$\delta = \left(\frac{t}{n} \right) \left(\frac{\phi_2}{\phi} \right). \quad (4.29)$$

4.8 Magnification

For finite object and image distances, magnification is defined as the ratio of image height to object height (as illustrated in Figure 4.12)

$$m = \frac{h'}{h} \quad (4.30)$$

Since h' is negative in the drawing, the magnification will be negative since:

$$\tan \theta = \frac{h}{l} = \frac{h'}{l'},$$

it is also true that:

$$m = \frac{l'}{l}$$

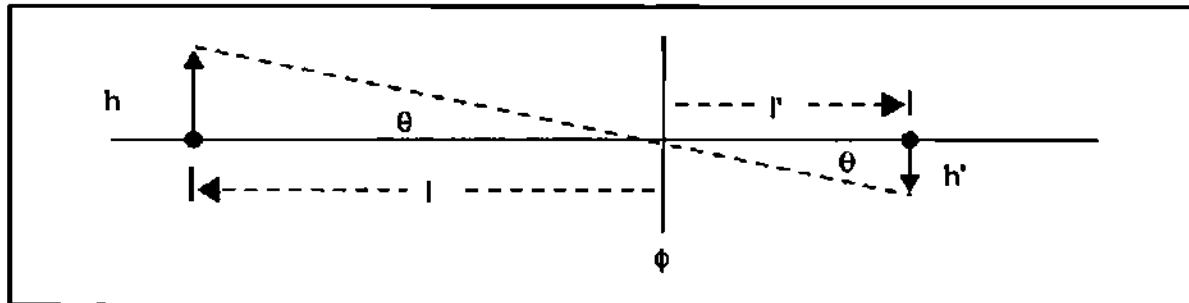


Fig. 4.12 Parameters relating to magnification.

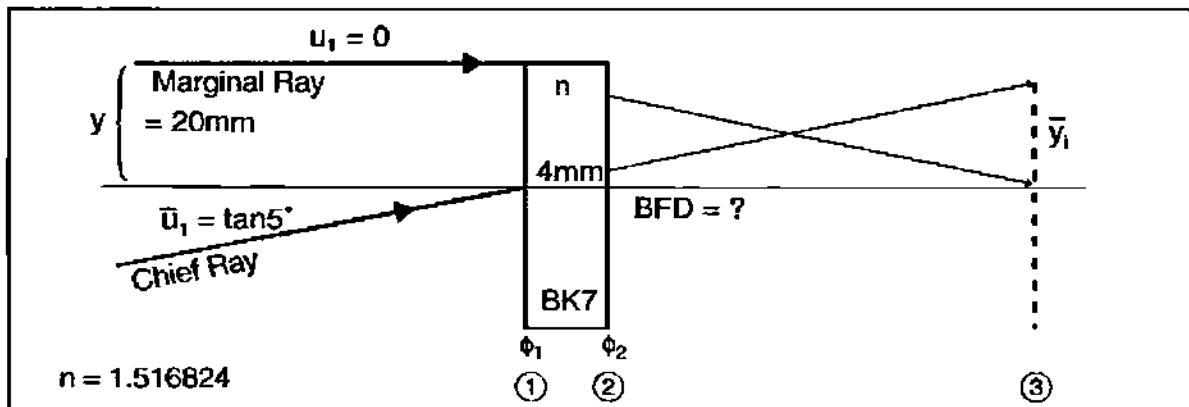


Fig. 4.13 Illustration for homework.

Since l is negative in the drawing, the magnification will be negative.

4.9 Homework

Returning to the singlet in the Homework for Chapter 1 (page 8) and referring to Figure 4.13:

- Calculate the surface powers.
- Do a paraxial ray trace through the lens to the image plane for the two rays indicated in the diagram.
- From the PRT data, find the back focal length (BFL).
- From the PRT data, find the image height y_3 .

Chapter 5

Stops and Pupils

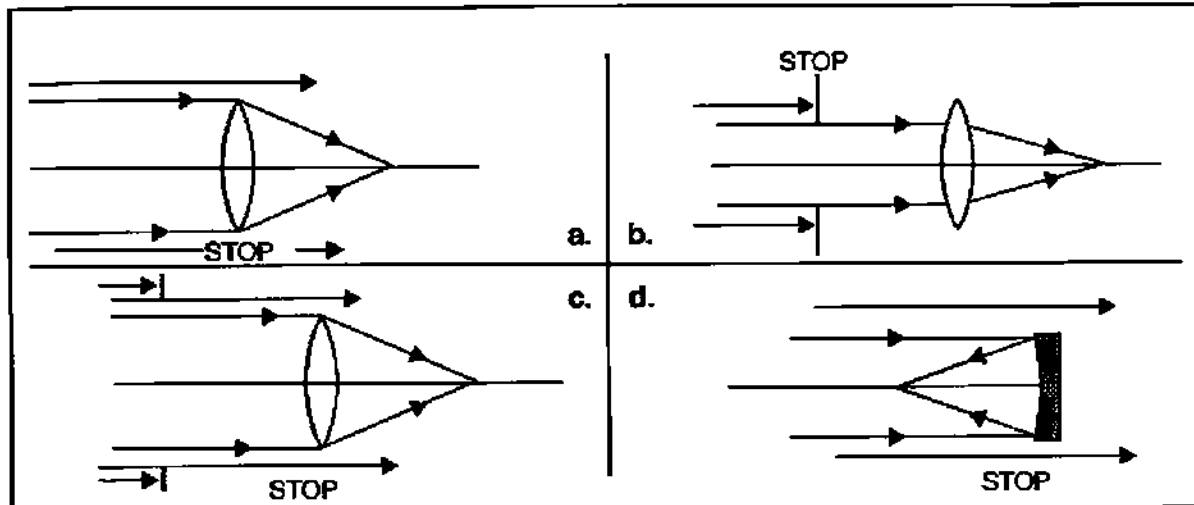


Fig. 5.1 Examples of stops.

5.1 Introduction

One of the most important concepts in optical design is that of the *stop* and its associated *pupils*. Most of us have used a stop (whether we knew it or not) when taking photographic pictures. Most good quality camera lenses have an internal adjustable iris by which one can control the exposure. This iris is a stop. It is not only used to change light levels at the image plane; designers use the stop's size and location to help control aberrations. You will see this application when you design a front landscape lens. The stop also defines two of the most important rays in optics: the marginal ray and the chief ray. When you do paraxial ray tracing from now on, these are the only rays that you will need to worry about. The ray heights and angles generated will be used to calculate aberrations.

5.2 Stop and Pupils

The stop is a hard physical aperture in the optical system. It is the *limiting aperture* of the system allowing some rays to pass through to the image, but blocking others. It may be defined by the diameter of an individual optic itself, or by an aperture plate (or iris) residing somewhere in the optical system. This is illustrated in Figure 5.1.

Let's look at Figure 5.1 *b* again. Because of the location of the stop in front

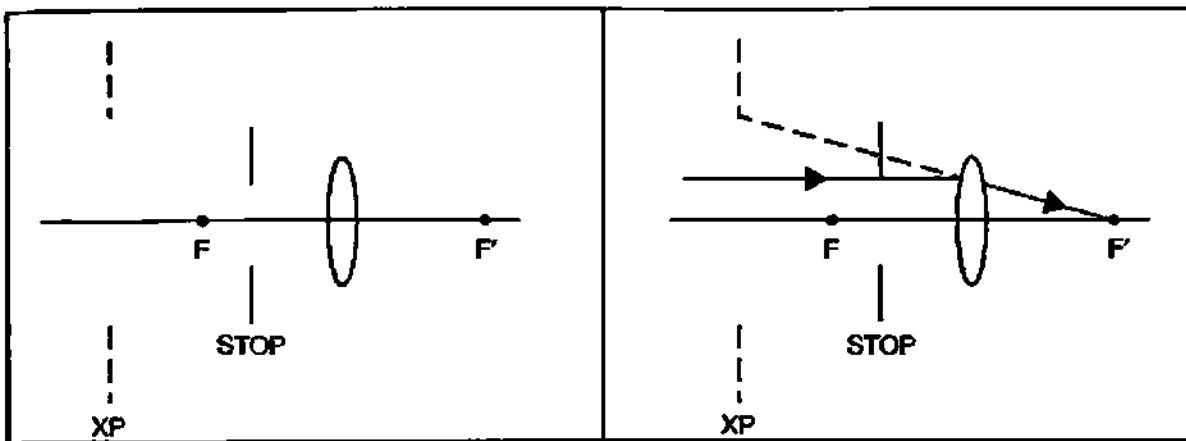


Fig. 5.2 Image of stop—the exit pupil.

Fig. 5.3 In image space, rays appear to be coming from the exit pupil.

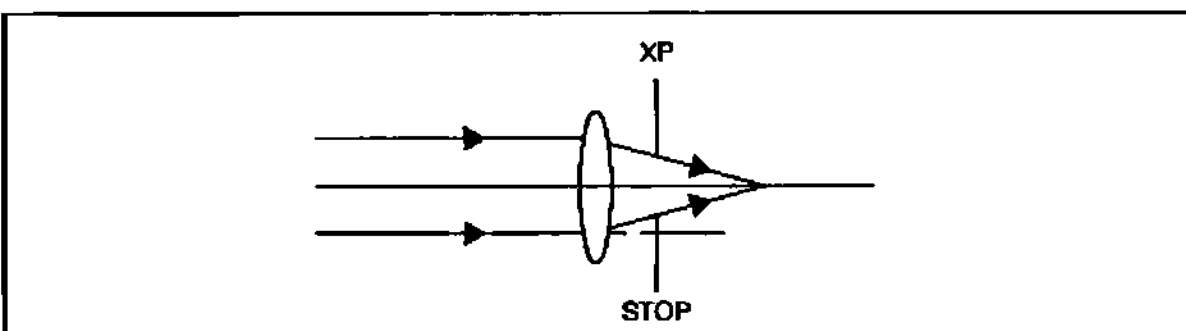


Fig. 5.4 Stop located after lens.

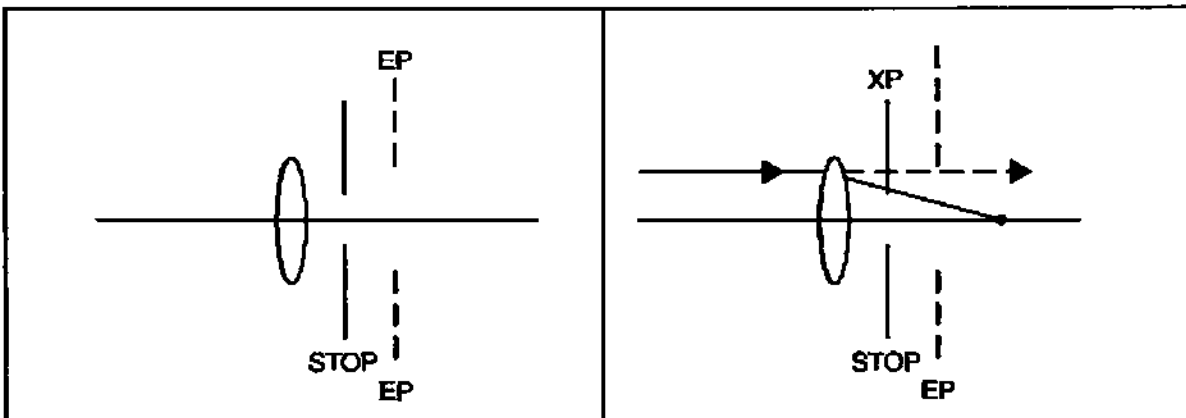


Fig. 5.5 Image of stop—the entrance pupil.

Fig. 5.6 In object space, rays appear limited by the entrance pupil.

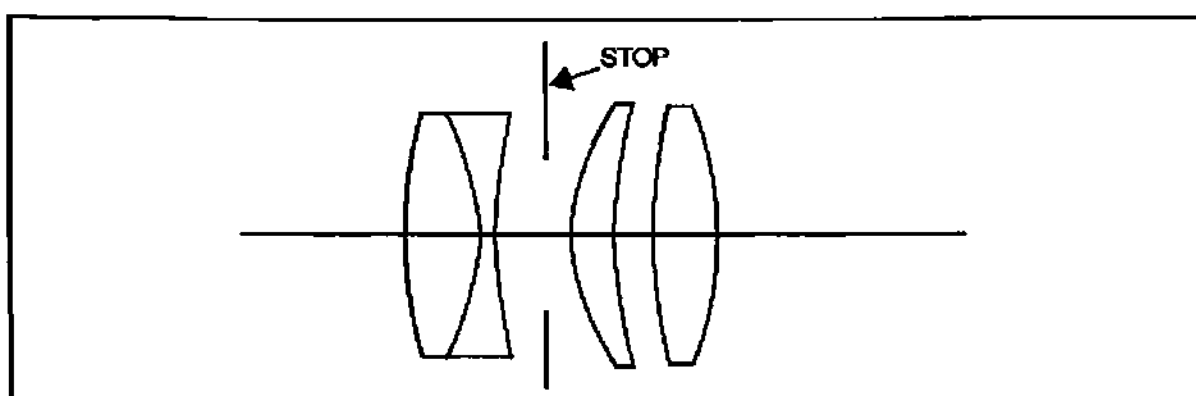


Fig. 5.7 Buried stop. From M. Klein, Optics (John Wiley and Sons). Reprinted with permission of John

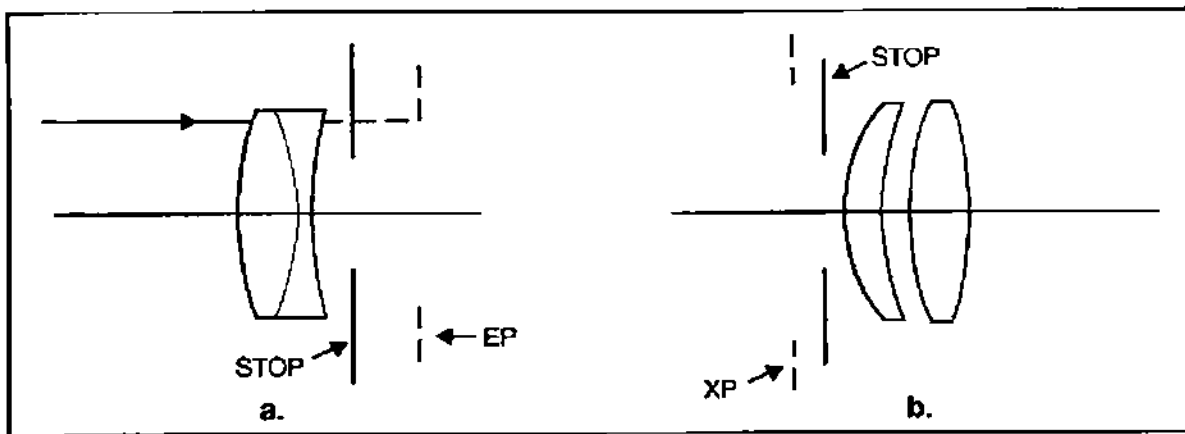


Fig. 5.8 Images of stop: a. the entrance pupil; b. the exit pupil. From M. Klein, Optics (John Wiley and Sons). Reprinted with permission of John Wiley and Sons, Inc.

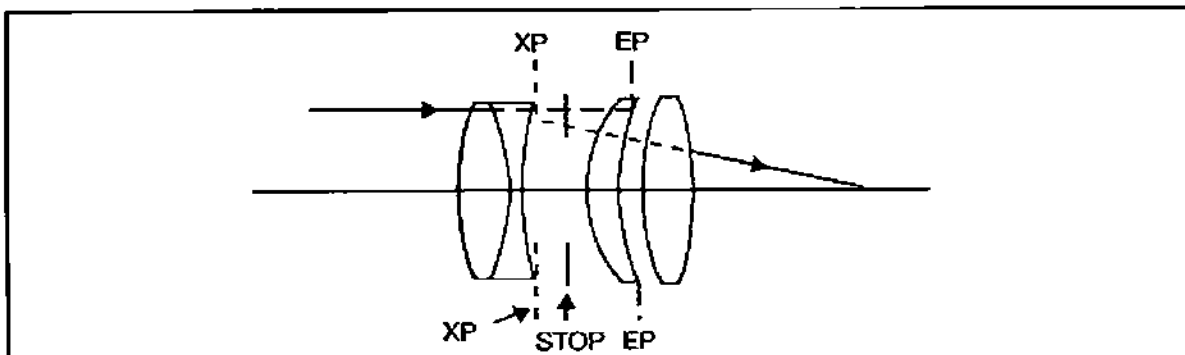


Fig. 5.9 Real ray bundle appears limited by virtual entrance pupil. From M. Klein, Optics (John Wiley and Sons). Reprinted with permission of John Wiley and Sons, Inc.

of the lens, it is also called the entrance pupil. Now consider the stop as an object to be imaged by the lens. The image of the stop (shown in Figure 5.2) is called the exit pupil. If you trace the real ray converging toward an image (due to an axial object at infinity) backward, it will track to the rim of the exit pupil, as shown in Figure 5.3.

Now consider the stop location shown in Figure 5.4. It comes *after* the lens. In this case, the stop is also the exit pupil. We can still consider the stop as an object to be imaged by the lens (just trace rays right to left this time). The stop image in this case is the entrance pupil (see Figure 5.5). Rays coming from an axial object at infinity will appear to be limited by the entrance pupil as shown in Figure 5.6.

Now consider the stop location in Figure 5.7. It is buried in the middle of the lens system. It is neither the entrance pupil nor exit pupil. However, we can still consider it as an object to be imaged. The stop image formed by all optics to the *left* of the stop is the entrance pupil, while the image of the stop formed by all optics to the *right* of the stop is the exit pupil. This is illustrated in Figure 5.8a and b.

For an axial object at infinity, the rays are aimed at the rim of the entrance pupil, while the rays appear to leave the rim of the exit pupil in image space as shown in Figure 5.9.

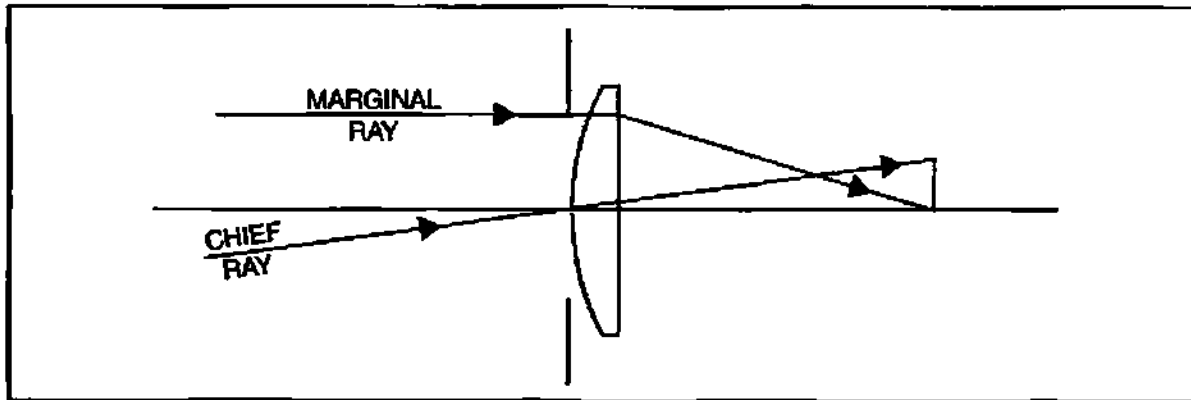


Fig. 5.10 Simple illustration of the marginal and chief ray.

5.3 Marginal and Chief Rays

For an axial object point, the ray that just brushes the *edge* or *rim* of the stop (and entrance pupil and exit pupil) is called the *marginal ray*. Now consider the off-axis point that defines the *maximum field angle*. The ray from this point that passes through the *center* of the stop is called the *chief ray*.¹ Figure 5.10 illustrates these two rays for a simple system.

By convention, the chief ray is inserted into the system with a positive angle (which implies that the off-axis object point is negative y). Also by convention, when the PRTE (Equations 4.1 and 4.2 on page 33) are applied to the chief ray, a bar is placed over the height and angle variables:

$$n'\bar{u}' = n\bar{u} - \bar{y}\Phi \quad (5.1)$$

$$\bar{y}_{j+1} = \bar{y}_j + \bar{u}'t \quad (5.2)$$

5.4 Locating Buried Stop Entrance and Exit Pupils Using PRTE

Suppose we are given the triplet with a buried stop shown in Figure 5.11. We want to trace the marginal and chief ray through the system. But to do that we need to aim the marginal ray at the edge of the entrance pupil and the chief ray at the center of the entrance pupil. How do we find these aim points? By finding the image of the stop due to all the optics to the left of the stop. We now go to the paraxial representation of the triplet as shown in Figure 5.12. We select two points on the stop: a point at the center and a point on the edge. From each point we launch a ray toward the optics on the left hand side. The launch angle is not critical. (It may also be easier to turn the picture around so that the rays are moving left to right as indicated in Figure 5.13.) Trace the ray from the center of the stop first. Trace it all the way through the truncated system. At the last surface, the ray will emerge at a

¹ Often the chief ray and principal ray are considered interchangeable. In this book, the chief ray will always refer to the *maximum field angle*. The principal ray, on the other hand, will refer to any field angle.

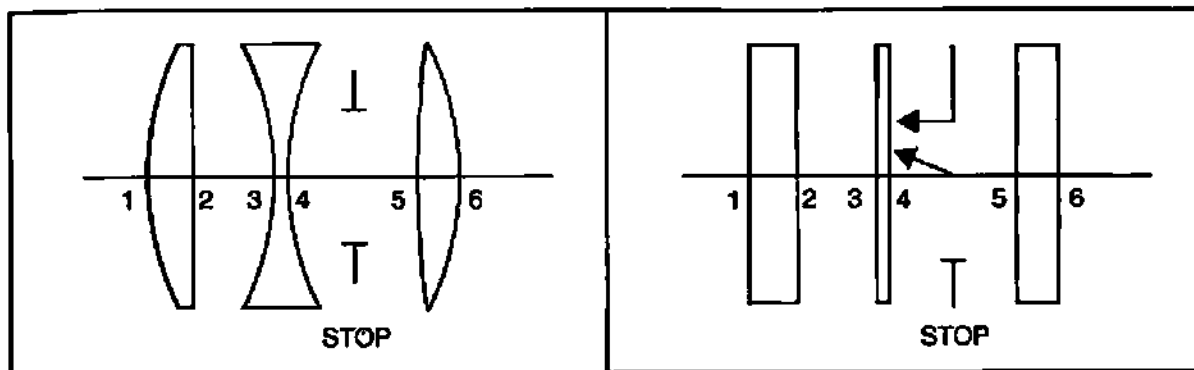


Fig. 5.11 Triplet with buried stop.

Fig. 5.12 Paraxial triplet with stop.

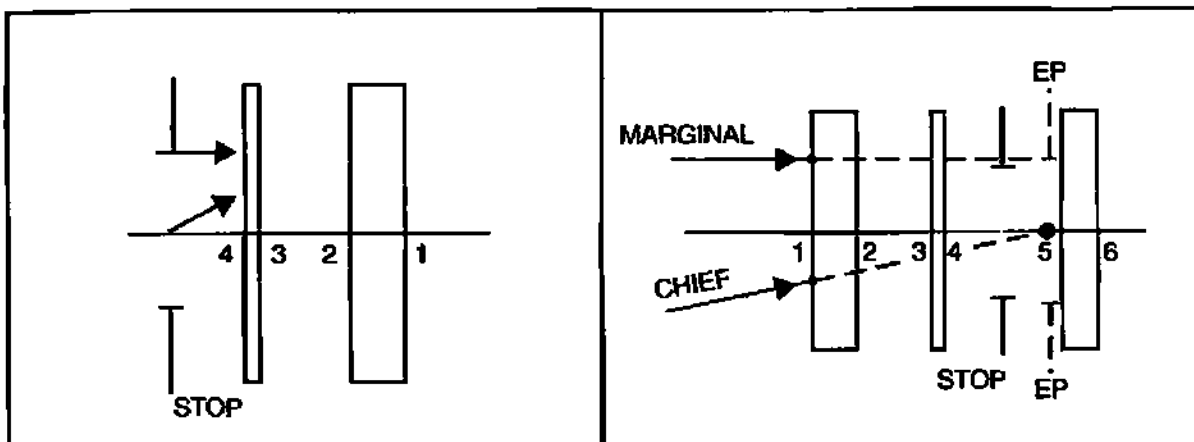


Fig. 5.13 Front portion of triplet turned around.

Fig. 5.14 Triplet with aim points located.

certain height and angle. Locate the image plane by tracing the ray to the surface where its height will be zero. (Note: This will likely be a virtual ray—or a ray that is backtracked.) This is the point where the ray crosses the optical axis. This will locate the axial position of the entrance pupil. But how big is the entrance pupil? To answer this question, trace the ray from the edge of the stop through the system to where it crosses the image plane defined by the previous ray. It will cross this plane at a certain height. This height defines the radius of the entrance pupil. So now we know the size and location of the entrance pupil. We turn the picture back around and incorporate it into the total system as shown in Figure 5.14. We now have our aim points for marginal and chief rays.

5.5 Pupil Size and F-Number

In Section 2.8.1 we saw how the f-number was related to the marginal ray angle in image space. This was done for a simple thin lens. However, that relationship is true even for complicated systems. Consider the system shown in Figure 5.15 where the stop is buried. Illustrated are the first and last paraxial surfaces, the entrance pupil, and the rear principal plane. The marginal ray is aimed at the entrance pupil. This ray emerges from the last surface at a certain height and angle.

Backtracking the image ray into the system, it crosses the projection of the

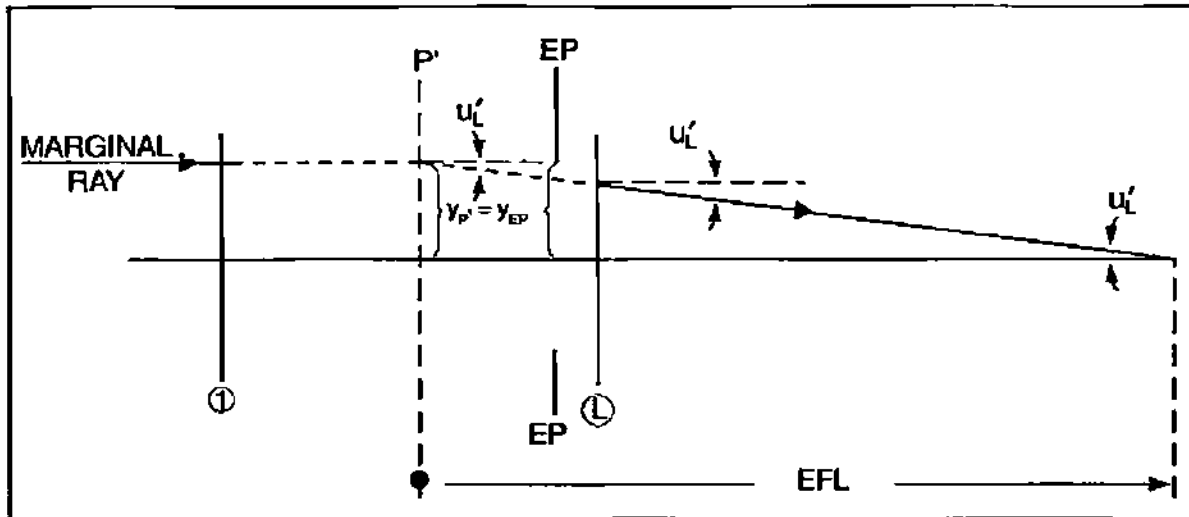


Fig. 5.15 General relation between marginal ray angle and f#.

object ray, which establishes the location of the rear principal plane. From the illustration (and being mindful of the sign convention established in Figure 3.1 on page 22) we see that:

$$u'_L = \frac{-y_{EP}}{\text{EFL}} \quad (5.3)$$

$$u'_L = -\left(\frac{\text{EPD}}{2}\right) / \text{EFL} \quad (5.4)$$

$$u'_L = \frac{-1}{2\left(\frac{\text{EFL}}{\text{EPD}}\right)} \quad (5.5)$$

$$u'_L = \frac{-1}{2(f/\#)} \quad (5.6)$$

Therefore,

$$f/\# = \frac{-1}{2 \tan U'_L} \quad (5.7)$$

Where U'_L is negative. Equation 5.7 shows the *general* relationship between the paraxial marginal ray angle and the paraxial f-number.

5.6 The Lagrange Invariant

Let us consider PRTEI for both the marginal and chief ray:

$$n'u' = nu - y\phi \quad (5.8)$$

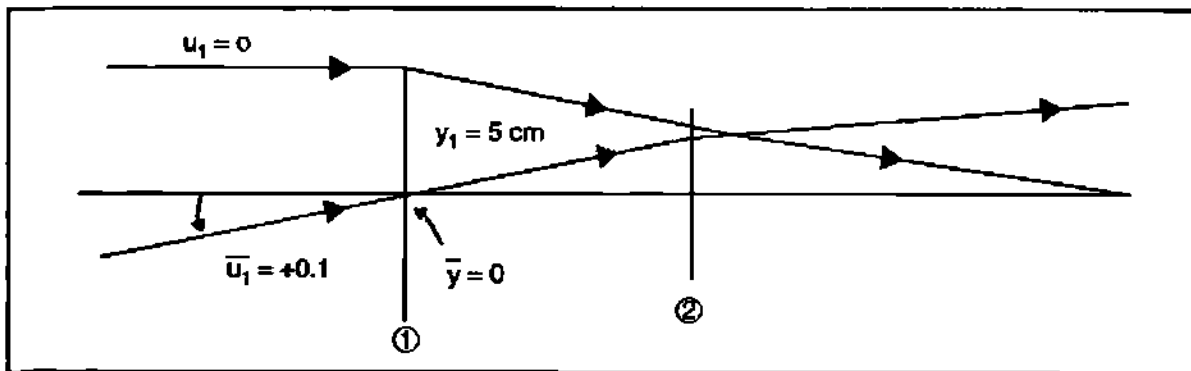


Fig. 5.16 Lagrange Invariant of Galilean Telescope.

$$n'u' = n\bar{u} - \bar{y}\phi . \quad (5.9)$$

Solve both for ϕ and equate:

$$\frac{(nu - n'u')}{y} = \frac{(n\bar{u} - n'\bar{u}')}{\bar{y}} . \quad (5.10)$$

Cross-multiply and rearrange terms:

$$n'(\bar{u}y - u'\bar{y}) = n(\bar{u}y - u\bar{y}) . \quad (5.11)$$

If we go to *any* plane in the optical system (a plane orthogonal to the optical axis) and compute either the left-hand side or the right-hand side value, we get the *same* number. This number is called the Lagrange Invariant, and we will designate it by the letter L . The importance of the Lagrange Invariant for us will be its application in thin lens calculations of off-axis aberrations.

Consider the Galilean telescope made up of thin lenses (shown in Figure 5.16). The first lens is both stop and entrance pupil. At the plane of the entrance pupil $L = \bar{u}y = +0.5$ cm. Had we examined any other plane we would obtain the same numerical value.

Note: It is customary to trace the chief ray to the center of the entrance pupil from the negative object field position so that the chief ray angle (\bar{U} or \bar{u}) is positive.

5.7 Homework

Given the triplet prescription as illustrated in Figure 5.17 and for an object at infinity with a $\bar{U} = 14^\circ$ field, find:

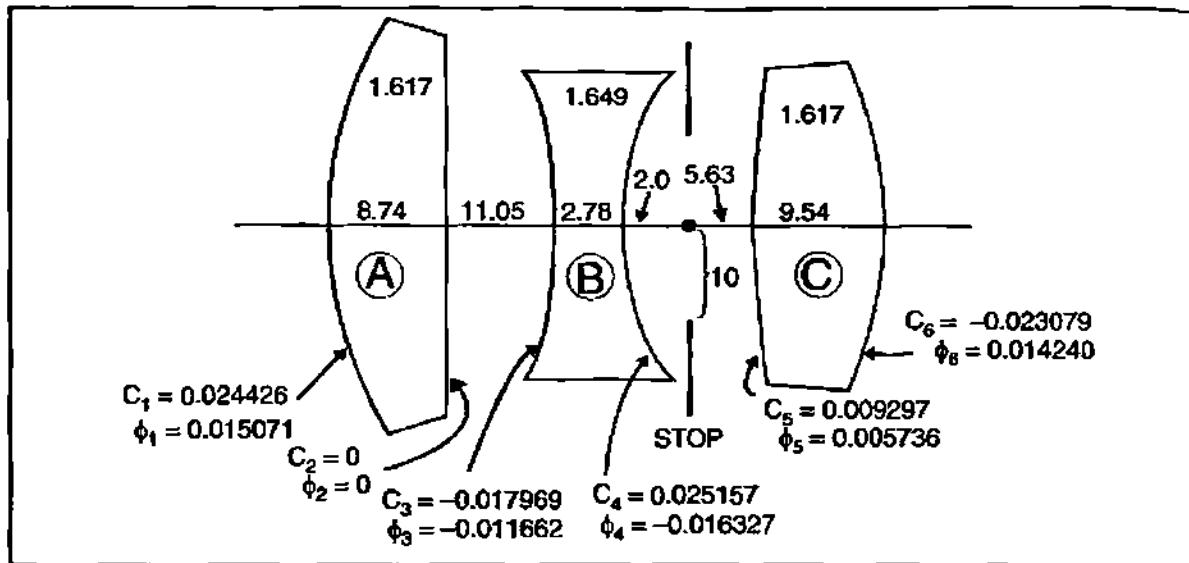


Fig. 5.17 From W. Smith, Modern Optical Engineering, (McGraw-Hill, 1990). Reprinted with permission from the McGraw-Hill companies.

- the size and location (relative to stop) of the entrance pupil using PRTE;
- the starting heights and angles on surface 1 for the marginal and chief rays, again using PRTE;
- draw an illustration of the lens showing data calculated in parts a and b.

Chapter 6

Glass, and the Landscape Lens

6.1 Introduction

Glass.... what a marvelous material. None of the modern cameras, camcorders, binoculars, telescopes, or CD players would work without glass (or plastic in some cases). In this chapter we will review those properties of glass which are of importance to the lens designer. We will then continue our discussion on the stop and see how its axial location can be used to control off-axis aberration. ZEMAX will then be used to illustrate the design of the classic rear landscape lens, after which you will try your hand at designing the front landscape lens.

6.2 Glass Properties

6.2.1 Refractive Index

Without a doubt, the refractive index is the single most important property of a glass. Without it, rays would not bend, lenses would not be possible, and, consequently, images would not be formed. The refractive index is the ratio of the speed of light in vacuum to its speed in the glass material.

$$n = \frac{c}{v} \quad (6.1)$$

Ray bending occurs at an interface between two media of different refractive indices as described by Snell's Law:

$$n_r \sin \theta_r = n_i \sin \theta_i \quad (6.2)$$

When this law is combined with spherically curved surfaces, a lens is born and all the wonderful images that go with it.

6.2.2 Dispersion

Now for the bad news. When a ray of collimated *white* light enters a glass lens, what emerges is an ensemble of rays of different colors, all focusing at different points along the optical axis, as illustrated in Figure 6.1. The EFL is wavelength dependent, and the spread of colors along the optical axis is called chromatic aberration. This results in poor image quality and a loss of resolution.

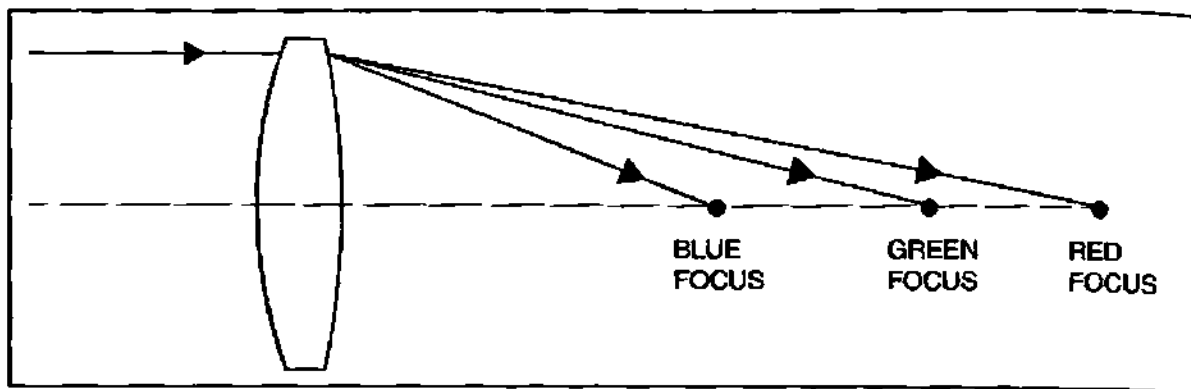


Fig. 6.1 Color dependence of the EFL.

**Table 6.1
Spectral Lines**

Wavelength (nm)	Identifier	Spectral Line
404.6	h	Hg (violet)
435.8	g	Hg (blue)
480	F'	Cd (blue)
486.1	F	H (blue)
546.1	e	Hg (green)
587.6	d	He (yellow)
589.3	D	Na (yellow)
643.8	C'	Cd (red)
656.3	C	H (red)
706.5	r	He (red)

The reason this happens is that the refractive index of glass is not constant but is a function of wavelength. This phenomenon is called *dispersion*. Typically, the index is higher in the blue and lower in the red. This means that a blue ray is bent more than a red ray at refractive interfaces (as is shown in Figure 6.1). It is said that Newton thought dispersion was an insurmountable problem for refractive optics, and was the main reason that drove him to accomplish imaging with mirrors—the Newtonian telescope.

6.2.3 How Can We Quantify the Dispersive Property of Glasses?

Before we answer that question we must make you aware of some traditions/conventions regarding the selection of standard wavelengths. To measure the refractive index accurately in olden times, you needed bright sources for the various colors in the visible spectrum. There were no lasers back then. What you had were ways of torching elements, like sodium, in bunsen burners, and then sending that light through a prism spectrometer. You'd pick a bright spectral line and feed that into a refractometer to get the index at that color. Keep in mind that the spectral peak of the eyeball response is at 555 nm (green) in daylight. At night, the dark-adapted peak shifts down to 513 nm. Table 6.1 shows the traditional spectral

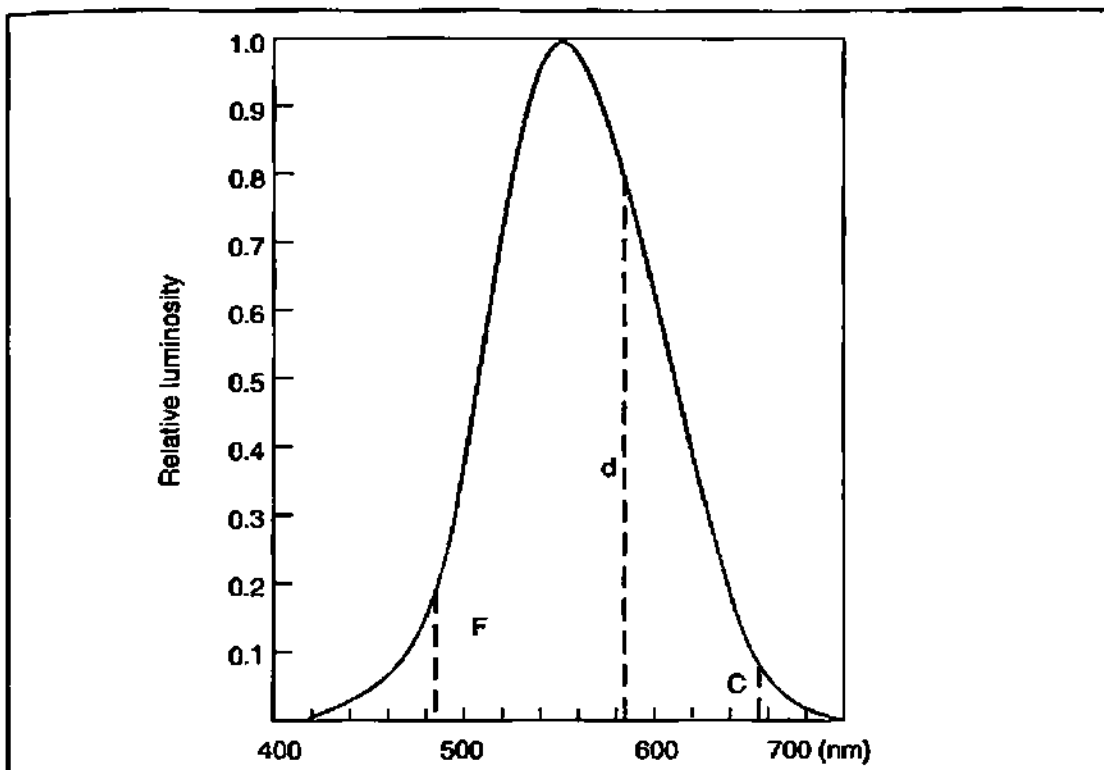


Fig. 6.2 Location of spectral lines on photopic response curve.

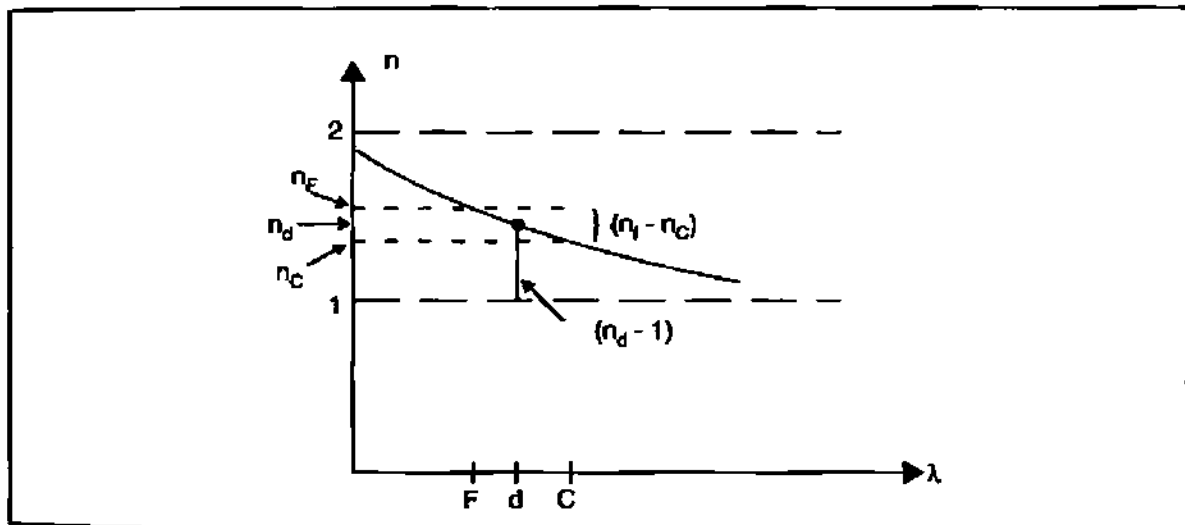


Fig. 6.3 Refractive index vs. wavelength for some generic optical glass.

lines used in refractive index measurements and consequently by lens designers. We will mainly use F , d , e , and C in this course. Figure 6.2 shows the location of these lines on the photopic (daylight) eye response curve.

Now let's go back to our original question about quantifying dispersion. In Figure 6.3 we show a generic spectral refractive index curve. On this curve we locate the index values due to the F , d , and C wavelengths. These are n_F , n_d , and n_C , respectively.

One measure of dispersion is to take the ratio:

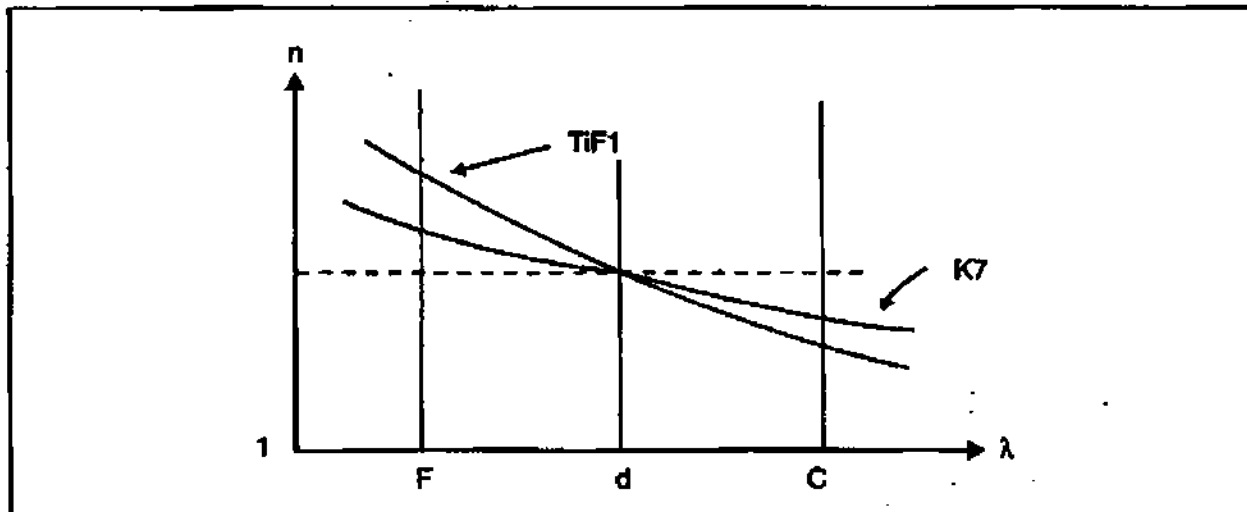


Fig. 6.4 Index spectrum of two Schott glasses.

$$D = \frac{n_F - n_C}{n_d - 1} \quad (6.3)$$

The numerator is the index difference between the extreme ends of the visible spectrum. The denominator is the difference between the material's mid-spectrum index value and its index value in vacuum (which is 1 for all wavelengths). The ratio yields a value much less than 1. As the numerator increases (more dispersion), D also increases. If the material had no dispersion (flat spectral response), D would be zero. Historically, however, this is not how dispersion was defined. Our predecessors chose the reciprocal of Equation 6.3 to represent dispersion. This representation is called the Abbe number, ν_d .

$$\nu_d = \frac{n_d - 1}{n_F - n_C} \quad (6.4)$$

In Figure 6.4 we show the index spectra for two Schott glasses with different dispersions but essentially the same mid-index value. Table 6.2 provides the pertinent information.

Although TiF1 has more dispersion (a bigger index difference between blue and red) than K7, it has the lower Abbe number.

There is a good physical reason for using the Abbe number for dispersion. You'll see why when we discuss chromatic aberration in more detail later on in Chapter 16.

6.2.4 Glass Chart

With so many optical glasses available to today's lens designer, it is difficult to keep track of them all. It would be nice to have some kind of summary format, a pictorial representation of glass materials and properties. Such a representation is shown in Figure 6.5 for the Schott glasses. A given glass is plotted on the map according to its mid-index value n_d and its Abbe number. The former is plotted as the ordinate; the latter as the abscissa. Higher dispersion glasses lie on the right

Table 6.2
Index Spectra for Two Scott Glasses

Glass	F	d	C	(n _F - n _C)	v _d
K7	1.51700	1.51112	1.50854	0.00846	60.42
TiF1	1.51820	1.51118	1.50818	0.01002	51.02

hand side. Those to the right of v_d = 50 are traditionally called flints, while those to the left are called crowns. The glass map is divided into subsections by the bold black boundary lines. These mainly refer to the chemical composition of the glass. We have been using BK7 in some of the exercises. More detailed information on BK7¹ is shown in Table 6.3.

6.2.5 Melt Data

In ZEMAX, as in most modern design codes, index and dispersion information on glass is resident within the code. The information may be in the form of a look-up table or, as in ZEMAX, may be retrievable via a polynomial equation whose coefficients represent the glass type. In either case, the glass information depends largely on the data supplied by the manufacturer, the same data from which glass maps and data charts are generated. As a designer you have to realize that the information contained in the glass map and data charts are approximate. The actual glasses from which your particular lens will be made will have slight differences in the index values compared to that found in the glass catalog. These differences can show up in the third decimal place or out. If your design is very sensitive to index value changes, or if the application is very critical, you will need to tweak the design to take the actual index values into account. Such information called "melt data," can be requested from the manufacturer. It is likely that all the curvatures will be slightly different in the revised design. Consequently, you need to do the tweaking *before* the optical shop actually starts grinding and polishing the lenses based on the old design.

6.2.6 Partial Dispersion

Partial dispersion is defined as:

$$P = \frac{n_F - n_d}{n_F - n_C} \quad (6.5)$$

If we plot P as a function of v_d for different glass types, we obtain the map shown in Figure 6.6. The interesting thing to note is how most of the glasses are clustered about a straight line. Partial dispersion will be useful in the design of apochromats which are used to correct secondary color (Chapter 18).

¹ Schott has replaced BK7 with N-BK7, and uses the Sellmeier dispersion formula for coefficients instead of the Schott dispersion formula coefficients shown in the table. However, BK7 is still listed in the ZEMAX glass library.

56 Chapter 6 Glass, and the Landscape Lense

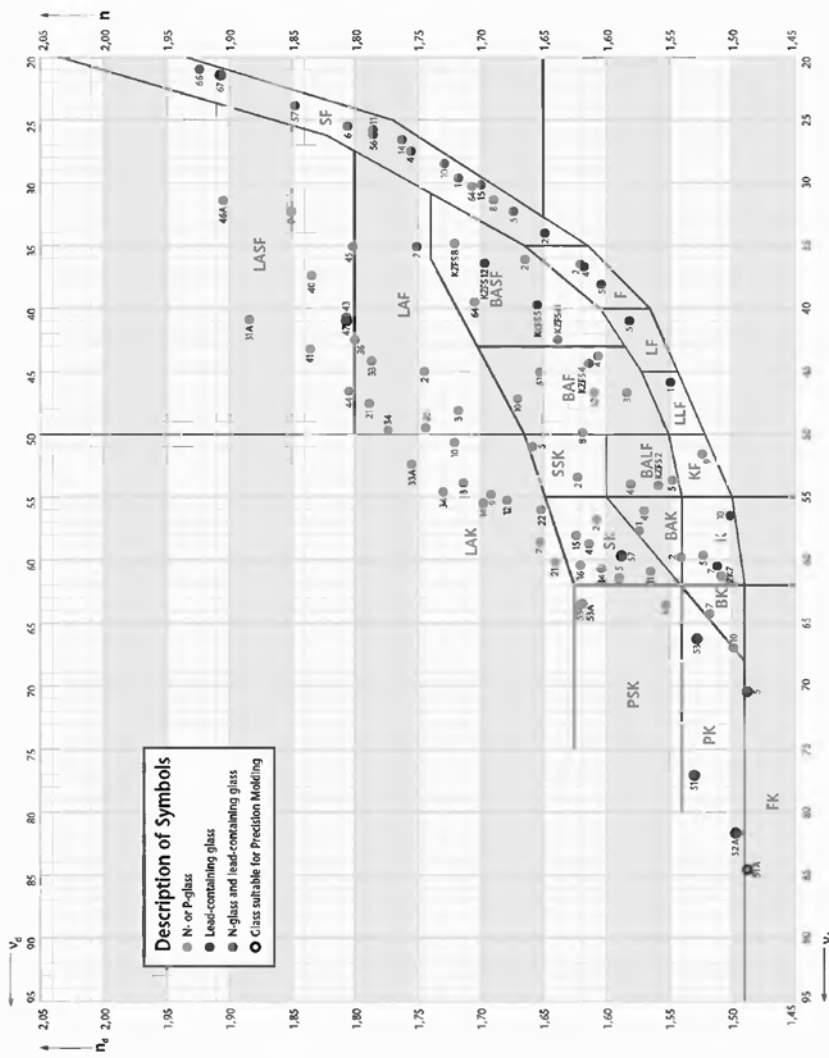


Fig. 6.5 This Schott Glass Chart is used with permission of Schott Glass Technologies. Readers are cautioned that this map was recreated from printed Schott maps by Willmann-Bell, Inc. and while it has been carefully checked and no known errors exist, it should be used with caution if it is used beyond the purpose of this book, which is solely illustrative. Accordingly, on projects that have economic implications, glass availability and specifications should be checked directly with Schott.

Section 6.2: Glass Properties 57

Table 6.3
BK7 Information

Y_t = 64.17

Table 6.3 BK7 Information			$v_d = 64.17$										
Refractive Indices			Relative Partial Dispersion				Internal Transmittance, T_i						
	λ [nm]		$P_{s,s}$	0.3097			λ [nm]	T_i (5 mm)	T_i (25 mm)				
$n_{325.4}$	2325.4	1.48929	$P_{C,C}$	0.5607			2325.4	0.89	0.57				
$n_{1970.1}$	1970.1	1.49500	$P_{d,C}$	0.3075			1970.1	0.968	0.85				
$n_{1529.6}$	1529.6	1.50094	$P_{e,d}$	0.2386			1529.6	0.997	0.985				
$n_{1060.0}$	1060.0	1.50669	$P_{g,F}$	0.5350			1060.0	0.999	0.998				
n_7	1014.0	1.50731	$P_{i,b}$	0.7478			700	0.999	0.998				
n_5	852.1	1.50981	$P_{F,d}$	0.6928			660	0.999	0.997				
n_4	706.5	1.51289	$P'_{s,s}$	0.3075			620	0.999	0.997				
n_{i^*}	656.3	1.51432	$P'_{C,C}$	0.6058			580	0.999	0.996				
n_{e^*}	643.8	1.51472	$P'_{d,C}$	0.2565			546.1	0.999	0.996				
$n_{632.8}$	632.8	1.51509	$P'_{e,d}$	0.2370			500	0.999	0.996				
n_D	589.3	1.51673	$P'_{g,F}$	0.4755			460	0.999	0.994				
n_d	587.6	1.51680	$P'_{i,b}$	0.7427			435.8	0.999	0.994				
n_c	546.1	1.51872	Constants of Dispersion Formula					420	0.998	0.993			
n_F	486.1	1.52238	A_0	2.2718929			404.7	0.998	0.993				
n_{F^*}	480.0	1.92283	A_1	$-1.0108077 \cdot 10^{-2}$			400	0.998	0.991				
n_g	435.8	1.52669	A_2	$1.0592509 \cdot 10^{-2}$			390	0.998	0.989				
n_h	404.7	1.53024	A_3	$2.0816965 \cdot 10^{-4}$			380	0.996	0.980				
n_i	365.0	1.53626	A_4	$-7.6472538 \cdot 10^{-6}$			370	0.995	0.974				
			A_5	$4.9240991 \cdot 10^{-7}$			365.0	0.994	0.969				
			Deviation of Relative Partial Dispersions ΔP from the "Normal Line"					350	0.986	0.93			
			$\Delta P_{s,s}$	0.0210			334.1	0.950	0.77				
			$\Delta P_{C,C}$	0.0083			320	0.81	0.35				
			$\Delta P_{d,C}$	-0.0009			310	0.59	0.07				
			$\Delta P_{e,d}$	-0.0008			300	0.26					
			$\Delta P_{g,F}$				290						
			$\Delta P_{i,b}$	0.0029			280						
Other Properties			Temperature Coefficients of Refractive Index										
			$\Delta n/\Delta T_{\text{relative}}$ [$10^{-6}/\text{K}$]				$\Delta n/\Delta T_{\text{absolute}}$ [$10^{-6}/\text{K}$]						
			[°C]	1060.0	s	C	e	g	1060.0	s	C	e	g
			-40/-20	2.2	2.3	2.5	2.7	3.1	0.2	0.3	0.4	0.6	1.0
			-20/ 0	2.2	2.3	2.6	2.8	3.3	0.5	0.6	0.8	1.0	1.5
			0/+20	2.3	2.4	2.7	2.8	3.4	0.9	1.0	1.2	1.3	1.9
			+20/+40	2.4	2.5	2.8	3.0	3.6	1.2	1.3	1.5	1.7	2.3
			+40/+60	2.5	2.6	2.9	3.1	3.8	1.3	1.4	1.7	1.9	2.6
			+60/+80	2.6	2.7	3.0	3.2	3.9	1.6	1.7	2.0	2.2	2.8

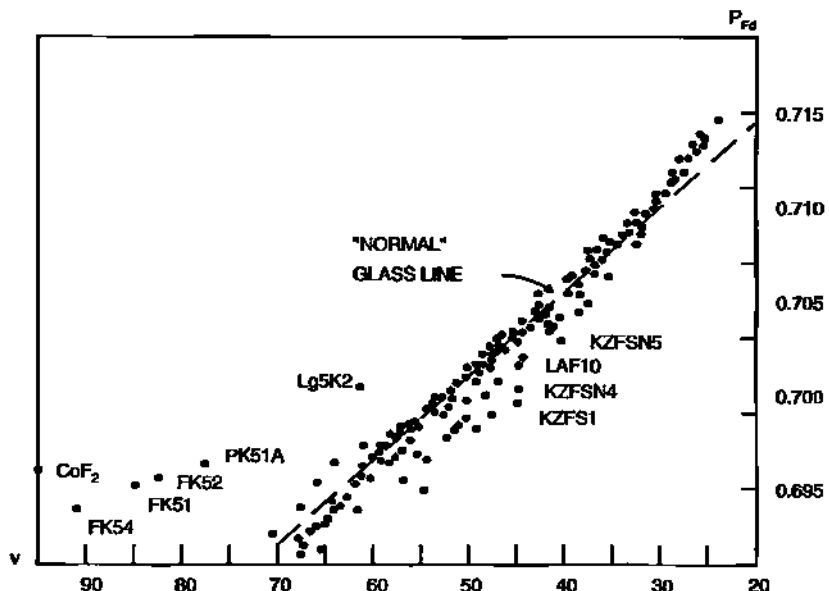


Fig. 6.6 The partial dispersion map. From W. Smith, Modern Lens Design (McGraw-Hill, 1992). Reprinted with permission from the McGraw-Hill Companies.

6.2.7 Practical Considerations

You believe you have a good design. Next ask yourself some practical questions. First, are any of the glasses in the design hard to work with; i.e., are any made from material that is difficult to grind or polish? Second, will your lens be used in a humid environment? If so, are any of the glasses hydrophilic? Third, are the glasses mildew resistant? Fourth, will your lens be subjected to temperature extremes? If so, how sensitive is the design to thermal environment? Will the mechanical structure supporting the lenses allow for thermal expansion of the elements without cracking them? These are some of the practical issues about which you must be knowledgeable as a serious designer.

6.3 Stop Shifting and Aberration Control

In the Homework for Chapter 3 (Section 3.7.1, page 29), you bent a singlet to minimize spherical aberration. Moving the stop around axially is not going to do anything for spherical aberration (assuming that lens radii are kept constant); however, it will have an impact on astigmatism and coma. We will talk more about off-axis aberrations in the next chapter. For now, we will rely on ZEMAX to show us what happens as the stop is moved.

Return to SING1o1b from Section 3.7.1. We will first reinstate the correct EFL (because of the offset introduced by the 4-mm glass thickness). Go to the

Section 6.3: Stop Shifting and Aberration Control 59

MFE and set:

Operand	Target	Weight
EFFL	400	1

Now place "V" on both radii. Put an M-solve on the thickness after the last glass surface (to get the BFD). Rename the file SINT1o1b.

SINT1o1b → Optimize → SINT1o1a

Note that the EFFL value is now 400. Although the curvatures have changed, note that the lens is still equiconvex. When we used the F-solve in Part 2 of Section 3.7 (page 29), the curvatures were different. Go to the MFE and set:

Operand	Target	Weight
EFFL	400	1
SPHA	(none)	0
COMA	(none)	0
ASTI	(none)	0

The zero weights mean we are simply monitoring these values. *No optimization will be done here.* Insert a surface in front of the lens. Make this surface the stop. This can be done by double-clicking on Standard and selecting Make Surface Stop. (Check the GEN box and make sure the EPD = 40.) Initially, let the thickness of the stop surface be zero. Hit Update in the MFE and note the current values of the operands. (Recall that the field angle is 5°.)

Operand	Value
EFFL	400
SPHA	1.713
COMA	-4.8702
ASTI	6.4049

The values of the aberrations shown are given in units of waves. Do not worry if you do not understand what the numbers mean right now. The important thing here is to see what happens to them as the stop is relocated. Note: It is important to let the diameter of the lens float. There should be no U in the semi-diameter solve column. We will now shift the stop away from the lens (by increasing its thickness in 10-mm increments) and monitor the changes in the operand aberration values. The results are plotted in Figure 6.7. As expected, the spherical aberration remains constant. Coma changes in a linear fashion, and actually goes through zero. Astigmatism appears parabolic over the same range, and goes

60 Chapter 6 Glass, and the Landscape Lens

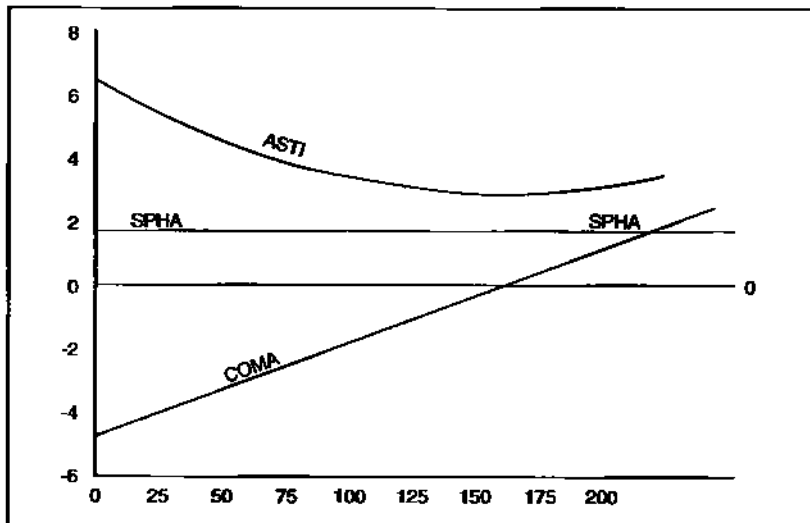


Fig. 6.7 Plot of the operand values COMA and ASTI as a function of stop shift.

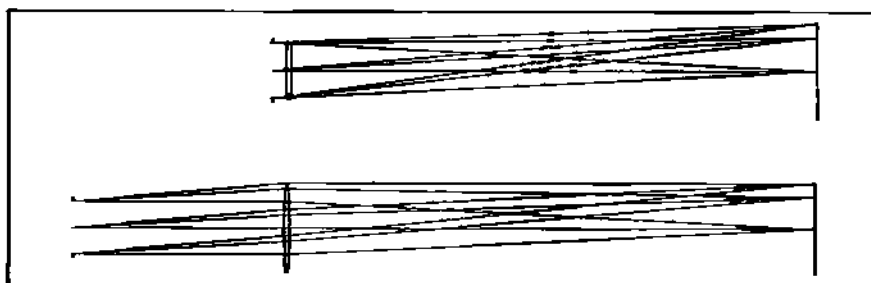


Fig. 6.8 Lens diameter increases as stop thickness increases.

through a minimum at about the same place where coma is zero.

Operand	Value
EFFL	400
Stop at 160 mm.	SPHA
	1.713
	COMA
	-0.07
	ASTI
	2.94

Note that the diameter of the lens has increased in size from 40 mm to over 68 mm (as shown in Figure 6.8). Now let ZEMAX locate the best stop position. Go to SINT1o1a. Remove V on the radii. Place V on the stop thickness. Start with zero stop thickness. In the MFE add TRAC [tools → default merit function {RMS/ Spot Radius/Centroid} → OK]. Rename WOLR1o1b. (Note: when you add TRAC to the MFE make sure it is inserted *below* your other resident operands. You will

Section 6.4: Wollaston Rear Landscape Lens 61

have to insert a "BLNK" line underneath them, highlight this line, and then insert TRAC.)

WOLR1o1b → Optimize → WOLR1o1a

Look at the stop thickness. It should now have a value of about 161.35... close to the value we see in the plot.

6.4 Wollaston Rear Landscape Lens

Now let's use optimization to find the best image plane as we let *both* lens bending and stop shifting do their work. Go to WOLR1o1a. Restore "V" to both radii. Rename WOLR2o1b.

WOLR1o2b → Optimize → WOLR1o2a

In this run we started with the stop offset found in WOLR1o1a. Let's see what happens if we start from zero stop thickness. Return to WOLR1o1b. Restore "V" to both radii. Rename WOLR3o1b.

WOLR1o3b → Optimize → WOLR1o3a

Now let's compare the two. The lenses are no longer equiconvex. The curvatures of the two lenses are very slightly different from each other. The stop locations are also different. (Note: Data obtained using ZEMAX version 7.2.)

PARAMETER	(1o2a) Value	(1o3a) Value
Stop at	163.821	163.9208
SPHA	1.9165	2.0156
COMA	-0.0297	-0.0307
ASTI	2.4126	2.1968

To achieve the best overall RMS spot size for the given aperture and field using lens bending and stop shifting, ZEMAX has allowed slightly higher spherical aberration in order to knock down coma and astigmatism by significant amounts. Starting points also matter. In this case, we get slightly better results when we start the optimization with zero stop thickness.

The classic Wollaston landscape lens is always shown as meniscus in shape. We can get that general shape by increasing our field. Go back to WOLR1o3b. Increase the field to 25°. We also need to increase our lens center thickness to 12 mm (so that surfaces do not end up crossing over each other).

Rename as WOLR1o4b.

WOLR1o4b → Optimize → WOLR1o4a

The resulting meniscus shape can be seen in Figure 6.9.

62 Chapter 6 Glass, and the Landscape Lens

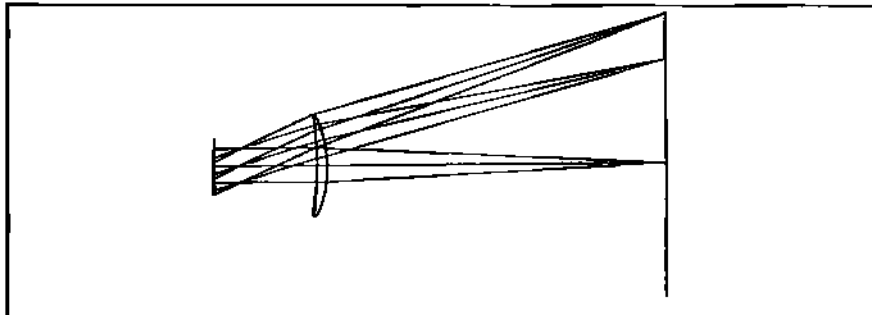


Fig. 6.9 The classic appearance of the Wollaston landscape lens.

6.5 Historical Note: William Wollaston

Lens designs do not pop out of thin air. A person is responsible for them. As we revisit some of the classic lenses, it is appropriate to say a few words about the designers who gave birth to them. The rear landscape lens just discussed is attributed to William Wollaston. Wollaston (shown in Figure 6.10) was born in England in 1766. He went to Cambridge and received a medical degree in 1793 but only practiced for a few years. His true interests were in science, particularly chemistry. He discovered a practical means of working platinum which made him rich. In optics he was the first to observe the dark lines in the solar spectrum; suggested the use of meniscus-shaped lenses for eyeglasses; and developed the meniscus lens with a stop in front (around 1812) for imaging distant objects for both viewing and drawing purposes. His landscape lens gave a much flatter field than the biconvex lenses used up until that time. When photography was introduced in 1839, the marriage between it and Wollaston's lens proved successful for nearly 60 years.

6.6 Homework

The front landscape will be your first real lens design problem using ZEMAX. Glass selection is an important part of the design process. Knowing what glasses to use for a particular lens type can mean the difference between meeting or not meeting a specification goal. Such knowledge is usually gained by trial and error. The designer will try a different glass (or glasses) in a lens system to see if there is any significant improvement in the *merit function* (Section 8.5). There are literally hundreds of glasses to choose from. Over the years, however, the designer gains an almost *intuitive feel* for what glasses are appropriate in a given situation. A student is not going to gain this ability in a one semester course. Consequently, specific glasses are assigned for the homework design problems in this book. However, once the assignment is finished, the student is encouraged to occasionally try other glass types to see what, if any, improvement is gained.

Design a *front* landscape lens:

$$\begin{array}{ll} EFL = 100 \\ f/15 \end{array}$$

$$\begin{array}{ll} \lambda = 0.587 \\ BK7 \end{array}$$

Section 6.6: Homework 63



Fig. 6.10 William Wollaston, inventor of the landscape lens.

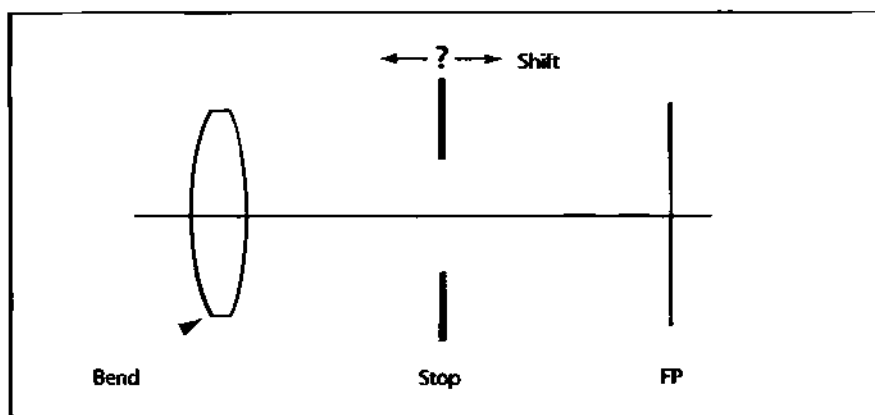


Fig. 6.11 Illustration for homework.

Calculate starting radii from thin lens power equation (assume lens is equiconvex). Insert radii into ZEMAX. Bend lens and shift stop to get the best RMS spot size on a flat image surface. (Note: Spot diagram settings use: square; centroid; Airy disk.) Use TRAC operand in MFE.

Target spot sizes: meet or beat:

Field	No DIS* RMS	DIS RMS
0°	23μm	18μm
10.5°	43	12
15°	65	20

*DIS: Dummy Image Surface (see page 30 paragraph number 8.)

64 Chapter 6 Glass, and the Landscape Lens

With the stop behind the lens, its diameter will have to change as a function of axial location in order to keep an f/15 imaging beam. With the rear landscape lens the stop diameter was fixed. Which option under GEN → Aper Type is now more appropriate to use?

You may also find that ZEMAX has a tendency to go back to the rear landscape configuration. To prevent that from happening you may find the operands MNCA and MXCA useful.

Note that the target RMS spot sizes are not rigid. As long as you are reasonably close, you're OK.

Suggested folder name: FRONTLAN; file name: LANF1o1b.

Practical Consideration: For this and subsequent design problems the semi-diameter of the surfaces should be allowed to float until the optimization cycle is complete over the full field. As a final step, "square up" the lens. This means, for example, surfaces of the same element should have the same diameter, and two elements in contact (like achromats) should both have the same diameter.

Chapter 7

Aberrations in General

7.1 Introduction

In the Homework for Chapter 3, you used optimization to reduce or eliminate aberrations such as spherical aberration, coma, and astigmatism. In Chapter 6 you saw how shifting the Stop could be used to help reduce coma and astigmatism. Until now these aberrations have just been numbers seen in the merit function editor with designations: SPHA, COMA, or ASTI. Although you should have had some previous exposure to these basic aberrations, we will now provide a qualitative review before proceeding any deeper into lens design. The aberrations will be described first in the image plane, and then in the exit pupil.

7.2 Diagnostic Plots

There are two diagnostic plots that you will be using throughout this course. These are the *ray fan plot*, and the *spot diagram*. Since we will be describing aberrations in terms of these plots, it will be helpful to gain some understanding of what these plots are about.

7.2.1 The Ray Fan Plot

Please refer to Figure 7.1a. We have an off-axis point source along the object's y-axis. From this source several rays are launched toward the optic in the plane defined by the optical axis and the point source (also known as the tangential plane). For the moment, consider the optic as a paraxial thin lens with the Stop at the lens. The ray that goes through the center of the Stop is, of course, the chief ray. The remaining rays are evenly spaced in the pupil plane along its y-axis. Two rays are at the pupil rim on either side of the chief ray. This distribution of rays in object space is called the (tangential) "ray fan." The chief ray continues on into image space and pierces the image plane at a certain height along its y-axis. The remaining rays converge toward the image plane and pierce it at various places along the y-axis.

Now let's plot a diagram where the abscissa represents the y-axis of the *pupil*, and the ordinate represents the y-axis of the *image plane*. Take a specific ray, say ray *a*. Plot its pupil position vs. image plane position as an x-y point on the diagram. However, for the image plane, we are not going to plot ray *a*'s displace-

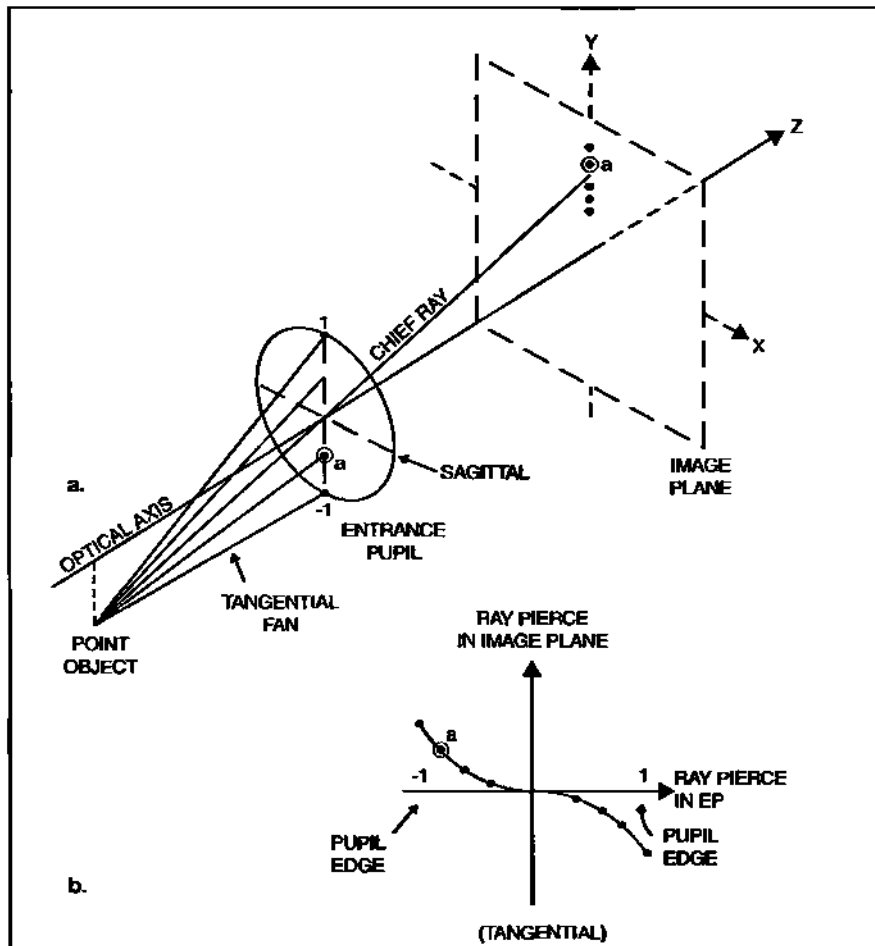


Fig. 7.1 Illustration of ray fan plot protocol.

ment from the optical axis. Rather we will plot ray a 's displacement *relative* to the chief ray pierce. In other words, the chief ray pierce defines the local zero for the y -axis of our diagram. We will do one other thing. Instead of plotting the actual pupil position of ray a , we will plot its normalized position (i.e., normalized by the radius of the pupil). The limits on the x -axis of our diagram will therefore be ± 1 . When we plot up all the rays according to the protocol just described, we generate what is called a (tangential) ray fan plot as illustrated in Figure 7.1 b. The shape of the ray fan plot depends upon the type and magnitude of the aberrations present in the system. For an unaberrated system, the ray fan plot would be a straight line coincident with the x -axis. (Note: a ray fan orthogonal to the tangential fan is called a sagittal fan and the corresponding plot is the sagittal ray fan plot.)

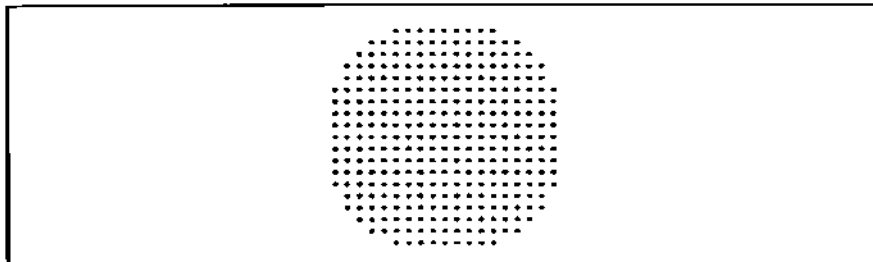


Fig. 7.2 Uniform grid on pupil defines ray pierce locations.

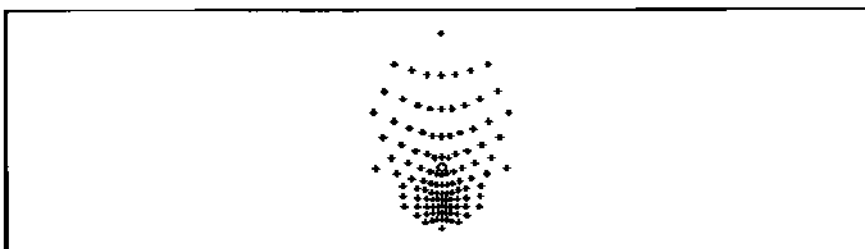


Fig. 7.3 An example of a spot diagram.

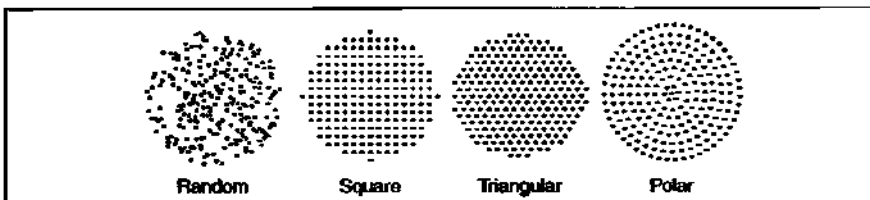


Fig. 7.4 Other pupil ray distributions. Reprinted with permission from Ruiten and van Venrooij, Telescope Optics (Willmann-Bell, 1988).

7.2.2 The Spot Diagram

Suppose we superimpose a uniform rectilinear grid over the entrance pupil as illustrated in Figure 7.2. From our off-axis point along the object's y -axis, we launch rays to pierce each grid point in the pupil. The rays emerge into image space and converge toward the image plane. Instead of having a one dimensional distribution of ray pierces (as in the ray fan), we have a two dimensional distribution, which is called a spot diagram (illustrated in Figure 7.3). The distribution of ray pierces depends on the aberrations in the system. The more compact the spot diagram, the less aberration is present. For an unaberrated system the spot diagram would appear as a single point.

Although the use of a uniform rectilinear grid in the entrance pupil is prevalent, other distributions are also utilized. These are illustrated in Figure 7.4.

7.3 Ray Description of Aberrations

7.3.1 Defocus

Consider rays incident on the pupil from an on-axis object point at infinity. A meridional fan is illustrated at the top of Figure 7.5. In this example we assume that no aberration is introduced by the lens. Rays are focused perfectly at the paraxial image plane. Please note that the only place where rays cross each other is at the paraxial focus. We now look at the ray distributions (spot diagrams and ray fan plots) in several designated planes about paraxial focus. The spot diagrams (for a polar distribution) are shown in the middle of Figure 7.5. The plane labeled 'c' is paraxial focus. All rays are coincident here and the spot diagram is just a point. In planes equidistant on either side of focus, the spot diagrams are symmetric. They get larger the further we move away from paraxial focus. However, the distribution in these defocus planes is just a geometrically scaled version of the pupil distribution.

Although defocus is not an aberration in the strict sense, its effects can be just as devastating. If the recording plane is not in the paraxial plane, then the geometrically scaled image of the object is convolved with a finite-sized blur spot which results in reduced resolution and loss of detail (recall Figure 1.4). As the separation between these planes increases, the blur spot gets larger and resolution decreases further.

The ray fan plots are shown on the lower part of Figure 7.5. Consider the marginal ray designated "ray 1." It brushes past the top edge of the stop, and is then bent by the lens. In defocus plane *a*, "ray 1" sits above the optical axis a certain amount—an amount which is indicated in plot (a). Going back to the stop, we follow the progress of all the other rays up to plane *a* and plot their respective heights relative to the optical axis. This shows up in plot (a) as a positively sloped straight line. At the paraxial plane *a* all ray heights are zero as indicated in plot (c). Plane *a* was *inside* of paraxial focus. If we go an equal distance *outside* of paraxial focus, we are in plane *e*. The plot of ray heights here is opposite that shown in plot (a). It is a straight line with negative slope. The linear nature of the ray fan plots having the same slope for both tangential and sagittal cross-sections is the "signature" of defocus.

7.3.2 Spherical Aberration

We now take the same meridional incident fan used in Section 7.3.1 and pass it through a lens having spherical aberration. Consider incident rays in Figure 7.6 (top) that are equidistant but on opposite sides of the optical axis. Unlike defocus, spherically aberrated rays do not all cross at paraxial focus. For example, the marginal ray pair (1 and -1) image closer to the lens than the ray pair (0.33 and -0.33) which image very near the paraxial focus of the lens. Thus for spherical aberration, different annular zones of the lens focus at different points along the optical axis. Spherical aberration is said to be a zonal aberration. The distance between paraxial and marginal focus is called "longitudinal spherical aberration." Such ray crossings are not confined to the optical axis. For example, "ray 0.66"

Section 7.3: Ray Description of Aberrations 69

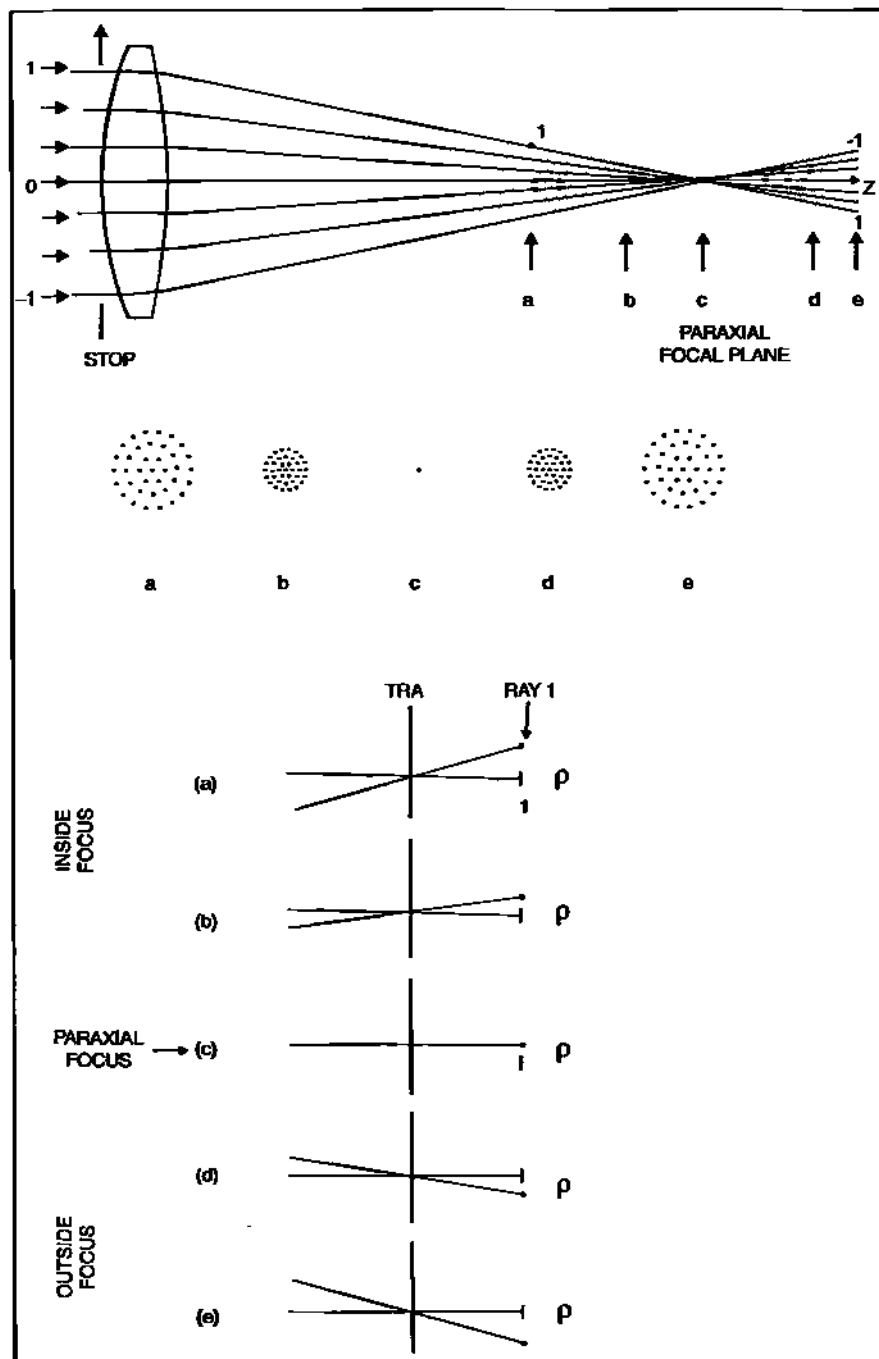


Fig. 7.5 Defocus: meridional plane (top); spot diagrams (center); ray fan plots (bottom). Reprinted with permission from Ruiten and van Venrooij, Telescope Optics (Willmann-Bell, 1988).

70 Chapter 7 Aberrations in General

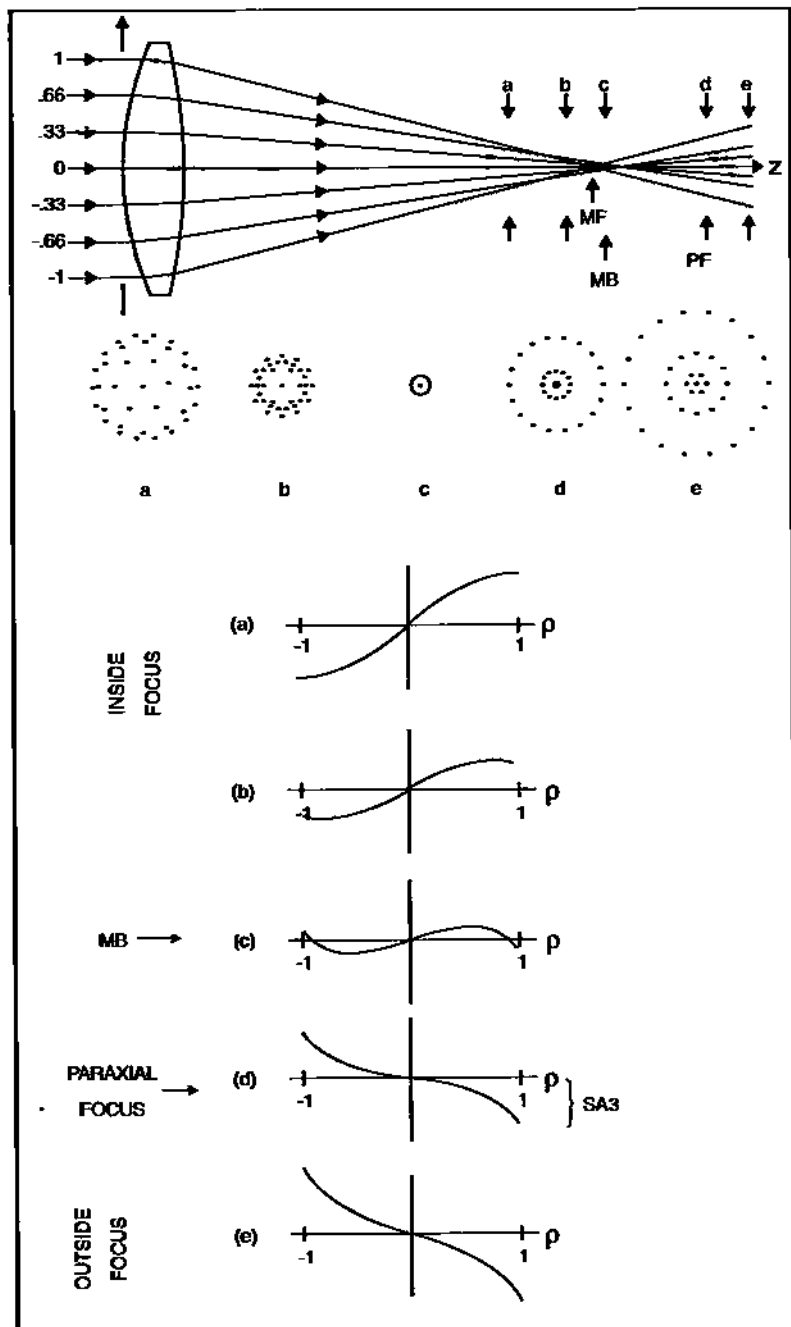


Fig. 7.6 Spherical Aberration: meridional plane (top); spot diagrams (center); ray fan plots (bottom). Reprinted with permission from Rutten and van Venrooij, Telescope Optics (Willmann-Bell, 1988).

Section 7.3: Ray Description of Aberrations 71

crosses “ray 1” in the meridional plane between image planes “a” and “b” as indicated. The ensemble of adjacent ray crossings is called the caustic. The point at which the marginal rays cross the caustic line defines a natural waist in the meridional ray plot. This axial position is called minimum blur.

The spot diagrams for planes “a–e” are shown in the middle of Figure 7.6. Notice that we no longer have geometrically scaled versions of the ray distribution in the pupil as we did with defocus. Each spot diagram is unique. In fact, spot diagrams for planes equidistant on either side of the paraxial plane “d” are no longer symmetric. Paraxial focus is no longer a point image but has a significantly sized blur circle. The smallest blur circle is at “c,” the minimum blur plane. This is the on-axis point that would have the highest resolution.

The corresponding ray fan plots for spherical aberration are shown at the bottom of Figure 7.6.

Notice that the plots now have a distinct “S” shape to them. At the paraxial plane ‘d’ there is no defocus and plot (d) is flat in its central region. The marginal ray positions on the plot have the *largest* transverse ray aberration (TRA) value and define the magnitude of the spherical aberration (SA3) present in the system. As we move away from paraxial focus, the plot is no longer flat in the central region, but takes on some slope which increases as the distance from paraxial focus increases. Note that there is one plot, plot (c), where the overall TRA has been minimized. This is at the minimum blur plane. We say that the spherical aberration has been balanced with defocus.

7.3.3 Coma

Instead of having the incident meridional fan parallel to the optical axis as in the previous two examples, we now tilt the collimated input beam to some off-axis angle as shown in Figure 7.7. If there were no aberration, all rays would come to the same focus in the paraxial plane, but that focus would be offset from the optical axis as defined by the chief ray pierce. Let’s assume that coma is the *only* aberration present. Coma, like spherical aberration, is a zonal dependent aberration. The marginal ray pair (1 and -1) focuses in the paraxial plane but at an offset furthest from the chief ray pierce. The ray pair (0.33 and -0.33) also focus in the paraxial plane but closer to the chief ray pierce. One can think of this as a variation in lateral magnification with zone.

Ray fan plots for the defocus planes indicated in the meridional diagram are shown at the bottom of Figure 7.7. Remember that the displacements are measured relative to the chief ray pierce. Note the quadratic character of the plots. This is most evident in the paraxial plane plot (c). The plot is symmetric, parabolic, and negative. Rays 1 and -1 have the same displacement from the chief ray. This is a maximum value for these marginal rays and defines the magnitude of the coma present (designated as CMA3). The ray fan plot departs from the true parabolic shape as we move to different defocus planes, but the quadratic character is still evident as the signature of coma.

Spot diagrams for the designated defocus planes are shown in the center of

72 Chapter 7 Aberrations in General

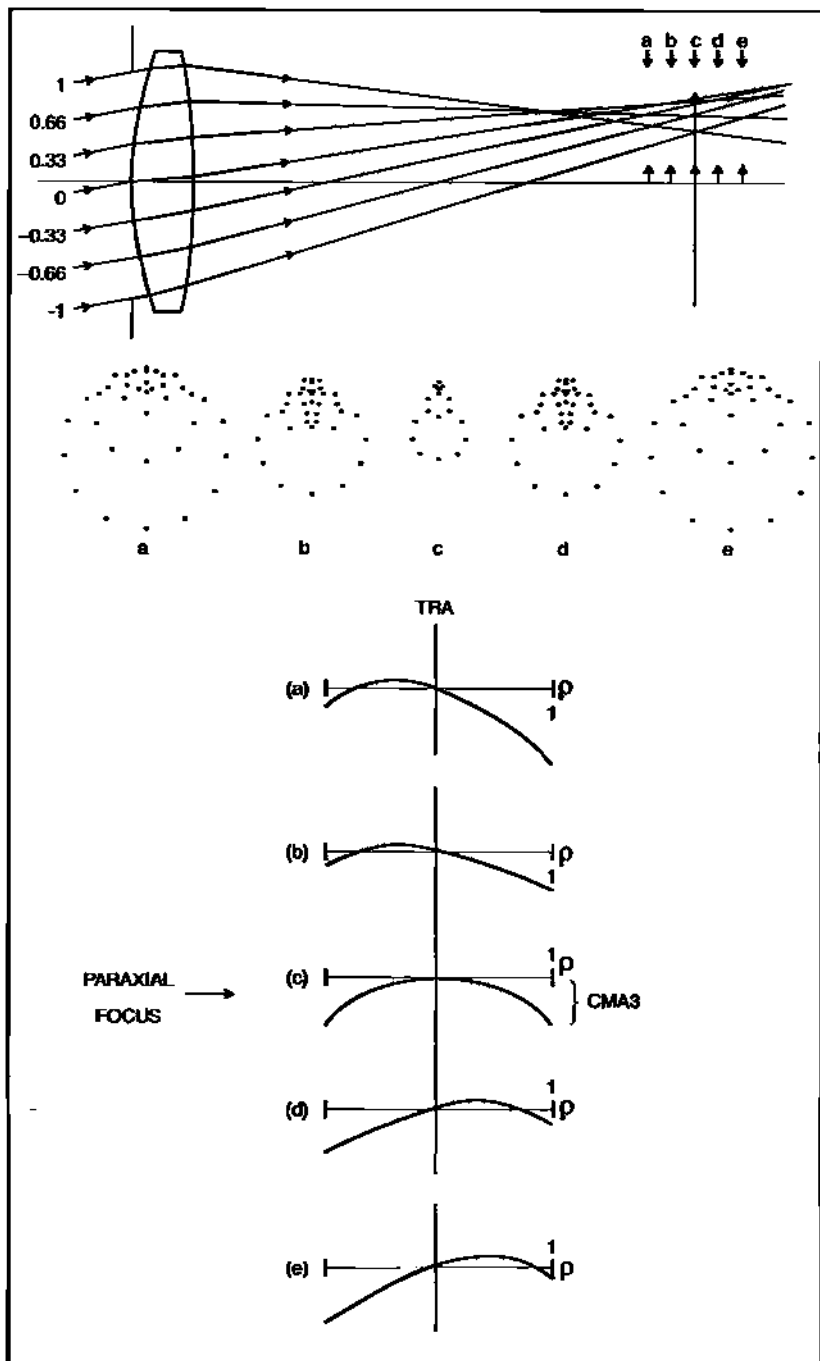


Fig. 7.7 Coma: meridional plane (top); spot diagrams (center); ray fan plots (bottom). Reprinted with permission from Ruitenberg and van Venrooij, Telescope Optics (Willmann-Bell, 1988).

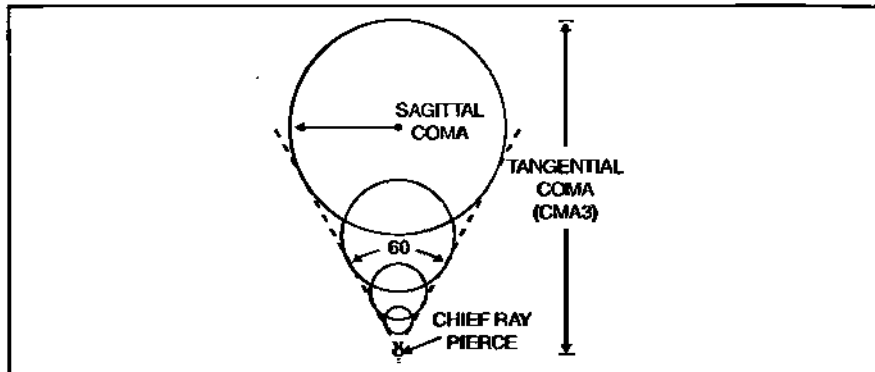


Fig. 7.8 Paraxial image of specific zones when coma is present.

Figure 7.7. At paraxial focus the spot diagram looks like an inverted ice cream cone. Unlike spherical aberration, all rays from a common zone do not all come to a focus at the same point. Only ray pairs from opposite sides of the zone cross at the same point in the paraxial plane. Zones are consequently imaged as rings in the paraxial plane. The ring diameter increases as the zone radius increases. The displacement of the ring center from the chief ray pierce also increases as the zone radius increases—hence the ice cream cone pattern as illustrated in Figure 7.8. This shape is evident even as we move to different defocus planes, but the pattern is most compact in the paraxial plane.

7.3.4 Astigmatism

Instead of showing a meridional plot for astigmatism, it is better to show a more three dimensional view of this aberration's behavior as illustrated in Figure 7.9 (top). We assume that astigmatism is the only aberration present. This time both the tangential and sagittal ray fans are illustrated. Astigmatism is not a zonal aberration like spherical aberration and coma. Rather, astigmatism results in a different focus point along the chief ray for the tangential and sagittal fans respectively. Astigmatism occurs because the two incident ray fans "see" different effective system powers. (There will be more about this when we discuss Coddington's equations later on.) All rays for each fan come to a perfect point focus. However, at the tangential focus point rays from the sagittal fan are out of focus. Hence a sharp line image *orthogonal* to the tangential plane is found. At the sagittal focus, rays from the tangential fan are out of focus resulting in a sharp line image lying in the tangential plane. The two line images are perpendicular to each other. (This can be easily seen by the spot diagrams for the several defocus planes indicated.) Without field curvature, the sagittal focus lies in the paraxial plane.¹

The shape of the spot diagrams evolve from elliptical forms on either side of

¹Note: There is a tangential image for each field point. The ensemble of such points defines the tangential image surface. Similarly, there is a sagittal image surface.

74 Chapter 7 Aberrations in General

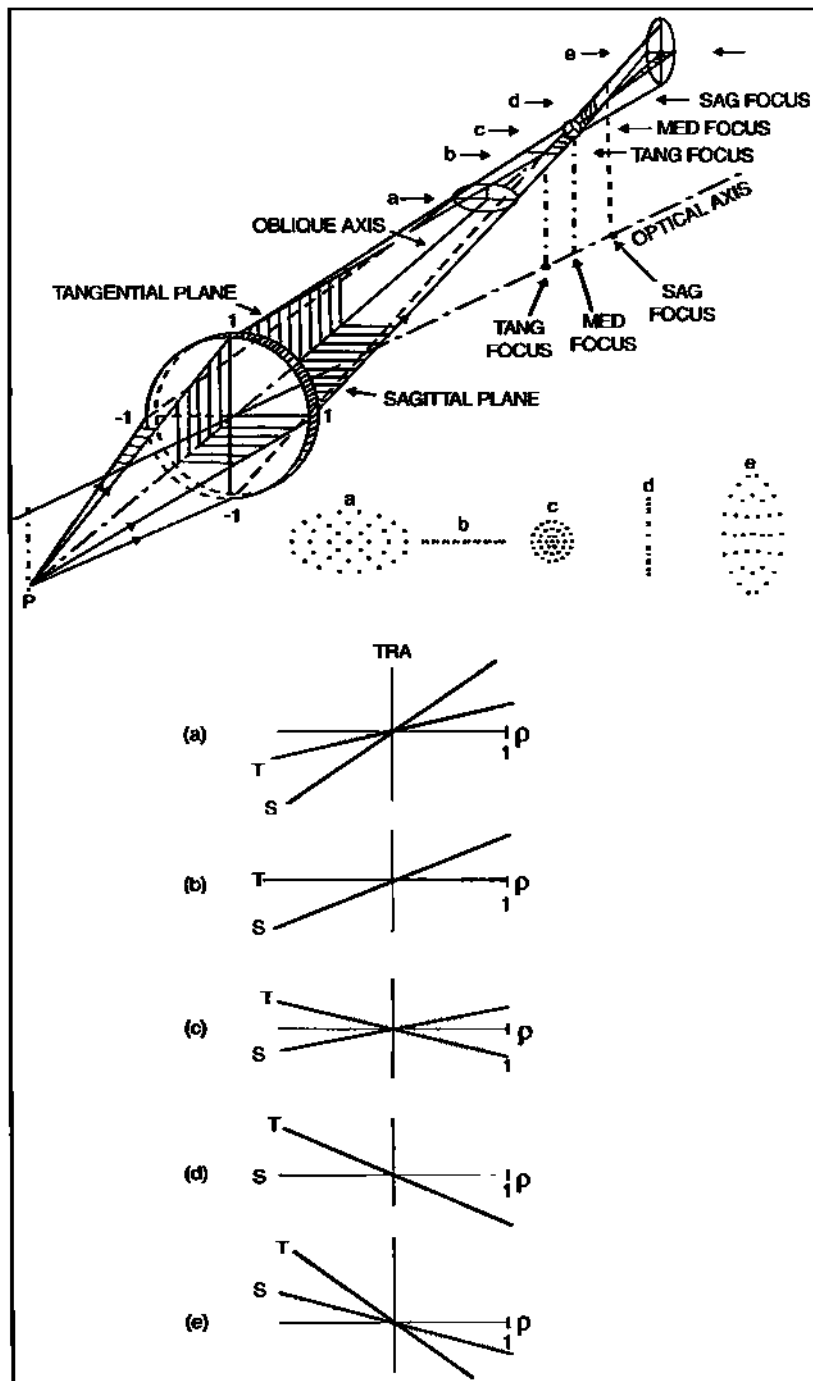


Fig. 7.9 Astigmatism: 3-D view (top); spot diagrams (center); ray fan plots (bottom). Reprinted with permission from Ruttel and van Venrooij, Telescope Optics (Willmann-Bell, 1988).

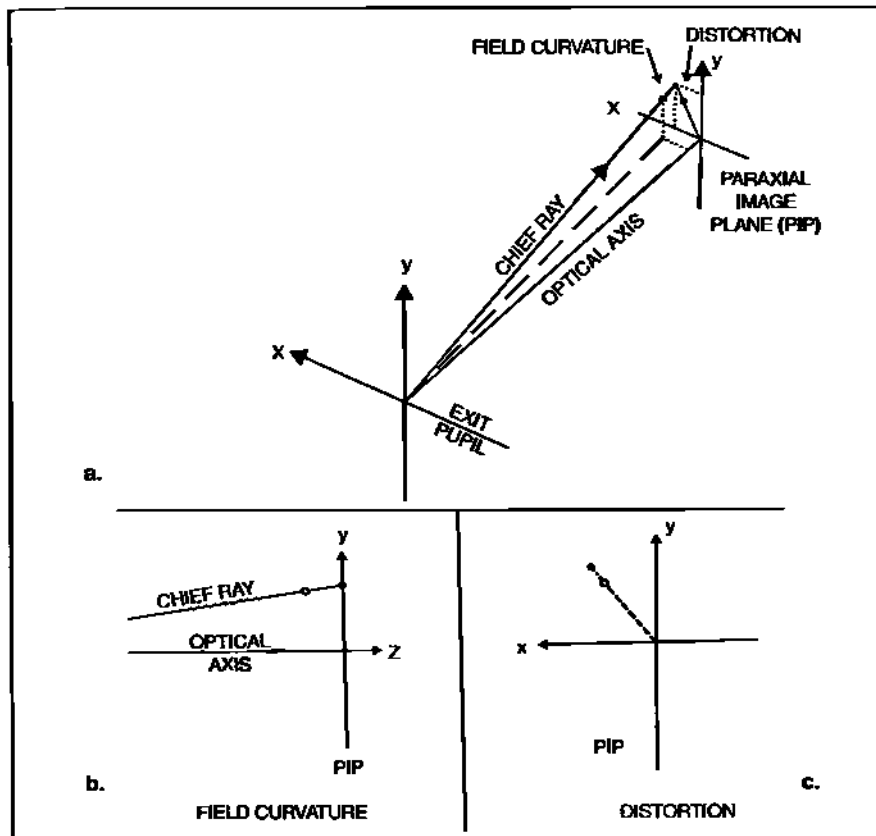


Fig. 7.10 Illustration of field curvature and distortion.

each line focus to a circular blur spot right between them. This image location is called medial focus and is defocus plane (c) in the drawing.

The ray fan plots are shown at the bottom of Figure 7.9. Two plots are shown for each defocus position—one for the tangential fan (dashed line) and one for the sagittal fan (solid line). Note that both plots are linear (which makes them similar to defocus as discussed in Section 7.3.1). But the two straight lines do not have the same slope. This is the signature of astigmatism in the ray fan plot pairs. Plot (b) is at the tangential focus because the slope of the T-plot is zero. Plot (d) is at the sagittal focus because the slope of the S-plot is zero. Plot (c) is at medial focus. Both the T and S plots have the same slope magnitude but of opposite sign.

7.3.5 Field Curvature and Distortion

There are two off-axis aberrations that do not affect the quality of a point image, only where it is located. In Figure 7.10a we show the chief ray emerging from the exit pupil. (The input to the entrance pupil is an off-axis collimated beam.) For an unaberrated system the chief ray pierces the paraxial plane as shown and all rays

76 Chapter 7 Aberrations in General

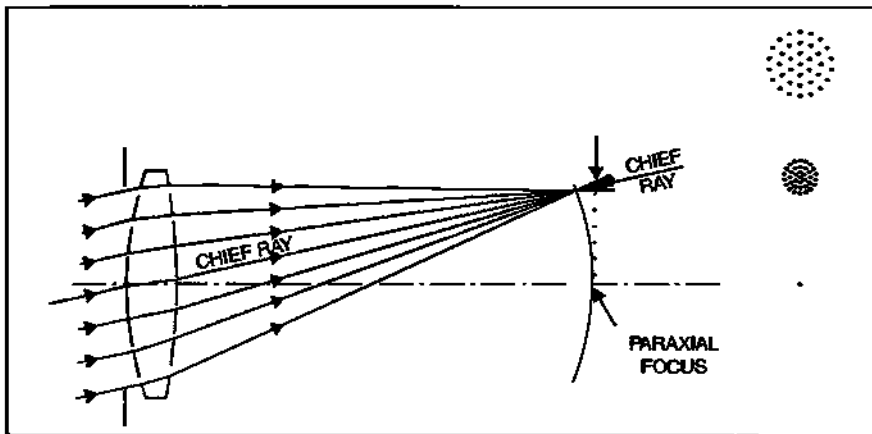


Fig. 7.11 Meridional plot illustrating field curvature. Reprinted with permission from Ruiten and van Venrooij, Telescope Optics (Willmann-Bell, 1988).

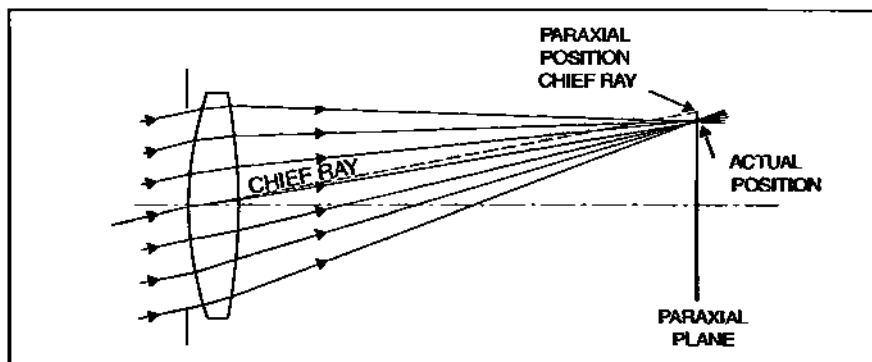


Fig. 7.12 Meridional plot illustrating distortion. Reprinted with permission from Ruiten and van Venrooij, Telescope Optics (Willmann-Bell, 1988).

cross at this location. However, if only field curvature is present, all rays will cross at a point along the chief ray which does not lie in the paraxial plane. This is also indicated in Figure 7.10b. If only distortion is present, all rays cross at a point in the paraxial plane but not at the ideal chief ray pierce. There is a lateral (radial) offset. This is also indicated in Figure 7.10c.

A meridional plot illustrating field curvature is shown in Figure 7.11. The displacement along the chief ray from the paraxial plane increases as the field angle is increased. This results in a curved image surface. Spot diagrams taken at various heights in the paraxial plane would show a steady increase in diameter.

A meridional plot for distortion is shown in Figure 7.12. A sharp image is formed in the paraxial plane. Spot diagrams as a function of height in the image plane will be true points. However, these points will be radially displaced from

Section 7.4: Wavefront Aberrations 77

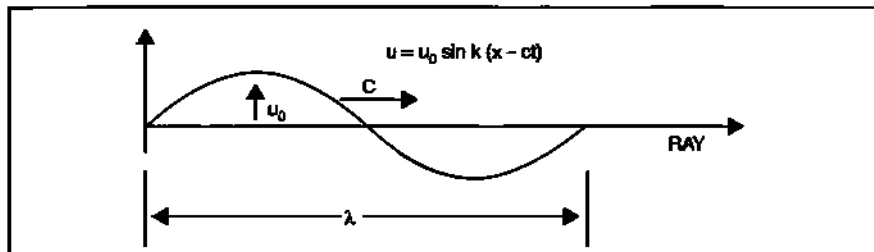


Fig. 7.13 Example of basic monochromatic wave structure propagating along a ray.

their ideal positions. This displacement increases with field angle.

7.4 Wavefront Aberrations

7.4.1 Description of Wavefront

Shadow casting phenomenon and the pinhole camera demonstrate in a simple manner that light travels in straight lines. The pinhole camera also helps define what is meant by a “ray of light.” Consider a point source of light emitting rays in all directions. Next, consider the ensemble of rays having a certain optical path length (OPL).

$$\text{OPL} = (\text{length}) \times (\text{refractive index}) \quad (7.1)$$

The OPL is a radius in this case and the ray tips lie on the surface of a sphere (centered on the point source.) This surface is a basic example of what is meant by a wavefront. (Note that rays and their associated wavefronts are always *orthogonal* to one another.) The wavefront is also called a phasefront. Light is an electromagnetic wave phenomenon. A ray can be thought of as the path along which the electric field strength u propagates in a sinusoidal manner with velocity c as described by Equation 7.2 and illustrated in Figure 7.13.

$$u = u_0 \sin \phi = u_0 \sin \left[2\pi \frac{(x - ct)}{\lambda} \right] \quad (7.2)$$

The field amplitude u is cyclic. Phase, ϕ , refers to some point in this cycle. For example, when $\phi = 90^\circ$, $u = u_0$. In an optical system, the temporal variation of the electric field is generally ignored. Ray paths connect the object and image, and the phase variations along those paths can be considered as “frozen-in.” What is of interest is the phase differences (or optical path difference, OPD) between different parts of the ray path, or between different rays. Such phase differences are, for our purpose, constant in time.

Consider the two rays from the point source shown in Figure 7.14. (Note: It is the nature of a point source that all rays leave the source having the same phase.) Along the ray path, the cyclic nature of light is indicated by the number of wave-

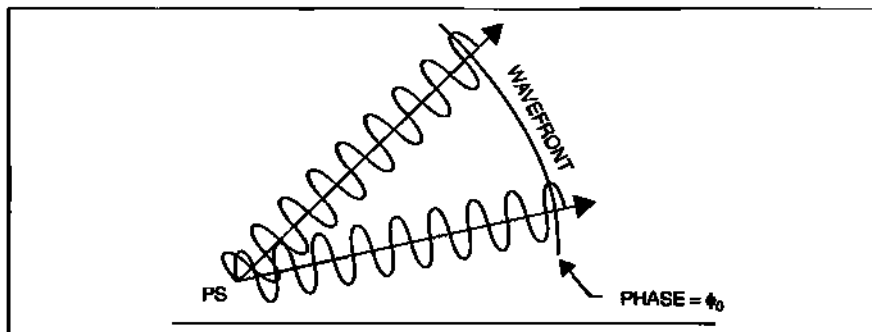


Fig. 7.14 Phase relationship between two rays.

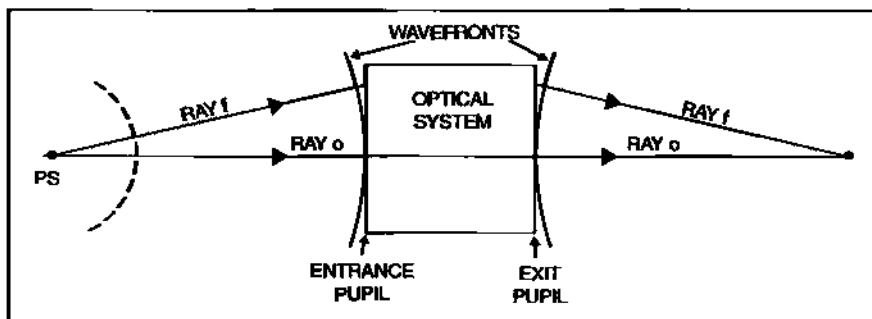


Fig. 7.15 Wavefront manipulation by a perfect optical imaging system.

lengths that fit the OPL.

At the surface of the wavefront, both rays have the same phase, ϕ_0 . If the point source is moved to infinity, then the wavefront observed will be flat. The rays (normal to this surface) will be parallel. (The parallel rays are said to form a collimated beam.) The spherical wavefront and flat wavefront are ideal constructions against which other wavefronts will be compared. In that context they will be called reference wavefronts.

7.4.2 Interaction Of Wavefronts With Optical Systems

Consider the ideal system shown in Figure 7.15. At the entrance pupil of the system is a diverging spherical wavefront centered on the object point. It is a surface of constant OPL. At the exit pupil of the system there is a collapsing or converging spherical wavefront centered on the image point. It too is a surface of constant OPL not only with respect to the image point but also with respect to the object point as well. A perfect optical imaging system is such that the OPL from the object point through the system to the image point is the same for any ray path.

Define an OPL on the axial ray between object and exit pupil, and let all other rays have this same OPL. Only a wavefront with a spherical surface can converge to a point. For an imperfect optical system these other rays do not termi-

Section 7.4: Wavefront Aberrations 79

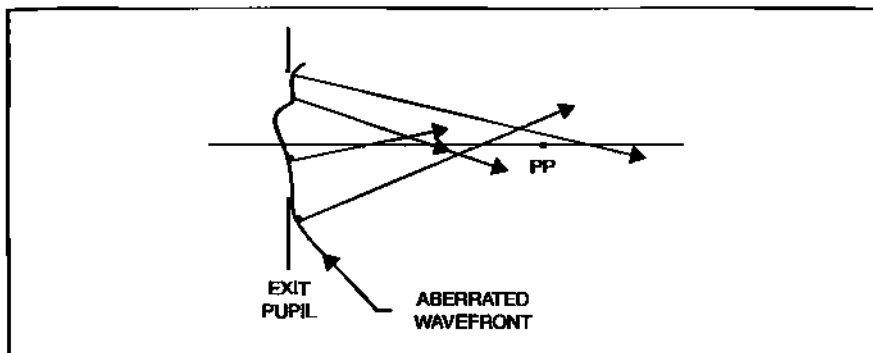


Fig. 7.16 Rays from a converging non-spherical wavefront cannot form a point image.

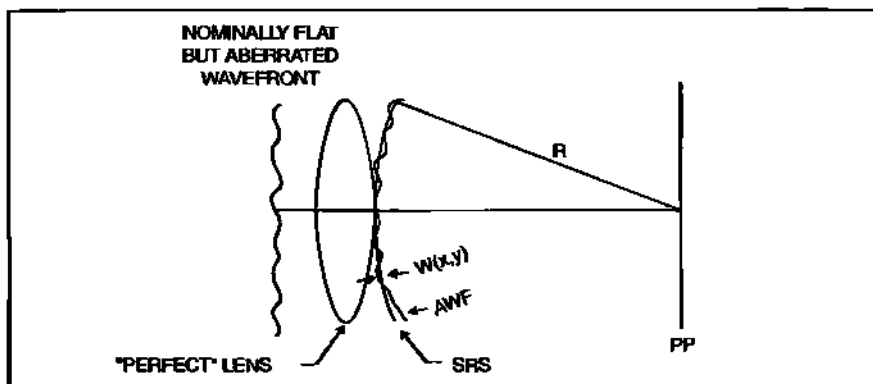


Fig. 7.17 Exit pupil aberration $W(x,y)$.

nate on the surface of a sphere (centered on the image point), hence no point image can be formed. This is illustrated in Figure 7.16. There is still a wavefront. All the rays terminating on its surface have the same phase. But this wavefront surface is non-spherical. Such a wavefront is said to be aberrated. The image formed by the aberrated wavefront will be spread out in a tiny volume about the ideal image point and cause a loss in resolution.

7.4.3 Wavefront Description

An aberrated wavefront can be described by comparing it to the ideal spherical wavefront, which we will call the reference wavefront. The reference wavefront is set up with its vertex tangent to the exit pupil, and its center of curvature coincident with the ideal image point. For each point in the exit pupil, we measure the *optical path difference*, W , between the spherical reference surface (SRS) and the aberrated wavefront (AWF) along the radius of the spherical reference surface. This is shown in Figure 7.17. A function $W(x,y)$ is obtained over the pupil which is now used as a description of the aberrated wavefront.

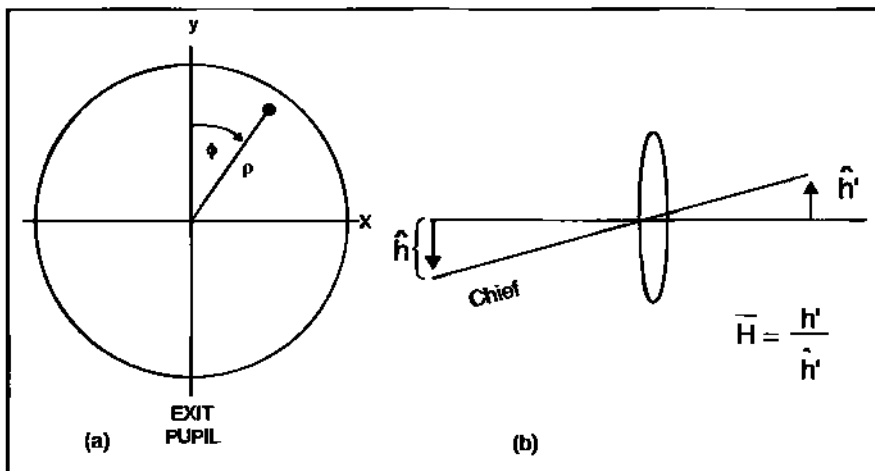


Fig. 7.18 Coordinate system for Seidel aberrations: (a) point location in exit pupil; (b) point location in image.

The OPD function $W(x, y)$ can be cast in a mathematical form by a polynomial. This is useful because each term in the polynomial describes a specific aberration and how much of it is present. There are two sets of polynomials that have been traditionally used for the description of aberrations in the exit pupil. In optical design the Seidel polynomial series is typically used. In optical testing the aberration content of a measured wavefront must be deciphered. The procedure commonly used is to fit the data with a Zernike polynomial.

Seidel polynomials use the polar coordinate system shown in Figure 7.18a. The Seidel polynomial can be described mathematically as follows:

$$W = \sum_{i,j,k} W_{ijk} \bar{H}^i \rho^j \cos^k \phi \quad (7.3)$$

In each term of the Seidel polynomial, W_{ijk} is the wavefront aberration coefficient whose value can be positive or negative. It has dimensions of length (usually in the units of the operational wavelength). The coefficient defines the maximum value the term can achieve. The subscripts ijk are a mnemonic device that ties the coefficient to a particular aberration term in the series. The subscripts refer to the powers on the other factors in that term. The factor \bar{H} is the fractional image height (as shown in Figure 7.18b). Its value ranges between 0 and 1. The fractional pupil radius, ρ , also ranges between 0 and 1. The other pupil coordinate is given by ϕ in the cosine term. The cosine has values between -1 and 1. The use of normalized pupil and field coordinates is a matter of convenience. Dimensionality is maintained by the coefficient W_{ijk} .

The Seidel aberrations are the five lower order terms in the polynomial where the sum $i + j = 4$. These are the most familiar aberrations: spherical aberration, coma, astigmatism, field curvature, and distortion. The first three affect the

Section 7.4: Wavefront Aberrations 81

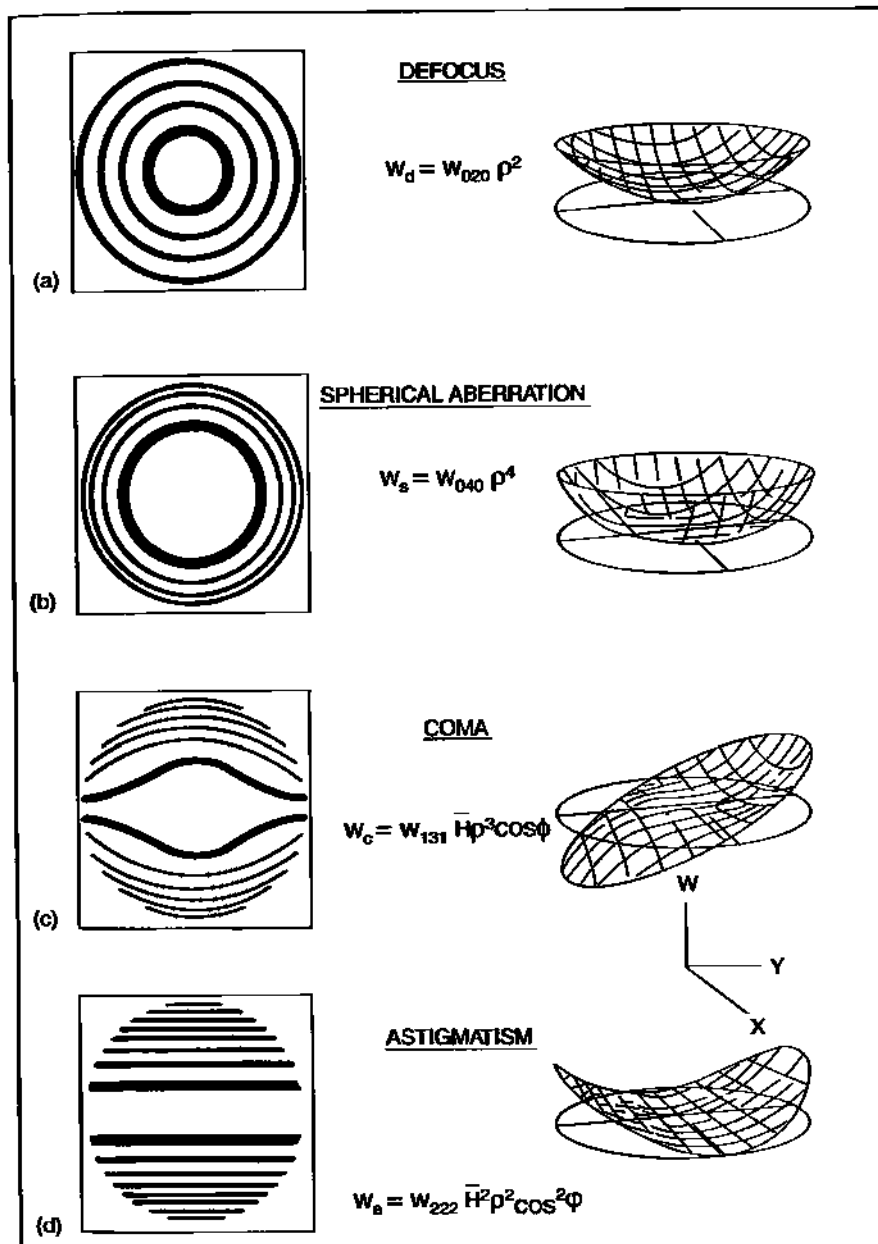


Fig. 7.19 Aberrations that affect the shape of the PSF: defocus and the Seidel's spherical, coma, and astigmatism.

82 Chapter 7 Aberrations in General

quality of the PSF. The last two affect its lateral and longitudinal position for off-axis field points.

Figure 7.19 shows the mathematical description of focus, spherical aberration, coma, and astigmatism along with contour and 3-D plots of their shape. W_{jk} can be calculated from a knowledge of the optical system geometry and a paraxial ray trace.

7.4.4 Wavefronts and Diffraction

In geometric optics, ray normals to $W(x,y)$ describe the ensemble of ray pierces in planes at or near paraxial focus. In physical optics, $W(x,y)$ plays the major role in describing the diffractive behavior of an image. In Fourier optics, the amplitude and phase in the exit pupil are described by:

$$\text{PUPIL FUNCTION: } p(x,y) = a(x,y)e^{ikW(x,y)} \quad (7.4)$$

The phase information is contained in $W(x,y)$. This is the aberration function that has been the topic of discussion in this chapter. The image point is related to the pupil function through the Fourier transform. The coherent point spread function is given by:

$$\text{CPSF} = k\mathcal{T}\{ p(x,y) \} = P(\xi, n) \quad (7.5)$$

The incoherent point spread function is given by:

$$\text{PSF} = P(\xi, n) \cdot P^*(\xi, n) \quad (7.6)$$

The latter is what is typically measured.

7.5 Connection Between Image Plane and Exit Pupil Aberrations

There is a definite connection between transverse ray aberrations as described in the image plane and the wavefront aberration in the exit pupil. This relation is given by the following equation:

$$T = - \left(\frac{R}{h \cdot r} \right) \left(\frac{dw}{dy} \right) \quad (7.7)$$

T is called the transverse ray aberration. Equation 7.7 will be discussed in more detail in Section 11.8.

Note: The Seidel aberrations are sometimes referred to as fourth order aberrations, and sometimes as third order. The former is applicable in the exit pupil; the latter, in the image plane. Equation 7.6 is the reason. The derivative drops the power of the aberration by one.

Section 7.6: Abbe Sine Condition 83

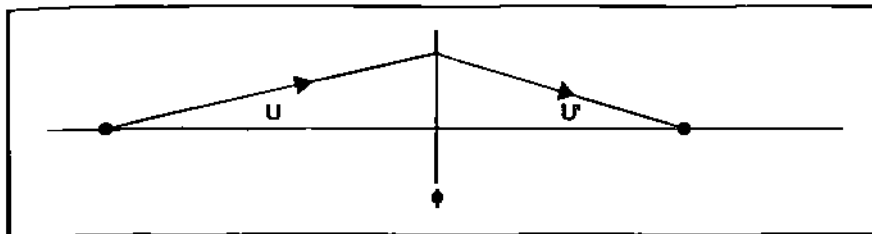


Fig. 7.20 Parameters relating to the Abbe sine condition.

7.6 Abbe Sine Condition

Coma is sometimes referred to as an offense against the Abbe sine condition. In other words, if a system has no coma, the sine condition would be satisfied. But what is this sine condition? It basically relates to lateral magnification, m (Section 4.8). Consider a thin lens with finite object/image conjugates as shown in Figure 7.20. The sine condition states that:

$$m = \frac{h'}{h} = \frac{\sin U}{\sin U'} \quad (7.8)$$

It means that the lateral magnification is independent of which annular zone in the lens that rays pass through.

Chapter 8

Solves and Merit Function

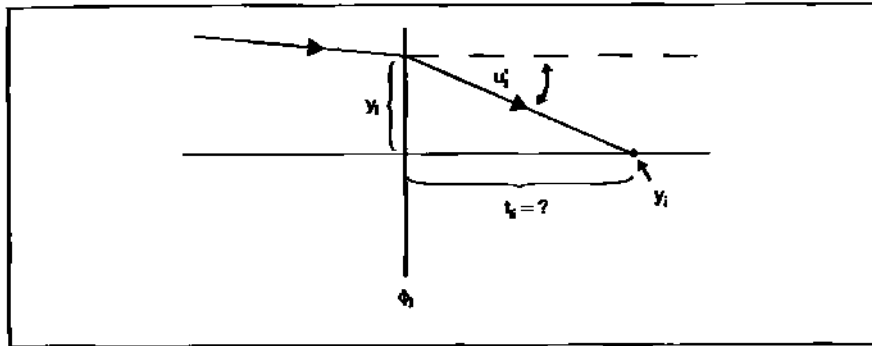


Fig. 8.1 Geometry used for *M*-solve.

8.1 Introduction

You have now gained some familiarity using ZEMAX to optimize and analyze simple systems (i.e., the singlet, and front and rear landscape lenses). In this chapter we will derive the basis for the two solves you have used, namely the *M* and *F* solves. We will also examine the general nature of the merit function, and discuss the TRAC merit function and its relation to RMS spot size.

8.2 The *M*-solve

The marginal ray *M*-solve is used to find the paraxial back image distance (or back focal length for an object at infinity). Figure 8.1 shows the marginal ray incident on the last optical surface of a lens system. The program solves the paraxial transfer equation for the thickness between the last surface and the image.

$$y_i = y_1 + u_i t_{1i} = 0$$

Therefore:

$$t_{1i} = \frac{-y_1}{u_i} \quad (8.1)$$

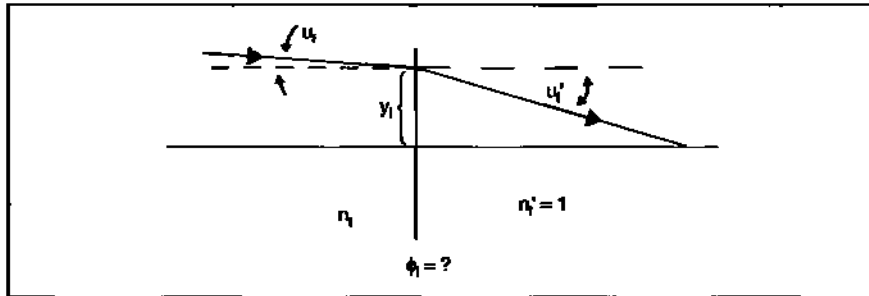


Fig. 8.2 Geometry used for F-solve.

8.3 The F-solve

The *F*-solve is used on the radius of curvature of the last optical surface. It solves for the radius which will yield a specified f-number. It is an easy way to lock in a specific EFL for a given entrance pupil diameter. Figure 8.2 shows the geometry we will be using. The refracted marginal ray angle is related to the f-number by:

$$u'_t = \frac{-1}{2(f/\#)} \quad (8.2)$$

Knowing the incident marginal ray angle, marginal ray height, refractive indices on either side of the interface, and the f-number, we can use the paraxial bending equation to solve for the power of the last optical surface.

$$\begin{aligned} \phi_t &= \frac{[n_t u_t - u'_t]}{y_t} \\ \phi_t &= \frac{n_t u_t - \left(\frac{-1}{2f/\#}\right)}{y_t} \end{aligned} \quad (8.3)$$

We also know that:

$$\phi_t = (1 - n_t) C_t \quad (8.4)$$

Equating Equations 8.3 and 8.4 and solving for C_t yields:

$$C_t = \frac{\phi_t}{1 - n_t} = \frac{n_t u_t + \frac{1}{2f/\#}}{y_t(1 - n_t)} \quad (8.5)$$

and

$$R_t = \frac{y_t(1 - n_t)}{n_t u_t + \frac{1}{2f/\#}} \quad (8.6)$$

Section 8.4: Rings and Arms 87

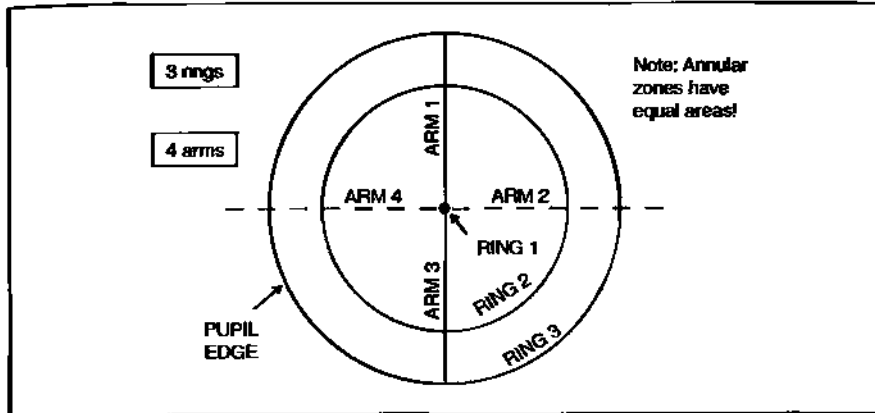


Fig. 8.3 Illustration of rings and arms in the pupil.

Merit Function Value: 4.85165164E-862

Num	Type	Int1	Int2	Hx	Hy	Px	Py	Target	Weight	Value	% Cont
1	TRAC	1	0.0000	0.0000	0.1679	0.2967	0.000000E+000	0.14544	3.05105E-003	0.026	
2	TRAC	1	0.0000	0.0000	0.3536	0.6124	0.000000E+000	0.23271	2.85887E-002	3.688	
3	TRAC	1	0.0000	0.0000	0.4718	0.8158	0.000000E+000	0.14544	6.77695E-002	12.952	
4	TRAC	1	0.0000	0.0000	0.3357	0.6000	0.000000E+000	0.14544	3.05105E-003	0.026	
5	TRAC	1	0.0000	0.0000	0.7871	0.0000	0.000000E+000	0.23271	2.85887E-002	3.688	
6	TRAC	1	0.0000	0.0000	0.9428	0.0000	0.000000E+000	0.14544	6.77695E-002	12.952	
7	TRAC	1	0.0000	0.0000	0.1679	-0.2967	0.000000E+000	0.14544	3.05105E-003	0.026	
8	TRAC	1	0.0000	0.0000	0.3536	-0.6124	0.000000E+000	0.23271	2.85887E-002	3.688	
9	TRAC	1	0.0000	0.0000	0.4718	-0.8158	0.000000E+000	0.14544	6.77695E-002	12.952	
10	TRAC	1	0.0000	0.0000	-0.1679	-0.2967	0.000000E+000	0.14544	3.05105E-003	0.026	
11	TRAC	1	0.0000	0.0000	-0.3536	-0.6124	0.000000E+000	0.23271	2.85887E-002	3.688	
12	TRAC	1	0.0000	0.0000	-0.4718	-0.8158	0.000000E+000	0.14544	6.77695E-002	12.952	
13	TRAC	1	0.0000	0.0000	-0.3357	0.0000	0.000000E+000	0.14544	3.05105E-003	0.026	
14	TRAC	1	0.0000	0.0000	-0.7871	0.0000	0.000000E+000	0.23271	2.85887E-002	3.688	
15	TRAC	1	0.0000	0.0000	-0.9428	0.0000	0.000000E+000	0.14544	6.77695E-002	12.952	
16	TRAC	1	0.0000	0.0000	-0.1679	-0.2967	0.000000E+000	0.14544	3.05105E-003	0.026	
17	TRAC	1	0.0000	0.0000	-0.3536	-0.6124	0.000000E+000	0.23271	2.85887E-002	3.688	
18	TRAC	1	0.0000	0.0000	-0.4718	-0.8158	0.000000E+000	0.14544	6.77695E-002	12.952	

Table 8.1

8.4 Rings and Arms

The default merit function TRAC (transverse ray aberration centroid) is quite powerful as an optimization tool. A selected number of rays are traced from each defined field point and for each defined wavelength. When this option is selected, the dialog box allows the user to define the ray group by defining the ray pierces in the entrance pupil. The rationale is illustrated in Figure 8.3.

This shows the entrance pupil with 3 rings: the center, a ring at 0.707 of the pupil radius, a ring at the pupil edge. Also shown are 4 arms. A ray pierce occurs wherever a ring and arm intersect. For the outer ring and the 0.707 ring there are four crossings each. At the center there are also four crossings but three are redundant. But the number of rays traced is $3 \times 4 = 12$. If you had three colors, there would be 12 rays for each color, i.e., 36 rays. If you had four field points, there would be 36 rays for each field point for a total of 144 rays. Table 8.1 shows the merit function listing for TRAC using 3 rings, and 6 arms for a single wavelength

88 Chapter 8 Solves and Merit Function

Merit Function Listing

File : A:\singlet\singlet6.ZMX

Title: Lens has no title.

Date : THU APR 29 2000

Merit Function Value: 4.05165179E-002

Num	Type	Int1	Int2	Hx	Hy	Px	Py	Target	Weight	Value	% Cont
1	TRAC		1	0.0000	0.0000	0.3357	0.0000	0.00000E+000	0.87266	3.05165E-003	0.158
2	TRAC		1	0.0000	0.0000	0.7871	0.0000	0.00000E+000	1.3963	2.85887E-002	22.128
3	TRAC		1	0.0000	0.0000	0.9428	0.0000	0.00000E+000	0.87266	6.77695E-002	77.714

Table 8.2

and field point.

While in the merit function editor (MFE), TRAC is inserted into the merit function by selecting: Tools → Default Merit Function → OK. Before you click on OK, make sure the dialog box is setup for RMS; Spot Radius; Centroid. For an axially symmetric system, the Assume Axial Symmetry box can be checked on. This will reduce the number of terms that show up in the MFE. The 18 terms in Table 8.1 will be reduced to just three (as shown in Table 8.2.) Note that the merit function value is the same for both tables.

8.5 The Merit Function

For this course the merit function (*MF*) is defined as follows:

$$(MF)^2 = \sum_i W_i (V_i - T_i)^2 / \sum_i W_i \quad (8.7)$$

where W_i is the weight, V_i is the current value, and T_i is the target value.

As an example, we will use the TRAC values in Table 8.2 (rounded off) along with Equation 8.7 to illustrate the computation of the *MF* (which will be in lens units). The data is for our standard test singlet.

$$(MF)^2 = \frac{0.8727(0.0031 - 0)^2 + 1.3693(0.0286 - 0)^2 + 0.8727(0.0678 - 0)^2}{3.1417}$$

$$(MF)^2 = 0.0000027 + 0.0003635 + 0.0012769$$

$$(MF)^2 = 0.0016431$$

$$MF = 0.0405353 \text{ mm} = 40.53 \text{ microns}$$

We will see shortly that this MF value is equivalent to the RMS spot radius obtained from the spot diagram.

The % contribution can be determined as follows:

Section 8.5: The Merit Function 89

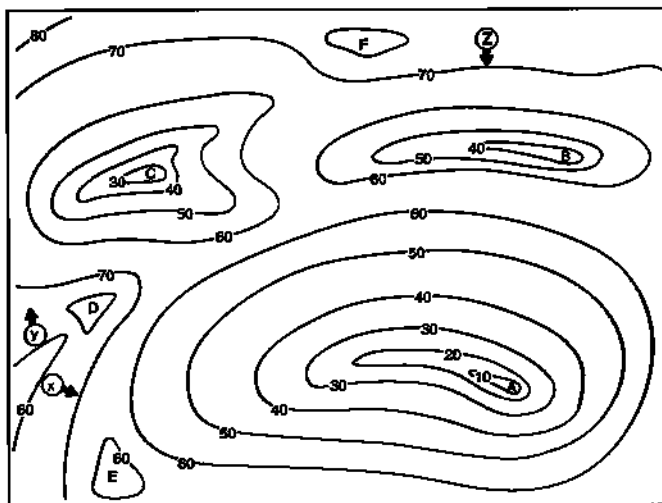


Fig. 8.4 Design space showing various optimization minima. From W. Smith, Modern Lens Design (McGraw-Hill, 1992). Reprinted with permission of the McGraw-Hill Companies.

$$\begin{aligned}
 \% \text{ Contribution: } & \frac{0.0000027}{0.0016431} + \frac{0.0003635}{0.0016431} + \frac{0.0012769}{0.0016431} = \\
 & 0.0016432 + 0.2223237 + 0.7771286 = 1.0010955 \\
 \text{or } & 0.16432\% + 22.23237\% + 77.1286\% = 100.10955\% \text{ [1]}
 \end{aligned}$$

The *MF* example given above is an extremely simple case. Most *MF*'s are much more complicated and include a wide variety of operands. The computation of the *MF* value follows the same procedure. However, a nice physical interpretation of the *MF* value no longer applies.

The *MF* value is a single number used to judge the overall quality or "goodness" of the design. The purpose of optimization is to drive this value to zero if at all possible. To do this certain parameters of the optical system must be set as variables (such as radii, thicknesses, etc.). The optimization engine plays with these variables to see which changes move the *MF* to lower values. It is a very iterative process. There is no guarantee that at the conclusion of the optimization run, the *MF* has attained the lowest possible value overall. It may be that the combination of operands and variables employed, and the starting point chosen, force the design into a local minimum, a minimum which may not be the lowest attainable. This is illustrated in Figure 8.4 for an *MF* (*z*-axis) based on two variables (*x* and *y* axes). Point *A* is the best solution. But if we started from Point *Z* we would end up at Point *B*—neither the deepest well nor the best design.

¹ Should sum to 100% but it does not because of round-off.

8.6 RMS Spot Size

Spot diagrams were introduced in the previous chapter as a way of visualizing the effect aberrations have on image quality. Another measure of quality that relies on the spot diagram is the RMS spot radius. The RMS spot radius is defined as:

$$RMS = \sqrt{\frac{\sum_i [(x_i - x_c)^2 + (y_i - y_c)^2]}{n}} \quad (8.8)$$

To illustrate the computation of RMS spot radius we will use the simple spot diagram in Figure 8.5. In this example, the reference point (x_r, y_r) is taken as $(0,0)$.

$$r_{RMS} = \sqrt{\frac{[3^2 + 2^2 + (-2)^2 + (-1)^2 + (+2)^2] + [1^2 + 3^2 + 2^2 + (-2)^2 + (-1)^2]}{5}}$$

$$r_{RMS} = \sqrt{4.4 + 3.8}$$

$$r_{RMS} = 2.86$$

Figure 8.6 shows spot diagrams for the standard singlet as a function of field angle. The number above each diagram is the field angle; below, the coordinate location in the image plane. The lower left data box contains the RMS and geometric spot radius for each field.

In RMS spot calculations, two reference points are commonly used: either the spot centroid, or the chief ray pierce. On-axis this distinction is meaningless. Off-axis, however, RMS spot radii can be significantly different depending on which reference is used (although the actual physical size and shape of the spot remains unchanged). This is illustrated in Figure 8.7 for our standard singlet at a field angle of 5° . The vertical separation (58 microns) of the x -coordinate axes is due to the difference in location between the centroid and chief ray. The RMS spot radius for the former is 196.146 microns; the latter, 204.702 microns.

Table 8.3 shows a comparison of RMS spot radius (centroid; square array) with the TRAC *MF* value for the standard singlet as a function of field angle. (Note that the *MF* was determined separately for each field angle.) The two values are essentially the same.

When TRAC is used in optimization, it will minimize the RMS spot size.

Table 8.3		
Field Angle	RMS Spot	MF
0°	40.7	40.5
3.5°	117.2	117.0
5°	196.1	196.0

The difference between RMS spot radius and geometric spot radius is illustrated in Figure 8.8. The latter has a radius which just encloses the outermost ray pierce in the pattern relative to the reference point.

Section 8.6: RMS Spot Size 91

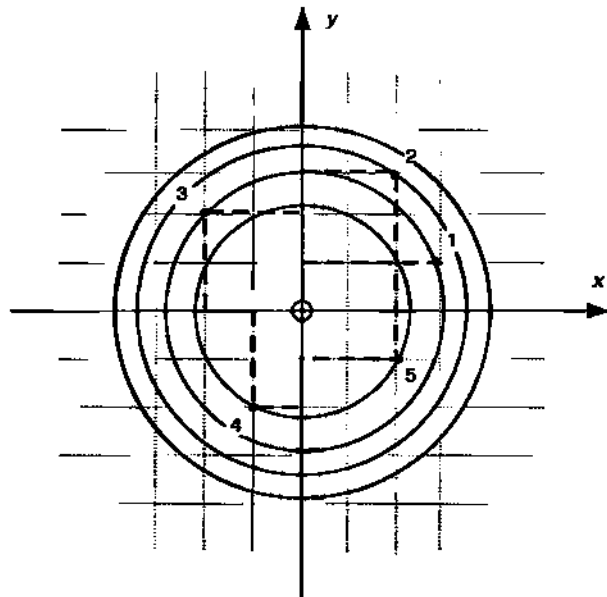


Fig. 8.5 Spot diagram for RMS calculation.

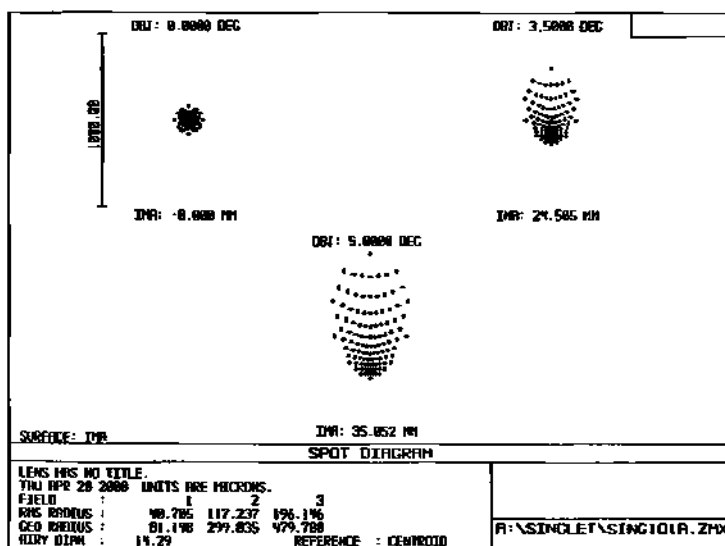


Fig. 8.6 Sample spot diagrams for standard singlet.

92 Chapter 8 Solves and Merit Function

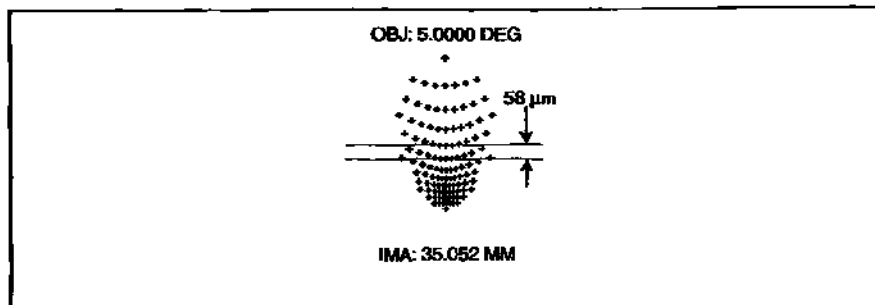


Fig. 8.7 Difference between spot diagrams centered on centroid vs. chief ray.

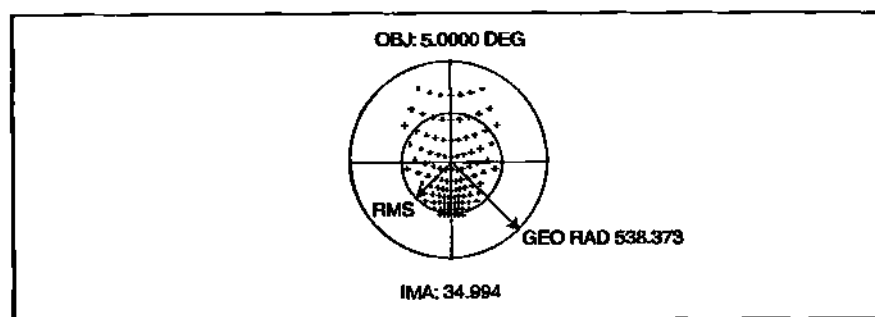


Fig. 8.8 Difference between RMS and geometric spot radii.

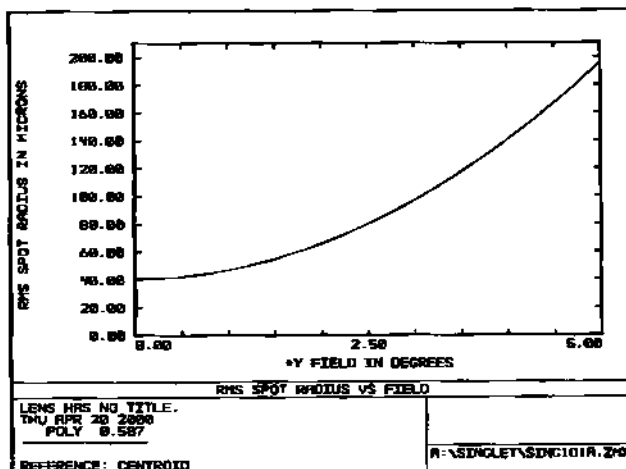


Fig. 8.9 Plot of RMS spot radius as a function of field angle.

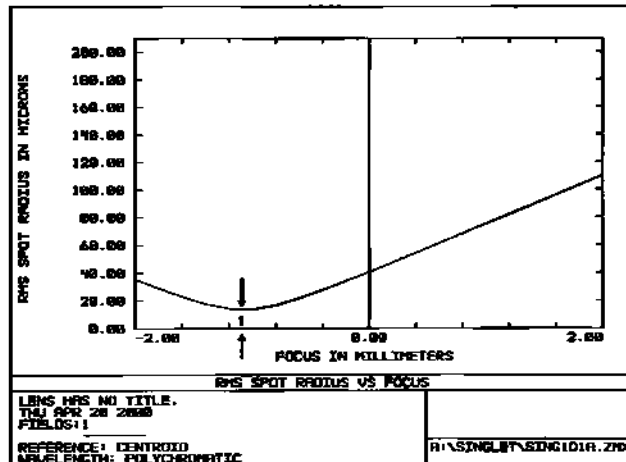


Fig. 8.10 Plot of RMS spot radius as a function of focus.

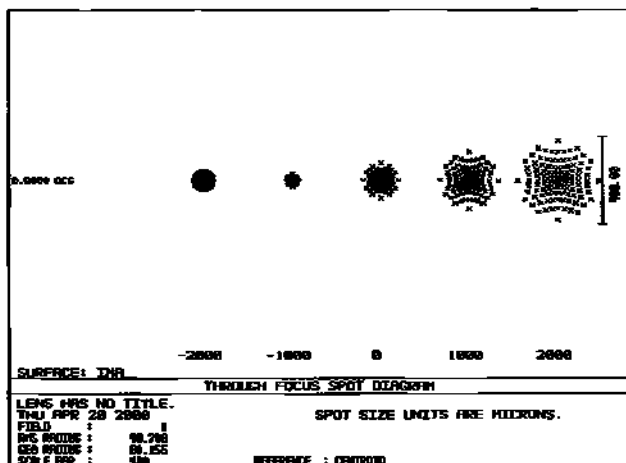


Fig. 8.11 Through focus spot diagrams.

8.7 RMS Spot Plots

There are two ways of plotting RMS spot size that prove useful in analyzing optical designs. The first is a plot of RMS vs. field angle as shown in Figure 8.9 (which corresponds to data in Figure 8.6). The second is RMS vs. focus as shown in Figure 8.10, and corresponds to the through focus plot in Figure 8.11. Note that the minimum in Figure 8.10 is *not* the “minimum blur” axial location we learned about in the last chapter (which is a minimum geometric spot radius).

Chapter 9

Splitting a Lens

9.1 Introduction

In Chapter 3 and its homework, you learned how to minimize spherical aberration by lens bending, and eliminating it by using an aspheric surface. The operands SPHA or TRAC were used in the merit function to accomplish this. In this chapter we will take up the topic of “lens splitting” as a means of achieving diffraction limited performance on-axis. Practical use of this technique can be found in “transmission spheres” in Fizeau interferometry, and in lithographic lenses. A homework exercise will be assigned in the former category.

9.2 Lens Splitting

9.2.1 Single Element

We will start with the following equiconvex singlet: 100 mm f/4. The lens material will be BK7 ($n = 1.5168$ at $\lambda = 0.587$ microns). Using the *thin* lens power equation, we calculate the starting radii of curvature that will be used in ZEMAX.

$$R_1 = 2(n - 1)/\phi \quad (9.1)$$

$$R_1 = 2(0.5168)/0.01 = 103.36 = -R_2$$

This lens is inserted into ZEMAX with a finite thickness of 7 mm. The merit function will contain two operands: EFL with a target of 100 mm, and SPHA with a target of zero. Variables will be placed on both radii. This optimization will strive to restore the proper focal length in the presence of the finite thickness, and bend the lens to minimize spherical aberration. The resulting singlet is shown in Figure 9.1. The EFL is 102.7, and the pupil spherical aberration $W_{040} = 9.64 \lambda$ (which can be read off directly from the merit function under “value”). This is a lot of spherical aberration, but it is the best that can be done with a singlet.

9.2.2 Double Element

The lens will now be split into two elements of equal power, i.e.,

$$\Phi_i = \frac{\Phi}{2} = \frac{0.01}{2} = 0.005 .$$

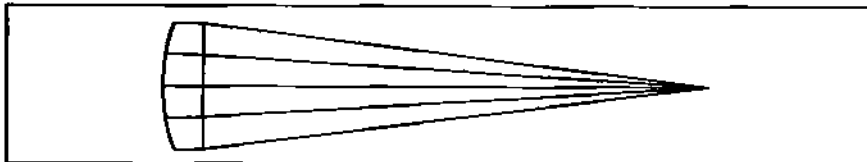


Fig. 9.1 Singlet bent for minimum spherical aberration.

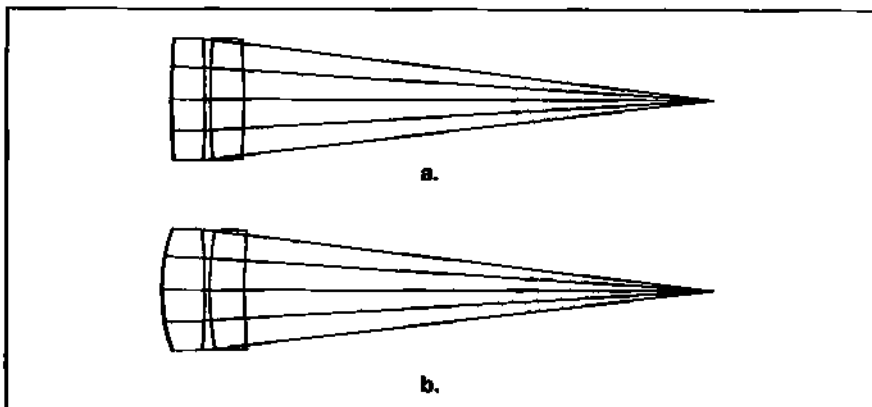


Fig. 9.2 Lens splitting: a. starting doublet; b. optimized doublet.

Once again we assume equal magnitude radii for all four surfaces.

$$R_1 = \frac{1.0336}{0.005} = 206.72 = R_3 = -R_2 = -R_4$$

These two lenses are inserted into ZEMAX with a 1 mm spacing between them. The starting layout is shown in Figure 9.2a. The same merit function is used, and all radii are made variables. After optimization, the focal length is approximately 100 mm, but $W_{040} = 2.04 \lambda$. By adding the second element and bending both, spherical aberration was reduced by almost a factor of five. The layout of the optimized system is shown in Figure 9.2b.

Note: Although the design started with two elements of *equal* power, the optimization process has transferred power between the elements. The first lens now has lower power than the second lens (where $\phi_1 = 0.004796$ and $\phi_2 = 0.005253$). This process has reduced the spherical aberration contribution of each element.

9.2.3 Triple Element

As a final example, the singlet will be turned into a triplet of the same power and f-number. The power of each component will be $\phi_i = \phi/3 = 0.01/3 = 0.00333$. The separation between elements is 1 mm. All components will be equiconvex with equal magnitude radii.

Section 9.2: Lens Splitting 97

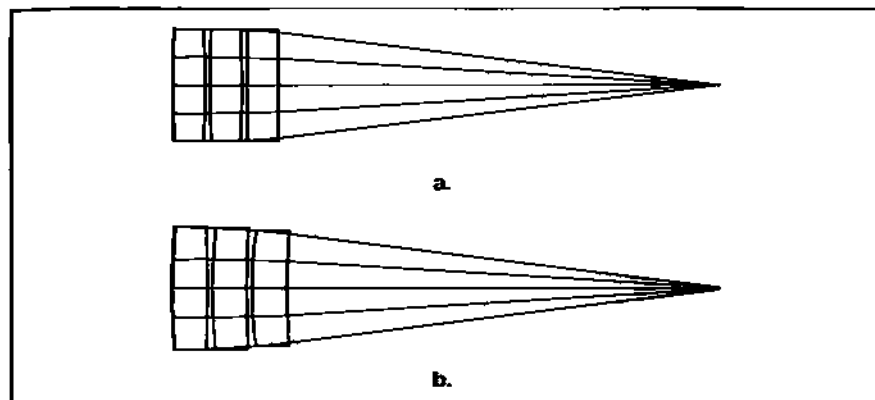


Fig. 9.3 *Lens splitting: a. starting triplet; b. optimized triplet.*

$$R_1 = \frac{(1.0336)}{0.00333} = 310.39 = R_3 = R_5 = -R_2 = -R_4 = -R_6$$

The starting layout is shown in Figure 9.3a. The operands in the merit function are still EFFL and SPHA. All radii are allowed to vary. After optimization the focal length is 100 mm, and $W_{040} = 0.51\lambda$. Spherical aberration has been reduced by a factor of 4. The optimized configuration is shown in Figure 9.3b. Note that the left-most element is biconvex, but the right-most element is meniscus and bent toward the image. This transitional lens shape behavior minimizes the spherical aberration contribution of each element.

Once again there is a redistribution of power among the elements. The new powers are:

$$\phi_1 = 0.003298; \phi_2 = 0.003355; \phi_3 = 0.003429.$$

The front element is weakest; the last, strongest.

Table 9.1 is a comparison of the surface by surface contribution to W_{040} for both the starting system and the optimized system. Also shown are the actual incidence angles at each surface.

As we proceed through the system, the optimized triplet has slightly higher spherical contributions at the air to glass interfaces than the starting triplet, but significantly lower values at the glass to air interfaces. The same behavior is found for the incidence angles. (The arrows beside the optimized values indicate whether they are higher or lower than the starting design.) If you sum the spherical contributions for each *element*, you will find that each element of the optimized design has significantly lower spherical than the starting design.

Figure 9.4 shows the spot diagrams for the optimized singlet, doublet, and triplet at the best RMS spot focus. (This was done by adding a dummy surface as the last surface and allowing its thickness to vary. Variables on all radii were removed. Only TRAC was used in the merit function.) The circle is the Airy disk

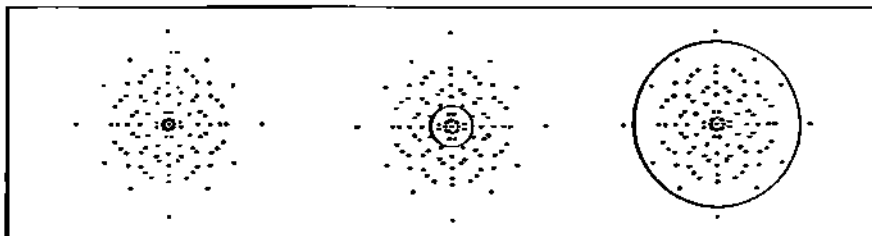


Fig. 9.4 Spot diagram comparison. Airy disk (circle) sets scale.

and has a diameter of 5.73 microns.

Table 9.1

Surface	Start		Optimized	
	W_{00}	Inc. Ang.	W_{00}	Inc. Ang.
1	0.03905	2.090803	0.19604↑	3.95395↑
2	0.56783	3.07819	0.18288↓	1.96774↓
3	-0.00010	0.10038	0.11318↑	5.02061↑
4	2.08014	4.57698	0.10856↓	1.31231↓
5	-0.18269	2.51304	-0.12219↑	6.10043↑
6	4.73832	5.99140	0.03174↓	0.65209↓
Σ	7.24256		0.51021	

9.3 Micro-lithography and Lens Splitting

The example of lens splitting given in Section 9.2 has many applications, e.g., in the field of integrated circuits. Higher circuit density on silicon chips means smaller and more powerful computers. The micro-lithography lens is the critical component in this industry. It must form an extremely high resolution distortionless image of a dense circuit pattern target onto a tiny format area. An example of a modern UV lithography lens is shown in Figure 9.5. This lens was designed for $\lambda = 0.365$ microns. Note the two lens groups that transition from meniscus shapes bent toward object space to meniscus shapes bent toward image space. This helps control not only spherical aberration but coma, astigmatism, and distortion as well.

9.4 Fizeau Interferometry

There are many interferometers used for optical testing. However, the Fizeau interferometer has become a standard method for evaluating the quality of optics. The basic layout of a Fizeau interferometer is shown in Figure 9.6.

A laser source is spatially filtered via a microscope objective and a pinhole. This pinhole is located at the focal point of a collimating lens. Between the pinhole and lens is a beam-splitter. The collimated beam immediately encounters a slightly wedged glass plate. This is the heart of the interferometer. The surface adjacent

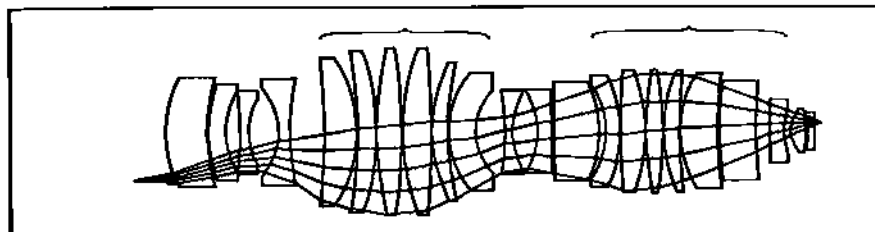


Fig. 9.5 A modern lithography lens. Courtesy Laser Focus World 31, no. 4 (April 1995): 113; © Penn-Well Publishing Co.

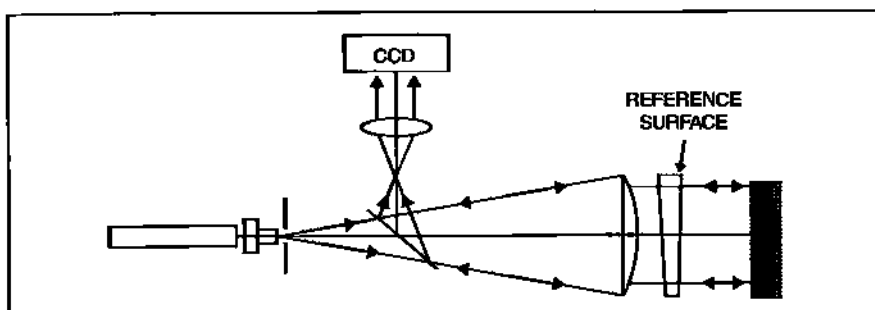


Fig. 9.6 Typical layout of a Fizeau interferometer.

to the collimating lens is of good optical quality. However, the next surface is of exceptional optical quality, $\lambda/20$ peak to valley (PV) or better. This is the reference surface and part of the collimated beam is reflected by this surface. Part of the collimated beam continues on to interrogate the test optic. The return beam contains information on aberration introduced by the test optic. The two wavefronts recombine inside the interferometer. The beam-splitter diverts the combined beams toward a recording medium, either film or a CCD. An intermediate lens together with the collimating lens forms an image of the test surface onto the recording plane. An observer will see a sharp image of the test surface with a fringe pattern running through it.

As an example, assume that the test object is a glass surface whose quality we wish to inspect. Suppose the test surface has a depression in it as illustrated in Figure 9.7. The flat wavefront from the interferometer is incident on the test surface and reflected back into the interferometer. Note that the reflected portion shown in Figure 9.7 has picked up *twice* the surface error inherent in the test surface. This aberrated wavefront returns through the reference plate to combine with reflected reference to form an interference pattern in the test object image plane.

A sample interferogram is shown in Figure 9.8. Each fringe is a contour as in a topographical map. Except here altitude above "sea level" (reference plane) is measured in waves of light. The height difference between each contour or

100 Chapter 9 Splitting a Lens

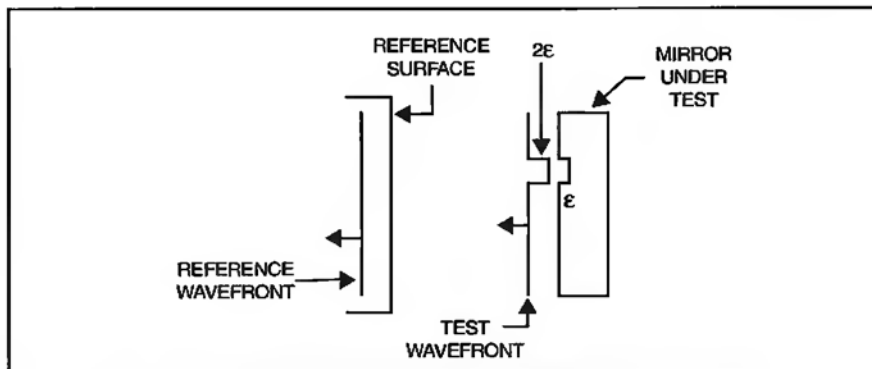


Fig. 9.7 Generation of test and reference wavefronts in a Fizeau interferometer.



Fig. 9.8 Interferogram of a "flat" mirror.

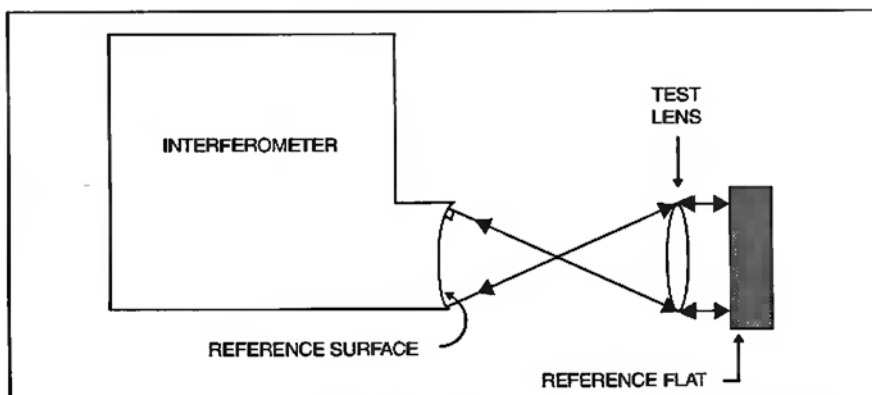


Fig. 9.9 Testing a lens with a transmission sphere.

Section 9.5: Homework 101

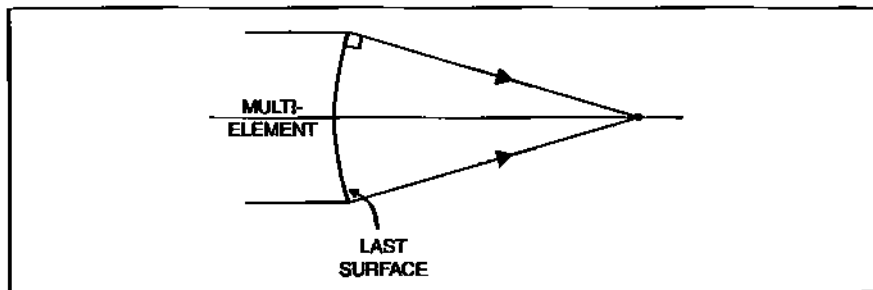


Fig. 9.10

fringe is 1 wave.

The setup for testing a lens is illustrated in Figure 9.9. Here a *transmission sphere* is being used. It is a specially designed positive power lens where rays emerging from the *last surface* (which is the reference surface) of the lens are *normal* to that surface. The test lens is aligned to the test beam and oriented so its rear focal point is coincident with the transmission sphere's focal point. The beam emerges from the lens as collimated light. A flat reference surface is needed to reflect the beam back. (We note that transmission spheres come in a variety of f-numbers and you must pick one that matches or overfills that of your test lens.)

9.5 Homework

Design a 4" diameter $f/7.8$ transmission sphere. The field angle is 0° . Use BK7 glass at a wavelength of 0.6328 microns. Let the thickness of each element be 0.5" separated by 0.2". Use as many elements (via splitting) to obtain diffraction limited performance, i.e., the spot diagram must be *completely* enclosed by the Airy disk. The following notes apply:

- a. Use TRAC, not SPHA.
- b. Use N-solve on last surface as an optimization run after spherical has been reduced. (The N-solve will help keep the rays *normal* to the last optical surface.)
- c. Use RAID operand to monitor incident ray angles on the last optical surface. (Note: Use three.)
- d. Use OPTH and DIFF operands to make the back focal distance equal to the effective focal length. (Note: You will need two OPTH entries in order for DIFF to work.)
- e. Suggested folder name: Fizeau. File name: Fizio1b, etc. where $i =$ the number of lens elements.

Chapter 10

Spherical Aberration

10.1 Introduction

In Section 7.4 we described the primary Seidel aberrations. We saw that W is a function of ρ , H , and ϕ . It is also dependent on the coefficient W_{jk} which specifies the size of the aberration. In ZEMAX we can access these coefficients by the path: Analysis → Calculations → Seidels. A printout of the resulting aberration coefficient list is shown in Listing 10.1. This list is for a singlet. The W_{jk} coefficients are in the second table. For a system having multiple surfaces, the procedure involves carrying out a paraxial ray trace of the system to obtain a knowledge of

Listing of Aberration Coefficient Data									
File : A:\Fscovpin.zmx Title: Lens has no title. Date : WED APR 24 2008									
Wavelength : 0.6818 microns									
Petzval radius : -71.5383									
Optical Invariant: 0.3500									
Seidel Aberration Coefficients:									
Surf	S1	COMA S2	AST1 S3	FCUR S4	DIST S5	CIA (CL)	CTR (CT)		
STD	0.00465	0.00239	0.00117	0.00171	0.00142	0.00000	0.00000		
Z	0.00113	-0.00121	0.00136	0.00000	-0.00139	0.00000	0.00000		
IMA	0.00000	0.00000	0.00000	0.00000	0.00000	0.00000	0.00000		
TOT	0.00599	0.00116	0.00247	0.00171	0.00063	0.00000	0.00000		
Seidel Aberration Coefficients in Waves:									
Surf	W048	W131	W222	W228	W311	W028	W131		
STD	16.11171	19.87622	9.75945	7.12195	11.88173	0.00000	0.00000		
Z	2.34188	-18.05154	10.78589	0.00000	-11.57386	0.00000	0.00000		
IMA	0.00000	0.00000	0.00000	0.00000	0.00000	0.00000	0.00000		
TOT	12.45351	9.82657	20.55534	7.12195	8.22785	0.00000	0.00000		
Transverse Aberration Coefficients:									
Surf	TSPN	TSOD	TICD	TSFC	TTFC	TDIS	TLAC		
STD	0.02981	0.01465	0.00395	0.01778	0.03216	0.00078	0.00060		
Z	0.00590	-0.00741	-0.02223	0.00795	0.02385	-0.00953	0.00000		
IMA	0.00000	0.00000	0.00000	0.00000	0.00000	0.00000	0.00000		
TOT	0.03672	0.00724	0.02173	0.02565	0.05596	0.00017	0.00000		
Longitudinal Aberration Coefficients:									
Surf	LSPH	LAST	LFCP	LFCS	LFCT	LAC			
STD	0.53316	0.25756	0.18776	0.31654	0.57410	0.00000			
Z	0.00465	0.15513	0.00000	0.09752	0.29255	0.00000			
IMA	0.00000	0.00000	0.00000	0.00000	0.00000	0.00000			
TOT	0.45837	0.37156	0.18276	0.31462	0.68638	0.00000			
Wavefront Aberration Coefficient Summary:									
	W048	W131	W222	W228P	W311	W028	W131		
TOT	12.4535	9.8267	20.5553	7.1226	8.2279	0.0000	0.0000		
	W228S	W228H	W228T						
TOT	17.40	27.88	37.95						

Listing 10.1 ZEMAX aberration coefficient data list.

ray heights and angles for the marginal and chief rays at each surface. This data is fed into aberration formulas from which the coefficients W_{ijk} are calculated for each surface. Once this is done the surface contributions are summed for each aberration type.

In this chapter we will concentrate on the boxed-in terms in Listing 10.1, which are for spherical aberration. We will derive the corresponding aberration formula and show how they are used to get the numbers displayed above.

10.2 Heuristic Approach to W_{jk}

Consider a collapsing aberrated wavefront (to point L) with an associated spherical reference surface pinned to it at the vertex as shown in Figure 10.1a. At the marginal ray the optical path difference is given by OPD_i . Next, the aberrated wavefront (AWF) encounters a convex spherical refracting surface as shown in Figure 10.1b. The wavefront and refracting surface are shown tacked together at the vertex. The OPD at the *marginal ray* between the two is given by the line segment $n\overline{QP}$ (where n is the refractive index of the incident medium). Figure 10.1c shows the wavefront just after it has entirely passed through the refracting surface. The OPD along the *axial ray* between the two is given by the line segment $n'\overline{VB}$ (where n' is the refractive index of the glass). Now we state that for all intents and purposes the following is true:

$$n\overline{QP} = n'\overline{VB} \quad (10.1)$$

(Remember that for a perfect imaging system the OPL between object and image points along any ray path is identical.) The refracted wavefront now consists of two aberration components—the part it had before it encountered the refracting surface and the part it picked up at that surface. The total aberration in the refracted wavefront is manifest once a reference sphere is attached at point B as shown in Figure 10.1d. The paraxial image point for the refracted wavefront and the center of curvature of its accompanying reference surface is at the point L' . Note that there is an axial offset between the vertices of the two aberrated wavefronts (and respective reference spheres given by the line VL). To compare the two wavefronts, this *DC* offset is removed. This has no effect other than putting the two wavefronts and reference spheres on a *common footing*. This shift is shown in Figure 10.1e. The refracting surface is reintroduced in Figure 10.1f.

Note that the OPL $n'\overline{VB}$ equals $n\overline{QP}$.

When we combine the wavefronts, reference spheres, and refracting surface together we obtain the illustration shown in Figure 10.2. The radii of the reference spheres are given by VL and $V'L'$ respectively. We also make the approximation that the line segments QP and $Q'P$ lie essentially on the same line.

We next obtain the OPD of the line segment between each wavefront and its respective reference sphere.

$$\text{OPD}_i = n(\overline{VL} - \overline{QPL}) \quad (10.2)$$

Section 10.2: Heuristic Approach to W_{jk} 105

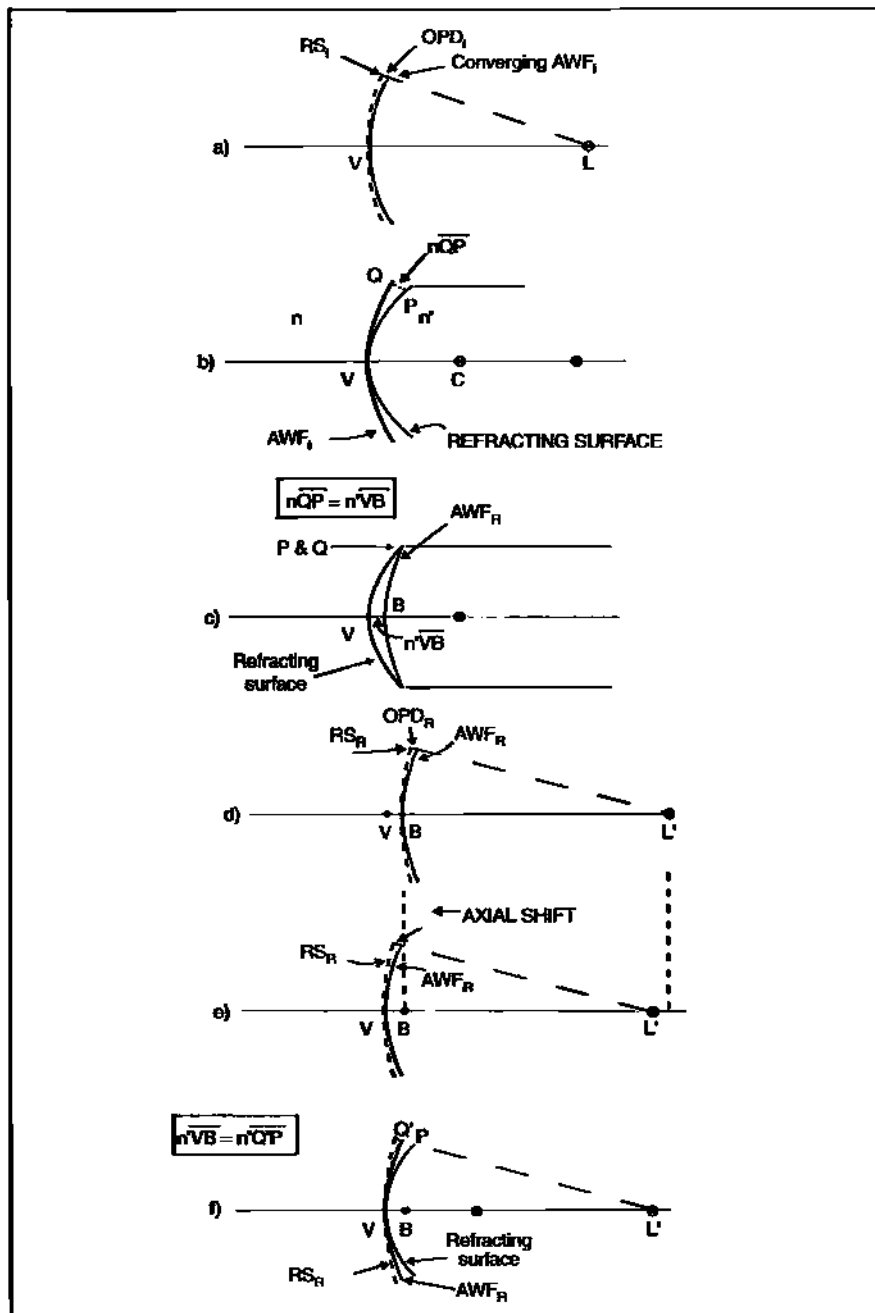


Fig. 10.1 Piecemeal buildup of wavefronts, reference spheres, and refracting surface.

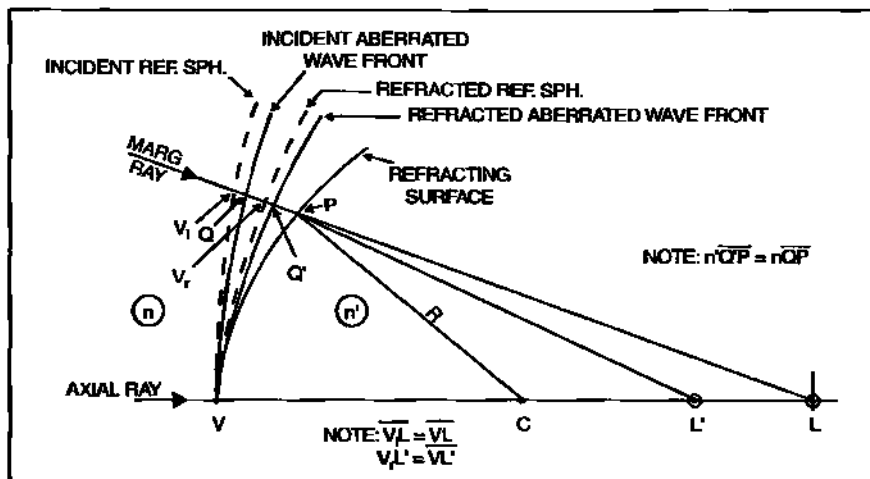


Fig. 10.2 Combination of wavefronts, reference spheres, and refracting surface.

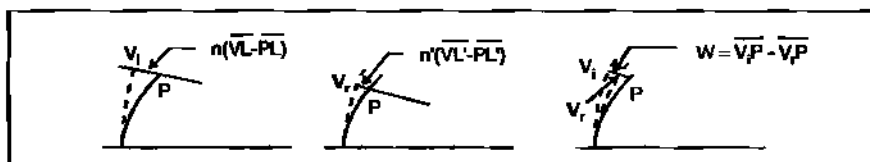


Fig. 10.3 Incident and refracted reference spheres and their difference.

$$OPD_r = n'(\overline{VL'} - \overline{Q'PL'}) \quad (10.3)$$

We are not interested in the aberration of the incident wavefront as such, but we are very interested in the amount of aberration picked up by its interaction with the refracting surface under consideration. To isolate this we form the difference:

$$W = OPD_r - OPD_i \quad (10.4)$$

When we expand out W , the terms $n'Q'P$ and nQP are equal and opposite, and hence cancel.

$$W = (n'\overline{VL'} - n'Q'P - n\overline{PL'}) - (n\overline{VL} - nQP - n\overline{PL}) \quad (10.5)$$

$$W = n'(\overline{VL'} - \overline{PL'}) - n(\overline{VL} - \overline{PL}) \quad (10.6)$$

The meaning of each of the remaining major terms is illustrated in Figure 10.3 as well as their difference.

Thus there are two equivalent viewpoints. W can be considered either as the difference between the OPDs of the incident and refracted aberrated wavefront compared to their respective reference spheres, or as the difference between the

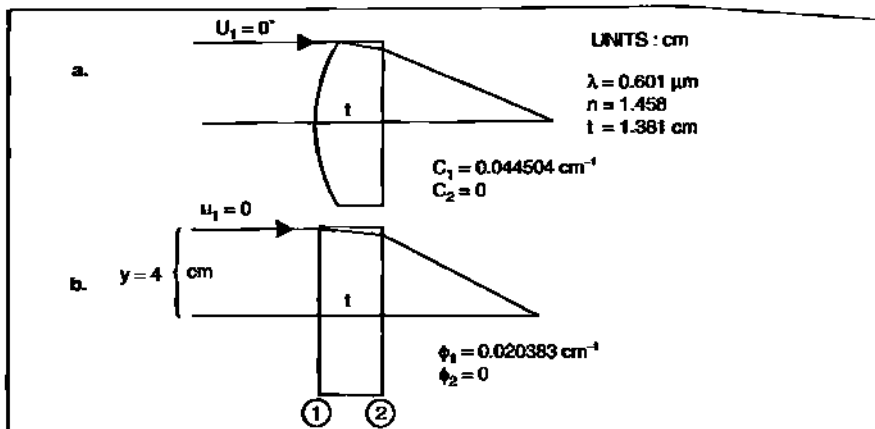


Fig. 10.4 Convex-plano lens: a. real lens; b. paraxial lens.

incident and refracted reference spheres compared to the refracting surface itself. In shorthand notation W becomes:

$$W = \Delta \{ n(\bar{VL} - \bar{PL}) \} \quad (10.7)$$

Equation 10.7 is the starting point for the derivation of the spherical aberration coefficient W_{040} that is presented in Section 10.7. As you will see, the math gets a bit messy. That is why we present only the coefficient derivation for spherical aberration in any depth and later simply state the results for the off-axis cases. One final point: we are interested in the *primary* Seidel term which is of fourth order. Terms higher than this will be discarded. The gist of Section 10.7 boils down to the following equation:

$$W_{040} = \frac{S_I}{8} = -A^2 y \Delta \left\{ \frac{u}{n} \right\} / 8 \quad (10.8)$$

W_{040} is a *wavefront aberration coefficient*. The factor S_I is called a *Seidel Coefficient*.

10.3 Example: W_{040} via Paraxial Ray Trace

We will calculate the spherical aberration contributed by the lens shown in Figure 10.4a. The first thing we have to do is a paraxial ray trace of the system. The paraxial form of the lens is shown in Figure 10.4b. (Note: in ZEMAX, use SILICA for the glass choice and let $\lambda = 0.601$.)

The paraxial ray trace results are:

Surface	y	u	u'
1	4	0	-0.055920
2	3.922774	-0.05592	-0.081531

Now we must utilize this information by applying Equation 10.8 to both surfaces.

First Surface:

$$1. \quad A_1 = n_1(u_1 + y_1 C_1)$$

$$A_1 = 1[0 + 4(0.044504)]$$

$$A_1 = 0.178016$$

$$2. \quad \Delta_1\{ u/n \} = \left[-\frac{0.05592}{1.458} - \frac{0}{1} \right]$$

$$\Delta_1\{ u/n \} = -0.038354$$

$$3. \quad S_{I1} = -(0.178016)^2(4)(-0.038354)$$

$$S_{I1} = 0.004862$$

Second Surface:

$$4. \quad A_2 = 1.458 \left[(-0.05592) + (3.9227744) \cdot 0 \right]$$

$$A_2 = -0.081531$$

$$5. \quad \Delta_2\{ u/n \} = \left[\frac{-0.081531}{1} - \frac{(-0.05592)}{1.458} \right]$$

$$\Delta_2\{ u/n \} = -0.043177$$

$$6. \quad S_{I2} = -(-0.081531)^2(3.9227744)(-0.043177)$$

$$S_{I2} = 0.001126$$

Next, the spherical aberration of the system is obtained by summing the contributions from all surfaces:

$$7. \quad S_I = \Sigma S_{Ii} = S_{I1} + S_{I2}$$

$$S_I = 0.004862 + 0.001126$$

Section 10.4: Thin Lens Form For W_{040} 109

$$S_I = 0.005988 \text{ cm} = 59.88 \mu\text{m}$$

Next, the system spherical aberration coefficient is determined from the Buchdahl coefficient:

$$8. \quad W_{040} = \frac{1}{8} \sum S_{ii}$$

$$W_{040} = 7.485 \mu\text{m}$$

Since the wavelength used for this ray trace was $\lambda = 0.601 \mu\text{m}$

$$9. \quad W_{040} = 12.454\lambda$$

Note that the coefficient values shown for surfaces 1 and 2 in the top boxed-in region in Listing 10.1 are the same as the S_{11} and S_{22} values just calculated in Steps 3 and 6. The sum in the top box is the same as that found in Step 7. The coefficient sum value in the bottom box in Listing 10.1 is essentially the same as that found in Step 9.

10.4 Thin Lens Form For W_{040}

In a *thin lens*, the y -height is the same for both surfaces. By algebraic manipulation and suitable substitutions a formula can be derived without *explicit* ray trace dependencies.

Thin Lens W_{040} Formula; (Derived in Section 11.10);

$$W_{040} = \left(\frac{1}{32}\right) y^4 \phi^3 \sigma_I \quad (10.9)$$

Structural Aberration Coefficient σ_I

$$\sigma_I = aX^2 - bXY + cY^2 + d \quad (10.10)$$

where

$$a = \frac{(n+2)}{n(n-1)^2} \quad c = \frac{3n+2}{n} \quad (10.11)$$

$$b = \frac{4(n+1)}{n(n-1)} \quad d = \left[\frac{n}{n-1}\right]^2$$

and where

$$Y = \frac{1+M}{1-M} \quad (10.12)$$

(M = magnification)

$$X = \frac{C_1 + C_2}{C_1 - C_2} \quad (10.13)$$

The quantity X is the shape factor which relates to lens bending as was discussed in Section 10.3. For a plano-convex lens $X = \pm 1$ depending on which surface faces the incoming light. For an object at infinity, $Y = 1$.

10.5 Example: W_{040} via Thin Lens Calculation

For the lens illustrated in Figure 10.4 the structural aberration coefficient σ_i given by Equation 10.10 is:

$$\sigma_i = (11.307)(1) - (14.724)(1)(1) + (4.372)(1) + 10.134$$

$$\sigma_i = 11.089$$

Using Equation 10.9 we can now determine W_{040} :

$$W_{040} = \left(\frac{1}{32}\right)(4)^4(0.020383)^3(11.089)$$

$$W_{040} = 0.000751 \text{ cm} = 7.51 \mu\text{m}$$

In waves:

$$W_{040} = 12.50\lambda$$

This is close to the value found in Step 9 in Section 10.3. The slight difference is due to the lens thickness being included in the one and not the other.

10.6 Off-Axis Aberration Coefficients

Table 10.1 provides a summary not only of the spherical aberration coefficients just derived and discussed in the preceding sections but contains the results for off-axis aberrations as well. There will be ample opportunity in subsequent chapters and problems to apply the latter formulations. I have foregone duplicating the derivation for the off-axis cases. Section 10.7 is enough to handle for now.

10.7 Derivation W_{040}

A. In this derivation we will call upon the binomial expansion:

$$(1 \pm x)^n \approx 1 \pm nx + \frac{n(n-1)}{2}x^2$$

where $x \ll 1$

Section 10.7: Derivation W_{tot} 111

Table 10.1

Aberration Type	Wavefront Coefficient	Relation to Seidel	Seidel Coefficient	Thin Lens and Mirror
Spherical	W_{040}	$\frac{1}{8}S_I$	$S_I = -\Sigma A^2 y \Delta \left(\frac{u}{n} \right)$	$S_I = \frac{1}{4}y^4 \phi^3 \sigma_I$
Coma	W_{131}	$\frac{1}{2}S_H$	$S_H = -\Sigma AB y \Delta \left(\frac{u}{n} \right)$	$S_H = \frac{1}{2}Ly^2 \phi^2 \sigma_H$
Astigmatism	W_{222}	$\frac{1}{2}S_M$	$S_M = -\Sigma B^2 y \Delta \left(\frac{u}{n} \right)$	$S_M = L^2 \phi \sigma_M$
Petzval Curv.	W_{220}	$\frac{1}{4}S_{IV}$	$S_{IV} = -L^2 \Sigma C \Delta \left(\frac{1}{n} \right)$	$S_{IV} = L^2 \phi \sigma_{IV}$
Distortion	W_{311}	$\frac{1}{2}S_V$	$S_V = -\Sigma \frac{B}{A} \left[CL^2 \Delta \left(\frac{1}{n} \right) - B^2 y \Delta \left(\frac{u}{n} \right) \right]$	$S_V = \sigma_V$

Where: $A = ni = n(u + yC)$ $B = n\bar{i} = n(\bar{u} + \bar{y}C)$ $L = \text{Lagrange Invariant}$

$$A = n'i' = n'(u' + yC) \quad B = n'\bar{i}' = n'(\bar{u}' + \bar{y}C) \quad L = n(\bar{u}y - u\bar{y})$$

Structural Aberration Coefficient	Thin Lens	Spherical mirror	OBJ. at	Y
σ_I	$aX^2 - bXY + cY^2 + d$	Y^2	∞	1
σ_H	$eX - fY$	$-Y$	Unit Mag.	0
σ_M	1	1	Recall:	
σ_{IV}	$\frac{1}{n}$	-1	$X = \frac{C_1 + C_2}{C_1 - C_2}$	
σ_V	0	0	$Y = \frac{1+M}{1-M}$	

$$\text{Where: } a = \frac{n+2}{n(n-1)^2} \quad b = \frac{4(n+1)}{n(n-1)} \quad c = \frac{3n+2}{n} \quad d = \frac{n^2}{(n-1)^2}$$

$$e = \frac{n+1}{n(n-1)} \quad f = \frac{2n+1}{n} \quad \Delta \left(\frac{u}{n} \right) = \left[\frac{u'}{n'} - \frac{u}{n} \right]$$

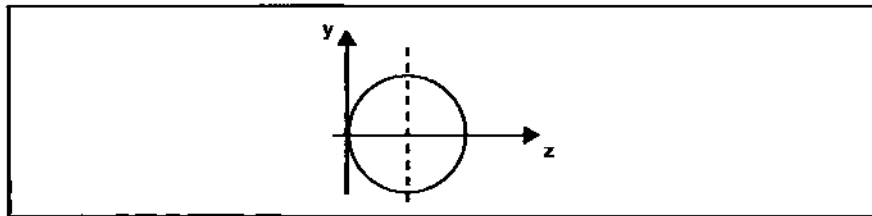


Fig. 10.5 Translated sphere.

- B. The equation used for spheres is that of a translated sphere. For example, the refracting surface in Figure 10.5 is given by:

$$y^2 + (z - R)^2 = R^2$$

$$z^2 - 2zR + y^2 = 0$$

- C. We will also need an expansion for z^2 . Solve the last equation for z using the quadratic formula.

Get:

$$z = R \left[1 - \sqrt{1 - \left(\frac{y}{R} \right)^2} \right]$$

Expand via binomial equation and keep the first two terms:

$$z \approx \left(\frac{1}{2} \frac{y^2}{R} + \frac{1}{8} \frac{y^4}{R^3} \right)$$

$$z^2 = \left(\frac{1}{2} \frac{y^2}{R} + \frac{1}{8} \frac{y^4}{R^3} \right)^2 = \frac{y^4}{4R^2} + \frac{y^6}{8R^4} + \frac{y^8}{64R^6}$$

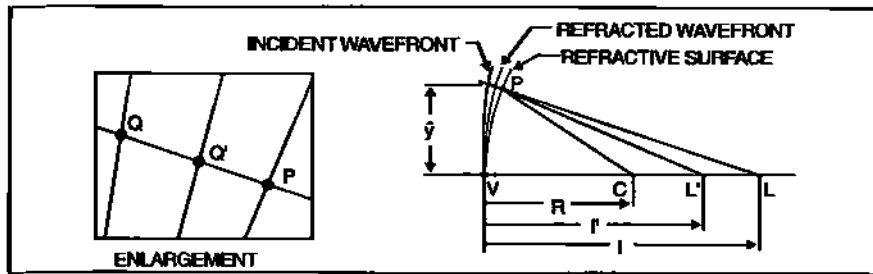
$$\therefore z^2 = \frac{y^4}{4R^2}$$

Refer to Figure 10.6

$$1. \quad W = \Delta \{ n[\overline{VL} - \overline{PL}] \}$$

$$2. \quad \overline{PL}^2 = (l - z)^2 + y^2 = l^2 - 2lz + (y^2 + z^2)$$

Substitute for z from (B):


 Fig. 10.6 Illustration for W_{obj} derivation.

$$\overline{PL}^2 = l^2 - 2l \left(\frac{y^2 + z^2}{2R} \right) + (y^2 + z^2)$$

$$\overline{PL}^2 = l^2 \left\{ 1 - \frac{(y^2 + z^2)}{lR} + \frac{(y^2 + z^2)}{l^2} \right\}$$

$$\text{Let: } \left\{ \frac{(y^2 + z^2)}{lR} - \frac{(y^2 + z^2)}{l^2} \right\} = J$$

$$\therefore \overline{PL} = l(1 - J)^{\frac{1}{2}}$$

3. Apply the binomial expansion to the last equation:

$$\overline{PL} \approx l \left(1 - \frac{J}{2} - \frac{J^2}{8} \right)$$

4. $\overline{VL} = l$

5. $[\overline{VL} - \overline{PL}] = l \left[\frac{J}{2} + \frac{J^2}{8} \right]$

6. Similarly:

$$[\overline{VL'} - \overline{PL'}] \approx l' \left[\frac{J'}{2} + \frac{J'^2}{8} \right]$$

7. Substitute 5 and 6 into 1:

$$W = n'l' \left[\frac{J'}{2} + \frac{J'^2}{8} \right] - nl \left[\frac{J}{2} + \frac{J^2}{8} \right]$$

$$W = \frac{1}{2}(n'l'J' - nlJ) + \frac{1}{8}(n'l'J^2 - nlJ^2)$$

$$W = \frac{1}{2}\Delta\{nlJ\} + \frac{1}{8}\Delta\{nlJ^2\}$$

8. But:

$$J = \frac{(y^2 + z^2)}{l} \left[\frac{1}{R} - \frac{1}{l} \right]$$

$$J^2 = \frac{(y^2 + z^2)^2}{l^2} \left[\frac{1}{R} - \frac{1}{l} \right]^2$$

$$9. W = \frac{1}{2}\Delta\left\{\frac{n}{R} - \frac{n}{l}\right\}(y^2 + z^2) + \frac{1}{8}\Delta\left\{\frac{1}{nl}\left[\frac{n}{R} + \frac{n}{l}\right]^2\right\}(y^2 + z^2)^2$$

10. Reconsider a marginal ray trace for a single refracting surface as per Section 4.5.

$$\frac{1}{l} = -\frac{u}{\hat{y}} ; \quad \frac{1}{nl} = \frac{1}{\hat{y}} \left(\frac{u}{n} \right)$$

$$\frac{1}{l'} = -\frac{u'}{\hat{y}} ; \quad \frac{1}{n'l'} = \frac{1}{\hat{y}} \left(\frac{u'}{n'} \right)$$

$$\frac{1}{R} = -\frac{\alpha}{\hat{y}}$$

where \hat{y} is the marginal ray height at the surface.

$$n'i' = ni$$

$$i = u - \alpha ; \quad i' = u' - \alpha$$

$$11. \quad \left[\frac{n}{R} - \frac{n}{l} \right] = -\frac{n\alpha}{\hat{y}} + \frac{nu}{\hat{y}} = \frac{n}{\hat{y}}(u - \alpha) = \frac{ni}{\hat{y}}$$

12. Similarly:

$$\left[\frac{n'}{R} - \frac{n'}{l'} \right] = \frac{n'i'}{\hat{y}}$$

$$13. \quad \frac{ni}{\hat{y}} = \frac{n'i'}{\hat{y}}$$

$$\text{Let } A = ni = n\hat{i}'$$

14. Note:

$$\Delta \left\{ \left[\frac{n}{R} - \frac{n}{l} \right] \right\} = \frac{A}{\hat{y}} - \frac{A}{\hat{y}} = 0$$

$$15. \quad \begin{aligned} \Delta \left\{ \frac{1}{nl} \left[\frac{n}{R} - \frac{n}{l} \right]^2 \right\} &= \frac{1}{n'l'} \left[\frac{n'}{R} - \frac{n'}{l'} \right]^2 - \frac{1}{nl} \left[\frac{n}{R} - \frac{n}{l} \right]^2 \\ &= \frac{1}{n'l'} \left(\frac{A^2}{\hat{y}^2} \right) - \frac{1}{nl} \left(\frac{A^2}{\hat{y}^2} \right) \\ &= \frac{A^2}{\hat{y}^2} \left[\frac{1}{n'l'} - \frac{1}{nl} \right] \end{aligned}$$

16. Substitute from step 10 for bracketed factor:

$$\Delta = \left\{ \frac{1}{nl} \left[\frac{n}{R} - \frac{n}{l} \right]^2 \right\} = -\frac{A^2}{\hat{y}^3} \Delta \left\{ \frac{u}{n} \right\}$$

$$17. \quad W = -\frac{1}{8\hat{y}^3} \Delta \left\{ \frac{u}{n} \right\} (y^2 + z^2)^2$$

18. Now get rid of z^2 ; substitute from (C):

$$y^2 + z^2 = y^2 + \frac{1}{4} \frac{y^4}{R^2}$$

$$(y^2 + z^2)^2 = \left(y^2 + \frac{1}{4} \frac{y^4}{R^2} \right)^2$$

$$\therefore (y^2 + z^2)^2 \approx y^4 + \frac{1}{2} \frac{y^6}{R^2} + \frac{1}{16} \frac{y^8}{R^4} \approx y^4$$

19. $W = -\frac{1}{8} \frac{A^2}{\hat{y}^3} \Delta \left\{ \frac{u}{n} \right\} y^4$

20. Now multiply by \hat{y}^4/\hat{y}^4 so that pupil is normalized. Let this normalized pupil function for spherical aberration be represented by W_4 :

$$\therefore W_4 = -\frac{1}{8} A^2 \hat{y} \Delta \left\{ \frac{u}{n} \right\} \left(\frac{y}{\hat{y}} \right)^4 \quad \text{where } W_{040} = -\frac{1}{8} A^2 \hat{y} \Delta \left\{ \frac{u}{n} \right\}$$

10.8 Homework

1. Using the PRTE data for the marginal ray from the Homework for Chapter 4 (page 42), calculate the Seidel coefficient S_1 for surfaces nos. 1 and 2.
2. Find the net S_1 for the system.
3. Calculate the wavefront aberration coefficient W_{040} in waves.
4. Now use the “thin lens” form of the Seidel coefficient to compute S_p and W_{040} where:

Shape factor $X = 0$

Magnification factor $Y = 1$

$c = 4.3186$; $d = 8.6141$

EFL = 400.66 mm

Chapter 11

Lens Bending and Aberration Balancing

11.1 Introduction

In the last chapter you saw how to calculate W_{040} by summing surface contributions. This was applied to a singlet. The thin lens form was also introduced and used on the same singlet. In the latter case, the formula was provided without any justification. In this chapter we'll tie up that loose end and show you how the thin lens form is hatched from the summation procedure. The thin lens form lends itself directly to demonstrating the effects of lens bending (first observed in Parts 3 and 7 of the Homework for Chapter 3). For a singlet, bending cannot remove all the spherical aberration present. However, by shifting the image plane (as was done in Part 8) a smaller RMS spot diagram was found. What happened here was that some of the spherical aberration was offset by defocus. This illustrates an important design principle called aberration balancing, and will be examined in more detail here.

11.2 The Thin Lens Form

We begin by writing out the Seidel summation for the *paraxial* biconvex lens shown in Figure 11.1*b*.

$$-S_i = \sum A_i^2 y_i \Delta_i \left\{ \frac{u}{n} \right\} \quad (11.1)$$

where:

$$A = nu + nyC = n'u' + n'yC$$

and

$$\Delta \left\{ \frac{u}{n} \right\} = \left(\frac{u'}{n'} \right) - \left(\frac{u}{n} \right)$$

The unprimes indicate values before the refracting surface and the primes are values after that surface. Expanding Equation 11.1 noting that for a thin lens $y_1 = y_2$,

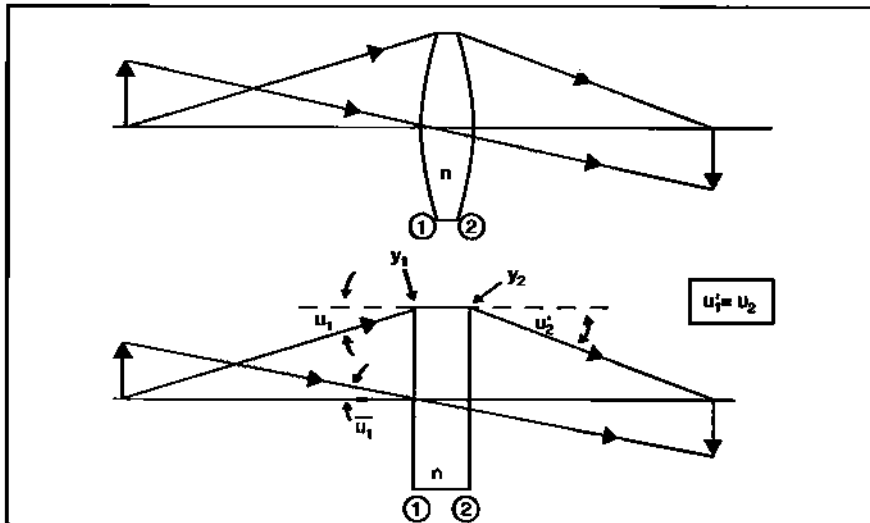


Fig. 11.1 Parameter illustration for deriving thin lens form.

$$-S_I = y \left\{ n_1^2 (u_1 + yC_1)^2 \left(\frac{u'_1}{n'_1} - \frac{u_1}{n_1} \right) + n_2^2 (u_2 + yC_2)^2 \left(\frac{u'_2}{n'_2} - \frac{u_2}{n_2} \right) \right\} \quad (11.2)$$

Also, for convenience, we will now let $n_1 = n'_1 = 1$ and $n_2 = n'_2 = n$.

$$-S_I = y \left\{ (u_1 + yC_1)^2 \left(\frac{u'_1}{n} - u_1 \right) + n^2 (u_2 + yC_2)^2 \left(\frac{u'_2}{n} - \frac{u_2}{n} \right) \right\} \quad (11.3)$$

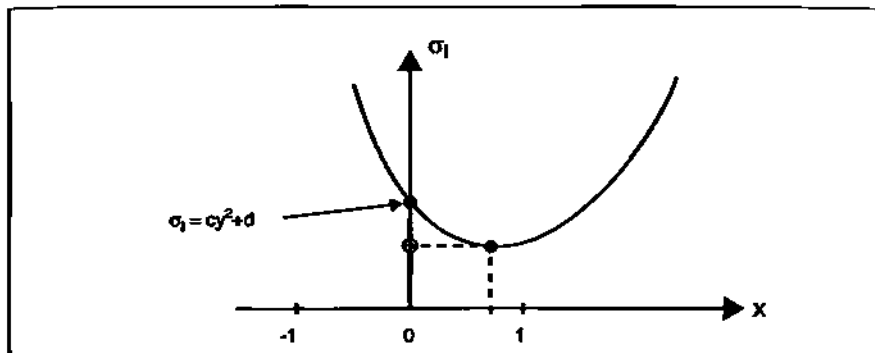
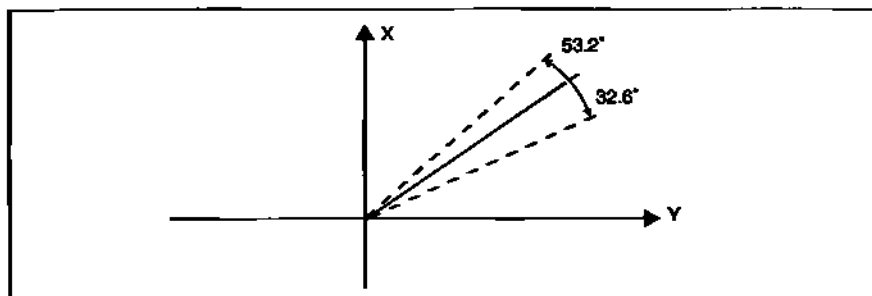
We make the substitution in the second term: $(u_2 + yC_2) = (n'_2/n_2)(u'_2 + yC_2)$ and rearrange:

$$-S_I = \left(\frac{y}{n} \right) \left\{ (u_1 + yC_1)^2 (u'_1 - nu_1) - (u'_2 + yC_2)^2 (u_2 - nu'_2) \right\} \quad (11.4)$$

The next step is to replace the factors within brackets with expressions containing the shape factor (X), the magnification factor (Y), and power (ϕ). These details will be found in Section 11.10. When everything is said and done, we arrive at the thin lens form for the Seidel coefficient:

$$-S_I = \left(\frac{1}{4} \right) y^4 \phi^3 [aX^2 - bXY + cY^2 + d] \quad (11.5)$$

where the quantity in brackets is called the structural aberration coefficient (σ_I). See Section 10.4 or Table 10.1 on page 111 for definition of parameter quantities.


 Fig. 11.2 Generic plot of σ_I .

 Fig. 11.3 Plot of derivative of σ_I .

11.3 Thin Lens Bending

Assuming that Y is constant, a plot of $\sigma_I(X)$ would yield an offset parabola as illustrated in Figure 11.2. Note that there is a low point where σ_I is a minimum. To find it we take the derivative and set it equal to zero:

$$\frac{d\sigma_I}{dX} = 2aX - bY = 0 \quad (11.6)$$

Solving for X :

$$X = \left(\frac{b}{2a} \right) Y \quad (11.7)$$

Inserting the values for a and b from Table 10.1 on page 111:

$$X = \frac{1}{2} \left[\frac{4(n+1)}{n(n-1)} \right] \left[\frac{n(n-1)^2}{n+2} \right] \cdot Y \quad (11.8)$$

$$X = 2 \frac{(n^2 - 1)}{(n + 2)} \cdot Y \quad (11.9)$$

Equation 11.7 gives us the lens shape that will minimize spherical aberration for a given object location. For example, for an object at infinity $Y = 1$ and $X = (b/2a)$. For an object at unit magnification, $Y = 0$ and $X = 0$ (equiconvex).

Consider a BK7 singlet with an object at infinity. Operating in d light, $n = 1.5168$. Consequently, $a = 8.6811$; $b = 12.8427$. Insert these values into Equation 11.7.

For minimum spherical: $X = 0.7397$

A generic plot of Equation 11.7 is shown in Figure 11.3. It is linear. However, its slope is confined to the range between 0.639 to 1.338 (or between 32.6° and 53.2°). This covers the range of refractive index values (between 1.45 and 1.90) for glasses used for lens design in the visible spectrum.

11.4 Focus Shift

In ZEMAX the best RMS spot size was found with the help of a dummy surface inserted between the M-solve surface and the IMG surface (see Part 8 of the Homework for Chapter 3, page 30). The optimization process relocated the dummy surface axially to find the best image plane. This was a focus shift. We now want to find an analytical expression for the focus shift which will then be used to illustrate aberration balancing.

Figure 11.4 shows two spherical wavefronts in the exit pupil. One is due to a flat wavefront entering the entrance pupil. This wavefront is brought to a focus at the paraxial focal plane. The other is due to a slightly converging wavefront at the entrance pupil. It is brought to a point image inside focus at distance δ . In the exit pupil, both spherical wavefronts have certain sag values (see Section 3.4). The difference in sag is equal (for all intents and purposes) to the OPD or (W_{020}) between the wavefronts at the edge of the pupil. We want to find a relationship between δ and W_{020} .

$$W_{020} = \text{Sag1} - \text{Sag2} \quad (11.10)$$

$$W_{020} = \left(\frac{r^2}{2} \right) \left[\frac{1}{R + \delta} - \frac{1}{R} \right] \quad (11.11)$$

$$W_{020} = \left(\frac{r^2}{2} \right) \left[\frac{-\delta}{R^2 + R\delta} \right] \quad (11.12)$$

But $R\delta \ll R^2$:

Section 11.5: Difference Between W_{020} and W_d 121

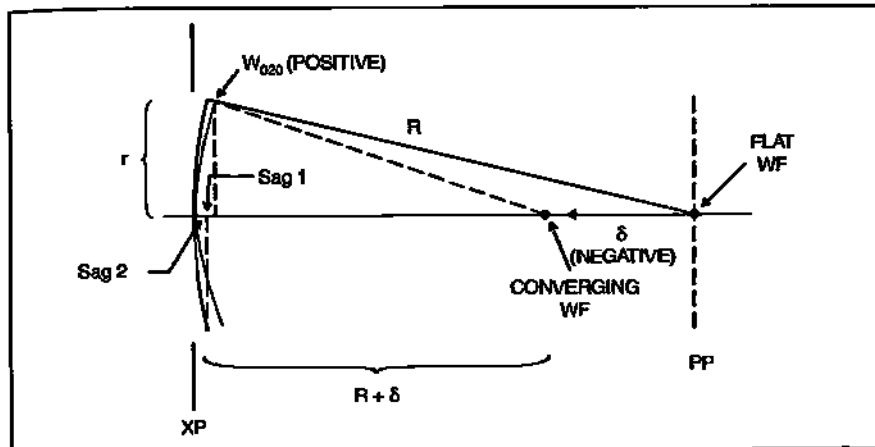


Fig. 11.4 Illustration for focus shift derivation.

$$W_{020} = \frac{1}{2} \left(\frac{r}{R} \right)^2 (-\delta) \quad (11.13)$$

Solving for δ :

$$\delta = -2 \left(\frac{R}{r} \right)^2 W_{020} \quad (11.14)$$

When the object distance $\rightarrow \infty$, $R \rightarrow f$ and $R/r \rightarrow 2$ f-number. Therefore, Equation 11.14 becomes:

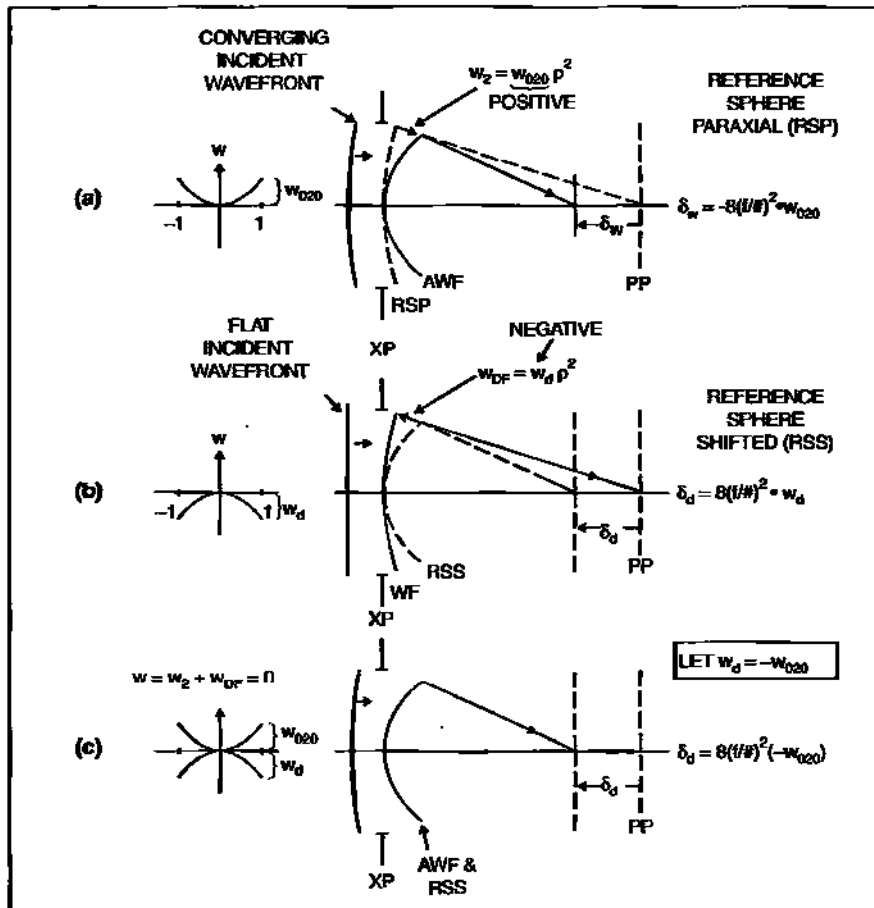
$$\delta = -8(f/\#)^2 W_{020} \quad (11.15)$$

Note: If wavefront is divergent, W_{020} is negative and δ is positive.

11.5 Difference Between W_{020} and W_d

Please refer to Figure 11.5 for the following discussion. Each part consists of an OPD plot on the left, a meridional plot in the middle, and a version of Equation 11.15 on the right. In Figure 11.5a we have a converging spherical wavefront incident on the imaging system. In the exit pupil we have the reference sphere centered on paraxial focus (RSP), and the actual wavefront (AWF) centered on its image point. At the pupil edge, the separation between the reference sphere with the AWF, W_{020} , is positive. The OPD plot shown is a positive plot. The location of the image point from paraxial focus is found from the equation shown on the right. Note that this is a *negative* separation.

Now suppose that the incident wavefront is flat. It will focus at the paraxial

Fig. 11.5 Illustrating the difference between w_{020} and defocus.

plane. But now we deliberately change our point of observation (reference sphere). We are introducing a focus shift or defocus. In Figure 11.5b the separation between the wavefront and the defocus reference sphere at the pupil edge, W_d , is negative. (Note that this time the wavefront is coincident with the paraxial reference sphere.) An OPD plot is shown on the left side. Note that the plot is *negative*. The location of the center of the defocus reference sphere relative to the image point in the paraxial plane is given by:

$$\delta_d = 8(f/#)^2 W_d \quad (11.16)$$

Note that this axial separation is negative because W_d is negative.

Now return to the scenario in Figure 11.5a. In order for us to get a sharp image we need to change the reference sphere by introducing a defocus which is equal but opposite (with respect to paraxial focus) to that on the AWF. This is

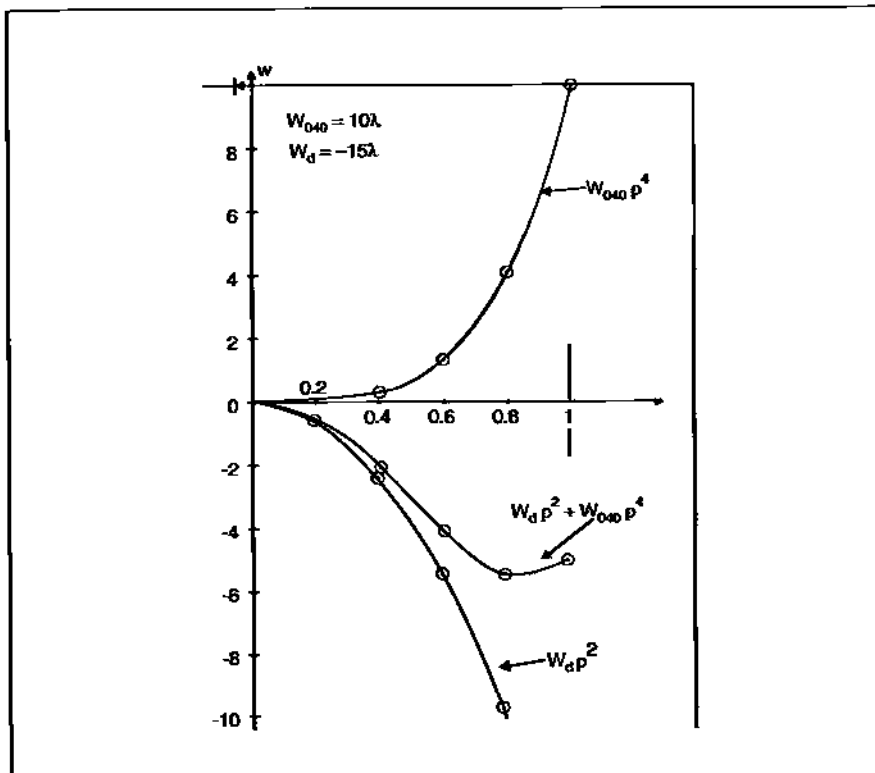


Fig. 11.6 Example of wavefront balancing by combining spherical with defocus.

illustrated in Figure 11.5 c. The OPD plot is shown on the left. By letting $W_d = -W_{020}$, the resultant OPD plot is flat and zero.

We will now use this same defocus technique to find the axial location of minimum blur when the exit pupil wavefront is afflicted with spherical aberration.

11.6 Aberration Balancing: Spherical Aberration and Defocus

If a system had no aberrations, then the best imaging plane would be the paraxial plane. With aberrations this is no longer so. With aberrations, point images are no longer possible. We then look for a place where the spot diagram induced by aberrations has the smallest lateral spread, such as the minimum blur spot shown in Figure 7.6. Anytime we explore regions away from the paraxial image, we are introducing a defocus. (Focus shifts can also be generated by moving the object point axially a bit. However, in this presentation defocus will generally mean exploring image space for a fixed object point.)

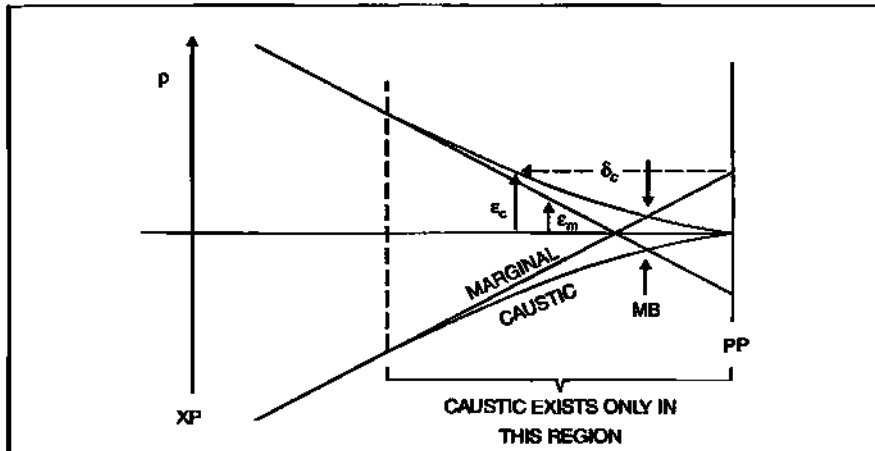


Fig. 11.7 Illustration of caustic envelope and marginal ray crossing.

We now combine spherical aberration and defocus mathematically so that we can find the position of the minimum blur (MB) spot.

$$W = W_{040} \rho^4 + W_d \rho^2 \quad (11.17)$$

This occurs when:

$$W_d = -\frac{3}{2} W_{040} \quad (11.18)$$

Example: Let $W_{040} = 10\lambda$; then $W_d = -15\lambda$. Equation 11.17 becomes

$$W = 10\lambda \rho^4 - 15\lambda \rho^2.$$

Each term is plotted in Figure 11.6 as well as W .

The axial location of the minimum blur waist with respect to the paraxial plane is:

$$\delta_d = 8(f/\#)^2 \left(-\frac{3}{2} W_{040} \right) \quad (11.19)$$

11.7 Basis For Equation

Figure 11.7 shows the meridional plane with the envelope of the caustic and the marginal rays displayed. The pair of equations describing the caustic axial location and radius are:

Section 11.8: Connection Between W_{040} and SA3 125

$$\delta_c = \left(\frac{2}{n}\right)\left(\frac{R}{r}\right)^2 \left[-6W_{040}p^2\right] \quad (11.20)$$

$$\varepsilon_c = -\left(\frac{R}{nr}\right) \left[-8W_{040}p^3\right]$$

The equation describing the marginal ray radius from the optical axis is given by:

$$\varepsilon_m = -\left(\frac{R}{nr}\right) \left[-12W_{040}p^2 + 4W_{040}\right] \quad (11.21)$$

At minimum blur, $\varepsilon_c = \varepsilon_m$.

Substituting Equation 11.20 for ε_c into Equation 11.21:

$$\left(\frac{R}{nr}\right) \left[-8W_{040}p^3\right] = \left(\frac{R}{nr}\right) \left[-12W_{040}p^2 + 4W_{040}\right] \quad (11.22)$$

$$-8W_{040}p^3 = -12W_{040}p^2 + 4W_{040}$$

Eliminating W_{040} and rearranging terms:

$$2p^3 - 3p^2 + 1 = 0 \quad (11.23)$$

Factoring:

$$(2p + 1)(p - 1)^2 = 0 \quad (11.24)$$

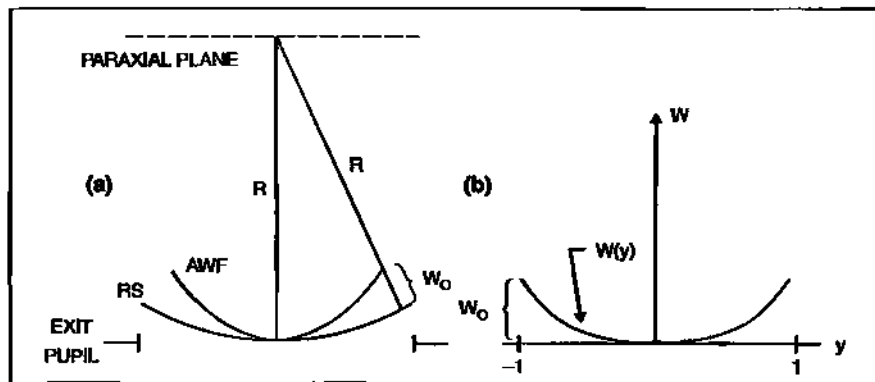
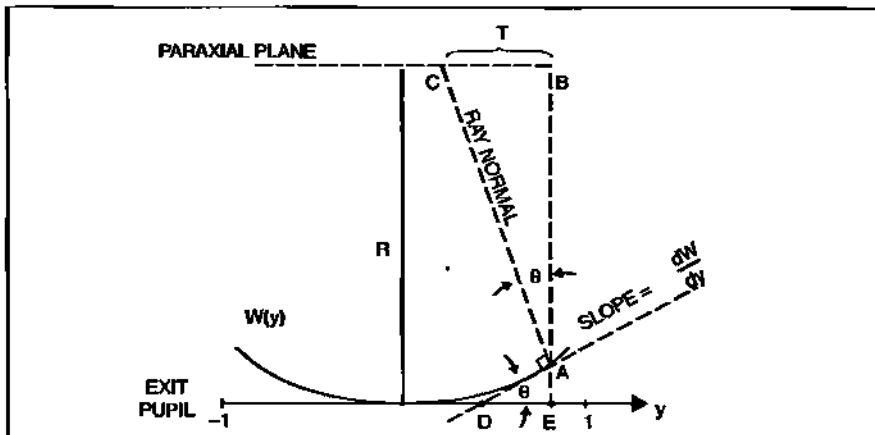
The roots are: $p = 1$ and $p = -\frac{1}{2}$; the latter value puts us in the MB plane. Inserting this root back into Equation 11.20 yields:

$$\delta_c = \left(\frac{2}{n}\right)\left(\frac{R}{r}\right)^2 \left[-\frac{3}{2}W_{040}\right] \quad (11.25)$$

$$\varepsilon_c = -\left(\frac{R}{nr}\right) \left[W_{040}\right]$$

11.8 Connection Between W_{040} and SA3

In Section 7.5 we stated that there was a definite connection between aberrations as described in the exit pupil and as described in the image plane. That connection was given by Equation 7.7. Because of the importance of this equation, a heuristic derivation will now be given. The refractive index is assumed to be 1. In Figure


 Fig. 11.8 a. Reference and actual wavefront; b. Plot of $W(y)$.

 Fig. 11.9 Construction for relating T and local wavefront tilt.

11.8a the pupil/focal plane system is rotated 90°. In b, $W(y)$ is plotted as a function of pupil position. The basic difference between a and b is that in b the reference sphere has been flattened out, thus removing the base curvature of the actual wavefront.

Now look at Figure 11.9. It has elements borrowed from both Figure 11.8a and b. The bottom part is from b and the top part is from a. The separation between them is the radius of curvature, R . (Note: Figure 11.9 is highly exaggerated because $W_0 \ll R$.) T is the transverse ray aberration (TRA).

Pick a spot, A, on the $W(y)$ curve. Now do three things:

1. find the tangent at Point A;
2. find the (ray) normal at Point A; and

Section 11.8: Connection Between W_{eff} and SA3 127

3. erect a perpendicular to the exit pupil and focal planes that passes through Point A.

The following observations can then be made:

1. $AE \ll AB$ so that AB is essentially equal to R (since W is measured in microns whereas R is measured in mm or cm);
2. $\angle BAC = \angle ADE$ by plane geometry (designate this angle Θ);
3. the slope or tangent at Point A, $dW/dy = \tan \Theta = -T/R$.

Therefore:

$$T = -R \tan \Theta = -R \frac{dW}{dy} \quad (11.26)$$

But we now want to cast this relationship into a form using normalized pupil coordinates. To do this, consider that W is a function of p which in turn is a function of y . So the derivative becomes:

$$\frac{dW}{dy} = \left(\frac{dW}{dp} \right) \left(\frac{dp}{dy} \right) \quad (11.27)$$

But:

$$p = \frac{y}{r} \quad (11.28)$$

And:

$$\frac{dp}{dy} = \frac{1}{r} \quad (11.29)$$

Therefore:

$$\frac{dW}{dy} = \left(\frac{dW}{dp} \right) \left(\frac{1}{r} \right) \quad (11.30)$$

Substitute Equation 11.30 into Equation 11.26:

$$T = -\left(\frac{R}{r} \right) \left(\frac{dW}{dp} \right) \quad (11.31)$$

This is identical to Equation 7.7 except for n .

Equation 11.31 was derived for a meridional plane and is valid for rotationally symmetric aberrations. For asymmetric aberrations there will be both T_x and T_y components.

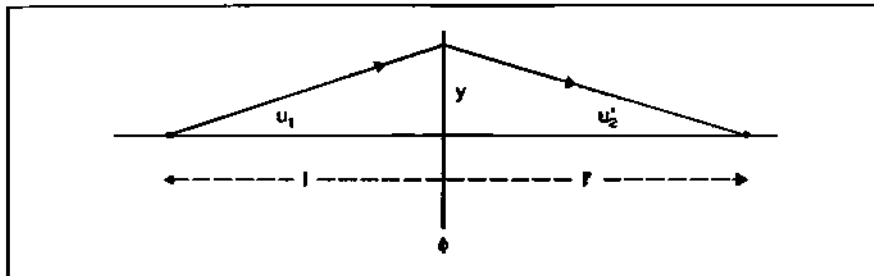


Fig. 11.10 Parameters used to verify Eq. 11.34.

11.9 Example With Spherical Aberration:

We saw in Figure 7.19 (page 81) that spherical aberration is described by $W = W_{040} \rho^4$. Employing Equation 11.31:

$$T = -\left(\frac{R}{nr}\right)\left[4W_{040}\rho^3\right] = SA3\rho^3 \quad (11.32)$$

where $SA3 = -(R/nr) 4 W_{040}$. If the object is at infinity: $SA3 = 8(f\text{-number}) W_{040}$. A plot of this function is shown in Figure 7.6d (page 70).

11.10 Derivation of Thin Lens Form

Picking up the derivation started in Section 11.2 at Equation 11.4, we will make use of the following relations:

$$X = \frac{C_1 + C_2}{C_1 - C_2} = \frac{\phi_1 - \phi_2}{\phi_1 + \phi_2} \quad (11.33)$$

$$Y = \frac{1+m}{1-m} = \frac{u'_2 + u_1}{u'_2 - u_1} \quad (11.34)$$

Equation 11.33 can be verified by direct substitution for the surface powers ϕ_1 and ϕ_2 . Equation 11.34 can be seen with the help of Figure 11.10.

Starting from:

$$Y = \frac{1+m}{1-m}$$

where:

$$m = \frac{l'}{l}; \quad l' = \frac{-Y}{u'_2}; \quad l = \frac{-Y}{u_1}.$$

Section 11.10: Derivation of Thin Lens Form 129

$$1 + m = 1 + \frac{l'}{l} = 1 + \frac{y/u'_2}{y/u_1} = 1 + \frac{u_1}{u'_2}$$

Similarly:

$$\left. \begin{aligned} 1 + m &= \left(\frac{1}{u'_2} \right) (u'_2 + u_1) \\ 1 - m &= \left(\frac{1}{u'_2} \right) (u'_2 - u_1) \end{aligned} \right\} \quad (11.35)$$

Inserting these into the starting expression, we arrive at Equation 11.34:

$$Y = \frac{u'_2 + u_1}{u'_2 - u_1} \quad (11.36)$$

From this result we can obtain an expression for u_1 in terms of Y and the system power (ϕ).

Similarly:

$$\left. \begin{aligned} u'_2 + u_1 &= (u_1 - y\phi) + u_1 \\ u'_2 - u_1 &= (u_1 - y\phi) - u_1 \end{aligned} \right\} \quad (11.37)$$

Substituting into Equation 11.34:

$$Y = \frac{2u_1 - y\phi}{-y\phi} \quad (11.38)$$

Now solve Equation 11.38 for u_1 :

Similarly:

$$\left. \begin{aligned} u_1 &= \frac{1}{2}(Y - 1)y\phi \\ u'_2 &= \frac{1}{2}(Y + 1)y\phi \end{aligned} \right\} \quad (11.39)$$

The next step is to find an expression for the curvatures in Equation 11.4 in terms of shape factor and power.

We start with the system power for a thin lens:

$$\phi = \phi_1 + \phi_2 \quad (11.40)$$

This is solved for ϕ_1 and Equation 11.33 is solved for ϕ_2 and inserted:

$$\phi_1 = \phi - \phi_2 \quad (11.41)$$

where:

$$\phi_2 = \left[\frac{1-X}{1+X} \right] \phi_1 \quad (11.42)$$

Inserting Equation 11.42 into Equation 11.41:

$$\phi_1 = \phi - \left[\frac{1-X}{1+X} \right] \phi_1 \quad (11.43)$$

$$\phi_1 + \left[\frac{1-X}{1+X} \right] \phi_1 = \phi$$

$$\left[\frac{(1+X) + (1-X)}{1+X} \right] \phi_1 = \phi$$

$$\phi_1 = \frac{(1+X)\phi}{2} \quad (11.44)$$

But we also know that:

$$\phi_1 = (n-1)C_1 \quad (11.45)$$

Combining Equations 11.44 and 11.45:

$$\left. \begin{array}{l} C_1 = \frac{(X+1)\phi}{2(n-1)} \\ C_2 = \frac{(X-1)\phi}{2(n-1)} \end{array} \right\} \quad (11.46)$$

Similarly: Now we have one set of replacement factors for Equation 11.4 by using the equation pairs from Equation 11.39 and Equation 11.46:

$$\left. \begin{array}{l} u_1 + yC_1 = -\frac{1}{2}(Y-1)y\phi + \frac{y(X+1)\phi}{2(n-1)} \\ u'_2 + yC_2 = -\frac{1}{2}(Y+1)y\phi + \frac{y(X-1)\phi}{2(n-1)} \end{array} \right\} \quad (11.47)$$

Equation 11.47 needs some modification before we use it in Equation 11.4.

$$u_1 + yC_1 = \frac{y\phi}{2} \left[\frac{1+X}{n-1} - (Y-1) \right]$$

Section 11.10: Derivation of Thin Lens Form 131

$$u_1 + yC_1 = \left[\frac{y\Phi}{2(n-1)} \right] [(1+X) - (n-1)(Y-1)]$$

$$u_1 + yC_1 = \left[\frac{y\Phi}{2(n-1)} \right] [X - (n-1)Y + n] \quad (11.48)$$

Let $M = X - (n-1)Y$:

$$\left. \begin{aligned} u_1 + yC_1 &= \left[\frac{y\Phi}{2(n-1)} \right] [M + n] \\ \text{Similarly: } u'_2 + yC_2 &= \left[\frac{y\Phi}{2(n-1)} \right] [M - n] \end{aligned} \right\} \quad (11.49)$$

We now work on the next set of replacement factors for Equation 11.4. Recall PRTEI and rearrange:

$$nu'_1 = u_1 - y\Phi$$

$$nu'_1 = u_1 - y(n-1)C_1$$

$$u'_1 = \frac{u_1}{n} - y(n-1)\frac{C_1}{n} \quad (11.50)$$

From Equation 11.4 we have the factor ($u'_1 - nu_1$). Substitute in Equation 11.50:

$$u'_1 - nu_1 = \frac{u_1}{n} - y(n-1)\frac{C_1}{n} - nu_1$$

Rearrange:

$$u'_1 - nu_1 = \left(\frac{1}{n} - n \right) u_1 - y(n-1)\frac{C_1}{n} \quad (11.51)$$

Now substitute in equations for u_1 and C_1 from Equations 11.39 and 11.46 respectively:

$$u'_1 - nu_1 = \left(\frac{1-n^2}{n} \right) \left[-\left(\frac{1}{2} \right) (Y-1)y\Phi \right] - \left[\frac{y(n-1)}{n} \right] \left[\frac{(X+1)\Phi}{2(n-1)} \right]$$

$$\begin{aligned} u'_1 - nu_1 &= \left(\frac{y\Phi}{2n} \right) [(Y-1)(n^2-1) - (X+1)] \\ u'_1 - nu_1 &= \left(\frac{y\Phi}{2n} \right) [(n^2-1)Y - X - n^2] \end{aligned} \quad (11.52)$$

Let $P = (n^2 - 1)Y - X$:

$$\begin{aligned} u'_1 - nu_1 &= \frac{y\Phi}{2n} (P - n^2) \\ u'_1 - nu_1 &= \frac{y\Phi}{2n} (P - n^2) \\ \text{Similarly: } u_2 - nu'_2 &= \frac{y\Phi}{2n} (P + n^2) \end{aligned} \quad (11.53)$$

The equation pairs 11.49 and 11.53 are now substituted into Equation 11.4:

$$-S_1 =$$

$$\begin{aligned} -S_1 &= \left(\frac{y}{n} \right) \left\{ \left[\left(\frac{y\Phi}{2(n-1)} \right)^2 (M+n)^2 \left[\left(\frac{y\Phi}{2n} \right) (P-n^2) \right] - \left[\frac{y\Phi}{2(n-1)} \right]^2 (M-n)^2 \left[\left(\frac{y\Phi}{2n} \right) (P+n^2) \right] \right\} \\ -S_1 &= \left(\frac{y}{n} \right) \left\{ \left(\frac{y^3\Phi^3}{4} \right) \left[\frac{1}{2n^2(n-1)^2} \right] [(M+n)^2(P-n^2) - (M-n)^2(P+n^2)] \right\} \end{aligned} \quad (11.54)$$

After squaring appropriate factors and canceling out terms Equation 11.54 becomes:

$$-S_1 = \left(\frac{y^4\Phi^3}{4} \right) \left[\frac{1}{2n^2(n-1)^2} \right] \{ 4nPM - 2n^2M^2 - 2n^4 \} \quad (11.55)$$

where:

$$PM = (n^2 + n - 2)XY - X^2 - (n-1)(n^2-1)Y^2 \quad (11.56)$$

and:

$$M^2 = X^2 - 2(n-1)XY + (n-1)^2Y^2 \quad (11.57)$$

Section 11.10: Derivation of Thin Lens Form 133

Now insert Equations 11.56 and 11.57 into the third factor group in Equation 11.55 and gather terms with common factors:

$$\begin{aligned} \{4nPM - 2n^2M^2 - 2n^4\} &= \{4n[(n^2 - 1) + (n - 1)] + 4n^2(n - 1)\} XY \\ &\quad - \{2n^2(n - 1)^2 + 4n(n^2 - 1)(n - 1)\} Y^2 \\ &\quad - \{4n + 2n^2\} X^2 \\ &\quad - 2n^4 \end{aligned} \tag{11.58}$$

Now let's multiply each coefficient of the common factor terms in Equation 11.58 through by the second factor group in Equation 11.55:

$$\left\{\frac{1}{2n^2(n-1)^2}\right\}\{4n[(n^2 - 1) + (n - 1)] + 4n^2(n - 1)\} = \frac{4n + 1}{n(n-1)} = b \tag{11.59}$$

$$\left\{\frac{1}{2n^2(n-1)^2}\right\}\{2n^2(n - 1)^2 + 4n(n^2 - 1)(n - 1)\} = \frac{3n + 2}{n} = c \tag{11.60}$$

$$\left\{\frac{1}{2n^2(n-1)^2}\right\}\{4n + 2n^2\} = \frac{2 + n}{n(n-1)^2} = a \tag{11.61}$$

$$\left\{\frac{1}{2n^2(n-1)^2}\right\}\{2n^4\} = \frac{n^2}{(n-1)^2} = d \tag{11.62}$$

Substituting Equations 11.59–11.62 into Equation 11.55:

$$-S_I = \left(\frac{y^4\Phi^3}{4}\right)\{-aX^2 + bXY - cY^2 - d\}$$

or:

$$S_I = \left(\frac{y^4\Phi^3}{4}\right)\{aX^2 - bXY + cY^2 + d\} = \frac{y^4\Phi^3}{4}\sigma_I \tag{11.63}$$

where:

$$\sigma_I = \{aX^2 - bXY + cY^2 + d\}$$

The wavefront coefficient is then given by:

$$W_{040} = \frac{1}{8} S_I$$

or:

$$W_{040} = \frac{1}{32} y^4 \phi^3 \sigma_I \quad (11.64)$$

Equation 11.64 is the thin lens form for Seidel spherical aberration.

11.11 Homework

In the homework for Chapter 10, you calculated the amount of spherical aberration, W_{040} , for the lens defined in the homework for Chapter 1. Now determine the *axial* location (relative to paraxial focus) of the minimum blur, and the diameter of the minimum blur circle.

$$\delta_{MB} = ?$$

$$D_{MB} = ?$$

Chapter 12

Symmetry and the Periscopic Lens

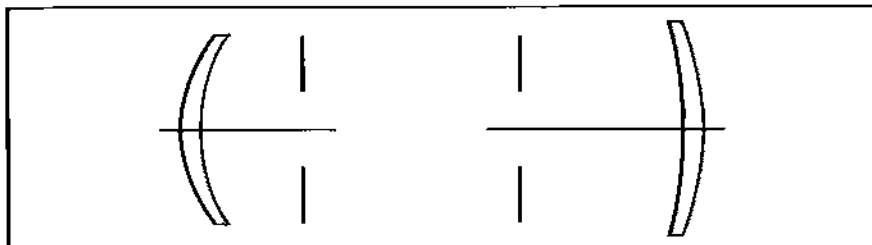


Fig. 12.1 *Front and rear landscape lenses.*

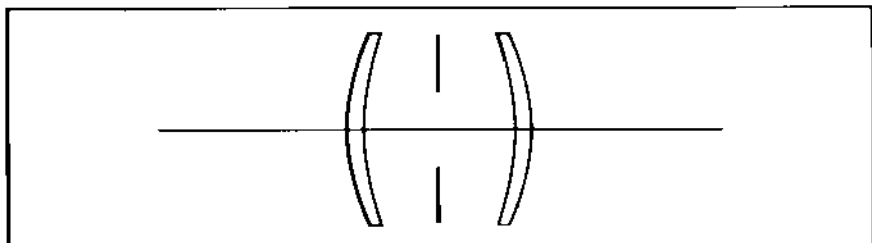


Fig. 12.2 *The periscopic lens.*

12.1 Introduction

In Chapter 5, the concept of the stop was introduced. In Chapter 6, stop position was seen to be critical to the design of both the front and rear landscape lenses (as illustrated in Figure 12.1). In Chapter 9, the design principle of lens splitting was introduced and was applied to reduce spherical aberration. In this chapter, all of these design elements will be combined. A singlet lens will be split into two separate lenses while maintaining the same system power. This is a symmetrical system and its optimization will lead us to the historically important periscopic lens, shown in Figure 12.2.

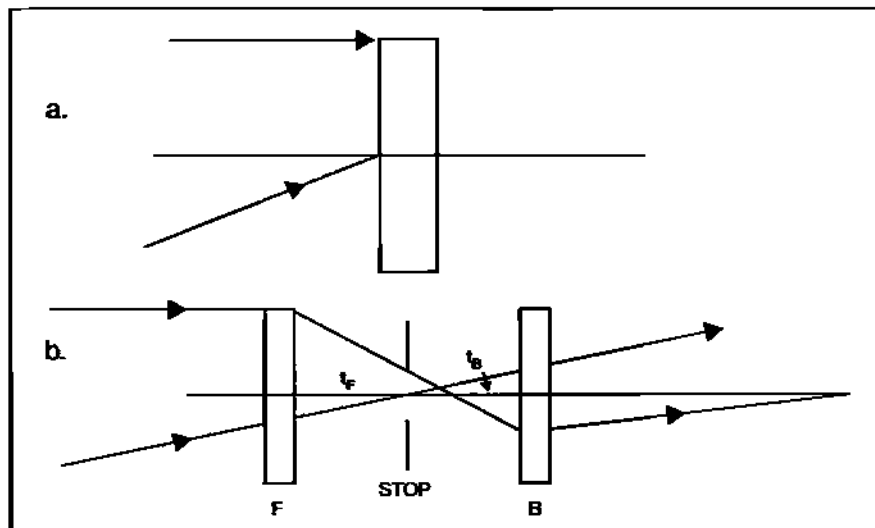


Fig. 12.3 a. Paraxial singlet; **b.** split symmetric system having same power.

12.2 Determining Starting Radii

Figure 12.3a illustrates the paraxial singlet parameters. The pre-design process is begun by splitting the power of this singlet between two separated elements. We will make use of the power equation for a two-element system derived in Section 4.6.2.

$$\Phi = \Phi_F + \Phi_B - t\Phi_F\Phi_B \quad (12.1)$$

The power of the front and back elements will be the same: $\Phi_F = \Phi_B$

$$\Phi = 2\Phi_F - t\Phi_F^2 \quad (12.2)$$

Solve Equation 12.2 for Φ_F via the quadratic equation:

$$\Phi_F = \left(\frac{1}{t}\right)[1 \pm \sqrt{1-t\Phi}] \quad (12.3)$$

Assuming equiconvex lenses, the radii are solved by using the power equation for a single refracting surface (derived in Section 4.6.3).

$$R_F = 2\frac{(n-1)}{\Phi_F} \quad (12.4)$$

Our paraxial design will appear as shown in Figure 12.3b which is a symmetric system with the stop right in the middle.

Section 12.3: Setting Up the Pre-Design In ZEMAX 137

SURFACE DATA SUMMARY:

Surf	Type	Comment	Radius	Thickness	Glass	Diameter
OBJ	STANDARD		Infinity	88.0		589.9146
1	STANDARD		343.02	15	SF2	181.4124
2	STANDARD		-343.02	98		98.14245
STD	STANDARD		Infinity	98 P		21.8792
4	STANDARD		343.02 P	15 P	SF2	99.0928
5	STANDARD		-343.02 P	111.7178 H		181.6993
INA	STANDARD	Infinity				155.5347

Merit Function Value: 6.18956988E+988

Num	Type	Int1	Int2	Hx	Hy	Px	Py	Target	Weight	Value	% Cont
1	EFFL		1					2.00000E+002	1	2.06198E+002	100.000
2	EFLY	1	2					0.00000E+000	0	2.65446E+002	0.000
3	PMAG		1					-1.00000E+000	0	-2.76645E+001	0.000
4	SPHA	8	1					0.00000E+000	0	5.14610E+001	0.000
5	CDIA	8	1					0.00000E+000	0	-0.27988E+000	0.000
6	ASTI	8	1					0.00000E+000	0	5.76729E+001	0.000
7	PERC		1					0.00000E+000	0	-4.68123E+003	0.000
8	DIST	8	1					0.00000E+000	0	5.79735E+000	0.000

Fig. 12.4 Starting prescription and merit function for perisopic lens.

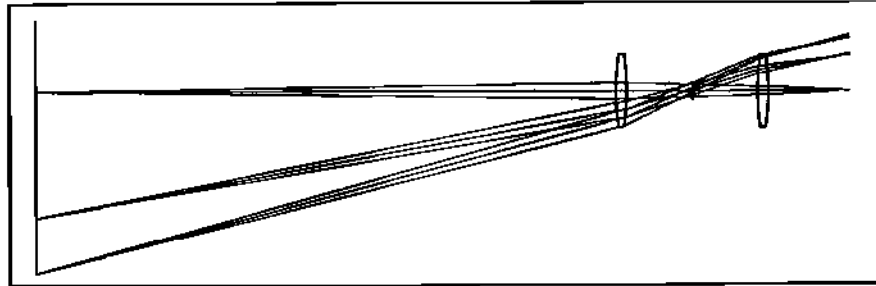


Fig. 12.5 Initial layout for perisopic lens.

12.3 Setting Up the Pre-Design In ZEMAX

Let us assume that the EFL of the perisopic lens will be 200 mm, and that the initial lens separation is 180 mm. So $\Phi_{P_+} = 0.0073$ and $\Phi_{P_-} = 0.0038$. We pick the latter. We will use Schott SF2 at $\lambda = 0.55$, which has an index of $n = 1.65174$. So $R_F = 343.02$. The glass thickness will be 15 mm. Field angles of 0° , 10.5° , and 15° will be employed. In the “Gen” box, we select the paraxial working f-number and insert 10.

The object will not initially be at infinity. We want to show certain features of the symmetric system which only show up clearly at unit magnification. For this we will employ the PMAG operand in the MFE. Our starting prescription (PERC101b) and MFE are shown in Figure 12.4. The layout is shown in Figure 12.5. Please note the use of the pickup solve (denoted by the letter P) on the back half of the lens. This “slaves” the back half of the lens to the front half. Regardless of how curvatures and airspace thickness changes in the front half, the P-solve will force the lens to remain symmetric.

The P-solve is accessed by double-clicking on the solve column just right of the parameter of interest. From the pop-up menu select “pickup.” Another menu appears where two numbers are requested. The first asks from which surface to

138 Chapter 12 Symmetry and the Perisopic Lens

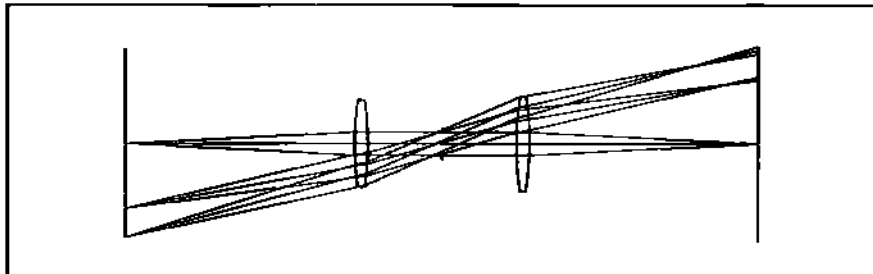


Fig. 12.6 Layout of symmetric system at unit magnification.

Merit Function Value: 3.72313262E-818											
Num	Type	Int1	Int2	Ix	Ly	Px	Py	Target	Weight	Value	% Cont
1	EFL		1					2.00000E+002	1	2.00000E+002	99.884
2	EFLY	1	2					0.00000E+000	0	2.65446E+002	0.000
3	PMAG		1					-1.00000E+000	1	-1.00000E+000	0.136
4	SPHA	8	1					0.00000E+000	0	1.95682E+000	0.000
5	COMA	8	1					0.00000E+000	0	4.22363E-010	0.000
6	ASTI	8	1					0.00000E+000	0	0.106805E+001	0.000
7	PETC		1					0.00000E+000	0	-4.50123E-003	0.000
8	BIST	8	1					0.00000E+000	0	-1.00000E+000	0.000

Fig. 12.7 MFE of the symmetric system showing zero coma.

pick the corresponding parameter value; the second, the sign to be assigned. In this problem radii will have the opposite sign; thicknesses, the same sign.

The MFE shows many more operands than are being actively utilized. Those with zero weight are serving as monitors. It is useful to watch what is happening to the Seidel aberration values before and after the various optimizations (without having to go through the "ANALYSIS" route). In particular, pay close attention to COMA (which is W_{131}).

The first thing we do is place a "V" on the airspace to tweak the system back to the target EFL of 200 mm.

PERC1o1b → Optimize → PERC1o1a

Next, we turn on PMAG (Target: -1; Weight: 1) and place a "V" on the object distance (and remove "V" on the airspace).

PERC1o2b → Optimize → PERC1o2a

The layout is shown in Figure 12.6. This is a unit magnification arrangement. Note that the object air thickness is equal to the back image distance (BID). Note the value of coma as shown in the MFE in Figure 12.7. It is now essentially zero. This is a natural consequence of a symmetric system operating at unit magnification. The coma introduced by the front half is canceled by that contributed by the rear half. Also, distortion and lateral color (although we have not discussed them yet) exhibit similar behavior.

Section 12.4: Object At Infinity 139

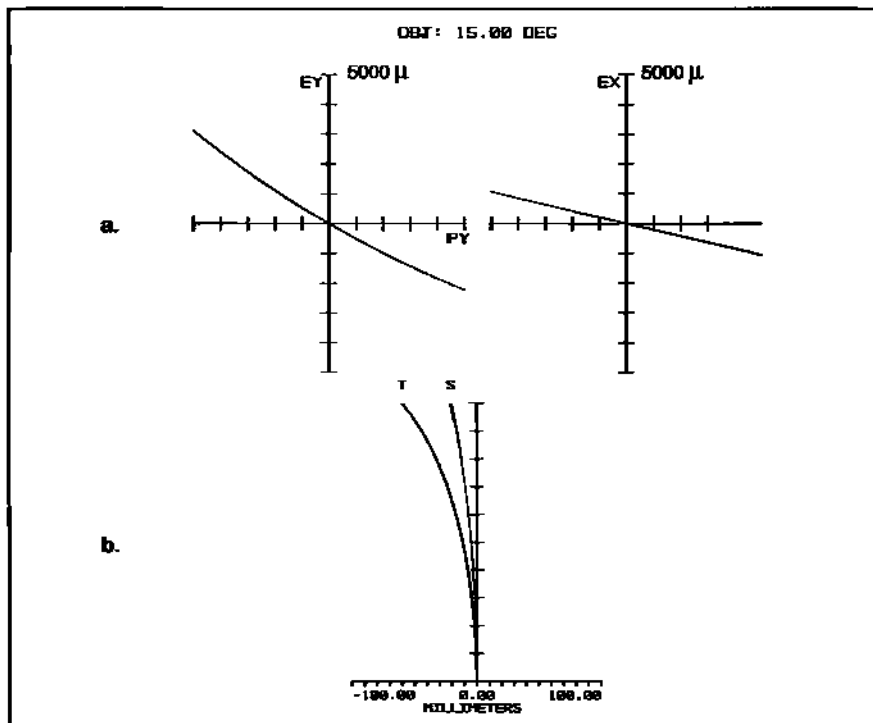


Fig. 12.8 Ray fan plots and field curvature prior to optimization.

12.4 Object At Infinity

Although symmetry works most effectively at unit magnification, it retains some benefit even when the object is moved to infinity. We now place variables on the front half curvatures and stop airspace, and insert the TRAC operands. Turn PMAG off. Prior to the optimization, RMS spot sizes (in microns) across the field are 8; 629; 1400. The main problem is astigmatism—56 waves of it. This is also grossly evident from the tangential and sagittal ray fan plots at full field as shown in Figure 12.8a. The slopes through the origin are dramatically different. The slight bow seen in the tangential plot is due to coma ($\sim 9\lambda$). Figure 12.8b shows the field curvature plot (scale of ± 100 mm).

PERC1o3b → Optimize → PERC1o3a

After the optimization spot sizes are 48; 76; 111: a major improvement. Astigmatism is still the dominant aberration but is now down to -8λ . Coma is at 3.6λ . The layout (shown in Figure 12.9) displays the classic perisopic form. Ray fan plots at the edge of the field are shown in Figure 12.10a, and the field curvature is shown in Figure 12.10b. Note the scale change for each.

The use of a dummy surface as a variable last surface, and a reduction in lens

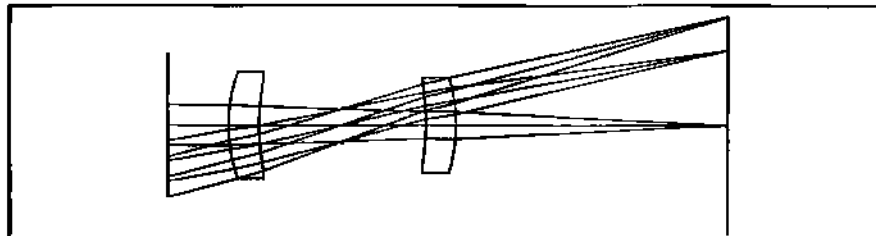


Fig. 12.9 Layout of lens after TRAC optimization.

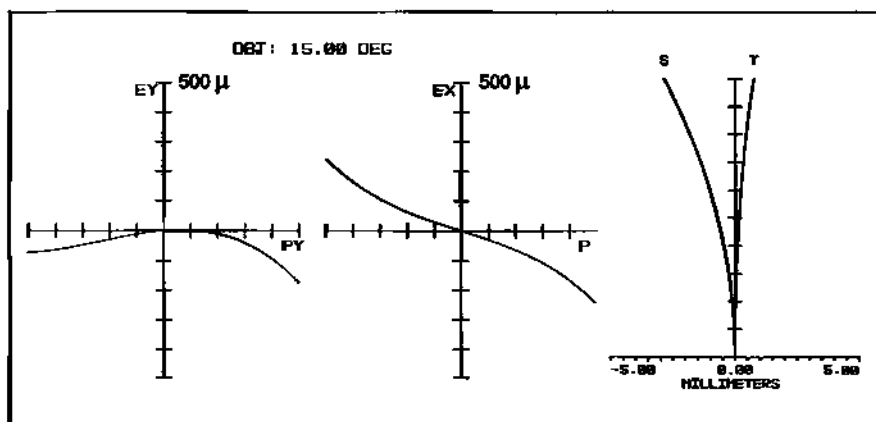


Fig. 12.10 Ray fan and field curvature plots after optimization.

thickness from 15 mm to 5 mm does add some improvement. Spot sizes are now 44; 33; 68.

PERC1o4b → Optimize → PERC1o4a

12.5 Field Flattening

In olden days, designers would often strive to flatten the tangential field since it often yielded better performance. This can be easily verified in Zemax by incorporating the FCGT operand in the MFE of PERC1o4a as shown in Figure 12.11. Note that FCGT is used three times—once for each field position.

PERC1o5b → Optimize → PERC1o5a

The field curvature plot in Figure 12.12a verifies that we achieved the flat tangential field, but spot sizes (72; 103; 141) are larger than found in PERC1o3a above. We can also flatten the sagittal field by using FCCS as a replacement operand for FCGT in PERC1o5b.

Section 12.6: Comparison With Rear Landscape Lens 141

Num	Type	Int1	Int2	Hx	Hy	PX	Py	Target	Weight	Value	% Cont
1	EFL		1					2.00000E+002	1	2.00000E+002	0.000
2	EFLY	2	3					0.00000E+000	8	3.38438E+002	0.000
3	PMAG		1					-1.00000E+000	8	0.00000E+000	0.000
4	SPHA	8	1					0.00000E+000	8	2.53262E+000	0.000
5	COMA	8	1					0.00000E+000	8	2.76688E+000	0.000
6	ASTI	8	1					0.00000E+000	8	-5.54512E+000	0.000
7	PETC		1					0.00000E+000	8	-3.48345E-003	0.000
8	DIST	8	1					0.00000E+000	8	2.87498E-001	0.000
9	FCGT	1	0.0000	0.0000				0.00000E+000	1	2.68628E+000	49.945
10	FCGT	1	0.0000	0.7876				0.00000E+000	1	2.06854E+000	31.223
11	FCGT	1	0.0000	1.0000				0.00000E+000	1	1.59758E+000	18.769

Fig. 12.11 Use of FCGT operand to flatten tangential field.

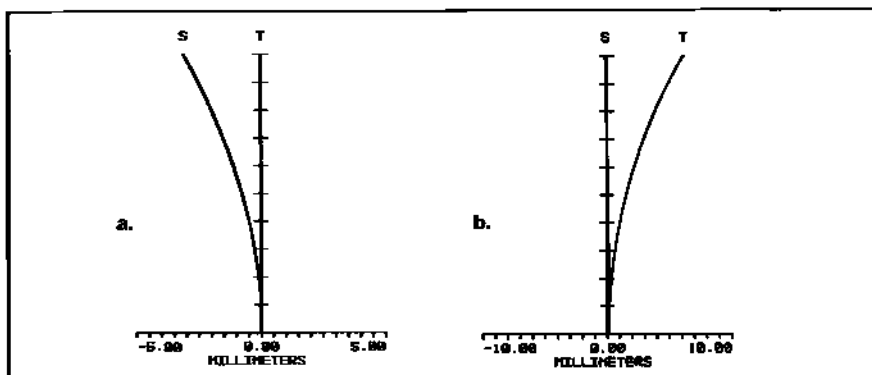


Fig. 12.12 Field curvature plots for flat tangential (a) and sagittal (b) fields.

PERC1o6b → Optimize → PERC1o6a

The resulting field curvature is shown in Figure 12.12b. Spot sizes here are 374; 333; 300—much worse than the flat tangential field case.

12.6 Comparison With Rear Landscape Lens

Have we gained anything by the perisopic design over its landscape counterparts? With the latter we had three variables: 2 curvatures and 1 airspace. With the symmetric perisopic design the same degrees of freedom are used on the front half. To make a proper comparison, WOLR1o4a (Section 6.4) is modified (SF2, $\lambda = 0.55$, $U = 15^\circ$) and reoptimized so that it has the same first order properties as the perisopic design.

WOLR1o5b → Optimize → WOLR1o5a

The resulting layout is shown in Figure 12.13. Spot sizes are 52; 28; 59, as compared to 44; 33; 68 for PERC1o4a. Field curvature plots are shown in Figure 12.14a and b, and ray fan plots at maximum field are shown in Figure 12.15a and b. The landscape lens is the lefthand plot in both.

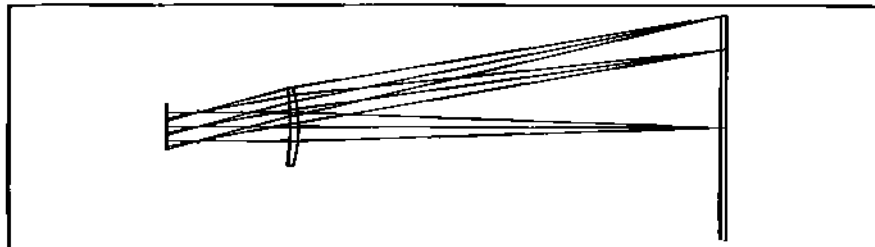


Fig. 12.13 Layout of modified rear landscape lens.

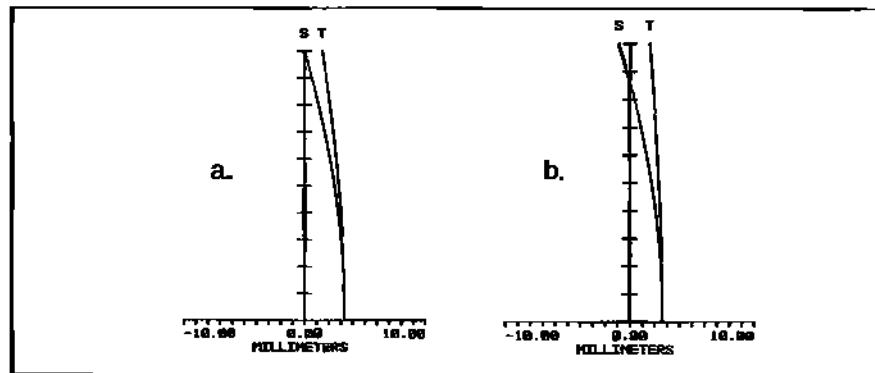


Fig. 12.14 Field curvature plots for: a. landscape lens; b. periscopic lens.

Seidel aberration content is shown in Table 12.1.

Table 12.1

	WOLR	PERC
SPHA	3.43λ	2.53λ
COMA	-0.19λ	2.77λ
ASTI	-3.45λ	-5.54λ
PETC	-0.0030	-0.0034
DIST	-1.52	0.29

The RMS spot is somewhat better on-axis for the periscopic lens, but the landscape is better off-axis. The field curvature plots give a slight edge to the landscape lens as well. The ray fan plots are on the same scale and approximately equivalent, although there is a lot more coma evident in the periscopic plot. On the other hand, the landscape lens shows better numbers in every category of Table 12.1 except for spherical aberration and distortion. All in all, the periscopic is not significantly improved over the rear landscape. However, when we remove the symmetry constraints on the former, things change dramatically.

Section 12.7: Breaking Symmetry 143

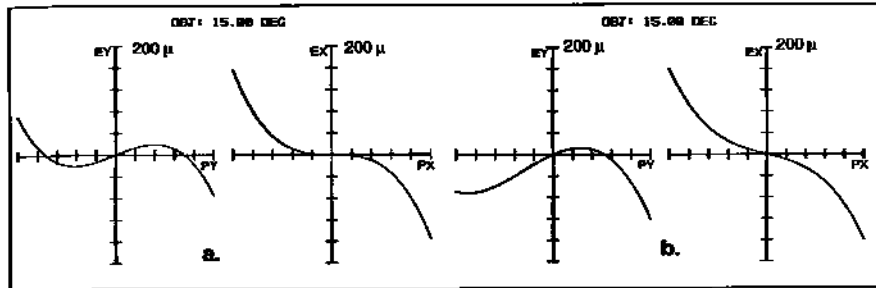


Fig. 12.15 Ray fan plots for: **a.** landscape lens; **b.** perisopic lens.

12.7 Breaking Symmetry

Let's see what improvement awaits us if we *unslave* the rear half from the front half of the perisopic lens. Since the object and image are no longer symmetric, it makes sense that some asymmetry in the lens might help us. If we start from PERC1o4a with variables on all curvatures, retain the dummy image surface, and use TRAC (no FCGTs):

PERC1o7b → Optimize → PERC1o7a

Spot sizes are 40; 27; 59. This is a slight improvement over PERC1o4a. Let's redo this from PERC1o4a but unslave the stop airspaces as well. Now all curvatures and airspaces are variable.

PERC1o8b → Optimize → PERC1o8a

The resulting layout is shown in Figure 12.16. The spot diagrams are shown in Figure 12.17. Spot sizes are now 7; 7; 9, and you can actually see the Airy disk in the plots. This is a dramatic improvement, and is due to having six degrees of freedom rather than three degrees. The ray fan plot at full field is shown in Figure 12.18a and the field curvature plot in Figure 12.18b.

Cautionary Note: In the above example we were able to get a good result by unslaving everything and making all curvatures and airspaces variable. Sometimes, however, this will not work. You might have to do things in several separate stages before a good result is obtained. In other words, a direct path to the deep minima may be blocked by a shallower minima. Somehow you have to get around the latter first. Properly staged optimizations can navigate around such an obstacle.

12.8 Historical Note: Carl Steinheil

Carl A. Steinheil (Figure 12.19) was born in Alsace in 1801. He studied under such men as Gauss and Bessel, the latter being his Ph.D. adviser. Steinheil received his doctorate at Konigsberg in 1825. By 1832, he was a professor of physics and mathematics in Munich. From 1849 to 1852, he helped set up a tele-

144 Chapter 12 Symmetry and the Periscopic Lens

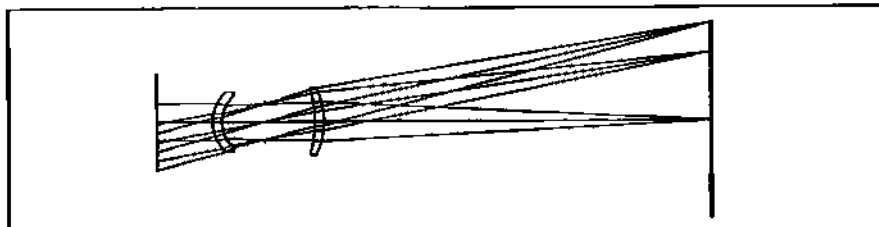


Fig. 12.16 Layout of the asymmetric periscopic.

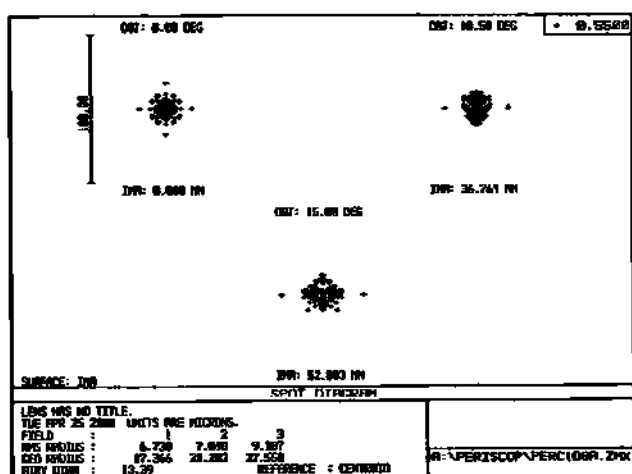


Fig. 12.17 Spot diagrams for asymmetric periscopic.

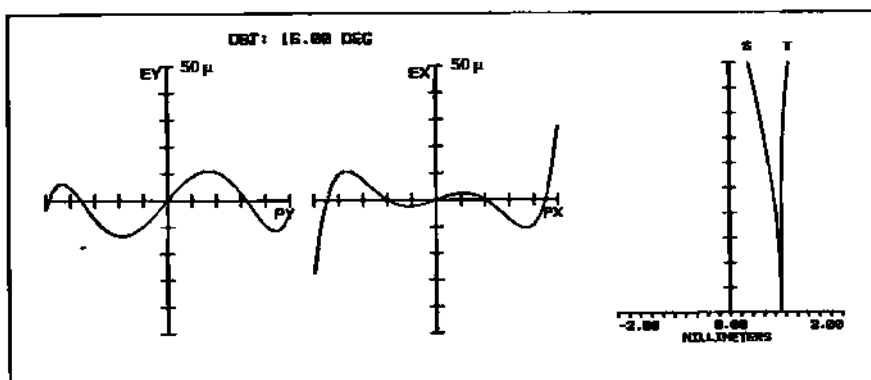


Fig. 12.18 a. Ray fan and b. field curvature plots for asymmetric periscopic.

Section 12.9: Homework 145



Fig. 12.19 Carl A. Steinheil (1801–1870).

graph system in Bavaria and Switzerland. In 1854 he established (in Munich) the Steinheil Optical Institute with the help of his son Adolph. In 1856, he collaborated with Foucault on the process of silver deposition on primary and secondary mirrors for telescopes. In 1865 Carl patented the design for an $f/15$ lens he called the Periskop (Figure 12.2). He died in 1870.

12.9 Homework

Design a periscopic lens:

- a. object at infinity
- b. EFL = 400 mm
- c. $f/15$
- d. Field angle: $\bar{U} = 25^\circ$
- e. Glass BK7; thickness = 12 mm.
- f. $\lambda = 0.587$
- g. Suggested folder name: Periscopic. File name: PERC1o1b, etc.
- h. Initial interlens airspace = 100 mm
- i. For RMS spot size use (square, centroid, Airy) under settings.

146 Chapter 12 Symmetry and the Periscopic Lens

1. Slave rear half to front half using the "P" command. Use TRAC to optimize lens. Meet or beat the following spot sizes:

Field	RMS
0°	138 μm
17.5°	92
25°	215

2. Try dummy image surface. Any improvement?
3. Use FCGT operands to flatten tangential field. Any improvement?
4. Unslave rear from front and reoptimize. Meet or exceed the following RMS spot sizes.

Field	RMS
0°	7 μm
17.5°	17
25°	21

Chapter 13

Coma and Astigmatism

13.1 Introduction

This chapter will continue the program started in Chapter 10. The ZEMAX aberration table is reprised here as Figure 13.1. This time, however, attention focuses on the transverse spherical aberration, coma, and astigmatism (indicated by the

Listing of Aberration Coefficient Data

File : A:\Fscovpln.zmx
Title: Lens has no title.
Date : MON APR 24 2000

Wavelength : 0.6810 microns
Petzval radius : -71.5303
Optical Invariant: 0.3500

Seidel Aberration Coefficients:

Surf	SPHA	S1	COMA	S2	ASTI	S3	FCUR	S4	DIST	S5	CLA (CL)	CTR (CT)
STO	0.00486		0.00239		0.00117		0.00171		0.00142		0.00000	0.00000
2	0.00113		-0.00121		0.00138		0.00000		-0.00139		0.00000	0.00000
IMA	0.00000		0.00000		0.00000		0.00000		0.00000		0.00000	0.00000
TOT	0.00599		0.00118		0.00247		0.00171		0.00003		0.00000	0.00000

Seidel Aberration Coefficients in Waves:

Surf	W040	W131	W222	W220	W311	W020	W111
STO	10.11171	19.87822	9.76945	7.12195	11.88173	0.00000	0.00000
2	2.34180	-10.05154	18.78589	0.00000	-11.57388	0.00000	0.00000
IMA	0.00000	0.00000	0.00000	0.00000	0.00000	0.00000	0.00000
TOT	12.45351	9.82667	28.55534	7.12195	0.22785	0.00000	0.00000

Transverse Aberration Coefficients:

Surf	TSPH	TSCO	TTCO	TSFC	TYFC	TDIS	TLAC
STO	0.02981	0.01465	0.04396	0.01770	0.03210	0.00870	0.00000
2	0.00690	-0.00741	-0.02223	0.00795	0.02385	-0.00053	0.00000
IMA	0.00000	0.00000	0.00000	0.00000	0.00000	0.00000	0.00000
TOT	0.03672	0.00724	0.02173	0.02565	0.05596	0.00017	0.00000

Longitudinal Aberration Coefficients:

Surf	LSPH	LAST	LFCP	LFCS	LFCT	LAC
STO	0.53316	0.25756	0.18776	0.31654	0.57410	0.00000
2	0.08469	0.19503	0.00000	0.09752	0.29255	0.00000
IMA	0.00000	0.00000	0.00000	0.00000	0.00000	0.00000
TOT	0.45037	0.37168	0.12878	0.31462	0.68630	0.00000

Fig. 13.1 ZEMAX aberration coefficient data list.

GENERAL LENS DATA:

Surfaces	:	3
Stop	:	1
System Aperture	:	Entrance Pupil Diameter = 8
Ray aiming	:	Off
Apodization	:	Uniform, factor = 0.00000E+000
Eff. Focal Len.	:	49.06042 (in air)
Eff. Focal Len.	:	49.06042 (in image space)
Back Focal Len.	:	48.11323
Total Track	:	49.49423
Image Space F/#	:	6.132552
Para. Wkng F/#	:	6.132552
Working F/#	:	6.065487
Image Space N.A.	:	0.0815321
Obj. Space N.A.	:	4e-010
Stop Radius	:	4
Parax. Ima. Hgt.	:	4.29223
Parax. Mag.	:	8
Entr. Pup. Dia.	:	8
Entr. Pup. Pos.	:	0
Exit Pupil Dia.	:	8
Exit Pupil Pos.	:	-49.06042
Field Type	:	Angle in degrees
Maximum Field	:	5
Primary Wave	:	0.601
Lens Units	:	Centimeters
Angular Mag.	:	1

Fig. 13.2 System first order properties for singlet.

boxed-in regions). The aberration formulations contained in Table 10.1 will be utilized to compute Seidel and wavefront coefficients for the singlet introduced in Section 10.3. In this way we will obtain some insight as to the manner in which ZEMAX generates the aberration numbers displayed in the table.

13.2 Transverse Spherical Aberration: SA3

We saw in Section 11.8 that the transverse ray aberration for spherical aberration is given by:

$$T = -\left(\frac{R}{r}\right)[4W_{040}p^3] = SA3p^3 \quad (13.1)$$

From Figure 13.1 we see that $W_{040} = 12.4535 \lambda = 0.00074846$ cm. From the first order properties shown in Figure 13.2 we see that the EFL = 49.0604 cm, and the EPD = 8 cm. Since the object is at infinity, $R = EFL$, and $r = EPD/2$. Inserting these values into Equation 13.1:

$$T = -\left(\frac{49.0604}{4}\right)[4(0.0007488)1] \quad (13.2)$$

$$T = -0.03672 \text{ cm} = -367.2 \mu\text{m} \quad (13.3)$$

Except for the sign, this is the value shown in the boxed-in region under the column TSPH. ZEMAX defines TSPH = $S_i/(2n'u')$, where u' is negative.

The ray fan plot is shown in Figure 13.3a, and the magnitude at the pupil

Section 13.2: Transverse Spherical Aberration: SA3 149

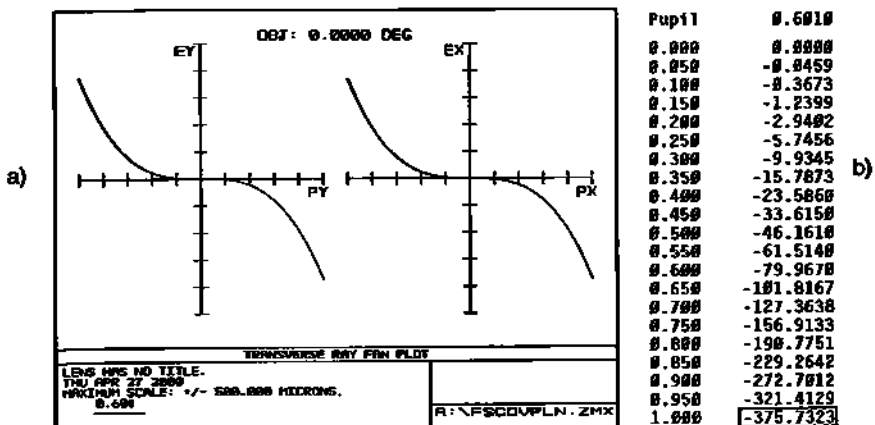


Fig. 13.3 a. Ray fan plot for singlet; b. ray fan data table.

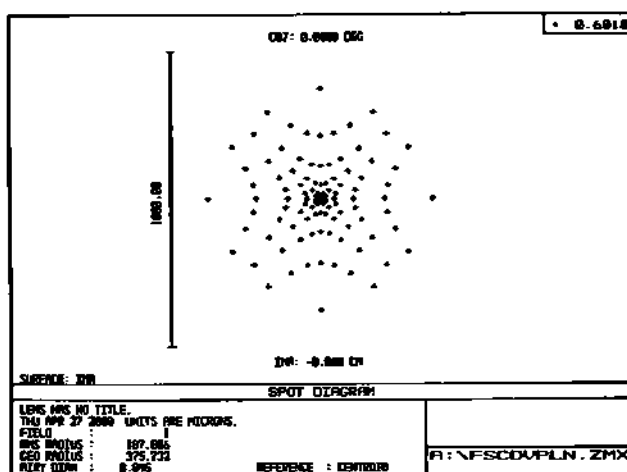


Fig. 13.4 Spot diagram for singlet.

Real Ray Trace Data:

Surf	X-coord	Y-coord	Z-coord	X-tangent	Y-tangent
OBJ	Infinity	Infinity	Infinity	0.0000000	0.0000000
1	0.000000E+000	4.000000E+000	3.588982E-001	0.0000000	-0.0566292
2	0.000000E+000	3.942119E+000	0.000000E+000	0.0000000	-0.0827151
3	0.000000E+000	-3.757323E-002	0.000000E+000	0.0000000	-0.0827151

Fig. 13.5 Ray trace data for real ray.

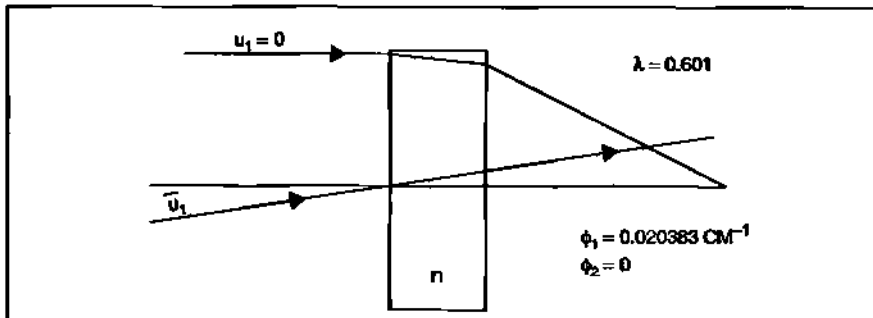


Fig. 13.6 Paraxial convex-plano thin lens.

edge appears to correspond to Equation 13.3. However, when the numbers are called up (via “text”), a discrepancy is seen (as indicated in Figure 13.3b). The value at the pupil edge is shown to be $375.7\mu\text{m}$. This value is also seen as the geometric radius in the spot diagram in Figure 13.4. Finally, when the ray trace is called up (Figure 13.6), the same number appears once again as the y-height in the image plane for the real ray.

The reason for the discrepancy is that the calculation for SA3 considers only Seidel aberration (fourth order in the exit pupil, third order in the image plane). The real ray is affected by *all* orders of aberration, and it is the real ray behavior that is reflected in both the ray fan and spot plots. In our case, sixth order spherical aberration is the main culprit.

13.3 ZEMAX Off-Axis Aberration Calculations

Figure 13.6 updates Figure 10.4b to include the chief ray. The PRT data for the chief ray is given in Table 13.1.

Table 13.1

Surface	\bar{y}	\bar{u}	\bar{u}'
1	0	0.087489	0.060006
2	0.082868	0.060006	0.087489

The Lagrange invariant (Section 5.6) is given by:

$$L = n[\bar{u}y - u\bar{y}] = \bar{u}y = 0.349955$$

We will also need some values previously determined in Section 10.3. These are:

$$\begin{aligned} A_1 &= 0.178016 \\ A_2 &= -0.081531 \\ \Delta_1(u/n) &= -0.038354 \\ \Delta_2(u/n) &= -0.043177 \end{aligned}$$

Section 13.3: ZEMAX Off-Axis Aberration Calculations 151

13.3.1 Coma (W_{131}) via Seidel Contributions

From Table 10.1, the surface-by-surface Seidel formulation for coma is given by:

$$S_H = -\sum B_i A_i y_i \Delta_i \left\{ \frac{u}{n} \right\} \quad (13.4)$$

All the information is on-hand except for the B_i values. From Table 10.1:

$$B = n(\bar{u} + \bar{y}C) \quad (13.5)$$

For surface 1:

$$B_1 = 1 \cdot [0.087489 + 0 \cdot (0.044504)] = 0.087489$$

For surface 2:

$$B_2 = 1.458[0.060006 + (0.082868) \cdot 0] = 0.087489$$

Now employing Equation 13.4:

First Surface:

$$S_{H1} = -(0.087489)(0.178016)4(-0.038354)$$

$$S_{H1} = +0.002389$$

Second Surface:

$$S_{H2} = -(0.087489)(-0.081531)(3.922774)(-0.043177)$$

$$S_{H2} = -0.001208$$

Surface Summation:

$$S_H = [S_{H1} + S_{H2}]$$

$$S_H = 0.001181 \text{ cm}$$

This is the value seen in Table 13.1 under the heading COMA S2.

Recalling that $W_{131} = S_H/2$ we have:

$$W_{131} = 0.0005904 \text{ cm}$$

$$W_{131} = 5.904 \mu\text{m}$$

$$W_{131} = 9.824 \lambda$$

This is essentially the value seen in Table 13.1 under the heading W_{131} . This is the magnitude of the aberration at the edge of the pupil.

13.3.2 Coma (W_{131}) via Thin Lens Formulation

From Table 10.1 we see that the thin lens formula for coma is given by:

$$W_{131} = \frac{1}{2}S_H = \frac{1}{2}\left[\frac{1}{2}Ly^2\phi^2\sigma_H\right] \quad (13.6)$$

Also from Table 10.1 we see that the structural aberration coefficient for coma is given by:

$$\sigma_H = eX - fY \quad (13.7)$$

Since the object is at infinity, the magnification factor $Y = 1$. Since the lens is convex-plano, the shape factor $X = 1$ as well. Inserting the values for e and f from Table 10.1, Equation 13.7 reduces to:

$$\sigma_H = e - f = \left[\frac{n+1}{n(n-1)}\right] - \left(\frac{2n+1}{n}\right) \quad (13.8)$$

Since the index is 1.458, σ_H becomes: $\sigma_H = 0.99507$.

We now have all the numbers needed to insert into S_H as found in Equation 13.6.

$$S_H = \frac{1}{2}(0.349955)4^2(0.020383)^3(0.99507)$$

$$S_H = 0.001157 \text{ cm}$$

The wavefront aberration coefficient W_{131} is given by:

$$W_{131} = \frac{1}{2}S_H = 0.000579 \text{ cm}$$

Therefore: $W_{131} = 9.63\lambda$.

This is close to the value found via the Seidel summation method. The difference is due to the fact that lens thickness was not taken into account.

13.3.3 Astigmatism (W_{222}) via Seidel Contributions

From Table 10.1, the surface-by-surface Buchdahl formulation for astigmatism is given by:

$$S_{II} = -\sum B_i^2 y_i \Delta_i \left\{ \frac{u}{n} \right\} \quad (13.9)$$

All the information is on hand.

First Surface:

$$S_{II1} = -(0.087489)^2(4)(-0.038354)$$

$$S_{III1} = +0.001174$$

Second Surface:

$$S_{III2} = -(0.087489)^2(3.922774)(-0.043177)$$

$$S_{III2} = +0.001296$$

Surface Summation:

$$S_{III} = [S_{III1} + S_{III2}]$$

$$S_{III} = 0.002470 \text{ cm}$$

This is the value seen in Table 13.1 under the heading ASTI S3.

Recalling that:

$$W_{222} = \frac{1}{2}S_{III},$$

we have:

$$W_{222} = 0.001235 \text{ cm}$$

$$W_{222} = 12.35 \mu\text{m}$$

$$W_{222} = 20.55 \lambda$$

This is the value seen in Table 13.1 under the heading W_{222} . This is the magnitude of the aberration at the edge of the pupil.

13.3.4 Astigmatism (W_{222}) via Thin Lens Formulation

From Table 10.1 we see that the thin lens formula for astigmatism is given by:

$$W_{222} = \frac{1}{2}S_{III} = \frac{1}{2}[L^2\phi\sigma_{III}] \quad (13.10)$$

Also from Table 10.1 we see that the value of $\sigma_{III} = 1$. Therefore, S_{III} becomes:

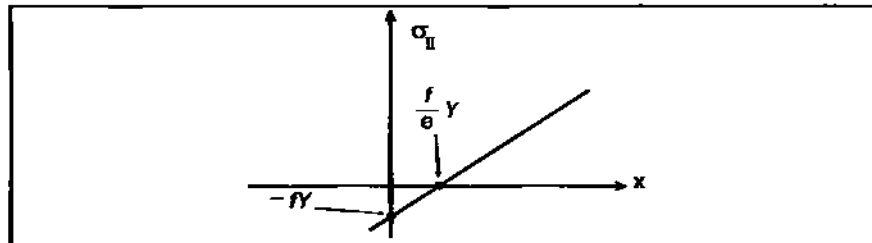
$$S_{III} = (0.349955)^2(0.020383) \cdot 1$$

$$S_{III} = 0.002496 \text{ cm}$$

The wavefront aberration coefficient is given by:

$$W_{222} = 0.001248 \text{ cm}$$

$$W_{222} = 20.76 \lambda$$

Fig. 13.7 Generic plot of σ_{II} .

Once again the difference between this and the summation result is due to lens thickness.

13.4 Coma and Lens Bending

In Chapter 11, we saw how the structural aberration coefficient σ_I lent itself to exploring the effects of lens bending to find the shape that minimized spherical aberration. A similar procedure can be used with the structural aberration coefficient for coma, σ_{II} . Figure 13.7 shows a generic plot for σ_{II} . It is a linear function described by:

$$\sigma_{II} = eX - fY \quad (13.11)$$

At the point where this plot crosses the abscissa, $\sigma_{II} = 0$. Therefore:

$$X = \left(\frac{f}{e}\right)Y \quad (13.12)$$

For an object at infinity, $X = (f/e)$. For an object at unit magnification, $X = 0$.

Consider a BK7 singlet with an object at infinity. Operating in d light, $n = 1.5168$. Consequently, $e = 3.2107$ and $f = 2.6593$. Inserting these values into Equation 13.12:

$$X = 0.8283$$

Recall from Section 11.3 that the shape factor for minimum spherical was $X = 0.7397$, which is not far from that for coma.

13.5 Coma and Astigmatism vs. F-Number and Field

Both coma and astigmatism increase as field angle increases and as aperture size grows. But how do coma and astigmatism compete with each other in the same arena? Under what conditions does one dominate the other? Consider the thin lens forms for coma and astigmatism as given by Equations 13.6 and 13.10 respective-

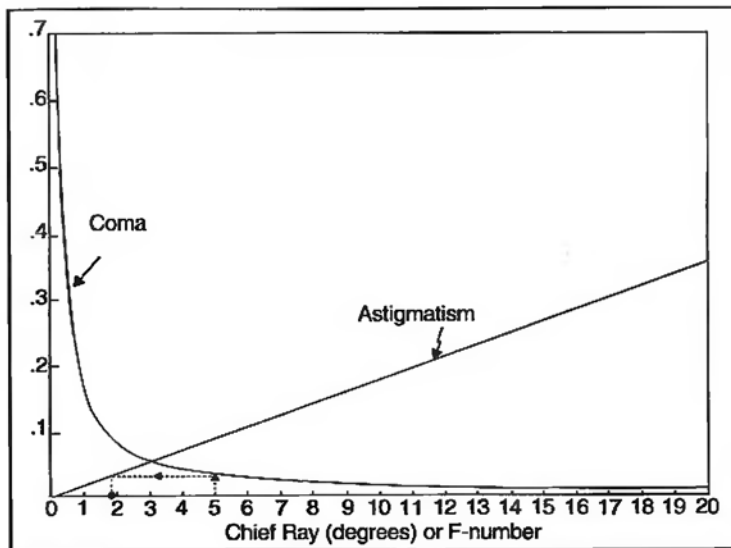


Fig. 13.8 Difference factor plot of coma and astigmatism for a plano-convex thin lens.

ly. For an object at infinity and stop at the lens, the Lagrange invariant is $L = \bar{u}y$. We will also use the relation f-number = $f/2y$. Equations 13.6 and 13.10 become:

$$W_{131} = \frac{1}{4}(\bar{u}y)\left(\frac{y}{f}\right)^2 \sigma_{II} = \frac{1}{4}\bar{u}y\left(\frac{2y}{f}\right)^2\left(\frac{\sigma_{II}}{4}\right) = \left[\frac{\bar{u}y}{4(f/\#)}\right] \cdot \left[\frac{\sigma_{II}}{4/\#}\right] \quad (13.13)$$

$$W_{222} = \frac{1}{2}(\bar{u}y)^2 \frac{\sigma_{III}}{f} = \frac{1}{2}(\bar{u}y)\left(\frac{2y}{f}\right)\left(\frac{\bar{u}\sigma_{III}}{2}\right) = \left[\frac{\bar{u}y}{4(f/\#)}\right] \cdot \left[\bar{u}\sigma_{III}\right] \quad (13.14)$$

From Equations 13.13 and 13.14 we see that coma and astigmatism have been reformatted into two factors: one factor is common to both (unshaded); the other, the source of difference (shaded). Assuming that σ_{II} and σ_{III} are constant, then, *relatively speaking*, coma varies inversely with f-number and astigmatism varies directly with \bar{u} .

As an example, let's plot the *difference part* for a thin plano-convex lens. The structural aberration coefficients become: $\sigma_{II} = (e-f)$ and $\sigma_{III} = 1$. As indicated in Table 10.1, both e and f are functions of the refractive index. Letting $n = 1.5$, $\sigma_{II} = 0.667$. The resulting plot is shown in Figure 13.8.

The numbers along the x -axis represent either the chief ray angle, \bar{U} , in degrees or f-number (depending upon which difference factor is being considered). Recall that:

$$\bar{u} = \tan \bar{U}.$$

As an example, suppose we have an $f/5$ system. Considering the x -axis as

158 Chapter 13 Coma and Astigmatism

f-number, locate 5 and then move vertically until you intercept the $0.667/(4f/\#)$ curve. From this point, move horizontally to the left until the chief ray curve is intercepted. Then drop straight down to the x -axis, which is now read as 1.75° . At this angle, coma and astigmatism have the same magnitude. Below this angle, coma is dominant. Above this angle, astigmatism is dominant.

13.6 Homework

Using the paraxial ray trace data from the Homework for Chapter 4 and the A-values computed in the Homework for Chapter 10, calculate the amount of coma and astigmatism (W_{131} and W_{222}) present for a 5° field.

$$W_{131} = ?$$

$$W_{222} = ?$$

Chapter 14

Field Curvature and Field Flattener

14.1 Introduction

In Section 7.3.5, two aberrations were introduced that affected the *position* of the point image without degrading its quality. These were field curvature and distortion. In this chapter, our attention will focus on the former. We will see how ZEMAX determines both the wavefront aberration value as well as the radius of the corresponding curved image surface. This will be followed by a discussion on the design of the optic known as the “field flattener.”

14.2 Petzval Curvature

Petzval curvature can be considered almost as a Platonic ideal. It is hardly ever something that can be directly measured or observed. Yet it has a big impact on the location of tangential and sagittal image surfaces, and must be controlled if flat field imaging is to be attained. Consider the spherical mirror illustrated in Figure 14.1. Note that the stop is located at the mirror. The chief ray strikes the stop/mirror vertex at an angle \bar{U} , and is reflected at an angle $-\bar{U}$. The incident and reflected chief rays are not coincident. Off-axis aberrations such as coma and astigmatism are introduced on the reflected beam.

Let's move the stop away from the mirror so that it now lies in the plane of the center of curvature as shown in Figure 14.2. The chief ray again strikes the stop vertex at angle \bar{U} , but continues on to strike the mirror surface a distance R away. This time, however, the angle of incidence on the mirror is zero. The incident and reflected chief rays are coincident. Because of the rotational symmetry about the chief ray, no off-axis aberrations are introduced. There is *no* coma or astigmatism on the reflected beam. There is just spherical aberration. The focus occurs along the reflected chief ray at a distance $R/2$. In fact, as the chief ray angle is varied, all the previous statements hold true. However, the image point traces out a curved focal surface (of radius $R/2$) as a function of chief ray angle. This is indicated in Figure 14.3. This curved image surface is the Petzval surface (and hence the name Petzval curvature). This is the rare case where the pure Petzval surface is physically realized. You can actually measure it.

Figure 14.4 illustrates the Petzval image surface for a refractive scenario. Once again the stop is located at the center of curvature. But now it is *buried* inside

158 Chapter 14 Field Curvature and Field Flattener

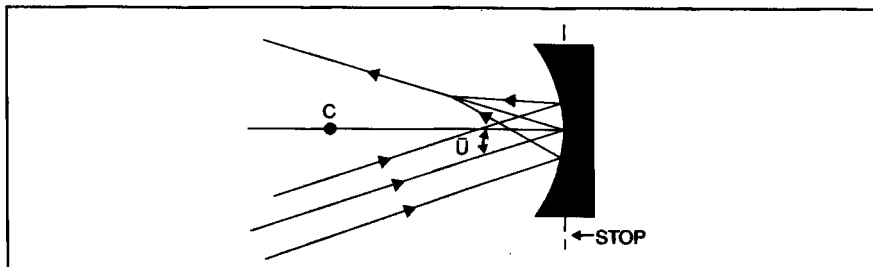


Fig 14.1 Off-axis imagery with the stop located at the mirror.

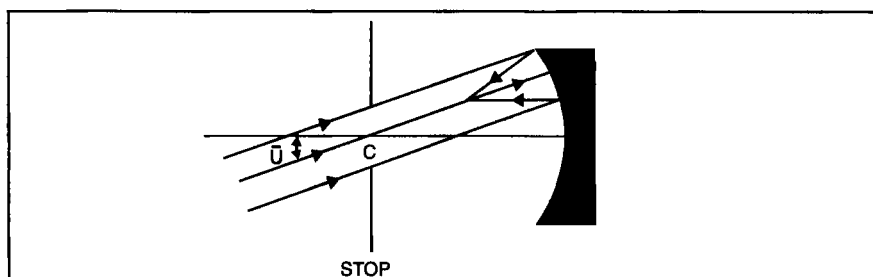


Fig 14.2 Off-axis imagery with stop at the center of curvature.

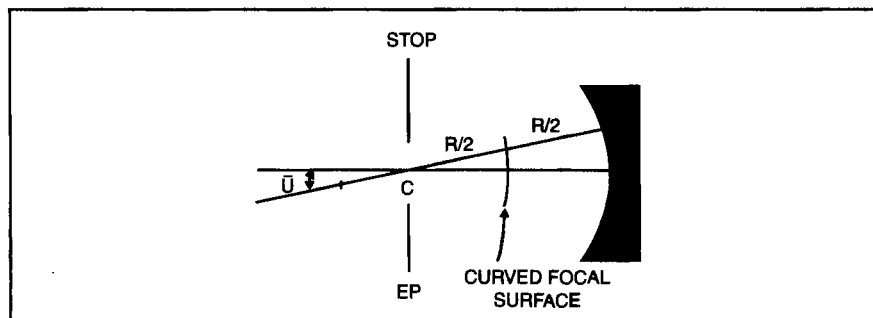


Fig 14.3 Generation of the curved Petzval image surface.

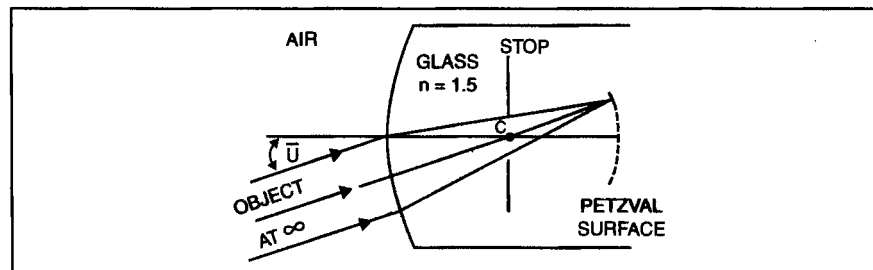


Fig 14.4 The Petzval image surface in a refractive medium.

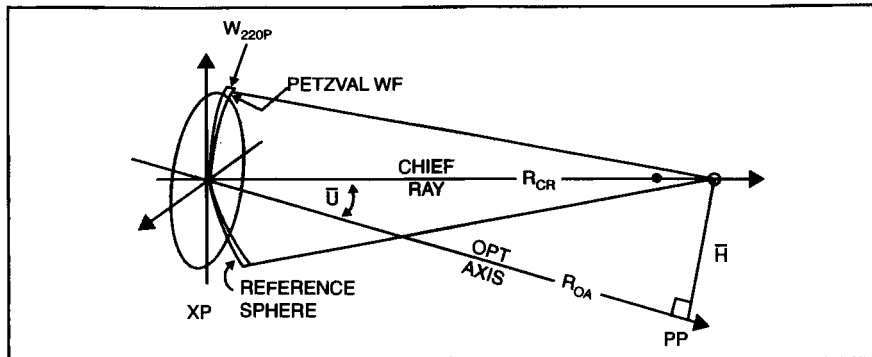


Fig 14.5 The Petzval wavefront and associated spherical reference wavefront.

the lens... and so is the Petzval image surface. The image, were it accessible, would have no coma or astigmatism. There would only be spherical and axial chromatic aberration.

14.3 The Petzval Wavefront Aberration

In Section 14.2 we discussed the curved image surface as a function of field angle. Now we look at the curved spherical wavefront in the exit pupil which gives rise to the focus point at a given field position. This is illustrated in Figure 14.5. There are two tilted spherical wavefronts shown. One is the aberrated Petzval wavefront; the other, the reference wavefront. The center of curvature of the latter lies in the paraxial plane. The center of curvature of the former lies inside paraxial focus but along the chief ray. The sag difference between the two wavefronts at the pupil edge is the coefficient W_{FC} and denotes the magnitude of the aberration. (Please note the similarity to the focus shift discussion in Section 11.4.)

14.4 The Petzval Aberration Coefficient and Petzval Sum

The Seidel wavefront polynomial term for Petzval field curvature is given by:

$$W_{FC} = \left[W_{220P} \bar{H}^2 \right] \cdot \rho^2 \quad (14.1)$$

This has the form of focus, but whose coefficient (the factor in brackets) is *field dependent*. The bracket factor is a maximum when $\bar{H} = 1$. The functional form for the coefficient W_{220P} is found in Table 10.1:

$$W_{220P} = \frac{1}{4} S_{IV} = -\left(\frac{L^2}{4}\right) \sum C_i \Delta \left\{ \frac{1}{n} \right\}_i \quad (14.2)$$

Given that the LaGrange Invariant, L , is constant, the magnitude of the Petz-

val coefficient is dependent solely on the local surface curvature and difference in refractive index.

Let's consider a *two-surface system* (such as a thin lens). In this case the summation becomes:

$$\begin{aligned} \sum C_i \Delta_i \left\{ \frac{1}{n} \right\}_i &= C_1 \left(\frac{1}{n} - 1 \right) + C_2 \left(1 - \frac{1}{n} \right) \\ &= \left(\frac{C_1}{n} \right) (1-n) + \left(\frac{C_2}{n} \right) (n-1) \\ &= \left(\frac{n-1}{n} \right) (-C_1 + C_2) \\ &= -\frac{[(n-1)(C_1 - C_2)]}{n} \end{aligned} \quad (14.3)$$

The factor in brackets is simply the power of a thin lens. Hence the sum becomes:

$$\sum C_i \Delta_i \left\{ \frac{1}{n} \right\}_i = -\frac{\Phi}{n} \quad (14.4)$$

Consequently, if we have a lens system consisting of several thin lenses:

$$W_{220P} = \left(\frac{L^2}{4} \right) \sum \frac{\Phi_i}{n_i} \quad (14.5)$$

The Petzval wavefront coefficient (and hence curvature) depends simply on the powers and refractive indices of the component elements. In order to have a reasonably flat field, this sum must be small.

14.5 Sample Calculation

Let us apply the formulation given by Equation 14.2 to our standard fused silica singlet. From Section 13.3 we have the LaGrange Invariant and lens curvature values:

$$W_{220P} = -\left(\frac{L^2}{4} \right) \sum C_i \left(\frac{1}{n} \right)_i$$

Section 14.6: Petzval Radius 161

Wavelength : 0.6010 microns
 Petzval radius : -71.5303
 Optical Invariant: 0.3500

Seidel Aberration Coefficients:

Surf	SPHA	S1	COMA	S2	ASTI	S3	FCUR	S4	DIST	S5	CLA (CL)	CTR (CT)
STO	0.00486	0.00239	0.00117	0.00171	0.00142	0.00000	0.00000	0.00000	0.00000	0.00000	0.00000	0.00000
2	0.00113	-0.00121	0.00130	0.00000	-0.00139	0.00000	0.00000	0.00000	0.00000	0.00000	0.00000	0.00000
IMA	0.00000	0.00000	0.00000	0.00000	0.00000	0.00000	0.00000	0.00000	0.00000	0.00000	0.00000	0.00000
TOT	0.00599	0.00118	0.00247	0.00171	0.00003	0.00000	0.00000	0.00000	0.00000	0.00000	0.00000	0.00000

Seidel Aberration Coefficients in Waves:

Surf	W040	W131	W222	W220	W311	W020	W111
STO	10.11171	19.87822	9.76945	7.12195	11.80173	0.00000	0.00000
2	2.34180	-10.05154	10.78589	0.00000	-11.57388	0.00000	0.00000
IMA	0.00000	0.00000	0.00000	0.00000	0.00000	0.00000	0.00000
TOT	12.45351	9.82667	20.55534	7.12195	0.22785	0.00000	0.00000

Fig 14.6 ZEMAX aberration data for standard singlet.

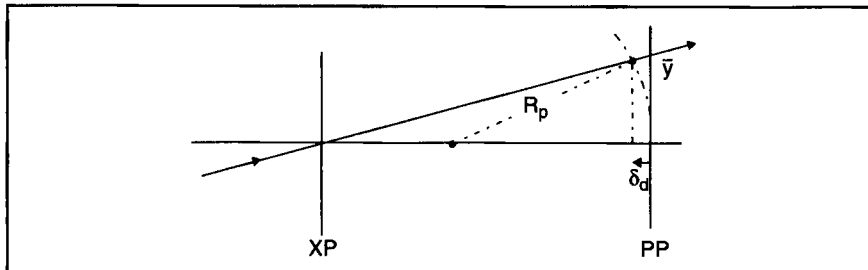


Fig 14.7 Radius of the curved Petzval image surface.

$$= -\frac{(0.349956)^2}{4} \left[(0.044504) \left(\frac{1}{1.458} - 1 \right) + 0 \right]$$

$$W_{220P} = 0.000428 \text{ cm} = 4.28 \mu\text{m}$$

$$\text{or } W_{220P} = 7.12\lambda \text{ (at } 0.601 \mu\text{m}) \quad (14.6)$$

The Seidel Coefficient S_{IV} :

$$S_{IV} = 4W_{220P} = 0.00171 \text{ cm} \quad (14.7)$$

The values given by Equations 14.6 and 14.7 are exactly the same as the aberration coefficient data supplied for this lens by ZEMAX in the boxed-in region shown in Figure 14.6.

14.6 Petzval Radius

What is the radius of the curved image surface discussed in Section 14.2 (and as

162 Chapter 14 Field Curvature and Field Flattener

illustrated in Figure 14.7)? We want to find R_P .

Along the principal ray shown in the figure, we first want to know the operator induced wavefront defocus, W_d , needed to null out the Petzval wavefront curvature, W_{220P} .

$$W = W_d y^2 + W_{220P} \bar{H}^2 y^2 = 0 \quad (14.8)$$

Therefore:

$$W_d = -W_{220P} \bar{H}^2 \quad (14.9)$$

Next, use is made of the focal shift equation obtained in Section 11.4:

$$\delta_d = 8(f/\#)^2 W_d \quad (14.10)$$

Substitute in Equation 14.9:

$$\delta = 8(f/\#)^2 \left[-W_{220P} \bar{H}^2 \right] \quad (14.11)$$

The last piece of the puzzle we need is the sag formula (Section 3.4). For the curved image surface:

$$\text{Sag}_P = \frac{1}{2} \left(\frac{(\bar{y})^2}{R_P} \right) \quad (14.12)$$

Now equate Equations 14.12 and 14.11:

$$\frac{1}{2} \left(\frac{(\bar{y})^2}{R_P} \right) = 8(f/\#)^2 \left[-W_{220P} \bar{H}^2 \right]$$

Solve this for R_P but first recall that $\bar{H} = \bar{y}/\hat{y}$ (where \hat{y} is the maximum image height):

$$R_P = - \left[\frac{\hat{y}^2}{16(f/\#)^2 W_{220P}} \right] \quad (14.13)$$

As an example, let's apply this result to the our standard silica singlet. Continuing the manual calculations (from Sections 10.3 and 13.3) using the PRTE we find:

a. f-number = 6.1326

b. $\hat{y} = 4.2923$ cm.

Inserting these values into Equation 14.13:

$$R_P = -71.536 \text{ cm.}$$

Section 14.7: Basic Theory of the Field Flattener 163

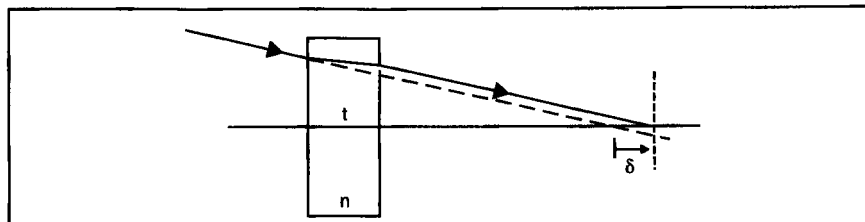


Fig 14.8 Focus shift introduced by a parallel plate in a converging beam.

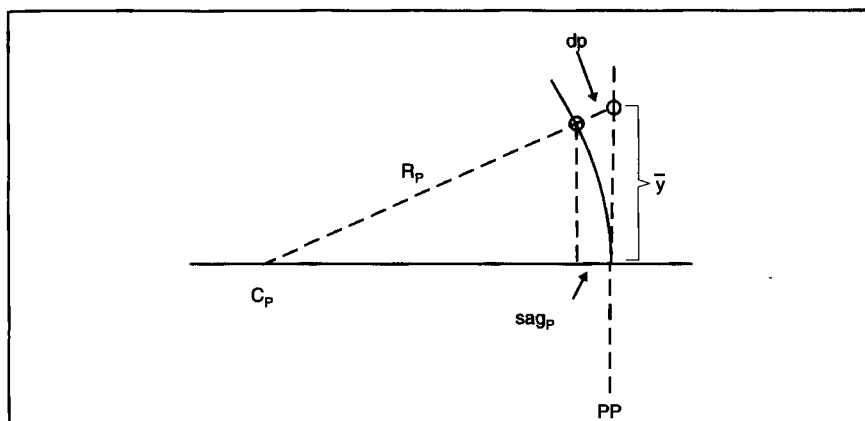


Fig 14.9 Petzval image surface and relevant parameters.

Note that this is essentially the “Petzval radius” value seen in Figure 14.6. Also, if we insert the PETC operand into the MFE, its value is the reciprocal of R_P .

14.7 Basic Theory of the Field Flattener

Given that:

- a. we have a lens with a curved image surface,
- b. most imaging sensors are flat, and
- c. the Petzval sum must be small for flat field applications;

what can be done to flatten Petzval curvature?

Consider a parallel plate in a converging beam as illustrated in Figure 14.8. Note that its effect is to shift the focus an amount δ away from the original focus position.

The equation describing the amount of axial shift will be derived later on (Section 23.4.1). For now we will just state the result:

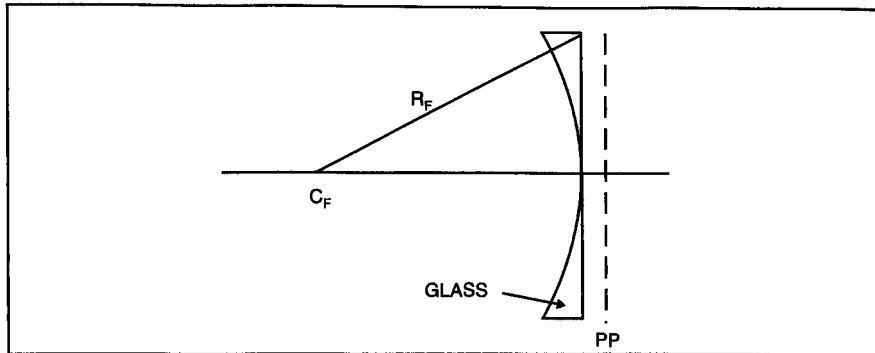


Fig 14.10 Idealistic field flattener.

$$\delta = \left(\frac{n-1}{n} \right) t \quad (14.14)$$

Solving for t :

$$t = \left(\frac{n}{n-1} \right) \delta \quad (14.15)$$

From Figure 14.9 we will make the approximation that $d_p \approx \text{Sag}_p$, where the latter is defined by Equation 14.12. Next, set the sag equal to a field dependent focus shift, that is:

$$\text{Sag}_p = \delta_p(\bar{y})$$

Now make use of Equation 14.15:

$$t(\bar{y}) = \left(\frac{n}{n-1} \right) \delta_p(\bar{y})$$

$$t(\bar{y}) = \left[\frac{n}{n-1} \right] \left[\frac{1}{2} \left(\frac{\bar{y}^2}{R_p} \right) \right] \quad (14.16)$$

This provides a variation in glass thickness as a function of paraxial image height. The idea is to introduce enough glass thickness to shift the local field focus back into the paraxial plane. This can be done with a thin concave-plano negative lens lying close to the image plane as shown in Figure 14.10. (Note: This is an idealistic lens since it has zero center thickness.)

What we need to find out now is the radius of curvature, R_F , of the concave side of the lens. This can be done by simply rearranging Equation 14.16.

Section 14.8: Homework 165

$$t(\bar{y}) = \frac{1}{2} \frac{(\bar{y})^2}{\left[(n-1) \frac{R_p}{n} \right]} \quad (14.17)$$

Equation 14.17 has the *look* of a sag equation provided the denominator is considered as a radius of curvature. In other words:

$$R_F = \left[\frac{(n-1)}{n} \right] R_p \quad (14.18)$$

In real life the simple field flattener discussed above does have a finite center thickness. However, it is only the thickness *difference* that plays a role in flattening the Petzval image field.

14.8 Homework

1. Manually calculate W_{220P} and R_p for the lens in the Homework for Chapter 1.
2. In ZEMAX, revisit SING1o1b from the Homework for Chapter 3 (page 28). Pull up the numbers on W_{220P} and R_p from the aberration table. Compare with manual calculation.
 - a. Manually design a field flattener using BK7 glass ($\lambda = 0.587 \mu\text{m}$).
 - b. Verify design by inserting it into ZEMAX. Let the center thickness of the flattener be 5 mm. Use "M" thickness solve to locate the paraxial image plane. (Should have about 1 mm separation.) Look at the "Petzval radius" value at the top of the aberration table. It should now be a very large number. Also, look at the PETC operand in the MFE. Its value should now be extremely small. (Note that the field flattener has hardly changed the astigmatism [ASTI], and that EFL $\neq 400$ mm.)
 - c. Now do the design over again using ZEMAX. Let ZEMAX find the necessary curvature on the front side of the flattener to make PETC in the MFE zero. Maintain the correct EFL.
 - d. Try using the FCUR operand as an alternative approach.

Chapter 15

Distortion

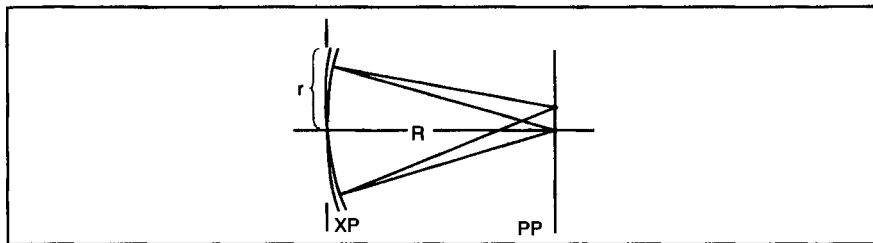


Fig. 15.1 Tilted spherical wavefronts.

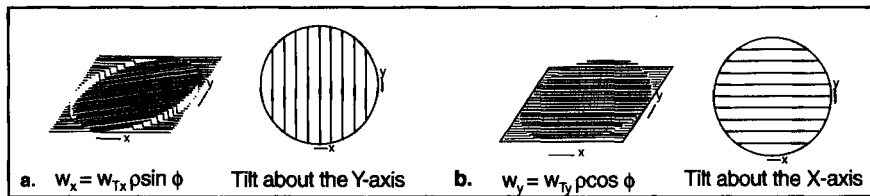


Fig. 15.2 Global wavefront tilt: a. about the y-axis; b. about the x-axis.

15.1 Introduction

This chapter will concentrate on the second aberration, which affects image point position rather than quality. Distortion is a *lateral* displacement of the image point from its ideal paraxial location. Low distortion is critical in lens systems requiring linearly scaled dimensional fidelity between object and image. Such systems include aerial mapping cameras, and micro-lithography cameras. We will examine distortion not only in the image plane but also in the exit pupil, and relate these quantitative results into the ZEMAX computations. But first we must introduce the concept of wavefront tilt and see how this is tied into an understanding of distortion.

15.2 Wavefront Tilt

In Section 11.4 we saw how two spherical wavefronts having different radii were related to generate a defocus offset, δ , in image space. In this section the two spherical wavefronts will have the *same* radius but differ in tilt as illustrated in

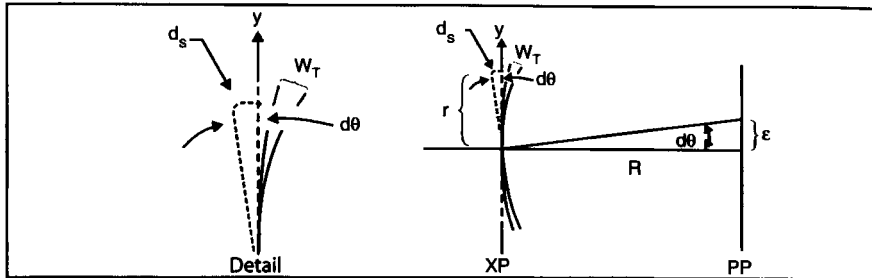


Fig. 15.3 Relating wavefront tilt to lateral displacement.

Figure 15.1. This will introduce a lateral offset in the image plane.

The mathematical description of two tilted wavefronts along either the x or y axes is shown in Figure 15.2 along with their respective OPD 3-D and contour maps.

Figure 15.3 will be used to help connect the lateral displacement in the image plane to the tilt between the two wavefronts in the exit pupil.

Tangents to both wavefront vertices are erected across the pupil aperture. Further, normals are erected to both vertices and carried out to the image plane. Note that the angle $d\theta$ separates both the tangents and the normals. The OPD at the pupil edge between the two wavefronts is given by W_T . This is essentially equal to the separation, d_s , between the tangents at the pupil edge, i.e.,

$$W_T = d_s \quad (15.1)$$

We also note that:

$$d\theta = \frac{d_s}{r} = \frac{W_T}{r} \quad (15.2)$$

In addition:

$$d\theta = \frac{\epsilon}{R} \quad (15.3)$$

Combining Equations 15.2 and 15.3:

$$W_T = \left(\frac{r}{R} \right) \epsilon \quad (15.4)$$

Equation 15.4 relates the wavefront tilt in the pupil to the lateral image displacement. We now have to generalize this a bit to account for small image displacements off-axis. This is illustrated in Figure 15.4.

Only the tangents and normals to the wavefronts are shown in Figure 15.4. Both wavefronts have a large off-axis tilt bias. Let the tilt bias for the reference

Section 15.3: Distortion 169

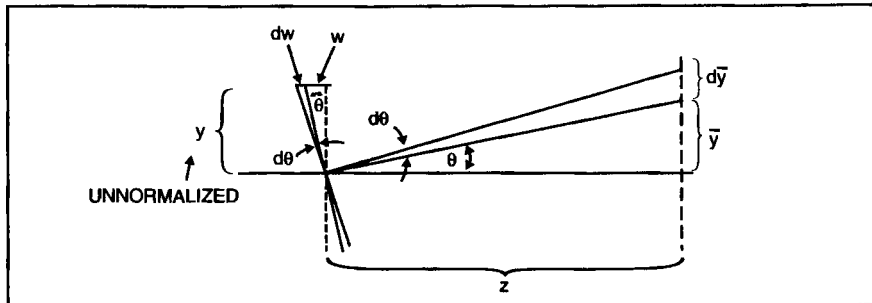


Fig. 15.4 Image displacement for an off-axis scenario.

wavefront be θ , and $(\theta + d\theta)$ for the actual wavefront. From the figure we see that:

$$\begin{aligned}\bar{y} &= z \tan \theta \\ w &= y \tan \theta\end{aligned}\tag{15.5}$$

Taking the derivatives of Equations 15.5:

$$\begin{aligned}d\bar{y} &= z \sec^2 \theta d\theta \\ dw &= y \sec^2 \theta d\theta\end{aligned}\tag{15.6}$$

Solving both for $\sec^2 \theta d\theta$ and equating:

$$\frac{d\bar{y}}{z} = \frac{dw}{y}\tag{15.7}$$

or

$$d\bar{y} = \left(\frac{z}{y} \right) dw\tag{15.8}$$

If we let $z = f$ and $y = d/2$ (where f is the focal length and d is the pupil diameter):

$$d\bar{y} = 2(f/\#)dw\tag{15.9}$$

So we see that the small lateral separation between image points is directly related to the system f-number and dw .

15.3 Distortion

The Seidel term describing wavefront distortion is given by:

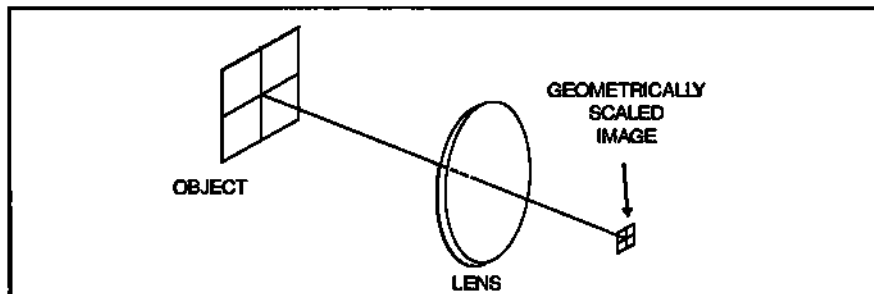


Fig. 15.5 Without distortion, image will be geometrically scaled version of object.

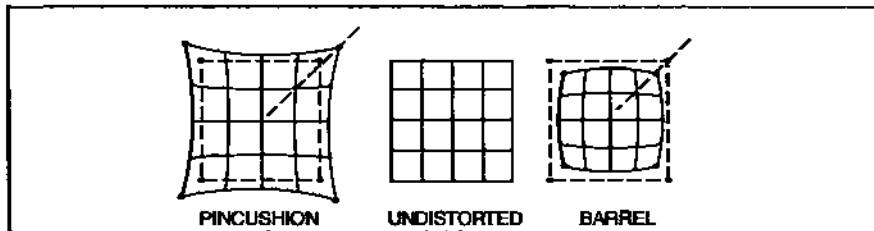


Fig. 15.6 With distortion, image will have either the barrel or pincushion form.

$$W_D = \left[W_{311} \bar{H}^3 \right] \rho \cos \theta \quad (15.10)$$

If we consider the factor in brackets as a “coefficient,” then Equation 15.10 looks exactly like the functional form for tilt. Since \bar{H} is part of this “coefficient,” *distortion can be considered as a field dependent tilt*. The angle $d\theta$ between the reference and aberrated wavefronts shown in Figure 15.4 increases as \bar{H} varies from zero to one.

We now apply Equation 11.31 to Equation 15.10, i.e.,

$$T = -\left(\frac{R}{r}\right) \frac{d}{d\rho}(W_D)$$

We will assume that $\phi = 0^\circ$. Therefore:

$$T = -\left(\frac{R}{r}\right) \left(W_{311} \bar{H}^3 \right) \quad (15.11)$$

Multiplying by $\frac{2}{2}$:

$$T = -\left(\frac{2R}{2r}\right) \left(W_{311} \bar{H}^3 \right) = -2(f/\#) \left(W_{311} \bar{H}^3 \right) \quad (15.12)$$

Equation 15.12 is identical to Equation 15.9 if we let $dw = -W_{311} \bar{H}^3$ and

Section 15.4: Example 171



Fig. 15.7 A simple unsymmetrical lens to illustrate distortion.

Real Ray Trace Data:

Surf	X-coord	Y-coord	Z-coord	X-tangent	Y-tangent
OBJ	Infinity	Infinity	Infinity	0.000000	0.0874887
1	0.000000E+000	-4.374433E+000	0.000000E+000	0.000000	0.0874887
2	0.000000E+000	0.000000E+000	0.000000E+000	0.000000	0.0874887
3	0.000000E+000	1.326955E+001	1.101526E-001	0.000000	0.0518523
4	0.000000E+000	1.386808E+001	-3.468421E-001	0.000000	0.0527831
5	0.000000E+000	[3.475958E+001]	0.000000E+000	0.000000	0.0527831

Paraxial Ray Trace Data:

Surf	X-coord	Y-coord	Z-coord	X-tangent	Y-tangent
OBJ	Infinity	Infinity	Infinity	0.000000	0.0874887
1	0.000000E+000	-4.374433E+000	0.000000E+000	0.000000	0.0874887
2	0.000000E+000	0.000000E+000	0.000000E+000	0.000000	0.0874887
3	0.000000E+000	1.325991E+001	0.000000E+000	0.000000	0.0520265
4	0.000000E+000	1.388423E+001	0.000000E+000	0.000000	0.0538495
5	0.000000E+000	[3.486274E+001]	0.000000E+000	0.000000	0.0538495

Fig. 15.8 Real and paraxial chief ray trace data.

$d\bar{y} = T$. Given the wavefront distortion coefficient W_{311} and f-number, T will vary in cubic fashion as H varies from 0 → 1. (Note that W_{311} can be determined from the Seidel coefficient S_y in Table 10.1.) For example, if a uniform grid object is imaged by an ideal lens, then the image will simply be a geometrically scaled version of the object as illustrated in Figure 15.5. However, if the lens suffers from distortion, then we get the familiar barrel and pincushion forms (depending on the sign of W_{311}) shown in Figure 15.6.

15.4 Example

As we saw with the perisopic lens (Chapter 12), a symmetric system at unit magnification has no distortion. To see a lot of distortion, an unsymmetric system like the one shown in Figure 15.7 can be used for illustrative purposes. This is a 400 mm f/10 BK7 lens operating in d-light. The stop is located 151.56 mm in front of the lens. Radii are 799.31 and -277.42 mm respectively. The lens is 12 mm thick.

As can be seen from Table 10.1, S_y is a bit messy to calculate manually so we'll let ZEMAX compute W_{311} using a chief ray angle of 5°. This turns out to be +8.86λ. Inserting the appropriate values into Equation 15.12 with $\bar{H} = 1$:

$$T = -2(10)(5.2\mu\text{m}) = -104 \mu\text{m} \quad (15.13)$$

Distortion in the image plane appears when the real chief ray picrce in the

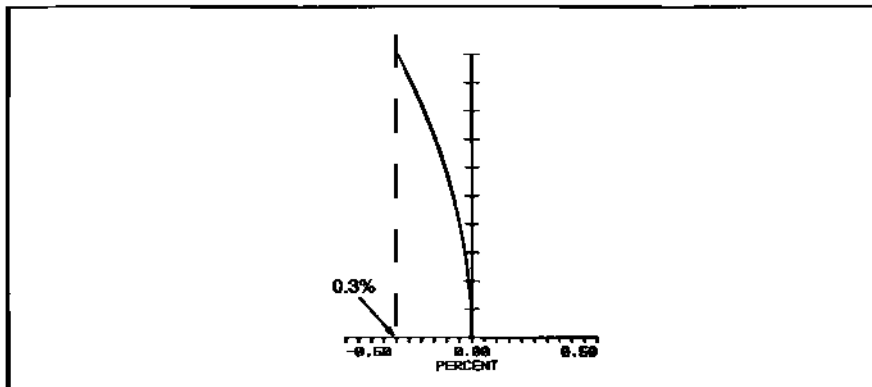


Fig. 15.9 Distortion plot.

paraxial image plane is different from that of the paraxial (or ideal) chief ray pierce. Data for the ZEMAX trace of the chief ray for our example is shown in Figure 15.8.

In particular, note the values on "line 5" under the "Y-coord" column for the real and paraxial rays. Taking their difference:

$$\bar{y}_{5r} - \bar{y}_{5p} = 34.75958 \text{ mm} - 34.86247 \text{ mm} = -0.10316 \text{ mm}$$

$$\Delta\bar{y}_{5r} = -103.2 \mu\text{m} \quad (15.14)$$

This is essentially the value shown in Equation 15.13.

A ZEMAX plot of distortion is shown in Figure 15.9. It is plotted as a percentage vs. field angle. In general, as the field angle increases, the percent distortion increases. But where does this percentage come from? How is it calculated?

Percent distortion is defined as:

$$D = \left(\frac{\bar{y}_r - \bar{y}_p}{\bar{y}_p} \right) \cdot 100\% \quad (15.15)$$

Using the example ray trace data:

$$D = \left(\frac{-0.1032}{34.86274} \right) \cdot 100\% = -0.296\% \approx -0.3\% \quad (15.16)$$

This is the value of the distortion at the field edge seen in the plot.

Next, we call up the MFE, making sure that the operand DIST is included. The MFE is shown in Figure 15.10.

Note the value of DIST. It is what we just calculated using Equation 15.15.

Section 15.5: Discussion 173

Merit Function Value: 8.00000000E+000										
Num	Type	Int1	Int2	Ix	Iy	Px	Py	Target	Weight	Value
1	EFFL		1					8.00000E+000	0	4.00000E+002
2	SPRA	0	1					8.00000E+000	0	2.88113E+000
3	COMA	0	1					8.00000E+000	0	-2.55253E-002
4	ASTI	0	1					8.00000E+000	0	1.84398E+000
5	DIST	0	1					8.00000E+000	0	-2.95911E-001
6	PETC		1					8.00000E+000	0	-1.65446E-003

Fig. 15.10 MFE for example.

Table 15.1
List of Sixth-Order Aberrations

1	$W_{600} \bar{H}^6$	PISTON (5th)
2	$W_{600} p^6$	SAS
3	$W_{242} \bar{H}^2 p^4 \cos^2 \phi$	Tangential Oblique Spherical Aberration
4	$W_{240} \bar{H}^2 p^4$	Sagittal Oblique Spherical Aberration
5	$W_{151} \bar{H} p^5 \cos \phi$	CMA5
6	$W_{311} \bar{H}^5 p \cos \phi$	DISTS
7	$W_{620} \bar{H}^4 p^2$	FLDCV5
8	$W_{422} \bar{H}^4 p^2 \cos^2 \phi$	ASTG5
9	$W_{331} \bar{H}^3 p^3 \cos \phi$	5 th Elliptical (cubic) Coma
10	$W_{333} \bar{H}^3 p^3 \cos^3 \phi$	5 th Linear Coma

15.5 Discussion

This chapter on distortion brings to a close a series of discussions on the Seidel (primary) monochromatic aberrations which began with an overview in Chapter 7 and continued in more detail through Chapters 10 and 11 (spherical aberration), Chapter 13 (coma and astigmatism), and Chapter 14 (Petzval curvature). We saw how to calculate the respective coefficients in the pupil, and connected these to behavior in the image plane. We also related and compared these computations to various ZEMAX analysis outputs. But as Equation 7.3 indicates, the aberration polynomial is an infinite series of terms. Our discussions have focused on the fourth order terms. In design problems, it is rarely worthwhile to drive these fourth order aberrations to zero because this leaves higher order terms unchecked. When TRAC is used to correct spherical, for example, it tries to balance *all* orders of that aberration. This results in a smaller overall RMS spot size. The next higher order aberrations are the sixth order and are shown (for information purposes only) in Table 15.1. (Note: no information is provided on the computation of the coefficients as was done for the fourth order in Table 10.1.)

Chapter 16

Axial Color and Achromats

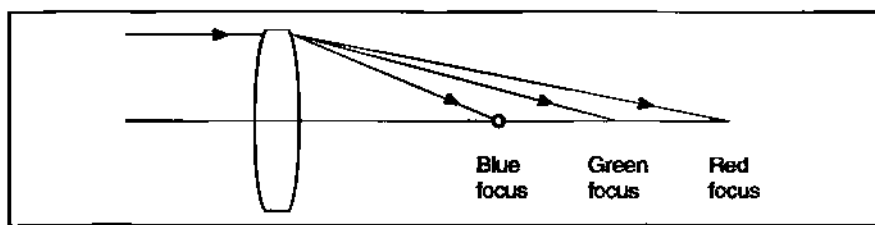


Fig. 16.1 Dispersion in a lens.

16.1 Introduction

In previous chapters our world was monochrome. Now, welcome to the wonderful world of color. For us, however, this adds another level of complexity to the design problem.

The problem is illustrated in Figure 16.1 for a singlet. Because the refractive index of glass varies as a function of wavelength, the lens focal length varies as a function of color. If we place our recording plane at the green focus, for example, the red and blue beams will have big blur circles and resolution will be greatly reduced. It is reported that Newton thought this to be an intractable problem for refractors. So he went off and invented the Newtonian reflective telescope.

In this chapter we will derive an equation for primary axial color which gives the actual separation between the red and blue foci seen in Figure 16.1. We will then discuss the solution to the problem—the achromat—and learn how to design it.

(*Suggestion:* This would be a good time to review the material on glass properties discussed in Section 6.2.)

16.2 Primary Axial Color

We saw in Section 4.6.3 that the power of a thin lens is given by:

$$\phi = (n - 1)(C_1 - C_2) \quad (16.1)$$

By taking the derivative of Equation 16.1, the change in power as a function of index can be obtained:

176 Chapter 16 Axial Color and Achromats

$$d\phi = (C_1 - C_2)dn \quad (16.2)$$

Now let $dn = n_F - n_C$, and insert into Equation 16.2.

$$d\phi = (C_1 - C_2)(n_F - n_C) \quad (16.3)$$

Multiply Equation 16.3 by $(n_d - 1)/(n_d - 1)$:

$$d\phi = (C_1 - C_2)(n_F - n_C) \left[\frac{n_d - 1}{n_d - 1} \right]$$

Rearrange:

$$d\phi = [(C_1 - C_2)(n_d - 1)] \left[\frac{n_F - n_C}{n_d - 1} \right] \quad (16.4)$$

Rewrite:

$$d\phi = \frac{\Phi_d}{v_d} = (\phi_F - \phi_C) \quad (16.5)$$

So we see that the power difference is equal to the power in d -light divided by the Abbe number.

This can be rewritten as:

$$\frac{d\phi}{\Phi_d} = \frac{1}{v_d} \quad (16.6)$$

Equation 16.6 will have more significance if it is reinterpreted in terms of focus. Recall that:

$$\phi = \frac{1}{f} \quad (16.7)$$

Taking the derivative:

$$d\phi = \left(\frac{-1}{f^2} \right) df \quad (16.8)$$

Dividing Equation 16.8 by Equation 16.7:

$$\frac{d\phi}{\phi} = \frac{-df}{f} \quad (16.9)$$

Substituting this into Equation 16.6 and rearranging:

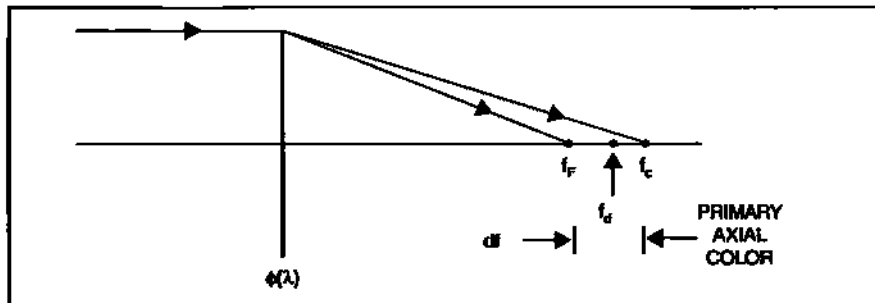


Fig. 16.2 Primary axial color.

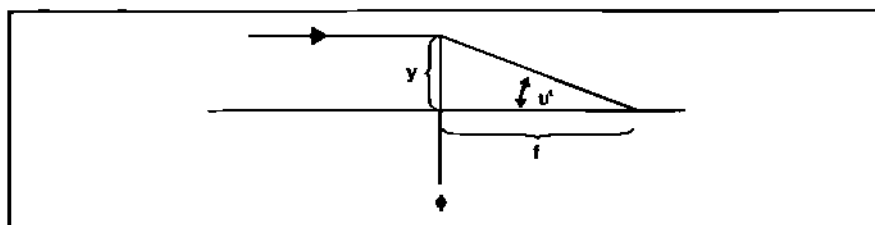


Fig. 16.3 Marginal ray and thin lens.

$$\frac{f_d}{df} = v_d \quad (16.10)$$

As illustrated in Figure 16.2, the ratio of the focal length in d -light to primary axial color is equal to the Abbe number. Equation 16.10 relates the Abbe number to something quite physical.

16.3 Derivation of C_L

We will now find another form for df that incorporates the marginal ray height and angle. This is a form which will be useful in the formulation of the wavefront aberration for color. Please refer to Figure 16.3.

Equate Equation 16.8 with Equation 16.6:

$$\left(\frac{1}{f^2} \right) df = -\frac{\phi_d}{v_d} \quad (16.11)$$

Multiply both sides by y^2 :

$$\left(\frac{y^2}{f^2} \right) df = -\frac{y^2 \phi_d}{v_d} \quad (16.12)$$

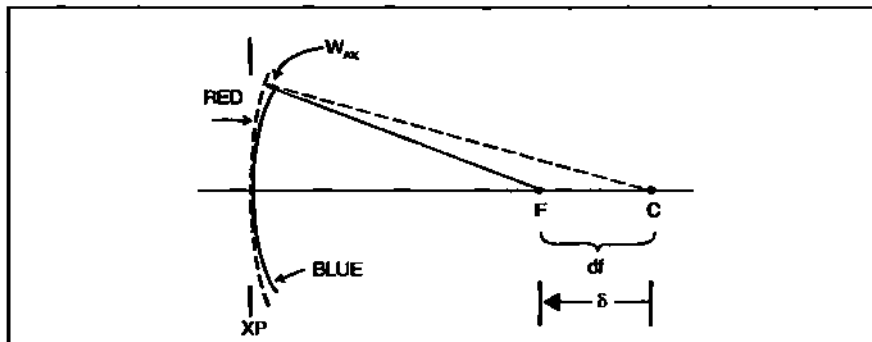


Fig. 16.4 Two spherical wavefronts of different color.

From Figure 16.3, $u' = y/f$. Therefore:

$$df = \left(\frac{1}{u'} \right)^2 \left(\frac{y^2 \phi_d}{v_d} \right) = \left(\frac{1}{u'} \right)^2 C_L \quad (16.13)$$

where C_L is defined by:

$$C_L = \frac{-y^2 \phi_d}{v_d} \quad (16.14)$$

16.4 The Wavefront Color Aberration W_{ax}

In Section 11.4 we developed a formalism which connected an OPD (W_{020}) in the exit pupil to an axial displacement in image space for two spherical wavefronts having slightly different radii of curvatures. We will make use of that formalism here, only this time the two wavefronts will be of different colors as illustrated in Figure 16.4.

The defocus equation from Section 11.4 is given by: $\delta = -8(f/\#)^2 W_{ax}$ (where W_{020} has been set equal to $-W_{ax}$). Next, equate this expression to Equation 16.13:

$$8(f/\#)^2 W_{ax} = \left(\frac{1}{u'} \right)^2 C_L \quad (16.15)$$

$$\text{But } f/\# = \frac{-1}{2(u')} :$$

$$8(f/\#)^2 W_{ax} = 4(f/\#)^2 C_L \quad (16.16)$$

Therefore:

Section 16.4: The Wavefront Color Aberration W_{ax} 179

Seidel Aberration Coefficients:

Surf	SPHA	S1	COMA	S2	ASTI	S3	FCUR	S4	DIST	S5	CLA (CL)	CTR (CT)
ST0	0.00051	0.00092	0.00166	0.00252	0.00757	-0.00514	-0.00929					
2	0.00757	-0.00674	0.00599	0.00252	-0.00757	-0.01845	0.00929					
IMA	0.00000	0.00000	0.00000	0.00000	0.00000	0.00000	0.00000	0.00000	0.00000	0.00000	0.00000	0.00000
TOT	0.00000	-0.00582	0.00765	0.00505	0.00000	-0.01558						

Longitudinal Aberration Coefficients:

Surf	LSPH	LAST	LFCP	LFCS	LFCT	LAXC
ST0	0.61712	4.03706	3.06171	5.00024	9.11730	-12.46740
2	1.51487	2.39632	0.50463	1.70279	4.09911	-4.17882
IMA	0.00000	0.00000	0.00000	0.00000	0.00000	0.00000
TOT	1.61659	3.06171	1.00926	2.54012	5.60182	-6.23370

Fig. 16.5 Aberration table containing data on color.

Merit Function Value: 6.614843×10^{-1}

Num	Type	Int1	Int2	Hx	Hy	Px	Py	Target	Weight	Value	% Cont
1	EFFL		2					400	1	400.6615	100.000
2	AXCL							0	0	[6.1943]	0.000

Fig. 16.6 Primary axial color as it shows up in the MFE.

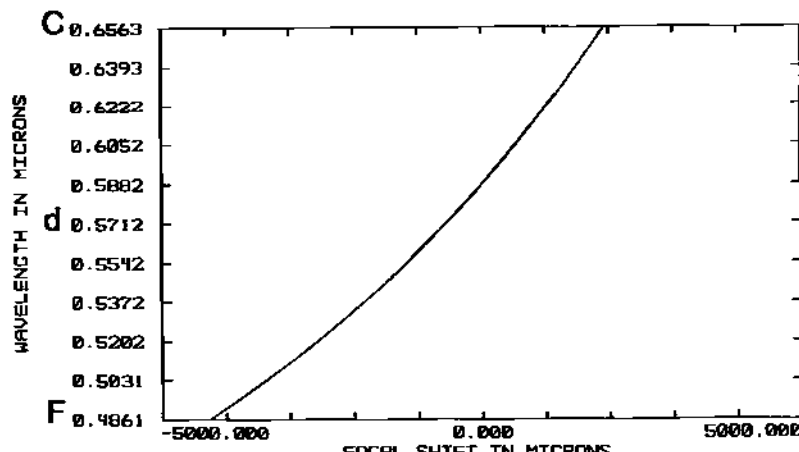


Fig. 16.7 ZEMAX plot of axial color.

$$W_{ax} = \frac{1}{2} C_L \quad (16.17)$$

Example: Let $f_d = 400$ mm and $y = 20$ mm. Let the glass be BK7 ($v_d = 64.17$).

$$C_L = -\left(\frac{0.0025}{64.17}\right)(20)^2 = -0.015584 \text{ mm}$$

$$W_{ax} = -0.007792 \text{ mm} = -7.792 \mu\text{m}$$

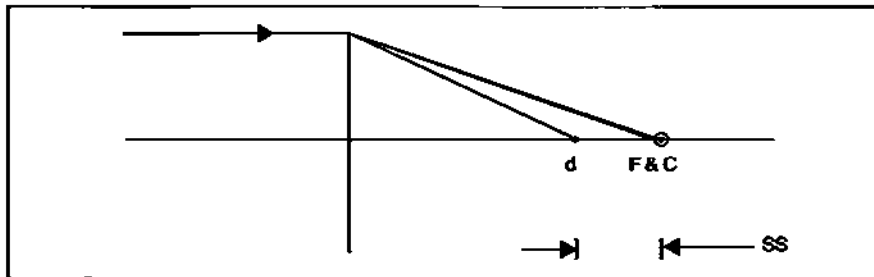


Fig. 16.8 Function of a thin lens achromat.

$$\delta_{ax} = -6.2336 \text{ mm}$$

$$-\left(\frac{f}{df}\right) = -\left(\frac{f}{\delta_{ax}}\right) = \frac{-400}{-6.2336} = 64.17 \text{ (the Abbe number)}$$

Modeling the above lens (SING101b) in ZEMAX generates the Seidel aberration data shown in Figure 16.5. Note the values under the column headings CLA (CL) and LAXC, which correspond to C_L and δ_{ax} given above. The slight differences are due to finite lens thickness.

The value of δ_{ax} can also be found in the MFE from the AXCL operand as shown in Figure 16.6, (which is the *M-solve* difference between *C* and *F* paraxial foci).

Of course the most dramatic way of presenting color data is the axial color plot accessed via: Analysis → Miscellaneous → Chromatic Focal Shift. The plot is shown in Figure 16.7. Note that the axial range between *F* and *C* light is simply δ_{ax} .

16.5 The Achromat

The achromat is a *doublet* consisting of two glasses with quite different refractive indices and dispersions. Its purpose is to counteract the deleterious effects of primary axial color by bringing *F* and *C* light to a common focus. For our pre-design we will consider two thin lenses in contact as shown in Figure 16.8.

16.5.1 Constraints

There are two constraints on achromat design. The first is that the doublet has the same power as the singlet.

$$\text{Constraint 1: } \phi = \phi_a + \phi_b \quad (16.18)$$

To obtain the second constraint, start by taking the derivative of Equation 16.18:

$$d\phi = d\phi_a + d\phi_b$$

Substituting in Equation 16.6:

$$d\phi = \frac{\phi_a}{v_a} + \frac{\phi_b}{v_b} \quad (16.19)$$

By setting $d\phi = 0$, we force F and C light together. Therefore the second constraint is written as:

$$\text{Constraint 2: } \frac{\phi_a}{v_a} + \frac{\phi_b}{v_b} = 0 \quad (16.20)$$

16.5.2 Achromat Powers

The purpose of the constraints is to allow the determination of the powers of the two lenses. First, solve Equations 16.18 and 16.20 for ϕ_b :

$$\begin{aligned} \phi_b &= \phi - \phi_a \\ \phi_b &= -\frac{v_b}{v_a} \phi_a \end{aligned} \quad (16.21)$$

Now equate these two expressions for ϕ_b :

$$\phi - \phi_a = -\frac{v_b}{v_a} \phi_a \quad (16.22)$$

Solve Equation 16.22 for ϕ_a :

$$\begin{aligned} \phi_a &= \left(\frac{v_a}{v_a - v_b} \right) \phi \\ \phi_a &= \left(\frac{v_a}{\Delta v} \right) \phi \\ \text{Similarly, } \phi_b &= -\left(\frac{v_b}{\Delta v} \right) \phi \end{aligned} \quad (16.23)$$

16.5.3 Achromat Example

Suppose we do a thin lens pre-design of an achromat having a system focal length of 400 mm ($\phi = 0.0025$). We'll use BK7 (Table 6.3 on page 57) and SF2 (Table 16.1 on page 183) having Abbe numbers of 64.17 and 33.85, respectively. Inserting this information into Equations 16.23, we find that:

$$\phi_a = 0.005291 \text{ and } \phi_b = -0.002791.$$

A quick check (using the first constant) shows that the sum of these powers is 0.0025, which is what we want.

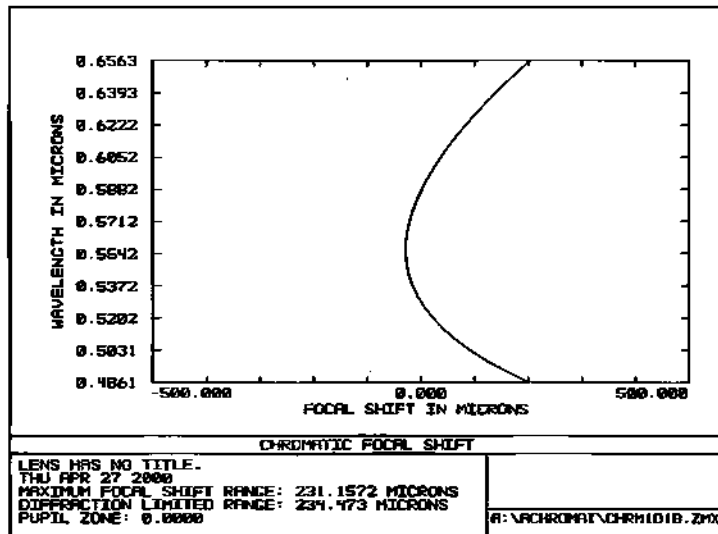


Fig. 16.9 Axial color for thin lens achromat.

Assuming that the positive lens is *equiconvex*, the radii can be found using Equation 4.22. These turn out to be $R_1 = 195.3506 = -R_2 = -R_3$, and $R_4 = -1234.7107$. Next, we insert these radii into ZEMAX with *zero* lens thicknesses. In the MFE, EFL is 399.992 mm and AXCL is 0.000233 mm, an extremely small number, essentially zero. The resulting axial color plot is shown in Figure 16.9. We can also verify that we have the right lens focal lengths (powers) by using EFLY for each lens (but incorporate a minuscule airspace between the two lenses). ZEMAX yields the following focal lengths: $f_a = 189$ mm and $f_b = -358.3$.

16.6 Homework

Manually calculate the powers, focal lengths, and radii for a 10-inch EFL $f/5$ achromat. Use the F, d, C spectrum. Use BK7 and SF2 Schott glasses. (Index and dispersion values can also be found by clicking on the “GLA” button and looking up the Schott catalog.)

Insert the thin lens (zero thickness) into ZEMAX and verify the calculated powers, the EFL, and the color correction.

Section 16.6: Homework 183

Table 16.1
SF2 Information

Note: Schott has replaced SF2 with N-SF2 but SF2 is still listed in ZEMAX glass library.

			$v_d = 33.85$		Internal Transmittance, T_i		
Refractive Indices		λ [nm]	Relative Partial Dispersion		λ [nm]	T_i (5 mm)	T_i (25 mm)
$n_{2325.4}$	2325.4	1.61008	$P_{s,t}$	0.2231	2325.4	0.94	0.74
$n_{1970.1}$	1970.1	1.61497	$P_{c,s}$	0.4806	1970.1	0.979	0.90
$n_{1529.6}$	1529.6	1.62058	$P_{d,C}$	0.2922	1529.6	0.999	0.994
$n_{1060.0}$	1060.0	1.62768	$P_{e,d}$	0.2367	1060.0	0.999	0.998
n_s	1014.0	1.62863	$P_{g,F}$	0.5885	700	0.999	0.999
n_c	852.1	1.63290	$P_{i,h}$	0.9384	660	0.999	0.998
n_d	706.5	1.63902	$P_{F,d}$	0.7076	620	0.999	0.998
n_e	656.3	1.64210	$P'_{s,t}$	0.2199	580	0.999	0.998
n_g	643.8	1.64297	$P'_{c,s}$	0.5189	546.1	0.999	0.998
$n_{632.8}$	632.8	1.64379	$P'_{d,C}$	0.2430	500	0.999	0.997
n_{D_1}	589.3	1.64752	$P'_{e,d}$	0.2334	460	0.998	0.992
n_j	587.6	1.64769	$P'_{g,F}$	0.5208	435.8	0.997	0.986
n_r	546.1	1.65222	$P'_{i,h}$	0.9250	420	0.997	0.983
n_F	486.1	1.66123	Constants of Dispersion Formula		404.7	0.995	0.973
$n_{F'}$	480.0	1.66238	A_0	2.6361862	400	0.994	0.970
n_g	435.8	1.67249	A_1	$-9.0087536 \cdot 10^{-3}$	390	0.989	0.948
n_h	404.7	1.68233	A_2	$2.5179779 \cdot 10^{-2}$	380	0.979	0.90
n_i	365.0	1.70029	A_3	$1.1171914 \cdot 10^{-3}$	370	0.965	0.84
			A_4	$-4.0112089 \cdot 10^{-5}$	365.0	0.954	0.79
			A_5	$6.6254840 \cdot 10^{-6}$	350	0.87	0.5
					334.1	0.49	0.03
					320	0.01	
					310		
					300		
					290		
					280		
			Deviation of Relative Partial Dispersion ΔP from the "Normal Line"		Temperature Coefficients of Refractive Index		
			$\Delta P_{c,t}$	-0.0019	$\Delta n / \Delta T_{\text{relative}}$ [$10^{-6}/\text{K}$]	$\Delta n / \Delta T_{\text{absolute}}$ [$10^{-6}/\text{K}$]	
			$\Delta P_{c,d}$	-0.0012	[°C]	1060.0	s C' e g
			$\Delta P_{F,d}$	0.0004	-40/-20	3.1	3.4 4.2 4.9 7.3 1.7 2.0 2.7 3.5 5.8
			$\Delta P_{g,F}$	0.0017	-20/ 0	3.1	3.4 4.2 4.9 7.3 1.9 2.2 2.9 3.7 6.1
			$\Delta P_{i,h}$	0.0122	0/+20	3.1	3.4 4.2 4.9 7.3 2.0 2.3 3.0 3.8 6.2
					+20/+40		
					+40/+60		
					+60/+80		

Chapter 17

Bending Achromats

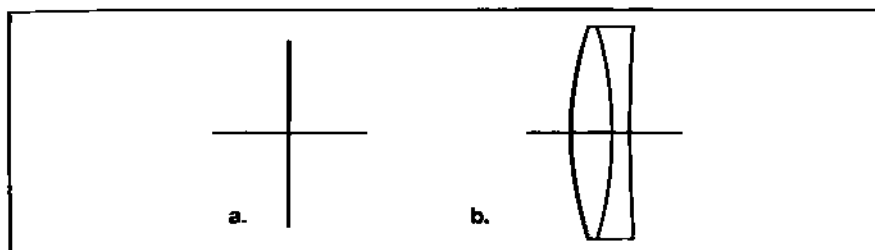


Fig. 17.1 Difference between a thin lens achromat (a); and a real achromat (b).

17.1 Introduction

The achromat designed in the Homework for Chapter 16 on page 182 is based on a thin lens approximation; i.e., this lens has no thickness (as per Figure 17.1a). A real achromat, one that would be designed in ZEMAX, has a finite thickness (as per Figure 17.1b). In this chapter we'll design a real achromat from the thin lens pre-design. We will also re-employ "lens bending" and see what happens to spherical aberration, coma, and astigmatism. We will also introduce another chromatic effect, called "lateral color."

17.2 Achromats in ZEMAX

Return to the design example in Section 16.5.3 (page 181). Insert this information into ZEMAX along with reasonable thicknesses for the lenses (e.g., 5 mm and 2 mm respectively), a minuscule airspace (e.g., 0.0001 mm), and an EPD of 40. Call this CHRM1o1b. Click on the SYS button. Note that the focal length is *not* 400. Go to Analysis → Miscellaneous → Chromatic Focal Shift. (Note: values under "settings" for "MAX SHIFT" and "PUPIL ZONE" are zero.) The plot shown in Figure 17.2 indicates that our axial color is off because the *F* and *C* foci do not coincide.

Our lens will have to be optimized to take into account the real thicknesses of the two elements. To do this, set variables on the first, second, and fourth radii. Slave the third radius to the second (using Pickup). In the MFE, use operands EFFL and AXCL set to targets of 400 and 0 respectively and weights of 1.

186 Chapter 17 Bending Achromats

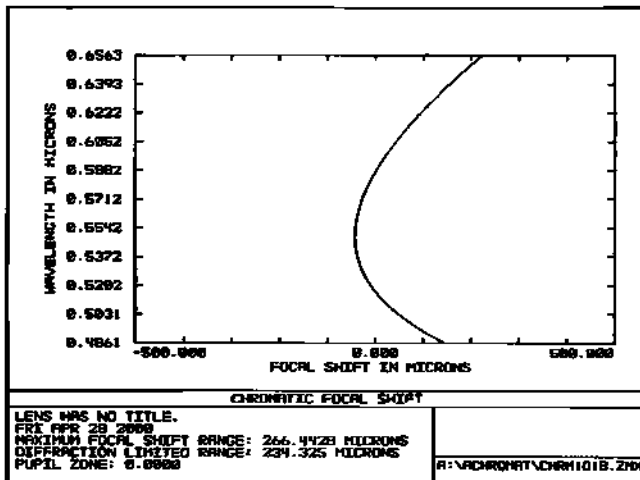


Fig. 17.2 Axial color for sample achromat after inserting finite glass thicknesses.

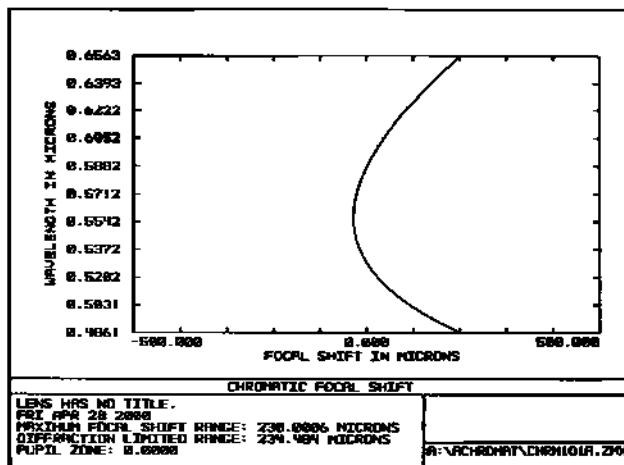


Fig. 17.3 Axial color of sample achromat after optimization.

Now run the optimization:

CHRM101b → Optimize → CHRM101a

After the optimization, the axial color plot shows proper correction as indicated in Figure 17.3. The curve has a quadratic appearance, and *F* and *C* foci are coincident. (Note: The separation between this common focus and the d-light focus is called "secondary spectrum.") Returning to SYS, the focal length is now 400.

The focal lengths for the components of the *thin* lens achromat calculated in

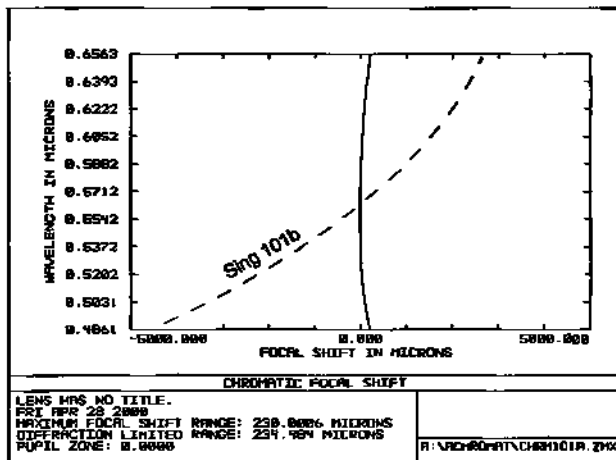


Fig. 17.4 Axial color for a singlet and achromat having the same power.

the Section 16.5.3 were $f_a = 189$ mm and $f_b = -358.3$ mm respectively. These will be slightly different for the optimized achromat with finite thickness. To see what the new component focal lengths are, use the operand EFLY. Use this operand twice—once for each element. Since this is for informational purposes only, set the weight to zero on both. It is at this point that the minuscule airspace comes into play. Why? Because the powers initially calculated via Equation 16.23 are for elements having air on both sides. (This minute airspace will not have any impact on performance *but should be removed when the design is finalized.*) The focal lengths for CHRM101a are now 188.62 and -354.24 respectively.

The improvement in axial color is shown in Figure 17.4. Note that the change is dramatic. The axial separation between F and d light is ~0.2 mm.

17.3 Achromat Bending and Seidel Spherical Aberration

Back in the Homework for Chapter 3, Parts 3 and 7, ZEMAX was used to minimize Seidel spherical aberration by “bending” the lens without changing its power. In Section 11.3, bending was examined in an analytical fashion via the behavior of the structural aberration coefficient σ_1 . This was an offset parabolic function (Figure 11.2) whose minimum value never quite made it to zero. Hence for a singlet, the best bending always leaves some finite value for W_{040} . In the homework just mentioned this was about 1λ .

An achromat can be bent just like a singlet. This means that the system power is maintained during the bending. Color correction is also maintained since this depends only on the power of the individual elements. A generic bending plot is illustrated in Figure 17.5 where W_{040} is plotted against the *curvature of the first surface of the achromat*. This is for an object at infinity. Note that the bending has

188 Chapter 17 Bending Achromats

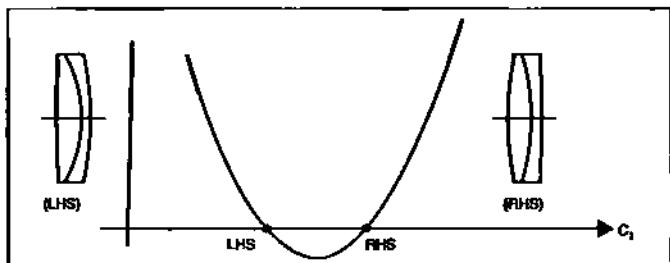


Fig. 17.5 Generic bending of achromat showing effect on spherical aberration.

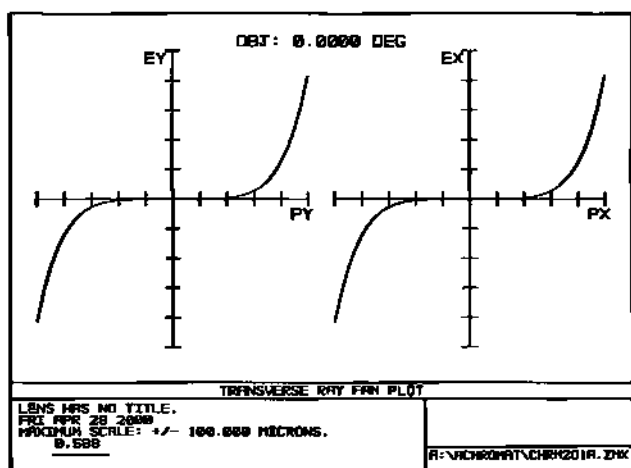


Fig. 17.6 Achromat exhibiting mainly fifth order spherical.

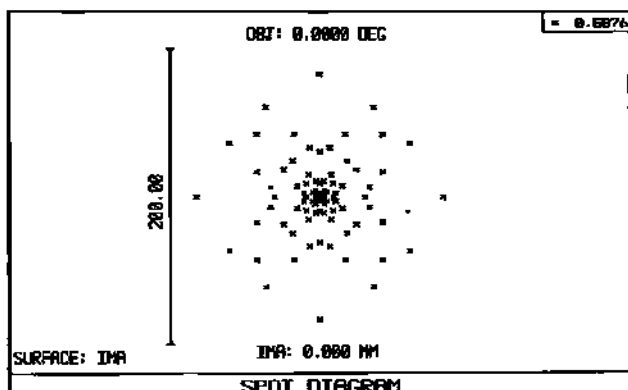


Fig. 17.7 Spot diagram for the f/3.3 achromat.

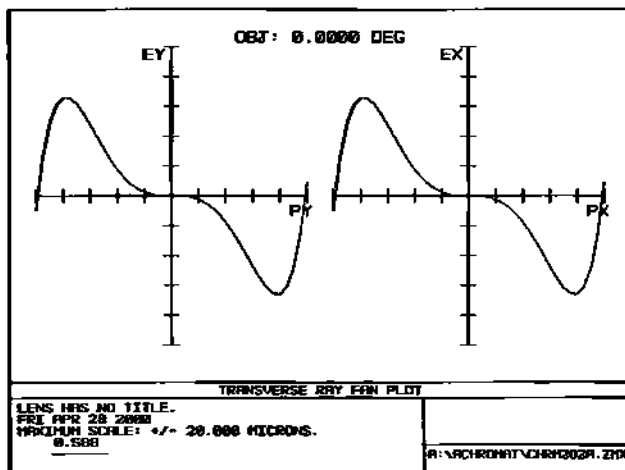


Fig. 17.8 Ray fan plot in which spherical aberration orders are balanced.

eliminated Seidel spherical completely—not just once but twice.

The right-hand zero solution is easily attained in ZEMAX by adding SPHA to the MFE for CHRM101a and setting its target value (with weight 1) equal to zero. The left-hand solution is a bit harder. You have to get close enough to it to begin with so that the optimization settles onto that solution; otherwise, ZEMAX will return you to the right-hand solution. One method is to change R_1 manually. Optimize the system *without* a variable on R_1 (with just EFFL and AXCL active). Monitor the value of SPHA. Continue by changing R_1 incrementally (based on an incremental change in C_1). You can actually plot out a curve similar to that shown in Figure 17.5. When SPHA gets small enough on the left side of this curve, reinstate the variable on R_1 , reactivate SPHA, and run the optimization. It will settle on the left-hand zero solution.¹

17.4 Higher Order Spherical

Figure 17.6 shows the ray fan plot for a right-hand solution in *d*-light for a 100 mm *f*/3.3 achromat. This is a much faster achromat than the *f*/10 we have been using. Although third order spherical has been zeroed out, the ray fan plot is not flat as might have been expected. What you are seeing is mostly the effect of fifth order spherical aberration. (The plot is a fifth order curve.)

The amount of fifth order is significant (because of the lower *f*-number) as can be seen by the spot diagram in Figure 17.7. It is by no means diffraction limited.

¹ Note: Effect of glass choice see: Kortes, H.D. and Hopkins, R.E., "Some Effects of Glass Choice in Telescope Doublets," JOSA, Vol. 49, No. 9, page 869 (1959).

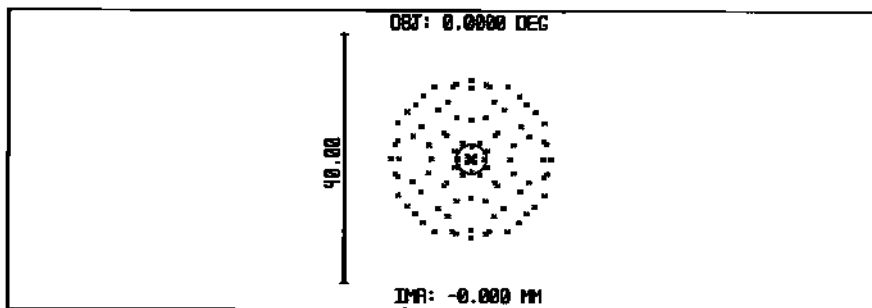


Fig. 17.9 Spot diagram after balanced optimization using TRAC.

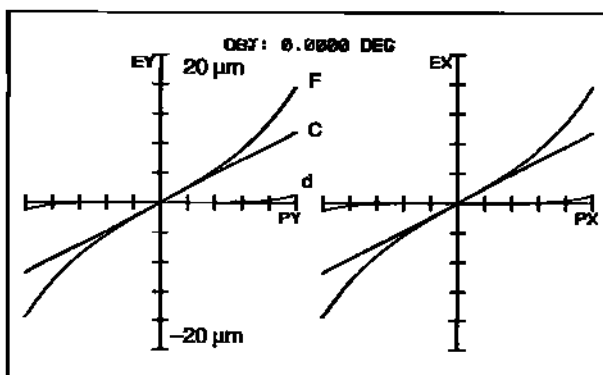


Fig. 17.10 Spherical aberration is color dependent.

The presence of higher order spherical is the main reason that TRAC should be used instead of SPHA in the optimization. TRAC retains some third order so as to *balance* fifth and seventh order. This results in a flatter ray fan plot as shown in Figure 17.8.

Now when we look at the spot diagram in *d*-light (Figure 17.9) the improvement is obvious. The relative size of the Airy disk (the circle on the plot) can be easily seen. It is not a tiny dot in the center of the pattern as it was in Figure 17.7.

17.5 Spherochromatism

Despite the fact that we are dealing with achromats, the right and left hand zero solutions for third order spherical aberration are valid for only one color. (If the standard visible spectrum is called up in ZEMAX, this color will be *d*-light. It will be accented as the "primary" color in the right-most column. You do have the freedom to select any color as the primary, but be aware that all numerical calculations are displayed only for the primary color.) This is dramatically illustrated by the three color ray fan plot (for the *f*/10 achromat) in Figure 17.10. The *d*-light plot is lying flat on the *x*-axis. This means we are at the *d*-light paraxial focal plane. There is a little bit of curl toward the edge of the pupil due to fifth order. The *F* and *C*-

Section 17.6: Achromat Bending and Coma and Astigmatism 191

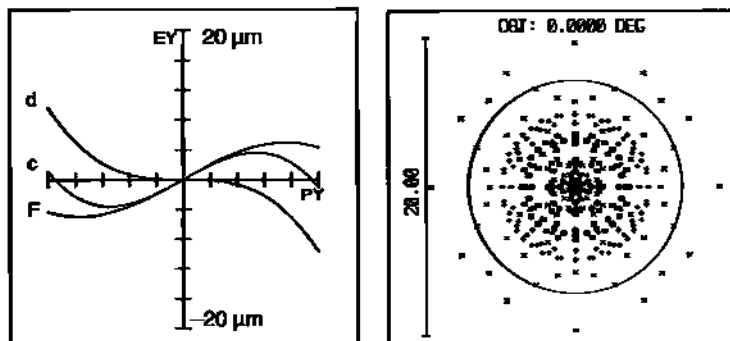


Fig. 17.11 An f/10 achromat optimized for color and spherical using TRAC.

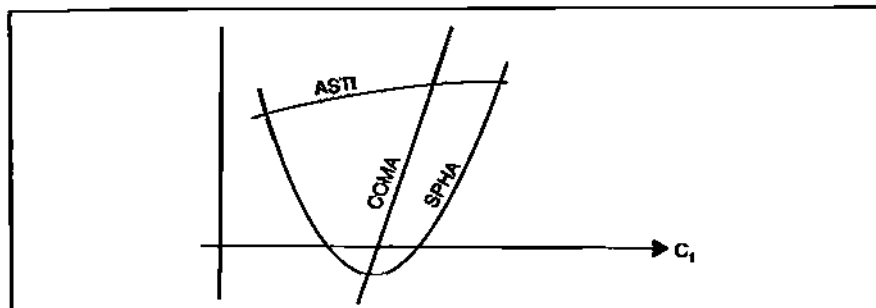


Fig. 17.12 Effect of lens bending on coma and astigmatism.

light plots are not flat since they are defocused relative to the d-light image plane. But they do have the *same* slope through the central portion of the plot, which is indicative of the achromatic correction. The C-light curve is practically a straight line. There is very little spherical of any order present. On the other hand, the F-light plot shows slightly more third order spherical and much more fifth order. (Actually, the SPHA values for F, d, and C are -0.00041, 0.0001, and 0.00016, respectively.)

Optimization of this lens via TRAC will color balance all orders of spherical. (But when doing this, turn off SPHA.) The resulting ray fan plot and spot diagram are shown in Figure 17.11.

17.6 Achromat Bending and Coma and Astigmatism

Coma and astigmatism are also influenced by lens bending as was seen in the Homework for Chapter 3 on page 28. What happens with the achromat? This is illustrated in Figure 17.12 where the values of COMA and ASTI (from the MFE) are superimposed on the SPHA (C_1) plot previously shown in Figure 17.5.

Unlike the parabolic shape of spherical, coma is linear. It has a zero value at

192 Chapter 17 Bending Achromats

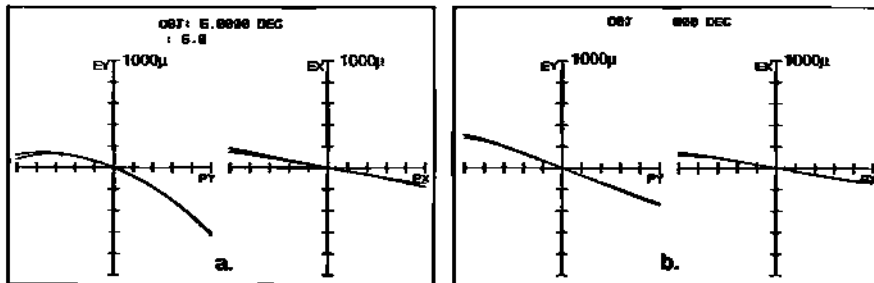


Fig. 17.13 An f/5 achromat corrected for a. spherical only; b. spherical and coma.

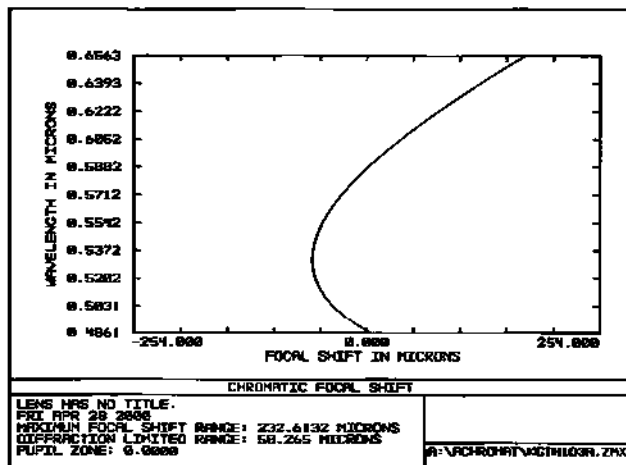


Fig. 17.14 Axial color for f/5 aplanatic achromat.

one point only, and in this example, it crosses the SPHA curve close to the SPHA minimum. Astigmatism is not strongly influenced by bending. It is a slowly varying function, almost linear but with a slight bowing.

17.7 The Aplanat

An *aplanat* is a lens which has no Seidel spherical aberration or coma. Consider the ray fan plot shown in Figure 17.13a for a 254-mm f/5 achromat. (This achromat has been optimized for EFL, color, and zero spherical using variables on the radii.) The plot shown is for the maximum field position of 5°. The difference in slope between the tangential and sagittal plots indicates astigmatism. The bow in the tangential plot is the signature of coma. Suppose we add to this achromat MFE that the operand COMA be zero as well. The ray fan plot resulting from the optimization is shown in Figure 17.13b. Note that the bow in the tangential plot is gone. The coma has been removed, but the astigmatism is about the same. Higher order spherical also remains. However, a price has been paid for this aplanatic so-

Section 17.8: Lateral Color 193

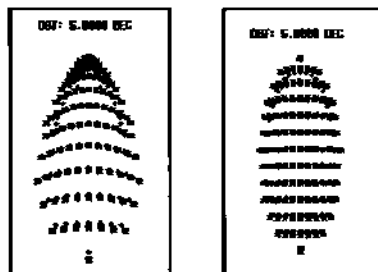


Fig. 17.15 Spot diagrams for an $f/5$ achromat 5° a. with spherical removed; b. with spherical and coma removed.

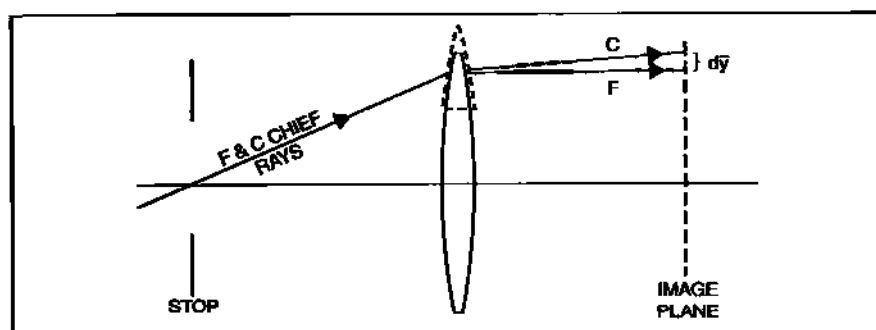


Fig. 17.16 The cause of lateral color.

lution. Remember that only three variables are being used to optimize four active operands. What has happened is that some ground has been surrendered on the color front. This is shown by the axial color plot in Figure 17.14.

The removal of coma is also obvious from the spot diagrams shown in Figure 17.15 (for the 5° field angle). The plot on the left side is prior to coma removal and has the typical comet flare signature. After optimization we are left with an elliptical shape, which is the astigmatism that remains.

17.8 Lateral Color

For the optimizations discussed in this chapter, the stop has been fixed at the first glass surface. In Chapter 19, achromatic lens bending coupled with stop shifting will be used to optimize a design (similar to what was done for the Wollaston lens in Chapter 6). But when the stop is shifted relative to the lens, a new color problem arises. This is illustrated in Figure 17.16 for a *singlet*. With a stop shift, the chief ray no longer passes through the center of the lens. Instead, it strikes the lens at an off-center location, which, in the meridional plot shown, is akin to a section of a prism. Prisms have long been used to spectrally separate light into its constituent colors for scientific work. But in the present context, the prism effect in the lens introduces an aberration called lateral color.

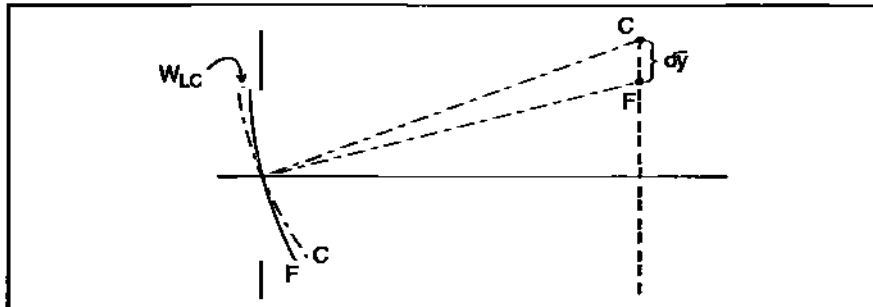


Fig. 17.17 Lateral color in the exit pupil.

When we look at this in terms of wavefronts in the exit pupil, we get the picture illustrated in Figure 17.17. Here the separate color wavefronts are tilted with respect to each other.

Figure 17.17 should strike a chord of recognition. Something very similar to this was discussed in connection with distortion (Chapter 15). The “OPD” for primary lateral color (between *F* and *C* light) in the pupil is given by:

$$W_{LC} = \frac{y\bar{y}\phi_d}{v_d} \quad (17.1)$$

where *y* and \bar{y} are the marginal and chief ray heights at the thin lens. The displacement in the paraxial image plane (*d*-light) between the *F* and *C* chief rays is then given by:

$$d\bar{y}_{CF} = 2(f/\#)W_{LC} \quad (17.2)$$

(See Section 30.8 for an application of Equation 17.2.)

17.9 Homework

Insert the achromat thin lens pre-design calculated in Chapter 16’s Homework into ZEMAX using lens thicknesses of 0.412" and 0.15" respectively (with a 0.0001" airspace between elements). Insert additional field angles at 3.5° and 5°. Optimize to restore proper EFL and achromatic correction. Using the bending technique outlined in Section 17.3 (page 187), generate and plot out the values of SPHA, COMA, and ASTI as a function of *C*₁. (Note the AXCL values.) Make sure you use enough *C*₁ range to catch both zero solutions for SPHA. Plots similar in appearance to Figure 17.12 should be obtained. Note the focal length values (EFLY₁₂ and EFLY₃₄) of the two components at the two SPHA zero solutions. They should be slightly different. Also, indicate on plot the values of *C*, at the zero SPHA crossings, and the zero coma crossing.

Chapter 18

Secondary Color

18.1 Introduction

In Section 17.2, ZEMAX was used to achieve perfect achromatic correction for the thin lens pre-design worked out in Section 16.5.3. This correction was shown in Figure 17.3. It was here that the first mention was made of secondary spectrum. We could see qualitatively what this meant by the bow in the color plot. This chapter will take a more quantitative approach to secondary spectrum. But first we must discuss the concept of partial dispersion in more detail.

18.2 Partial Dispersion

Figure 18.1 shows the variation in refractive index as a function of wavelength for the two glasses used in the achromat design—BK7 and SF2. Index values at *F*, *d*, and *C* light are indicated.

As can be seen from the figure, there is more index variation over the *F–C* spectrum for SF2 than for BK7 (0.0191 vs. 0.008054). This is also obvious from the steepness in the former's slope. However, the primary measure of dispersion (reciprocal dispersion actually) is the Abbe number, v_d , which was introduced in Section 6.2.2.

$$v_d = \frac{n_d - 1}{n_F - n_C} \quad (18.1)$$

The Abbe number represents the *full* dispersion over the spectrum from blue to red light. However, when we arrive at a final mathematical form for secondary spectrum, it will be expressed in terms of a *partial* dispersion. As its name implies, partial dispersion is a measure of dispersion over *any subset* of the visible spectrum. Partial dispersion is a ratio of the refractive index difference over the subset divided by that for the full spectrum. Typical subsets are over *F–d* and *d–C*:

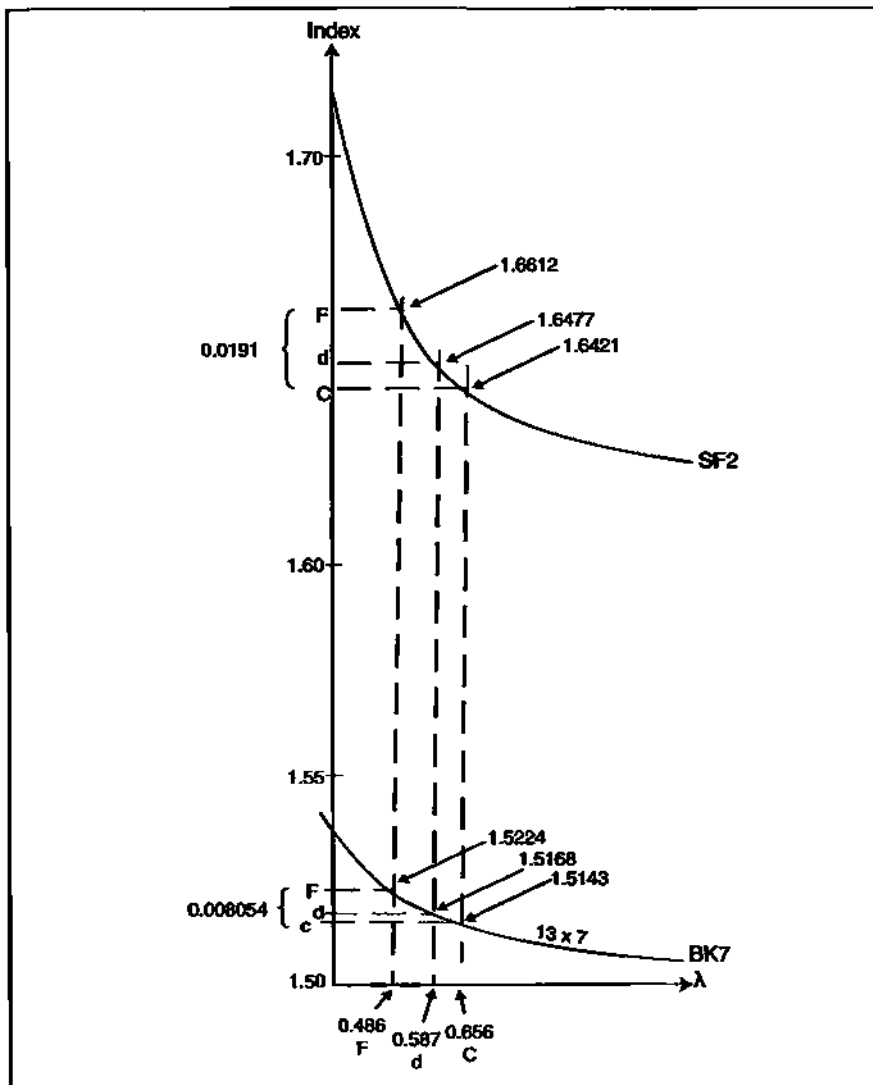


Fig. 18.1 Index vs. wavelength for BK7 and SF2.

$$\left. \begin{aligned} P_{Fd} &= \frac{n_F - n_d}{n_F - n_C} \\ P_{dC} &= \frac{n_d - n_C}{n_F - n_C} \end{aligned} \right\} \quad (18.2)$$

Section 18.2: Partial Dispersion 197

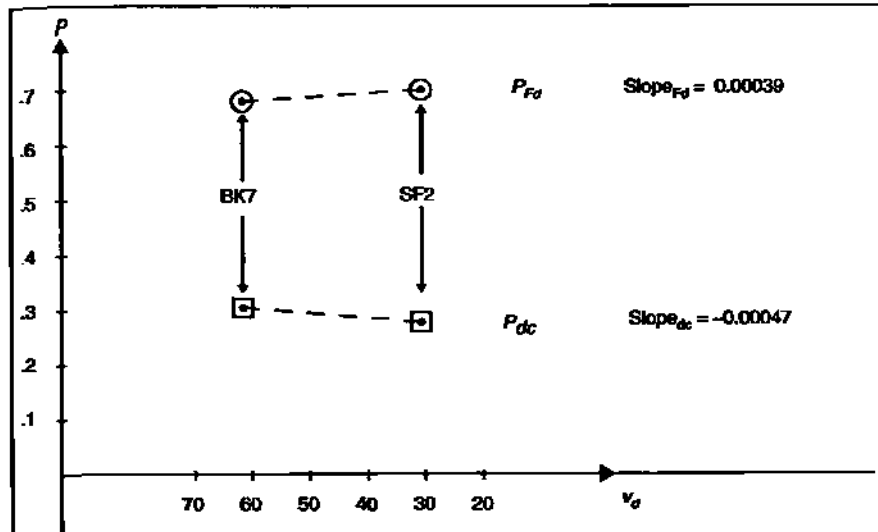


Fig. 18.2 Partial dispersion plot for BK7 and SF2.

Also note that:

$$P_{Fd} + P_{dc} = 1 \quad (18.3)$$

and that:

$$P_{Fd} \geq P_{dc} \quad (18.4)$$

i.e., there is more dispersion on the blue side than on the red side.

For example, the partial dispersions for SF2 and BK7 are:

	P_{Fd}	P_{dc}
SF2	0.7078	0.2922
BK7	0.6928	0.3075

Partial dispersion is often plotted against the Abbe number as shown in Figure 18.2.

Note that both slopes in the figure are shallow with the $F-d$ branch being positive while the $d-C$ branch is negative. Slope is given by:

$$\text{Slope} = \frac{\Delta P}{\Delta v_d} \quad (18.5)$$

where the $F-d$ branch is 0.00039, and the $d-C$ branch is -0.00047.

The plot lines in Figure 18.2 are for two glasses. Suppose we populate the

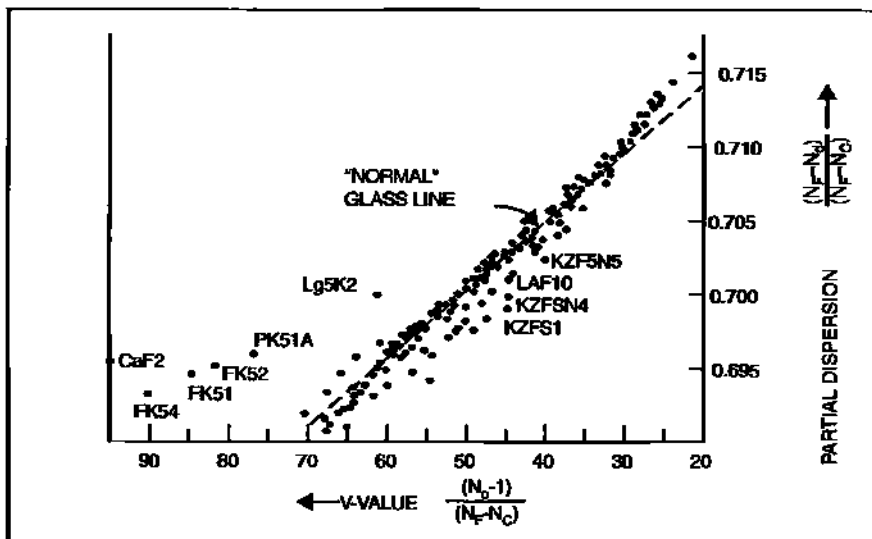


Fig. 18.3 Partial dispersion vs. Abbe number for F-d light. From W. Smith, Modern Lens Design (McGraw-Hill, 1992). Reprinted with permission of the McGraw-Hill Companies.

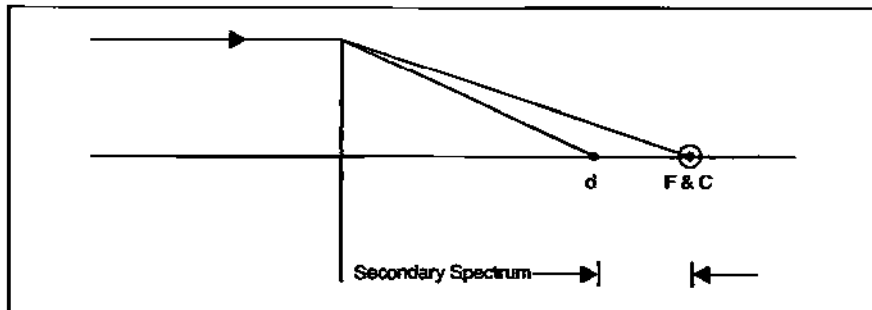


Fig. 18.4 Thin lens achromat illustrating secondary spectrum.

F-d branch with all the Schott glasses as shown in Figure 18.3. Note how most of the glasses are clustered about a straight line called the *normal glass line*. (This will have significance in reducing secondary spectrum as we shall soon see.) The slope of this line is about 0.0004.

18.3 Achromat Secondary Spectrum

Figure 18.4 illustrates a *thin lens achromat* and the axial separation between the d-light focus and the coincident foci for F and C-light. This axial separation is the secondary spectrum of interest here.

For convenience of labeling we will represent the thin lens by the lens shown

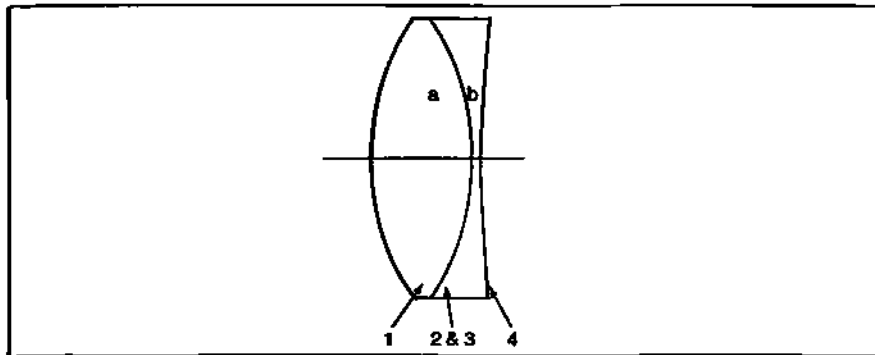


Fig. 18.5 Labeling representation for thin lens achromat.

in Figure 18.5.

We start the derivation with the powers for the achromat components in *d*-light (Section 16.5.2):

$$\left. \begin{aligned} \phi_a &= \frac{v_a}{\Delta v} \phi \\ \phi_b &= -\frac{v_b}{\Delta v} \phi \end{aligned} \right\} \quad (18.6)$$

Next, we write down the expressions for the component powers in terms of indices and curvatures (Section 4.6.3):

$$\left. \begin{aligned} \phi_a &= (n_{da} - 1)(C_1 - C_2) \\ \phi_b &= (n_{db} - 1)(C_3 - C_4) \end{aligned} \right\} \quad (18.7)$$

Now equate Equations 18.6 and 18.7 for the *a*-component:

$$(n_{da} - 1)(C_1 - C_2) = \left(\frac{v_a}{\Delta v} \right) \phi \quad (18.8)$$

Solve for the curvature difference:

$$(C_1 - C_2) = \left(\frac{v_a}{\Delta v} \right) \left(\frac{\phi}{n_{da} - 1} \right) \quad (18.9)$$

Substitute in the expression for the Abbe number from Equation 18.1:

$$(C_1 - C_2) = \left[\frac{n_{da} - 1}{(n_{Fa} - n_{Ca})\Delta v} \right] \left(\frac{\phi}{n_{da} - 1} \right) \quad (18.10)$$

Cancel out the factor $(n_{da} - 1)$:

$$(C_1 - C_2) = \frac{\phi}{[\Delta v(n_{Fa} - n_{Ca})]} \quad (18.11)$$

In a similar manner:

$$(C_3 - C_4) = \frac{-\phi}{[\Delta v(n_{Fb} - n_{Cb})]} \quad (18.12)$$

The power of two thin lenses in contact (Section 4.6.3) is given by: $\phi = \phi_a + \phi_b$

Substituting in Equations 18.7 in *d*-light:

$$\phi_d = (n_{da} - 1)(C_1 - C_2) + (n_{db} - 1)(C_3 - C_4) \quad (18.13)$$

There is a similar expression in *C*-light:

$$\phi_C = (n_{Ca} - 1)(C_1 - C_2) + (n_{Cb} - 1)(C_3 - C_4) \quad (18.14)$$

Now find the power difference between Equations 18.13 and 18.14:

$$\Delta\phi_{dC} = \phi_d - \phi_C \quad (18.15)$$

$$\Delta_{dC} = [(n_{da} - 1) - (n_{Ca} - 1)](C_1 - C_2) + [(n_{db} - 1) - (n_{Cb} - 1)](C_3 - C_4) \quad (18.16)$$

$$\Delta\phi_{dC} = (n_{da} - n_{Ca})(C_1 - C_2) + (n_{db} - n_{Cb})(C_3 - C_4) \quad (18.17)$$

Substitute into Equation 18.17 the curvature differences from Equations 18.11 and 18.12:

$$\Delta\phi_{dC} = (n_{da} - n_{Ca}) \left[\frac{\phi}{\Delta v(n_{Fa} - n_{Ca})} \right] - (n_{db} - n_{Cb}) \left[\frac{\phi}{\Delta v(n_{Fb} - n_{Cb})} \right] \quad (18.18)$$

Substitute in the expression for partial dispersion found in Equation 18.2 for *d-C* light:

$$\Delta\phi_{dC} = P_{dCa} \left(\frac{\phi_d}{\Delta v} \right) - P_{dCb} \left(\frac{\phi_d}{\Delta v} \right) \quad (18.19)$$

$$\Delta\phi_{dC} = (P_{dCa} - P_{dCb}) \left(\frac{\phi_d}{\Delta v} \right) \quad (18.20)$$

$$\Delta\phi_{dC} = \left(\frac{\Delta P_{dC}}{\Delta v} \right) \phi_d \quad (18.21)$$

Section 18.3: Achromat Secondary Spectrum 201

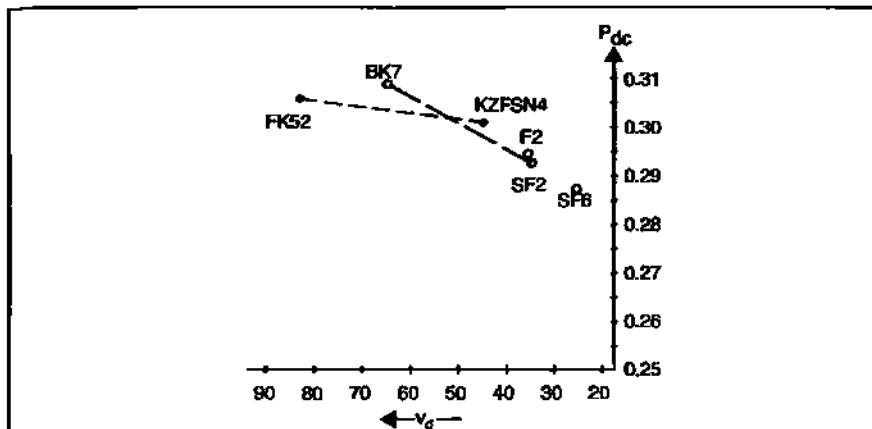


Fig. 18.6 Partial dispersion plot for selected glasses.

Equation 18.21 tells us that the power difference between *d*-light and *C*-light is the ratio of the partial dispersion difference to the Abbe number difference—that quantity being multiplied by the system power in *d*-light. Let's recast this in terms of focal length. Utilizing Equation 16.10 from Section 16.1:

$$\frac{\Delta\phi_{dC}}{\phi_d} = -\frac{\Delta f_{dC}}{f_d} \quad (18.22)$$

Combining this with Equation 18.21 we obtain:

$$\frac{-\Delta f_{dC}}{f_d} = \frac{\Delta P_{dC}}{\Delta v} \quad (18.23)$$

The secondary spectrum is then given by:

$$\Delta f_{dC} = -\left(\frac{\Delta P_{dC}}{\Delta v}\right)f_d \quad (18.24)$$

where the quantity in parentheses is the partial dispersion *slope* (Equation 18.5) for the two glasses.

Example: What is the secondary spectrum for the achromat designed back in Section 16.5.3?

Using the P_{dc} from Section 18.2:

$$\Delta f_{dC} = -\left(\frac{0.0153}{30.32}\right)(400)$$

$$\Delta f_{dC} = -0.2018 \text{ mm} = -201.8 \mu\text{m}$$

So the secondary spectrum is almost $202\mu\text{m}$. The negative sign indicates that the d -light focus is in front of the C -light (and F -light) focus.

Equation 18.24 tells us that one way to reduce secondary spectrum is to look for a glass pair in which ΔP_{dC} is fairly small while Δv is fairly large. Figure 18.6 illustrates this point.

Had we picked FK52 and KzFSN4 for our glasses, the secondary spectrum becomes:

$$\Delta f_{dC} = -\left(\frac{0.0043}{37.5}\right)(400)$$

$$\Delta f_{dC} = -45.9 \mu\text{m}$$

which is about a fourth the secondary spectrum seen for BK7 and SF2.

Why not use FK52 and KzFSN4 or something similar? Because there are other factors to consider, such as the effect on higher-order aberrations, susceptibility to environmental factors, manufacturability, and cost.

18.4 ZEMAX Corrected Achromat

Returning to CHRM101a in Section 17.2, the secondary spectrum can be found in several ways. In the “Lens Data Editor” we see that the back focal distance (BFD) in d -light is 395.5449 mm. Click on the WAV button and reset the primary wavelength to either F - or C -light. The new BFD is 395.7466 mm. The difference between these two BFDs is the secondary spectrum.

$$\Delta \text{BFD}_{dC} = -201.7 \mu\text{m} = \Delta f_{dC}$$

This is the same value found in the example above using BK7 and SF2. Another method is to measure the secondary spectrum directly off the axial plot as indicated in Figure 18.7. You can also go to Settings → Text and obtain a table of values from which the secondary spectrum can be interpolated (as shown in Listing 18.1).

18.5 When Is Secondary Spectrum Worrisome?

One way to gauge a potential secondary color problem is by comparing its image blur size to the diffractive Airy core. (This assumes, of course, that spherical aberration is not the limiting factor.) Consider the marginal ray in d -light and where it pierces the F - and C -light image plane as shown in Figure 18.8. From Section 5.5 we know that:

$$u_d' = \frac{1}{2(f/\#)} \quad (18.25)$$

From Figure 18.8, we also see that:

Section 18.5: When Is Secondary Spectrum Worrisome? 203

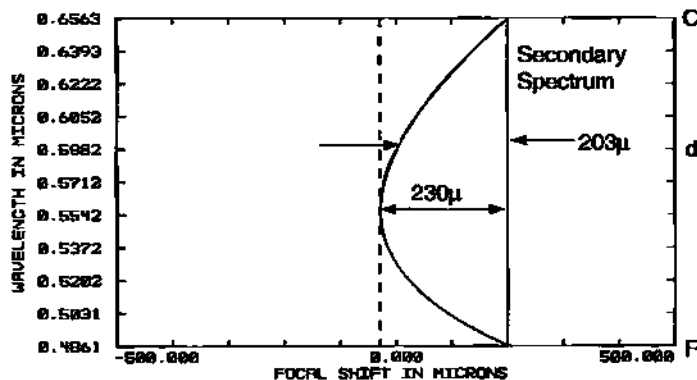


Fig. 18.7 Measuring secondary spectrum directly from color plot.

Wavelength	Shift
0.486133	0.29178768
0.491864	0.15989759
0.497475	0.12342626
0.503147	0.09184128
0.508818	0.06473533
0.514489	0.04174171
0.520161	0.02252911
0.525832	0.00679883
0.531503	-0.00572267
0.537175	-0.01527885
0.542846	-0.02209374
0.548517	-0.02637622
0.554189	-0.02829388
0.559860	-0.02983857
0.565531	-0.02573587
0.571283	-0.02154971
0.576974	-0.01568812
0.582545	-0.00800441
0.588217	0.00112993
0.593888	0.01178432
0.599559	0.02362832
0.605221	0.03681882
0.610902	0.05119942
0.616573	0.06669983
0.622245	0.08325531
0.627916	0.10068621
0.633587	0.11929758
0.639259	0.13867843
0.644938	0.15898889
0.650601	0.17992517
0.656273	0.20170768

Listing 18.1

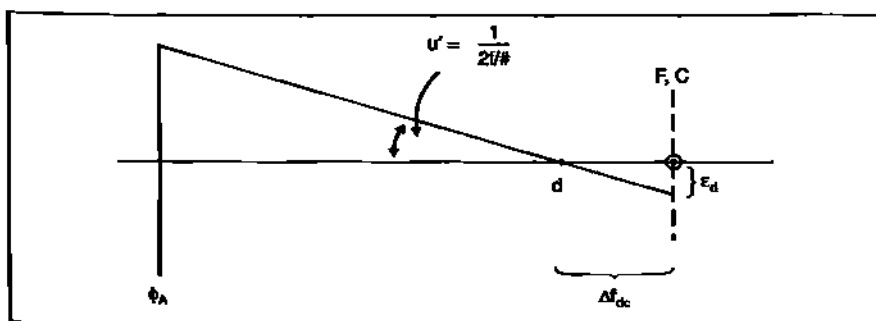


Fig. 18.8 Secondary spectrum image blur ϵ_d .

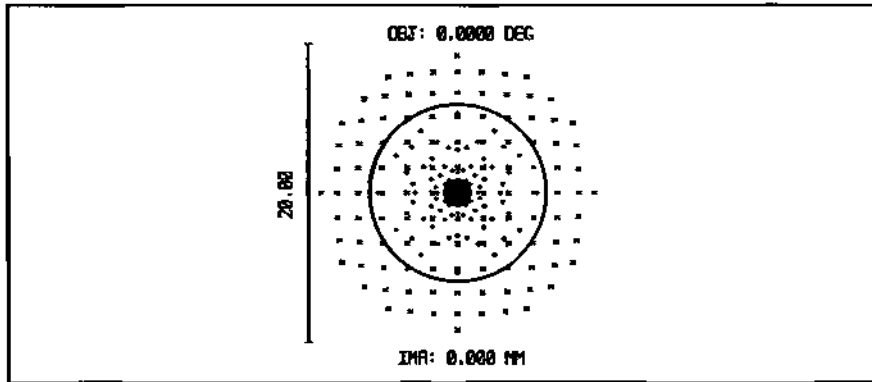


Fig. 18.9 Spot diagram at F and C focus plane for f/10 achromat corrected for color and 3rd order spherical.

$$u'_d = \frac{\epsilon_d}{\Delta f_{dc}} \quad (18.26)$$

Equating Equations 18.25 and 18.26 we obtain the radial image blur size due to secondary color:

$$\epsilon_d = \frac{\Delta f_{dc}}{2(f/\#)} \quad (18.27)$$

For our 400 mm f/10 BK7 and SF2 achromat:

$$\epsilon_d = \frac{-201.8 \text{ } \mu\text{m}}{20} = -10 \text{ } \mu\text{m}$$

The diffractive Airy disk diameter is given by:

$$\text{Airy} = 2.44\lambda(f/\#) \quad (18.28)$$

The next thing to do is compare the secondary spectrum blur *diameter* with the Airy core diameter:

$$\frac{2\epsilon_d}{\text{Airy}} = \frac{\left(\frac{\Delta f_{dc}}{f/\#}\right)}{2.44\lambda(f/\#)}$$

$$\frac{2\epsilon_d}{\text{Airy}} = \frac{\Delta f_{dc}}{2.44\lambda(f/\#)^2} \quad (18.29)$$

For our 400 mm achromat:

$$\frac{2\epsilon_d}{\text{Airy}} = \frac{20 \text{ } \mu\text{m}}{14.3 \text{ } \mu\text{m}} = 1.4$$

Section 18.6: Flat Field Achromat 205

Look at the spot diagram in Figure 18.9 This is our 400 mm $f/10$ achromat corrected for Seidel spherical (right-hand solution) as well as color. The plane of observation is the F - and C -light paraxial plane. The Airy disk is surrounded by a larger halo due to secondary color—the spots outside the Airy disk are due solely to d -light. So in this lens, resolution will be limited not by diffraction but by secondary color. When secondary color limits performance, that's the time to think about reducing it.

18.6 Flat Field Achromat

Petzval curvature was discussed in Chapter 14. For a system of thin lenses we found the following constraint (Equation 14.4), which we adopt for the two lens achromat:

$$\frac{\phi_a}{n_a} + \frac{\phi_b}{n_b} = 0 \quad (18.30)$$

The second color constraint found in Chapter 16 was given by:

$$\frac{\phi_a}{v_a} + \frac{\phi_b}{v_b} = 0 \quad (18.31)$$

Solve each constraint for ϕ_a :

$$\phi_a = -\left(\frac{n_a}{n_b}\right)\phi_b \quad (18.32)$$

$$\phi_a = -\left(\frac{v_a}{v_b}\right)\phi_b \quad (18.33)$$

Now equate these two expressions:

$$\frac{v_a}{v_b} = \frac{n_a}{n_b} \quad (18.34)$$

Rearrange:

$$\frac{v_a}{n_a} = \frac{v_b}{n_b} \quad (18.35)$$

The condition expressed by Equation 18.35 permits a flat Petzval field achromat.

18.7 Homework

- a. Manually calculate the magnitude of the secondary spectrum for the achromat in the Homework for Chapter 16.

206 Chapter 18 Secondary Color

- b. For the ZEMAX color-corrected achromat in the Homework for Chapter 17 (for zero field), find the value of the secondary spectrum using ZEMAX.



Chapter 19

Large Air-Spaced Achromat and French Landscape Lens

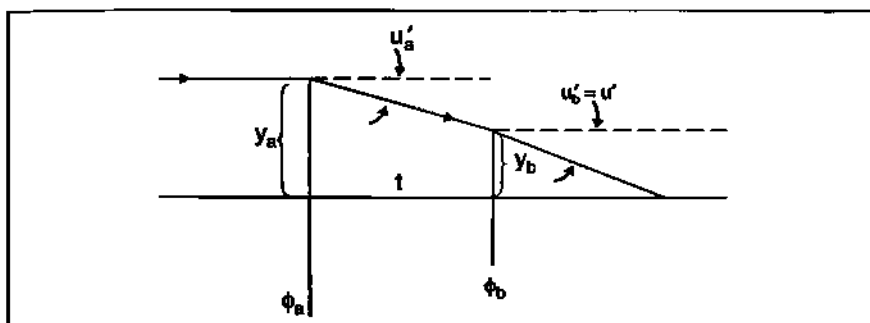


Fig. 19.1 Widely separated thin lens achromat.

19.1 Introduction

In our discussions on color correction thus far we have concentrated on the contact or cemented achromat. This is about to change. We will show how to color correct for two *widely* spaced thin lenses. Such a corrected lens is called a dialyte. We will then discuss the 3-lens apochromat and its role in reducing secondary spectrum. The apochromat is subject to three separate constraints, two of which have seen duty on the achromat. We will delve into the nature of this third constraint. (The actual design of an apochromat will take place in Chapter 21.) Then we move on to a discussion of the Chevalier lens, which is the achromatic equivalent of the Wollaston. This will be the subject of a homework exercise.

19.2 Separated Thin Lens Achromat

19.2.1 Dispersion Constraint Modification

The dispersion constraint in Equation 16.20 on page 181 must be reformulated to take into account the different marginal ray heights between the two lenses. This is illustrated in Figure 19.1.

Recall from Section 16.3 the formulation for primary axial color:

$$df = -\left(\frac{1}{u'^2}\right) \left(\frac{y^2 \Phi}{v} \right) \quad (19.1)$$

For the *two* separated thin lenses this becomes:

$$df = -\left(\frac{1}{u'^2}\right) \left[\left(\frac{y_a^2 \Phi_a}{v_a} \right) + \left(\frac{y_b^2 \Phi_b}{v_b} \right) \right] \quad (19.2)$$

To make this pair of lenses achromatic requires that:

$$\left[\left(\frac{y_a^2 \Phi_a}{v_a} \right) + \left(\frac{y_b^2 \Phi_b}{v_b} \right) \right] = 0 \quad (19.3)$$

Note that when $t = 0$, $y_a = y_b$ (which cancel out). We are then left with the original achromatic constraint (Equation 16.20 on page 181).

The two constraints for the separated achromat are therefore:

$$\left. \begin{aligned} \Phi_a + \Phi_b - t\Phi_a\Phi_b &= \Phi \\ \frac{y_a^2 \Phi_a}{v_a} + \frac{y_b^2 \Phi_b}{v_b} &= 0 \end{aligned} \right\} \quad (19.4)$$

Note that we are using the “thick” lens formulation for system power from Equation 4.18 on page 38.

19.2.2 Determining Component Powers

As was done for the cemented achromat, we will use the constraints in Equation 19.4 to determine the powers of Φ_a and Φ_b . Using the first paraxial ray trace equation (PRTE No. 1) from Equation 4.1 on page 33 we know that:

$$u'_a = -y_a \Phi_a \quad (19.5)$$

The height on the second lens is given by PRTE No. 2 (from Equation 4.2 on page 33):

$$y_b = y_a + u'_a t \quad (19.6)$$

Substituting Equation 19.5 into Equation 19.6:

$$y_b = y_a + (-y_a \Phi_a)t$$

or

Section 19.2: Separated Thin Lens Achromat 209

$$y_b = (1 - \Phi_a t) y_a \quad (19.7)$$

Let t equal some multiplier of the first lens' focal length:

$$t = \kappa f_a = \frac{\kappa}{\Phi_a} \quad (19.8)$$

Substitute this in for t in Equation 19.7:

$$y_b = (1 - \kappa) y_a \quad (19.9)$$

Also, substitute Equation 19.8 into the power constraint shown in Equation 19.4 (top):

$$\Phi = \Phi_a + (1 - \kappa) \Phi_b \quad (19.10)$$

Substitute Equation 19.9 into the second constraint shown in Equation 19.4 (bottom) and cancel out y_a :

$$\frac{\Phi_a}{v_a} + (1 - \kappa)^2 \frac{\Phi_b}{v_b} = 0 \quad (19.11)$$

Solve Equation 19.10 for Φ_a :

$$\Phi_a = \Phi - (1 - \kappa) \Phi_b \quad (19.12)$$

Insert Equation 19.12 into Equation 19.11 and solve for Φ_b :

$$\left[\frac{\Phi - (1 - \kappa) \Phi_b}{v_a} \right] + \left[\frac{(1 - \kappa)^2 \Phi_b}{v_b} \right] = 0 \quad (19.13)$$

$$\left(\frac{\Phi}{v_a} \right) - \left[\frac{(1 - \kappa)}{v_a} - \frac{(1 - \kappa)^2}{v_b} \right] \Phi_b = 0 \quad (19.14)$$

$$\Phi_b = \frac{\frac{\Phi}{v_a}}{\left(1 - \kappa \right) \left[\frac{1}{v_a} - \frac{(1 - \kappa)}{v_b} \right]} \quad (19.15)$$

$$\Phi_b = \frac{\Phi}{\left(1 - \kappa \right) \left[1 - \left(1 - \kappa \right) \frac{v_a}{v_b} \right]} \quad (19.16)$$

As a check, rewrite Equation 19.16:

$$\phi_b = \frac{v_b \phi}{(1-\kappa) [v_b - (1-\kappa)v_a]}$$

Now let $\kappa = 0$:

$$\phi_b = \frac{v_b \phi}{v_b - v_a} = \frac{v_b}{\Delta v_{ab}} \phi$$

We see that ϕ_b reduces to the power found for the contact (or cemented) achromat in Equation 16.23 on page 181 (bottom).

Now we have to find ϕ_a . Substitute Equation 19.15 into Equation 19.12:

$$\phi_a = \phi - (1-\kappa) \left\{ \frac{\frac{\phi}{v_a}}{(1-\kappa) \left[\frac{1}{v_a} - \frac{(1-\kappa)}{v_b} \right]} \right\} \quad (19.17)$$

The $(1-\kappa)$ cancels out, and the system power can be brought outside as a separate factor:

$$\phi_a = \left\{ 1 - \frac{1}{v_a \left[\frac{1}{v_a} - \frac{(1-\kappa)}{v_b} \right]} \right\} \phi \quad (19.18)$$

Through algebraic manipulation we will evolve this expression for ϕ_a into a more useful form:

$$\phi_a = \left\{ 1 - \frac{v_b}{[v_b - (1-\kappa)v_a]} \right\} \phi \quad (19.19)$$

$$\phi_a = \left\{ \frac{v_b - (1-\kappa)v_a - v_b}{v_b - (1-\kappa)v_a} \right\} \phi \quad (19.20)$$

$$\phi_a = \left\{ \frac{-(1-\kappa)v_a}{v_b - (1-\kappa)v_a} \right\} \phi \quad (19.21)$$

As a check, let $\kappa = 0$:

$$\phi_a = \frac{-v_a \phi}{v_b - v_a} = \left(\frac{v_a}{\Delta v_{ab}} \right) \phi$$

We see that ϕ_a reduces to the power found for the contact (or cemented) achromat in Equation 16.23 on page 181 (top).

19.2.3 One-Glass Achromat

Here's an interesting curiosity for you. Let $v_a = v_b$ in 19.21. This means we are using the same glass for each lens. Equation 19.21 then becomes:

$$\phi_a = \left\{ \frac{-(1-\kappa)}{1-(1-\kappa)} \right\} \phi \quad (19.22)$$

which reduces to:

$$\phi_a = \left[\frac{(1-\kappa)}{\kappa} \right] \phi \quad (19.23)$$

The power of the second element given by Equation 19.16 becomes:

$$\phi_b = \frac{\phi}{(1-\kappa)[1-(1-\kappa)]}$$

which becomes:

$$\phi_b = \frac{\phi}{\kappa(1-\kappa)} \quad (19.24)$$

For example, if ϕ is positive and κ is positive and greater than 1, ϕ_a is always positive and ϕ_b is always negative. The good news is that we have achieved achromatism with just one glass type. The bad news is that the image will not be real, but virtual. Take the ratio of the front power over the rear power:

$$\frac{\phi_a}{\phi_b} = \frac{-(1-\kappa)\phi}{\kappa} \cdot \frac{\kappa(1-\kappa)}{\phi} = -(1-\kappa)^2 \quad (19.25)$$

The power of ϕ_b is then given by:

$$\phi_b = \left[\frac{-1}{(1-\kappa)^2} \right] \phi_a \quad (19.26)$$

For example, if $\kappa = 1.5$, then $\phi_b = -4\phi_a$, the power of the first lens is 4x weaker than the rear lens. Since the former is positive, the rear lens increases the divergence of the beam incident on it. The image will be virtual. So you will not be able to record an image on a piece of film or on a CCD. However, this type of

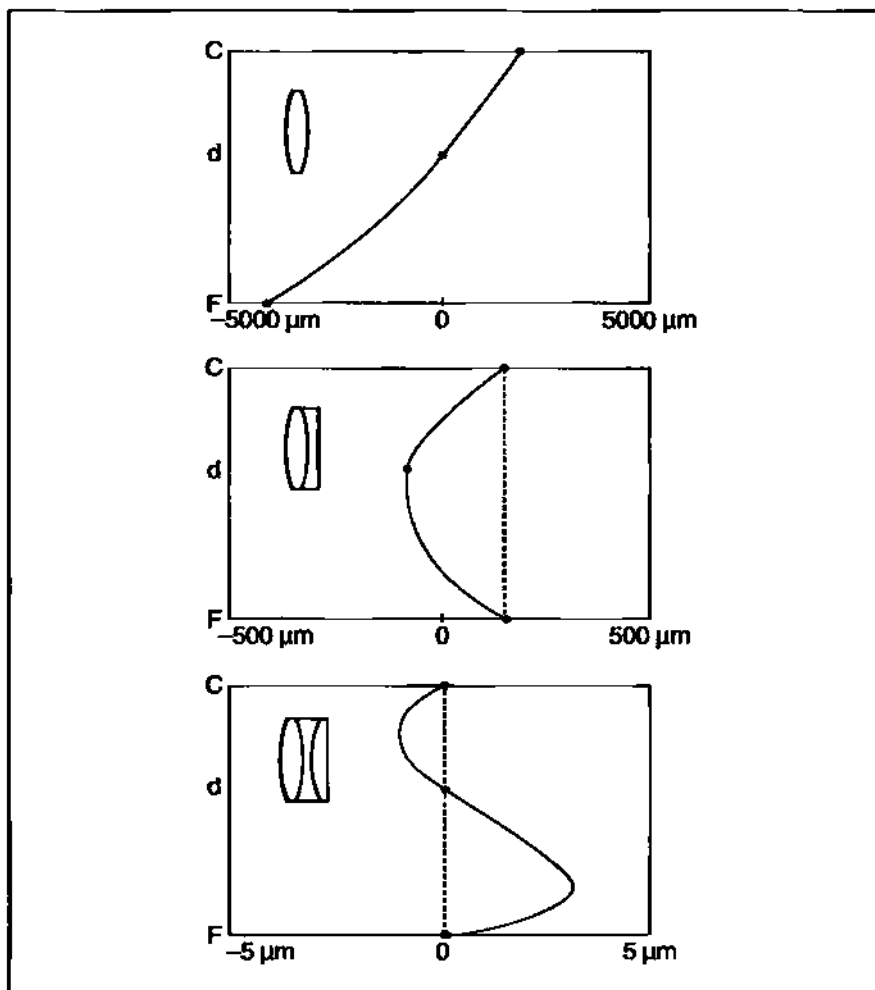


Fig. 19.2 The color correction path.

system is useful if it feeds into another. For example, if you view the virtual image with your eye, a real image will form on the retina.

19.3 The Apochromatic Constraint

Figure 19.2 summarizes and neatly illustrates where we've been with regard to color correction and where we have yet to go. The top figure shows the problem of primary axial color in a singlet. Below that we see the benefits of achromatic correction and the problem of secondary color. Secondary color can be greatly reduced by resorting to a three-glass system called an apochromat. This is illustrated

Section 19.3: The Apochromatic Constraint 213

in the bottom figure. Such a lens has a common focus for *three* colors across the visible spectrum instead of two (as in the achromat). The residual color problem is called tertiary spectrum.

We will be discussing apochromats in more detail in Chapter 21. As you will recall, the achromat had a set of two constraints (Section 16.5.1). The apochromat, on the other hand, has a set of three constraints that will be used to determine element powers. Our goal here is to provide a basis for the use of the *third* apochromatic constraint. But we will begin this process by first working with a singlet.

19.3.1 Partial Primary Axial Color

The power of a thin singlet is given by:

$$\phi = (n - 1)(C_1 - C_2) \quad (19.27)$$

Power difference is obtained via the differential:

$$d\phi = (C_1 - C_2)dn \quad (19.28)$$

Let $dn = (n_d - n_c)$ and substitute into Equation 19.28:

$$d\phi = (C_1 - C_2)(n_d - n_c) \quad (19.29)$$

But $(n_d - n_c) = P_{dc}(n_F - n_c)$ from Equation 18.2 on page 196. Insert this into Equation 19.29:

$$d\phi = (C_1 - C_2)P_{dc}(n_F - n_c) \quad (19.30)$$

Rewrite:

$$d\phi = (C_1 - C_2)P_{dc}(n_F - n_c) \left[\frac{n_d - 1}{n_d - 1} \right] \quad (19.31)$$

The Abbe number $v = (n_d - 1)/(n_F - n_c)$. Substitute into Equation 19.31:

$$d\phi = (C_1 - C_2)(n_d - 1) \left(\frac{P_{dc}}{v} \right) \quad (19.32)$$

But $(C_1 - C_2)(n_d - 1)$ is the power as expressed in Equation 19.27. So Equation 19.32 becomes:

$$d\phi = \left(\frac{P_{dc}}{v} \right) \phi \quad (19.33)$$

Utilizing Equation 16.10 on page 177 to recast this in terms of focal length:

$$\frac{\Phi}{d\phi} = \frac{-f}{df} = \frac{v}{P_{dc}} \quad (19.34)$$

This is similar to the expression for primary color (Equation 16.10 on page 177) except for the presence of the partial dispersion P_{dc} . Let's return to our 400 mm f/10 BK7 singlet. (SING1c1b optimized for EFL in d-light with both radii as variables.) Using the *M-solve* in ZEMAX, we find the back focal lengths for colors F, d, and C (simply by assigning primary wavelength status to each in succession). We generate the following data table:

Wavelength	BFD (mm)	ΔBFD (mm)
F	394.439	-4.261
d	398.700	-1.922
C	400.622	

Let's go back to Equation 19.34 and rewrite it as:

$$df = -\left(\frac{P_{dc}}{v}\right)f \quad (19.35)$$

Recall that for BK7, $P_{dc} = 0.3086$; $v = 64.17$

$$df = -\left(\frac{0.3086}{64.17}\right)400 = -1.9236 \text{ mm}$$

which is essentially the ΔBFD just found between d and C light. In other words, Equation 19.35 provides us a *partial* primary color value.

19.3.2 Partial Primary Color Applied to Doublets and Triplets

For a thin lens doublet the system power is given by:

$$\phi = \phi_a + \phi_b \quad (19.36)$$

The differential partial power is given by:

$$d\phi_{dc} = d\phi_{a,dc} + d\phi_{b,dc} \quad (19.37)$$

or by:

$$d\phi_{dc} = \left(\frac{P_{dc}}{v}\right)_a \phi_a + \left(\frac{P_{dc}}{v}\right)_b \phi_b \quad (19.38)$$

A similar procedure is use for a thin lens triplet:

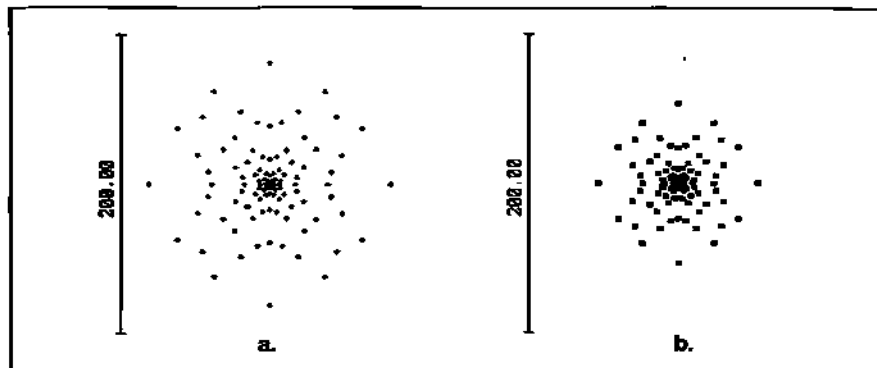


Fig. 19.3 Spot sizes at F and C focus for: (a) F-light; (b) C-light.

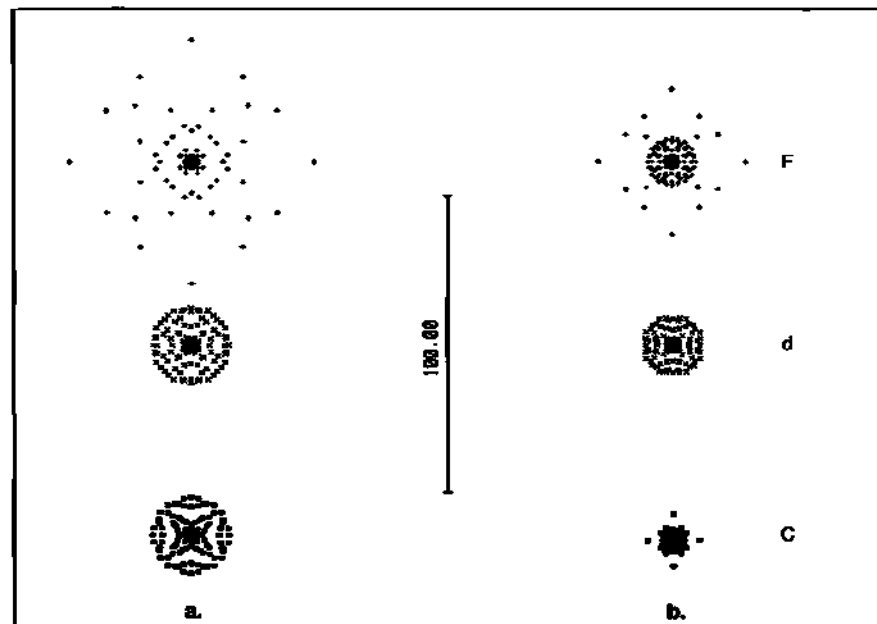


Fig. 19.4 Spot sizes at d-focus for F, d, C-light using TRAC with: (a) AXCL on; (b) AXCL off.

$$d\Phi_{dC} = \left(\frac{P_{dC}}{v} \right)_a \Phi_a + \left(\frac{P_{dC}}{v} \right)_b \Phi_b + \left(\frac{P_{dC}}{v} \right)_c \Phi_c \quad (19.39)$$

Equation 19.39 is the basis for the third constraint used in connection with apochromatic design.

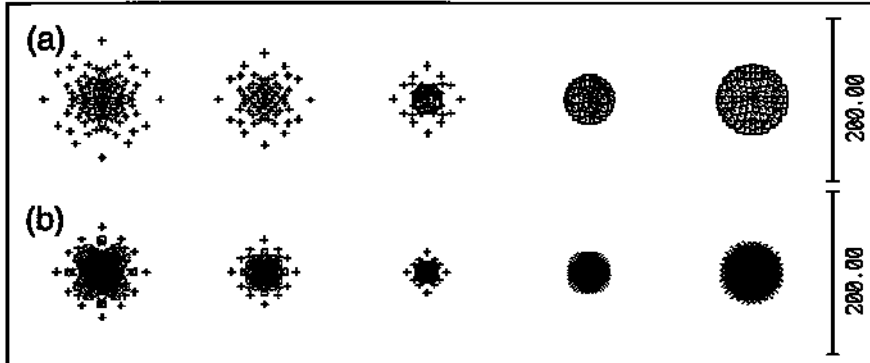


Fig. 19.5 All colors combined through focus spot plots: (a) AXCL on; (b) AXCL off.

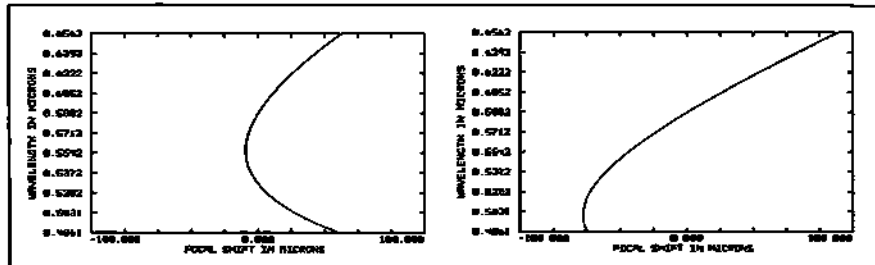


Fig. 19.6 Axial color, TRAC optimization: (a) with AXCL on; (b) with AXCL off.

19.4 Color Correction vs. Spot Size

The operand AXCL is a *point-like* constraint. It forces two colors (usually F and C) to focus at the same point. This does *not* mean, however, that the *spot sizes* of the two colors are the same at this point as illustrated in Figure 19.3 (for a 100-mm $f/4$ achromat). This has an important implication for the TRAC operand.

Suppose we optimize the 100-mm $f/4$ on-axis with EFFL, AXCL, and TRAC active. Afterwards, we look at the spot sizes for F_d , and C light in the d focal plane. Next, we repeat the process with AXCL turned off. The results are shown in Figure 19.4.

For every color, TRAC *without* AXCL results in a smaller spot size. This holds true for through focus spots as well (as shown in Figure 19.5).

But what has happened to the axial color? This is shown in Figure 19.6. With AXCL active, the color correction is right on. When AXCL is off, the color correction is itself off quite a bit.

As can be seen, absolute achromatic color correction has been sacrificed to achieve smaller spot sizes. If our goal is to get the visible spectrum for a star source onto a very small detector, then sacrificing some color correction is a good trade-off.

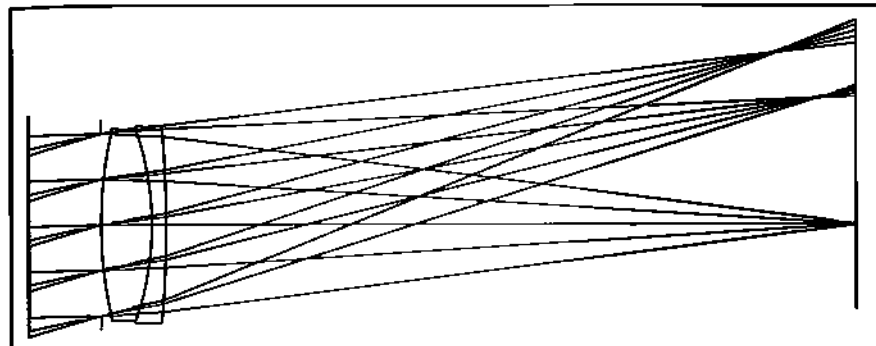


Fig. 19.7 Achromat (100 mm f/4) with 15° field showing strong field curvature.

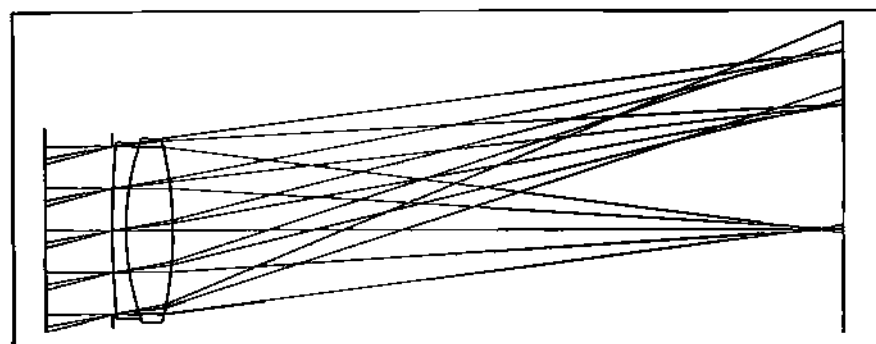


Fig. 19.8 Same achromat but reversed. Main problem now is coma.

19.5 The Chevalier Lens

Figure 19.7 shows a 100-mm $f/4$ achromat with a 15° field. (This is the same lens previously discussed in Section 17.4, just stopped down a bit.) Note that this lens is exhibiting strong tangential field curvature. Flip this lens around as shown in Figure 19.8. (When we do this the axial color is off and has to be retweaked.) The field is flatter but the main problem now is coma.

This observation was initially made by Charles Chevalier (Figure 19.9). He was a maker of telescopes and microscopes, and he needed to come up with a decent flat field lens for the budding field of photography after 1839.

In Chapter 6, we saw that stop location had a significant impact on the off-axis aberrations of a singlet. Similar behavior is observed for an achromat, and Chevalier made use of this. To beat down the coma, Chevalier placed a stop in front of one of his “used in reverse” telescope objectives. Let’s do this for the 100-mm $f/4$ in Figure 19.8. We’ll let ZEMAX find the optimum stop location using TRAC, and the only variable will be the thickness of the airspace after the stop surface. (Of course we will keep EFPL and AXCL on-line as well.) The result is



Fig. 19.9 Charles Chevalier, inventor of the French landscape lens.

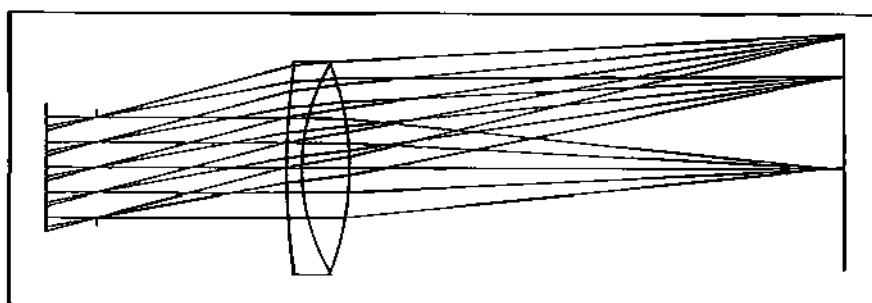


Fig. 19.10 Coma reduced by optimizing position of stop.

shown in Figure 19.10. It's the rays passing through the lower part of the lens in Figure 19.8 that give rise to the coma problem. The location of the stop in Figure 19.10 gets rid of these rays simply by blocking (or vignetting) them.

We saw in Chapter 17 that achromatic bending had a strong impact on spherical aberration and coma, and a somewhat lesser effect on astigmatism. Chevalier was aware of Wollaston's meniscus-shaped landscape lenses (Chapter 6). He realized that the combination of stop shift and lens bending could result in a compact wide field lens useful for photography. The resulting lens came to be known as the French Landscape lens.

19.6 Homework

Now you are ready to combine the lessons learned about achromat design (to control color) with stop shift (to help control off-axis aberration) together with lens

Section 19.6: Homework 219

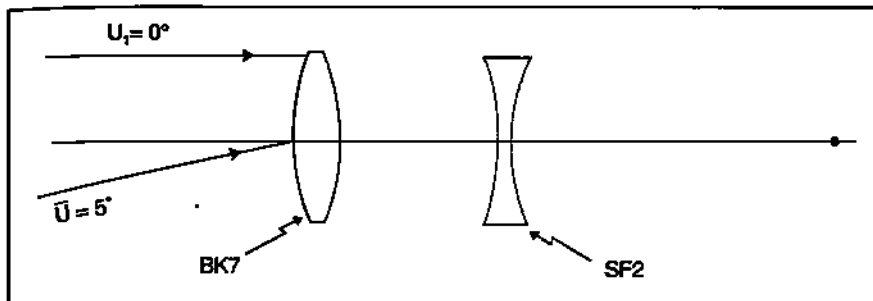


Fig. 19.11

bending (to control spherical, coma, and astigmatism). You will not flip the achromat around as Chevalier had done. But you will keep the stop out in front as he did. You will find that, of the two zero SPHA solutions found in Homework for Chapter 17, only one will serve as a viable starting point for the design.

1. Using ZEMAX, design an *achromatic* French landscape lens (crown in front; stop in front). The lens is to be a 10" focal length $f/10$ covering a $\pm 25^\circ$ field. (Note: You may want to work your way out to this field in several steps updating TRAC as you go.) Use Schott BK7 and SF2. Achromatic correction over the F, d, C spectrum. Tangential field should be reasonably flat. Try to attain (or better) the following RMS spot size targets (use settings: square; centroid):

Field	RMS Spot
0°	$102\mu\text{m}$
17.5°	119
25°	246

Suggested folder name: Chevalier, etc. File name: CHEV101b, etc.

2. Design and optimize a 400-mm EFL $f/10$ dialyte achromat (Figure 19.11) over the F, d, C spectrum with $\kappa = 0.1$. The field angle is $\bar{U} = 5^\circ$. Use BK7 and SF2. Let the positive lens be 5 mm thick; the negative, 3 mm. To start with, let the positive lens be equiconvex; the negative lens, also equiconcave. Folder name: Dial; file name Dial101b, etc. Meet or exceed the following RMS spot specifications (use settings square, centroid):

Field	RMS Spot
0°	$102\mu\text{m}$
3.5°	48
5°	135

Chapter 20

Mid-Term Exam

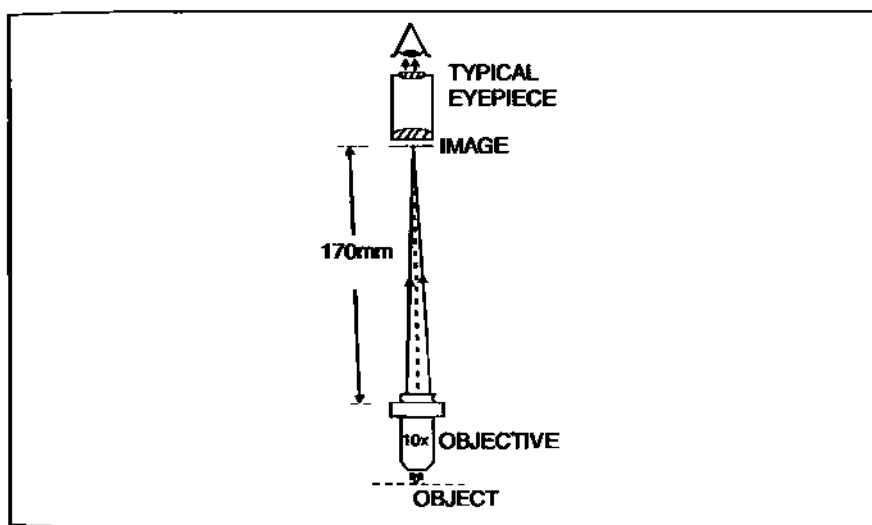


Fig. 20.1 Typical microscope system.

20.1 Introduction

This exam involves the design of a 10x microscope objective. It will consist of two parts. Part I will be a manual thin lens pre-design to obtain a starting prescription. Part II will involve the insertion of this starting prescription into ZEMAX and the optimization of the design. Before the exam is given, some general information about the design protocol will be provided.

20.2 The Microscope

Figure 20.1 illustrates the microscope system along with pertinent distances. The objective forms a magnified image of the object. The magnification is usually inscribed directly on the objective barrel as 5x; 10x; etc. The image lies in the focal plane of the eyepiece. Consequently, the light emerging from the eyepiece is collimated. The eye (focused for infinity) then forms a secondary image on the retina.

All the photographic lens designs in this book assume an object at infinity.

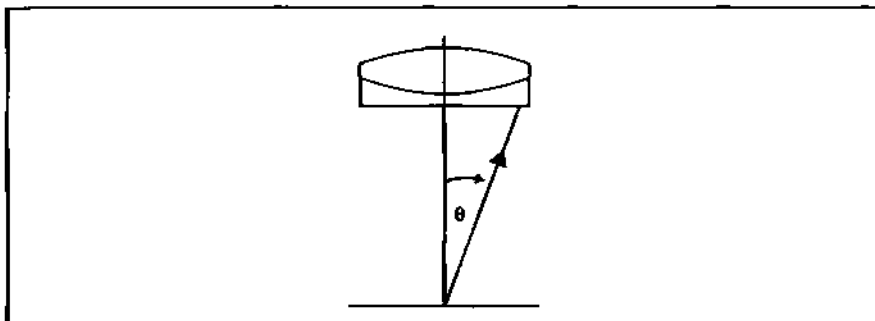


Fig. 20.2 Numerical aperture for objective.

Table 20.1
Typical microscope objectives.

Mag	NA	EFL(mm)	Work Dist.(mm)
5x	0.12	24.8	27.4
10x	0.25	14.6	7.3
20x	0.54	8.4	1.6
40x	0.60	4.6	0.8

in which case the image lies in the rear focal plane. For the microscope, however, the object is just outside the front focal plane, and the image lies *very* far from the rear focal plane. No matter what power objective is used, the image plane (for standard microscopes) will always be located the same distance from the objective's shoulder (either 160 mm or 170 mm).

For photographic lenses, the light gathering capability is indicated by the f-number. The smaller the f-number for a given focal length, the larger the entrance pupil, and hence, more irradiance in the image. For microscope objectives, the light gathering capability is given by the object space numerical aperture. This is the second number found inscribed on the objective barrel, e.g., 0.25.

The numerical aperture is defined as:

$$NA = n \sin \theta \quad (20.1)$$

The refractive index, n , is usually that of air. The exception is high power oil immersion objectives (and then you use the index value for oil). Figure 20.2 illustrates how θ is measured.

As the numerical aperture increases (assuming the same magnification), the irradiance in the image increases. However, it is more usual to find the NA increasing with increasing magnification as indicated in Table 20.1. The NA increases because the focal length gets shorter resulting in a smaller working distance. Although more light is gathered it is spread out over a larger image, and the image irradiance appears to decrease.

Lower power objectives such as the 5x tend to be simple achromats (opti-

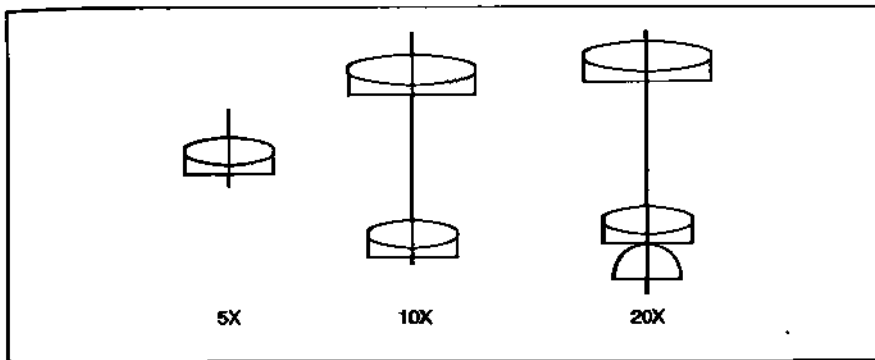


Fig. 20.3 Assorted microscope objective designs.

mized for the appropriate conjugates). As the power of the objective increases, the number of elements also increases in order to maintain good resolution at the proper image conjugate. Figure 20.3 illustrates some typical designs.

20.3 Design Overview and Helpful Hints

The mid-term involves the design of a 10X, 0.25 objective. This is a separated double achromat system. This is a challenging design and intended to be a learning experience. So an outline of the design with a few salient hints should help you get through this. As with photographic lenses, the design will proceed from the long conjugate to the short conjugate. This means that the objective is designed in reverse fashion to the way it is actually used (as illustrated in Figure 20.4).

20.3.1 Part I: Thin Lens Pre-Design

For the pre-design we will assume that the two achromats are both thin. Figure 20.5 shows what information is known and what remains to be learned. There is a lot of the latter.

1. You have enough information to determine the value of u_3 . The next thing you'll need to find is the value of u_1 . You can make use of the illustration in Figure 20.6 to help you do this. Also, keep in mind that $|y_0/y_3| = 10$.
2. You now need to find the *total bend* on the marginal ray upon its passage through the system. Conceptually, you can replace the two lenses with a "system" thin lens as shown in Figure 20.7. This illustration should help you determine the total ray deviation (TRD_m).
3. The reason this design has two lenses is to split the TRD_m between the elements so that the workload is shared between them. This helps reduce incidence angles on surfaces, which in turn will reduce aberration contributions. So split the TRD_m evenly between ϕ_1 and ϕ_2 .
4. Knowing the amount of bend that ϕ_1 must accomplish, you can employ

224 Chapter 20 Mid-Term Exam

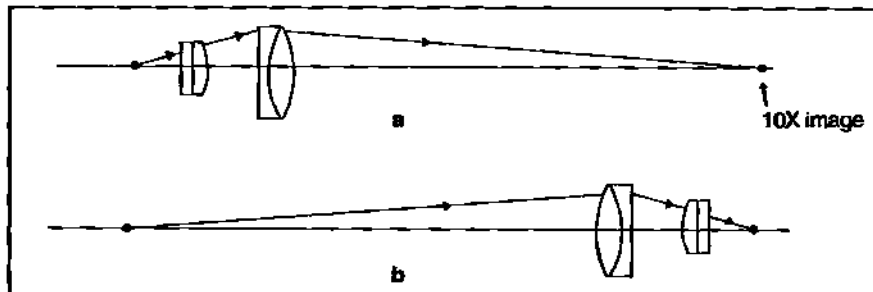


Fig. 20.4 Microscope objective: (a) as used; (b) as designed.

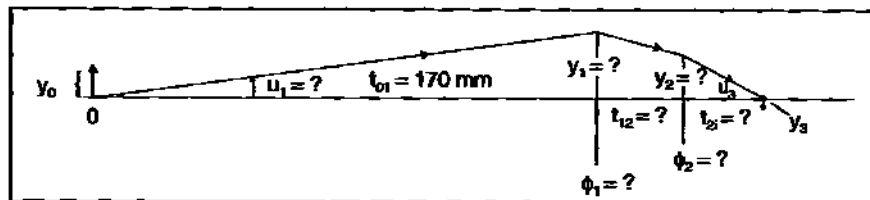


Fig. 20.5 Known and unknown parameters.

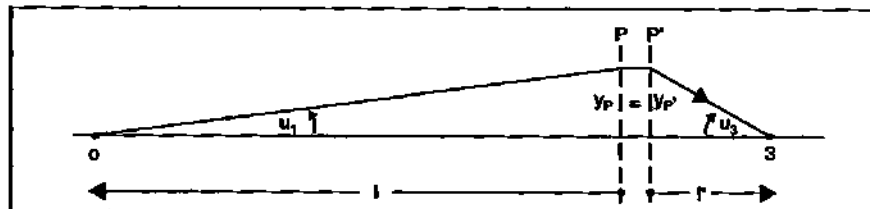


Fig. 20.6 An aid in determining u_1 .

- the PRTE to find power of the first achromat.
5. Now employ the PRTE to find out where the marginal ray crosses the optical axis after this first bend as indicated in Figure 20.8.
 6. Take *half* the distance found in (5) and place ϕ_2 at this location.
 7. Next, use the PRTE to find the power of the second achromat.
 8. You now have enough information here to determine the power and EFL of the *system*.
 9. Achromatize ϕ_1 and ϕ_2 for F and C light.
 10. Assuming that the achromat positive lens is equiconvex, calculate the starting radii for all surfaces for each achromat of the objective.

20.3.2 Part II: ZEMAX Design Optimization

1. Insert the prescription for each achromat separately into ZEMAX and op-

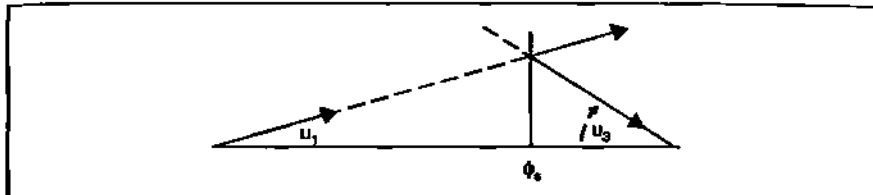


Fig. 20.7 An aid in determining TRD_m

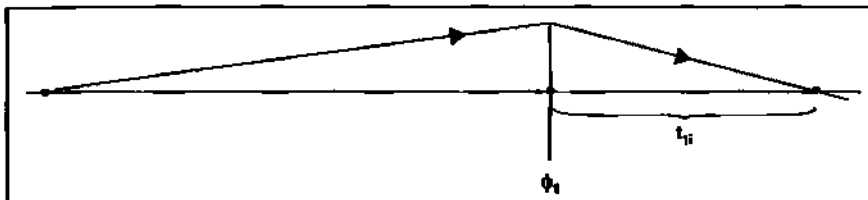


Fig. 20.8 Separation between ϕ_1 and the marginal ray crossing.

imize for EFL and AXCL. You can assume an object at infinity for both. Suggested file names for this step are:

MACH1o1b and MACH2o1b etc.

2. Combine the optimized achromat designs with an object located 170 mm from the first surface of ϕ_1 . Now optimize system so that you end up with a color corrected 10x, 0.25 objective. Suggested file name is MCR1o1b etc.
3. After each optimization run, always check your layout to see if it makes sense and that lens surfaces are not crossing one another. Each achromat should have a common diameter.

20.4 Mid-Term Exam

Design a 10x, 0.25 NA microscope objective for the F, e, C spectrum. Glass type and lens thickness information is provided in Figure 20.9.

PART I: Manually calculate the powers of the two achromats, their separation, color correction and starting radii of glass surfaces. Make use of the PRTE. Note that:

$$v_e = \frac{n_e - 1}{n_F - n_C}$$

Values for n_e can be found from the BK7 and SF2 data sheets in Chapters 6 and 16 respectively.

Table 20.2 lists the parameters you will need to find in Part I in order to

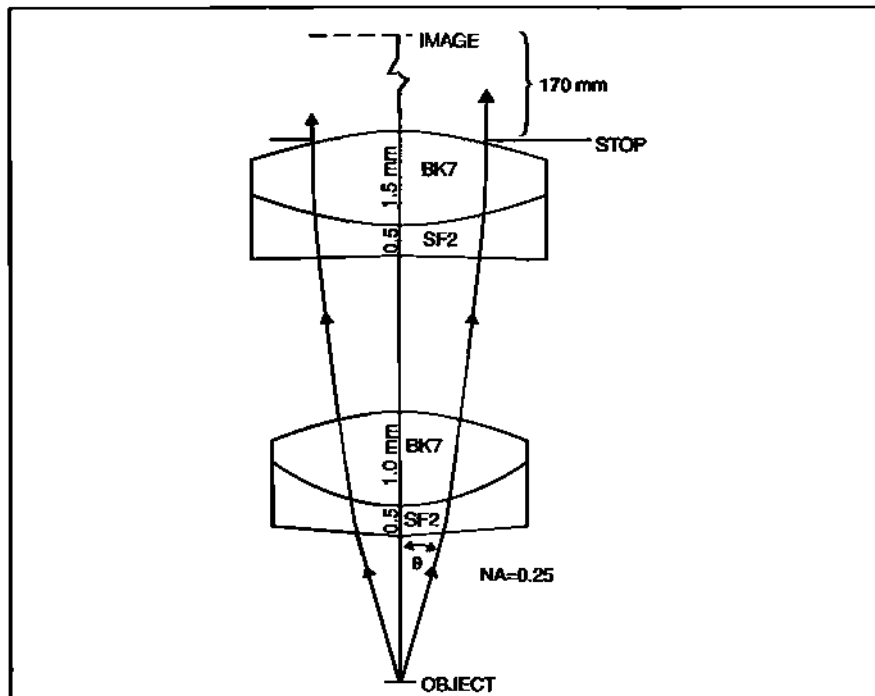


Fig. 20.9 Glass type and lens thickness for 10X objective design.

proceed with Part II.

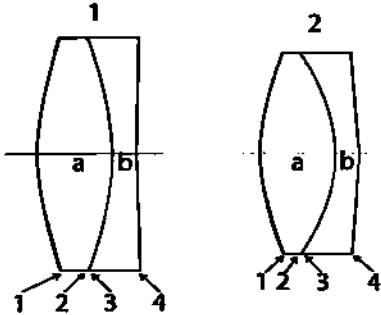
PART II: Insert starting prescription determined in Part I and install in ZEMAX. Use 1° field. Optimize system so that you end up with a color corrected 10x, 0.25 objective. (Note: the resulting system should be diffraction limited on-axis in e-light.)

20.5 Where Do We Go From Here

By now you have a decent understanding of the paraxial ray trace equations and how they're used for first and third order analysis, and in thin lens pre-design. You know how to calculate Seidel aberrations and understand ray fan and OPD plots. You have learned the importance of design principles such as lens bending, stop size, stop shift, lens splitting, and symmetry. You know how to do an achromatic correction. You are now starting to get comfortable with ZEMAX. You know how to enter a prescription, assign variables, build a merit function, perform an optimization, and analyze the resulting design using tools like ray fan plots, spot diagrams, field curvature and distortion plots, and axial color plots. You know what the numbers mean when you call up ray trace and aberration data tables.

All the things you have learned in the first half of the course will be applied

Section 20.5: Where Do We Go From Here 227

Table 20.2	
1) $u_1 =$	5) $\epsilon_{1i} =$
2) TRD =	6) $y_2 =$
3) $u'_1 =$	7) $\phi_2 =$
4) $\phi_1 =$	8) $\phi =$
Starting Powers and Radii	
	
$\phi_{1a} =$	$\phi_{2a} =$
$\phi_{1b} =$	$\phi_{2b} =$
$R_{1a1} =$	$R_{2a1} =$
$R_{1a2} =$	$R_{2a2} =$
$R_{1a3} =$	$R_{2a3} =$
$R_{1a4} =$	$R_{2a4} =$

again and again in the second half, and we will build on that knowledge base. For example, you will take the Chevalier lens and fold it into a periscopic design known as the Rapid Rectilinear lens. You will apply dialyte theory to the design of a symmetric achromatic anastigmat known as the Celor lens. This will then find an application in the design of a Cooke triplet. You will also work on the design of a famous portrait lens known as the Petzval lens. There will also be other topics sandwiched in between like telescope and eyepiece design, the use of aspherics, and various image quality criteria.

Chapter 21

APOCHROMAT

21.1 Introduction

The three-element apochromat was briefly introduced in Chapter 19. An apochromat reduces secondary color by bringing *three* colors (like *F*, *d*, *C*) to a common focus. The axial plot for the primary color of a singlet is fairly linear. The secondary color plot of an achromat has a quadratic appearance. In an apochromat, the axial plot of tertiary color tends to be cubic over the corrected spectrum. In this chapter the theory of the apochromat will be developed. This will lead to the determination of element powers which in turn leads to the calculation of starting radii for insertion into ZEMAX. An example will be given for a *cemented* apochromat.

21.2 Apochromatic Constraints

As we saw in Section 16.5.1, a thin lens *achromat* has two constraint equations:

$$\left. \begin{aligned} \phi_1 + \phi_2 &= \phi \\ \frac{\phi_1}{v_1} + \frac{\phi_2}{v_2} &= 0 \end{aligned} \right\} \quad (21.1)$$

The thin lens *apochromat*, on the other hand, has three constraining equations:

$$\left. \begin{aligned} \phi_1 + \phi_2 + \phi_3 &= \phi \\ \left(\frac{1}{v_1}\right)\phi_1 + \left(\frac{1}{v_2}\right)\phi_2 + \left(\frac{1}{v_3}\right)\phi_3 &= 0 \\ \left(\frac{P_1}{v_1}\right)\phi_1 + \left(\frac{P_2}{v_2}\right)\phi_2 + \left(\frac{P_3}{v_3}\right)\phi_3 &= 0 \end{aligned} \right\} \quad (21.2)$$

The first constraint is on power. The second constraint is on primary color, and the third on secondary color. The latter was derived in the Section 19.3. A

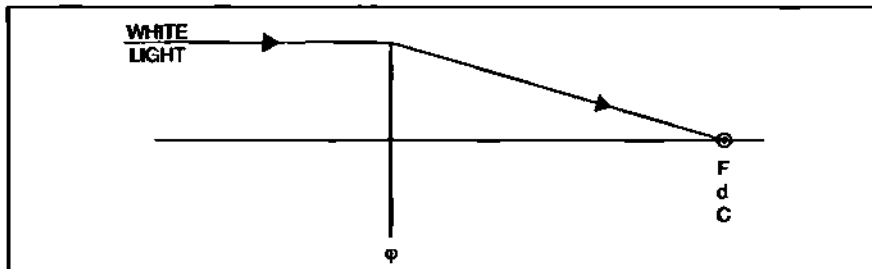


Fig. 21.1 Paraxial thin lens apochromat.

paraxial thin lens apochromat for the visible spectrum is illustrated in Figure 21.1. Because the lenses have zero thickness they are shown together as a single vertical line. Note that in this example, F , d , C light are brought to a common focus.

21.3 Apochromatic Power Solution

The constraints in Equation 21.2 consist of three equations and three unknowns. There is enough information to solve for the component powers. The algebraic technique of determinants can be used to find them. We start by finding the determinant for the set of equations shown in Equation 21.2.

$$D = \begin{vmatrix} 1 & 1 & 1 \\ \frac{1}{v_1} & \frac{1}{v_2} & \frac{1}{v_3} \\ \frac{P_1}{v_1} & \frac{P_2}{v_2} & \frac{P_3}{v_3} \end{vmatrix} \quad (21.3)$$

Expanding:

$$\begin{aligned} D &= \left(\frac{P_3}{v_2 v_3} - \frac{P_2}{v_3 v_2} \right) - \left(\frac{P_3}{v_1 v_3} - \frac{P_1}{v_3 v_1} \right) + \left(\frac{P_2}{v_1 v_2} - \frac{P_1}{v_2 v_1} \right) \\ D &= \frac{\Delta P_{32}}{v_2 v_3} + \frac{\Delta P_{13}}{v_1 v_3} + \frac{\Delta P_{21}}{v_1 v_2} \end{aligned} \quad (21.4)$$

There are three more determinants that need to be generated. The first is:

$$D_1 = \begin{vmatrix} \phi & 1 & 1 \\ 0 & \frac{1}{v_2} & \frac{1}{v_3} \\ 0 & \frac{P_2}{v_2} & \frac{P_3}{v_3} \end{vmatrix} \quad (21.5)$$

which reduces to:

$$D_1 = \left[\frac{\Delta P_{32}}{v_2 v_3} \right] \phi \quad (21.6)$$

The second determinant is:

$$D_2 = \begin{vmatrix} 1 & \phi & 1 \\ \frac{1}{v_1} & 0 & \frac{1}{v_3} \\ \frac{P_1}{v_1} & 0 & \frac{P_3}{v_3} \end{vmatrix} \quad (21.7)$$

which becomes:

$$D_2 = \left[\frac{\Delta P_{13}}{v_1 v_3} \right] \phi \quad (21.8)$$

The last determinant is given by:

$$D_3 = \begin{vmatrix} 1 & 1 & \phi \\ \frac{1}{v_1} & \frac{1}{v_2} & 0 \\ \frac{P_1}{v_1} & \frac{P_2}{v_2} & 0 \end{vmatrix} \quad (21.9)$$

and this becomes:

$$D_3 = \left[\frac{\Delta P_{21}}{v_2 v_1} \right] \phi \quad (21.10)$$

The power of the first element, ϕ_1 is given by:

$$\phi_1 = \frac{D_1}{D} = \frac{\left[\frac{\Delta P_{32}}{v_2 v_3} \right] \phi}{\frac{\Delta P_{32}}{v_2 v_3} + \frac{\Delta P_{13}}{v_1 v_3} + \frac{\Delta P_{21}}{v_1 v_2}} \quad (21.11)$$

$$\phi_1 = \frac{\Delta P_{32} \phi}{\Delta P_{32} + \frac{\Delta P_{13} v_2}{v_1} + \frac{\Delta P_{21} v_3}{v_1}} \quad (21.12)$$

Multiply the denominator by v_1/v_1 . ϕ_1 which then becomes:

$$\phi_1 = \frac{v_1 \Delta P_{32} \phi}{v_1 \Delta P_{32} + v_2 \Delta P_{13} + v_3 \Delta P_{21}} \quad (21.13)$$

In a similar fashion ϕ_2 and ϕ_3 are given by:

$$\phi_2 = \frac{v_2 \Delta P_{13} \phi}{v_1 \Delta P_{32} + v_2 \Delta P_{13} + v_3 \Delta P_{21}} \quad (21.14)$$

$$\phi_3 = \frac{v_3 \Delta P_{21} \phi}{v_1 \Delta P_{32} + v_2 \Delta P_{13} + v_3 \Delta P_{21}} \quad (21.15)$$

21.4 Calculation Example

Let's calculate the thin lens powers for a 400-mm EFL apochromat using the glasses (with the properties) listed in Table 21.1, and the ΔP_{ij} listed in Table 21.2.

Table 21.1

	Vendor	Glass	v_d	P_{AC}	n_d
1)	Schott	SSKNS	50.88	0.302094	1.658477
2)	Ohara	FPL53	94.97	0.308158	1.438763
3)	Schott	BAK1	57.55	0.304724	1.572529

Table 21.2

ΔP_{32}	-0.003434
ΔP_{13}	-0.002630
ΔP_{21}	+0.006064

Substituting in the Table values, the denominator in Equation 21.13 is found to be:

$$v_1 \Delta P_{32} + v_2 \Delta P_{13} + v_3 \Delta P_{21} = -0.174722 - 0.249771 + 0.348983 = -0.07551$$

Inserting into Equation 21.13:

$$\phi_1 = \frac{v_1 \Delta P_{32} \phi}{-0.07551} = \frac{-0.0004368}{-0.07551}$$

Therefore:

$$\phi_1 = 0.005785 \text{ or } f_1 = 172.869 \text{ mm}$$

Following the same procedure for Equations 21.14 and 21.15:

$$\phi_2 = 0.008269 \text{ or } f_2 = 120.927 \text{ mm}$$

$$\phi_3 = -0.011554 \text{ or } f_3 = -86.548 \text{ mm}$$

Section 21.4: Calculation Example 233

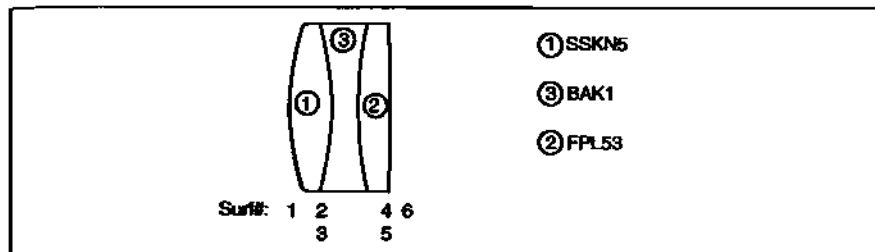


Fig. 21.2 Arrangement of apochromatic components.

(Note that the sum of the three powers equals 0.0025.)

Now that the powers of the three components have been found, we must next determine the starting curvatures for these lenses. Since color correction does not depend on the order in which the components are placed, we are going to sandwich the negative component between the positive components as indicated in Figure 21.2. We'll also let this negative component be equiconcave.

$$\phi_3 = (n_3 - 1)(C_3 - C_4)$$

where $C_4 = -C_3$,

$$\phi_3 = 2C_3(n_3 - 1)$$

$$C_3 = \frac{-0.11554}{(2)(0.572529)}$$

$$C_3 = -0.01009 \text{ or } R_3 = -R_4 = -99.105 \text{ mm}$$

Next we'll find the radius of the first surface.

$$\phi_1 = (n_1 - 1)(C_1 - C_2)$$

where $C_2 = C_3$,

$$C_1 = \frac{\phi_1}{n_1 - 1} + C_2$$

$$C_1 = \frac{0.005785}{0.658477} - 0.01009$$

$$C_1 = -0.001304 \text{ or } R_1 = -766.533 \text{ mm}$$

The final step is to find the power on the last surface.

$$\phi_2 = (n_2 - 1)(C_5 - C_6)$$

$$C_6 = C_5 - \frac{\phi_2}{(n_2 - 1)}$$

But $C_5 = C_4$; therefore:

$$C_6 = 0.01009 - \frac{0.008269}{0.438763}$$

$$C_6 = -0.008756 \text{ or } R_6 = -114.205$$

We now have our starting radii for insertion into ZEMAX.

21.5 ZEMAX Optimization

Now it's time to optimize the color correction in ZEMAX. First, insert the radii computed in Section 21.4 along with the selected glasses (over the F , d , C spectrum). To check the focal lengths computed above, I will let the lenses have zero thickness. But I will introduce a tiny airspace (0.001 mm) between the lenses. Keep in mind that the apochromat designed in Section 21.4 was for thin lenses (zero thickness) with air on *all* sides. In the MFE, I use EFLY three times—once for each lens. This will give me the focal length of each lens. Listing 21.1 is the resulting MFE. The focal lengths shown here are essentially the same as those calculated in Section 21.4.

Now we add real thickness to the lenses (say 10 mm, 5 mm, and 10 mm respectively). The layout is shown in Figure 21.3. The axial color is shown in Figure 21.4. As can be seen, the addition of thickness throws the color correction significantly off.

Unfortunately, the operand AXCL will not help us in color correcting this lens. That operand is designed to bring two colors to a common back focus. We want to bring F , d , and C to a common focus. How can we do this? One way the correction can be accomplished is by using the operands PARR and DIFF. The MFE for this utilization is shown in Listing 21.2. In our case, PARR is used to specify a paraxial radial ray height in the image plane for the different ray colors of interest. We have to specify some radial ray height *in the pupil* in order for this to work. I've used $p_y = 0.1$. The image surface is Surf. No. 7. PARR is used in two pairs, one pair per two colors. Note that no weight is assigned. The operand DIFF is then used on each PARR pair. The target is zero with weight one. Variables are on the radii as shown in the pre-optimized Listing 21.3.

The state of color correction after the optimization run is shown in Figure 21.5. The curve is cubic through the spectral region of interest. Note that the curve does pass through the F , d , C spectral points. Also, note that the tertiary spectrum is a max of 4 microns compared to the secondary spectrum of 203 microns for a 400-mm EFL achromat (discussed in Section 18.3).

Our only purpose here was to demonstrate a method for obtaining color correction in a three lens apochromat. This lens still needs to be optimized for

Section 21.5: ZEMAX Optimization 235

Merit Function Value: 6.8445233E-002

Num	Type	Int1	Int2	Hx	Hy	Px	Py	Target	Weight	Value	% Cont
1	EFFL		2					4.00000E+002	1	3.99932E+002	100.000
2	EFLY	1	2					0.00000E+000	0	1.72855E+002	0.000
3	EFLY	3	4					0.00000E+000	0	-8.65582E+001	0.200
4	EFLY	5	6					0.00000E+000	0	1.26932E+002	0.000

Listing 21.1 MFE listing the thin lens apochromat system.

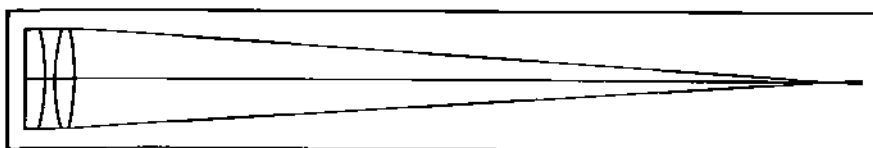


Fig. 21.3 Preliminary apochromatic design after insertion of glass thicknesses.

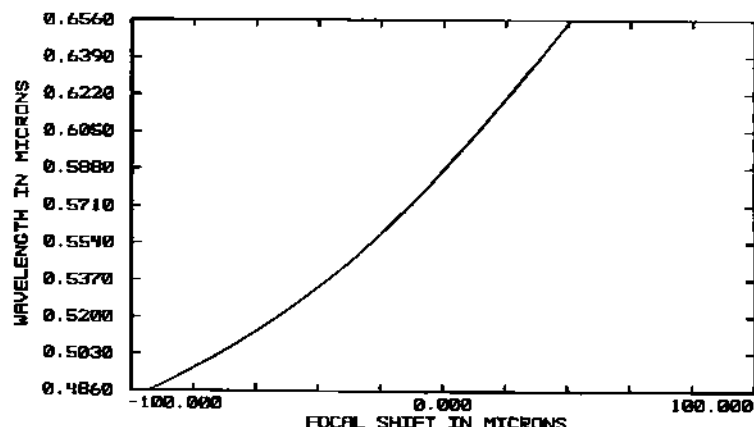


Fig. 21.4 Axial color of preliminary design.

Merit Function Value: 4.84862372E+000

Num	Type	Int1	Int2	Hx	Hy	Px	Py	Target	Weight	Value	% Cont
1	EFFL		2					4.00000E+002	1	3.91682E+002	100.000
2	EFLY	1	2					0.00000E+000	0	1.71832E+002	0.000
3	EFLY	3	4					0.00000E+000	0	-8.57625E+001	0.000
4	EFLY	5	6					0.00000E+000	0	1.22686E+002	0.000
5	PARR	7	1	0.0000	0.0000	0.0000	0.1000	0.00000E+000	0	6.82788E-004	0.000
6	PARR	7	2	0.0000	0.0000	0.0000	0.1000	0.00000E+000	0	8.88178E-016	0.000
7	DEFF	6	5					0.00000E+000	1	-5.82788E-004	0.000
8	PARR	7	2	0.0000	0.0000	0.0000	0.1000	0.00000E+000	0	8.88178E-016	0.000
9	PARR	7	3	0.0000	0.0000	0.0000	0.1000	0.00000E+000	0	2.68646E-004	0.000
10	DIFF	9	8					0.00000E+000	1	2.68646E-004	0.000

Listing 21.2 MFE listing for three color correction.

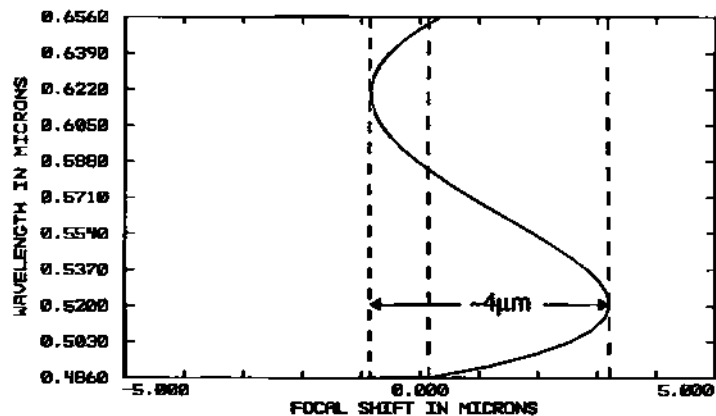


Fig. 21.5 Apochromatic correction for example system.

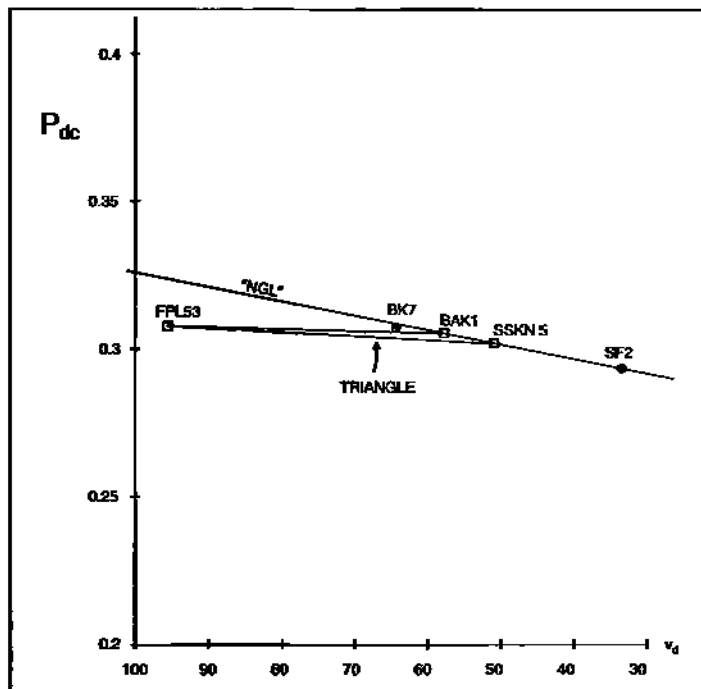


Fig. 21.6 Triangle on partial dispersion plot for glasses used in example.

spherical aberration, and coma (if a finite field is introduced). The success of lens bending to reduce these aberrations is dependent on the glass choices made. Some glass selections may prove of limited value as far as bending is concerned even though secondary color correction is achieved.

When color correction is accomplished in an apochromat (or achromat) the

Section 21.5: ZEMAX Optimization 237

SURFACE DATA SUMMARY:

Surf	Type	Comment	Radius	Thickness	Glass	Diameter	Conic
OBJ	STANDARD		Infinity	Infinity		0	0
STO	STANDARD		-766.533 V	10	SSKN5	50	0
2	STANDARD		-99.105 V	0.001		50.18751	0
3	STANDARD		-99.105 P	5	BAK1	50.18718	0
4	STANDARD		99.105 V	0.001		50.17223	0
5	STANDARD		99.105 P	10	FPL53	50.17255	0
6	STANDARD		-114.2652 V	397.2723		50.36112	0
IMA	STANDARD		Infinity			2.121979	0

Listing 21.3

back focal length is the same for all three colors, not the effective focal length. In the apochromatic example just presented, the EFLs for F , d , C are 399.9250, 400, and 400.0343 mm respectively.

Glass selection for apochromats is more critical than it is for achromats. The wrong choices could lead to excessive curvatures on some surfaces. Tighter curvatures means larger angles of incidence, and the latter generates more aberration (especially in the higher orders). There is a rule of thumb, however, which helps to steer clear of such problems. It involves the partial dispersion glass chart (Section 18.2). The rule of thumb goes as follows: two of the glasses for the achromat can lie on (or near) the "normal glass line" but the third should be well off it. (The two glasses selected from the normal glass line can be considered as a single artificial glass whose partial dispersion matches that of the third, more exotic glass choice.) Connecting the three glasses with straight lines yields a triangle. This is illustrated in Figure 21.6 for the glasses used in the example. The rule suggests that maximizing the area of this triangle will lead to a more successful design overall.¹

¹ Note: Two glass apochromats are possible. See Smith, G. H., *Practical Computer-Aided Lens Design*, Willmann-Bell, Inc., 1998.

Chapter 22

Eyepiece Design

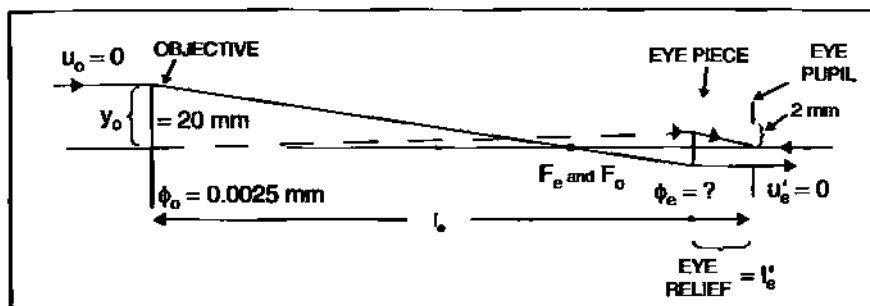


Fig. 22.1 First-order layout of telescope system.

22.1 Introduction

The mid-term exam involved the design of a microscope objective. Of course, a complete microscope also includes an eyepiece to couple the observer's eye to the image formed by the objective. The eyepiece collimates the light from this image. Consequently, the eye is effectively looking at something at infinity. Unlike microscope objectives, which look at small things close-up, telescope objectives (which can be achromats or apochromats) look at big things very far away—things which are for all intents and purposes at infinity. Still, it is necessary to couple the observer's eye to the image formed by the telescope objective just as it was for the microscope objective. Designs for telescope and microscope eyepieces are quite similar except the former are larger in size. In this chapter we will design a basic Ramsden eyepiece. The latter also introduces the functionality of something called a "field lens."

22.2 First Order Layout of Eyepiece

Figure 22.1 is the first order layout of our example telescope system. The objective has a 400-mm EFL and operates at $f/10$. The eyepiece performs two functions: first, it recollimates the light; second, it forms an image of the objective that more or less matches the pupil diameter of the iris. Note: This image is also the

240 Chapter 22 Eyepiece Design

exit pupil. For low power telescopes such as those used in riflescopes, there is a practical third consideration. The objective image needs to be far enough behind the eyepiece so that it will not hit the eye during recoil. This is called "eye relief."

We will use the PRTE to find pertinent parameters. The first step is to find the marginal ray angle after refraction by the objective.

We begin by using the bending equation:

$$u'_o = u_o - y_o \phi_o$$

$$u'_o = 0 - 20(0.0025) = -0.05 = u_e \quad (22.1)$$

Let us assume that the iris diameter is 4 mm. We can now determine the power of the eyepiece by again using the bending equation:

$$u'_e = u_e - y_e \phi_e = 0$$

Solving for ϕ_e :

$$\phi_e = \frac{u_e}{y_e} = \frac{-0.05}{-2}$$

$$\phi_e = 0.025 \quad (22.2)$$

or:

$$f_e = 40 \text{ mm}$$

Next we must determine the eye relief. We already know the magnification. It is the ratio of the iris diameter to the objective diameter:

$$m = \frac{4}{40} = -0.1 \quad (22.3)$$

But the magnification is also equal to the conjugate distances, i.e.,

$$m = \frac{l'_e}{l_e} \quad (22.4)$$

where $l_e = -(f_o + f_e) = -440 \text{ mm}$. Therefore,

$$l'_e = 44 \text{ mm}$$

We will assume that the eyepiece is a convex-plano lens ($C_2 = 0$) made out of BK7. Knowing ϕ_e we can easily determine the radius of the convex surface.

$$\phi_e = (n_d - 1)C_1$$

$$C_1 = \frac{0.025}{0.5168} = 0.048375 \quad (22.5)$$

Section 22.3: Insertion into ZEMAX 241

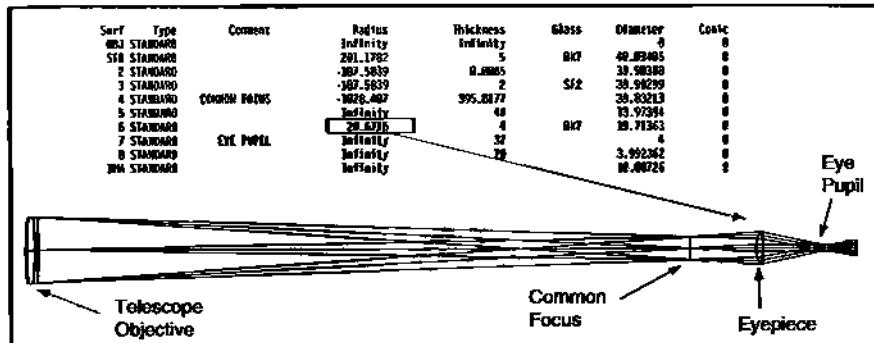


Fig. 22.2 Telescope layout in ZEMAX.

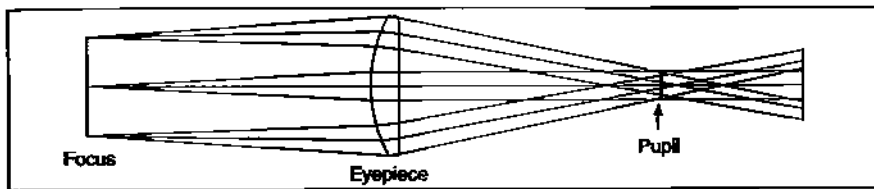


Fig. 22.3 Close-up of eyepiece region.

or

$$R_1 = 20.6716 \text{ mm}$$

22.3 Insertion into ZEMAX

For our objective we will use the 400 mm EFL achromat designed in Section 17.2. We will also give the singlet eyepiece some reasonable thickness, say 4 mm. The system is shown in Figure 22.2, (along with the prescription) for a $\pm 1^\circ$ field. Figure 22.3 is a close-up of the eyepiece region.

The paraxial image of the objective formed by the eyepiece lies at a distance of 41.405 mm from its plano surface. However, what is shown in Figure 22.3 is the place where the recollimated real ray beams from the three field points *overlap*. This occurs empirically at a distance of 37 mm from the plano surface. This is where the pupil of the eye would be located for viewing.

If we double the field, the eyepiece lens must increase both in diameter and thickness to accept all the rays. Further, the field extremes are no longer properly recollimated due to severe aberration. These points are illustrated in Figure 22.4.

If the field is increased further, the size and thickness of the eyepiece gets larger and the induced aberrations worsen. Also, many rays from the field extremes start missing the convex surface altogether.

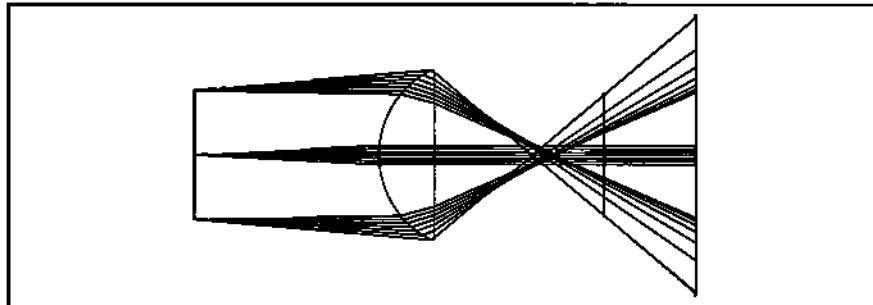
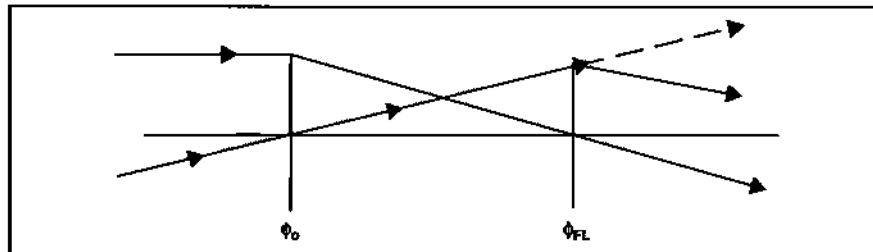
Fig. 22.4 Eyepiece geometry when field is $\pm 2^\circ$.

Fig. 22.5 Paraxial illustration of telescope objective plus field lens.

22.4 Field Lens

Consider the paraxial layout shown in Figure 22.5. The diagram shows the telescope objective with another lens located right at its focal plane. This is called a field lens. If we look at the bending equation for rays passing through the field lens, we'll note an interesting effect:

$$u'_f = u_{fi} - y_f \Phi_f \quad (22.6)$$

The y -height at the field lens for all rays entering the objective *parallel* to the optical axis is zero at the field lens location. That means that y_f in Equation 22.6 is zero, which in turn means that all these rays leave the field lens at the *same* angle they entered it with.

Now look at the off-axis rays. As the field angle increases, the y -height of these rays (which are focused at the field lens) increases. This means that u'_f is no longer equal to u_{fi} , and bending does take place.

Let's now illustrate this point via ZEMAX. We place a plano-convex BK7 lens close to the objective's focal plane. We will watch the behavior of the various field beams as they pass through this lens on their way to the eyepiece. The only change that will be made is the power of the field lens. This will be done by simply changing the curvature of the convex surface (Surf. no. 7). The results are shown in Figure 22.6. The field beams leave the focal plane of the objective and immediately encounter the field lens. They then proceed to the *plane* of the recollimat-

Section 22.4: Field Lens 243

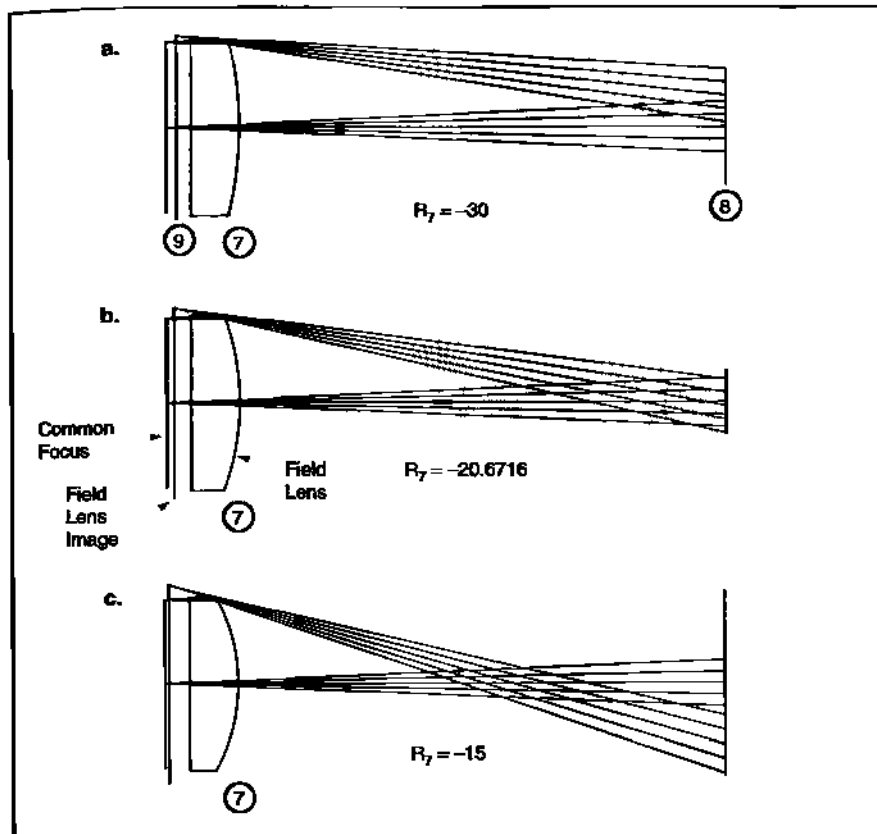


Fig. 22.6 Steering of field beams by field lens.

ing lens (Surf. no. 8). (Note, the recollimating lens is not present in this model.) The beams then proceed to their paraxial focus location (Surf. no. 9), which is virtual in this case.

The on-axis beam remains on-axis after interacting with the field lens with little disturbance to its divergence no matter the radius placed on Surf. No. 7. However, the off-axis beam is greatly affected by the radius change; not in divergence but in *direction*. In fact, we can find a radius that steers the off-axis beam tight on top of the on-axis beam at the plane of the recollimating lens.

It is now time to reinsert the recollimating lens and see how it interacts with the redirected beams from the field lens. This is illustrated in Figure 22.7.

For $R_7 = -15$ mm, the $\pm 1^\circ$ field beams cross in front of the recollimating lens. If we place our eyeball behind the recollimating lens we would not see the full field. For the field that we do see, the brightness would fall off with the field because of vignetting by the iris. For $R_7 = -20.67$ mm, the fields cross in the middle of the recollimating lens. Problems would be similar to the previous case

244 Chapter 22 Eyepiece Design

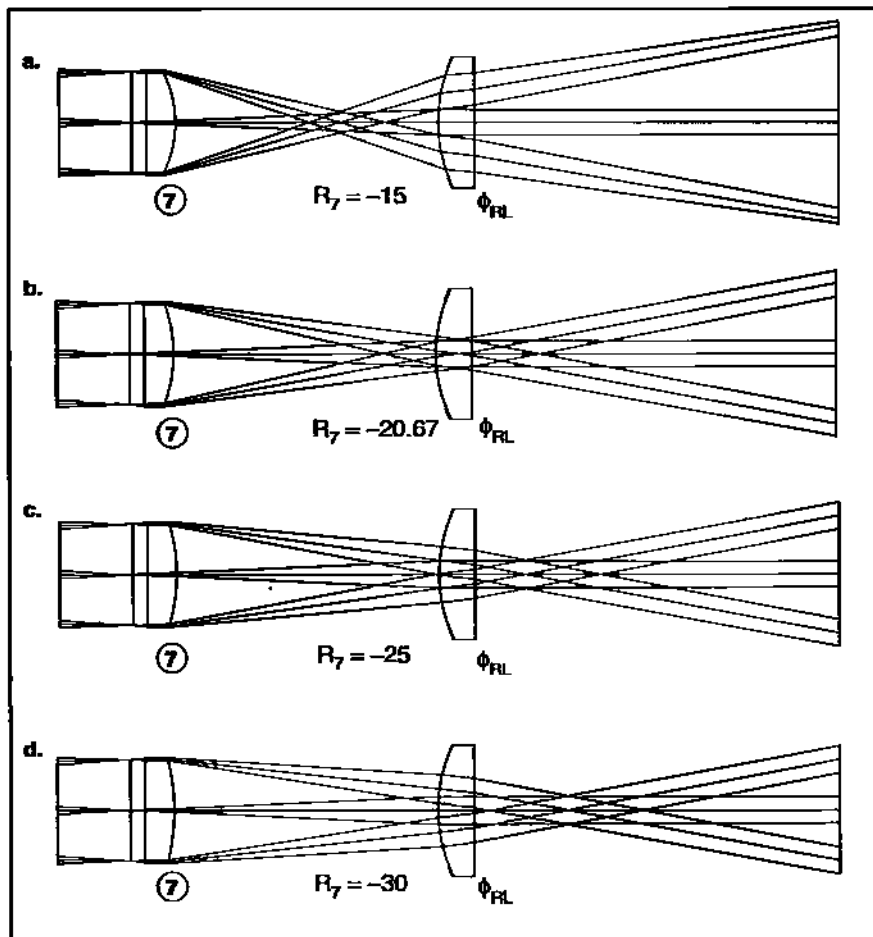


Fig. 22.7 Interaction of recollimating lens with power change in field lens.

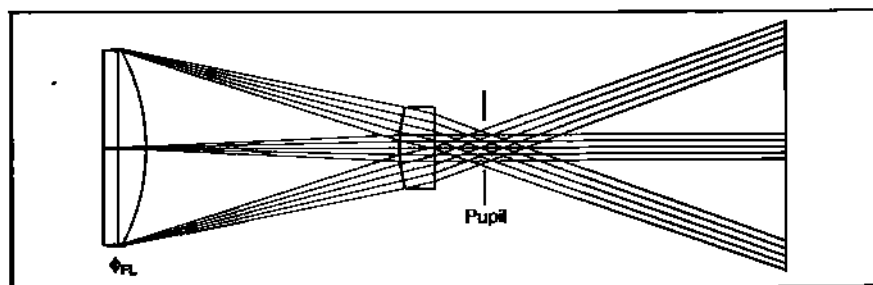


Fig. 22.8 Behavior of eyepiece system for $\pm 2^\circ$ field.

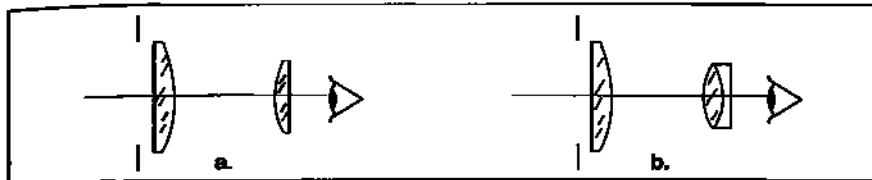


Fig. 22.9 a. Ramsden eyepiece; b. Kellner eyepiece.

but not as severe. For $R_7 = -25$ mm, the collimated field beams cross behind the recollimating lens. We finally have a position for the iris pupil which can view the entire field without vignetting. The eye relief can be controlled by R_7 . It can be pushed further out by increasing the radius as shown for the case where $R_7 = -30$ mm. Note also that the diameter of the recollimating lens needed to collect all field beams also depends on R_7 .

If we increase the field to $\pm 2^\circ$, the field lens will double its diameter but the recollimating lens diameter change is modest. This is shown in Figure 22.8.

22.5 The Ramsden and Kellner Eyepieces

The classic Ramsden eyepiece consists of two plano-convex lenses with plano sides facing outward. One lens is the field lens; the other, the recollimating lens as illustrated in Figure 22.9a. It is an economical eyepiece that finds use in both telescopes and microscopes. It has a further advantage in that a reticle can be placed at the “real” object surface of the eyepiece. It does have some problems with lateral color, but over modest fields this can be overlooked. Achromatizing the recollimating lens to reduce lateral color leads to a variant on the Ramsden design known as the Kellner eyepiece. The latter is illustrated in Figure 22.9b.

22.6 The Ramsden Eyepiece and Eye Model

Let’s return to Figure 22.8 and add a very simple model of the human eye. At the pupil (defined by the crossing of the recollimated field beams) we introduce an idealized lens called a *paraxial* surface type in ZEMAX. (This lens forms an image without introducing any aberration of its own.) To add this lens we first insert another surface before the image surface. Next, double-click on *standard* on this new surface. A menu box will appear. Select Surface Type. A submenu will then appear. Select Paraxial then OK. On the paraxial surface line we must insert numerical values under the Thickness column and Focal Length column (which appears on the right side of the conic header). The eye focal length is about one inch. Since the lens units are in millimeters, insert 25.4 at both locations.

The retina lies on a curved surface. Let ZEMAX find this curvature by placing “v” on the image surface under the radius header. This will be the only variable. Use the default TRAC in the MFE and no other operands. The result is

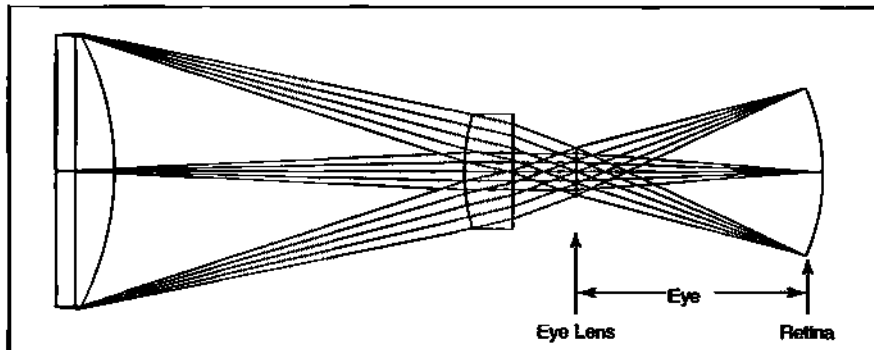


Fig. 22.10 Ramsden eyepiece with model eyeball.

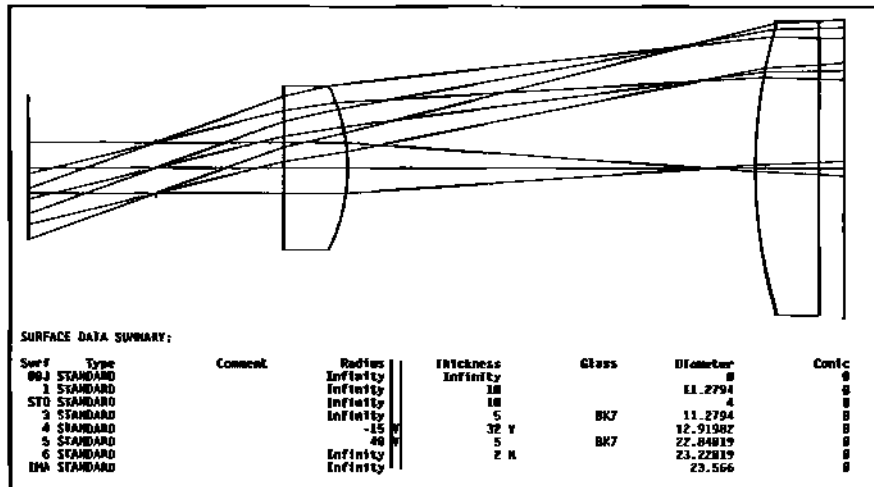


Fig. 22.11 Starting layout and prescription for Ramsden example.

shown (Surfaces 5–11) in Figure 22.10. In this case, the retina radius is -21.724 mm for a $\pm 2^\circ$ field.

22.7 Ramsden Design Example Using ZEMAX

In the mid-term exam you designed a microscope objective. It was designed from the long to the short conjugate (opposite to the operational use). The Ramsden eyepiece can be designed using a similar approach: starting with collimated fields entering a stop (iris pupil) followed by the recollimating lens and field lens.

Let the stop diameter be 4 mm and the eye relief distance be 10 mm. The field will be 20° . We'll let the 5-mm thick plano-convex lenses be BK7 with an initial interlens separation of 32 mm. Set the convex surface radius of the recollim-

Section 22.7: Ramsden Design Example Using ZEMAX 247

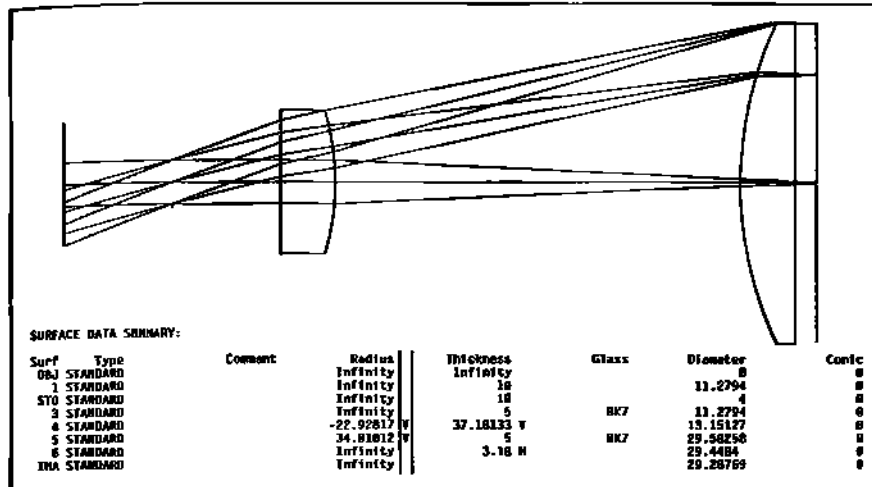


Fig. 22.12 Optimized layout (and prescription) for Ramsden example.

mating lens so that the lens focuses in front of and near the field lens. Set the radius on the convex surface of the field lens to 40mm. Set the distance from the flat surface of the field lens to the image plane at 2 mm. Set variables on the convex surfaces and the interlens airspace. Spectrum will be F , d , C-light.

Now let's work on the merit function. The singlet eyepiece designed in Section 22.2 had an EFL of 40 mm. We'll use this for our Ramsden. Set EFL to a target of 40 mm with weight 1. You may have noticed that real eyepieces have a numeral value stamped on them followed by "X". This is the *angular* magnification of the eyepiece. Consequently, we will make use here of the AMAG operand. The eyepiece we are designing will have a 10X value. But since this is being designed in reverse (so we do not have to contend with an image at infinity), we set AMAG to a target of 0.1 with weight 1. Finally, to get the best RMS spot values at the defined distance for the image plane, default TRAC is incorporated into the MFE. Figure 22.11 shows the starting layout along with the prescription. Figure 22.12 shows the layout after running the optimization.

Chapter 23

Field Lens and Windows

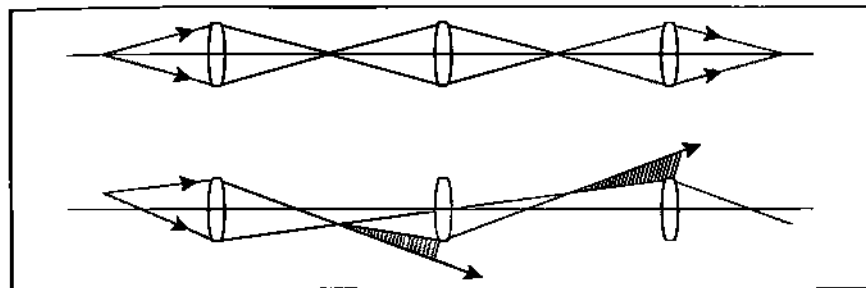


Fig. 23.1 Simple relay system.

23.1 Introduction

The eyepiece designed in the last chapter showed the important role played by the on-board field lens. In this chapter we will continue with a qualitative description of field lens application in relay systems. After this we will move onto a discussion of the zero-power system known as the window. Many optical systems operate by viewing the subject of interest through a window. In aerial reconnaissance, for example, the window serves both a structural and optical function. It is part of the aircraft fuselage in the former; part of the camera system in the latter. In many test systems the window separates the optical metrology instruments from a hostile environment, such as a vacuum or deep water. We will examine the effect windows have on image quality.

23.2 Field Lenses in Relay Systems

Suppose you have to design an optical system in which an initial image of some object must be transferred to the final sensor through a long tube or tunnel. The long tube may be a submarine periscope or a medical endoscope. A common way of transferring the image is by using a unit magnification relay system. Recall that unit magnification systems are symmetrical and aberrations such as coma, distortion, and lateral color are automatically compensated. (We saw this behavior with the periscopic lens in Chapter 12 when it was operated at unit magnification.) A

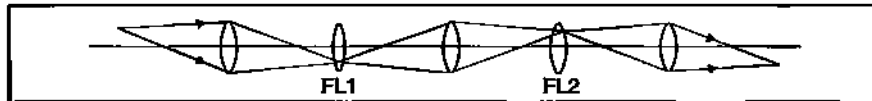


Fig. 23.2 Incorporation of field lenses into the relay system.

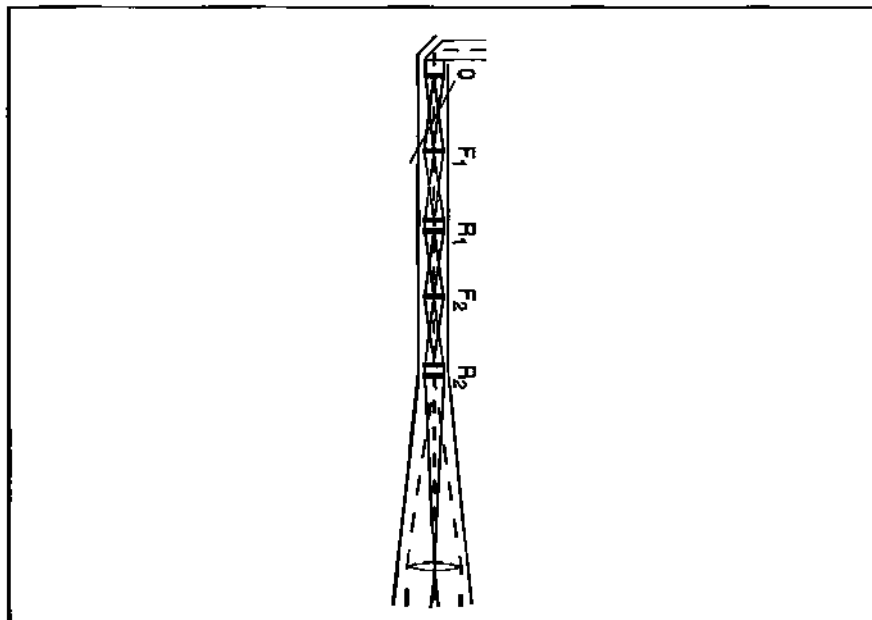


Fig. 23.3 Periscope. Figure from "The Telescope" in Optical Systems Design by Rudolph Kingslake, © 1983 by Academic Press, reproduced by permission of the publisher.

simple relay is shown in Figure 23.1.

All the light collected from the on-axis point by the first lens makes it through the entire relay to the final image point without loss (assuming 100% transmission). However, light collected by the first lens from an off-axis point does not make it through the relay unscathed. A certain percentage of the light is lost through vignetting at both the second and third relays. The further off-axis we go, the more light is vigneted. The final image will be bright in the center with illumination decreasing with increasing field.

This relative illumination problem can be resolved by incorporating field lenses as illustrated in Figure 23.2. A field lens is located at each intermediate image plane formed by the relays. The main design consideration with field lenses is having just the right amount of power so that the beam is steered fully onto the aperture of the following relay. But this has little effect on the power of the relay system.

Field lenses are not complicated; they're usually just simple equiconvex

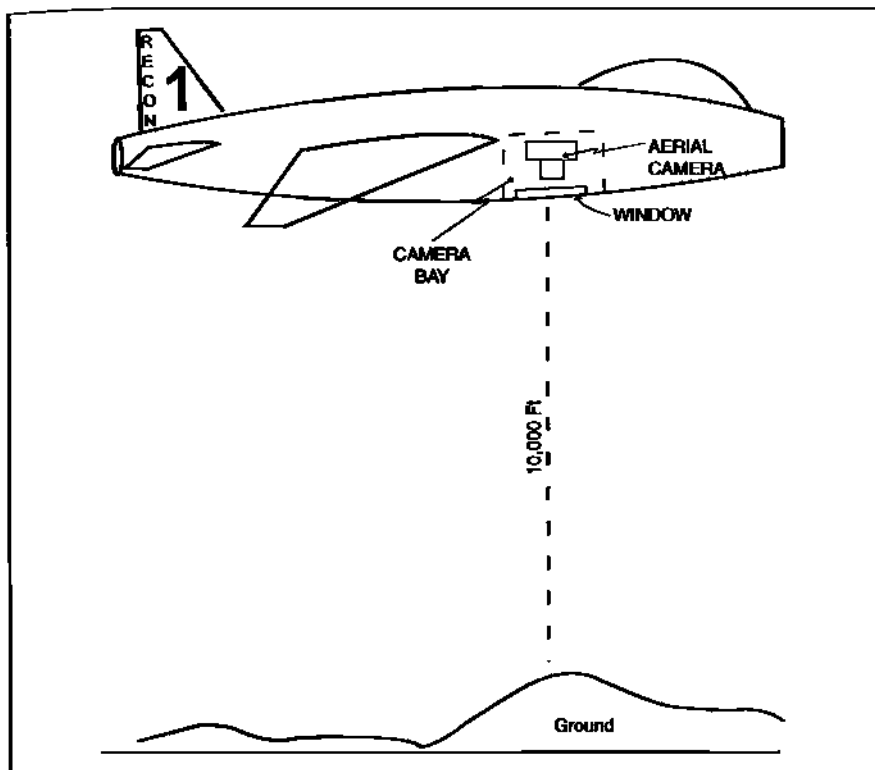


Fig. 23.4 In aerial reconnaissance, the window is part of the overall optical system.

lenses. This can be seen in the upper portion of a submarine periscope as shown in Figure 23.3. The objective views the target ship (through a right-angle prism) and forms the primary image. The latter must be relayed down inside the vessel for inspection. The first field lens is located with the primary image. This is followed by the first relay group which forms a secondary image. Another field lens is located at the secondary image. This is followed by the second relay group. A third field lens is located at this tertiary image. This process is repeated several more times until the final image is viewed via an eyepiece.

23.3 Windows

In the introduction, I mentioned windows in an aerial reconnaissance role. Figure 23.4 illustrates an operational scenario. The camera system looks out through the window at a ground scene of interest. The rays entering the window from various field points are essentially collimated. The window itself appears as a simple parallel plate of glass. As such it should not introduce any aberration, and hence have no impact on image quality. However, closer inspection of the window via inter-

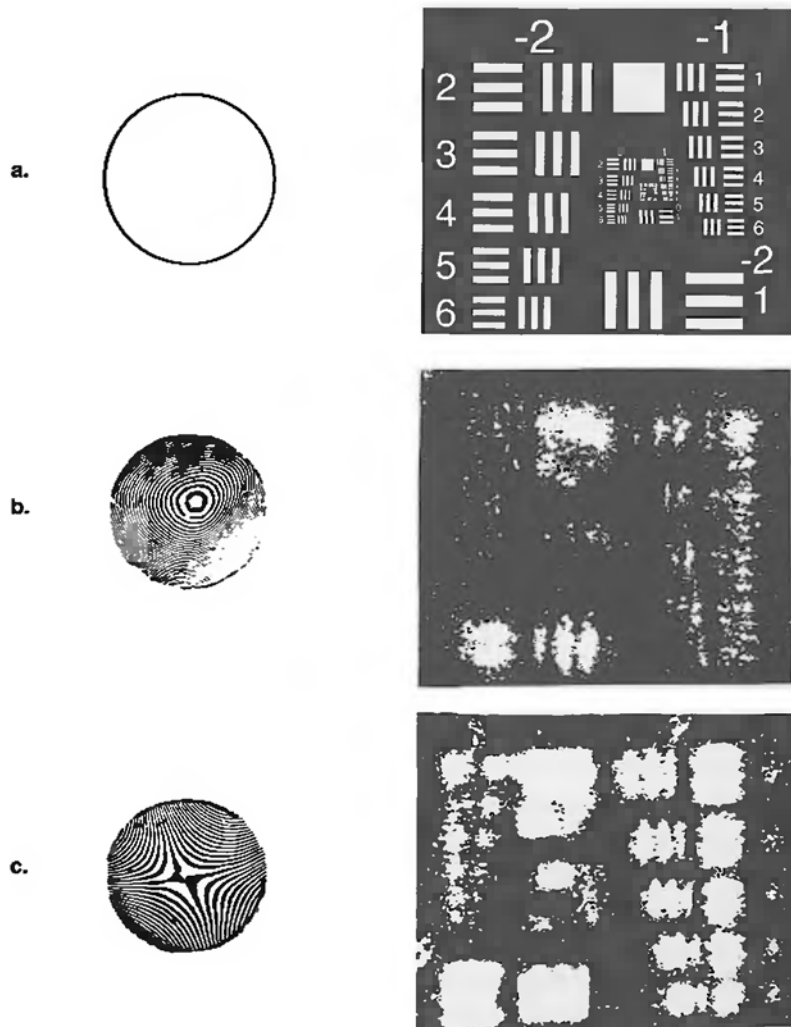


Fig. 23.5 The effect of OPD variations in the window have on image quality.

ferometry may show surprising and unwelcome imperfections. Figure 23.5 shows the effect various real windows have on image quality. The lefthand column shows the interferogram whose fringes can be considered as an OPD contour map in the entrance pupil. (This is similar to Figure 7.19 which showed OPD in the exit pupil for various aberrations.) The right column shows the windows effect on imagery. In (a) the window is perfect. The OPD is uniform across the pupil resulting in a null fringe. The image quality is degraded only by aberration in the imaging lens. In (b) the window OPD looks like defocus and the resulting image is fuzzy. In (c) the window OPD looks astigmatic and near medial focus. It blurs the image.

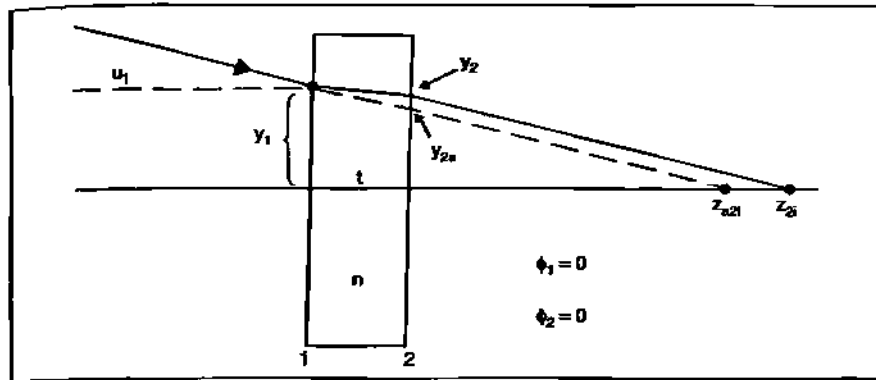


Fig. 23.6 Defocus introduced by parallel plate in a converging beam.

Obviously, (a) is the best choice for installation in front of the lens. Note: a window that has a small amount of pure wedge (yielding a uniform density, straight line fringe pattern) tilts the wavefront. This introduces a small lateral shift of the image relative to the camera format. There is some lateral color but it is generally negligible and image quality is unaffected.

23.4 Aberrations Introduced by Perfect Windows

23.4.1 Focus Shift

When a perfect parallel plate is placed in the collimated space prior to the lens, it introduces no aberration affecting image quality. However, if that same perfect window is placed *behind* the lens in the *converging* beam, it will introduce aberration. The major effect is defocus. The amount can be derived using the PRTE. Figure 23.6 illustrates the geometry.

We have the marginal ray converging on the first window surface with incident angle u_1 and height y_1 . The "bending" equation is used to find the refracting angle u'_1 . Since the surface has zero power:

$$u'_1 = \frac{u_1}{n} = u_2 \quad (23.1)$$

The height on the second window surface is via the "transfer" equation:

$$y_2 = y_1 + \left(\frac{u_1}{n} \right) t \quad (23.2)$$

Employing the bending equation again on the second zero power surface:

$$u'_2 = nu_2 = n\left(\frac{u_1}{n}\right) = u_1 \quad (23.3)$$

Where does this ray cross the optical axis? Using the transfer equation:

$$\begin{aligned} y_i &= 0 = y_2 + u'_2 z_{2i} \\ z_{2i} &= \frac{-y_2}{u'_2} \end{aligned} \quad (23.4)$$

Had the glass window *not* been there, where would the marginal ray cross the optical axis? The air thickness will still be t .

$$y_{a2} = y_1 + u_1 t \quad (23.5)$$

Where does this ray cross the optical axis?

$$z_{a2i} = \frac{-y_{a2}}{u_1} \quad (23.6)$$

The difference between the two marginal ray crossings (with and without the window) is given by:

$$\Delta z = z_{2i} - z_{a2i} \quad (23.7)$$

Substituting in Equations 23.4 and 23.6:

$$\Delta z = -\left(\frac{1}{u_1}\right)(y_2 - y_{a2}) \quad (23.8)$$

Substituting in Equations 23.2 and 23.5 and simplifying:

$$\begin{aligned} \Delta z &= -\left(\frac{t}{u_1}\right)\left(\frac{u_1}{n} - u_1\right) \\ \Delta z &= \left(\frac{n-1}{n}\right)t \end{aligned} \quad (23.9)$$

So the main disturbance introduced by the window is a focus offset. If this is not accounted for, imagery will be degraded.

For example, let the window have $n = 1.5168$ and $t = 2$ cm:

$$\Delta z = 0.681 \text{ cm}$$

The corresponding ZEMAX example is shown in Figure 23.7. In Part *a*, a 2-cm thick airspace is delineated behind the 100-mm $f/3.3$ achromat (Section 17.4).

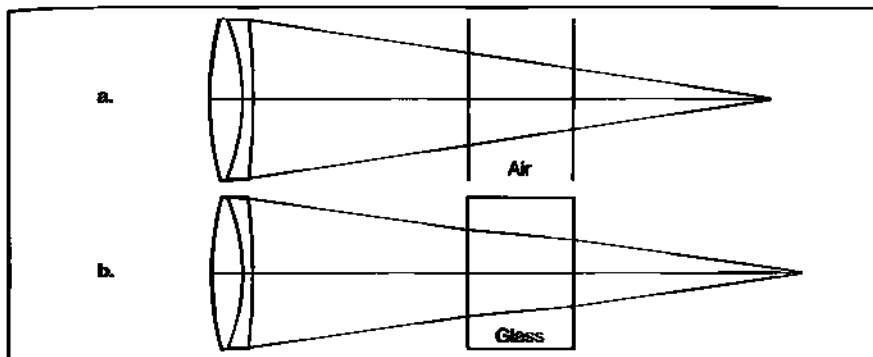


Fig. 23.7 Focus shift introduced by BK7 window.

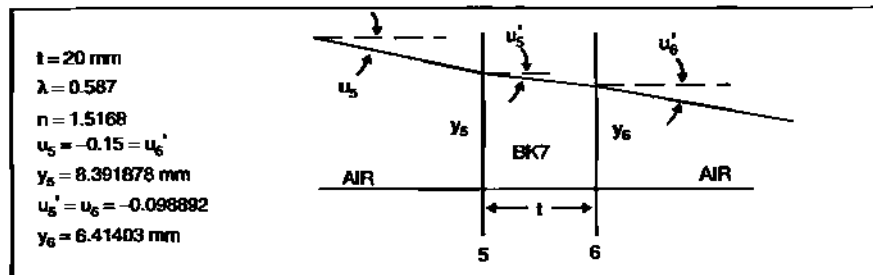


Fig. 23.8 Paraxial trace through window.

In *b*, this same space is filled with BK7 glass. The shift in focus is evident and amounts to 6.81 mm.

23.4.2 Spherical Aberration

Aside from the defocus, the window also introduces spherical aberration. We can calculate the amount via the Seidel coefficient S_1 (Table 10.1) for both window surfaces using paraxial ray trace data. A paraxial trace of the marginal ray through the 100-mm, *f*/3.3 achromat and window (located 40 mm behind the lens) yields the data shown in Figure 23.8.

For the first window surface (which is surface no. 5 after the achromat) the Seidel coefficient is given by:

$$S_{15} = -A_5^2 y_5 \Delta_5 \left\{ \frac{u}{n} \right\} \quad (23.10)$$

where:

$$A_5 = n_5(u_5 + y_5 C_5) = u_5$$

256 Chapter 23 Field Lens and Windows

Surf	SPHA	S1
ST0	0.05235	
2	1.80564	
3	-1.98607	
4	0.11429	
5	-0.01601	}
6	0.01224	} -0.00377
IMA	0.00000	
TOT	-0.01758	

Fig. 23.9 ZEMAX calculated Seidel Coefficient S_i for window.

since $n_3 = 1$ and $C_3 = 0$, and:

$$\Delta_5 \left\{ \frac{u}{n} \right\} = \frac{u'_5}{1.5168} - \frac{u_5}{1} = 0.084802$$

So:

$$S_{15} = -(-0.15)^2 (8.391878)(0.084802)$$

$$S_{15} = -0.016012$$

For the second window surface (Surf. no. 6) the Seidel coefficient is given by:

$$S_{16} = -A_6^2 y_6 \Delta_6 \left\{ \frac{u}{n} \right\} \quad (23.11)$$

where:

$$A_6 = n_6 u_6 = (1.5168)(-0.098892) = -0.149999$$

and:

$$\Delta_6 \left\{ \frac{u}{n} \right\} = -0.084802$$

So:

$$S_{16} = -(-0.149999)^2 (6.41403)(-0.084802)$$

$$S_{16} = 0.012238$$

The total contribution introduced by the window is:

$$S_{fw} = S_{15} + S_{16} \quad (23.12)$$

Section 23.4: Aberrations Introduced by Perfect Windows 257

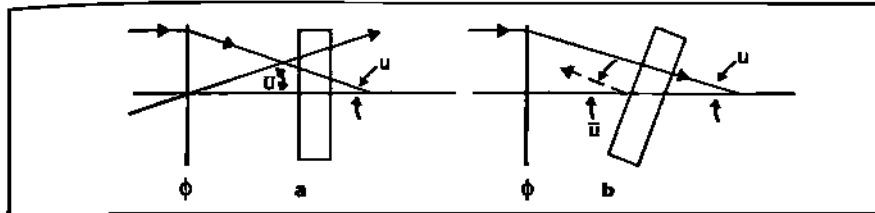


Fig. 23.10 Window surface: (a) normal to system optical axis; (b) tilted with respect to system optical axis.

Table 23.1	
Aberration	Seidel Coefficient
Spherical	$S_{IW} = Nu^4$
Coma	$S_{IIW} = Nu^3 \bar{u}$
Astigmatism	$S_{IIIW} = Nu^2 \bar{u}^2$
Petzval Curvature	$S_{IVW} = 0$
Distortion	$S_{VW} = Nu \bar{u}^3$

$$S_{IW} = -0.016012 + 0.012238$$

$$S_{IW} = -0.003774 \text{ mm}$$

Therefore, the spherical aberration introduced by the window is:

$$W_{040} = \frac{S_{IW}}{8} \quad (23.13)$$

$$W_{040} = -0.472 \mu\text{m} = -0.804\lambda$$

This is a significant amount of spherical aberration contributed by the “perfect” window.

The numerical values calculated for S_{IW} and S_{VW} can be easily verified in ZEMAX by going to:

Analysis → Calculations → Seidel.

Look at the values displayed for surfaces 5 and 6 as shown in Figure 23.9. Their sum equals -0.00377 .

23.4.3 Simple Formulas for Window Seidel Coefficients

Fortunately there is an easier way of determining window Seidel aberration content for *both* on and off-axis conditions. The formulas shown in Table 23.1 turn it

258 Chapter 23 Field Lens and Windows

into a simple calculation.¹ N in Table 23.1 is given by:

$$N = \frac{(1-n^2)_t}{n^3} \quad (23.14)$$

The geometries are illustrated in Figure 23.10 for a window *a* whose surface is normal to the system optical axis but not the chief ray; *b* for a window tilted with respect to the optical axis (and no chief ray).

Note that these formulas are independent of y-height. This means that the aberrations are unaffected by the axial location of the window in the converging beam. To illustrate we will use the same window example from Section 23.2. Using the data from Figure 23.8 we first calculate N from Equation 23.14.

$$N = \left(\frac{1 - 1.5168^2}{1.5168^3} \right) 20$$

$$N = -7.454$$

Then:

$$S_{IW} = (-7.454)u_5^4$$

$$S_{IW} = (-7.454)(-0.15)^4$$

$$S_{IW} = -0.003774 \text{ mm}$$

which is the same value obtained in Equation 23.12 via the ray trace approach.

If we have a chief ray incident at 10° or have the window tilted 10°, then the coma, astigmatism, and distortion are:

$$S_{HW} = +0.004436 \text{ mm};$$

$$S_{UW} = -0.005214 \text{ mm};$$

$$S_{VW} = +0.00613 \text{ mm}.$$

23.5 Tilted Window in ZEMAX

A tilted window can be introduced into ZEMAX by making use of the coordinate break surface option. The window is sandwiched between two coordinate breaks. It is done in the following way:

1. insert two new surfaces: one just before the front window surface, another one just after the back window surface;

¹ Note: derivations of the formulas in Table 23.1 can be found in Chapter 3 of *Aberration Theory Made Simple* by V. Muhnjan (SPIE Tutorial Text TT-6, 1991).

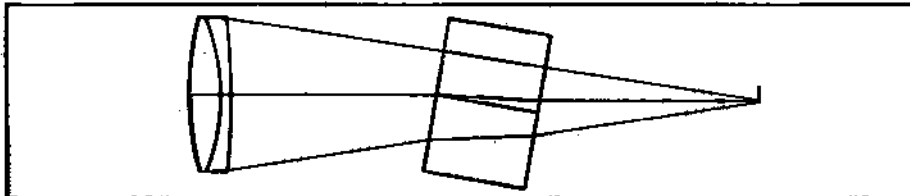


Fig. 23.11 Tilted window example in ZEMAX.

2. go to the first new surface and double-click on standard;
3. from surface type menu click on the “down arrow” icon;
4. select coordinate break from the menu;
5. click on OK;
6. repeat this procedure on the second new surface;
7. go back to the first coordinate break and move right until you come to the box under the heading Tilt About X;
8. insert the desired angle (in degrees);
9. staying in the same column, move down to the second coordinate break;
10. insert the negative of the first angle (which restores the original coordinate system orientation).

The result of these steps is shown in Figure 23.11. Note that there is zero thickness for the first coordinate break and the marginal ray solve was placed on the second coordinate break (and zero thickness on the second window surface). Also, use L3D instead of Lay to get the layout.

23.6 Effect on Axial Color

One final point before departing windows. The original achromatic correction for the 100 mm $f/3.3$ is upset by the addition of a window in the converging path. Figure 23.12a shows the original correction for the lens alone. Figure 23.12b shows the imbalance caused by the window. To restore achromatism, the optimization must be conducted with the window in place. Figure 23.12c shows the result of this reoptimization.

23.7 Homework

Using the singlet from the Homework for Chapter 3 (file name: Sing1o1b), insert a 25.4 mm thick BK7 window in the convergent beam 100 mm behind the lens.

- a. Using ZEMAX, find the contribution to S_t due to the window.
- b. Using the equation for S_{tw} , calculate the contribution of the window.
- c. How do a and b compare?

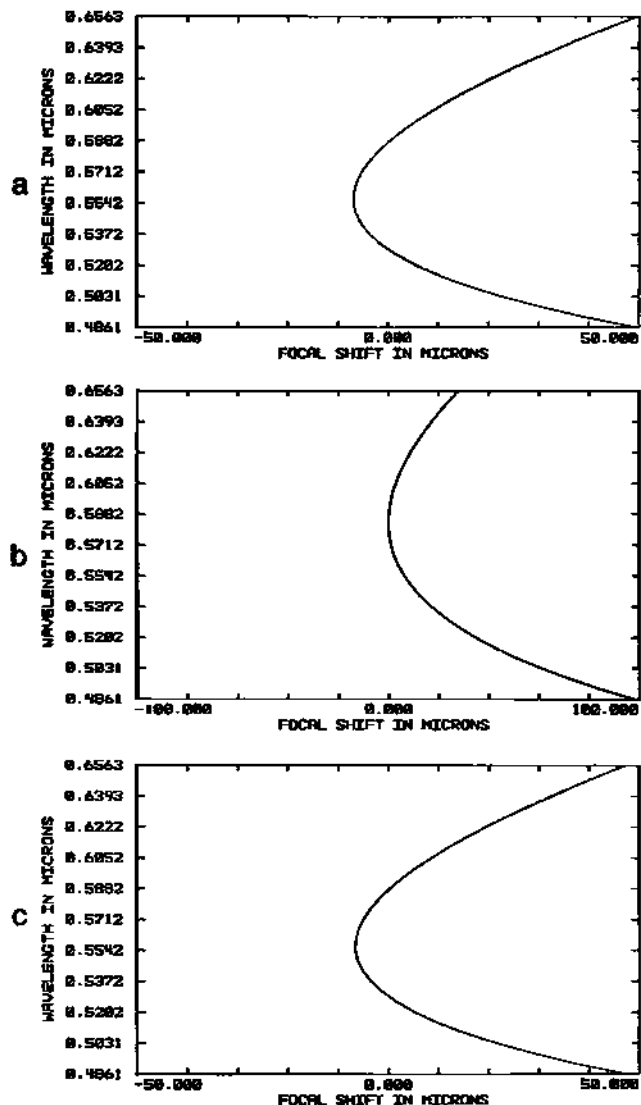


Fig. 23.12 Axial color of 100 mm f/3.3: (a) lens optimized, no window; (b) window present; (c) reoptimization of lens with window in place.

Chapter 24

Mirrors and Corrector Plates

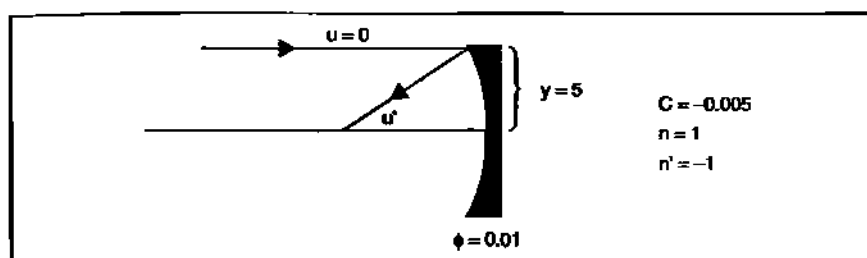


Fig. 24.1 Primary mirror: 100-mm f/10.

24.1 Introduction

In Chapter 3 we introduced the concept and mathematical description of aspheric surfaces. This was done mainly to acquaint you with the conic constant feature in ZEMAX and facilitate the solution of Step 6 in the Homework for Chapter 3 (page 30). In this chapter we will see how a surface conic constant can be designed so that spherical aberration is removed from a concave mirror. We will also utilize a specially designed "parallel plate" (called a Schmidt plate) to remove spherical aberration introduced by a spherical concave mirror.

24.2 The Parabolic Mirror

The image of a star formed by a perfect *spherical* primary mirror will be degraded due to spherical aberration introduced by the mirror itself, simply due to the operational geometry. (That same mirror will image a point source located at its center of curvature without any spherical aberration.) We want to modify the design of the primary so that a star will be imaged without spherical aberration. This can be done by modifying the mirror surface with an appropriate conic constant. But how does one find that conic constant? Consider the 100-mm f/10 mirror illustrated in Figure 24.1.

Applying the bending equation, we first find the value of the marginal ray angle after reflection:

$$n u' = n u - y \phi \quad (24.1)$$

$$-u' = 0 - 5(0.01)$$

$$u' = +0.05$$

Next, we employ the Buchdahl surface summation formulation from Table 10.1, but with an extra term that accounts for the conic constant (K) surface modification. (Recall that $K = -\epsilon^2$.)

$$S_i = -\sum_i \left[A^2 y \Delta \left\{ \frac{u}{n} \right\} - K C^3 y^4 \Delta \{ n \} \right] \quad (24.2)$$

We're dealing with a single surface, and S_i will be set to zero so that Equation 24.2 can be solved for K :

$$A^2 y \Delta \left\{ \frac{u}{n} \right\} - K C^3 y^4 \Delta \{ n \} = 0 \quad (24.3)$$

For our mirror surface:

$$A = n(u + yC) = yC = 5(-0.005) = -0.025$$

$$\Delta \left\{ \frac{u}{n} \right\} = \left[\frac{0.05}{-1} - 0 \right] = -0.025$$

$$\Delta \{ n \} = [-1 - 1] = -2$$

Inserting the above into Equation 24.3:

$$\begin{aligned} (-0.025)^2(5)(-0.05) - K(-0.005)^3(5)^4(-2) &= 0 \\ -0.000156 - (0.000156)K &= 0 \end{aligned}$$

Then, solving for K :

$$(0.000156)K = -0.000156$$

Therefore:

$$K = -1$$

This is the conic constant of a parabola.

For an axial point source at *infinity* the parabola forms an image without aberration. (However, if you move that point source to the mirror's center of curvature, the resulting image will be corrupted by spherical aberration.)

24.3 Aberration Content Comparison

In this section we want to compare the Seidel aberration content on- and off-axis for a 400-mm $f/10$ optic. The optic will be either a thin lens, a spherical mirror, or a parabolic mirror. The field angle will be 5° , and the object is at infinity. The equiconvex thin lens has the same power and aperture as the singlet used in the very first exercise. The glass is BK7 and the index is that in d -light. The thin lens forms in Table 10.1 can be used to determine the aberration coefficients. The LaGrange invariant (needed for the off-axis calculations) is the same for all three optics. It is found from:

$$L = \bar{u}y = (0.087489)(20) = 1.74977$$

Alternatively, one can use ZEMAX to determine the Seidel aberration coefficients. The results obtained using either method are shown in Table 24.1.

Table 24.1

Aberration	Thin Lens	Spherical Mirror	Parabolic Mirror
W_{00}	1.72λ	0.14λ	0
W_{11}	-4.95λ	-1.86λ	-1.86λ
W_{22}	6.52λ	6.52λ	6.52λ
W_{20}	2.15λ	-3.26λ	-3.26λ
W_{31}	0	0	0
AXCL	-6.102 mm	0	0
Petz. Rad.	-606.7 mm	400 mm	400 mm

For the *same* power, f-number, and field, the thin lens introduces far more spherical aberration and coma than the mirrors. All generate the same amount of astigmatism. The mirrors have more field curvature (which is also evident by their tighter Petzval radii). Primary axial color exists only for the lens.

24.4 Aspheric Correction of Lens

Shortly you will use Equation 24.2 to determine the conic constant needed to remove Seidel spherical aberration in a lens in a manner similar to that recently employed on the concave mirror in Section 24.2. The same technique was used on a 100-mm $f/5$ convex-plano lens to generate the ray fan plots shown in Figure 24.2.

Before putting an aspheric correction on the convex surface, the amount of spherical aberration present in the lens is shown by the b -curve. The amount of SA3 (using the scale on the right) is about 120 microns. After the aspheric design correction was installed, the third order spherical was completely removed. This is shown by the a -curve. But wait a minute. That curve is not flat. What's going on? The a -curve is not third order but fifth order spherical. And the scale employed is also different—it is the one on the left. The amount of SA5 is about 0.25 microns.

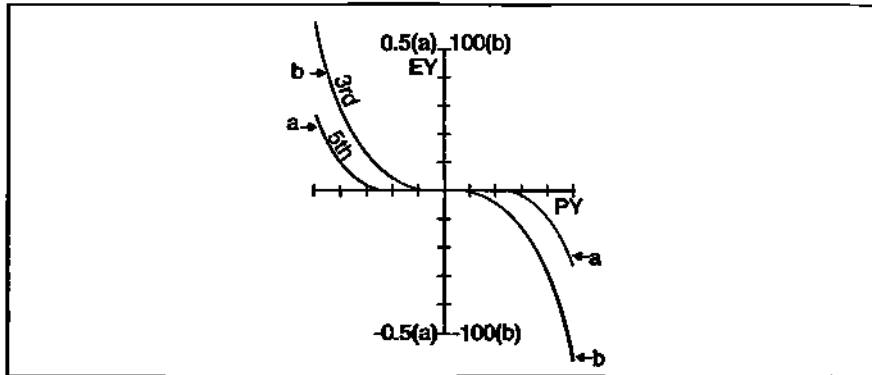


Fig. 24.2 Ray fan plots before and after aspheric correction.

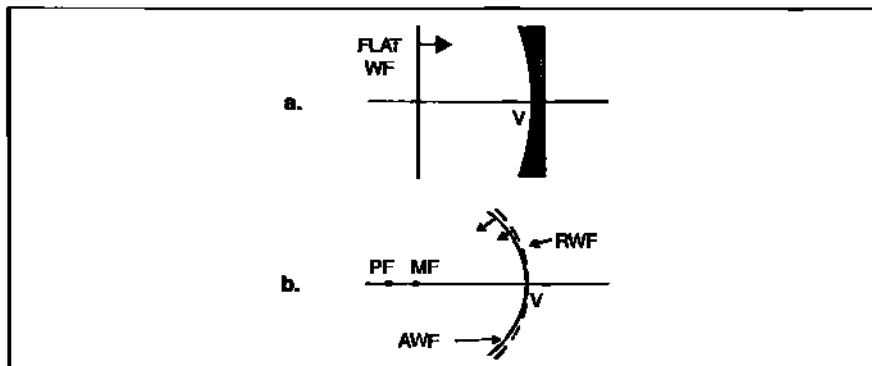


Fig. 24.3 Spherical aberration introduced by mirror on flat input wavefront.

24.5 Corrector Plate for Spherical Mirrors

24.5.1 Qualitative Description

We know that a flat input wavefront sent into a spherical mirror, as in Figure 24.3a, will result in a converging beam with spherical aberration as illustrated in Figure 24.3b. Note that the aberrated wavefront *leads* the reference wavefront.

However, if we could find a way of preconditioning the input wavefront such that it *lags* the reference wavefront by just the right amount as illustrated in Figure 24.4a, then the output wavefront will be a spherical wavefront (with no spherical aberration) as per Figure 24.4b.

24.5.2 Quantitative Description

Figure 24.5a shows a collimated beam incident on a parallel plate of thickness t . Figure 24.5b shows a collimated beam incident on a parallel airspace having the same thickness.

The optical path length through the plate is:

$$\text{OPL}_p = nt \quad (24.4)$$

Section 24.5: Corrector Plate for Spherical Mirrors 265

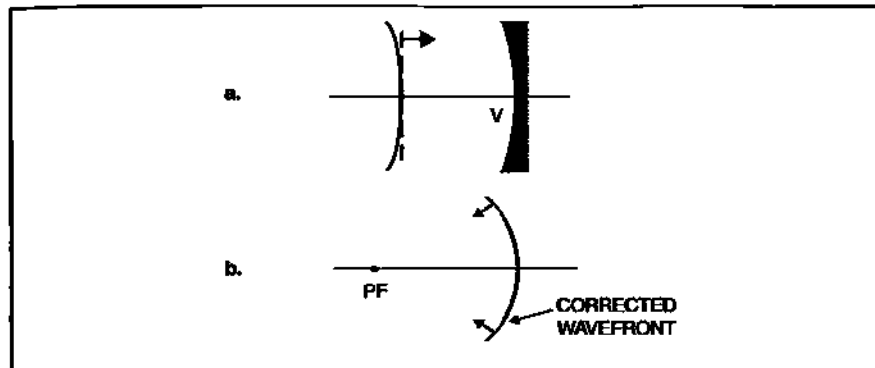


Fig. 24.4 Imposing spherical aberration on an incoming flat wavefront prior to incidence on the mirror.

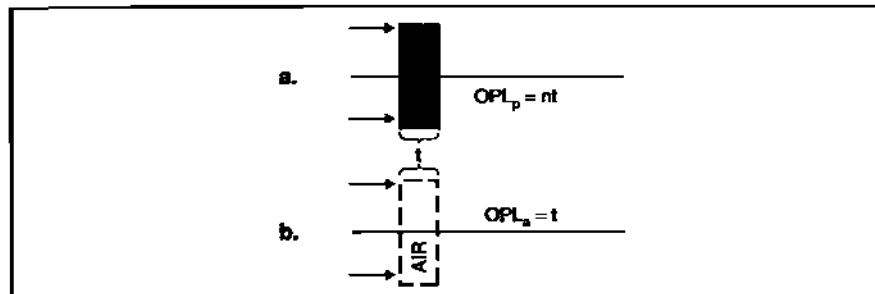


Fig. 24.5 Beam incident on: (a) parallel glass plate; (b) air-space.

The optical path through the airspace is given by:

$$OPL_A = t \quad (24.5)$$

Consequently, the optical path difference (OPD) introduced by the presence of the plate (as compared to that same thickness without the plate) is given by:

$$OPD = OPL_p - OPL_A$$

$$OPD = (n - 1)t \quad (24.6)$$

Recall from Table 10.1 that the Seidel coefficient for spherical aberration is given by:

$$W_{040} = \left(\frac{1}{32}\right)y^4\phi^3\sigma_i \quad (24.7)$$

Note: For a spherical mirror $\sigma_i = 1$.

We will now equate Equations 24.6 and 24.7:

$$OPD = -W_{040}$$

$$(n - 1)t = -\left(\frac{1}{32}\right)y^4\phi^3 \quad (24.8)$$

Solve for t :

$$t = -\left(\frac{\phi^3}{32(n - 1)}\right)y^4 \quad (24.9)$$

Equation 24.9 gives us the *variation* in thickness needed in the plate to generate spherical aberration equal (but *opposite*) to that introduced by the spherical mirror.

As an example, suppose we have a spherical mirror 30 cm in diameter with $\phi = 0.016584 \text{ cm}^{-1}$. (This is an *f/2* system.) For an object at infinity, the spherical aberration generated by this mirror is 72.2 microns. Suppose our plate has an index of 1.5151. Utilizing Equation 24.9:

$$t = -\left(\frac{0.016584^3}{32(0.5151)}\right)y^4$$

$$t = -(2.767 \times 10^{-7})y^4$$

This is how the thickness of the plate must vary to cancel the spherical aberration introduced by the mirror. At the edge of the plate this additional thickness (over and above the base thickness of the parallel plate) amounts to 140 microns. This type of corrector plate is known as the Schmidt Corrector.

24.5.3 Schmidt Plate in ZEMAX

Let's insert the mirror used in Section 24.5.2 into ZEMAX. It receives a collimated axial input. The spherical aberration present on the reflected wavefront is evident on the OPD plot shown in Figure 24.6. The OPD at the edge of the pupil is 113.2 waves. For a Helium-Neon (HeNe) laser light source this is 71.6 microns.

Next, we insert a BK7 plate (2 cm thick) in front of the mirror close to its center of curvature as shown in Figure 24.7. We'll change the "surface type" on the front surface of the plate from "standard" to "even asphere" (double-click on Standard → Surface Type → Even Asphere.). Moving right on this row we arrive at column headings "2nd order term," "4th order term," "6th order term," etc. We'll make the "4th order term" a variable. (The prescription is also shown in Figure 24.7.)

In the MFE, we insert SPHA with target = 0 and weight = 1. After the optimization is run, the value of the "4th order term" is shown in Figure 24.8. It is the same as that calculated in Equation 24.9.

The OPD after the optimization is shown in Figure 24.9. It shows a tremendous improvement because all the Seidel spherical has been removed. What is left is mainly sixth order, 2.75 waves of it.

Section 24.6: Spectral Effects 267

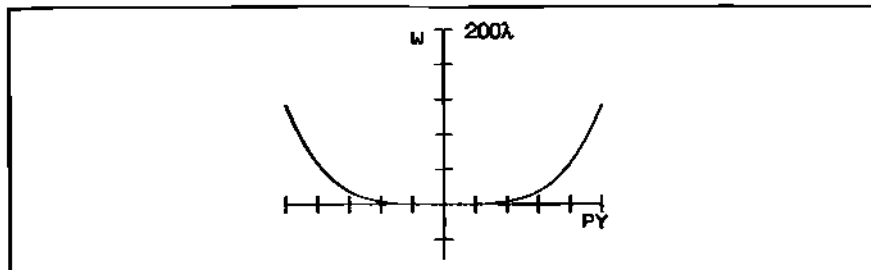


Fig. 24.6 OPD plot of wavefront reflected from spherical mirror.

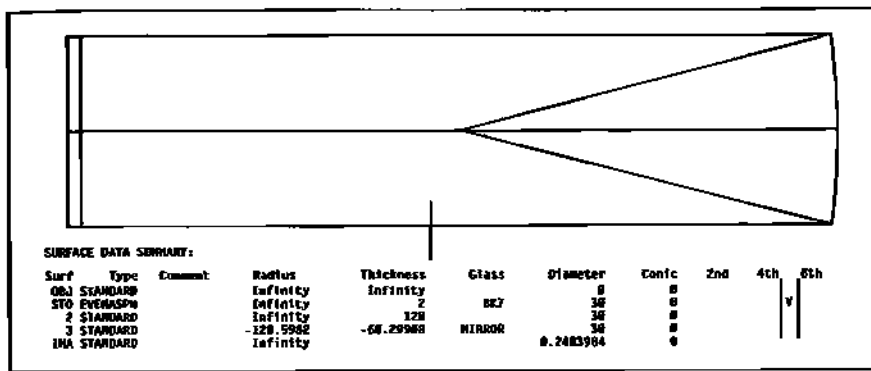


Fig. 24.7 Initial layout of mirror with parallel plate.

SURFACE DATA DETAIL:

```

Surface OBJ   : STANDARD
Surface STO   : EVENASPH
Coeff on r  2 : 6
[Coeff on r  4 : -2.7671673e-897]
Coeff on r  6 : 6
Coeff on r  8 : 6
Coeff on r 10 : 6
Coeff on r 12 : 6
Coeff on r 14 : 6
Coeff on r 16 : 6
Surface 2   : STANDARD
Surface 3   : STANDARD
Surface IMA  : STANDARD

```

Fig. 24.8 Value assigned to "4th order term" after optimization.

24.6 Spectral Effects

The optimization run above was for a single color, *HeNe*. If we now insert the standard visible spectrum (*F*, *d*, *C*-light), some color problems crop up. Using the "zoom" feature on the ZEMAX layout, we greatly magnify the region around the paraxial focus. What you see may be surprising. After all, a mirror is insensitive to color, but the glass plate is not. Figure 24.10 shows the focal region. There is a small residual axial color shift between *F*, *d*, and *C* focus points due to the Schmidt plate. This color effect is seen in the OPD plot shown in Figure 24.11.

Note that this spectral effect is associated mainly with the residual sixth

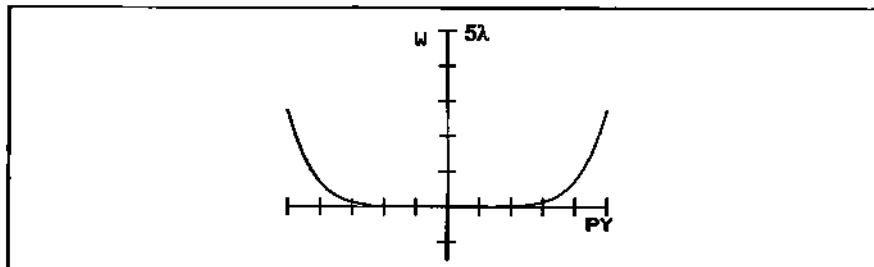


Fig. 24.9 OPD plot after plate correction.

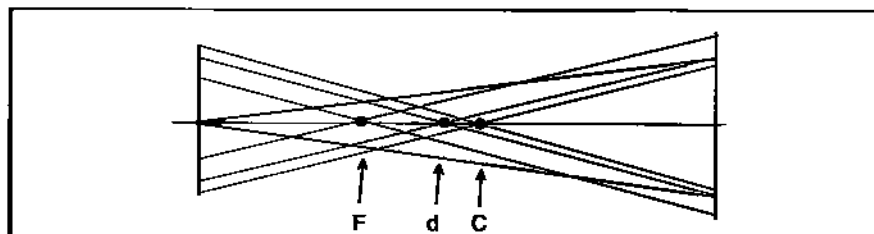


Fig. 24.10 Zoomed region around paraxial focus showing color shift.

order spherical. Its influence can be significantly reduced by adding a base power to the front plate surface. In ZEMAX we set a variable on the radius of Surf No. 1 and remove the variable on the fourth order coefficient. In the MFE, SPHA is turned off and TRAC is introduced. After the optimization, the resulting radius on Surf No. 1 is shown in Figure 24.12. The corresponding OPD plot is shown in Figure 24.13. The scale is now 1λ instead of 5λ .

24.7 Applications

Recall from Section 14.2 that when a stop is placed at the center of curvature of a spherical mirror (as illustrated in Figure 24.14) no coma or astigmatism is generated off-axis. The focal surface is curved and the only aberration present is spherical.

If we now place a Schmidt plate at the stop, the spherical aberration is eliminated. If the recording surface is curved to match the curved focal surface, then good quality imaging will result. Such a system is illustrated in Figure 24.15. Schmidt telescopes have extremely wide fields when compared to standard type telescopes such as Cassegrains. They are used for sky survey work. The 48-inch Schmidt telescope atop Palomar Mountain is perhaps the most famous example. It is shown in Figure 24.16.

Section 24.7: Applications 269

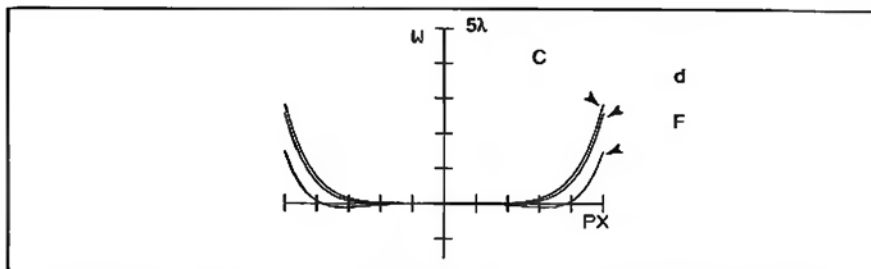


Fig. 24.11 OPD plot showing color effect of Schmidt plate.

SURFACE DATA SUMMARY:						
Surf	Type	Comment	Radius	Thickness	Glass	Diameter
06J	STANDARD		Infinity	Infinity		0
STD EVENASPH		V	5984.279	2	6K7	38
2	STANDARD		Infinity	128		38.00167
3	STANDARD		-128.5982	-59.92718	MIRROR	38.09877
JHA STANDARD			Infinity			.3819d7662

Fig. 24.12 Post-optimization prescription.

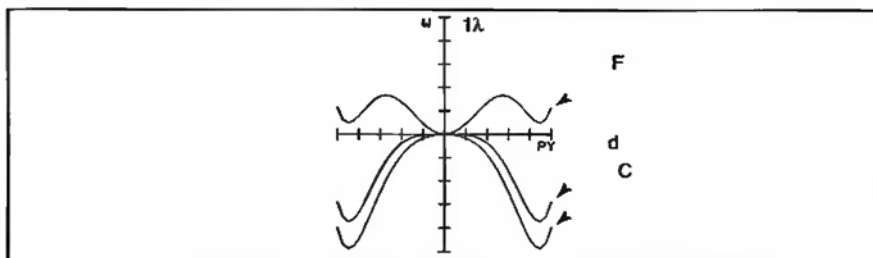


Fig. 24.13 OPD plot with color corrected Schmidt plate.

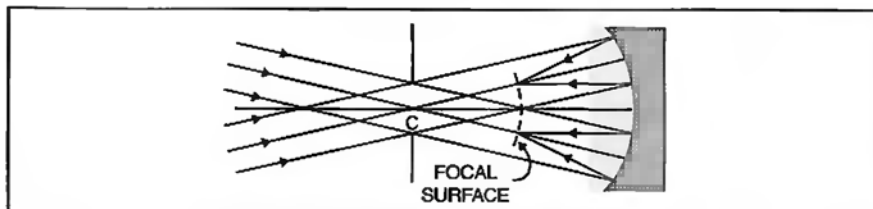


Fig. 24.14 No coma or astigmatism is present for off-axis fields.

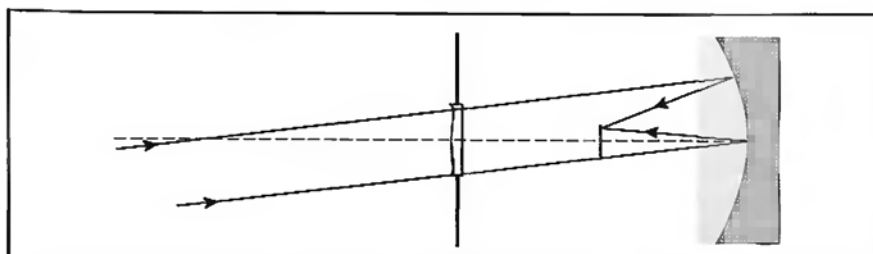


Fig. 24.15 Illustration of a Schmidt telescope.

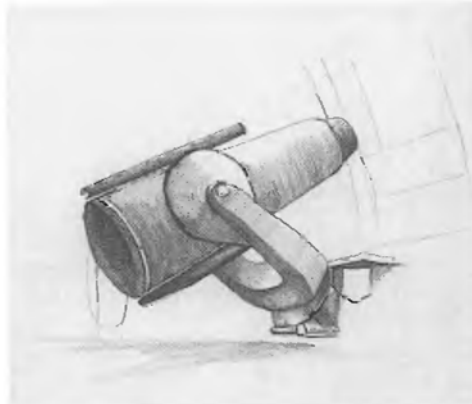


Fig. 24.16 The 48" Schmidt telescope on Palomar Mountain.



Fig. 24.17 Bernhard Schmidt (1879–1935).

24.8 Historical Note: Bernhard Schmidt

The man responsible for developing this important correction technique was Bernhard Schmidt (Figure 24.17). Though born in Estonia in 1879 he lived most of his life in Germany. He was a one-armed optician because of an unfortunate accident with gunpowder as a youth. He became a “lefty” by necessity. At one point during WWI he was a POW briefly, but his skill as an optician was highly valued, so he was allowed to continue working at his craft. His first corrector plate for a spherical mirror was made in 1930. It was a marvelous accomplishment. For job security reasons he did not tell anybody about the technique he used. He took that secret to the grave in 1935.

24.9 Homework

Using the S_i information from the Homework for Chapter 10:

- a. Calculate the conic constant, K , required on surface No. 2 to make the system $S_f = 0$.
- b. Compare this K value to the conic constant obtained in Step 6 of the Homework for Chapter 3.

Chapter 25

Symmetric Achromat and Vignetting

25.1 Introduction

In this chapter, we begin to look at our first truly complex photographic lens design. It will be a symmetric system about a central stop. You can think of it as an achromatic perisopic design or as a symmetric French Landscape lens. We will first discuss the general design approach and apply it to a specific system. This will then lead to a discussion of the compact symmetric system known as the Rapid Rectilinear. The actual design of the Rapid Rectilinear will be a homework assignment.

25.2 Basic Design Approach

Suppose we want to design a 10" f/8 symmetric achromatic system for a 20° half field. Where do we begin? We begin by designing the rear half first. This half will be designed as a 20" EFL achromat (object at infinity). Why? So that when both halves are put together, the resulting EFL will be in the neighborhood of 10 inches (recall that $\phi = \phi_1 + \phi_2$). We also want to use the lefthand spherical aberration solution (Section 17.3). The stop will lie somewhere to the left of the rear half. Its axial location will be initially selected to provide a flat tangential field (Section 12.5). TRAC will not be used at this stage because it will try to knock down coma. Instead, we are going to rely on system symmetry to help us deal with that aberration. After the rear half is designed, the front half is added to generate the symmetric system. The rear half is then slaved to the front half and the system is optimized.

25.3 Application of Design Approach

The glasses Schott BK7 and SF2 will be used for the 10" f/8 design. We first determine the powers of the positive and negative components for a 20" EFL using Eqs. 16.23 in Section 16.5.2. These turn out to be: $\phi_a = 0.10582 \text{ mm}^{-1}$; $\phi_b = -0.05582 \text{ mm}^{-1}$ (or $f_a = 9.45 \text{ mm}$; $f_b = -17.9147 \text{ mm}$). Go into ZEMAX. Make the positive lens equiconvex. Pick some radius (e.g., 4") for the first surface. Slave the second and third surfaces to the first. Insert some long radius for the fourth surface (e.g., 100"). Both lenses have zero thickness. Put variables on the first and

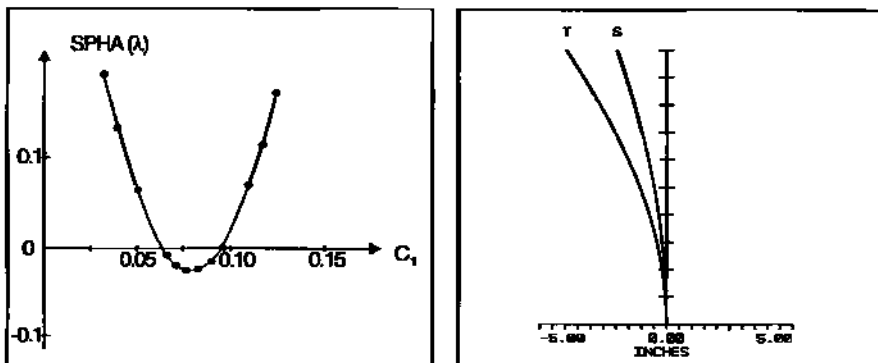


Fig. 25.1 Bending plot for 20" f/16 achromat (BK7 and SF2).

Fig. 25.2 Field curvature plot for LHS.

fourth surfaces. In the MFE insert EFFL with target 20" and weight 1. Insert AXCL with target 0, weight 1. Insert EFLY twice to watch the powers on the positive and negative components. Weight these at zero. Insert SPHA with weight 0. Set EPD = 1.25" in the GEN menu. This will yield an f/16 system (after optimization). (When the two halves are put together this will become f/8.) Select the visible spectrum (F , d , C) in the WAV menu. Field can be zero for now. Run the optimization. You should get a 20" f/16 thin lens achromat having the component powers calculated above. The radius on the first surface should be 9.7675". The second and third surfaces should be -9.7675". The fourth surface should be -61.741". (Note: If you calculate the curvatures manually using Equation 4.22, you will obtain the same radii.)

Next, we add some reasonable thickness (say 0.5" and 0.2" respectively). Put a 0.0001" thickness between the second and third surfaces. With the positive lens held as an equiconvex, re-optimize the lens for the finite thicknesses using $\text{EFFL} = 20"$ and $\text{AXCL} = 0$. After the optimization, spherical aberration is low at 0.03λ . Inserting the 20° field, we find that coma is around 3.5λ , and astigmatism is over 55λ .

We remove the "pickup" for radius on the second surface and place a variable on it. The variable on the first surface is removed and is adjusted manually. The lens is optimized after each manual adjustment. Only EFFL and AXCL are turned on. A "bending plot" is generated (per Section 17.3), and shown in Figure 25.1. The left-hand solution is selected because the stop will be on the left side of the lens. Coma for this solution is now about -3λ , and astigmatism is still high at 53λ ; field curvature (shown in Figure 25.2) is also hefty.

Astigmatism is our biggest problem now. We want to knock it down. As we saw in the Homework for Chapter 17 (page 194) lens bending does not impact astigmatism in any dramatic way. On the other hand, stop location does. We'll do this by shifting the stop position under FGCT (Section 12.5) operand control. This will flatten the field and reduce the astigmatism at the same time. In the MFE, the

Section 25.3: Application of Design Approach 273

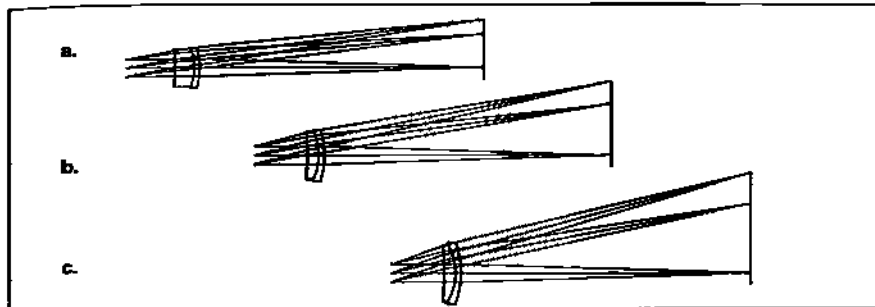


Fig. 25.3 Post-optimization layout for field angle: (a) 10°; (b) 14°; (c) 20°.

SURFACE DATA SUMMARY:

Surf	Type	Comment	Radius	Thickness	Glass	Diameter	Conic
OBJ	STANDARD		Infinity	Infinity		0	0
STD	STANDARD		Infinity	3.686456	V	1.25	0
2	STANDARD		-28.41068	0.8	BK7	3.866715	0
3	STANDARD		-3.912662	0.0001		4.84301	0
4	STANDARD		-3.912662	0.4	SF2	4.843031	0
5	STANDARD		-6.89464	20.55438	H	4.369121	0
IMA	STANDARD		Infinity			14.23974	0

Listing 25.1 Prescription for layout in Figure 25.3 (c).

Merit Function Value: 5.42417886E-883

Num	Type	Int1	Int2	Hx	Hy	Px	Py	Target	Weight	Value	% Const
1	EFFL		2					2.00000E+001	1	2.00000E+001	0.000
2	EFLY	2	3					0.00000E+000	0	9.21423E+000	0.000
3	EFLY	4	5					0.00000E+000	0	-1.81838E+001	0.000
4	AXCL							0.00000E+000	1	9.55257E-004	0.625
5	SPHA	0	2					0.00000E+000	0	1.66759E+000	0.200
6	CORR	0	2					0.00000E+000	0	-3.54657E+000	0.000
7	ASTI	0	2					0.00000E+000	0	-1.28979E+001	0.000
8	FGCT	2	0.0000	0.0000				0.00000E+000	1	-1.58684E-007	0.000
9	FGCT	2	0.0000	0.7000				0.00000E+000	1	-1.06106E-002	79.444
10	FGCT	2	0.0000	1.0000				0.00000E+000	1	5.41547E-003	19.936

Listing 25.2 MFE data for layout in Figure 25.3 (c).

only operands active will be EFFL, AXCL, and FGCT (three of them). When the stop starts shifting to the left, the lens diameter will have to increase to accept the full field. This also means that the lens thickness (particularly the positive component) will have to increase to avoid lens surfaces crossing each other within this larger diameter. Consequently, an incremental approach will be taken. The full 20° field will not be used during the first optimization run. Rather, we'll start with 10° and work our way out in a couple of steps. After each run, the lens component thicknesses will be tweaked. Figure 25.3a-c shows the post-optimization layouts for this three-stepped "increasing field" approach.

The prescription data for Figure 25.3c is shown in Listing 25.1. The stop is located about 3.7" in front of the lens. The positive component has a thickness of 0.8" and the negative component 0.4". MFE data is shown in Listing 25.2. Note

274 Chapter 25 Symmetric Achromat and Vignetting

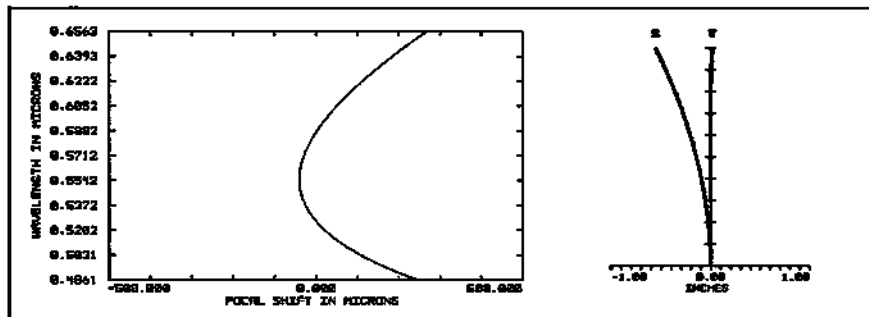


Fig. 25.4 Left: axial color for Fig. 25.3 (c); right: field curvature for Fig. 25.3 (c).

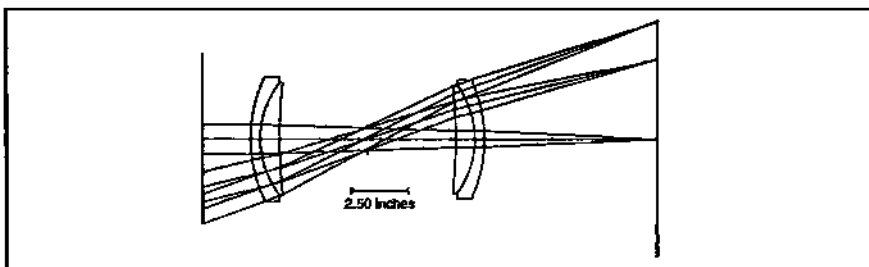


Fig. 25.5 Starting symmetric design (SYMA101b).

SURFACE DATA SUMMARY:

Surf	Type	Comment	Radius	Thickness	Glass	Diameter	Conic
0.82	STANDARD		Infinity	Infinity		7.128939	
1	STANDARD		Infinity	2		5.241868	
2	STANDARD		6.89461V	8.4	SF2	4.785942	
3	STANDARD		3.91271V	0.0081		4.745986	
4	STANDARD		3.91271P	8.8	EK7	4.646296	
5	STANDARD		28.41871V	0.68651V		1.073661	
5T0	STANDARD		Infinity	0.68651V		4.436425	
7	STANDARD		-28.41871P	8.8	EK7	4.562312	
8	STANDARD		-3.91271P	0.0081		6.562341	
9	STANDARD		-3.91271P	8.4	SF2	4.998794	
10	STANDARD		-6.89461P	7.23891W		9.921942	
IMA	STANDARD		Infinity				

Listing 25.3 Prescription for starting symmetric design (SYMA101b).

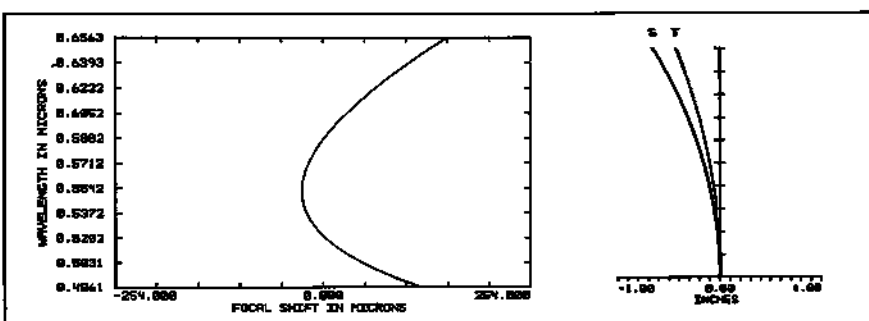


Fig. 25.6 Right: color for SYMA101b; left: field curvature for SYMA101b.

Section 25.3: Application of Design Approach 275

Table 25.1 RMS spot sizes			
Field	SYMA1o1b	SYMA1o1a	SYMA1o1v
0°	18 μm	91 μm	55 μm
14°	244	192	138
20°	499	325	275
ARMS	254	203	156

that spherical has increased to $\sim 1.7\lambda$. Astigmatism is down to -12λ .

We still have good axial color, and the tangential field is flat, as shown in Figure 25.4. This provides a reasonable starting point for our symmetric lens, SYMA1o1b (shown in Figure 25.5), the prescription for which is shown in Listing 25.3. Note how the rear half is slaved to the front half via the “pickup” command.

From the system data this is a 13.32" f/10.65. Color correction is still pretty good (as shown in Figure 25.6, left), but we lost some ground on the field curvature front (as per Figure 25.6, right). SPHA is $\sim 0.8\lambda$; ASTI $\sim -11\lambda$; COMA $\sim 4.3\lambda$. (But recall that for a symmetric system at *unit magnification*, coma, distortion, and lateral color will disappear.)

This system will now be optimized. Variables will be placed on the second, third, and fifth radii and on the fifth thickness. In the MFE, EFFL (=10") and AXCL will be on, FCGT will be off, and TRAC will be added.

SYMA1o1b → Optimize → SYMA1o1a

The layout for SYMA1o1a is shown in Figure 25.7. Axial color is good, and the tangential field is reasonably flat. Both are shown in Figure 25.8. The stop is 1.67" from either lens half.

We can find the best overall image plane by inserting a dummy surface just before the IMA plane and placing a variable on its thickness and removing all other variables. After optimization (SYMA1o1a), the BFD = 6.72" and the best image plane sits $-0.117"$ in front of the paraxial image plane. The layout is the same as Figure 25.7 except for the added variable plane.

Despite the fact that fourth order coma has increased to 12.4λ and ASTI to -35.6λ , the *overall* improvement in RMS spot size (after both optimization procedures are run) is shown in Table 25.1. This can be seen via a simple average of the RMS shown at the bottom.

The optimization procedure used to obtain SYMA1o1a essentially restricts the symmetry solution to the paraxial image plane. However, if we restore all the variables removed when the dummy surface was added, *but also keep the variable dummy surface (SYMA2o1b)*, an entirely different solution presents itself.

SYMA2o1b → Optimize → SYMA2o1a

The layout is shown in Figure 25.9. Note that this is a far more *compact* system. (This entire lens could fit within the stop airspace of lens SYMA1o1a back

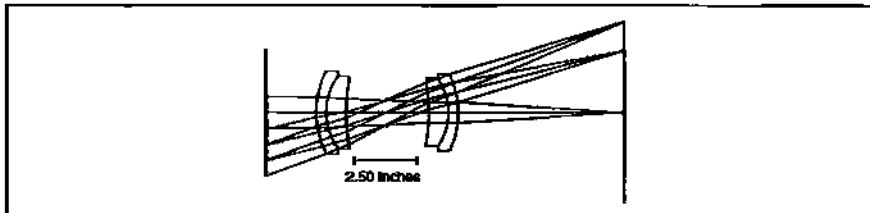


Fig. 25.7 Layout of SYMA1o1a.

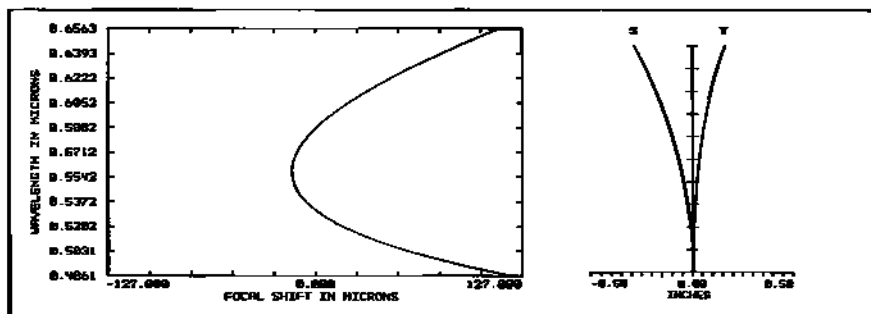


Fig. 25.8 Left: color for SYMA1o1a; right: field curvature for SYMA1o1a.

Table 25.2 RMS spot sizes		
Field	SYMA2o1a	SYMA2o2a
0°	125 μm	138 μ
14°	94	96
20°	196	207
ARMS	138	147

in Figure 25.7.) The length of the lens is 3.25", and the stop airspace is now 0.84" instead of 3.34". The BFD = 8.56" and the best image plane sits -0.2416" in front of it. Color is identical to that in Figure 25.8 (left), and the tangential field is a bit flatter than in Figure 25.8 (right).

If we *thin* the lenses (especially the crown) and reoptimize, we get the result in Figure 25.10. The overall length of the lens has increased slightly to 3.61" but the stop airspace has increased significantly to 2". Color is unchanged. A comparison of field curvatures and distortion is shown in Figure 25.11. RMS spot sizes are compared in Table 25.2.

Performance-wise, SYMA2o1a and SYMA2o2a are fairly equivalent. The SYMA2o2a is likely the best choice, particularly because of the extra room in the stop airspace. This is normally where an iris mechanism is located, and frequently the shutter mechanism is located here as well.

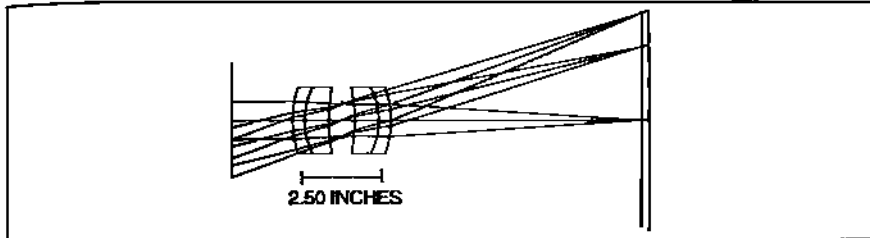


Fig. 25.9 Layout of SYMA2o1a.

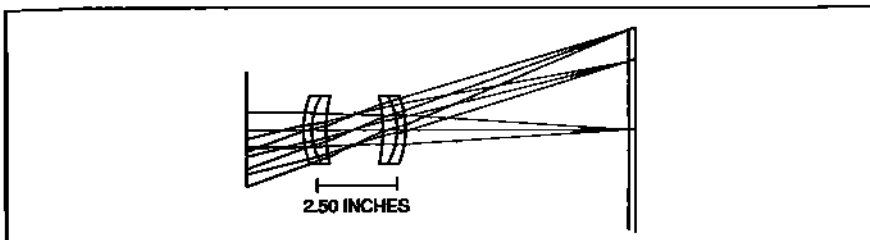


Fig. 25.10 Layout of SYMA2o2a (thinner lenses).

25.4 Area Weighted RMS

The average RMS used in Tables 25.1 and 25.2 is simple but crude. A better way of getting one number that is representative of spot diagram performance over the entire field is to use an area weighted RMS (or AWRMS). For a particular field position, the spot lies in the middle of an annular zone having a certain area. This is illustrated in Figure 25.12.

The AWRMS is then found via the following formulation:

$$\text{AWRMS} = \left(\frac{1}{A} \right) \sum_i A_i \times \text{RMS}_i. \quad (25.1)$$

Each spot RMS is multiplied by the area of the zone it occupies. All the terms are summed-up and then divided by the total area of the format.

25.5 Breaking Symmetry

What were the number of variables we had to play with in designing the symmetric achromat? There were 3 lens radii, one interlens airspace, and the dummy image surface. With those we had to control: EFL, color, spherical aberration, coma, astigmatism, field curvature, and distortion. So we had 5 degrees of freedom to control 7 parameters (not to mention higher order aberrations like sixth order spherical, elliptical coma, and oblique spherical). This means that in some ways what we gain in one area, we lose in another. For a completely symmetric

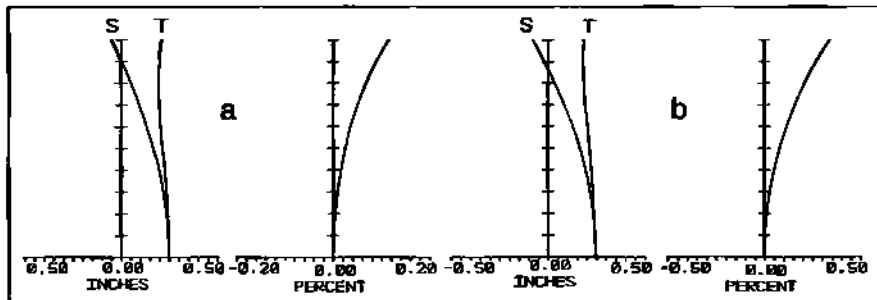


Fig. 25.11 Field curvature and distortion for: (a) SYMA2o1a; (b) SYMA2o2a.

system which includes object-image symmetry (unit magnification), coma, distortion, and lateral color are eliminated automatically. That leaves 5 parameters to control with 5 variables which gives us a better shot at greatly improving image quality.

As we saw once before with the periscopic lens (Section 12.7), we can gain quite a bit of ground by breaking the symmetry of the lens. This is a reasonable thing to do when the object-image conjugates are themselves unsymmetric. But we have to be careful how this is done. It matters where we start from, and in what order things are done. This can best be illustrated by an example.

If we start with SYMA1o1v and place variables on *both* the front and the rear half radii (leaving the airspace alone):

ASYM1o1b → Optimize → ASYM1o1a

ASYM1o1a is shown in Figure 25.13. The radii are so large in the front half that they are essentially acting like a window and all the work is being done by the rear half. If I start from ASYM1o1b and include the front airspace as a variable (with the rear half airspace still slaved to the front half), but also add MNCA = 0.1" to the MFE to keep the halves from crashing together:

ASYM2o1b → Optimize → ASYM2o1a

ASYM2o1a is shown in Figure 25.13. The lenses are relatively thick and the stop airspace is down to 0.46". If I start from SYMA2o2a with variables on all radii (except the two slaved interlens curvatures) and a variable on the front half stop airspace (rear half slaved):

ASYM3o1b → Optimize → ASYM3o1a

ASYM3o1a is shown in Figure 25.13. This time the rear half is not working as hard as the front half (looking almost like a pair of bent parallel plates), and the crown on the front half would have to be thickened.

If we start from SYMA2o1a, unslave the rear half, freeze the stop airspace,

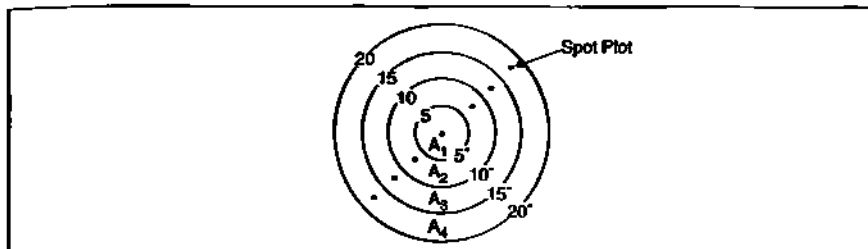


Fig. 25.12 Geometry for determining AWRMS.

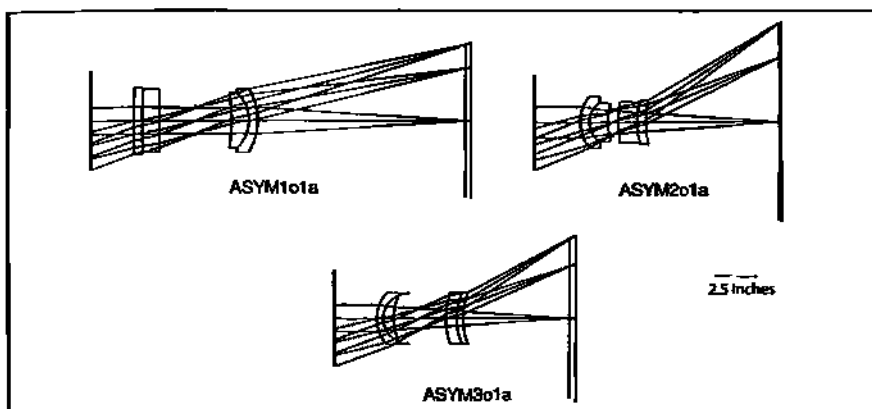


Fig. 25.13 Assorted asymmetric lenses based on different starting points and variable assignment.

Table 25.3 RMS Spot Sizes	
Field	ASYM4o1a
0°	71
14°	64
20°	73
ARMS	69

but leave the dummy image plane free to move about:

ASYM4o1b → Optimize → ASYM4o1a

ASYM4o1a is shown in Figure 25.14. It is similar to ASYM2o1a except the former's interlens airspace is twice as big. The interlens radius on the front half is rather tight (which may present some fabrication problems). Color is accurate. Tangential and sagittal field curvatures are reasonably flat. Distortion is higher. Both are shown in Figure 25.15. But the RMS spot sizes are much improved, as seen in Table 25.3. The actual spot diagrams are shown in Figure 25.16.

ASYM4o1a could certainly stand more tweaking, but the main purpose of the

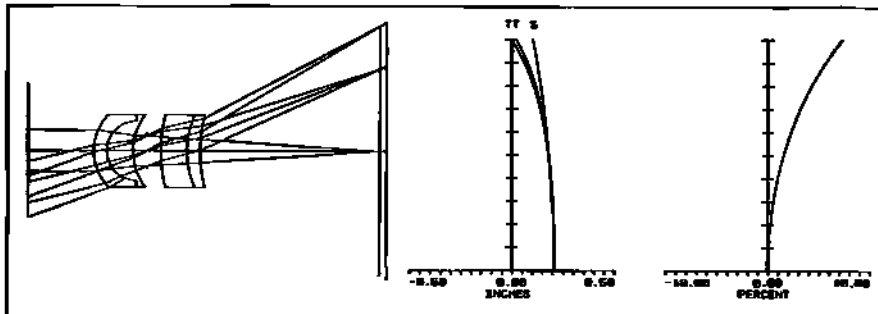


Fig. 25.14 Layout of ASYM4o1a.

Fig. 25.15 Field curvature and distortion for ASYM4o1a.

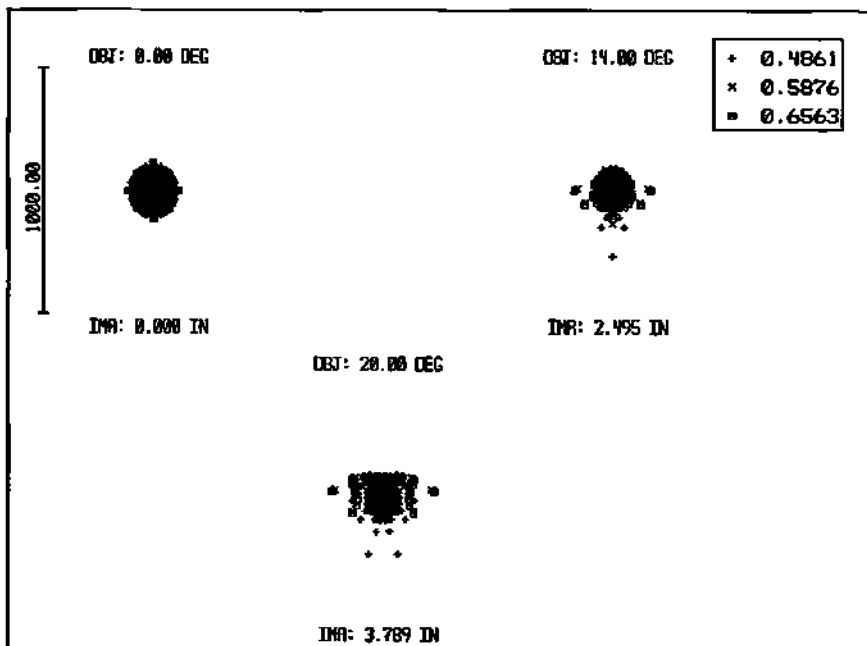


Fig. 25.16 Spot diagrams for ASYM4o1a.

exercise was to show the benefits (and some pitfalls) of symmetry breaking. In general, you can get a much better performing lens by allowing an initial symmetric design to go asymmetric (provided the lens is not working at unit magnification).

25.6 Vignetting

Let's go back to SYMA1o1b to illustrate an important ZEMAX point. The "entrance pupil diameter" in the GEN menu was set to 1.25". This imposes a

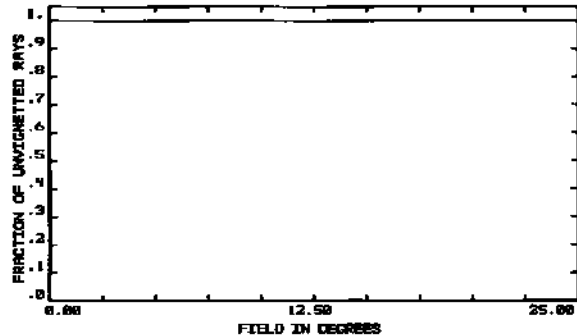


Fig. 25.17 Vignetting plot of SYMA101b without hard aperture.

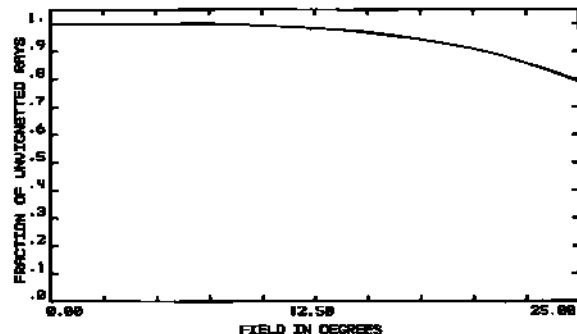


Fig. 25.18 Vignetting plot of SYMA101b with hard aperture invoked.

certain diameter on the stop surface. If only the 0° field is activated, the semi-diameter of the stop (as seen in the LDE) is 0.4698. But if we increase the field out to 25° , the semidiameter of the stop *increases* in size to 0.6217". In other words, the stop opens up to allow *all* the off-axis rays to pass. A real physical stop does not do that. Now let's go into (Analysis → Illumination → Vignetting Plot). The result is the flat plot shown in Figure 25.17. This shows that no rays have been blocked or vignetted.

The stop thus far has been used to define the system f-number. It has not been used as a "hard aperture" which simulates a real physical stop which can vignette rays. To do this: double-click on the stop surface under Surface Type → Aperture Type → Circular Aperture → Max Radius (= 0.47) → OK. An asterisk will appear beside STO to indicate that this is now a hard aperture. (Also, set the semi-diameter size to 0.4698" so the layout will show the actual size of hard aperture.) Now go back to the vignetting plot. The influence of the hard aperture stop can now be seen as indicated in Figure 25.18. (Note: To get a smooth looking plot you will have to go into Options → Settings and increase the ray density. In the present case, default was 7 and I increased it to 27. Also note that a hard aperture can be placed

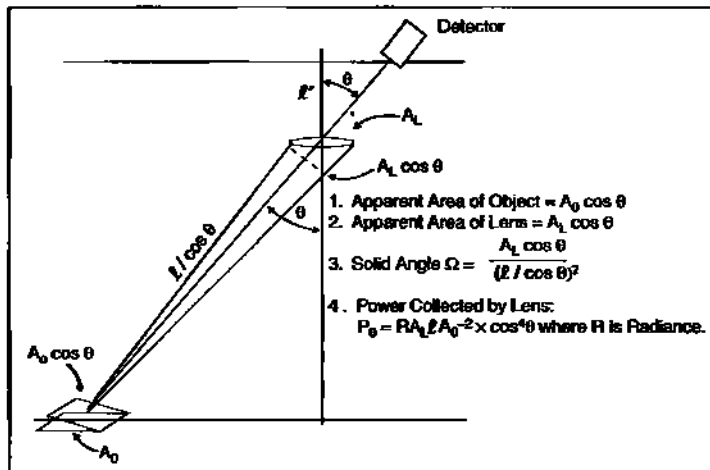


Fig. 25.19 Brief derivation of cosine fourth Law.

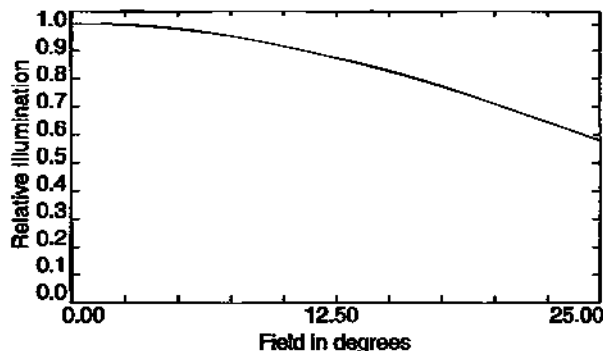


Fig. 25.20 Relative illumination plot of SYMA10b without vignetting.

on *any* surface in the lens system, not just the stop surface.)

25.7 Relative Illumination

Given a uniform object field (Lambertian), relative illumination fall off (or RIF) is basically the ratio of off-axis image irradiance to on-axis image irradiance. In ZEMAX the range is from 0–1. In other parlance it is given as a percentage. For a perfect thin lens looking at a distant uniform object field, the RIF follows a cosine fourth falloff law. (A basic derivation of this is presented in Figure 25.19.) Please note that this “law” has nothing to do with vignetting. For example, SYMA10b without the hard aperture has a RIF as shown in Figure 25.20. There is no vignetting but there is significant illumination falloff. If we now turn the hard

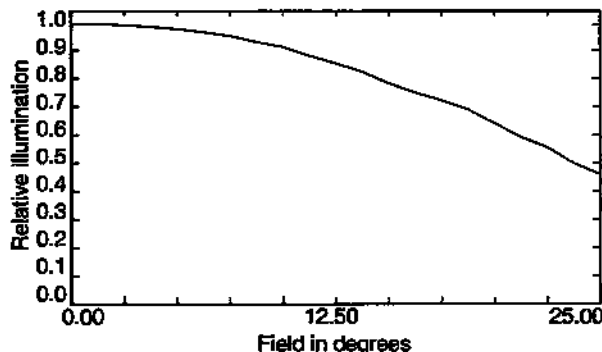


Fig. 25.21 *Relative illumination plot of SYMA10lb with vignetting.*

aperture back on, the RIF plot for SYMA10lb is much worse as can be seen from Figure 25.21. (Relative illumination is also affected by pupil distortion and image plane distortion.)

As a designer, you want to avoid steep RIF curves because you do not want to saturate a sensor in the middle of the format and/or starve it for photons in the outer field. You should also note that as the stop airspace increases, RIF problems generally worsen. Which brings us to the Rapid Rectilinear.

25.8 The Rapid Rectilinear

The Rapid Rectilinear is one of history's most successful lenses. It was designed by John Dallmeyer and introduced to the public in 1866. It had a long run—approximately 60 years. It is a symmetric achromat. But unlike the design worked out in this chapter, the classic Rapid Rectilinear made use of two glasses whose Abbe numbers were not that far apart (although their refractive indices were quite different). This allows for a more compact wide field lens design, and a flatter illumination field. In our design example, BK7 and SF2 glasses were used. Their index difference in *d*-light is 0.130889, and the difference in Abbe number is 30.32. By contrast your homework design problem uses glasses whose index difference is 0.05281 and whose Abbe difference is 6.88.

25.9 Historical Note: John Henry Dallmeyer

John Dallmeyer (Figure 25.22) was born in Westphalia in 1830. He trained as an optician. In 1851 he went to live in England, married into a wealthy family, and was able to start his own business when his father-in-law left him a small fortune. Dallmeyer set up a shop to design and build photographic lenses. He was quite good at it and received many European honors. Dallmeyer died in 1883.



Fig. 25.22 John H. Dallmeyer, father of the Rapid Rectilinear.

25.10 Homework

Design a 10" f/8 "Rapid Rectilinear" photographic lens to cover a 20° field. Design the lens for the F , e , C spectrum. Use Schott LF1 and F1 glasses (LF1 glass chart is shown in Table 25.4). Do the thin lens pre-design of the rear half first as was illustrated in this chapter. Instead of "walking over" to the lefthand solution for zero SPHA by manually adjusting C_1 (or R_1), try using FCGT (at full field) starting from the righthand solution. You must have the stop sitting in front of the rear half (about 1" initially) with the airspace fixed. After optimization you will have a lens meniscus to the left. SPHA will still be a couple of waves, but you will have the right-shaped achromat for the rear half. You can assemble the symmetric lens from this point and continue the design from there without FCGT. Insert this design into ZEMAX, adjust, and then add the front half. Optimize the design. Do not let the airspace between the front and rear halves go below 0.6". We need this much space for an iris and shutter mechanism. Strive for good color, and a reasonably flat tangential field. Meet or exceed the target RMS spot sizes shown below (use settings: square; centroid). I suggest you use the folder name: Rapidrect; file names: REAR1o1b, etc.; RAPR1o1b, etc.; ASYM1o1b, etc.

Field	SYM RMS	ASYM RMS
0°	112 μm	98 μm
14°	72	63
20°	176	165

After you have a symmetric design you are happy with, let the lens go asymmetric. See what you can do with it.

Section 25.10: Homework 285

Table 25.4

LF1 Information

Refractive Indices			Relative Partial Dispersion			Internal Transmittance, T_i		
	λ [nm]		$P_{s,i}$	0.2445		λ [nm]	T_i (5 mm)	T_i (25 mm)
$n_{2325.4}$	2325.4		$P_{c,i}$	0.5020		2325.4	0.93	0.70
$n_{1970.1}$	1970.1		$P_{d,C}$	0.2967		1970.1	0.990	0.95
$n_{1529.6}$	1529.6		$P_{e,d}$	0.2374		1529.6	0.998	0.990
$n_{1060.0}$	1060.0	1.55829	$P_{z,F}$	0.5714		1060.0	0.998	0.990
n_s	1014.0	1.55905	$P_{t,b}$	0.8724		700	0.999	0.995
n_z	852.1	1.56234	$P'_{s,i}$	0.2415		660	0.999	0.995
n_r	706.5	1.56687	$P'_{C,s}$	0.5421		620	0.999	0.995
n_C	656.3	1.56910	$P'_{d,C'}$	0.2470		580	0.999	0.995
n_F	643.8	1.56973	$P'_{e,d}$	0.2345		546.1	0.999	0.995
$n_{632.8}$	632.8	1.57032	$P'_{z,F'}$	0.5063		500	0.999	0.995
n_D	589.3	1.57297	$P'_{t,b}$	0.8619		460	0.998	0.990
n_J	587.6	1.57309	Constants of Dispersion Formula			435.8	0.998	0.990
n_r	546.1	1.57629	A_0	2.4217647		420	0.998	0.990
n_F	486.1	1.58256	A_1	-8.5906079 · 10 ⁻³		404.7	0.997	0.990
n_F'	480.0	1.58335	A_2	1.7651245 · 10 ⁻²		400	0.997	0.990
n_z	435.8	1.59025	A_3	5.8415074 · 10 ⁻³		390	0.996	0.980
n_b	404.7	1.59684	A_4	-1.6884537 · 10 ⁻⁵		380	0.994	0.970
n_t	365.0	1.60858	A_5	2.7259662 · 10 ⁻⁶		370	0.992	0.961
Other Properties			Deviation of Relative Partial Dispersion ΔP from the "Normal Line"			365.0	0.991	0.955
$\alpha_{300-700C} [10^{-6}/K]$	8.5		$\Delta P_{c,i}$	-0.0005		350	0.984	0.92
$\alpha_{20-300C} [10^{-6}/K]$	9.7		$\Delta P_{C,s}$	-0.0001		334.1	0.93	0.70
T_g [°C]	435		$\Delta P_{F,F'}$	0.0002		320	0.55	0.05
$T_{10\%}$ [°C]	612		$\Delta P_{t,b}$	0.0007		310	0.19	
c_p [J/g - K]			Temperature Coefficients of Refractive Index			300		
λ [W/m - K]			$\Delta n/\Delta T_{relative} [10^{-6}/K]$			290		
ρ [g/cm ³]	3.16		1060.0	s	C'	e	g	
E [10 ³ N/mm ²]	60		-40/-20					
μ	0.221		-20/ 0					
HK	390		0/+20	1.6	1.8	2.2	2.7	3.8
R	1		+20/+40	1.6	1.8	2.2	2.7	3.8
CR	1		+40/+60	1.6	1.8	2.2	2.7	3.8
FR	0		+60/+80	1.6	1.8	2.2	2.7	3.8
SR	1							
AR	2.0							

Important Note: Some versions of ZEMAX do not have LF1 glass in their libraries. In that case you will need to manually load the $n(\lambda)$ data contained in the lefthand column in Table 25.4 on page 285. This can be done in the following manner. Click on Gla button. The Catalog: box is on the upper left. Select Schott for this box. Go to the lower right and click on Fit Data. The Fit Index Data menu will appear.

1. Insert Table 25.4 on page 285 data into its left-most columns.
2. On the right-hand side go to Name: and insert LF1 in the box currently labeled New Glass.
3. Make sure Schott appears in the Form: box. Now click on box labeled Fit. (This will fit a polynomial to the $n(\lambda)$ data you inserted. ZEMAX does not store that data, only the coefficients of the fitting polynomial.)
4. Click on Add box. (LF1 will be added to the Schott catalog.)
5. Click on Exit. Now you are back in the Gla menu.
6. Click on Save on the lower left and then Exit.

Chapter 26

Telescopes

26.1 Introduction

In this chapter we will take a break from refractive systems and look at a totally different kind of photographic objective—one that depends on reflective components. The objects of interest are not terrestrial but astronomical. For astronomical reflective telescopes, aspheres are the rule rather than the exception; consequently, we will continue the application of aspheric surfaces from Chapter 24. One of the most attractive features of mirror systems is their inherent freedom from chromatic aberration problems. On the downside, telescopes have a much narrower field-of-view (usually a degree or so). In this chapter, we will confine ourselves to two-mirror systems.

26.2 Telescope Types

26.2.1 Newtonian Form

The Newtonian telescope (named after its inventor Sir Isaac Newton) consists of a *parabolic* primary mirror and a flat fold mirror oriented at 45° (as illustrated in Figure 26.1). (Newton himself used a spherical primary *circa* 1668.) We saw back in Section 24.2 that the parabolic mirror introduced no spherical aberration when viewing a very distant object, and stars certainly qualify as being distant. Also, Newton felt compelled to use this system design because he was fairly certain that the chromatic problems in lenses presented an insurmountable problem. (He would be proven wrong with the invention of the achromat.)

26.2.2 Cassegrain Form

The Cassegrain form (invented by the Frenchman S.G. Cassegrain *circa* 1672) consists of a concave primary mirror and a convex secondary mirror as illustrated in Figure 26.2. Table 26.1 lists the common variations of this very successful and versatile form.

The Ritchey-Chrétien is aplanatic (corrected for spherical and coma) and has a wider field as a result. The only advantage that the Dall-Kirkham has is the spherical secondary which is easier to make and test. It has been used in HEL (high energy laser) beam propagation applications in which the telescope is used in reverse.

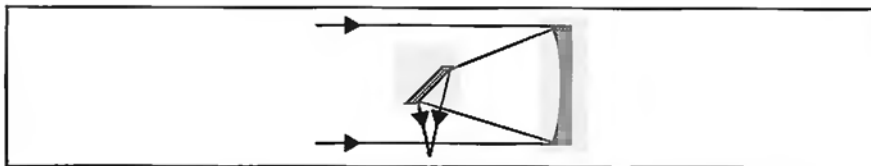


Fig. 26.1 Newtonian telescope.

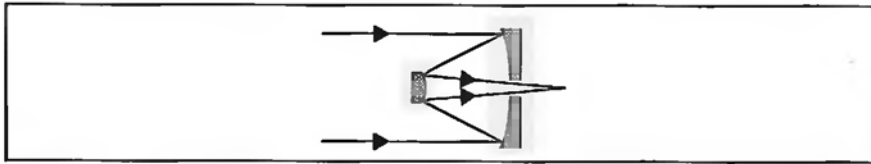


Fig. 26.2 Cassegrain telescope.



Fig. 26.3 The 200-inch Hale telescope.

Table 26.1
Variations of the Cassegrain

Type	Primary	Secondary
1. Classic	Parabolic	Hyperbolic
2. Ritchey-Chrétien	Hyperbolic	Hyperbolic
3. Dall-Kirkham	Elliptical	Spherical

Perhaps the most famous classic Cassegrain is still the 200" Hale Telescope on Palomar Mountain, which is shown in Figure 26.3. The pyrex primary mirror blank was cast in 1936 by Corning. The 5-meter diameter mirror blank weighed 20 tons. Five tons of glass were removed in the grinding process to get the base radius of curvature. Polishing to the parabolic shape removed another quarter ton.

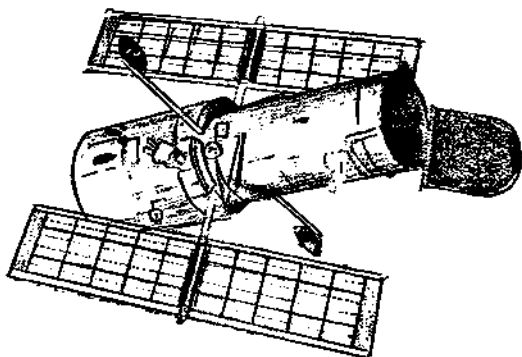


Fig. 26.4 The Hubble Space Telescope.

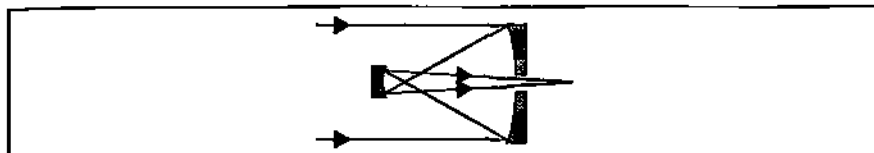


Fig. 26.5 Gregorian telescope form.

Construction of the telescope was interrupted by WWII, but first light was finally achieved in 1948.

The most famous Ritchey-Chrétien is not on earth at all. It is in orbit—the Hubble Space Telescope (shown in Figure 26.4). The HST got off to a bumpy start with the discovery that first light images were plagued by severe spherical aberration. This was tracked down to the primary mirror. The primary mirror was of excellent quality. It had one of the smoothest surfaces ever made. Unfortunately, it was polished to the wrong conic constant due to a spacing error in the reflective null corrector used in the metrology. The problem was fixed during the first servicing mission with the installation of the COSTAR corrective optics. Since then the HST has given excellent performance, and has made many discoveries.

26.2.3 Gregorian Form

The Gregorian form (invented in 1663 by James Gregory) consists of a concave primary mirror and a concave secondary mirror as illustrated in Figure 26.5. The most common type has a parabolic primary and an elliptical secondary. Note that the Gregorian has an internal focus, and is longer than the Cassegrain. The concave secondary is also easier to fabricate and test.

26.2.4 Schmidt Telescope

The Schmidt telescope consists of a spherical primary mirror with a Schmidt corrector plate (Section 24.5) located at the primary's radius of curvature. If no

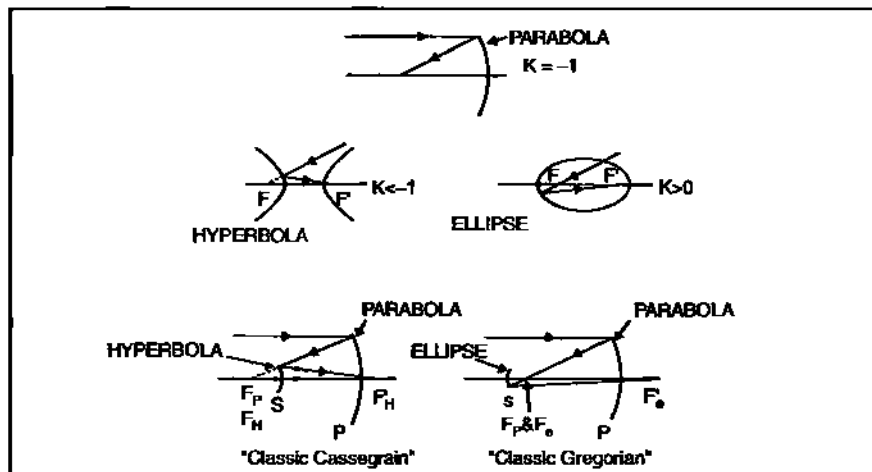


Fig. 26.6 Aspheric on secondary needed to complement parabolic primary.

other components are employed we have what is known as a Schmidt camera, i.e., the image falls on a curved film plate (as was illustrated in Figure 24.15). This is a very wide field system used for deep sky surveys.

26.2.5 Complementary Aspheres in Telescopes

Given a parabolic primary, Figure 26.6 illustrates how different aspheres on the secondary give rise to the two “classic” telescope forms.

26.3 Designing a Cassegrain

Let's design a modest-size Cassegrain telescope suitable for use by an amateur astronomer. Initially we're thinking about a 25-cm diameter primary. We'd also like it to be reasonably fast, say $f/2$. That means a radius of curvature of 100 cm. By happenstance, a friend in an optical shop has a 30-cm diameter parabolic mirror in storage (left over from a previous project). Its radius is 120.598 cm, and already has a 5.124-cm diameter hole in it. But best of all, it's free.

26.3.1 Secondary Mirror and First Order Properties of System

Now we work on the secondary. For our example we will make it as big as the hole in the primary (though usually it is somewhat larger). Next we need to find out how far it has to be from the primary, and what radius of curvature it needs to put the image a reasonable distance on the far side of the primary. For our calculations we'll use the “unfolded” paraxial version of the telescope as shown in Figure 26.7.

Using the PRTE bending equation, we find the angle of the marginal ray coming off the primary.

Section 26.3: Designing a Cassegrain 291

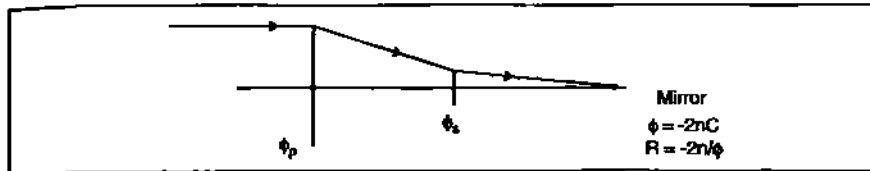


Fig. 26.7 Unfolded "paraxial" Cassegrain.

$$u'_p = \frac{-y_p \phi_p}{n'} \quad (26.1)$$

$$u'_p = \frac{-15(0.016584)}{1}$$

$$u'_p = -0.24876 \text{ cm} = u_s$$

Next, we have to find the distance at which the marginal ray just strikes the edge of the secondary. For this we use the PRTE transfer equation.

$$y_s = y_p + u_s t_{ps} \quad (26.2)$$

Solving for t_{ps} :

$$t_{ps} = \frac{y_s - y_p}{u_s}$$

$$t_{ps} = \frac{2.562 - 15}{-0.24876}$$

$$t_{ps} = 50 \text{ cm}$$

We know that the image has to be thrown more than 50 cm to get it to a comfortable distance behind the primary. A little experimentation with the secondary power shows us that $\phi_s = -0.08$ ($R_s = 25$ cm) will do the trick. Using the bending equation again:

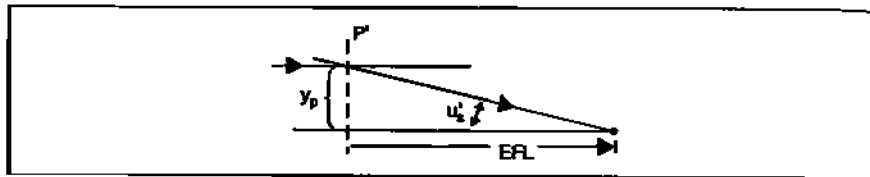
$$u'_s = u_s - y_s \phi_s \quad (26.3)$$

$$u'_s = -0.24876 - (2.562)(-0.08)$$

$$u'_s = -0.0438$$

Applying the transfer equation once again (where $y_i = 0$):

$$t_l = \frac{-y_s}{u'_s} \quad (26.4)$$

Fig. 26.8 P' and EFL.

$$t_i = \frac{-2.562}{-0.0438}$$

$$t_i = 58.493 \text{ cm} = \text{BFD}$$

Back-tracing the image-space marginal ray until it crosses the object-space marginal ray (as indicated in Figure 26.8) defines the location of P' , and hence, the EFL. Using the transfer equation yet again:

$$t'_P = \frac{y_P}{u'_S} \quad (26.5)$$

$$t'_P = \frac{15}{-0.0438}$$

$$t'_P = 342.4657 \text{ cm} = \text{EFL}$$

Since the stop is at the primary, it is also the EPD (entrance pupil diameter). The system f-number can be found by:

$$f/\# = \frac{\text{EFL}}{\text{EPD}} \quad (26.6)$$

$$f/\# = \frac{342.4657}{30}$$

$$f/\# = 11.415$$

The only first order properties left are the location and size of the exit pupil. We do this by letting the secondary image the stop (which is at the primary). Using the Gaussian lens formula (Equation 4.3), the stop image (t'_S) is -10 cm from the secondary (as per Figure 26.9), and the magnification (t'_S/t_S) is 0.2. This makes the exit pupil 6 cm in diameter.

Now we can refold the system. The result (with pertinent axial distances indicated) is shown in Figure 26.10.

26.3.2 Conic Constant Design

The on-axis beam converging toward the secondary from the primary is perfectly spherical. We must now design a conic constant for the secondary so that the beam

Section 26.3: Designing a Cassegrain 293

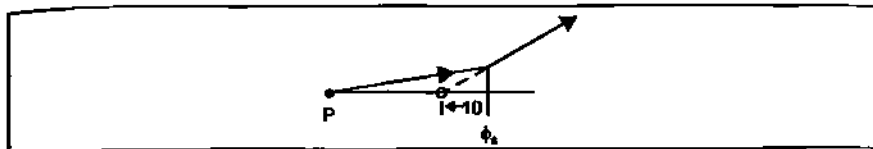


Fig. 26.9 Secondary imaging primary.

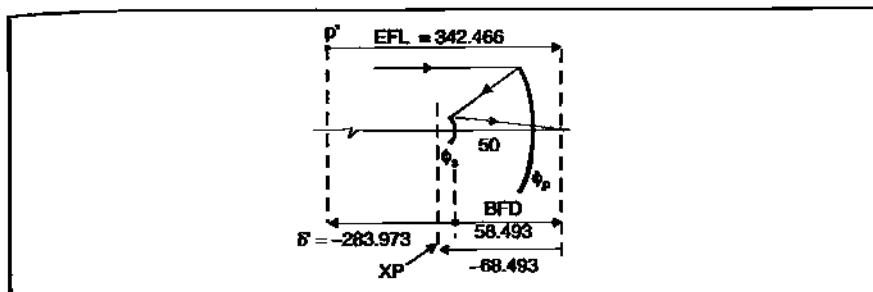


Fig. 26.10 Refolded Cassegrain.

reflected from it is also perfectly spherical. To do this we make use of Equation 24.3 once again and apply it to the secondary.

$$K_S = \frac{A_S^2 y_S \Delta_S \left\{ \frac{u}{n} \right\}}{C_S^3 y_S^4 \Delta_S \{ n \}} \quad (26.7)$$

where

$$A_S = n'(u_S + y_S C_S);$$

$$\Delta_S \left\{ \frac{u}{n} \right\} = \frac{u'_S}{n'_S} - \frac{u_S}{n_S};$$

$$\Delta_S \{ n \} = n'_S - n_S.$$

But there is a curveball here. In the ray trace we were only concerned about the power of the components. Equation 26.7 involves curvatures. Curvatures are absolute quantities. Their sign depends only on whether they point to the right or left (refer back to the sign conventions in Figure 3.2). The power of a component is also an absolute. It is either positive or negative. This brings us to the relation between power and curvature via the equation: $\phi = -2nC$. For the primary, C_p is negative but the power is positive. However, for the secondary, both quantities are negative. This can only happen if the airspace from the primary to the secondary is considered to be *negative*. With this in mind let's calculate the values for Equa-

tion 26.7:

$$A_s = (-1)[0.24876 + (2.562)(-0.04)] = -0.14628$$

$$\Delta_s \left\{ \frac{u}{n} \right\} = \left[-0.0438 - \frac{0.24876}{-1} \right] = 0.20492$$

$$\Delta_s(n) = 1 - (-1) = 2$$

Inserting into Equation 26.7:

$$A_s^2 y_s \Delta_s \left\{ \frac{u}{n} \right\} = (-0.14628)^2 (2.562)(0.20492) = 0.011234$$

$$C_s^3 y_s^4 \Delta_s \{ n \} = -0.04^3 (2.562)^4 (2) = -0.005515$$

Therefore:

$$K_s = \frac{0.011234}{-0.005515}$$

$$K_s = -2.037$$

Referring back to Table 3.1, we see that this is a hyperbolic surface.

26.4 Cassegrain in ZEMAX

It is now time to load our predesign into ZEMAX. Our initial entry will *not* include the conics on either surface, nor will we worry about obscurations and holes just yet. The resulting layout and prescription are shown in Figure 26.11. Note that: (a) the radii are both negative; (b) the stop is on the primary; (c) MIRROR is placed in the "Glass" column for both the primary and secondary; (d) the thickness following the primary is negative; and (e) the *collimated* rays pass through the secondary as if were not there. Also, the M-solve places the image surface in the paraxial plane. Instead of a focus point, we have a blur spot ~1 cm in diameter. This is due to the large amount, 105λ ($\lambda = 0.55 \mu\text{m}$), of spherical aberration present when using just spherical mirrors. The OPD plot and spot diagram are shown in Figure 26.12.

We now insert the conic constants. The new layout is shown in Figure 26.13. The marginal rays are being focused in the paraxial plane. The OPD plot and spot diagram are shown in Figure 26.14. Note the scale change in the OPD plot. The spot diagram says it all; the system is diffraction limited on-axis.

Now let's take into account the hole in the primary. On the primary surface: double-click on Standard → Aperture Type → Circular Aperture → (Replace the Min Radius with 2.562) → OK. The result of this is shown in Figure 26.15.

Section 26.4: Cassegrain in ZEMAX 295

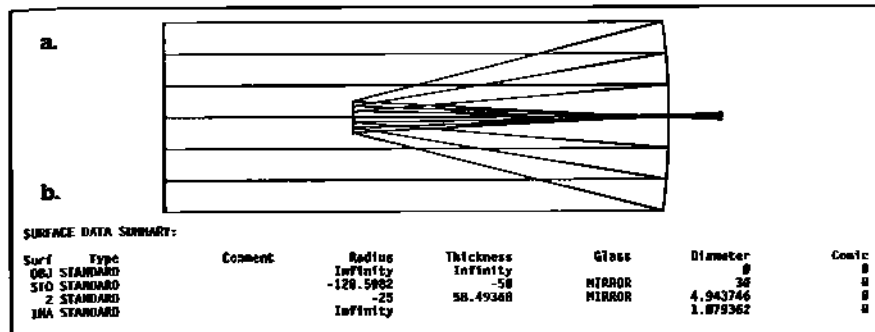


Fig. 26.11 Layout and prescription for spherical mirror Cassegrain.

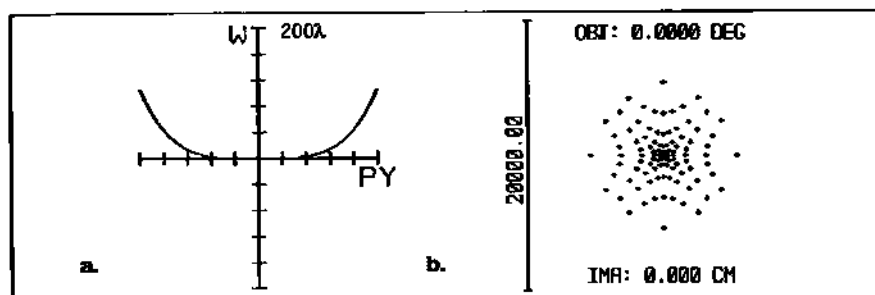


Fig. 26.12 OPD plot and spot diagram of spherical mirror Cassegrain.

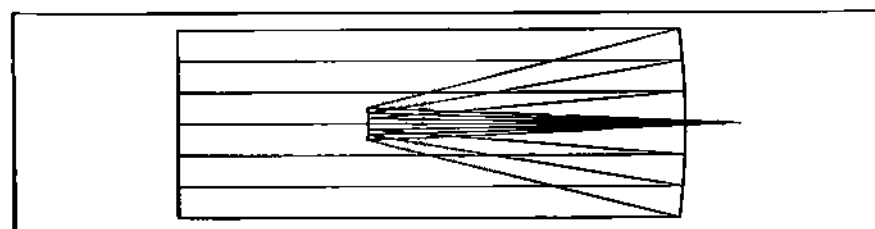


Fig. 26.13 Classic Cassegrain with proper conic constants installed.

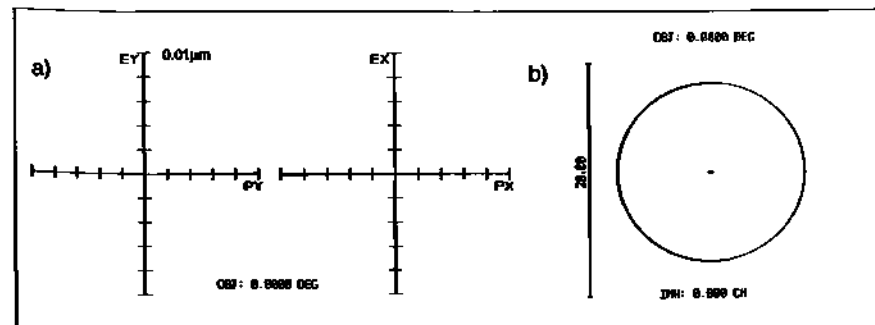


Fig. 26.14 OPD plot and spot diagram after installation of conic constants.

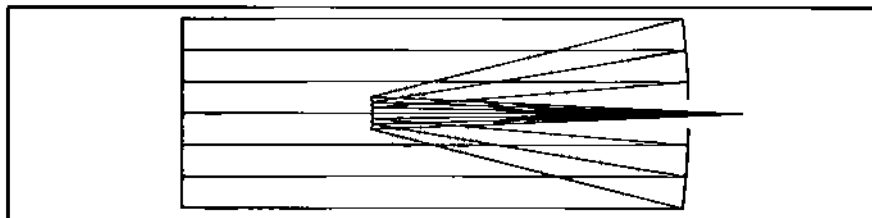


Fig. 26.15 Hole in primary.

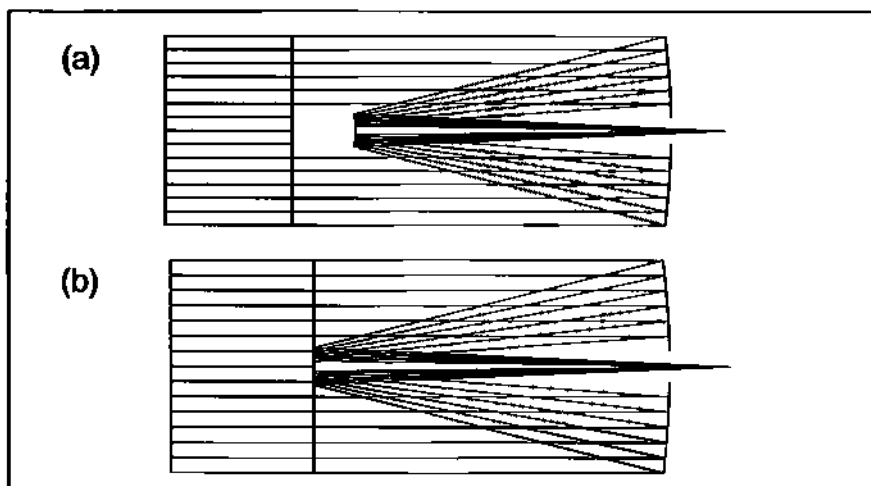


Fig. 26.16 Central obscuration.

For the obscuring effect of the secondary, insert another dummy surface in front of the primary (with an initial 60 cm thickness). This will now be Surf No. 2. On this surface: double-click on Standard → Aperture Type → Circular Obscuration → (Replace the Max Radius with 2.562) → OK. The result of this is shown in Figure 26.16a. The 60-cm thickness was selected in order to clearly see the effect of the obscuration. Now change that thickness to 50 cm to make the obscuration *coincident* in space with the secondary as shown in Figure 26.16b.

26.5 Other Design Considerations

26.5.1 Effect of Central Obscuration

All the telescope types mentioned in Section 26.2 have one thing in common—a central obscuration. Aside from the obvious reduction in light throughput, these obscurations have an impact on image resolution. The reason is the shape of the *diffraction point spread function* (PSF) which is affected by the relative size of the obscuration to the full primary (or entrance pupil) aperture. This point is illustrat-

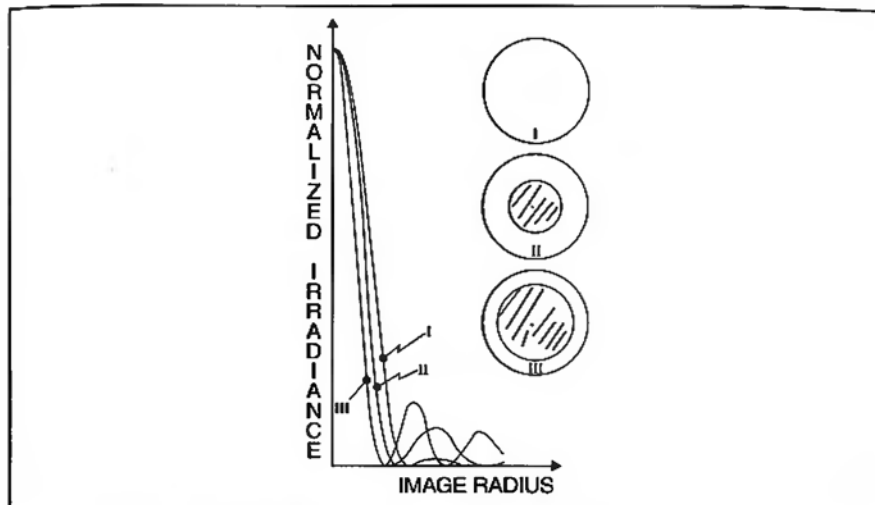


Fig. 26.17 PSF profiles as a function of central obscuration size.

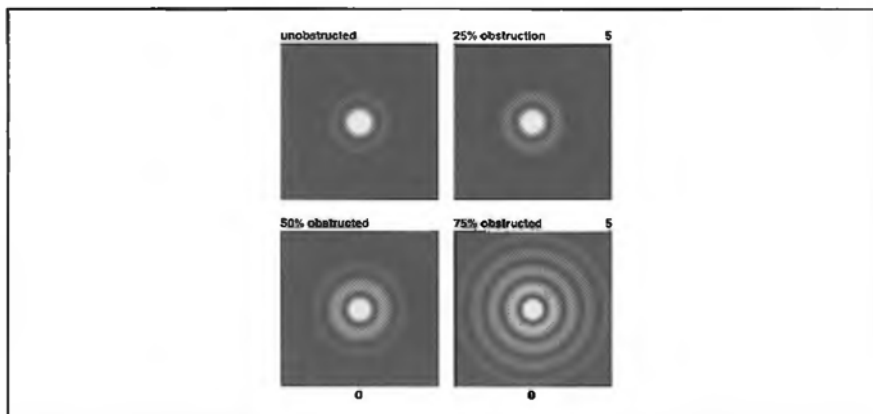


Fig. 26.18 PSF as a function of central obscuration size. Reprinted with permission from H.R. Suiter, Star Testing Astronomical Telescopes (Willmann-Bell, 1994).

ed in Figure 26.17. Shown are the normalized profiles across a diameter of the PSF as a function of obscuration ratio ($\text{DIAM}_{\text{OB}}/\text{DIAM}_{\text{EPD}}$) compared to a system with no central obscuration. As the ratio increases, the core diameter decreases (which seems good), but more power is being sucked from the core and pumped into the surrounding diffraction rings (which is bad). This effectively increases the size of the PSF which in turn reduces resolution. This brightening of the rings (at the expense of the core) is seen more dramatically in Figure 26.18. For our telescope the obscuration ratio is not bad at 17%. (The Hubble has about a 13% obscuration.)

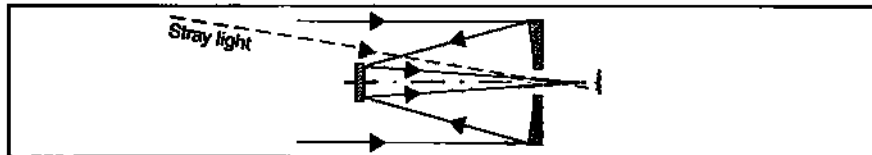


Fig. 26.19 Source of non-image forming light in a Cassegrain.

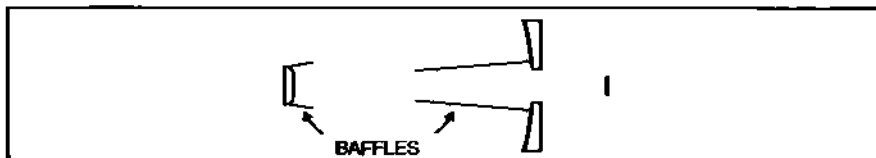


Fig. 26.20 Example of baffles to suppress stray light in Cassegrain.

26.5.2 Stray Light and Baffles

It is quite possible for a ray of light from some off-axis field point to slip past the secondary, go through the hole in the primary, and hit the imaging sensor without ever interacting with the primary and secondary. This is illustrated in Figure 26.19. This is non-image forming light. It creates unwanted background illumination which reduces image contrast and, hence, resolution. For this reason telescopes incorporate light baffles to eliminate or minimize the effect of stray light. An example is shown in Figure 26.20. The famous stray light code APART found its inception in stray light prediction and suppression (including baffle design and scatter from matte black finishes) for the Hubble. It is not our purpose here to get into the nitty-gritty of baffle design, only to point out its importance to the overall telescope system design.

26.6 Historical Note: G.W. Ritchey and H.J. Chrétien

Your homework problem will involve the design of a Ritchey-Chrétien telescope. This was a major improvement of the Cassegrain type, and resulted from a fruitful collaboration between an American and a Frenchman. The improvement can be seen in Figure 26.21, which shows spot diagrams as a function of field for both the Classic and Ritchey-Chrétien Cassegrains. The main problem with the Classic is third order coma. This has been eliminated in the Ritchey-Chrétien. Though the latter telescope results in superior performance, the mirrors are much more difficult to fabricate. Ritchey and Chrétien figured out a practical way to do this.

George W. Ritchey (Figure 26.22) was born in 1864, raised in Ohio, and later attended the University of Cincinnati. His father's interest in astronomy rubbed off on George... so much so that he set up a small optics shop in his home to make his own mirrors. He developed his skills over the years, and eventually became Director of the Mt. Wilson optics shop which was located in Pasadena, California. Not only could Ritchey build telescopes, he also knew how to use them since he was also a professional astronomer.

Section 26.7: Homework 299

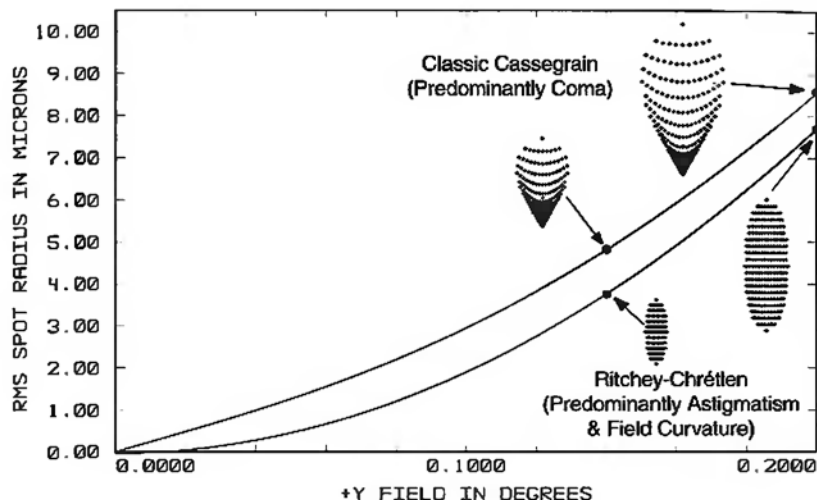


Fig. 26.21 Spot diagram comparison between Classic and Ritchey-Chrétien Cassegrains.



Fig. 26.22 George Ritchey (1864–1945).



Fig. 26.23 Henri J. Chrétien (1879–1956).

Ritchey met the French optician Henri J. Chrétien at Mt. Wilson. Chrétien was visiting the US to learn more about telescope design. Chrétien (Figure 26.23) was born in Paris in 1879. By 1910 he was married, had 3 children, and was chief of astrophysics at Nice. He helped found the famous Institut d'Optique in Paris in 1917.

26.7 Homework

Using the base mirror radii and mirror separation used in this chapter for the Cassegrain telescope, use ZEMAX to turn it into an *aplanatic* Ritchey-Chrétien. Let the field angle be $\pm 1^\circ$. Suggest using folder name: Cassegrain; file name: RICH1o1b, etc.

Chapter 27

Relating Defocus, Astigmatism, and Field Curvature

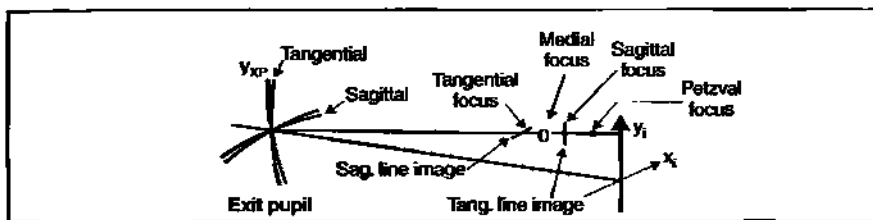


Fig. 27.1 Relative locations of line foci, medial focus, Petzval focus to paraxial focus.

27.1 Introduction

In ZEMAX the paraxial image plane is located by using the M-solve. The best RMS spot size plane is usually found with a dummy image surface whose thickness is a variable coupled to the merit function via a set of operands (like TRAC). Any other focal plane can be explored by removing the variable on the dummy thickness and setting that thickness to any arbitrary value desired. This is an operator induced defocus. The latter was discussed in terms of the pupil wavefront aberration, W_d , in Section 11.5. It was then employed to locate minimum blur when spherical aberration was present. In Chapter 14, we learned about Petzval curvature and how to calculate its coefficient W_{220P} . In that same chapter, we also saw how to combine defocus W_d and W_{220P} to locate the Petzval surface. In this chapter, we will build upon these traditions and use W_d to explore image space when both astigmatism and Petzval curvature are present. This will enable us to quantitatively determine the locations of the line foci and medial focus relative to the Petzval surface and the paraxial plane as illustrated in Figure 27.1.

27.2 Wavefront Description of Aberrations in Cartesian Coordinates

The Seidel wavefront aberrations (including defocus) are given in polar form by:

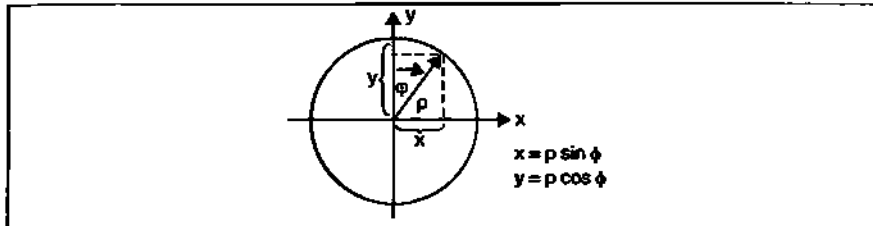


Fig. 27.2 Relation between polar and Cartesian descriptions.

$$W = W_d \rho^2 + W_{040} \rho^4 + W_{131} \bar{H} \rho^3 \cos \phi + W_{222} \bar{H}^2 \rho^2 \cos^2 \phi + \\ W_{220} \bar{H}^2 \rho^2 + W_{311} \bar{H}^3 \rho \cos \phi \quad (27.1)$$

This can be converted to Cartesian form with help from the illustration in Figure 27.2.

The Seidel aberrations can now be written as:

$$W = W_d (x^2 + y^2) + W_{040} (x^2 + y^2)^2 + W_{131} \bar{H} (x^2 + y^2) y + \\ W_{222} \bar{H}^2 y^2 + W_{220P} \bar{H}^2 (x^2 + y^2) + W_{311} \bar{H}^3 y \quad (27.2)$$

27.3 Wavefront Gradients in Cartesian Form

The wavefront slopes in Cartesian form can be found by taking the derivatives of Equation 27.2 with respect to both x and y , i.e., $\partial W/\partial x$ and $\partial W/\partial y$. These partial derivatives are shown in Table 27.1.

Table 27.1 Slopes of Wavefront Aberrations in Cartesian Form		
Aberration	$\partial W/\partial x$	$\partial W/\partial y$
Defocus	$2W_d x$	$2W_d y$
Spherical	$4W_{040} (x^2 + y^2)x$	$4W_{040} (x^2 + y^2)y$
Coma	$2W_{131} \bar{H} xy$	$W_{131} \bar{H} (x^2 + 3y^2)$
Astigmatism	0	$2W_{222} \bar{H}^2 y$
Field Curvature	$2W_{220P} \bar{H}^2 x$	$2W_{220P} \bar{H}^2 y$
Distortion	0	$W_{311} \bar{H}^3$

27.4 Defocus, Astigmatism, and Petzval Curvature in Pupil

It will be useful for us to *define* another field curvature coefficient W_{fc} which combines astigmatism with Petzval:

$$W = W_{fc} \bar{H}^2 (x^2 + y^2)$$

where:

$$W_{fc} = \frac{1}{2} W_{222} + W_{220P} \quad (27.3)$$

Note that the astigmatism piece of this coefficient is incorporated into a term that has *rotational symmetry*.

The interrelationship between defocus, astigmatism, and field curvature is then given by:

$$W = W_d (x^2 + y^2) + W_{222} \bar{H}^2 y^2 + W_{fc} \bar{H}^2 (x^2 + y^2) \quad (27.4)$$

Substituting Equation 27.3 into Equation 27.4:

$$W = W_d (x^2 + y^2) + W_{222} \bar{H}^2 y^2 + \left(\frac{1}{2} W_{222} + W_{220P} \right) \bar{H}^2 (x^2 + y^2) \quad (27.5)$$

Therefore, along the *y*-axis (Figure 27.2) we have:

$$W_y = \left[W_d + \left(\frac{3}{2} \right) W_{222} \bar{H}^2 + W_{220P} \bar{H}^2 \right] y^2 \quad (27.6)$$

and along the *x*-axis:

$$W_x = \left[W_d + \frac{1}{2} W_{222} \bar{H}^2 + W_{220P} \bar{H}^2 \right] x^2 \quad (27.7)$$

The agenda now is to set W_d equal to various combinations of W_{222} and W_{220P} along both *x* and *y* axes.

1. Petzval focus: Let $W_d = -W_{220P} \bar{H}^2$. Then Equation 27.6 becomes:

$$W_y = \left(\frac{3}{2} \right) W_{222} \bar{H}^2 y^2$$

and the slope is:

$$\frac{\partial W_y}{\partial y} = 3 W_{222} \bar{H}^2 y$$

Then Equation 27.7 becomes:

$$W_x = \frac{1}{2} W_{222} \bar{H}^2 x^2$$

and the slope is:

(27.9)

$$\frac{\partial W_x}{\partial x} = W_{222} \bar{H}^2 x$$

2. Sagittal focus: let $W_d = -\left(\frac{1}{2}W_{222} + W_{220P}\right)\bar{H}^2$

Then Equation 27.6 becomes:

$$W_y = W_{222} \bar{H}^2 y^2$$

and the slope is:

(27.10)

$$\frac{\partial W_y}{\partial y} = 2W_{222} \bar{H}^2 y$$

Then Equation 27.7 becomes:

$$W_x = 0$$

and the slope is:

(27.11)

$$\frac{\partial W_x}{\partial x} = 0$$

3. Tangential focus: Let $W_d = -\left[\frac{3}{2}W_{222} + W_{220P}\right]\bar{H}^2$

Then Equation 27.6 becomes:

$$W_y = 0$$

and the slope is:

(27.12)

$$\frac{\partial W_y}{\partial y} = 0$$

Then Equation 27.7 becomes:

$$W_x = -W_{222} \bar{H}^2 x^2$$

and the slope is:

(27.13)

$$\frac{\partial W_x}{\partial x} = -2W_{222} \bar{H}^2 x$$

Section 27.5: Making the Connection to Image Space 305

4. Medial focus: Let $W_d = -[W_{222} + W_{220P}]H^2$

Then Equation 27.6 becomes:

$$W_y = \frac{1}{2}W_{222}H^2y^2$$

and the slope is:

(27.14)

$$\frac{\partial W_y}{\partial y} = W_{222}H^2y$$

Then Equation 27.7 becomes:

$$W_x = -\frac{1}{2}W_{222}H^2x^2$$

and the slope is:

(27.15)

$$\frac{\partial W_x}{\partial x} = -W_{222}H^2x$$

27.5 Making the Connection to Image Space

With the proper relations set up in the exit pupil for the wavefront aberrations W_x and W_y , and their slopes $\partial W_x / \partial x$ and $\partial W_y / \partial y$, we can now transfer their influence into image space. First, we'll look at longitudinal locations, and then at image sizes and shapes.

27.5.1 Image Focus Locations Along Chief Ray

Recall from Sections 11.4–11.5 that: $\delta = 8(f/\#)^2 W_d$ (where δ was measured on-axis from the paraxial focal plane). However, in the cases to be presented here, δ is measured along the chief ray, \bar{U}' , in image space.

For the Petzval focus:

$$\delta_p = 8(f/\#)^2 [-W_{220P}H^2] \cos \bar{U}' \quad (27.16)$$

Sagittal focus:

$$\delta_s = 8(f/\#)^2 \left[-\left(\frac{1}{2}W_{222} + W_{220P} \right) H^2 \right] \cos \bar{U}' \quad (27.17)$$

Tangential focus:

$$\delta_t = 8(f/\#)^2 \left[-\left(\frac{3}{2}W_{222} + W_{220P} \right) H^2 \right] \cos \bar{U}' \quad (27.18)$$

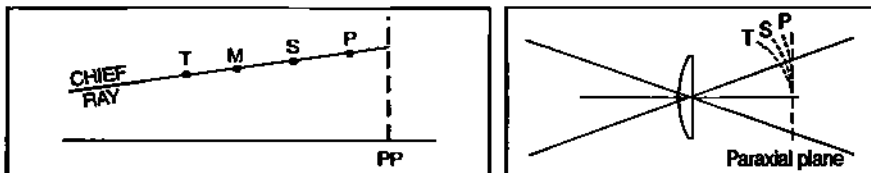


Fig. 27.3 Relative location of foci along chief ray.

Fig. 27.4 Focal surfaces for thin lens.

Medial focus:

$$\delta_M = 8(f/\#)^2 \left[-\left(W_{222} + W_{220P} \right) \bar{H}^2 \right] \cos \bar{U}' \quad (27.19)$$

The relative ordering of these focus locations depends on the signs of the Petzval and astigmatism coefficients. (Note: See Section 27.7 for an explanation of the appearance of the $\cos \bar{U}'$)

27.5.2 Example

As an example we'll use the sample singlet from Section 13.3.4 and Section 14.5. Here the coefficient values were: $W_{222} = 12.48 \mu\text{m}$ and $W_{220P} = 4.28 \mu\text{m}$. The f-number is $f/6.13$. So the factor in front of the bracketed terms in the above focus equations: $8(f/\#)^2 = 300.61$. We'll also set $\bar{H} = 1$, i.e., maximum field, which in this case is 5° . The results are shown in Table 27.2 and illustrated in Figure 27.3.

Table 27.2 Focus locations for sample singlet	
Petzval focus:	$\delta_p = -1.282 \text{ mm}$
Sagittal focus:	$\delta_s = -3.150 \text{ mm}$
Tangential focus:	$\delta_t = -6.888 \text{ mm}$
Medial Focus:	$\delta_M = -5.019 \text{ mm}$

If we plotted out each focal surface as a function of field, we would get a plot like that shown in Figure 27.4. Each of these focal surfaces is parabolic in shape because all are quadratic with field angle.

Note that the tangential focal surface is further from the Petzval surface than the sagittal focal surface. In fact, along the chief ray (or any principal ray), the tangential focus is a factor of three further away than the sagittal focus. This can be demonstrated as follows:

First, find the difference between the Petzval and tangential foci:

$$\delta_p - \delta_t = 8(f/\#)^2 \left[-W_{220P} \bar{H}^2 + \frac{3}{2} W_{222} \bar{H}^2 + W_{220} \bar{H}^2 \right] \cos \bar{U}'$$

Section 27.5: Making the Connection to Image Space 307

$$\delta_p - \delta_T = 8(f/\#)^2 \left(\frac{3}{2} W_{222} \bar{H}^2 \right) \cos \bar{U}'$$

or:

$$\delta_{PT} = 3 \left\{ 8(f/\#)^2 \left[\frac{1}{2} W_{222} \bar{H}^2 \right] \right\} \cos \bar{U}' \quad (27.20)$$

Second, find the difference between the Petzval and sagittal foci:

$$\delta_p - \delta_S = 8(f/\#)^2 \left[-W_{220P} \bar{H}^2 + \frac{1}{2} W_{222} \bar{H}^2 + W_{220P} \bar{H}^2 \right] \cos \bar{U}'$$

$$\delta_p - \delta_S = 8(f/\#)^2 \left[\frac{1}{2} W_{222} \bar{H}^2 \right] \cos \bar{U}'$$

or:

$$\delta_{PS} = 1 \left\{ 8(f/\#)^2 \left[\frac{1}{2} W_{222} \bar{H}^2 \right] \right\} \cos \bar{U}' \quad (27.21)$$

By comparing Equations 27.20 and 27.21, an important relationship is seen:

$$\delta_{PT} = 3\delta_{PS} \quad (27.22)$$

27.5.3 Separation Between Tangential and Sagittal Foci

One of the things that can be easily measured in the lab is the separation between the sagittal and tangential foci. In the present context this can be done by taking the difference between Equations 27.17 and 27.18.

$$\delta_T - \delta_S = \delta_{TS} = -8(f/\#)^2 W_{222} \bar{H}^2 \cos \bar{U}' \quad (27.23)$$

Referring to Table 10.1, W_{222} for a *thin lens* can be written as:

$$W_{222} = \frac{1}{2} L^2 \phi \quad (27.24)$$

In air the Lagrange invariant,

$$L = (\bar{u}y - \bar{y}u)$$

For an object at infinity, or stop at the optic:

$$L = \bar{u}y \quad (27.25)$$

Inserting this into Equation 27.24:

$$W_{222} = \frac{1}{2}(\bar{u}y)^2\phi \quad (27.26)$$

where y is the actual (unnormalized) aperture radius.

Inserting Equation 27.26 into Equation 27.23:

$$\delta_{TS} = -4(f/\#)^2(\bar{u}y)^2\phi\bar{H}^2\cos\bar{U}' \quad (27.27)$$

Substituting in for the f-number:

$$\delta_{TS} = -4(f/2y)^2(\bar{u}y)^2\frac{1}{f}\bar{H}^2\cos\bar{U}'$$

$$\delta_{TS} = -f\bar{u}^2\bar{H}^2\cos\bar{U}' = -f\bar{H}^2\tan^2\bar{U}'\cos\bar{U}' \quad (27.28)$$

At full field $\bar{H} = 1$:

$$\delta_{TS} = -f\frac{\sin^2\bar{U}'}{\cos^2\bar{U}'}\cos\bar{U}'$$

$$\delta_{TS} = -f\tan\bar{U}'\sin\bar{U}'. \quad (27.29)$$

Note that δ_{TS} is aperture independent.

The sample lens (used in the example in Section 27.5.2) has a focal length of 490.6 mm. Applying Equation 27.28 for an angle of 5°:

$$\delta_{TS} = -(490.6)(0.087489)(0.087156)$$

$$\delta_{TS} = -3.741 \text{ mm}$$

which is essentially the value obtained by taking the difference between the tangential and sagittal foci values in Table 27.2.

We made a point by noting that δ_{TS} is aperture independent. As it turns out, *all* the δ values in Equations 27.16 through 27.19 are aperture independent. This can be easily verified by substituting Equation 27.26 into the various δ -equations along with the equation for the Petzval coefficient:

$$W_{220P} = \frac{(\bar{u}y)^2}{4n_L f} \quad (27.30)$$

where n_L is the refractive index of the lens. (Also, please keep in mind that the aperture value y as used in determining the magnitude of aberration *coefficients* [as in Equations 27.26 and 27.30] is the real physical aperture radius. It is not normalized. But y and x as used in the aberration polynomial equation [as in Equation 27.2] are normalized.)

Section 27.5: Making the Connection to Image Space 309

The results of these substitutions are:

$$\left. \begin{aligned} \delta_P &= -\frac{1}{2}\bar{f}\bar{u}^2 \left[\frac{1}{n_L} \bar{H}^2 \cos \bar{U}' \right] \\ \delta_S &= -\frac{1}{2}\bar{f}\bar{u}^2 \left[1 + \frac{1}{n_L} \bar{H}^2 \cos \bar{U}' \right] \\ \delta_T &= -\frac{1}{2}\bar{f}\bar{u}^2 \left[3 + \frac{1}{n_L} \bar{H}^2 \cos \bar{U}' \right] \\ \delta_M &= -\frac{1}{2}\bar{f}\bar{u}^2 \left[2 + \frac{1}{n_L} \bar{H}^2 \cos \bar{U}' \right] \end{aligned} \right\} \quad (27.31)$$

27.5.4 Image Sizes at Respective Focal Planes

To get information about image dimensions and shapes in the various focal planes of interest, the pertinent wavefront slopes in the X and Y directions are multiplied by: $-R/nr$ (Section 11.8). This generates the relevant transverse ray aberration equations listed in Table 27.3.

Table 27.3 Transverse Ray Aberration in Defined Focal Planes		
Focus	T_y	T_x
Petzval	$\frac{-R}{nr}(3W_{222}\bar{H}^2y)$	$\frac{-R}{nr}(W_{222}\bar{H}^2x)$
Sagittal	$\frac{-R}{nr}(2W_{22}\bar{H}^2y)$	$\frac{-R}{nr}(0)$
Tangential	$\frac{-R}{nr}(0)$	$\frac{-R}{nr}(-2W_{22}\bar{H}^2x)$
Medial	$\frac{-R}{nr}(W_{222}\bar{H}^2y)$	$\frac{-R}{nr}(-W_{222}\bar{H}^2x)$

Using our sample lens once again, the value of the scaling coefficient is: $-R/nr = -12.265$. If we go to full field, $\bar{H} = 1$. The results of inserting these values into Table 27.3 are shown in Table 27.4.

Table 27.4 Transverse Ray Aberration in Defined Focal Planes		
Focus	T_y (μm)	T_x (μm)
Petzval	-459.94 y	-153.31 x
Sagittal	-306.62 y	0
Tangential	0	306.62 x
Medial	-153.31 y	153.31 x

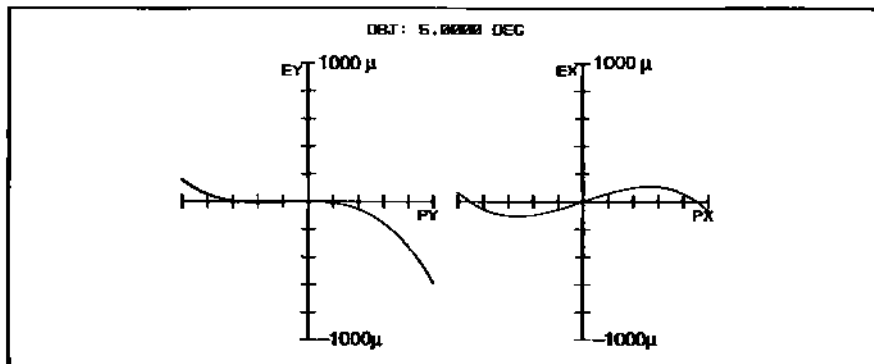


Fig. 27.5 Tangential and sagittal ray fan plots at tangential focus.

Sagittal fan, field number 2 = 5.0000 deg

Pupil	0.6916
-1.000	66.3945
-0.950	27.7199
-0.900	-5.3739
-0.850	-33.2187
-0.800	-56.1394
-0.750	-74.4566
-0.700	-88.4626
-0.650	-98.5267
-0.600	-104.6922
-0.550	-107.8784
-0.500	-107.7687
-0.450	-104.6987
-0.400	-99.4957
-0.350	-91.8843
-0.300	-82.3363
-0.250	-71.1333
-0.200	-58.5546
-0.150	-44.8756
-0.100	-30.3739
-0.050	-15.3249
0.000	0.0000
0.050	15.3249
0.100	30.3739
0.150	44.8756
0.200	58.5546
0.250	71.1333
0.300	82.3363

Table 27.5 Sagittal ray fan at tangential focus.

At the tangential focus located -6.914 mm from the paraxial plane along the chief ray, we have (if spherical and coma are neglected) a sagittal-line image 613.24 microns in length (at full normalized aperture: $y = 1$). At the sagittal focus there is a tangential line image of the same length. At medial focus, there is a circular blur with a diameter of 306.62 microns. Also note that, unlike the δ -locations, these image sizes are very much aperture dependent.

27.6 Checking Out the Image Predictions in ZEMAX

The problem we'll face when we try to verify the predictions in Table 27.2 and Table 27.4 is the presence of spherical aberration and coma in this lens. Recall that this singlet has 7.51 microns of spherical aberration (Section 10.5), and 5.8 microns of coma (Section 13.3.2) at 5° . This is a thin lens prediction. In ZEMAX this requires setting the lens thickness to zero. There are two ways to approach this

Section 27.6: Checking Out the Image Predictions in ZEMAX 311

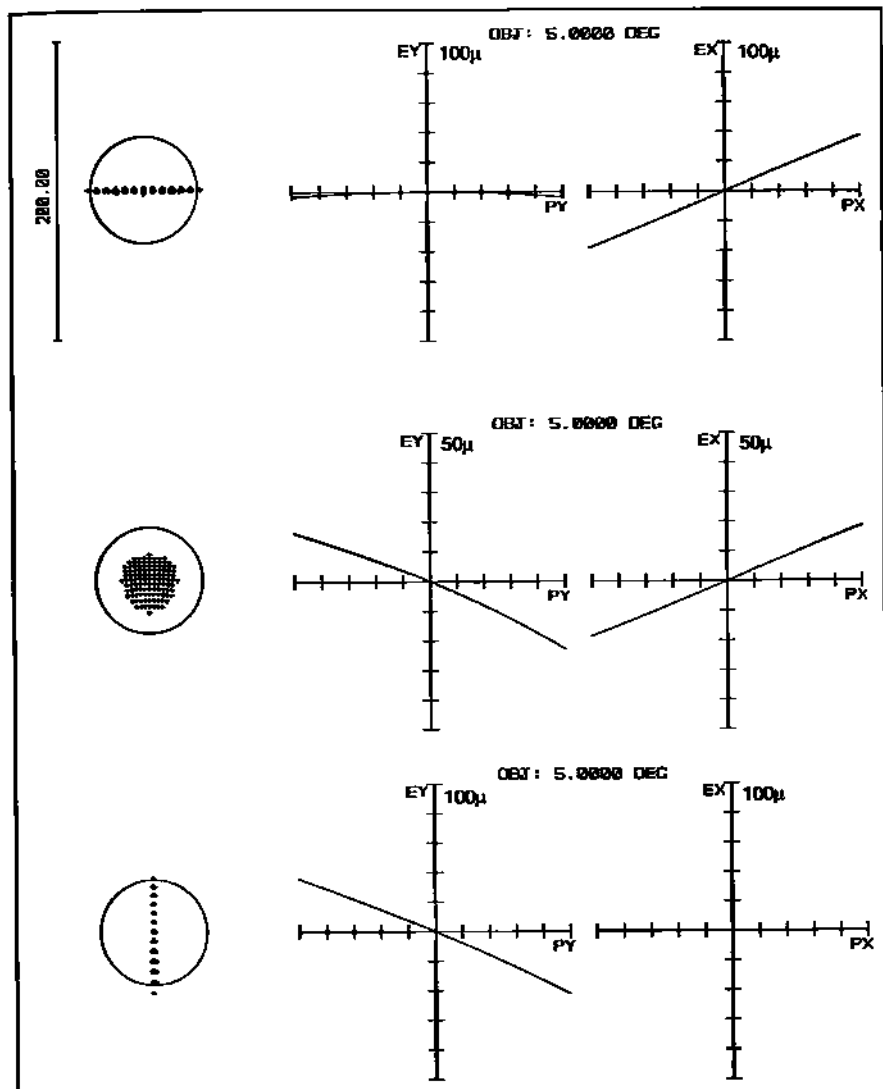


Fig. 27.6 Spot diagrams and ray fan plots at tangential, medial, and sagittal foci.

problem. The first way is to examine the ray fan plots. In ZEMAX we'll insert a dummy surface after the line containing the M-solve. To place ourselves at the tangential focus, we take the δ_T value from Table 27.2 and multiply it by $\cos 5^\circ$ to get the focal shift we need along the optical axis. The ray fan plot at the tangential focus is shown in Figure 27.5.

The left side of the plot is the tangential fan. Note that this plot is flat and zero in the central part of the aperture. Over the full aperture we can see the S-

shape signature of spherical aberration, and the quadratic bend indicating the presence of coma. The sagittal fan is on the right side of the plot. Spherical is very obvious here. Coma is not. The astigmatism is also obvious by the linear slope passing through the central part of the lens. This is the part that we want to look at more carefully. Go to **Settings → View Text** on the plot. This will pull up the numbers that are plotted in Figure 27.5. The numbers for the sagittal fan at 5° are shown in Table 27.5.

The slope through the origin is: $\tan \theta = E_x/P_x = 15.324 / 0.05$. If there were no spherical or coma, this slope would continue as a straight line out to the aperture edge (where $P_x = 1$). The value of E_x at this point would be: $E_x = 306.48$ microns, which is very close to the value you will find listed under T_x at the tangential focus in Table 27.4.

The second way of approaching the problem is by playing with the aperture size. Let's compare the coefficients for the three aberrations of interest here:

$$\text{Spherical: } W_{040} = \frac{1}{32} \left(\frac{\sigma_i}{f^3} \right) y^4$$

$$\text{Coma: } W_{131} = \frac{1}{4} \left(\frac{\bar{u} \sigma_H}{f^2} \right) y^3$$

$$\text{Astigmatism: } W_{222} = \frac{1}{2} \left(\frac{\bar{u}^2}{f} \right) y^2$$

Spherical has a y to the *fourth* dependence; coma, y to the *third*; astigmatism, y to the *second*.

By shrinking the aperture down we can greatly reduce the effect of spherical and coma relative to astigmatism. This will change the sizes of the line images but not their axial locations. Figure 27.6 is a montage of ray fan plots and spot diagrams as a function of focus position (from Table 27.2) for a 1-cm diameter aperture. All plots are for 5°. In the spot diagrams, we clearly see the sagittal line image at the tangential focus, and the tangential line image at sagittal focus. (Note: The circle defines the Airy disk.) At medial focus, the blur spot is not quite circular due to the little bit of coma still present. The ray fan plots are linear except for a hint of coma bow in the tangential (or E_y plots). They behave as expected. At tangential focus the E_y fan is flat and the E_x fan is straight with a positive slope; the reverse prevails at the sagittal focus.

27.7 Basis for the Use of $\cos \bar{U}'$

Referring to Figure 27.7 and recalling the derivation from Sections 11.4 and 11.5:

$$\delta_R = 2 \left(\frac{R}{r} \right)^2 W_d \quad (27.32)$$

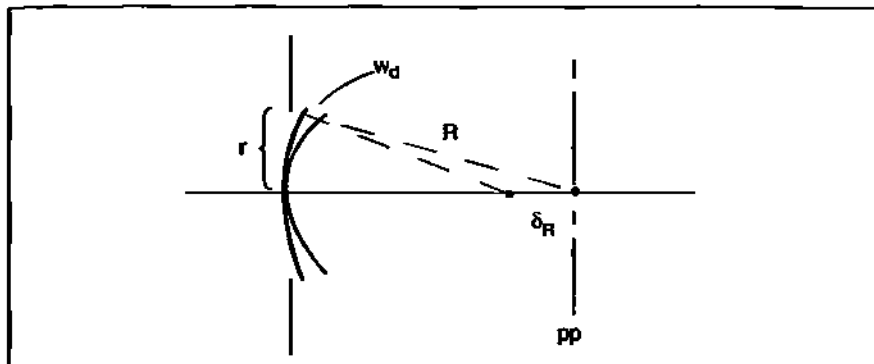


Fig. 27.7 Relation between W_d and δ_R for on-axis focus shift.

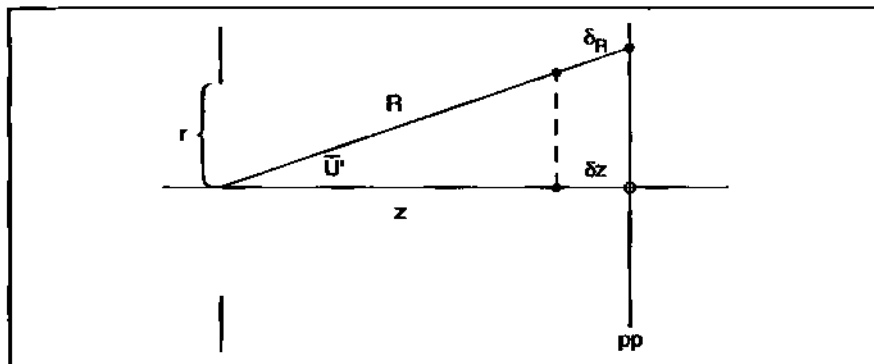


Fig. 27.8 Off-axis focus shift geometry.

OR,

$$\delta_R = 8(f/\#)^2 W_d . \quad (27.33)$$

Now consider the off-axis case shown in Figure 27.8.
Note that:

$$\frac{\delta_R}{R} = \frac{\delta_z}{z} \quad (27.34)$$

and:

$$\cos \bar{U}' = \frac{z}{R} = \frac{\delta_z}{\delta_R} . \quad (27.35)$$

On-axis we have (akin to Equation 27.32):

$$\delta_z = 2 \left(\frac{z}{r} \right)^2 W_d. \quad (27.36)$$

Substitute Equation 27.35 into Equation 27.36:

$$\delta_z = 2 \left(\frac{R \cos \bar{U}'}{r} \right)^2 W_d. \quad (27.37)$$

Rewriting:

$$\delta_z = 2 \left(\frac{R}{r} \right)^2 W_d \cos^2 \bar{U}'. \quad (27.38)$$

In terms of f-number:

$$\delta_z = 8(f/\#)^2 W_d \cos^2 \bar{U}'. \quad (27.39)$$

From Equations 27.35:

$$\delta_z = \delta_R \cos \bar{U}' \quad (27.40)$$

Equating Equations 27.39 and 27.40 we find that:

$$\delta_R = 8(f/\#)^2 W_d \cos \bar{U}'. \quad (27.41)$$

27.8 Homework

1. For a spherical mirror ($EFL = 32''$; $D = 10''$) with an object at infinity and stop at the mirror, where $\delta = -8(f/\#)^2 W_d$ for the mirror:
 - a. Find the values for: δ_p , δ_T , and δ_M at 15° .
 - b. Show that δ_S is zero for *any* field angle.
 - c. Find the value for δ_{TS} at 15° .

Chapter 28

Celor Lens

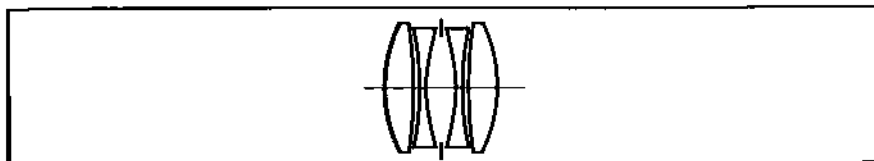


Fig. 28.1 The Celor lens.

28.1 Introduction

In Chapter 25 we discussed the design of an “achromatic periscopic” or “symmetric French Landscape” lens. In this chapter, we will discuss another classic design called the Celor lens (which is also known as a symmetric dialyte). The Celor lens is shown in Figure 28.1. It is a symmetric lens with a pair of *airspaced achromats*. The airspace provides a new degree of freedom.

The airspace means that the individual lens powers must increase to preserve the color correction. This can also be done in such a way as to lower the Petzval sum. As before, this lens design starts with the rear half. The idea behind this design is as follows. The rear half has five degrees of freedom: two lens powers, two lens bendings, and the airspace. These are used to hold the system focal length, maintain color correction, reduce the Petzval sum, control spherical aberration, and astigmatism. When the two halves are combined, coma, distortion, and lateral color are also reduced because of the symmetry.

28.2 Generalized Power

Before discussing the design, we need to obtain a different expression for the rear half power.

In Section 4.6.2 we found that the power for a two-element system (shown in Figure 28.2) could be expressed as:

$$\Phi = \Phi_1 + \Phi_2 - t\Phi_1\Phi_2 \quad (28.1)$$

However, we need to find a more general expression for power which eliminates the explicit thickness dependence, and is applicable to multi-element systems. We begin with the bending equation at the first surface for an object at infinity.

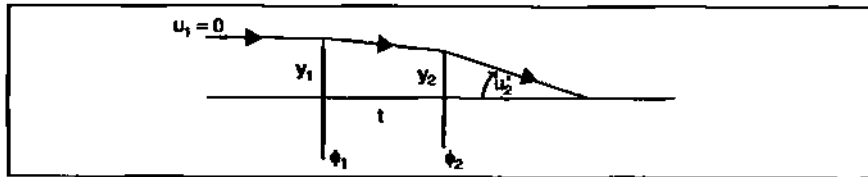


Fig. 28.2 Two element system.

$$u_1' = -y_1 \phi_1 = u_2 \quad (28.2)$$

At the second surface:

$$u_2' = u_2 - y_2 \phi_2 \quad (28.3)$$

Substitute Equation 28.2 into Equation 28.3:

$$u_2' = -y_1 \phi_1 - y_2 \phi_2 \quad (28.4)$$

However:

$$u_2' = \frac{-y_1}{\text{EFL}} = -y_1 \phi \quad (28.5)$$

Substituting Equation 28.5 into Equation 28.4:

$$-y_1 \phi = -y_1 \phi_1 - y_2 \phi_2$$

or:

$$\phi = \left(\frac{1}{y_1} \right) [y_1 \phi_1 + y_2 \phi_2] \quad (28.6)$$

In general:

$$\phi = \left(\frac{1}{y_1} \right) \sum_i y_i \phi_i \quad (28.7)$$

Equation 28.7 is the generalized power constraint.

28.3 Celor Lens Constraints

The following constraints are imposed on the design of the Celor rear half:

$$\left. \begin{array}{l} 1. \quad \phi = \left(\frac{1}{y_a} \right) (y_a \phi_a + y_b \phi_b) \\ 2. \quad \frac{y_a^2}{v_a} \phi_a + \frac{y_b^2}{v_b} \phi_b = 0 \\ 3. \quad \frac{\phi_a}{n_a} + \frac{\phi_b}{n_b} = \phi_p \end{array} \right\} \quad (28.8)$$

The first constraint is the generalized power condition derived in the previous section. The second constraint is on color and was previously derived in Section 19.2.1. The third constraint is from the Petzval sum developed in Section 14.4.

28.4 Derivation of Celor Equation

We will now derive an equation through which the power of the negative element is determined.

From Constraint No. 1 we have:

$$y_b = \frac{(\phi - \phi_a)y_a}{\phi_b} \quad (28.9)$$

Substitute Equation 28.9 into Constraint No. 2 and then do some rearranging:

$$\frac{y_a^2}{v_a} \phi_a + \frac{\phi_b}{v_b} \left[\frac{(\phi - \phi_a)y_a}{\phi_b} \right]^2 = 0 \quad (28.10)$$

$$\frac{y_a^2}{v_a} \phi_a + \left[\frac{(\phi - \phi_a)^2 y_a^2}{v_b \phi_b} \right] = 0$$

$$\frac{y_a^2}{v_a} \phi_a + \left(\frac{y_a^2}{v_b \phi_b} \right) (\phi^2 - 2\phi\phi_a + \phi_a^2) = 0$$

$$\frac{y_a^2}{v_b \phi_b} \phi_a^2 + \left(\frac{y_a^2}{v_a} - \frac{2y_a^2 \phi}{v_b \phi_b} \right) \phi_a + \frac{y_a^2 \phi^2}{v_b \phi_b} = 0$$

Now multiply through by ϕ_b :

$$\frac{y_a^2}{v_b} \phi_a^2 + \left(\frac{y_a^2 \phi_b}{v_a} - \frac{2y_a^2 \phi}{v_b} \right) \phi_a + \frac{y_a^2 \phi^2}{v_b} = 0$$

Divide through by y_a^2 :

$$\frac{1}{v_b} \phi_a^2 + \left(\frac{\phi_b}{v_a} - \frac{2\phi}{v_b} \right) \phi_a + \frac{\phi^2}{v_b} = 0 \quad (28.11)$$

From Constraint No. 3:

$$\phi_b = \left(\phi_p - \frac{\phi_a}{n_a} \right) n_b \quad (28.12)$$

Substitute Equation 28.12 into Equation 28.11 and rearrange:

$$\begin{aligned} & \frac{1}{v_b} \phi_a^2 + \left[\left(\phi_p - \frac{\phi_a}{n_a} \right) n_b - \frac{2\phi}{v_b} \right] \phi_a + \frac{\phi^2}{v_b} = 0 \\ & \frac{1}{v_b} \phi_a^2 + \frac{\phi_p n_b}{v_a} \phi_a - \frac{n_b}{n_a v_a} \phi_a^2 - \frac{2\phi}{v_b} \phi_a + \frac{\phi^2}{v_b} = 0 \\ & \left(\frac{1}{v_b} - \frac{n_b}{n_a v_a} \right) \phi_a^2 + \left(\frac{\phi_p n_b}{v_a} - \frac{2\phi}{v_b} \right) \phi_a + \frac{\phi^2}{v_b} = 0 \end{aligned}$$

Now multiply through by $(v_a v_b)$:

$$\left(v_a - \frac{n_b v_b}{n_a} \right) \phi_a^2 + (\phi_p n_b v_b - 2\phi v_a) \phi_a + v_a \phi^2 = 0 \quad (28.13)$$

Equation 28.13 is the Celor lens equation.

28.5 Celor Rear Half Lens Powers

The quadratic formula can be used to solve for ϕ_a :

$$\phi_a = \frac{-b \pm \sqrt{b^2 - 4ac}}{2a} \quad (28.14)$$

$$\left. \begin{aligned} a &= v_a - \frac{n_b}{n_a} v_b \\ b &= \phi_p n_b v_b - 2\phi v_a \\ c &= v_a \phi^2 \end{aligned} \right\} \quad (28.15)$$

where:

Section 28.5: Celor Rear Half Lens Powers 319

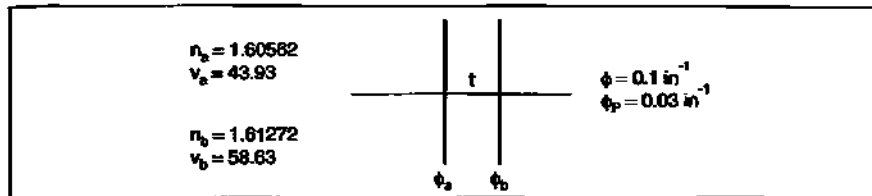


Fig. 28.3 Celor paraxial thin lens rear half.

This will yield two solutions for ϕ_a . Pick the negative solution. Insert this into Constraint No. 3 in Section 28.3 and solve for ϕ_b . Next, use Equation 28.1 to find the separation between the two elements.

An example will help. Figure 28.3 shows the thin lens version of the rear half of the Celor.

The index (*d*-light) and dispersion values are indicated as are the system power and the Petzval sum.

Using the Equation 28.15 set:

$$a = \left[43.93 - \left(\frac{1.61272}{1.60562} \right) (58.63) \right] = -14.96$$

$$b = 1.61272(58.63)(0.03) - 2(43.93)(0.1) = -5.95$$

$$c = 43.93(0.01)^2 = 0.4393$$

Inserting these parameters into Equation 28.14 yields: $\phi_{a+} = -0.4614$ and $\phi_{a-} = 0.0636$. Since element *a* has to be negative we pick ϕ_{a+} . This value is inserted into the third constraint and solved for ϕ_{b+} . So $\phi_{b+} = 0.5118$. Using these values for ϕ_{a+} and ϕ_{b+} we can now solve for the separation between the two components.

$$t = \frac{\phi_{a+} + \phi_{b+} - \phi}{\phi_{a+}\phi_{b+}}$$

$$t = \frac{-0.4614 + 0.5118 - 0.1}{(-0.4614)(0.5118)}$$

$$t = 0.21''$$

For initial curvatures for insertion into ZEMAX, one can assume that the negative component is equi-concave and the positive component is equi-convex. We can calculate these curvatures either from Equation 4.22, or by setting up variables and a merit function in ZEMAX to do it for us.

If we look at *b* in Equation 28.15 we see that $(\phi_p n_b v_b)$ will always be much less than $(2\phi v_a)$ because we usually want the Petzval sum to be low. So there is no reason why we can not set $\phi_p = 0$ to begin with. Applying this to the example just given: $\phi_{a+} = -0.6336$ ($f_{a+} = -1.5783$); $\phi_{b+} = 0.6364$ ($f_{b+} = 1.5713$); $t = 0.241''$. The

320 Chapter 28 Celor Lens

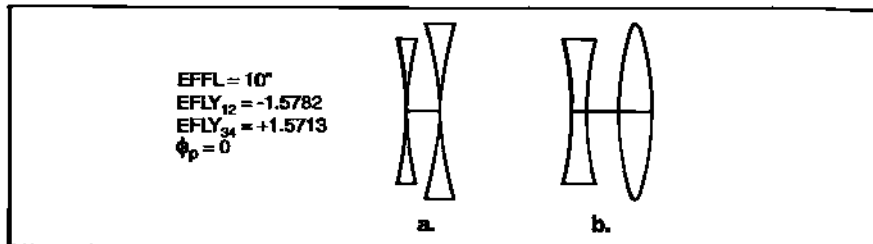


Fig. 28.4 Celor lens rear half: (a) thin lenses; (b) thick lenses.

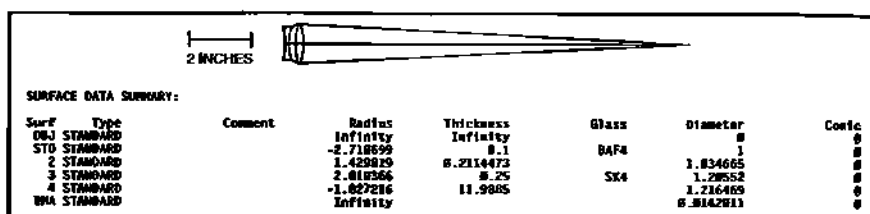


Fig. 28.5 Layout of CELO1o2a.

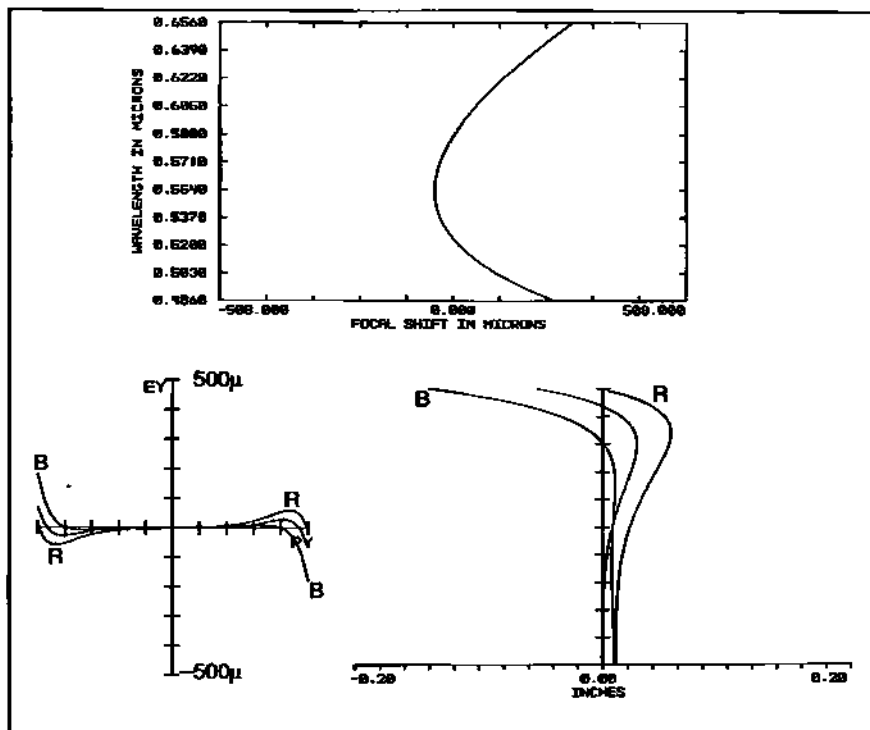


Fig. 28.6 CELO1o2a: axial color; ray fan; longitudinal aberration.

radii calculated from this solution provide a valid point of departure for ZEMAX.

28.6 Celor ZEMAX Design Procedure

In our example, the focal length of the rear half design is 10" (which implies that the focal length we're aiming for in the symmetric system is 5"). Once we have the rear half thin lens pre-design for the Celor, we can insert the computed radii and thickness into ZEMAX. We'll also set our EPD = 1" (or $f/10$). The thin lens design in ZEMAX for our example is shown in Figure 28.4a. (You can verify the system and individual lens focal lengths by using EFL and EFLYs in the MFE.) The layout when reasonable glass thicknesses (0.1" and 0.25" respectively) are added is shown in Figure 28.4b.

When real thicknesses are added we must tweak the lens to get back our target EFL and color correction. This is done by setting EFL = 10" and AXCL = 0 in the MFE. Variables are placed on radii on the first and third surfaces, and the airspace thickness. Radii on the second and fourth surfaces are slaved via pick-up to the first and third surfaces respectively. This will yield an equi-concave and a equi-convex negative and positive element. After optimization, the new element powers are: EFLY₁₂ = -1.53; EFLY₃₄ = 1.6032.

CELO1o1b → Optimize → CELO1o1a

We must now deal with the spherical aberration which is hefty ($\sim 107\lambda$). This will be done using lens bending. All surface radii are allowed to vary, but the individual lens powers will be tied down to their current EFLY values. The airspace will also be allowed to vary. So weights on the EFLYs will be turned on, as well as SPHA which will be targeted to zero.

CELO1o2b → Optimize → CELO1o2a

The design, after this optimization, is shown in Figure 28.5 along with the prescription. Axial color, ray fan, and longitudinal aberration plots are shown in Figure 28.6.

We have not used the longitudinal aberration plot before. This is an on-axis plot and provides another way of looking at spherical aberration. Go back and look at the meridional drawing at the top of Figure 7.6. The 0.33 ray in the pupil crosses the optical axis at a different longitudinal position (relative to the paraxial plane) than the 0.66 ray. If we plot a ray's pupil position along the ordinate and the axial crossover point along the abscissa, we get the longitudinal aberration plot shown on the bottom right in Figure 28.6.

We now add some field; not a lot, say 5°. We'll also add an aperture stop out in front of the lens pair, say 0.25". Add COMA and ASTI to the MFE and note that we have -7.6λ of coma and 6.7λ of astigmatism. We saw before (Section 6.3) that axial stop location has an impact on off-axis aberrations. But that's not going to help us here. Actually, we have enough degrees of freedom in the lens pair to knock down the astigmatism. (The coma knockdown should be handled

once symmetry is established.) There are two ways of going about this. Both require variables on all radii and the inter-lens airspace. The stop airspace is left fixed. In the MFE we also turn off the EFLYs (by setting weight to zero). In the *first* way, we turn-on ASTI = 0, making sure COMA is turned off. In the *second* way, ASTI is off as well as COMA, but FCGT (used three times—one for each defined field position) is turned on.

CELO1o3b → Optimize → CELO1o3a

After either optimization is run, AXCL, SPHA, and ASTI are all extremely low, but coma has increased to about -33λ . But symmetry will eventually help us there. The layout (either method) is shown in Figure 28.7.

Now it is time to assemble the symmetric system, CELO1o4b. This is shown in Figure 28.8. The rear half is *slaved* to the front half via the “pickup” option. The EFL of the system is 6.8”. Still at 5° field, coma has dropped about an order of magnitude (to 4.4λ) because of symmetry, while astigmatism has increased slightly to $\frac{3}{4}\lambda$.

We'll do our first optimization of the system to get the target EFL of 5” and restore good color correction. Variables will be on *all* front half radii and the front inter-lens airspace.

CELO1o4b → Optimize → CELO1o4a

The next step is to activate TRAC in the MFE. The variables on the front half negative element are removed, leaving the positive element radii and inter-lens airspace as variables. (If you do not turn off the negative radii at this point, TRAC tends to slam the positive and negative elements into [and inside] each other as shown in Figure 28.9a. If we let all radii vary on the front half as well as the lens and *stop* airspace, the separation between front and rear halves will double, and the lens airspace will be non-negative as shown in Figure 28.9b.) In addition, we will also turn on the stop airspace and allow it to vary. This will help lower both coma and astigmatism further as well as improve field flatness. RMS spot sizes will also improve. In doing this, however, we must make sure that there is enough room in the stop airspace after the optimization to accommodate not only a variable stop (iris), but also a shutter mechanism. For example, we may need at least 0.4-inch between the two halves for this.

CELO1o5b → Optimize → CELO1o5a

Suppose our desired field is 15°. The safest procedure is to work our way out there gradually, i.e., reoptimize CELO1o5a for a 10° field (CLEO1o6a). Then take the next step out to 15°, (CELO1o7a). *Update TRAC each time you change the field.* After each optimization, check the layout to make sure it is accurate (for example, no lens surfaces running into each other). Figure 28.10 shows the sequence of results from CELO1o5a through CELO1o7a. It should look fine up through 10°. But at 15° things go wrong in a hurry. Figure 28.11 shows the tangential ray fan and spot diagram at 15°. Note the steep upturn on the left side of the

Section 28.6: Celor ZEMAX Design Procedure 323

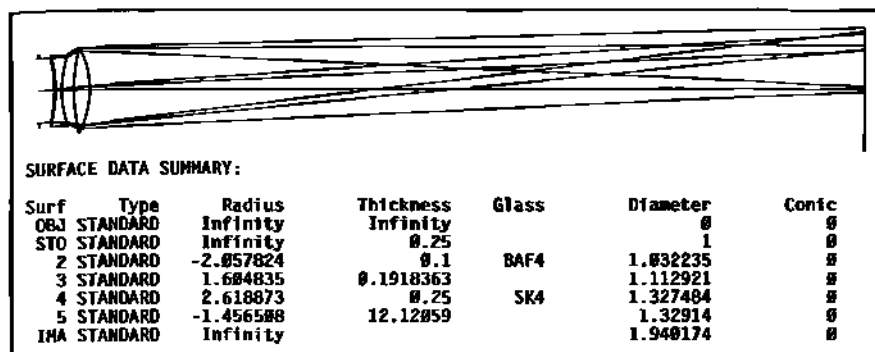


Fig. 28.7 Layout after third optimization run to reduce astigmatism.

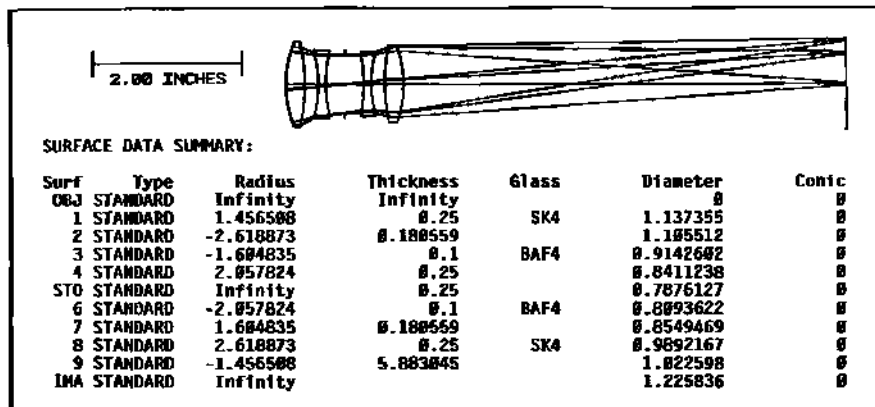


Fig. 28.8 CELO1o4b: symmetrized version of CELO1o3a.

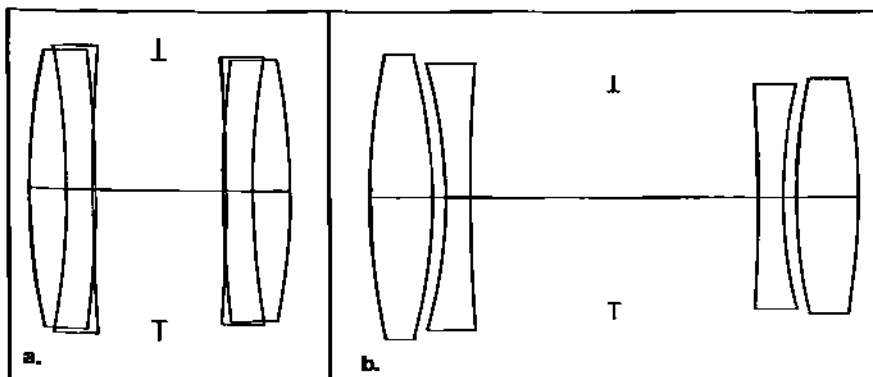


Fig. 28.9 Layout when: (a) negative radii are allowed to vary; (b) all radii and airspaces are allowed to vary.

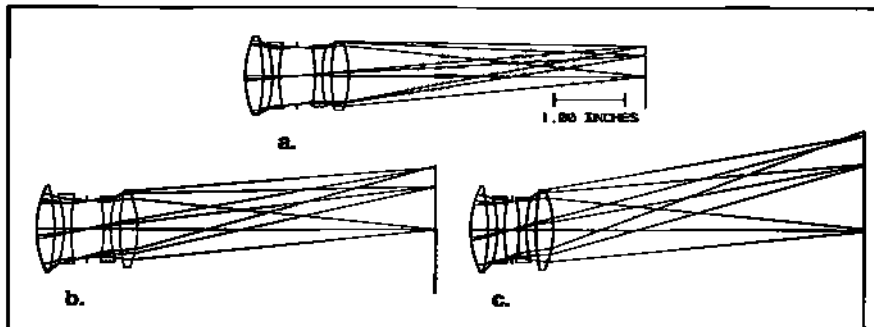


Fig. 28.10 Layouts for optimized results from CELO1o5a to CELO1o7a.

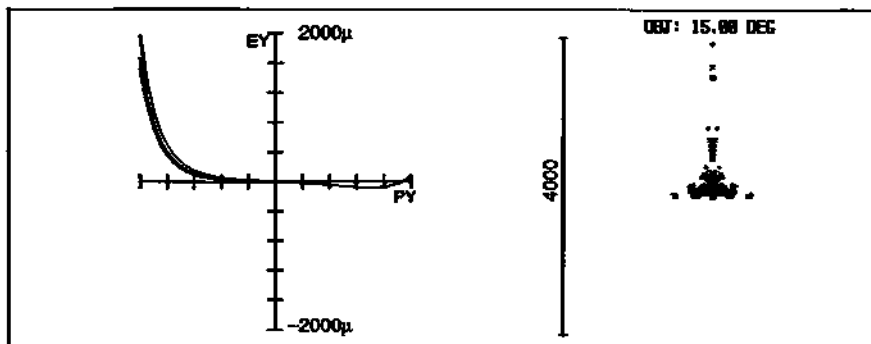


Fig. 28.11 Ray fan and spot diagram at 15° for CELO1o7a.

ray fan (which corresponds with a centered vertical slice through the spot diagram). Also, the two halves are too close together ($0.27''$) to allow room for the intended mechanisms.

At this point, we will go back to CELO1o7b and make the following changes: freeze the stop air-space on the front half of $0.2''$ and allowed all radii on the front half to vary as well as the inter-lens airspace. The layout for CELO1o8a is shown in Figure 28.12.

CELO1o8b → Optimize → CELO1o8a

CELO1o8a has good color correction, a fairly flat tangential field, and low distortion (under $\frac{1}{2}\%$). Ray fan plots are shown in Figure 28.13. Astigmatism's not too bad, but third-order coma is back and is particularly obvious at mid-field in the tangential plot. Higher-order spherical can also be seen on-axis.

Longitudinal spherical aberration is low as can be seen from its plot in Figure 28.14. Note that at zero pupil height d-light is located at the zero position on the abscissa while F- and C-light are displaced to the right. This separation between the colors is a direct measure of the secondary spectrum (Section 18.3). CELO1o8a

Section 28.6: Celor ZEMAX Design Procedure 325

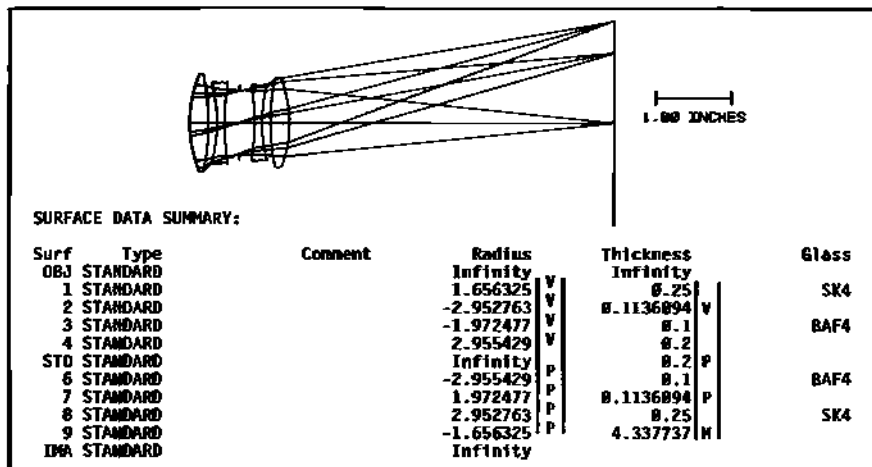


Fig. 28.12 Layout and prescription for CELO1o8a.

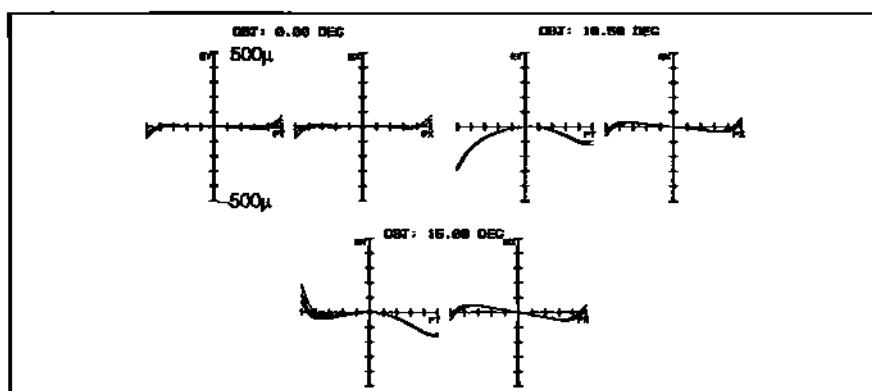


Fig. 28.13 Ray fan and spot diagram at 15° for CELO1o8a.

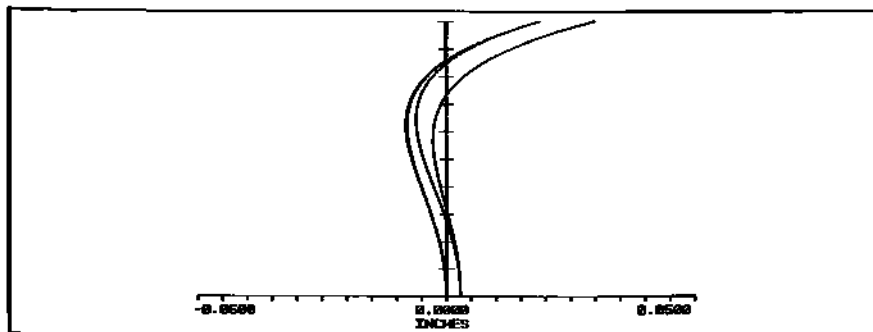


Fig. 28.14 Longitudinal aberration for CELO1o8a.

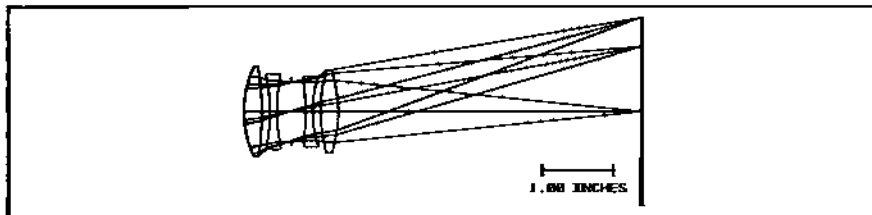


Fig. 28.15 Layout of CELO1o12a.

is pretty much the best one can do based on the strict symmetry conditions imposed. There may be marginal gains here and there, but nothing very dramatic. To improve things further requires symmetry-breaking. This will be done without any obvious departure from the general Celor form. Table 28.1 provides a summary of RMS spot sizes as a function of field (out to 15°) for both symmetric and unsymmetric cases starting with CELO1o7a.

The MFE is the same for each.

Table 28.1 RMS Spot Sizes for Various Celor Configurations						
Field	SYM		UNSYM			
	1o7a	1o8a	1o9a	1o10a	1o11a	1o12a
0	189	19	15	16	11	11
0.7	169	65	41	35	28	28
1	254	63	45	32	27	23

All unsymmetric cases start with variable changes made to 1o8a. For CELO1o9a, variables are placed on the front and rear positive lens radii and nothing else. For CELO1o10a, variables are placed on all front half radii and on the rear positive lens. The rear half negative lens is still slaved to the front. The front inter-lens spacing is also allowed to vary (and the rear half spacing is still slaved). CELO1o11a is the same as CELO1o10a except for the addition of a dummy image surface whose thickness is allowed to vary. For CELO1o12a, all radii are allowed to vary as well as the front inter-lens airspace and a dummy image surface. CELO1o12a is shown in Figure 28.15.

28.7 Historical Note: Emil von Hoegh

Emil von Hoegh (Figure 28.16), a Dane, was born in 1865. Not much is known about his education, but he eventually lived in Berlin where he worked for Barnburg Instruments. Later on he became the chief optical designer for the German company Goerz, a major manufacturer of photographic objectives. He got the job because of a six element symmetric anastigmat design he had developed on his own time. Details are sketchy, but the negotiations may have gone something like this: "Here's my anastigmat. Build a prototype. If it's any good, you can sell the

Section 28.8: Homework 327



Fig. 28.16 *Emil von Hoegh, designer of the Celor anastigmat.*

lens provided you hire me.” Goerz accepted the challenge. They built the prototype and found it had very good performance. Goerz hired von Hoegh. They also applied for and received the patent on von Hoegh’s design (and named the lens “Dagor”). Von Hoegh designed many lenses during his time at Goerz. Among these was the famous Celor which came on the market in 1899. He died in 1915.

28.8 Homework

Design a 10” EFL $f/6$ Celor photographic lens for $\bar{U} = 20^\circ$ field. Let $\phi_p = 0.003$. Design the lens for F , d , C spectrum. Use Schott BAF4 and SK4 glasses. Do the thin lens pre-design of the rear half first as was illustrated in this chapter. Obtain starting radii and insert into ZEMAX. Initial thicknesses are 0.2” and 0.55” for the negative and positive lenses respectively. Tweak as needed and then add the front half. We require at least a one-inch separation between front and rear halves for iris and shutter mechanisms. Strive to maintain good color and a reasonably flat tangential field. Meet or beat the target RMS spot sizes shown below for a *symmetric* system. Please use settings: square; centroid.

Field	SYM RMS	ASYM RMS
0	26 μm	25 μm
14°	155	97
20°	138	69

After you have a satisfactory symmetric design, let the lens go asymmetric and see what kind of spot sizes you can attain. Remember, the general Celor form must be maintained.

Suggested folder name: CELOR; file name: CELR1o1b, etc.

Chapter 29

Coddington's Equations

29.1 Introduction

In Chapter 27, we saw how to use the operator-induced defocus W_p to find the longitudinal locations and image sizes at the tangential and sagittal foci. Predictions were confirmed in ZEMAX using ray fan plots and spot diagrams. We did not utilize ZEMAX's field curvature plot (obtained via Analysis → Miscellaneous → Field Curv/Dist). The reason is that the field curvature plots in ZEMAX are not generated based on pupil aberration W and the wavefront slopes: $\partial W_y / \partial y$ and $\partial W_x / \partial x$. The tangential and sagittal foci locations are found via paraxial ray traces about a principal ray across both the X and Y pupil axes. This approach has its basis in what are known as Coddington's Equations, the subject of this chapter.

29.2 Coddington

In 1829, H. Coddington published a set of equations by which the location of the tangential and sagittal images along the principal ray could be determined. It is an extension of Gaussian or first order optics to off-axis imaging. This is illustrated in Figure 29.1. An object point sits vertically below the optical axis. A "narrow-beam" *tangential* ray fan "illuminates" a *short* vertical line segment (centered about optical axis) along the Y-axis of the entrance pupil. A similar *sagittal* fan

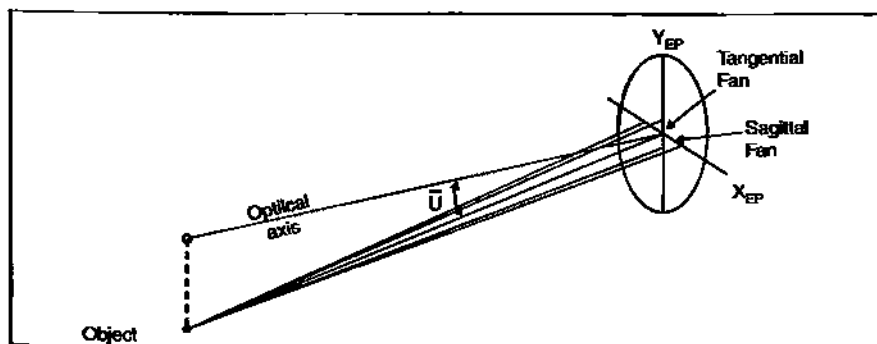


Fig. 29.1 Paraxial tangential and sagittal ray fans relative to entrance pupil.

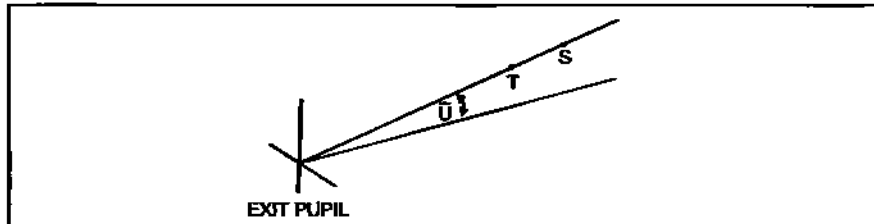


Fig. 29.2 Paraxial tangential and sagittal image points along the principal ray.

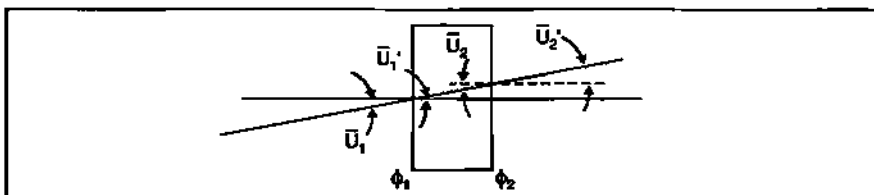


Fig. 29.3 Oblique power for thin lens.

illuminates a short line segment along the pupil's X-axis. Rays in both fans are considered to be paraxial in nature. If astigmatism is present, each fan will come to a different focus along the principal ray in image space as illustrated in Figure 29.2.

29.3 Oblique Power

Recall from Section 4.5 that the power for a single refracting surface is given by:

$$\phi = (n' - n)C_1 \quad (29.1)$$

In Coddington's equations, this concept is extended or modified to explicitly include the off-axis angle. It is termed the oblique power. For a single refracting surface:

$$\Phi_{OB} = (n' \cos \bar{U}' - n \cos \bar{U})C_1 \quad (29.2)$$

The reason these power differences occur between on-axis and off-axis object points is that the latter "see" different effective surface curvatures as the field angle increases.

The oblique power for a *thin* lens can be found with the aid of Figure 29.3. (Note: Although this is for a thin lens, some thickness has been added to the paraxial drawing for tracking purposes.)

$$\Phi_{OB} = \Phi_{OB1} + \Phi_{OB2} \quad (29.3)$$

Inserting the individual surface powers:

$$\phi_{OB} = (n \cos \bar{U}' - \cos \bar{U}_1)C_1 + (\cos \bar{U}'_2 - n \cos \bar{U}_2)C_2 \quad (29.4)$$

Multiplying out:

$$\phi_{OB} = nC_1 \cos \bar{U}' - C_1 \cos \bar{U}_1 + C_2 \cos \bar{U}'_2 - nC_2 \cos \bar{U}_2 \quad (29.5)$$

But $\bar{U}_1 = \bar{U}'_2$ (set both equal to \bar{U}), and $\bar{U}'_2 = \bar{U}_2$ (set both equal to \bar{U}'). Then Equation 29.5 becomes:

$$\phi_{OB} = nC_1 \cos \bar{U}' - C_1 \cos \bar{U} + C_2 \cos \bar{U} - nC_2 \cos \bar{U}' \quad (29.6)$$

Rearranging the terms:

$$\phi_{OB} = (n \cos \bar{U}' - \cos \bar{U})C_1 - (n \cos \bar{U}' - \cos \bar{U})C_2 \quad (29.7)$$

Pulling out the common factor:

$$\phi_{OB} = (n \cos \bar{U}' - \cos \bar{U})(C_1 - C_2) \quad (29.8)$$

29.4 Coddington's Equations

Recall that the Gaussian formula (Section 4.3) in air is given by:

$$\frac{-1}{l} + \frac{1}{l'} = \Phi \quad (29.9)$$

Substituting Equation 29.1 into Equation 29.9:

$$\frac{-1}{l} + \frac{1}{l'} = (n-1)(C_1 - C_2) \quad (29.10)$$

When compared to a ray trace through the system (which uses paraxial rays or rays very close to the optical axis), Equation 29.10 accurately predicts the axial image location (where the paraxial ray crosses the optical axis). Coddington's equations for a *thin lens* have a form similar to Equation 29.10.

Coddington's equations for thin lens are:

$$\text{Tangential: } \frac{-1}{l_t} + \frac{1}{l'_t} = \frac{(n' \cos \bar{U}' - n \cos \bar{U})(C_1 - C_2)}{\cos^2 \bar{U}} \quad (29.11)$$

$$\text{Sagittal: } \frac{-1}{l_s} + \frac{1}{l'_s} = (n' \cos \bar{U}' - n \cos \bar{U})(C_1 - C_2)$$

Coddington's equations can then be written in pseudo-Gaussian form as:

$$\frac{-1}{l_t} + \frac{1}{l'_t} = \Phi_t$$

(29.12)

$$\frac{-1}{l_s} + \frac{1}{l'_s} = \phi_s$$

where:

$$\left. \begin{aligned} \phi_t &= \frac{\Phi_{OB}}{\cos^2 U} \\ \phi_s &= \phi_{OB} \end{aligned} \right\} \quad (29.13)$$

29.5 Thin Lens Example

Let's calculate the tangential and sagittal image locations for our standard lens as illustrated in Figure 29.4.

The first thing we do is calculate the oblique power. From Section 13.3 we know that $\bar{n}' = 0.060006$ which gives us an angle $U' = 3.434^\circ$.

$$\phi_{OB} = (1.458 \cos 3.434^\circ - \cos 5^\circ)(0.044504 - 0)$$

$$\phi_{OB} = (0.459187)(0.044504)$$

$$\phi_{OB} = 0.020436 \text{ cm}^{-1} \quad (\text{or } f_{OB} = 48.934 \text{ cm}) \quad (29.14)$$

We'll let the object be at infinity:

$$\frac{1}{l'_t} = \phi_t = \frac{\Phi_{OB}}{\cos^2 5^\circ}$$

$$\frac{1}{l'_t} = \frac{0.020436 \text{ cm}^{-1}}{0.992404}$$

$$\frac{1}{l'_t} = 0.020592 \text{ cm}^{-1}$$

Therefore:

$$l'_t = 48.561 \text{ cm} \quad (29.15)$$

In a similar manner:

$$\frac{1}{l'_s} = 0.020436 \text{ cm}^{-1}$$

and:

$$l'_s = 48.934 \text{ cm} \quad (29.16)$$

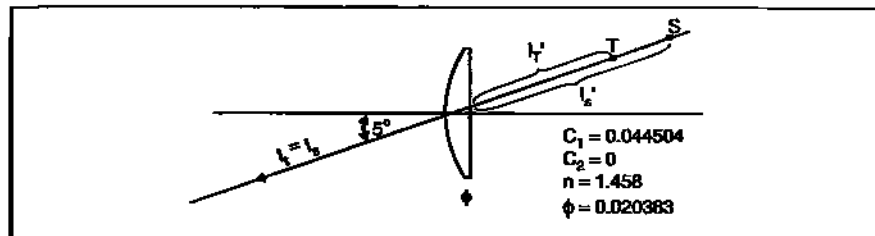


Fig. 29.4 Application of Coddington's equations to our standard lens.

Note that l'_T and l'_S are measured from the vertex of the thin lens out along the principal ray to the respective foci. (Recall that the δ_T and δ_S measurements were made from the paraxial plane.)

The separation between the two foci is given by:

$$\Delta l' = l'_S - l'_T = 0.372 \text{ cm} \quad (29.17)$$

29.6 Thin Lens Expression for $\Delta l'$

When the object is at infinity:

$$l'_T = \frac{\cos^2 \bar{U}}{\Phi_{OB}} \quad (29.18)$$

and:

$$l'_S = \frac{1}{\Phi_{OB}} \quad (29.19)$$

Subtracting the Equation 29.18 from Equation 29.19:

$$\Delta l' = \frac{1 - \cos^2 \bar{U}}{\Phi_{OB}} \quad (29.20)$$

Using a trigonometric relation:

$$\Delta l' = \frac{\sin^2 \bar{U}}{\Phi_{OB}} \quad (29.21)$$

or:

$$\Delta l' = f_{OB} \sin^2 \bar{U} \quad (29.22)$$

As an example we will apply this formula to the standard lens at 5° :

$$\Delta l' = (48.934)(0.007596) = 0.372 \text{ cm}$$

which is the same value shown by Equation 29.17.

29.7 Coddington's Equations and Mirrors

The oblique power for a mirror is given by:

$$\Phi_{OB} = (n' \cos \bar{U}' - n \cos \bar{U})C \quad (29.23)$$

This equation is simplified by noting that in air, $n = 1$ and $n' = -1$

$$\Phi_{OB} = -2C \cos \bar{U} \quad (29.24)$$

This can be written in terms of focal length:

$$\Phi_{OB} = \frac{\cos \bar{U}}{f} \quad (29.25)$$

For an object at infinity, Equations 29.18 and 29.19 become:

$$l'_t = \frac{\cos^2 \bar{U}}{\left(\frac{\cos \bar{U}}{f}\right)} = -f \cos \bar{U} \quad (29.26)$$

$$l'_s = -\frac{1}{\left(\frac{\cos \bar{U}}{f}\right)} = \frac{-f}{\cos \bar{U}} \quad (29.27)$$

Both l'_t and l'_s are measured from the mirror vertex and are *negative*, and both are aperture-independent. These distances are illustrated in Figure 29.5. Also note that l'_s always places the sagittal focus (with its associated tangential line image) in the paraxial focal plane.

Next, we find the difference between l'_t and l'_s :

$$\Delta l' = l'_s - l'_t = \left(\frac{-f}{\cos \bar{U}}\right) + f \cos \bar{U} \quad (29.28)$$

$$\Delta l' = f \left[\frac{-1}{\cos \bar{U}} + \cos \bar{U} \right]$$

$$\Delta l' = -f \left(\frac{1 - \cos^2 \bar{U}}{\cos \bar{U}} \right)$$

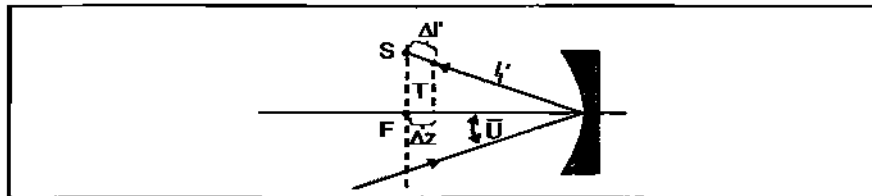


Fig. 29.5 Location of tangential and sagittal foci relative to mirror vertex.

$$\Delta l' = \frac{-f \sin^2 \bar{U}}{\cos \bar{U}}$$

$$\Delta l' = -\left(f \tan \bar{U}\right) \sin \bar{U} \quad (29.29)$$

29.8 Comparison of $\Delta l'$ and δ_{TS} for Mirrors

Recall Equation 27.29 (page 308).

$$\delta_{TS} = -\left(f \tan \bar{U}'\right) \sin \bar{U}' \quad (29.30)$$

This is the same form as Equation 29.9. Table 29.1 provides a comparison for a concave spherical mirror with EFL = 400 mm, and object at infinity.

Table 29.1 $\Delta l'$ and δ_{TS} for Mirror		
\bar{U}	$ \delta_{TS} $	$ \Delta l' $
2.5°	0.762 mm	0.762 mm
5°	3.050	3.050
10°	12.247	12.248
15°	27.740	27.740
20°	49.794	49.794

29.9 Field Curvature Plot in ZEMAX

Figure 29.6 shows the layout for our mirror example in 5° increments out to 20°. You can easily see the arc of the tangential foci. The corresponding field curvature plot for the mirror is shown in Figure 29.7.

The ZEMAX field curvature plot is based on *real* rays. In the tangential plane, a ± pair of real rays, hugging very close to the principal ray, are traced through the system to the point where they cross in image space. A similar pair of real rays is traced in the sagittal plane. What is plotted in Figure 29.7 is the distance (Δz) of the respective foci from the paraxial plane *along the optical axis* and *not* along the principal ray. Simply dividing Δz at each field point by the

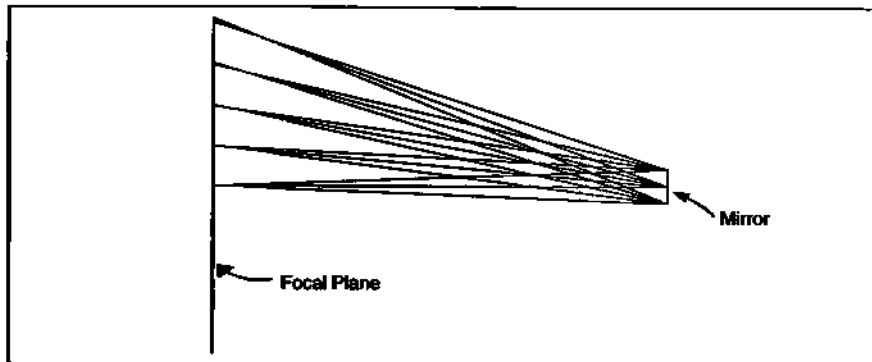


Fig. 29.6 Layout of sample mirror with multiple fields.

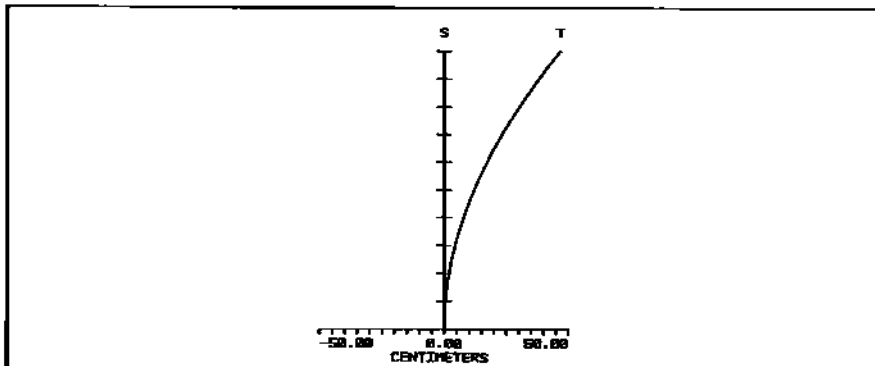


Fig. 29.7 Field curvature plot for mirror.

cosine of the field angle yields the separation along the principal ray. These results are shown in Table 29.2. Note that the divided values are very close to the magnitudes predicted by δ_{rs} or $\Delta l'$.

29.10 Toric Surfaces

Is there a way to design a mirror for off-axis use without having a separation between the tangential and sagittal foci, thus improving image quality and resolution? The answer is: "Yes!" If the mirror has a toric surface, $\Delta l'$ can be made zero.

A toric mirror is not rotationally symmetric. It has two different radii of curvatures along orthogonal directions as illustrated in Figure 29.8. We need to determine what those radii need to be in order to make $\Delta l' = 0$ for a specific operational field angle.

For example, go back and look at Equations 29.26 and 29.27 where $l_t = l_s = \infty$. What we also want is:

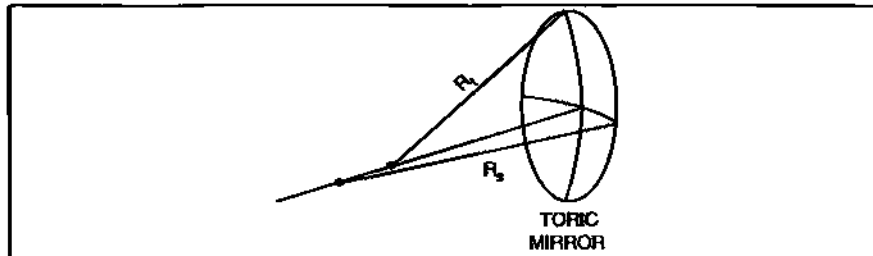


Fig. 29.8 Toric mirror.

Table 29.2
 $\Delta t'$ vs. Δz for Mirror

\bar{U}	Δz	$\frac{\Delta z}{\cos \bar{U}}$
0°	0 mm	0 mm
5°	3.037	3.049
10°	12.059	12.245
15°	26.791	27.736
20°	46.786	49.789

$$l'_t = l'_s \quad (29.31)$$

where:

$$\left. \begin{aligned} l'_t &= \frac{-\cos^2 \bar{U}}{\Phi_{OBt}} \\ l'_s &= \frac{-1}{\Phi_{OBs}} \end{aligned} \right\} \quad (29.32)$$

Note the subscripts on the oblique powers! Substituting Equation 29.32 into Equation 29.31:

$$\frac{\cos^2 \bar{U}}{\Phi_{OBt}} = \frac{1}{\Phi_{OBs}}$$

or: (29.33)

$$\Phi_{OBt} = \Phi_{OBs} \cos^2 \bar{U}$$

Now substitute in Equation 29.24 for the oblique powers:

$$-2C_t \cos \bar{U} = -2C_s \cos^3 \bar{U} \quad (29.34)$$

Solving for C_t :

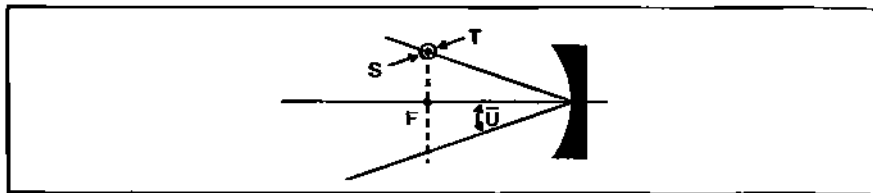


Fig. 29.9 Toric mirror used to correct astigmatism.

$$C_t = C_s \cos^2 \bar{U} \quad (29.35)$$

or in terms of radii:

$$R_t = \frac{R_s}{\cos^2 \bar{U}} \quad (29.36)$$

If the mirror is made so that the ratio of the sagittal to tangential radii is:

$$\frac{R_s}{R_t} = \cos^2 \bar{U} \quad (29.37)$$

then $\Delta I'$ will equal zero for the given operational field angle \bar{U} as illustrated in Figure 29.9.

One application of toric mirrors is in monochromators. In the design shown in Figure 29.10, the collimating and focusing mirrors (before and after the grating) are often toric surfaces to remove astigmatism.

29.11 Aberration Generator

In most design problems the goal is to beat down the aberrations as much as possible. However, there are occasions when it is necessary to design a system that deliberately introduces specific aberration(s) onto a wavefront. Such a system is known as an aberration generator. The wavefront it produces is sent into another optical system to test that system's response to the aberration. A perfect example of this was seen during the Hubble recovery program. Hubble aberration generators were built by several organizations (such as NASA and ESA), which simulated the huge spherical aberration (of proper magnitude and sign) that was inherent on the crippled telescope. The purpose of the aberration generator was to test how good the corrective fixes were before they were launched into orbit and incorporated into the Hubble. This was how the COSTAR optics were tested and approved. These aberration generators also simulated Hubble's off-axis aberrations such as astigmatism.

Let's pose the following problem: Design an aberration generator to produce mainly astigmatism with very little coma (say about a twentieth of the astigmatism). It must be done with one reflective component. Why would we want to do

Section 29.11: Aberration Generator 339

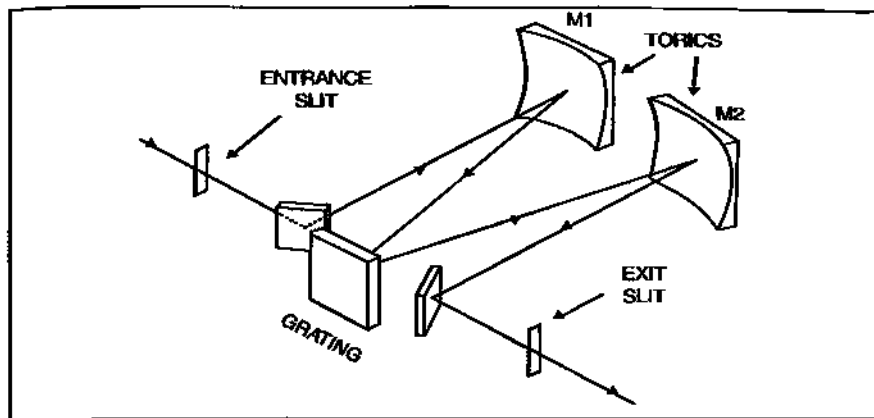


Fig. 29.10 Monochromator with toric mirrors. Reprinted with permission of Chromex, Inc.

this? One reason might be to calibrate a wavefront sensor.

To solve this design problem we'll use a concave spherical mirror. We need to figure out what f-number and field angle to use. For this we will make use of equations developed in Section 13.5:

$$W_{131} = \Gamma \left[\frac{\sigma_H}{4(f/\#)} \right] \quad (29.38)$$

$$W_{222} = \Gamma(\bar{u}\sigma_H)$$

where:

$$\Gamma = \frac{\bar{u}y}{4f/\#}$$

The first problem is solved by taking the ratio of coma to astigmatism:

$$\frac{W_{131}}{W_{222}} = \Upsilon$$

Substituting in Equation 29.38:

$$\left[\frac{1}{4\bar{u}f/\#} \right] \left| \frac{\sigma_H}{\sigma_{H\#}} \right| = \Upsilon \quad (29.39)$$

where we are interested more in *magnitude* than sign.

For a mirror with an object at infinity and stop at the mirror: $\sigma_H = -1$ and $\sigma_{H\#} = 1$ (Table 10.1).

Therefore:

$$\left| \frac{\sigma_H}{\sigma_{II}} \right| = 1 \quad (29.40)$$

Substituting into Equation 29.39:

$$\left[\frac{1}{4\bar{u}(f/\#)} \right] = \Upsilon$$

or:

$$\bar{u}(f/\#) = \frac{1}{4\Upsilon} \quad (29.41)$$

Let $\Upsilon = 0.05$:

$$\bar{u}(f/\#) = 5$$

For example, let f-number = 20, which means that $\bar{u} = 0.25$ ($\bar{U} = 14.036^\circ$), and $\Gamma = 0.003125y$. Inserting these values into Equation 29.38 yields:

$$\begin{aligned} |W_{131}| &= \frac{0.003125y}{80} = 0.000039y \\ |W_{222}| &= (0.003125)(0.25) = 0.000781y \end{aligned} \quad (29.42)$$

Note that the ratio $|W_{131}|/|W_{222}| = 0.05$, which is what we wanted, but the coefficient magnitude depends on the pupil radius y . Letting $y = 25$ mm: $|W_{131}| = 0.98 \mu\text{m}$; $|W_{222}| = 19.52 \mu\text{m}$. Since this is an f/20 mirror, the radius of curvature is 2 meters!

29.12 Homework

A concave spherical mirror (illustrated in Figure 29.11) has a point source located off-axis, but located in the plane of the mirror's center of curvature. Using Coddington's equations:

- a. Locate the tangential and sagittal image points.
- b. What is $\Delta l'$?
- c. What is $\Delta l'$ if you halve the aperture? If you double the aperture?

Note that the general Gaussian formula (Equation 4.3, page 35) for a mirror in air becomes:

$$-\frac{1}{l} + \frac{(-1)}{l'} = \phi$$

or

Section 29.12: Homework 341

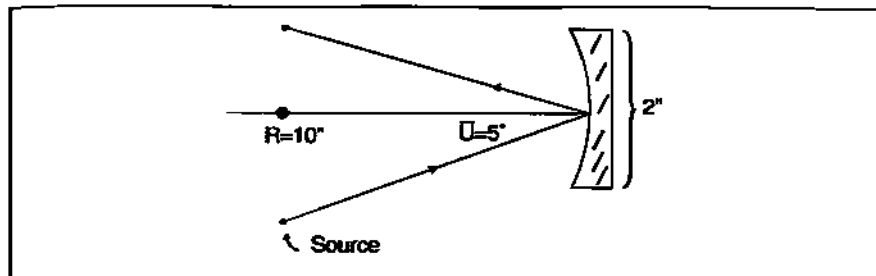


Fig. 29.11 Illustration for the Homework.

$$\frac{1}{l} + \frac{1}{l'} = -\frac{1}{f} \quad (29.43)$$

This is in keeping with the sign convention in Section 3.2.

Chapter 30

Triplet Lens and Image Compactness

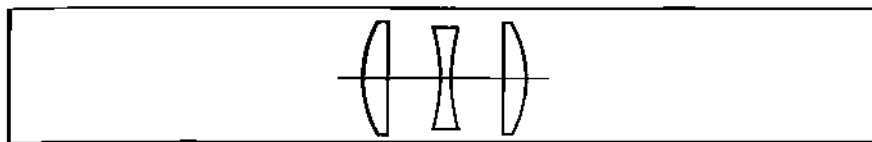


Fig. 30.1 Typical triplet.

30.1 Introduction

In Chapter 28, we learned how to go about designing von Hoegh's Celor lens. Although the Celor is historically important in its own right, there is an ulterior motive for its inclusion in this course—the Cooke Triplet. This is not a triplet in the apochromatic sense (as per Chapter 21). In the triplet to be discussed here all three elements are separated as shown in Figure 30.1. Also note that the central negative element is sandwiched between two positive elements having the same index.

The triplet design is often the high point (and end point) of many lens design courses. There are very good reasons for this. The triplet is the first lens to come our way which has enough inherent degrees of freedom to successfully combat all the Seidel aberrations while maintaining the proscribed EFL and achromatism. Our approach to the triplet design is nonstandard but effective. The methodology used to design the Celor will be applied to the design of the triplet.

In this chapter, we will initiate a series of discussions on the general topic of image quality. The first will be on image compactness which is related to RMS spot size. We will also revisit lateral color (Section 17.8).

30.2 Philosophy Behind Triplet Lens Design

Recall that the Petzval sum (Section 14.4) is given by:

$$W_{220P} = \left(\frac{L^2}{4}\right) \sum \left(\frac{\Phi}{n}\right)_i \quad (30.1)$$

and that the power for a two element system is given by:

$$\Phi = \Phi_1 + \Phi_2 - i\Phi_1\Phi_2 \quad (30.2)$$

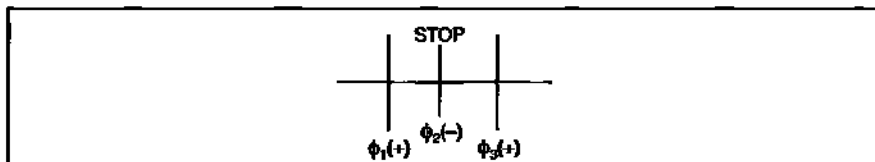


Fig. 30.2 Basic thin lens triplet.

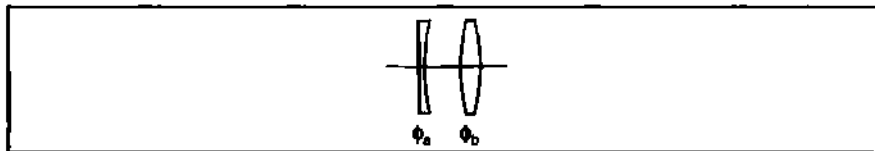


Fig. 30.3 Initial appearance of triplet rear half.

From Equation 30.1 we see that a system of two elements (with the same index) having equal but opposite powers will have a zero Petzval sum. From Equation 30.2 we see that the power of that system can be controlled by t , the separation between elements. Unfortunately, this system will be highly asymmetric. Coma, distortion, and lateral color will be the culprits. To make the system more symmetric, one can split the positive lens. A positive lens (with approximately half the power of the original) can be placed in front of the negative element. Another half-power positive lens can be placed equi-distant behind it (as illustrated by the thin lens design in Figure 30.2).

If the stop is at the negative element, we actually have three powers, three lens bendings, and two lens spacings to play with. This provides enough flexibility to do a decent design job.

30.3 Outline of Triplet Design

Once an EFL and f-number are selected for the triplet, its design begins with the rear half. What rear half you ask? There are only three lenses. True, but Figure 30.3 illustrates what we have in mind.

The first surface of the rear half negative element is flat and will remain flat. It is also the stop surface. All the power associated with the negative element will be carried by its second surface.

You calculate the powers and lens separation for ϕ_a and ϕ_b just as you did before with the Celor. You determine the radii with the help of Equation 4.22. The negative element will be plano-concave; the positive element, equi-convex. Insert these radii into ZEMAX along with appropriate lens thicknesses. Follow the Celor procedures for optimizing the rear half with the proviso that the first surface (which is flat) is *not* a variable.

Symmetrize the system by adding on the front half. Note: This means that



Fig. 30.4 H. Dennis Taylor, father of the Cooke Triplet.

the plano-side of the front negative element is in direct contact (no airspace) with the plano-side of the rear half negative element. The stop is sandwiched between them. Slave the rear half to the front half.

Continue optimizing this symmetric system over the full field as was done with the Celor.

After you have reached the point of diminishing returns with the symmetric system, unslave the rear half from the front half allowing the system to become asymmetric. Note: the stop is still buried inside the negative element. Although fabricating such an arrangement is entirely achievable using an opaque thin film coating, this stop would not be adjustable. Further, a shutter mechanism would be entirely out of the question. Most real triplets have the stop located outside of, but near the negative element.

30.4 Historical Note: H. Dennis Taylor

H. Dennis Taylor (Figure 30.4) was born in England in 1862. In his professional career, he eventually became the optics manager at Cooke and Sons located in York. Taylor designed his famous triplet lens in 1893, an accomplishment that should have made the company ecstatic. But no—their mainline business was building telescopes and they opted not to manufacture a photographic lens. Fortunately, the company allowed Taylor to find someone else to build his lens. That turned out to be Taylor and Hobson in Leicester.

Surprisingly, Taylor designed his triplet without tracing any rays whatsoever—a fact he was quite proud of. He worked strictly from algebraic formulations. He authored the book *A System of Applied Optics* in 1906. Incidentally, before

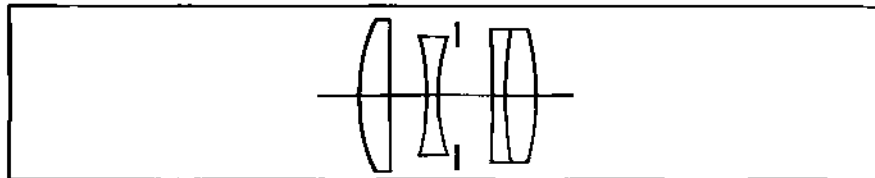


Fig. 30.5 Triplet variant, the Tessar lens.

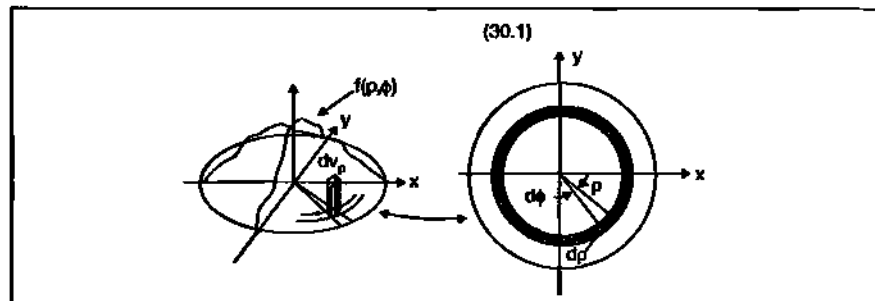


Fig. 30.6 Finding the average volume within unit circle.

there was such a thing as thin film coatings, Taylor was one of the first to recognize that tarnished lenses transmit more light than new lenses. This led to the development of anti-reflection coatings used in all modern day photographic lenses. Taylor died in 1943 at the age of 81.

30.5 An Important Triplet Variant

Perhaps the most important variant on the triplet is the Tessar lens illustrated in Figure 30.5. The positive rear element has been split and is now an achromatic doublet. (You can also think of the Tessar as a front-end dialyte coupled with a rear-end achromat.) Splitting the rear positive element provides an extra surface curvature and thus an additional degree of freedom. Given a Tessar and triplet (both having the same EFL, f-number, and field coverage), the former will show better performance.

30.6 Image Quality I

30.6.1 Average Volume Over Unit Circle

Suppose we have some function $f(p, \phi)$ defined over a unit circle as illustrated in Figure 30.6.

The parallelepiped indicated in the figure is a sub-volume and is described by:

$$dV_p = f(p, \phi)p dp d\phi \quad (30.3)$$

The volume enclosed within the annulus is given by:

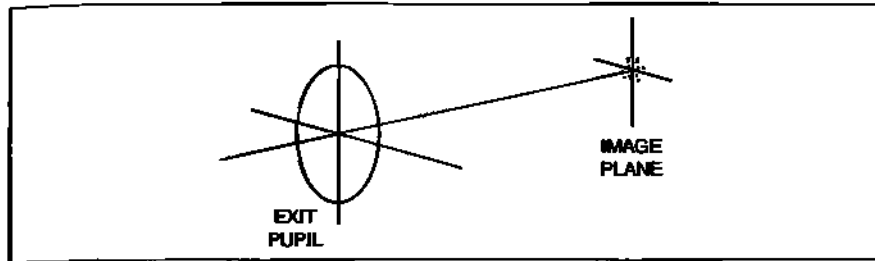


Fig. 30.7 Aberrated exit pupil and associated spot diagram.

$$dV_a = \int_0^{2\pi} f(\rho, \phi) \rho \, d\rho \, d\phi \quad (30.4)$$

Finally, the total volume within the unit circle is given by:

$$V = \int_0^{2\pi} \int_0^1 f(\rho, \phi) \rho \, d\rho \, d\phi \quad (30.5)$$

What we want, however, is the average value of V over the unit circle. Consequently, we must divide Equation 30.5 by the area of the unit circle, which is π .

$$V = \left(\frac{1}{\pi}\right) \int_0^{2\pi} \int_0^1 f(\rho, \phi) \rho \, d\rho \, d\phi \quad (30.6)$$

30.6.2 Image Compactness

Figure 30.7 shows the exit pupil of an optical system and its paraxial image plane. The system is aberrated as indicated by the spot diagram in the image plane. Each pierce point represents a certain transverse ray aberration error (Section 11.8) described by:

$$T = -\left(\frac{R}{r}\right) \frac{\partial W}{\partial \rho} \quad (30.7)$$

Image compactness is defined by:

$$C = \left(\frac{1}{\pi}\right) \int_0^{2\pi} \int_0^1 T^2 \rho \, d\rho \, d\phi \quad (30.8)$$

The similarities between Equations 30.8 and 30.6 should be obvious. C is the average volume of T^2 over the normalized exit pupil. The value of C increases as aberration increases. When aberrations are small, the image is more compact and C is small. Inserting Equation 30.7 into Equation 30.8:

$$C = \left(\frac{1}{\pi}\right)\left(\frac{R}{r}\right)^2 \int_0^1 \int_0^{2\pi} \left(\frac{\partial W}{\partial p}\right)^2 p \, dp \, d\phi \quad (30.9)$$

If W is rotationally symmetric:

$$C = 2\left(\frac{R}{r}\right)^2 \int_0^1 \left(\frac{\partial W}{\partial p}\right)^2 p \, dp \quad (30.10)$$

We now define a parameter which we'll call *compactness* and is given by:

$$\sigma_c = \sqrt{C} \quad (30.11)$$

30.6.3 Calculation Example

In this example we will determine the image compactness of a rotationally symmetric set of aberrations, namely defocus and spherical aberration.

$$W = W_d p^2 + W_{040} p^4 \quad (30.12)$$

Then:

$$\frac{\partial W}{\partial p} = 2W_d p + 4W_{040} p^3 \quad (30.13)$$

Taking the square:

$$\left(\frac{\partial W}{\partial p}\right)^2 = 16W_{040}^2 p^6 + 4W_d^2 p^2 + 16W_d W_{040} p^4 \quad (30.14)$$

Now insert Equation 30.14 into Equation 30.10:

$$C = 2\left(\frac{R}{r}\right)^2 \int_0^1 [16W_{040}^2 p^6 + 4W_d^2 p^2 + 16W_d W_{040} p^4] p \, dp \quad (30.15)$$

After the integrations:

$$C = 2\left(\frac{R}{r}\right)^2 \left[2W_{040}^2 + W_d^2 + \frac{8}{3}W_d W_{040} \right] \quad (30.16)$$

Next, we complete the square:

$$C = \left(\frac{R}{r}\right)^2 \left[2\left(W_d + \frac{4}{3}W_{040}\right)^2 + \frac{4}{9}W_{040}^2 \right] \quad (30.17)$$

Note that C is a minimum when:

Merit Function Value: 1.63847872E-002											
Num	Type	Intcl	Int2	Hx	Hy	Px	Py	Target	Weight	Value	% Cont.
1	TRAC	1		0.0000	0.0000	0.1679	0.2987	0.0000E+000	0.14544	1.63847872E-002	6.739
2	TRAC	1		0.0000	0.0000	0.3536	0.6124	0.0000E+000	0.14544	1.63847872E-002	3.738
3	TRAC	1		0.0000	0.0000	0.4710	0.8156	0.0000E+000	0.14544	2.84193E-002	6.739
4	TRAC	1		0.0000	0.0000	0.3357	0.6124	0.0000E+000	0.14544	1.92418E-002	6.739
5	TRAC	1		0.0000	0.0000	0.7071	0.9989	0.0000E+000	0.14544	1.16391E-002	3.738
6	TRAC	1		0.0000	0.0000	0.3428	0.6000	0.0000E+000	0.14544	2.84193E-002	7.198
7	TRAC	1		0.0000	0.0000	0.1679	0.2987	0.0000E+000	0.14544	1.82418E-002	6.739
8	TRAC	1		0.0000	0.0000	0.3536	0.6124	0.0000E+000	0.14544	1.63847872E-002	3.738
9	TRAC	1		0.0000	0.0000	0.4710	0.8156	0.0000E+000	0.14544	2.84193E-002	7.198
10	TRAC	1		0.0000	0.0000	0.1679	0.2987	0.0000E+000	0.14544	1.82418E-002	6.739
11	TRAC	1		0.0000	0.0000	0.3536	0.6124	0.0000E+000	0.14544	1.16391E-002	3.738
12	TRAC	1		0.0000	0.0000	0.4710	0.8156	0.0000E+000	0.14544	1.82418E-002	7.198
13	TRAC	1		0.0000	0.0000	0.3357	0.6124	0.0000E+000	0.14544	1.92418E-002	6.739
14	TRAC	1		0.0000	0.0000	0.7071	0.9989	0.0000E+000	0.14544	1.16391E-002	3.738
15	TRAC	1		0.0000	0.0000	0.9429	0.6000	0.0000E+000	0.14544	2.84193E-002	7.198
16	TRAC	1		0.0000	0.0000	0.1679	0.2987	0.0000E+000	0.14544	1.82418E-002	6.739
17	TRAC	1		0.0000	0.0000	0.3536	0.6124	0.0000E+000	0.14544	1.63847872E-002	3.738
18	TRAC	1		0.0000	0.0000	0.4710	0.8156	0.0000E+000	0.14544	2.84193E-002	7.198

SURFACE DATA SUMMARY:											
Surf	Type	Comment	Radius	Thickness	Glass	Diameter	Conic	Obj STANDARD	Std STANDARD	2 STANDARD	IMA STANDARD
	OBJ STANDARD		Infinity	Infinity							
	STD STANDARD		-600	-600							
	2 STANDARD		Infinity	0.0000	MIRROR	1.00					
	IMA STANDARD		Infinity	0.52260241	V						

Listing 30.1 Merit function and prescription for mirror compactness example.

$$W_d = -\frac{4}{3} W_{040} \quad (30.18)$$

so:

$$C = \left(\frac{R}{r}\right)^2 \left(\frac{4}{9} W_{040}^2\right) \quad (30.19)$$

and:

$$\sigma_C = \frac{R}{r} \left(\frac{2}{3} W_{040}\right). \quad (30.20)$$

30.6.4 Numerical Example

Suppose we have a 400-mm f/4 spherical mirror. Let the object be an on-axis point source at infinity. Using the spherical aberration formula for a thin lens/mirror from Table 10.1, we find that $W_{040} = 3.05 \mu\text{m}$. Inserting this value into Equation 30.20:

$$\sigma_C = \frac{400}{50} \left[\left(\frac{2}{3}\right)(3.05) \right] = 16.27 \mu\text{m}$$

30.6.5 ZEMAX Example

We now insert the mirror example from the previous section into ZEMAX. We'll set $\lambda = 0.55 \mu\text{m}$. In the MFE we'll use the TRAC default by itself. In the LDE the only variable will be on the image distance. Listing 30.1 shows the MFE and the LDE after the optimization has been run.

Note the value of the Merit Function. It is $16.38 \mu\text{m}$. This is essentially the compactness value calculated in Section 30.6.4. In Sections 8.5 and 8.6 we saw that when TRAC is used by itself for a given field point, the MFE value is equiv-

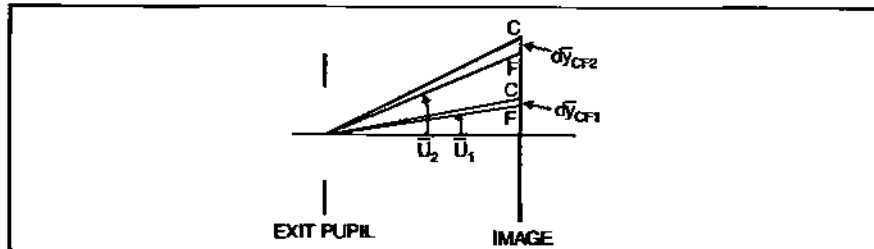


Fig. 30.8 Lateral color displacements for two different field angles.

alent to the RMS spot size. This also means that compactness, σ_C , is equivalent to the RMS spot size.

30.7 Axial Location of σ_C

From Sections 11.4 and 11.5 we found a handy relation between defocus as applied to *axial* image locations and the corresponding wavefront OPD in the exit pupil. For a mirror, this is given by:

$$\delta = -8(f/\#)^2 W_d \quad (30.21)$$

The value of δ at the plane of minimum compactness in our example is obtained by substituting Equation 30.18 into Equation 30.21:

$$\delta = -8(f/\#)^2 \left(\frac{4}{3} W_{040} \right) \quad (30.22)$$

Substituting in the numerical values for the mirror:

$$\delta = -8(4)^2 \left[-\left(\frac{4}{3} \right)(3.05) \right] = 520.5 \mu\text{m} = 0.520 \text{ mm}$$

Now compare this value of δ to the boxed-in thickness value in the prescription shown in Listing 30.1. It is essentially the same value.

30.8 Lateral Color Revisited

Lateral color was introduced in Section 17.8. There we saw how the vertical displacement (d_y_{CF}) between F and C (blue and red) light in the image plane was connected to two spherical wavefronts in the exit pupil. One wavefront was in F-light; the other, C-light. The two wavefronts were tilted with respect to each other. The displacement in the image plane is measured between the F-chief ray pierce to the C-chief ray pierce. Figure 30.8 illustrates displacements for two different field angles.

If we return to Section 17.8 and insert Equation 17.1 into Equation 17.2, we

Section 30.8: Lateral Color Revisited 351

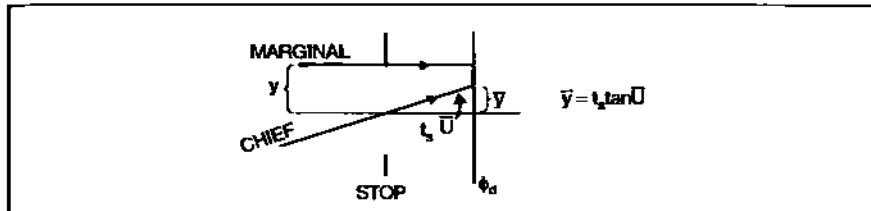


Fig. 30.9 Relation between chief ray height on lens and field angle.

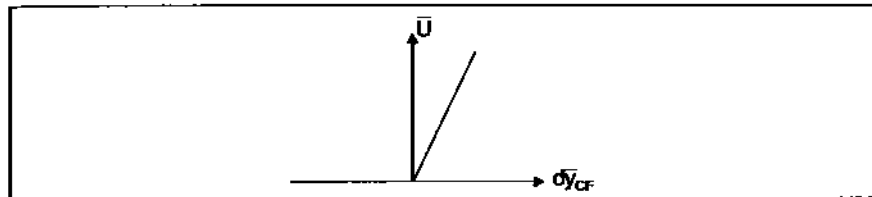


Fig. 30.10 Lateral color plot.

get:

$$dy_{CF} = 2(f/\#) \left(\frac{\Phi_d}{V_d} \right) y \bar{y} = \frac{\bar{y}}{V_d} \quad (30.23)$$

Note that this equation is *linear* in \bar{y} , which in turn is directly related to the field angle as shown in Figure 30.9. The chief ray height, \bar{y} , is related to the field angle \bar{U} via:

$$\bar{y} = t_s \tan \bar{U} \quad (30.24)$$

A graph of lateral color plots the $d\bar{y}_{CF}$ displacements as a function of field angle (usually normalized) as shown in Figure 30.10. The plot is linear. If the displacement is positive (C pierce above F pierce), then the plot lies on the right-hand side of the ordinate.

Let's do an example. We'll calculate the lateral color for a 10" f/10 thin lens made of BK7 glass ($V_d = 64.17$). The 1" diameter stop is located 1" in front of the lens. The field angle is 20°. Substituting values into Equation 30.23 (which is a paraxial thin lens type equation):

$$d\bar{y}_{CF} = \frac{\bar{y}}{V_d} = \frac{0.364}{64.17} = 0.00567'' \quad (30.25)$$

Now let's insert this lens into ZEMAX. Correct radii can be found by first assigning arbitrary radii (equal but opposite), placing variables on both radii, setting EFL = 10" in the MPE with weight 1, and then running the optimization. Let the lens thickness be zero. Insert the stop 1" in front of the lens, set the field

352 Chapter 30 Triplet Lens and Image Compactness

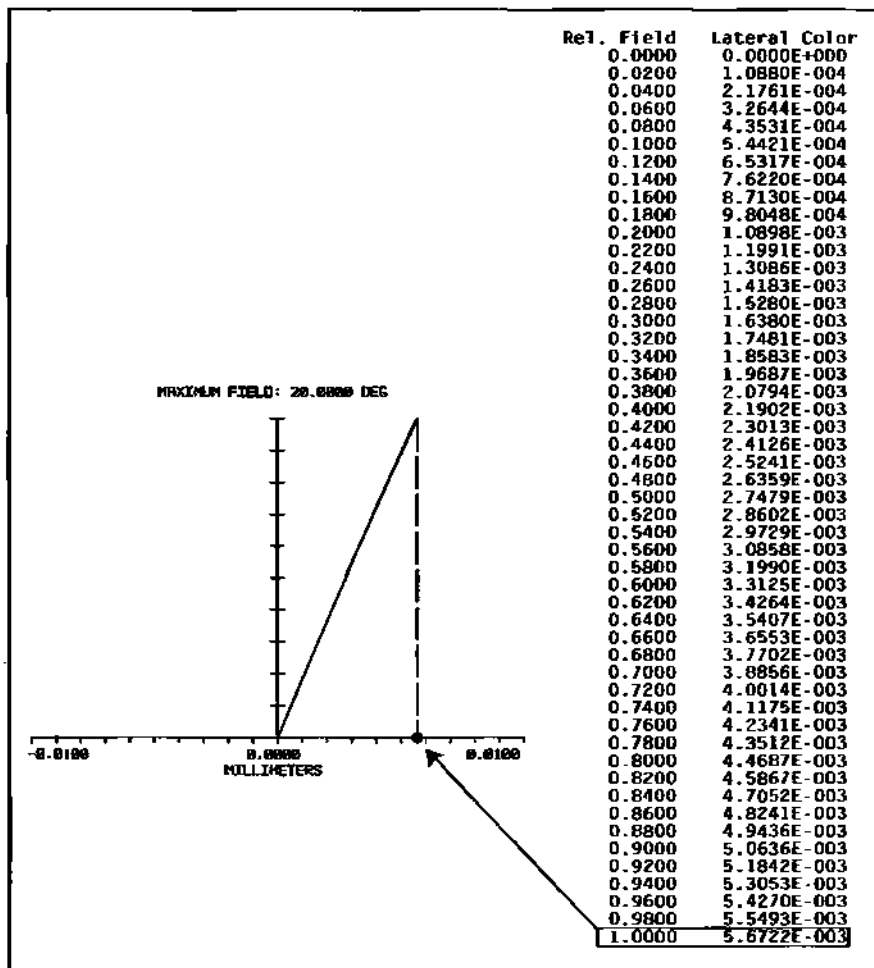


Fig. 30.11 Lateral color plot and listing for thin lens example.

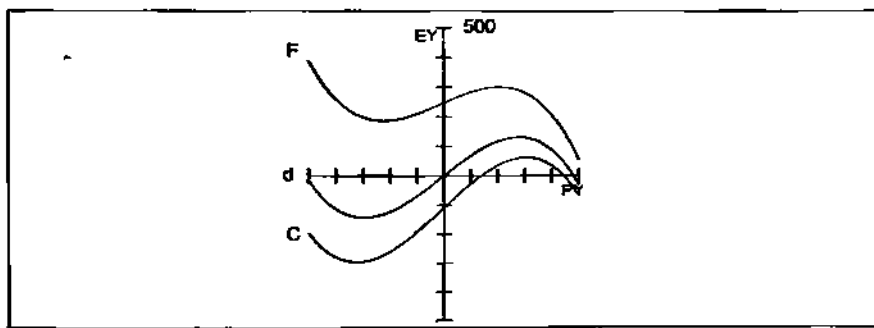


Fig. 30.12 Lateral color effects in ray fan plot.

Section 30.9: Homework 353

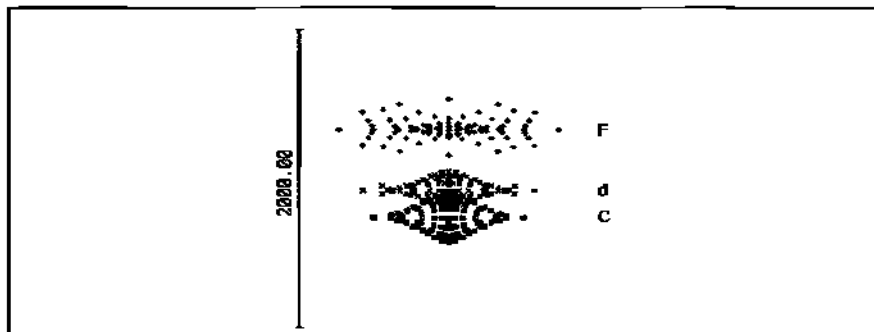


Fig. 30.13 Lateral color effect on spot diagrams.

to 20° . Once this is done we can call up the color plot (Figure 30.11) by going to Analysis → Miscellaneous → Lateral Color. Also included in the figure is the listing (Lateral Color → Text).

From the ZEMAX plot and listing, note that the value of $\overline{dy_{CF}}$ at 20° is 0.0056727". This is the same value calculated manually via Equation 30.25. Note: As real thickness is added to the lens, the value of LACL will depart somewhat from the thin lens value.

Lateral color makes its presence known in ray fan plots by vertically displaced curves as shown in Figure 30.12. In spot diagrams, the spot ensembles for different colors are also displaced vertically as shown in Figure 30.13. (Note: The last two figures are not based on the previous example.)

30.9 Homework

1. Calculate the form for image compactness for coma.
2. Design a 10" EFL f/5 triplet for a $\pm 20^\circ$ field. Design the lens for the F , d , C spectrum. Use Schott F4 and SK16 for the negative and positive components respectively. Strive to maintain good color and a reasonably flat field. Do the thin lens rear half pre-design (as per the Celor) but make it a 10" EFL f/10. $\phi_{rz} = -0.03$. Insert starting radii into ZEMAX. Use initial glass thicknesses of 0.1 and 0.3 inches respectively. When the rear half is sufficiently optimized, assemble the symmetric system. (For this exercise, keep the stop buried in the middle of the negative element.) Note that the system EFL is close to 5". Optimize the system for 5". When the symmetric system is fully optimized rescale the lens to a 10 focal length using Tools → Make Focal. After rescaling, meet or exceed the target RMS spot sizes for the symmetric and asymmetric cases as shown

354 Chapter 30 Triplet Lens and Image Compactness

below (use settings: square; centroid). For the triplet, it is the asymmetric case which is of main importance here. Suggest using folder name: triplet

Field	SYM	ASYM
	RMS	RMS
0°	108µm	35
14°	147	71
20°	225	68

and file name: TRIP101b, etc.

Note: For the symmetric case you may notice something strange on the ray fan plot. As you know, Seidel spherical is constant over the field. But here it seems that spherical at 20° is much larger than at 0°. What you are seeing is the effect of oblique spherical aberration (refer to Table 15.1).

Chapter 31

Strehl Ratio

31.1 Introduction

If you will recall from Chapter 9, as we improved the performance of the transmission sphere by reducing the amount of spherical aberration, the spot diagram became more and more compact. In fact, if the transmission sphere were completely unaberrated, geometric optics predicts a point image. But long before this happens, diffraction begins taking its toll. This was seen in Figure 9.4. As aberration decreased, the diffractive Airy core (defined by the circle) increased in *relative* size to the spot diagram. Image compactness (discussed in Chapter 30) is no longer a reliable predictor of image quality for small aberrations. As a metric it is much too coarse. Something finer is needed in a realm where diffraction effects can no longer be ignored. In this chapter, we will look at Strehl ratio and wavefront variance as new image quality evaluators.

31.2 Image Quality II

31.2.1 Strehl Ratio

If we have a perfect imaging system, the image of a point object is a spread out blob whose structure is due to the diffractive interaction of light with the stop. The shape and size of the blob are directly related to the shape of the stop (or exit pupil), system f-number, and wavelength.

If we have an unobscured circular stop, the resulting image blob is shown in Figure 31.1. It is called the Airy pattern. The diameter of its core or Airy disk is given by:

$$D_A = 2.44\lambda(f/\#) \quad (31.1)$$

When a small amount of rotationally symmetric aberration is present, power is removed from the core and redistributed into the surrounding rings. A larger percentage of the power goes into the first ring. Figure 31.2 compares profiles across perfect and imperfect diffraction patterns. You can see that the central peak of the aberrated pattern is lower than the unaberrated pattern. However, when we look at peak power in the first rings, the reverse is true.

The Strehl ratio is defined as the ratio of the *central* intensity in the aberrated

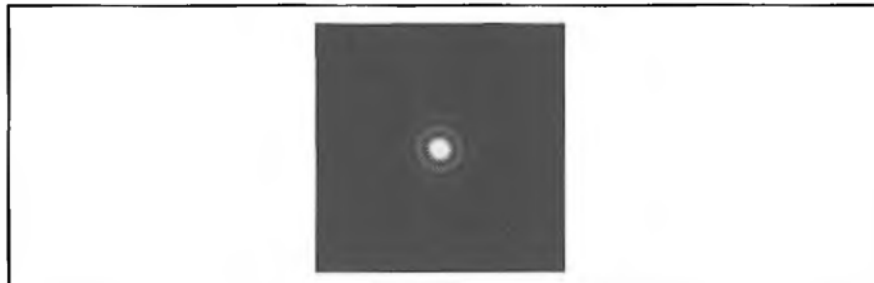


Fig. 31.1 Airy pattern for circular aperture. Reprinted with permission from Star Testing Astronomical Telescopes by H.R. Suiter (Willmann-Bell, Inc, 1994).

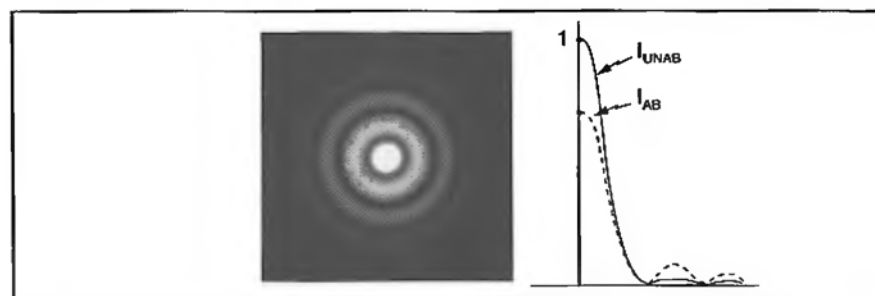


Fig. 31.2 Profiles across diffraction patterns having small, or no aberration. Aberrated image also shown. Compare to Figure 31.1. Diffraction pattern reprinted with permission from Star Testing Astronomical Telescopes by H.R. Suiter (Willmann-Bell, Inc, 1994).

pattern to the *central* intensity in the unaberrated pattern:

$$S = \frac{I_{ab}}{I_{unab}} \quad (31.2)$$

The Strehl ratio will have values ranging from 1 (for a perfect system) to 0 (for a system having significant aberration). Equation 31.2 provides a good qualitative understanding of what Strehl is; however, it is not very useful for actually calculating values. Equation 31.3 is more helpful in this regard, assuming uniform pupil irradiance:

$$S = \exp[-(k\sigma)^2] \quad (31.3)$$

where $k = 2\pi/\lambda$, and σ^2 is the wavefront variance.

The square root of the wavefront variance is σ , the standard deviation or RMS wavefront.

Equation 31.3 can also be rewritten as an expansion. Recall that:

Table 31.1 Comparison of S_a and S as function of σ		
σ	S	S_a
0.01 λ	0.990	0.990
0.02 λ	0.961	0.961
0.03 λ	0.915	0.911
0.04 λ	0.854	0.842
0.05 λ	0.782	0.753
0.06 λ	0.701	0.645
0.08 λ	0.532	0.369
0.10 λ	0.373	0.014
0.12 λ	0.242	-0.42

$$e^x = 1 + x + \frac{x^2}{2!} + \frac{x^3}{3!} + \text{etc} \quad (31.4)$$

Applying this to Equation 31.3:

$$S = 1 - (k\sigma)^2 + \frac{1}{2}(k\sigma)^4 - \frac{(k\sigma)^6}{6} + \text{etc.} \quad (31.5)$$

If aberrations are really small, Equation 31.3 can be approximated by:

$$S_a \approx 1 - (k\sigma)^2 \quad (31.6)$$

Since Equation 31.6 is commonly seen, Table 31.1 provides a comparison between S_a and S for various values of σ . This will help define the range over which S_a has validity. We'll let the wavelength be $\lambda = 0.6328$. Therefore, $k = 9.93$. As you can see from the table, you probably would not want to trust S_a past $\sigma = 0.05 \lambda$. Also note from Equation 31.2 that the true Strehl ratio can never go negative.

31.2.2 Wavefront Variance

The key component of the Strehl formula is the wavefront variance defined by:

$$\sigma^2 = \text{Var}\{W\} = \langle W^2 \rangle - \langle W \rangle^2 \quad (31.7)$$

where W is the pupil aberration function that we have been using throughout the course.

In a manner similar to the formal definition of image compactness (Equation 30.8), the formal expressions for the two constituent parts of wavefront variance are given by:

$$\langle W \rangle^2 = \left[\left(\frac{1}{\pi} \right) \int_0^{2\pi} \int_0^1 W \rho d\rho d\phi \right]^2 \quad (31.8)$$

and:

$$\langle W^2 \rangle = \left(\frac{1}{\pi} \right) \int_0^{2\pi} \int_0^1 W^2 \rho d\rho d\phi \quad (31.9)$$

31.2.3 Calculation Example

As we did with image compactness, we will now generate an expression for σ^2 for a wavefront consisting of a mixture of defocus and spherical aberration.

$$W = W_d \rho^2 + W_{040} \rho^4 \quad (31.10)$$

The expression for $\langle W \rangle$ is given by:

$$\langle W \rangle = \left(\frac{1}{\pi} \right) \int_0^{2\pi} d\phi \int_0^1 (W_d \rho^2 + W_{040} \rho^4) \rho d\rho \quad (31.11)$$

The angle integral can be brought outside to the left of the radial integral because W is rotationally symmetric.

$$\langle W \rangle = 2 \left[W_d \int_0^1 \rho^3 d\rho + W_{040} \int_0^1 \rho^5 d\rho \right] \quad (31.12)$$

$$\langle W \rangle = \frac{1}{2} W_d + \frac{1}{3} W_{040} \quad (31.13)$$

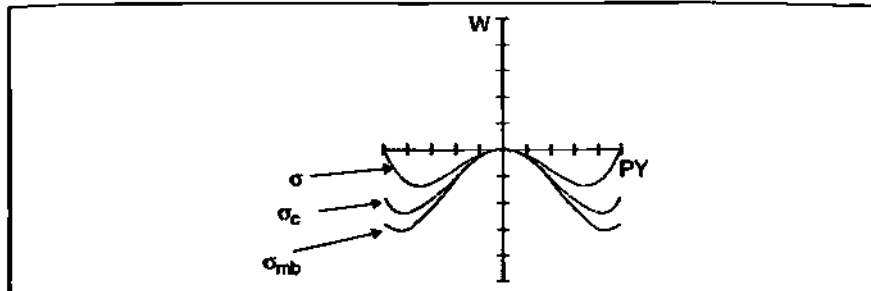
Taking the square:

$$\langle W \rangle^2 = \frac{1}{4} W_d^2 + \frac{1}{3} W_d W_{040} + \frac{1}{9} W_{040}^2 \quad (31.14)$$

The expression for $\langle W^2 \rangle$ is given by:

$$\langle W^2 \rangle = \left(\frac{1}{\pi} \right) \int_0^{2\pi} d\phi \int_0^1 (W_d \rho^2 + W_{040} \rho^4)^2 \rho d\rho \quad (31.15)$$

$$\langle W^2 \rangle = 2 \int_0^1 (W_d^2 \rho^4 + 2 W_d W_{040} \rho^6 + W_{040}^2 \rho^8) \rho d\rho \quad (31.16)$$

Fig. 31.3 Shape of $W(p)$ for the various image quality criteria.

$$\langle W^2 \rangle = 2 \left[W_d^2 \int_0^1 p^5 dp + 2 W_d W_{040} \int_0^1 p^7 dp + W_{040}^2 \int_0^1 p^9 dp \right] \quad (31.17)$$

Evaluating the integrals:

$$\langle W^2 \rangle = \frac{1}{3} W_d^2 + \frac{1}{2} W_d W_{040} + \frac{1}{5} W_{040}^2 \quad (31.18)$$

Inserting Equations 31.14 and 31.18 into Equation 31.7 we obtain:

$$\sigma^2 = \left(\frac{1}{3} W_d^2 + \frac{1}{2} W_d W_{040} + \frac{1}{5} W_{040}^2 \right) - \left(\frac{1}{4} W_d^2 + \frac{1}{3} W_d W_{040} + \frac{1}{9} W_{040}^2 \right) \quad (31.19)$$

$$\sigma^2 = \frac{1}{12} W_d^2 + \frac{1}{6} W_d W_{040} + \frac{4}{45} W_{040}^2. \quad (31.20)$$

Completing the square:

$$\sigma^2 = \frac{1}{12} (W_d + W_{040})^2 + \frac{1}{180} W_{040}^2. \quad (31.21)$$

The wavefront variance $\text{Var}(W)$ or σ^2 is a *minimum* when $W_d = -W_{040}$. Therefore:

$$\sigma^2 = \frac{1}{180} W_{040}^2 \quad (31.22)$$

and:

$$\sigma = 0.0745 W_{040}$$

Table 31.2 lists the various best image criteria obtained thus far for a combination of spherical aberration and defocus. Figure 31.3 shows the shape of $W(p)$ for these different criteria.

Table 31.2 Image quality criteria for $(W_d p^2 + W_{040} p^4)$		
Refer to Section	Criteria	Wavefront Relation
11.6 and 11.7	Minimum Blur	$W_d = -\frac{3}{2}W_{040}$
30.6.3	Image Compactness	$W_d = -\frac{4}{3}W_{040}$
31.2.3	Wavefront Variance	$W_d = -W_{040}$

31.2.4 Numerical Example

Let's calculate the wavefront variance at "best Strehl focus" for the same spherical mirror used in the image compactness example (Section 30.6.4). Recall that that was a 400 mm EFL mirror operating at $f/4$.

With an axial point object at infinity, $W_{040} = 3.05$ microns. Inserting this value into Equation 31.22:

$$\sigma^2 = \left(\frac{1}{180}\right)(3.05)^2 = 0.05168 \mu\text{m}^2$$

Therefore:

$$\sigma = 0.2275 \mu\text{m}$$

The value of σ in *waves* at $\lambda = 0.55 \mu\text{m}$ is:

$$\sigma_\lambda = 0.41364\lambda$$

Using Equation 31.3 we can compute the Strehl ratio at $\lambda = 0.55 \mu\text{m}$:

$$S = \exp\left\{-\left(\frac{2\pi}{0.55}\right)^2(0.05168)\right\} = \exp\{-6.745\} = 0.0012$$

This is an extremely poor Strehl. Image quality will be very bad.

31.2.5 Axial Location of σ

Making use of Equation 30.21 once again, we can locate where along the optical axis (relative to paraxial focus) the best Strehl image lies. We'll set $W_d = -W_{040}$.

$$\delta_s = -8(f/\#)^2(-W_{040}) \quad (31.23)$$

$$\delta_s = -8(4)^2(-3.05 \mu\text{m})$$

$$\delta_s = 390.4 \mu\text{m} = 0.39 \text{ mm}$$

Section 31.2: Image Quality # 361

Merit Function Value: 4.1397999E-001										
No	Type	Intx1	Intx2	Rx	Ry	Px	Py	Target	Height	Value
1	OPDX	1	0.0000	0.0000	0.1670	0.2947	0.00000E+000	0.16544	3.6971E+000	3.693
2	OPDX	1	0.0000	0.0000	0.3536	0.6124	0.00000E+000	0.23271	-4.6284E+000	9.259
3	OPDX	1	0.0000	0.0000	0.4710	0.8158	0.00000E+000	0.16544	3.70551E+000	3.715
4	OPDX	1	0.0000	0.0000	0.3357	0.6000	0.00000E+000	0.16544	3.69717E+000	3.693
5	OPDX	1	0.0000	0.0000	0.7071	0.8000	0.00000E+000	0.23271	-4.62842E+000	9.259
6	OPDX	1	0.0000	0.0000	0.9428	0.8000	0.00000E+000	0.16544	3.70531E+000	3.715
7	OPDX	1	0.0000	0.0000	0.1679	0.2997	0.00000E+000	0.16544	3.69717E+000	3.693
8	OPDX	1	0.0000	0.0000	0.3536	0.6124	0.00000E+000	0.23271	-4.62842E+000	9.259
9	OPDX	1	0.0000	0.0000	0.4710	0.8158	0.00000E+000	0.16544	3.70531E+000	3.715
10	OPDX	1	0.0000	0.0000	0.1679	0.2997	0.00000E+000	0.16544	3.69717E+000	3.693
11	OPDX	1	0.0000	0.0000	0.3536	0.6124	0.00000E+000	0.23271	-4.62842E+000	9.259
12	OPDX	1	0.0000	0.0000	0.4710	0.8158	0.00000E+000	0.16544	3.70531E+000	3.715
13	OPDX	1	0.0000	0.0000	0.3357	0.6000	0.00000E+000	0.16544	3.69717E+000	3.693
14	OPDX	1	0.0000	0.0000	0.7071	0.8000	0.00000E+000	0.23271	-4.62842E+000	9.259
15	OPDX	1	0.0000	0.0000	0.9428	0.8000	0.00000E+000	0.16544	3.70531E+000	3.715
16	OPDX	1	0.0000	0.0000	0.1679	0.2997	0.00000E+000	0.16544	3.69717E+000	3.693
17	OPDX	1	0.0000	0.0000	0.3536	0.6124	0.00000E+000	0.23271	-4.62842E+000	9.259
18	OPDX	1	0.0000	0.0000	0.4710	0.8158	0.00000E+000	0.16544	3.70531E+000	3.715

SURFACE DATA SUMMARY:										
Surf	Type	Comment	Radius	Thickness	Glass	Diameter				
OBJ STANDARD			infinity	infinity						
STO STANDARD			-888	-498	MIRROR	100				
2 STANDARD			infinity	0.398903	V	9.197643				
IMA STANDARD			infinity			0.69872822				

Listing 31.1 MFE and LDE for locating Strehl plane.

31.2.6 Wavefront Variance in ZEMAX

Insert the above mirror example into ZEMAX. There is only one field (on-axis). Set the wavelength to 0.55. In the MFE select: Tools → Default Merit Function → RMS/Wavefront/Centroid. This will insert a group of OPDX values (instead of TRAC). These OPDX operands should be the only operands turned on in the MFE. In the LDE put a dummy surface just before the IMA surface. Place a variable on the dummy surface thickness. When the optimization is run, the dummy surface will shift to the best Strehl focal plane. The results of this exercise are shown in Listing 31.1 which shows both the MFE and the LDE. Note the value of the merit function and compare it to the value of σ_x calculated in Section 31.2.4. Also note the thickness value on surf. No. 2 in the LDE. Compare this to δ_s calculated in Section 31.2.5. The values are essentially the same.

It is worth briefly reviewing in a qualitative way the sign difference in δ_s between lenses and mirrors. A biconvex thin lens and a concave spherical mirror both have positive, sometimes called “undercorrected” (by people with gray hair), spherical aberration. To find the best image planes in either case we must shift from the paraxial plane *toward* the optic. One of the optics community’s conventions (Section 3.2) is that light always travels from left-to-right. So both the lens and mirror are illuminated by a source on their left. After refraction in the lens the light continues moving left-to-right from the exit pupil to the image plane as illustrated in Figure 31.4a. From paraxial focus we must shift our observation plane toward the left (toward the lens) to locate any of the “best” image planes discussed thus far. That means the deltas are negative (according to convention). After reflection from the mirror, light travel has reversed itself moving right-to-left. The paraxial plane relative to the exit pupil now lies on the left side. So if we take Figure 31.4a and flip it 180° (using the exit pupil as the point of rotation), we get the result shown in Figure 31.4b. The “best” image planes are to the right of the

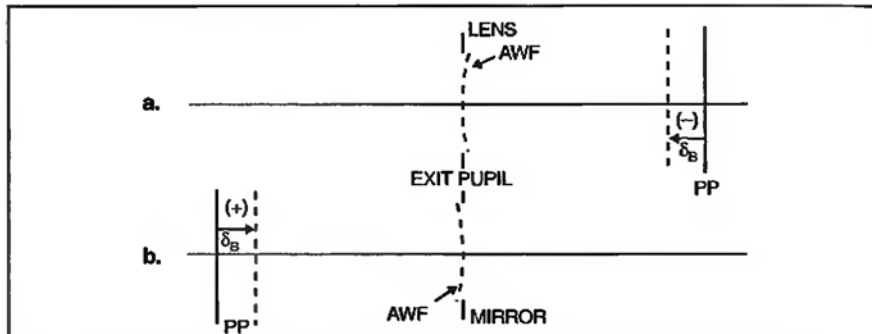


Fig. 31.4 Relative locations and signs of "best image" planes for: (a) thin lens; (b) mirror.

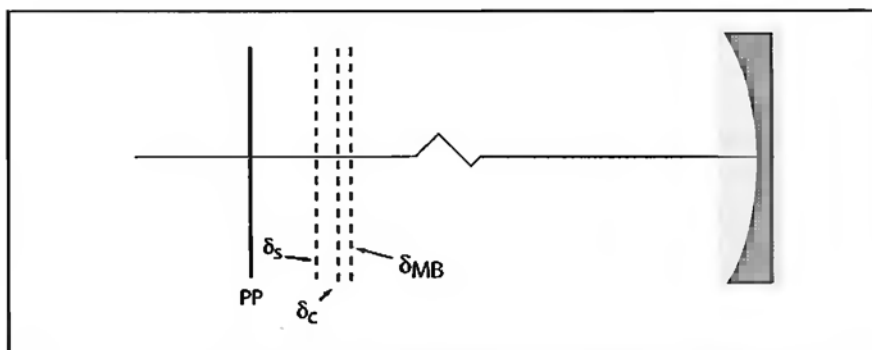


Fig. 31.5 "Best image" locations for minimum blur, image compactness, and Strehl as determined in ZEMAX for the mirror.

paraxial plane and the deltas are positive.

31.3 Minimum Blur in ZEMAX

To locate the axial location of minimum blur (where the marginal ray crosses the caustic) in ZEMAX, keep everything the same as it was in the LDE (Section 31.2.6). However, in the MFE:

Tools → Default Merit Function → PTV/Spot Radius/Centroid

After the optimization, you'll find that the dummy surface thickness is now: +0.5879 mm. Using Equation 30.19 once again, we find:

$$\delta_{MB} = -8(4)^2 \left[-\frac{3}{2}(3.05 \text{ } \mu\text{m}) \right] = 585.6 \mu\text{m} = 0.586 \text{ mm.}$$

The relative locations of these various "best image" planes for this mirror are illustrated in Figure 31.5.

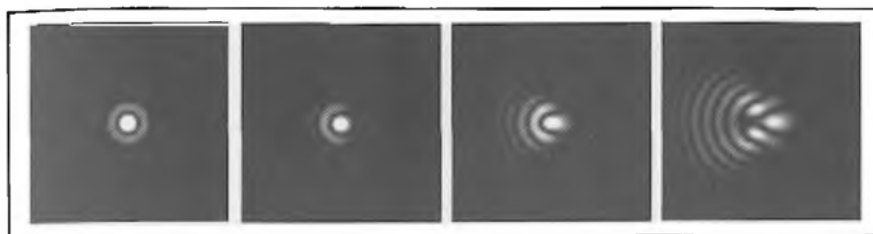


Fig. 31.6 Image behavior in best focus for increasing coma. Reprinted with permission from Star Testing Astronomical Telescopes by H.R. Suiter (Willmann-Bell, Inc. 1994).

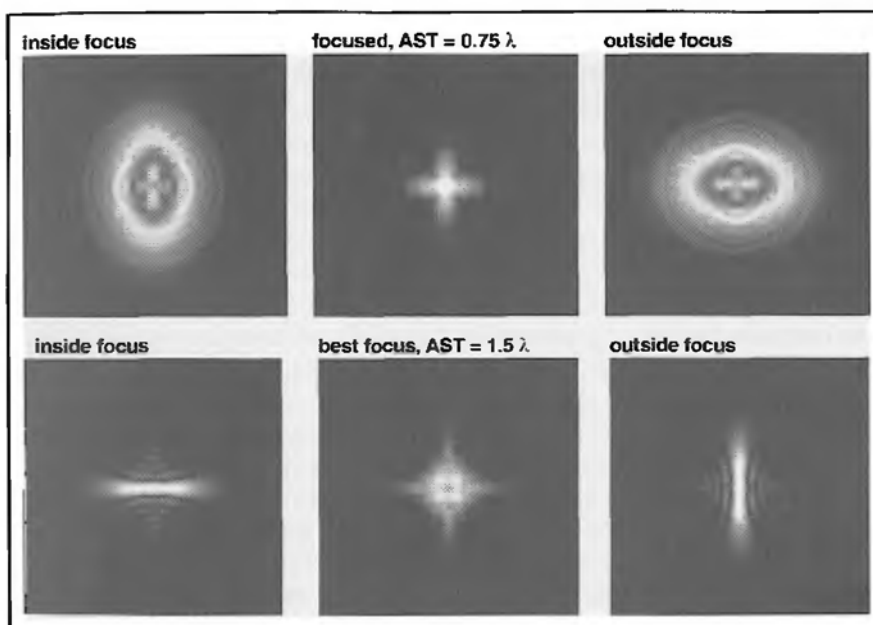


Fig. 31.7 Appearance of astigmatic image in the sagittal, medial, and tangential focal planes for $\frac{3}{4}\lambda$ (top) and 1.5λ , respectively. Note top row images are magnified relative to bottom row. Reprinted with permission from Star Testing Astronomical Telescopes by H.R. Suiter (Willmann-Bell, Inc. 1994).

31.4 Wavefront Variance for Asymmetric Aberrations

In the examples used thus far we have concentrated on rotationally symmetric aberrations (and their corresponding images). Table 31.3 shows the value of σ^2 for coma and astigmatism. Figure 31.6 shows how the asymmetry in the paraxial image plane builds up as the amount of coma is increased. The asymmetry in an astigmatic image at the sagittal, medial, and tangential image planes is shown in Figure 31.6 for $\frac{3}{4}\lambda$ and 1.5λ .

Table 31.3 Wavefront variance for the asymmetric aberrations.	
Aberration	σ^2
Coma	$0.1250 W_{131}^2$
Astigmatism	$0.0625 W_{222}^2$

31.5 Homework

1. Go through the calculation steps (similar to Section 31.2.3) to show how the wavefront variance values in Table 31.3 were obtained. (Note: $\bar{H} = 1$.)
2. Using the equations found in (1) calculate the Strehl ratio if you have 1 wave a) coma; and b) astigmatism.

Chapter 32

Axial Intensity and Depth of Focus

32.1 Introduction

In Chapter 30, we discussed *image compactness* (Section 30.6) as an image quality measure and saw how this was related to RMS spot size in ZEMAX. *Image compactness* is a lateral measure of quality in the plane of the image. This was followed in Chapter 31 with a discussion of two related image quality criteria: *Strehl ratio* (Section 31.2.1) and *wavefront variance* (Section 31.2.2). Strehl is a point-like measure in the image plane whereas wavefront variance is evaluated at and across the exit pupil. The latter two image quality measures were needed in the realm where diffraction spreading of the image was as important as that due to aberration. As an example, we applied the criteria to a combination of spherical aberration and defocus. Each criteria (including *minimum blur*) gave a different “opinion” of what constituted the “best” image, and where that image plane was located relative to the paraxial plane. In this chapter, we are going to explore Strehl behavior more fully along the optical axis and not limit ourselves to just a single plane defined by Equation 31.23. This will get us involved with depth of focus issues. In addition, all the criteria discussed thus far are for single point objects. We’re going to expand this here to include a pair of point objects in order to initiate a discussion on *Resolution* as an image quality measure for objects having finite extent.

32.2 Image Quality III

32.2.1 Axial Intensity

In this section, we’re going to derive an expression for the distribution of intensity along the optical axis in and around the paraxial image plane. This will not be a geometric optics derivation, but rather one based on diffraction. This will be accomplished using Fourier Optics techniques. Recall from Section 7.4.4 that the amplitude and phase distribution in the exit pupil was expressed as:

$$p(x,y) = a(x,y) e^{ikW(x,y)} \quad (32.1)$$

We’re going to assume a circular pupil having uniform *unit* amplitude, so $a(x,y) = \text{CYL}(r/d)$. The expression on the right is just shorthand notation. What it means is shown in Figure 32.1. Think of it as a round pill box, of radius = a .

Suppose the thin lens we used to focus the light is perfect. No aberration is introduced on the wavefront. The wavefront at the exit pupil is spherical. Figure 32.2 shows the ray and wavefront representations of this focusing.

So the wavefront expression for the exit pupil function now becomes:

$$p(r) = CYL\left(\frac{r}{d}\right) \exp\left[-i\left(\frac{\pi}{\lambda f}\right)r^2\right] \quad (32.2)$$

where the $\exp[]$ portion represents the spherical phasefront (wavefront).

To propagate this wavefront to the image plane, we need to take the Fourier transform of Equation 32.2. Actually what we really need is the Fourier-Fresnel (Hankel) transform.

$$u(\rho) = \mathcal{F}\{p(r)\} \quad (32.3)$$

$$u(\rho) = 2\pi \int_0^\infty CYL\left(\frac{r}{d}\right) \exp\left[-i\left(\frac{\pi}{\lambda f}\right)r^2\right] \exp\left[i\left(\frac{\pi}{\lambda z}\right)r^2\right] J_o(2\pi\rho r)r dr \quad (32.4)$$

where $J_o(2\pi\rho r)$ is a Bessel function, and ρ is a spatial frequency.

Since $CYL(r/d) = 0$ for $r > a$, Equation 32.4 can be rewritten as:

$$u(\rho) = 2\pi \int_0^a \exp\left[-i\left(\frac{\pi}{\lambda}\right)\left(\frac{1}{f} - \frac{1}{z}\right)r^2\right] J_o(2\pi\rho r)r dr \quad (32.5)$$

$$u(\rho) = 2\pi \int_0^a \exp\left[-i\left(\frac{\pi}{\lambda}\right)\left(\frac{z-f}{fz}\right)r^2\right] J_o(2\pi\rho r)r dr \quad (32.6)$$

Since $z \sim f$:

$$u(\rho) = 2\pi \int_0^a \exp\left[i\left(\frac{\pi}{\lambda}\right)\left(\frac{f-z}{f^2}\right)r^2\right] J_o(2\pi\rho r)r dr \quad (32.7)$$

Let's work in normalized pupil space ($\mathcal{R} = r/a$) and let $\delta = f-z$.

$$u(\rho) = 2\pi a^2 \int_0^1 \exp\left[i\left(\frac{\pi}{\lambda}\right)\left(\frac{\delta}{f^2}\right)a^2 \mathcal{R}^2\right] J_o(2\pi\rho a \mathcal{R}) \mathcal{R} d\mathcal{R} \quad (32.8)$$

Axial amplitude is obtained from Equation 32.8 by setting $\rho = 0$, and $J_o(0) = 1$:

$$u(0) = 2\pi a^2 \int_0^1 \exp\left[ikW\mathcal{R}^2\right] \mathcal{R} d\mathcal{R} \quad (32.9)$$

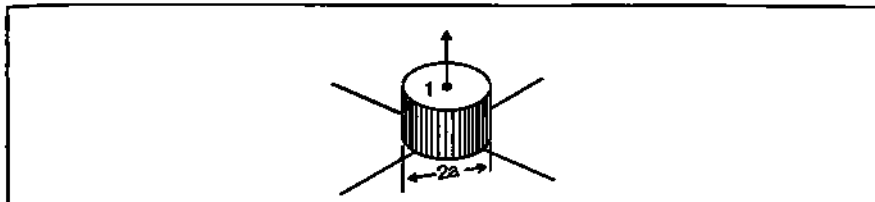


Fig. 32.1 Unit amplitude across circular exit pupil. From Linear Systems, Fourier Transforms, and Optics by J. D. Gaskill, © John Wiley and Sons, 1978. Reprinted by permission of John Wiley and Sons, Inc.

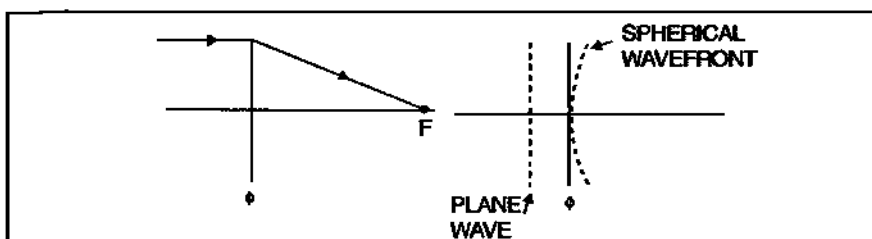


Fig. 32.2 Thin lens focusing for collimated source: a. ray; b. wavefront.

where we have set $kW = (\pi/\lambda)(a^2/f^2)\delta$

Now we introduce a change of variables. Let $x = \mathcal{R}^2$

$$dx = 2\mathcal{R}d\mathcal{R} \quad (32.10)$$

Substituting Equations 32.10 into Equation 32.9

$$u(0) = \pi a^2 \int_0^1 \exp[ikWx] dx \quad (32.11)$$

Recall that:

$$\int e^{bx} dx = \frac{e^{bx}}{b} \quad (32.12)$$

Therefore:

$$u(0) = \pi a^2 \left[\frac{\exp(i kW)}{ikW} \right]_0^1 \quad (32.13)$$

$$u(0) = \pi a^2 \left[\frac{\exp(i kW) - 1}{ikW} \right] \quad (32.14)$$

Recall the Euler relation:

$$e^{i\theta} = \cos\theta + i\sin\theta \quad (32.15)$$

Using this relation in Equation 32.14:

$$u(0) = \left(\frac{\pi a^2}{kW}\right) \left[\frac{(\cos kW + i\sin kW) - 1}{i} \right] \quad (32.16)$$

Now multiply numerator and denominator by i :

$$u(0) = \frac{\pi a^2}{kW} [\sin kW - i(\cos kW - 1)] \quad (32.17)$$

This is still an expression for on-axis amplitude. To get on-axis intensity:

$$I(0) = u(0)u^*(0)$$

where u^* is the complex conjugate.

$$I(0) = \left(\frac{\pi a^2}{kW}\right)^2 [\sin^2 kW + (\cos kW - 1)^2] \quad (32.18)$$

Equation 32.18 reduces to:

$$I(0) = 2\left(\frac{\pi a^2}{kW}\right)^2 [1 - \cos kW] \quad (32.19)$$

But

$$1 - \cos 2\theta = 2\sin^2\theta \quad (32.20)$$

Using Equation 32.20 in Equation 32.19:

$$I(0) = (\pi a^2)^2 \left[\frac{\sin^2\left(\frac{kW}{2}\right)}{\frac{kW}{2}} \right]^2 \quad (32.21)$$

The expression in brackets is known as the “sinc-squared function.” We can rewrite Equation 32.21 as:

$$I(0) = I_0 \text{sinc}^2\left(\frac{kW}{2}\right) \quad (32.22)$$

Figure 32.3 illustrates the shape of Equation 32.22. Remember, this is axial intensity as a function of defocus, W_d , in the exit pupil. It's the signal you would get out of a point detector as it is moved along the optical axis through paraxial focus.

If we substitute in the value for k ($= 2\pi / \lambda$) in Equation 32.22, the equation

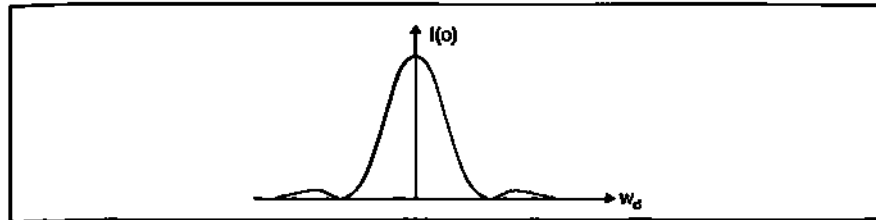


Fig. 32.3 Axial intensity for unaberrated imaging optical system.

can be written as:

$$I(0) = I_0 \left[\frac{\sin \pi \left(\frac{W}{\lambda} \right)}{\pi \left(\frac{W}{\lambda} \right)} \right]^2 \quad (32.23)$$

Note that when $W = \pm \lambda$, $I(0) = 0$. These are the first zeros on either side of paraxial focus as indicated in Figure 32.3.

Figure 32.3 is plotted in terms of waves of defocus along the abscissa. Let's get this in terms of actual axial displacements, δ , in image space. Recall from Equation 32.9 where we had set:

$$kW_d = \left(\frac{\pi}{\lambda} \right) \left(\frac{a^2}{f^2} \right) \delta \quad (32.24)$$

Insert the value of k and cancel common factors:

$$2W_d = \left(\frac{a^2}{f^2} \right) \delta = \left(\frac{1}{4} \right) \left(\frac{2a}{f} \right)^2 \delta \quad (32.25)$$

But $(2a/f) = (f/\#)^{-1}$. Therefore:

$$\delta = 8(f/\#)^2 W_d \quad (32.26)$$

Equation 32.26 should look familiar to you. It is the same as Equation 11.16, which was used as recently as Chapters 30 and 31. Equation 32.26 tells us that the axial spread of the sinc-squared function goes as the square of the f-number. As the f-number increases, the axial spread of $I(0)$ also increases. Conversely, the smaller the f-number, the more compact $I(0)$ is about the paraxial plane.

Let's suppose we have an $f/5$ system. The first zeros on either side of the paraxial plane are separated by:

$$\Delta\delta = 2[8(5)^2(1\lambda)] = 400\lambda$$

Let $\lambda = 0.6328 \text{ } \mu\text{m}$; then:

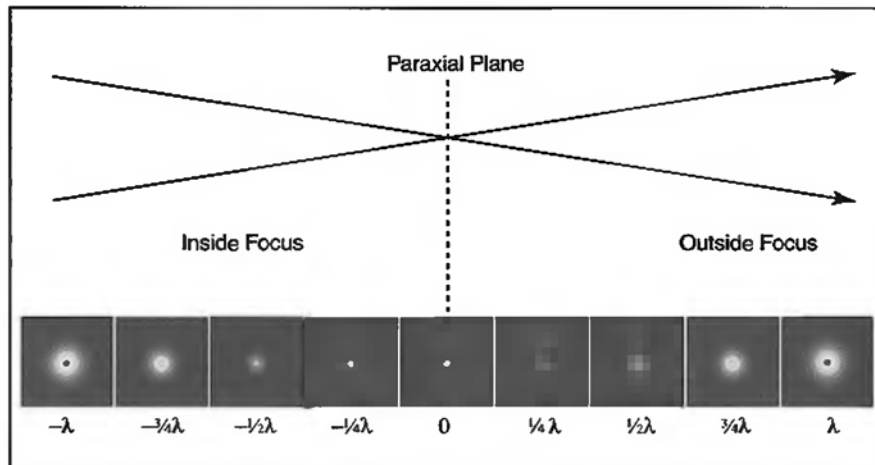


Fig. 32.4 Through-focus images for an aberrationless optical system.

$$\Delta\delta = 253.12 \text{ } \mu\text{m}$$

We know what the *axial* intensity looks like for a perfect system. What do the corresponding images look like? Figure 32.4 shows images taken about paraxial focus at equal but, opposite δ locations including points where $W_d = \pm \lambda$. The latter can be identified in the figure by the tiny black dot (zero intensity) right in the middle of the pattern. Also note that the patterns symmetric about the paraxial plane are identical in appearance. At the paraxial plane we have the Airy pattern (also called the star image).

32.2.2 Diffractive Depth of Focus

Lord Rayleigh came up with the quarter wave rule-of-thumb. In an upcoming section you will hear more about it. But right now we are going to use it to help define what is meant by the diffractive depth of focus (DDOF). For this we set $W_d = \pm \lambda/4$. Insert this value into Equation 32.26:

$$\delta_D = 8(f/\#)^2 \left(\frac{\pm \lambda}{4} \right)$$

Diffractive depth of focus:

$$\delta_D = \pm 2(f/\#)^2 \lambda \quad (32.27)$$

Going back to Equation 32.23 and substituting in $W_d = \lambda/4$:

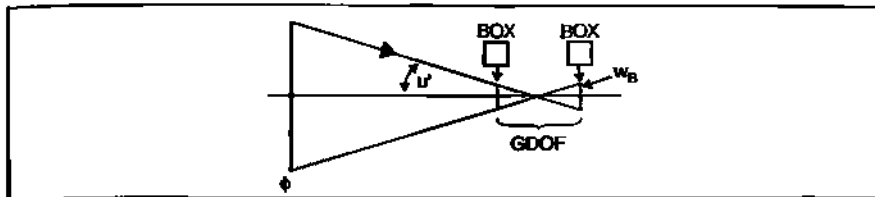


Fig. 32.5 Geometric DOF for "perfect" system.

$$I_D(0) = I_0 \left(\frac{\sin \frac{\pi}{4}}{\frac{\pi}{4}} \right)^2$$

$$I_D(0) = I_0 \left(\frac{\sin 45^\circ}{0.7854} \right)^2$$

$$I_D(0) = 0.81 I_0 \quad (32.28)$$

The axial intensity is down to 81% of its peak value at the extremes of the Rayleigh depth of focus. What this means in practical terms is that at either extreme the image still looks Airy-like to the observer.

32.2.3 Geometric Depth of Focus

Figure 32.5 shows a "perfect" thin lens forming a point image. The entrance pupil (which for convenience is square) is uniformly illuminated. If we go on either side of paraxial focus, we will see a smaller version of the pupil, i.e., a uniform square of light. How big this box is depends on how far our plane of observation is from the focal plane. The geometric depth of focus (GDOF) will be determined by these box sizes.

Suppose the half-width of the box is w_B . From the illustration we see that this box width can be related to the f-number via the marginal ray angle:

$$u' = \frac{w_B}{\left(\frac{GDOF}{2} \right)} = \frac{1}{2(f/\#)} \quad (32.29)$$

Therefore:

$$GDOF = 4(f/\#)w_B \quad (32.30)$$

Of course, the key question is how big is w_B , but that's pretty much up to the designer and the customer to decide. "How much can you stand?" There is no hard and fast rule as there was in the definition of DDOF. In imaging arrays, the "box" should be about the pixel size.

Let's move on to a simple aberrated system due to focus error. This is illus-

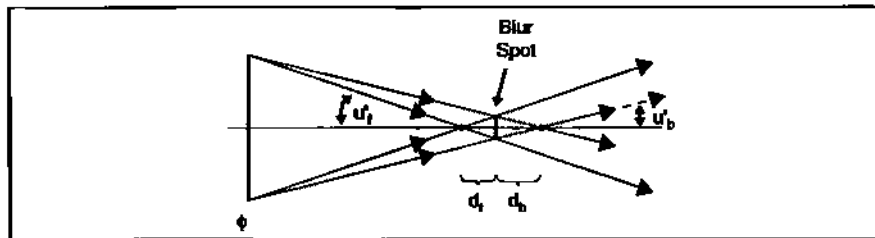


Fig. 32.6 Geometric DOF for aberrated system.

trated in Figure 32.6. Instead of a nice point image at the paraxial plane, we have a square blur spot. This can come about either because the light leaving the exit pupil is focusing short of the paraxial plane, or beyond it.

From the figure:

$$u'_f = \frac{w_B}{d_f} \quad (32.31)$$

and:

$$u'_b = \frac{w_B}{d_b}$$

But:

$$GDOF = d_f + d_b \quad (32.32)$$

Substitute Equations 32.31 into Equation 32.32:

$$GDOF = w_B \left(\frac{1}{u'_f} + \frac{1}{u'_b} \right) \quad (32.33)$$

$$GDOF = 2w_B (f/\# + f_b/\#)$$

But $f/\#$ is about the same as $f_b/\#$:

$$GDOF \sim 4w_B (f/\#) \quad (32.34)$$

which is the same expression as obtained for the unaberrated case.

The GDOF only makes sense when you are nowhere near the diffraction-limit, and are looking at highly structured finite-sized objects (like resolution targets used in optical testing).

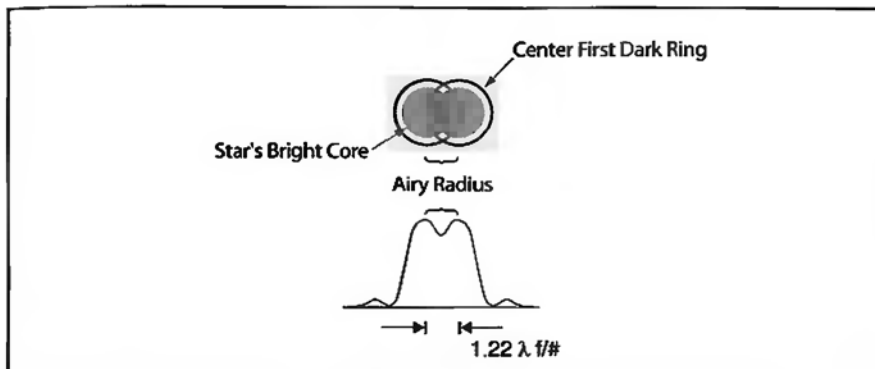


Fig. 32.7 Star image resolution.

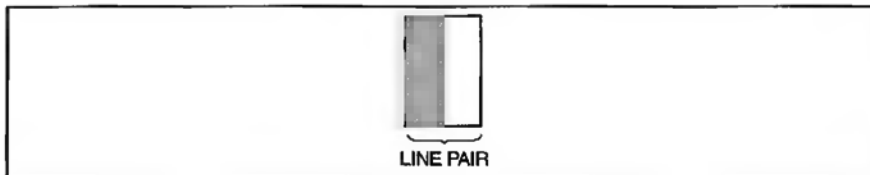


Fig. 32.8 Example of a line pair.

32.2.4 Resolution

32.2.4.1 Star Sources

When you look at stars through a telescope (or at any image of point source pairs), ask yourself this question: how close together can these *images* be and still be distinguishable as two separate points or stars? This is a resolution question. Figure 32.7 illustrates the Rayleigh criterion answer if the imaging system is diffraction-limited. Shown at the top are the images of two stars. The images are overlapping but still distinguishable. Below the image is the corresponding irradiance profile. This profile shape occurs when the center of the first dark ring of one image is centered on the peak irradiance of the other. This means that the separation between the peaks is the radius of the Airy disk.

$$r_A = 1.22\lambda f/\# \quad (32.35)$$

If we have an $f/10$ system and $\lambda = 0.55 \mu\text{m}$: $r_A = 6.71 \mu\text{m} = 0.0067 \text{ mm}$. The reciprocal of the Airy radius *expressed in mm* is the resolution:

$$R = (1.22\lambda f/\#)^{-1} \quad (32.36)$$

The resolution for the $f/10$ example is 149.25 line pairs/mm.

OK... but what's this line-pair business? This goes back to the structure of resolution patterns used in optical testing. A line pair is a dark/light bar pair as

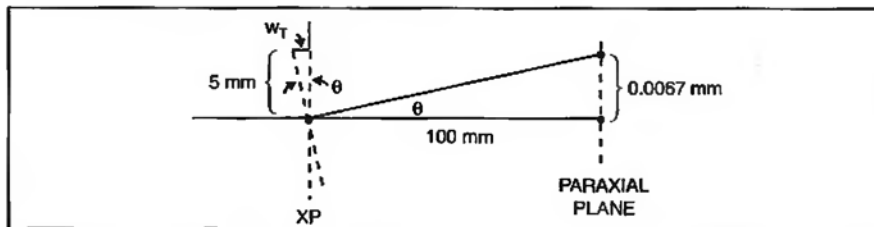


Fig. 32.9 Geometry for determining wavefront tilt.

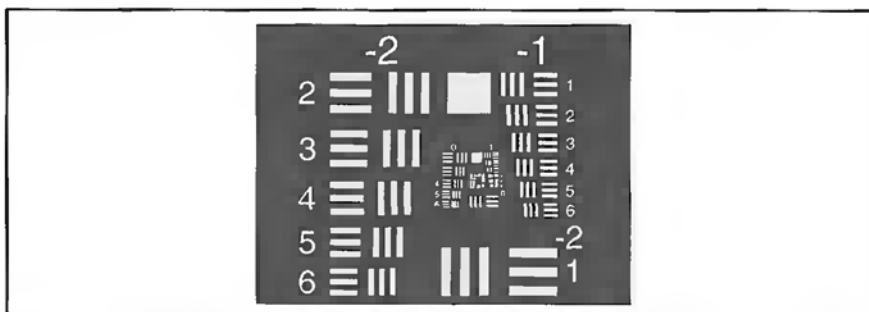


Fig. 32.10 Air Force ‘sixth root of two’ resolution target.

shown in Figure 32.8. For our example, the width of the line pair is made equal to the radius of the Airy disk. How many line pairs 0.0067 mm wide can you fit into a 1 mm length? The answer: 149.

To get separated star images in the image requires two spherical wavefronts with some small tilt between them (Section 15.2). For our $f/10$ example, how much tilt is there? Suppose our $f/10$ system has an EFL = 100 mm and a EPD = 10 mm. Figure 32.9 shows the geometry.

From the figure the following relationship holds:

$$\tan \theta = \frac{0.0067}{100} = \frac{W_T}{5} \quad (32.37)$$

So:

$$W_T = 0.000335 \text{ mm} = 0.335 \mu\text{m}$$

which in waves at 0.55 μm is:

$$W_T = 0.61\lambda$$

32.2.4.2 Broad Sources

Photographic systems generally view broad source targets, extended objects. A typical target used to evaluate photographic objectives is shown in Figure 32.10. It is called the Air Force ‘sixth root of two’ resolution target. It is made up of sets



Fig. 32.11 Fully resolved line pair (a); unresolved line pair due to defocus (b).

of 2½ line pairs (vertical and horizontal) of decreasing size (hence increasing resolution). This target is usually located in the focal plane of a collimator. The objective under test views the light from the collimator and forms a geometrically scaled image of the resolution target (corrupted by any inherent aberrations in the objective). An observer viewing the image via a microscope looks for the smallest group he can resolve and reads out this resolution as so many line pairs/mm.

The GDOF discussed in Section 32.2.3 takes on more meaning in terms of a resolution target image. You can now ask how much defocus will make a certain line pair-set unresolvable. This is illustrated (via profiles) in Figure 32.11.

32.2.5 Rayleigh Rules

In this chapter there were two distinct rules utilized with Lord Rayleigh's name tagged to them. The one used in Section 32.2.4.1 was a point (star) source *resolution* criterion. The other rule, the quarterwave, was used in Section 32.2.2 in the context of the diffractive depth of focus. The quarter-wave criteria stems from Rayleigh's investigation of optical imaging system performance. How much error can be tolerated in an imaging instrument before its effects on image quality are noticeable? He concluded that if the wavefront error was no greater than $\lambda/4$ peak-valley, image quality, in a practical sense, would not be degraded. In the image plane this meant that a little bit of power would leave the Airy disk, brightening the first bright ring. In other words, the Strehl ratio (Section 31.2.1) drops to about 80%.

32.3 Strehl in ZEMAX

Unless a design for an imaging system approaches diffraction-limited performance, there is not much point in looking at Strehl values. Within the context of this course, only a few designs were diffraction-limited. These included the aspheric singlet (Part 6 of the Homework for Chapter 3), the Fizeau transmission sphere (Lecture 9 Homework), and the Ritchey-Chrétien telescope (Lecture 26 Homework). None of the photographic objectives were anywhere near diffraction-limited.

There are a few places in ZEMAX where Strehl ratio information can be called upon. In terms of the wavefront:

Analysis → Calculations → Zernike Coefficients

The Strehl ratio value is in the block of data appearing just above the listing of the Z-coefficients.

376 Chapter 32 Axial Intensity and Depth of Focus

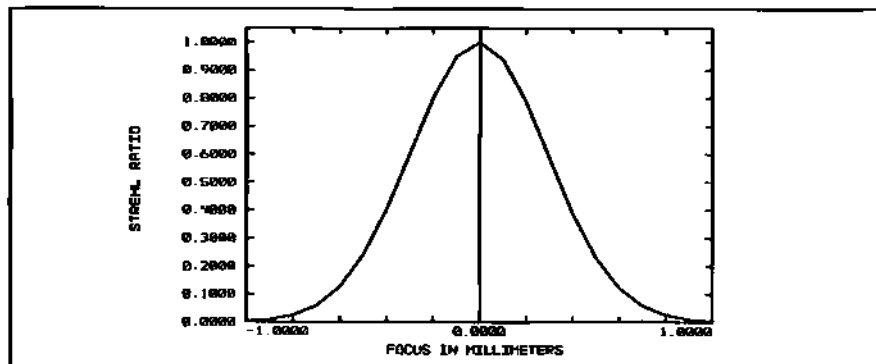


Fig. 32.12 Axial intensity or Strehl ratio as a function of focus for Cassegrain telescope.

For diffractive-depth-of-focus information:¹

Analysis → RMS → RMS vs. Focus → Settings → Data → Strehl Ratio → OK

You can play with the focus range within the Settings menu by changing the numbers in the Min Focus and Max Focus blocks. A sample plot for a Cassegrain telescope is shown in Figure 32.12.

¹For Version 5.0 and 5.5 you must also insert Options between RMS vs Focus and Settings.

Chapter 33

Petzval Lens

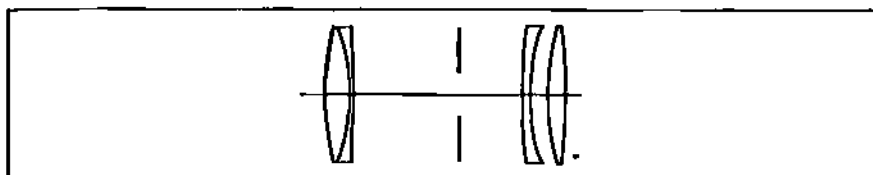


Fig. 33.1 Traditional Petzval lens form.

33.1 Introduction

Beginning with the Rapid Rectilinear in the Homework for Chapter 25, designs have started with the rear half. Once this part of the procedure was accomplished, the lens was made symmetric about the stop by adding the identical (but reversed) front half. The rear half was then slaved to the front half and the optimization of the symmetric lens continued. In this chapter, we will break with this tradition. The homework assignment in this chapter will be the design of a Petzval portrait lens (illustrated in Figure 33.1). This is not a symmetric lens. Rather it is the marriage of a standard front-end achromat with a Celor-like rear-end (or inverted dialyte) with the stop lying between them.

The Petzval lens resulted from an industry-sponsored competition for a prize. This was in the early days of the photographic process. Back then the Chevalier lens (Section 19.5) was in common use. Exposure times were very long because the lens was fairly slow (large f-numbers). While doing portraits, people (especially children) tended to fidget if exposure times exceeded a few seconds. The result is some blurring of the image due to object movement. This does not help customer satisfaction. The new industry wanted and needed a faster lens, hence the contest. Petzval's design was an f/3.6, about twenty times faster than the lenses then on the market.

33.2 Paraxial Thin Lens Petzval Design

Let's first consider the thin lens form of the Petzval lens, which consists of two separated positive elements. A key feature is that each element bends the marginal ray the same amount as indicated in Figure 33.2. In addition, the marginal ray height at ϕ_2 is half that at ϕ_1 , i.e., $y_2 = \frac{1}{2}y_1$. (Recall that something similar was done

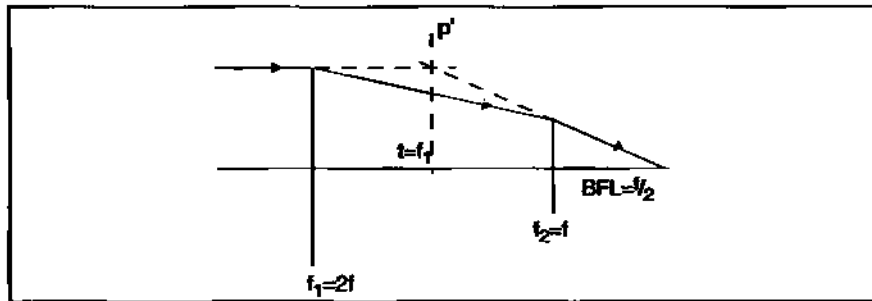


Fig. 33.2 Thin lens Petzval.

for the midterm.)

Applying the bending equation to the first element:

$$u'_1 = u_1 - y_1 \phi_1 \quad (33.1)$$

$$u'_1 = -y_1 \phi_1 = u_2 \quad (33.2)$$

The bending at the second surface is given by:

$$u'_2 = u_2 - y_2 \phi_2 = 2u'_1 \quad (33.3)$$

or:

$$2u_2 = u_2 - y_2 \phi_2$$

$$u_2 = -y_2 \phi_2 \quad (33.4)$$

Substitute Equation 33.2 into Equation 33.4:

$$y_1 \phi_1 = -y_2 \phi_2 \quad (33.5)$$

or:

$$\frac{y_1}{y_2} = \frac{\phi_2}{\phi_1} = \frac{f_1}{f_2} \quad (33.6)$$

Recall from Section 28.2:

$$\phi = \left(\frac{1}{y_1} \right) (y_1 \phi_1 + y_2 \phi_2) \quad (33.7)$$

Substitute Equation 33.5 into Equation 33.7:

$$\phi = \left(\frac{1}{y_1} \right) (2y_1 \phi_1)$$

Section 33.2: Paraxial Thin Lens Petzval Design 379

$$\phi = 2\phi_1 \quad (33.8)$$

or:

$$\phi_1 = \frac{1}{2}\phi \quad (33.9)$$

or:

$$f_1 = 2f \quad (33.10)$$

So the focal length of the front element of the Petzval lens is twice its system focal length.

Let's go back to Equation 33.6 and substitute in that y -height constraint on the second element:

$$\frac{\frac{y_1}{(y_1)}}{\left(\frac{y_1}{2}\right)} = \frac{f_1}{f_2}$$

$$f_2 = \frac{f_1}{2} \quad (33.11)$$

Substitute in Equation 33.10:

$$f_2 = f \quad (33.12)$$

The second element focal length equals the system focal length.

Now we need to figure out the separation between the elements. We'll make use of Equation 4.18 from Section 4.6.2.

$$\phi = \phi_1 + \phi_2 - t\phi_1\phi_2 \quad (33.13)$$

Using Equation 33.9:

$$\phi = \frac{1}{2}\phi + \phi_2 \left(1 - \frac{1}{2}t\phi\right) \quad (33.14)$$

Solving for ϕ_2 :

$$\phi_2 = \frac{\phi}{2} \left[1 - \left(\frac{t\phi}{2}\right)\right]$$

$$\phi_2 = \frac{\phi}{2 - t\phi} \quad (33.15)$$

Rewriting Equation 33.15 in terms of focal lengths:

$$f_2 = 2f - t \quad (33.16)$$

Substituting in Equation 33.12 and solving for t :

$$t = f \quad (33.17)$$

The separation between elements equals the system focal length.

The BFL can be found using the transfer equation:

$$y_3 = y_2 + u'_2 t_{BFL} = 0 \quad (33.18)$$

$$t_{BFL} = \frac{-y_2}{u'_2}$$

But $u'_2 = 2u_2$ from Equations 33.2 and 33.3

$$t_{BFL} = \frac{-y_2}{2u_2} \quad (33.19)$$

Substituting in Equation 33.4:

$$t_{BFL} = \frac{-y_2}{2(-y_2\phi_2)} = \frac{1}{2\phi_2} \quad (33.20)$$

Substituting in Equation 33.12:

$$t_{BFL} = \frac{1}{2}f = BFL \quad (33.21)$$

The back focal length is half the system focal length.

33.3 Outline of Petzval Design Procedure on ZEMAX

We will assume that the front achromat is a given. This means that during optimization there are no variables assigned to the front achromat. It is what it is. Our main job will be designing the rear half (at the proper spacing from the front half) so that the overall aberration of the assembled system is reduced.

Since we know the front achromat focal length, we also know that the focal length of the rear half will be half this. We can then employ the Celor equations (Section 28.5) to determine the powers of the two rear half elements and their spacing. The thin lens radii can then be calculated from these powers. (We will initially assume that the positive lens is equiconvex, and the negative lens is equiconcave.) There is a caveat to these calculations. If ϕ_p is set to zero in the Celor power equations, you will discover that the resulting radii are fairly short for the homework problem. An alternative is to assign a finite value to ϕ_p . How much? Anywhere from an order of magnitude down from the rear half power up to a fifth its value. The radii will loosen up and the interlens spacing will increase.

With care, you can still work with the radii found by setting ϕ_p to zero. Insert these values into ZEMAX. Add real thickness. Optimize to restore the proper

Section 33.4: Historical Note: Joseph M. Petzval 381

EFL, and color correction with variables on radii and airspace. You will likely find that spherical aberration is rather large. You can knock it down using on-axis TRAC but freeze airspace. The lens at this point is ready for integration with the front achromat.

There are two important design constraints. The first is that the stop will be held *midway* between the two lens groups. This is done by slaving the rear-stop airspace to the front-stop airspace. The second constraint is that the ratio of the system focal length to the back focal length be equal to two. Use TTHI to generate the BFL value. Use DIVI to ratio EFL to TTHI. DIVI's target value should be 2.

The assembled lens must now be restored to its first order Petzval conditions. Put variables on all rear half radii and the front-stop airspace. Use EFLY to maintain the rear half focal length at its design value. Use AXCL to restore color correction.

After the above optimization, beat down and balance all orders of spherical using TRAC. Place variables on all rear half radii and the front-stop airspace.

The next optimization series deals with the *gradual addition of field*. You will likely find that going to full-field all at once will lead to warnings that certain operands cannot be computed. Walking your way out to full-field in several steps will avoid such problems. (Do not forget to update TRAC each time you change field entries.)

The final optimization is just tidying things up. The rear positive lens can be thinned if it looks too fat. The rear negative lens diameter can be made the same diameter as the rear positive lens. You can insert a dummy image surface with a variable on its thickness to see if it buys you anything. Your final design should look similar in form to that shown in Figure 33.1. The resulting lens will probably have a fairly flat sagittal field, but considerable ground will have been lost on the color front. The latter is due largely to the second constraint. If you reoptimize after turning off both EFLY on the rear half and DIVI, color correction will be restored and the RMS spot sizes will show considerable improvement. Although the lens form will still look Petzval-like, you will note that the BFL is equal to or greater than the separation between halves, and the rear half focal length is no longer 5".

33.4 Historical Note: Joseph M. Petzval

Petzval (Figure 33.3) was born in Hungary in 1807. After a two-year stint at the University of Budapest as a mathematics professor, he moved on to a similar position at the University of Vienna where he stayed thereafter. Oddly, Petzval knew nothing about designing lenses at the time a colleague told him about the prize being offered for a faster lens. Undaunted, Petzval threw his hat into the ring. He had help from the Austrian army though. To defray the tedium of ray tracing, the army folks who calculated trajectories for artillery undertook this task under Petzval's direction. It took six months before a satisfactory design was achieved. The lens was built and tested in 1840. It received high marks. But the prize, a platinum



Fig. 33.3 Joseph M. Petzval, inventor of the Petzval portrait lens.

medal, went to Chevalier for another lens he designed. Ironically, by the process of natural selection, portrait photographers preferred Petzval's lens by far—so much so that Chevalier's new lens became extinct. That's the good news. The bad news is that Petzval lost control over the rights to his lens. Pretty soon everyone was making Petzval lenses without acknowledging or compensating the inventor.

33.5 Image Quality IV

There is a rule-of-thumb in optics which goes like this: when aberrations are small, use diffractive predictions for image quality; but when aberrations are large, use geometric predictions. Sounds reasonable. But how small is small, and how large is large? At what point do we transition from one regime to the other? Let's explore this question. For an unaberrated optical imaging system, geometric optics predicts a *point* image as illustrated in Figure 33.4a. For the same system diffractive optics predicts a symmetric patch of light called the Airy pattern (assuming a circular exit pupil) as shown in Figure 33.4b. But for either approach, the location of the best image plane is the same—the paraxial plane. If we move to either side, image quality deteriorates.

Geometrically, the blur circle increases in diameter the further away one moves from the paraxial plane as indicated in Figure 33.5. The diffractive patch also increases in diameter to either side as can be seen by referring back to Figure 32.4.

Now let's contaminate our imaging system with aberration. We'll use spherical aberration as our guinea pig. Now the best image plane is no longer the paraxial plane, and the patterns, whether geometric or diffractive, are no longer symmetric about this plane as indicated in Figure 33.6 for the geometric example, and Figure 33.7 for the diffractive example.

Where is the best image plane relative to paraxial focus now that we have

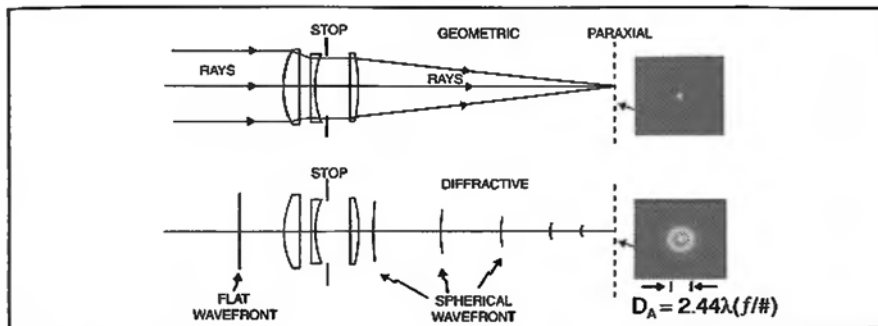


Fig. 33.4 Best image location for an unaberrated imaging system is the paraxial plane: a. geometric; b. diffractive.

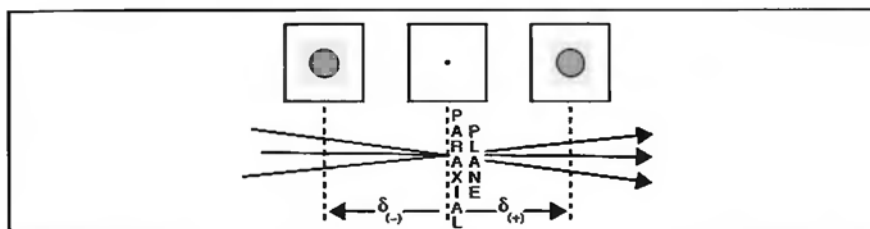


Fig. 33.5 Geometric blur diameter increases symmetrically about paraxial focus (No aberration).

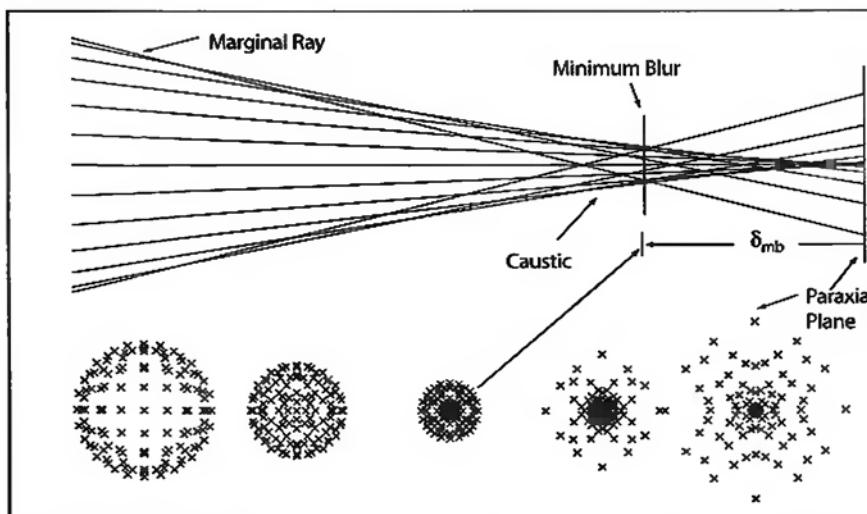


Fig. 33.6 Spherically aberrated imaging system showing non-symmetric spot diagrams about paraxial focus.

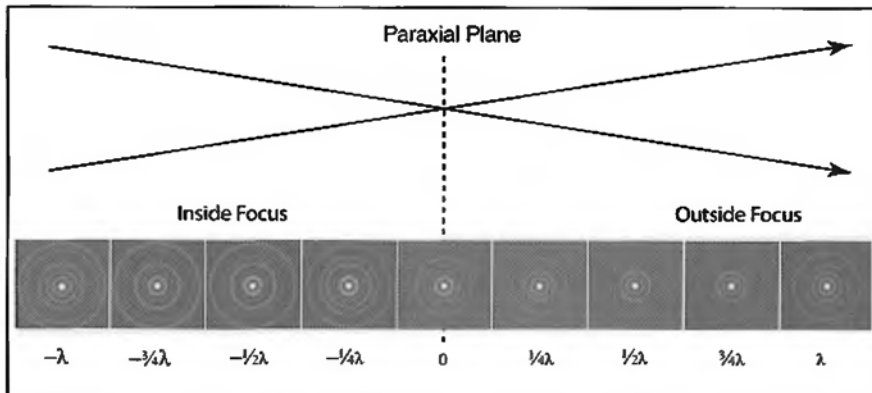


Fig. 33.7 Spherically aberrated imaging system showing non-symmetric point spread functions about paraxial focus.

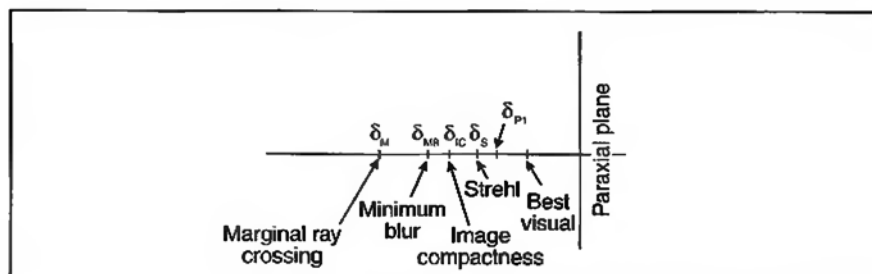


Fig. 33.8 Relative location of best image planes for spherically aberrated (3λ) system.

spherical aberration in our system? It depends on which image quality criteria (geometric or diffractive) one uses as listed in Table 33.1 and illustrated in Figure 33.8.

We have discussed the first three image quality criteria in Table 33.1 already. Let's say a few words about the last two. The first peak is obtained from axial intensity plots, which can be generated either theoretically or experimentally. Best visual is subjective and empirical. An observer views the star image through a microscope and sets the focus for what appears to be the most Airy-like pattern. To do this the observer minimizes the number of diffraction rings; keeps the first dark ring as dark as possible; minimizes the power in the first bright ring.

The range explored here is $\lambda/2$ to 3λ , which would certainly seem to cover the transition region we are interested in. The data presented here was generated with the same singlet used as an example for calculating spherical aberration in Section 10.3. In the present case, the plano-side faces a collimated HeNe beam. The amount of spherical aberration was controlled by a variable iris stop in front of the lens. Table 33.2 provides information on stop size and axial displacement for the first three criteria.

Table 33.1
Best Image Plane Criteria.

Criteria	Axial Location
1) Minimum Blur (<i>MB</i>)	$\delta_{MB} = 8(f/\#)^2 \left[-\frac{3}{2}W_{040} \right]$
2) Image Compactness (<i>IC</i>)	$\delta_{IC} = 8(f/\#)^2 \left[-\frac{4}{3}W_{040} \right]$
3) Strehl (<i>S</i>)	$\delta_S = 8(f/\#)^2 \left[-W_{040} \right]$
4) 1 st Peak (<i>P₁</i>)	(Via axial intensity plots)
5) Best Visual (<i>BV</i>)	$\delta_{BV} = 8(f/\#)^2 \left[-0.531 W_{040} \right]$ (empirical)

Table 33.2
Spherical aberration, stop size, and axial displacement.

<i>W₀₄₀</i>	Stop Radius	<i>f/#</i>	δ_{MB}	δ_{IC}	δ_S
$\lambda/2$	1.310 cm	18.72	-1.330 mm	-1.831 mm	-0.887 mm
λ	1.558	15.74	-1.881	-1.672	-1.245
2λ	1.853	13.24	-2.662	-2.367	-1.775
3λ	2.051	11.96	-3.258	-2.896	-2.172

Recall from Section 32.2.1 that the axial intensity plot for an unaberrated system is a sinc-squared function. Now look at Figure 33.9. Down its left side are *theoretical axial* intensity plots over a range of spherical aberration values from a half wave to 3 waves. (These plots are to the same scale.) At a half wave the plot still looks sinc-squarish, but the center of the pattern has drifted to the left of paraxial focus. As more and more aberration is added, this drift increases, and the shape of the pattern changes drastically (though the pattern still retains a symmetry axis which is defined by $W_d = -W_{040}$). It has been found both theoretically and empirically that the first well-defined axial peak (P_1) of the pattern relative to the paraxial plane locates the best image plane. (In this case, the best image means most Airy-like.)

To the right of each axial plot in Figure 33.9 are *experimental radial* intensity scans of the point spread function in the best image planes defined by the various criteria in Tables 33.1 and 33.2. At a half wave the plots identified as *S* and *P₁* are Airy-like, and are actually coincident. At a wave, *S* and *P₁* are still Airy-like and coincident. However, above one wave these two planes start noticeably separating, and only *P₁* retains an Airy-like form. Plane *P₁* always has the highest peak intensity among the various criterion. *BV* retains its Airy-like form throughout, but its peak intensity is always lower than *P₁*. The geometric criteria *IC* and *MB* are out of the ball game from the very beginning.

The first half of the rule-of-thumb does apply to the diffractive Strehl criteria out to one wave. The second half of the rule-of-thumb about large aberration does

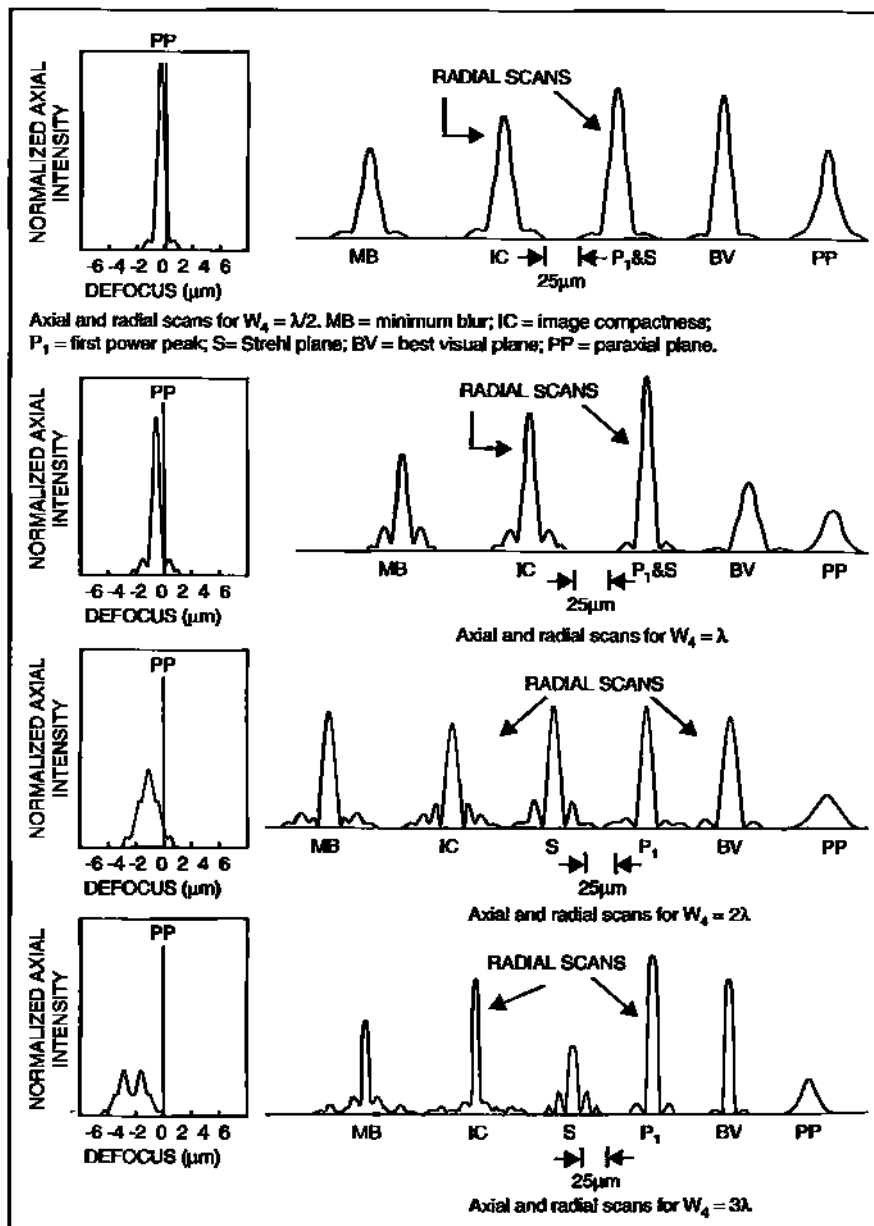


Fig. 33.9 Theoretical axial intensity scans (left column), and measured radial intensity scans at various criteria planes for best image for various amounts of spherical aberration. For the axial profiles the abscissa values are given in terms of exit pupil OPD in microns. Peterson, P. and Geary, J. "Intermediate Spherical Aberration," Optical Engineering, pp. 1232-1240, Vol. 25, No. 11 (1986).

Section 33.6: Homework 387

Table 33.3
Front achromat

Surf. no.	Radius	Thick.	Glass	Semi-Diam
1	2.971"	0.5"	K7	1.15"
2	-2.971"	0.12"	LF7	1.15"
3	10.3491"			1.15"

Table 33.4

Strict Petzval		Relaxed Petzval	
Target Spot Sizes		Target Spot Sizes	
Ü	RMS	Ü	RMS
0°	28	0°	21
7°	78	7°	37
10°	125	10°	47

not apply to the geometric criteria *JC* or *MB*. Neither one isolates the best image plane. The winner in this little exercise for locating the best image plane is P_1 (as determined via axial intensity scan data). P_1 reliably locates the best star image over the entire range of aberration magnitudes small or large. Consequently, the rule-of-thumb does not apply to the P_1 criterion at all.

33.6 Homework

Design a 5" EFL *f*/5 Petzval lens for a 10° half-field. Use the Celor equations to determine the powers of the rear half elements. Glass for the rear half will be LF7 and K7 respectively. Let $\phi_{pz} = 0$. The stop must be in the middle of the airspace between the two halves. In addition, the ratio EFL/BFL must equal two. For the initial assembly of the front and rear halves, let the airspace between the halves be 4.4".

For this homework problem you will not have to design the front achromat. The achromat is a 10" EFL *f*/4.35 lens (prescription is given in Table 33.3). The achromat is color corrected for *F*, *d*, C-light, so the rear half must be corrected for the same spectrum.

After working on the strict case, relax the constraints (e.g., by turning off EFLY and DIVI) and reoptimize.

As usual, meet or beat the RMS spot sizes in Table 33.4 and use settings: square; centroid.

Suggested folder name: Petzval; file name: Petz1o1b, etc.

Chapter 34

MTF: Image Quality V

34.1 Introduction

In Section 30.6, we initiated an image quality series with a discussion on *image compactness*. This criteria is basically what the default operand TRAC utilizes in ZEMAX for optimization. This was followed in Section 31.2 with an investigation of the diffractive criteria *wavefront variance* and *Strehl*. This led into an examination of axial intensity (or axial variation of Strehl) in Section 32.2 and its connection to depth of focus issues. This also involved us in a study of resolution with both point and broad sources. All the various image quality criteria thus far were assembled together in Section 33.5 to see which were most pertinent in the context of big and small aberrations in establishing the location of the best image plane. This chapter will complete the series of discussions on image quality by introducing an entirely different kind of metric, one that is especially pertinent to the imaging of finite-sized objects. This is the modulation transfer function, or MTF.

34.2 What is Modulation?

Suppose our object is a sinusoidal bar pattern as indicated in Figure 34.1. If we could get right up to the object and scan it with a small sampling aperture, we would obtain a profile across this pattern as shown in Figure 34.2.

The mathematical description of an object profile can be given in complex notation by:

$$f(x) = b_0 + b_1 \exp\{i2\pi\nu_0 x\} \quad (34.1)$$

The maximum value of Equation 34.1 is:

$$f_{\max}(x) = b_0 + b_1 \quad (34.2)$$

The minimum value is:

$$f_{\min}(x) = b_0 - b_1 \quad (34.3)$$

Modulation (or contrast) of this profile is defined by:

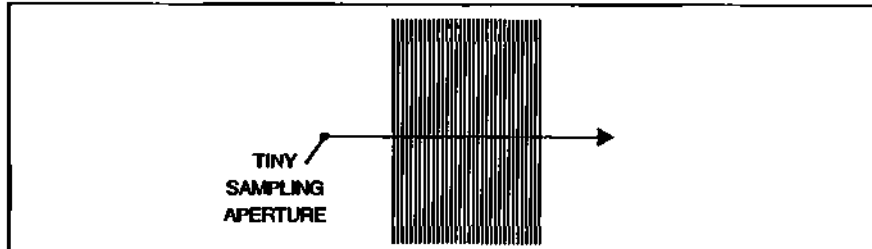


Fig. 34.1 Sinusoidal object pattern.

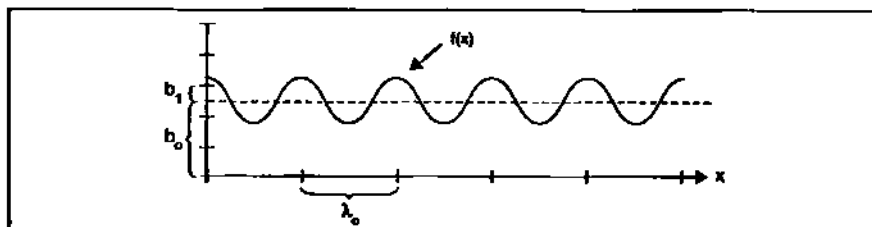


Fig. 34.2 Profile of sinusoidal object pattern.

$$M = \frac{f_{\max}(x) - f_{\min}(x)}{f_{\max}(x) + f_{\min}(x)} \quad (34.4)$$

Inserting the max and min values from Equations 34.2 and 34.3:

$$M = \frac{(b_0 + b_1) - (b_0 - b_1)}{(b_0 + b_1) + (b_0 - b_1)} \quad (34.5)$$

Simplifying Equation 34.5:

$$M_0(v_0) = \frac{b_1}{b_0} \quad (34.6)$$

Equation 34.6 is the inherent modulation (contrast) of the object.

Let us suppose that we are working at unit magnification (to avoid scaling issues). If the imaging system is perfect, then the sinusoidal pattern of the image will look exactly the same as the object. A profile across the image will mimic that of the object. However, if the imaging system is imperfect, then two things can happen to the pattern: a) its modulation can decrease; b) the image can be shifted laterally from its ideal or paraxial location.

34.3 Convolution and Fourier Transform

For an aberrated system, the star image (of a point object) is a lateral blob of light as indicated in Figure 34.3. We'll call this blob the point spread function (PSF). If we are imaging a finite-sized object through the same aberrated system, the result-

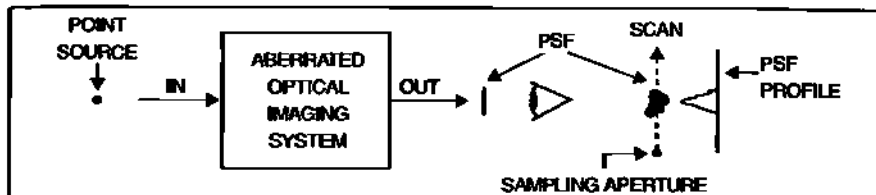


Fig. 34.3 Star image due to aberrated optical system.

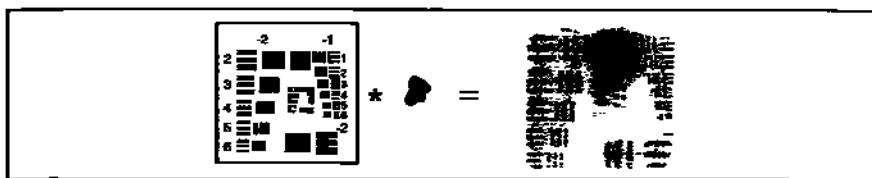


Fig. 34.4 Convolution of aberrated PSF with perfect geometric image.

ing image can be thought of as taking each point in the perfect image and replacing it with the aberrated PSF (suitably scaled for local irradiance) as illustrated in Figure 34.4.

Mathematically this can be thought of as the *convolution* of the aberrated PSF with the perfect image. Let's illustrate this using a *one-dimensional* analog (so that we can use it in conjunction with the analysis already done in Section 34.2). The aberrated star image will be represented by $h(x)$ (the incoherent PSF). The convolution is then given by:

$$g(x) = \int_{-\infty}^{\infty} f(\alpha)h(x-\alpha)d\alpha \quad (34.7)$$

In shorthand notation, the above convolution is represented by:

$$f(x) * h(x) = g(x) \quad (34.8)$$

Often times it is easier to calculate the convolution indirectly by way of the Fourier Transform, defined as:

$$F(v) = \int_{-\infty}^{\infty} f(x) \exp\{-i2\pi vx\} dx \quad (34.9)$$

In shorthand notation, the Fourier Transform will be represented by $\mathcal{F}\{ \cdot \}$. Equation 34.9 then looks like:

$$\mathcal{F}(v) = \mathcal{F}\left\{ f(x) \right\} \quad (34.10)$$

In this shorthand, the Fourier Transform of Equation 34.8 becomes:

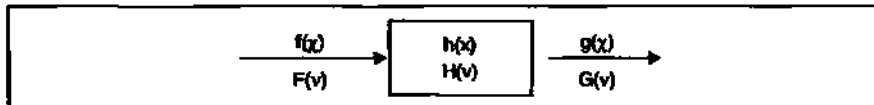


Fig. 34.5 Transferring the object through the optical imaging system.

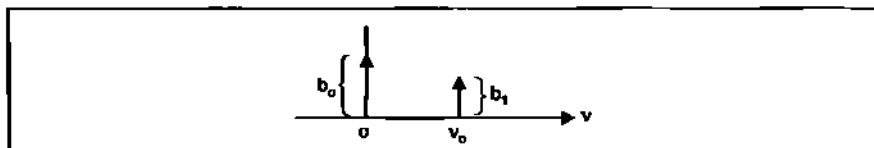


Fig. 34.6 The Fourier Transform of the object.

$$\mathcal{F}\{g(x)\} = \mathcal{F}\left\{f(x) * h(x)\right\} \quad (34.11)$$

or:

$$G(v) = F(v) \cdot H(v) \quad (34.12)$$

Note that the convolution operation becomes a product in frequency space. This is what makes the transition from real space computationally worthwhile. It is often easier to calculate this product rather than the integral.

34.4 The Optical Transfer Function

We will now transfer our object function, $f(x)$, through the imaging system as indicated in Figure 34.5 using the Fourier technique.

The Fourier Transform of the object is given by:

$$F(v) = \mathcal{F}\{f(x)\} = \mathcal{F}\left\{b_0 + b_1 \exp(i2\pi v_0 x)\right\} \quad (34.13)$$

$$F(v) = b_0 \mathcal{F}\{1\} + b_1 \mathcal{F}\{\exp(i2\pi v_0 x)\}$$

$$F(v) = b_0 \delta(v - 0) + b_1 \delta(v - v_0) \quad (34.14)$$

where $\delta()$ is the delta-function. Its meaning in spatial frequency space is illustrated in Figure 34.6.

Now lets look at the image as expressed by the product in Equation 34.12:

$$G(v) = F(v) \cdot H(v) = b_0 \delta(v - 0) H(v) + b_1 \delta(v - v_0) H(v) \quad (34.15)$$

It is a property of the delta-function called "sifting" that allows us to rewrite Equa-

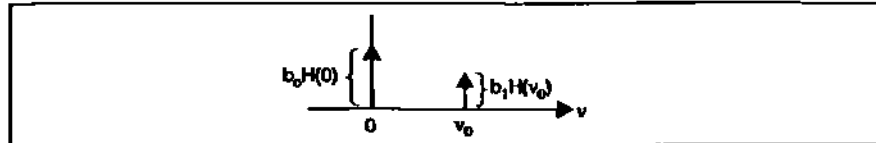


Fig. 34.7 The Fourier Transform of the image.

tion 34.15 as:

$$G(v) = b_0 H(0) \delta(v - 0) + b_1 H(v_0) \delta(v - v_0) \quad (34.16)$$

This function is illustrated in Figure 34.7.

Now we need to get back to the image in real space. This is done by taking the *inverse* transform, $\mathcal{F}^{-1}\{\cdot\}$, of $G(v)$:

$$g(x) = \mathcal{F}^{-1}\{G(v)\} = b_0 H(0) \mathcal{F}^{-1}\{\delta(v - 0)\} + b_1 H(v_0) \mathcal{F}^{-1}\{\delta(v - v_0)\} \quad (34.17)$$

$$g(x) = b_0 H(0) \cdot 1 + b_1 H(v_0) \cdot \exp(i2\pi v_0 x) \quad (34.18)$$

The image modulation at the spatial frequency v_0 is given by:

$$M_i(v_0) = \frac{g_{\max}(x) - g_{\min}(x)}{g_{\max}(x) + g_{\min}(x)} \quad (34.19)$$

where:

$$g_{\max}(x) = b_0 H(0) + b_1 H(v_0) \quad (34.20)$$

$$g_{\min}(x) = b_0 H(0) - b_1 H(v_0) \quad (34.21)$$

Inserting Equations 34.20 and 34.21 into Equation 34.19:

$$M_i(v_0) = \left[\frac{H(v_0)}{H(0)} \right] \left[\frac{b_1}{b_0} \right] \quad (34.22)$$

Substituting in Equation 34.6:

$$M_i(v_0) = \left[\frac{H(v_0)}{H(0)} \right] M_o(v_0) \quad (34.23)$$

So the modulation in the image at the spatial frequency v_0 is a product of “that thing in brackets” and the “modulation in the object.”

If we conduct the same procedure for all sinusoidal object spatial frequencies, we can write Equation 34.23 as:

$$M_i(v) = \left[\frac{H(v)}{H(0)} \right] M_o(v) \quad (34.24)$$

and “that thing in brackets” is called the Optical Transfer Function, i.e.:

$$\text{OTF}(v) = \left[\frac{H(v)}{H(0)} \right] \quad (34.25)$$

where:

$$H(v) = \int_{-\infty}^{\infty} h(x) \exp(-i2\pi vx) dx \quad (34.26)$$

and:

$$H(0) = \int_{-\infty}^{\infty} h(x) dx \quad (34.27)$$

Equation 34.26 is the Fourier Transform of the PSF, and Equation 34.27 is the area underneath the PSF. The latter is a normalizing quantity.

$H(v)$ is complex and can be written (using the Euler relationships) as:

$$H(v) = \int_{-\infty}^{\infty} h(x) \cos(2\pi vx) dx - i \int_{-\infty}^{\infty} h(x) \sin(2\pi vx) dx \quad (34.28)$$

As a consequence, the OTF is also complex and can be written as:

$$\text{OTF}(v) = v(v) - iw(v) \quad (34.29)$$

where:

$$v(v) = \frac{\int_{-\infty}^{\infty} h(x) \cos(2\pi vx) dx}{\int_{-\infty}^{\infty} h(x) dx} \quad (34.30)$$

and:

$$w(v) = \frac{\int_{-\infty}^{\infty} h(x) \sin(2\pi vx) dx}{\int_{-\infty}^{\infty} h(x) dx} \quad (34.31)$$

Equation 34.29 can also be written as:

Section 34.4: The Optical Transfer Function 395

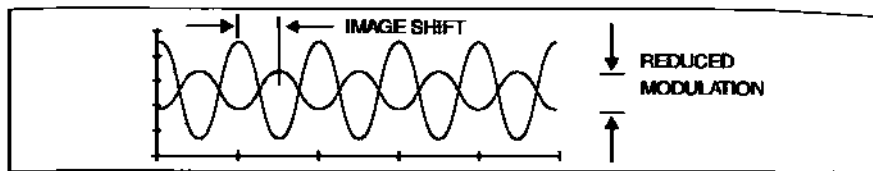


Fig. 34.8 Effects of the MTF and PTF on image.

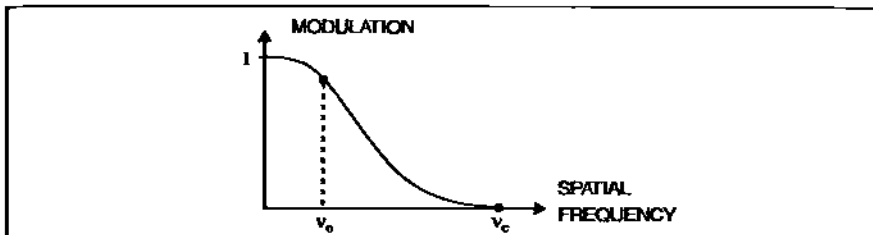


Fig. 34.9 Typical MTF plot.

$$OTF(v) = MTF(v) \exp\left\{-iPTF(v)\right\} \quad (34.32)$$

where:

$$MTF(v) = \sqrt{v^2(v) + w^2(v)} \quad (34.33)$$

and:

$$PTF(v) = \tan^{-1}\left[\frac{w(v)}{v(v)}\right] \quad (34.34)$$

Equation 34.33 is the *modulation transfer function* which is responsible for the reduction in image modulation (or contrast). Equation 34.34 is the *phase transfer function* which is responsible for the lateral shifting of the pattern.

Figure 34.8 illustrates (for one spatial frequency) the effects of the MTF and PTF on an image obtained through an aberrated system as compared to an unaberrated image.

If the PSF is asymmetric, this will result in a PTF which introduces a lateral shifting of the sinusoidal pattern. Rotationally symmetric PSFs (or even functions) do not, in general, cause such shifting. (Although as one increases the PSF size due to defocus, there are abrupt lateral shifts in the pattern of a half-wave due to PTF having a phase change from 0° to 180° .)

The MTF has values ranging between zero and one. A typical MTF plot is illustrated in Figure 34.9. The spatial frequency where the MTF goes to zero (the first time) is called the cut-off frequency.

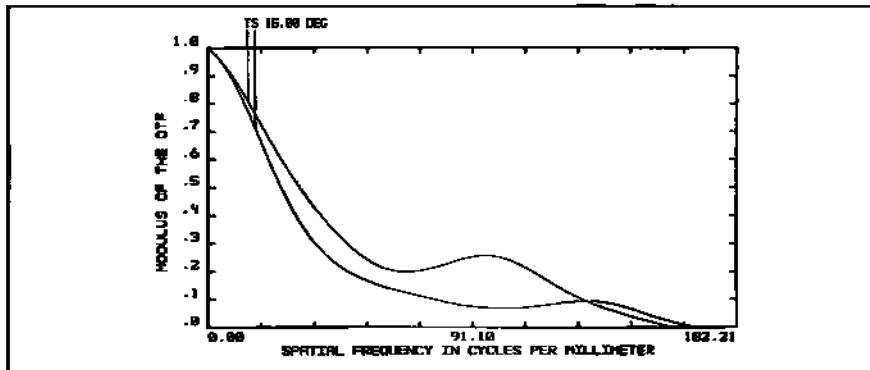


Fig. 34.10 Tangential and sagittal profile MTFs for PERC108a.

34.5 MTF in ZEMAX

The MTF is used in ZEMAX both as a diagnostic and as an optimization tool. The former is called up by: Analysis → MTF → Modulation Transfer Function. For example, the MTF at full field for the perisopic lens PERC108a (Section 12.7) is shown in Figure 34.10. Two MTF profile plots are shown: one for the tangential MTF; the other, sagittal MTF.

Note that the two MTF plots are quite different. The reason for this is that the PSFs become asymmetric off-axis. The widths and profiles of the PSF along the tangential and sagittal directions are different. So the convolution of these profiles with the paraxial (or geometric) image will result in different amounts of smearing in the two directions. This means that the resolution in the two directions will also be different.

In this course, we have used TRAC as our workhorse optimization tool. When the P-V wavefront error gets down to about 1 wave (or near the diffraction limit), then it is appropriate to start using MTF optimization. This optimization can be accomplished using the MTFT (or MTFS or MTFA) operands. However, the SE version of ZEMAX does not support MTF optimization. You need the XE or EE versions of the program. MTF optimization is an appropriate topic for a more advanced lens design course and will not be pursued here any further.

34.6 MTF and Symmetry

Because of the nature of the object used in Figure 34.1 we were able to explain OTF and MTF in a one-dimensional manner (which made the math somewhat easier to digest). However, the PSF is a three-dimensional entity. It has coordinates x and y . At those coordinates there is a third number, the local irradiance, which defines the height. So the PSF is a small self-contained and bounded mountain jutting up from the XY-plane (as illustrated in Figure 34.11). Since the OTF is the Fourier Transform of this 3-D function, the MTF is 3-D as well (as illustrated in

Section 34.6: MTF and Symmetry 397

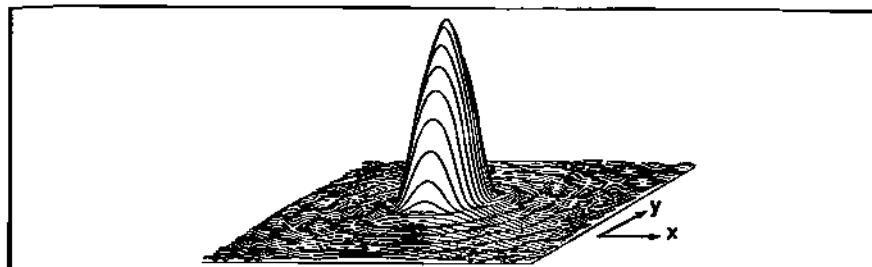


Fig. 34.11 The PSF is 3-dimensional.

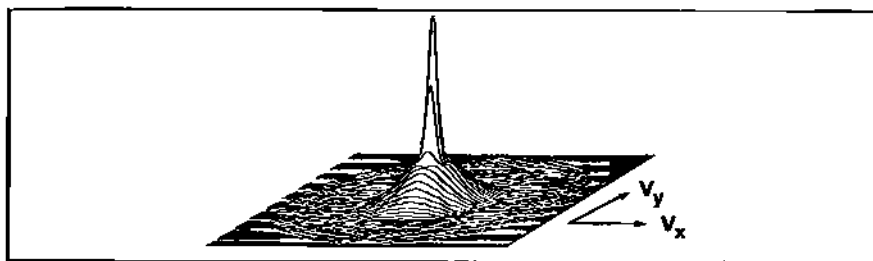


Fig. 34.12 The MTF is also 3-dimensional.

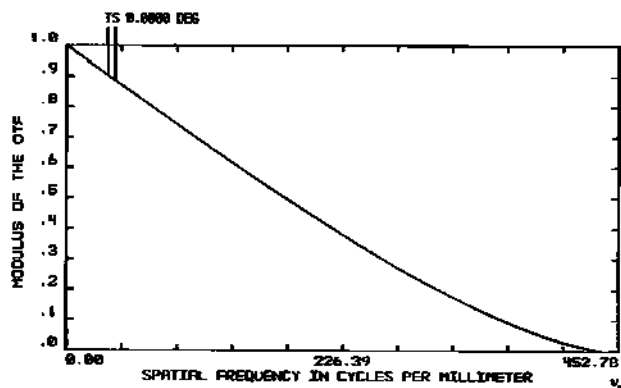


Fig. 34.13 Diffraction-limited MTF for circular pupil.

Figure 34.12); only its coordinates (v_x, v_y) are in spatial frequency units, and the height is the local modulation value. If the PSF is rotationally symmetric, the MTF is rotationally symmetric. If the PSF is asymmetric, so also is the MTF.

Using a series of objects (like that of Figure 34.1) but of different spatial frequencies, the MTF profile obtained for one orientation of the objects is sufficient if the PSF is symmetric. If the PSF is not symmetric, then the sinusoidal objects used to obtain the MTF profile must be oriented (and scanned) in several

different directions to build up a picture of the asymmetry in the MTF.

In most applications, the designer will be working with rotationally symmetric optical systems. The MTF for a perfect diffraction limited imaging system with a circular exit pupil is shown in Figure 34.13. This represents the ideal MTF against which the real system must be compared.

Chapter 35

Null Lens Design

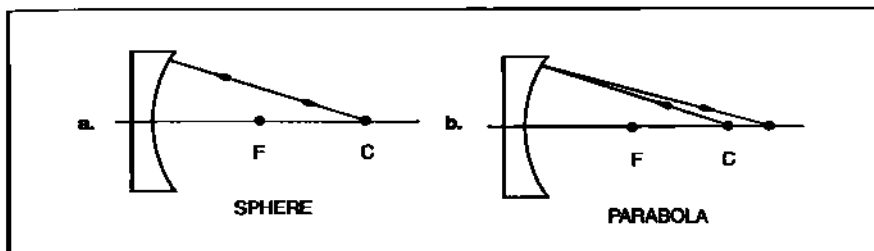


Fig. 35.1 A center of curvature point source is imaged: a) without spherical aberration; b) with spherical aberration.

35.1 Introduction

Back in Chapter 9, we discussed lens splitting as a means of *eliminating* spherical aberration from our imaging system. A practical application of this technique was found in the Homework for Chapter 9 where you designed a transmission sphere for a Fizeau interferometer. In this chapter, we will look at another attachment to an interferometer that deliberately *introduces* spherical aberration. It is called a *null lens*, and it is used to test aspheric (e.g., parabolic) primary mirrors.

From past discussions on concave mirrors, you know that spherical aberration is introduced when a spherical mirror images a point object at infinity. If the mirror is parabolic, no spherical aberration is introduced into the image. Now move the point source to the mirror center of curvature as illustrated in Figure 35.1. The unaberrated image is now generated by the spherical mirror. The parabola, on the other hand, introduces spherical aberration. The amount introduced increases as the f-number of the parabola decreases. The departure from sphere (Section 3.6) can get so large that interferometric testing without the mediation of a null lens is impossible.

35.2 Spherical Aberration Generated by a Parabolic Mirror

Looking at Figure 35.1b, how much spherical aberration is introduced on the reflected wavefront? Recall from Table 10.1 that:

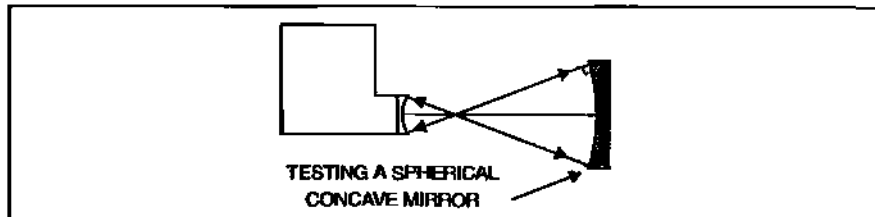


Fig. 35.2 Fizeau interferometer test of spherical mirror.

$$W_{040} = \frac{1}{32} y^4 \phi^3 \sigma_I \quad (35.1)$$

where σ_I is modified to include the effect of the conic constant:

$$\sigma_I = Y^2 + K \quad (35.2)$$

When a mirror is tested at its radius of curvature, the test is being conducted at unit magnification, in which case $Y = 0$, and, consequently, $\sigma_I = K$. So Equation 35.1 becomes:

$$W_{040} = \frac{1}{32} y^4 \phi^3 K \quad (35.3)$$

For a parabola:

$$W_{040} = \frac{1}{32} y^4 \phi^3 \quad (35.4)$$

Suppose we have to test a 364 cm EFL parabola 91 cm in diameter. Utilizing Equation 35.4, we find that it has $-27.77 \mu\text{m}$ or -43.88λ (at HeNe) of spherical aberration.

35.3 Test Configuration For Concave Mirrors

Figure 35.2 illustrates a Fizeau interferometric configuration for testing a spherical mirror. The transmission sphere forms a point image at the mutual center of curvature of the mirror and transmission sphere. Assume for the moment that the mirror is a perfect sphere. Rays from the point image arrive at the mirror *normal* to its surface. They are reflected back upon themselves, pass through the center of curvature and enter the interferometer via the transmission sphere. The resulting fringe pattern will show a *null* (uniform) fringe. If the mirror's shape is not perfect, then the rays arriving at the mirror will not be exactly normal to its surface. Reflected rays will not pass exactly through the center of curvature. The interference pattern resulting from this imperfection will show up as a finite number of distinct fringes.

Now replace the sphere with a *perfect* parabola. The center of curvatures of

Section 35.4: Purpose Of Null Lens in Testing Parabolic Mirrors 401

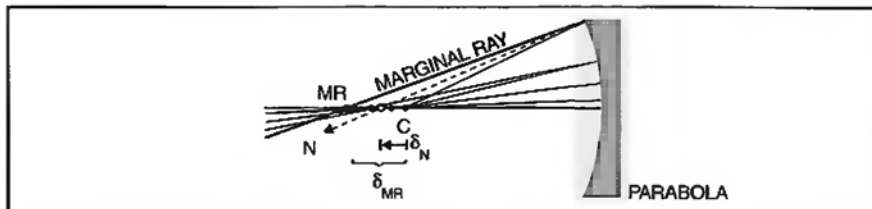


Fig. 35.3 Rays reflected from a perfect parabola in a center of curvature test arrangement.

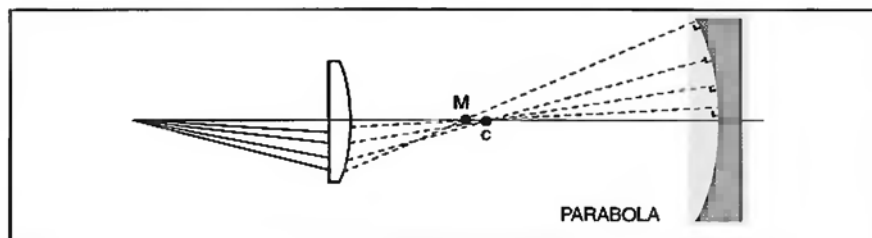


Fig. 35.4 Null lens matches surface normal axial locations and angles.

both the transmission sphere and the parabola are coincident. Strictly speaking, however, only the axial incident ray is normal to the mirror surface. Moving radially outward, the departure from *normality* for incident rays increases. This lack of *normality* is responsible for the spherical aberration generated by the mirror (as calculated in Section 35.2). What we are after in the test is the surface figure (or error in the shape) of the mirror. All that spherical aberration just clutters things up and gets in the way, especially if we are looking for surface departures of a tenth-wave or so.

Figure 35.3 shows the behavior of the rays reflected from different annular zones on the perfect parabolic mirror. The distribution of zonal foci begins at the center of curvature for the paraxial zone. As the annular zone diameter on the mirror increases, the foci move from the center of curvature along the optical axis away from the mirror. The marginal zone focuses furthest from the mirror.

35.4 Purpose Of Null Lens in Testing Parabolic Mirrors

Suppose we erect *surface normals* for each annular zone on the parabolic mirror and project them toward the optical axis. They will all intersect the optical axis but not at the same spot. Each zone has its own intersection point. If you look at Figure 35.3 once again, you'll note that we have also included the *surface normal* for the marginal zone (at the rim of the mirror). It crosses the optical axis to the left of (and furthest from) the center of curvature.

For a spherical mirror, all the surface normals strike at the same spot, the center of curvature. Not so for a parabolic mirror. As a consequence, we need an interface between the perfect point image formed by the transmission sphere on

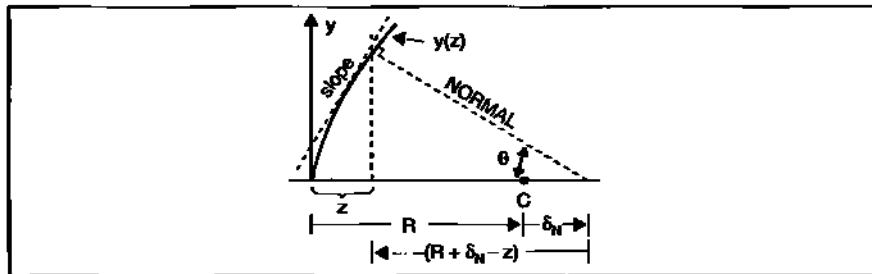


Fig. 35.5 Finding the surface normals.

one side and the axial line of surface normal intersection points of the parabola on the other. This interface is called the *null lens*, a simple version of which is illustrated in Figure 35.4. Note that it must accomplish two distinct tasks simultaneously. It must match the axial distribution of surface normal intersection points. It must also match the angles of the surface normals at each intersection point. Only then will the rays from the Fizeau test point arrive normal (perpendicular) to the parabolic mirror surface and the spherical aberration of the mirror nullified.

35.5 Derivation of Surface Normals for Parabolic Mirror

We want to find the distribution (δ_N) of surface normal crossings along the optical axis relative to the center of curvature as illustrated in Figure 35.5.

Our starting point will be the aspheric equation derived in Section 3.5 (pages 23–27):

$$z = \frac{R}{P} \left[1 - \sqrt{1 - \frac{P}{R^2} \cdot y^2(z)} \right] \quad (35.5)$$

Taking the derivative dz/dy :

$$1 = -\left(\frac{R}{P}\right)\left(\frac{-P \cdot y}{R^2}\right) \left[1 - P\left(\frac{y}{R}\right)^2 \right]^{\frac{1}{2}} \left(\frac{dy}{dz} \right) \quad (35.6)$$

Solving Equation 35.6 for dy/dz :

$$\frac{dy}{dz} = \frac{R}{y} \sqrt{1 - P\left(\frac{y}{R}\right)^2} = \text{slope} \quad (35.7)$$

Knowing the tangents to the mirror surface we can now determine the surface normals. The surface normal is given by:

Section 35.5: Derivation of Surface Normals for Parabolic Mirror 403

$$N = \frac{-1}{\left(\frac{dy}{dz}\right)} \quad (35.8)$$

Inserting Equation 35.7:

$$N = \frac{\frac{-y}{R}}{\sqrt{1 - P^2 \left(\frac{y}{R}\right)^2}} \quad (35.9)$$

or:

$$\sqrt{1 - P^2 \left(\frac{y}{R}\right)^2} = \frac{-y}{RN} \quad (35.10)$$

Rewriting Equation 35.5:

$$\sqrt{1 - P^2 \left(\frac{y}{R}\right)^2} = 1 - \left(\frac{P}{R}\right)z \quad (35.11)$$

Now equate Equations 35.11 and 35.10:

$$\frac{-y}{RN} = 1 - \left(\frac{P}{R}\right)z \quad (35.12)$$

Solve for N :

$$N = \frac{y}{Pz - R} \quad (35.13)$$

But from Figure 35.5:

$$\tan \theta = \frac{y}{-(R + \delta_N - z)} = N \quad (35.14)$$

Equate Equations 35.14 and 35.13:

$$\frac{y}{Pz - R} = \frac{y}{-(R + \delta_N - z)} \quad (35.15)$$

Solve for δ_N :

$$\delta_N = (1 - P)z \quad (35.16)$$

or substituting Equation 3.5 (from page 23):

$$\delta_N = (1 - P) \left[\frac{y^2}{2R} + \frac{Py^4}{8R^3} + \text{etc} \right] \quad (35.17)$$

For a parabola $P=0$:

$$\delta_N = z = \frac{y^2}{2R} = \text{sag} \quad (35.18)$$

The distribution of normal intercepts along the optical axis follows the same law as the sag (sag was discussed in Section 3.4).

Substituting $\delta_N = z$ into Equation 35.14, it becomes:

$$\tan \theta = \frac{-y}{R} \quad (35.19)$$

Solve Equation 35.19 for y and insert into Equation 35.18:

$$\delta_N = \frac{(-R \tan \theta)^2}{2R} \quad (35.20)$$

$$\delta_N = \frac{R}{2} \tan^2 \theta \quad (35.21)$$

Equation 35.21 relates the normal distribution along the axis with the angles that the normals make with respect to the axis.

As an example, we'll apply Equations 35.18 and 35.21 to the sample parabola from Section 35.2. Its base radius of curvature is $R = 728$ cm. The results are displayed in Table 35.1.

Table 35.1 Surface Normal Axial and Angular Distribution.			
y (cm)	δ_N (cm)	$\tan \theta$	θ
11.375	0.0889	0.015622	0.895°
22.750	0.3555	0.031252	1.790°
34.125	0.7998	0.046879	2.684°
45.500	1.4219	0.062494	3.576°

From Table 35.1 we see that the *marginal* normal intersects the optical axis 1.4219 cm from the center of curvature. There is another way to find this separation value. Recall that a wavefront is always perpendicular to rays. We can think of an equivalent wavefront associated with the surface normals. In Section 35.2 we found that the spherical aberration wavefront coefficient value for our sample parabola was: $W_{040} = -27.77 \mu\text{m}$. The equivalent value for the surface normal wavefront is: $W_{040N} = \frac{1}{2} W_{040} = -13.88 \mu\text{m}$ (or -21.93λ at HeNe). If you calculate the departure from sphere (discussed in Section 3.6) for this parabola, you will get the same value; in other words, $W_{040N} = \text{DFS}$.

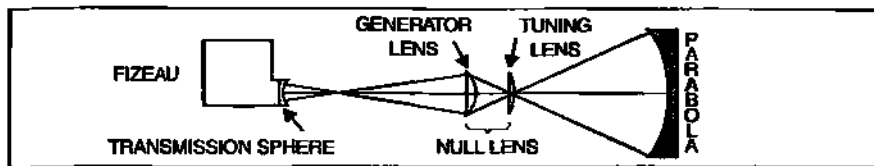


Fig. 35.6 Fizeau test of parabola with intermediate Offner null lens.

From Section 11.5:

$$\delta = 8(f/\#)^2 W_d \quad (35.22)$$

For an object at infinity the f-number of the parabola is $f/4$. But for a point object at the center of curvature, its *effective* f-number is doubled. From Section 5.5 recall that:

$$f/\# = \frac{1}{2 \tan U'} . \quad (35.23)$$

In this case the marginal ray angle is found by dividing the mirror aperture radius by its radius of curvature: $\tan U' = 45.5 / 728 = 0.0625$. Inserting this into Equation 35.23:

$$f_e/\# = \frac{1}{2(0.0625)} = 8$$

You may remember from Section 11.6 that the minimum blur location relative to paraxial focus was found by setting $W_d = -(3/2)W_{040}$. The location of the marginal ray crossing is found by setting $W_d = -2W_{040}$. In the present context, however, we want to find where the marginal *normal* intersects the optical axis—so we want to set $W_d = -2W_{040N}$. Inserting all this information into Equation 35.22:

$$\delta_N = -8(f_e/\#)^2 (2W_{040N}) = -8(8)^2 (-27.77) = 1.4218 \text{ cm} .$$

This is the same number found in Table 35.1 at full aperture radius.

35.6 The Offner Null Lens

The design we are going to work on here is the Offner null lens.¹ It consists of two singlets (usually plano-convex) as illustrated in Figure 35.6. The test point is the focus (and center of curvature) of the Fizeau transmission sphere. Rays from this point are relayed by the null lens to the region of the mirror center of curvature but with the right axial and angular distribution to match the surface normals of the parabola. After reflection, the rays should return back along the same path through

¹ Offner, Abe, "A Null Corrector for Paraboloid Mirrors," *Applied Optics*, Vol. 2, No. 2 pp. 153–155 (1963).

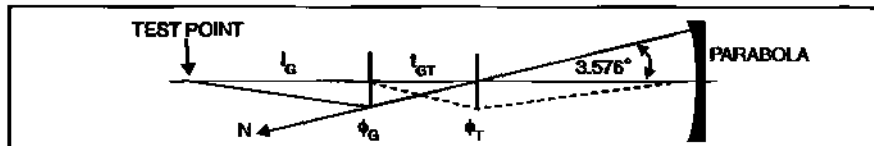


Fig. 35.7 First order layout of null lens.

the null lens to image at the test point. This image should be perfect if the parabola is perfect. Light proceeds back into the interferometer where the wavefront is compared against the reference wavefront from the front surface of the transmission sphere. If the mirror surface is not perfect then the return wavefront will have aberrations on it. The aberrations will make themselves known by the behavior of the fringe pattern.

Let's call the first singlet in the null lens the *generator* because it will generate most of the spherical aberration. The second lens we'll call the *tuner* because it will tune the axial and angular ray distribution to match the parabola's surface normals. (Note that the *tuner* is located at or near the mirror center of curvature.)

35.6.1 Predesign

We will design a null lens for the 364-cm EFL 91-cm parabola discussed in Section 35.2. The thin lens layout is illustrated in Figure 35.7.

As drawn, the marginal surface normal passes through the center of the tuner aperture at 3.576°, and then proceeds to the generator lens. The aperture of the generator will be defined once the spacing between the tuner and generator, t_{GT} , is set. It is crucial that the generator lens be placed beyond the parabola's surface normal caustic (which is half that of the ray caustic). We must have a fairly good correlation between surface normal pierces at the pupil and at the generator lens aperture. Within the caustic region, this correlation is lost because the surface normals become intertwined. The length of the ray caustic is given by:

$$\delta_C = 48(f/\#)^2 W_{040} \quad (35.24)$$

Using the effective f-number:

$$\delta_C = 48(8)^2(-27.77\mu\text{mm}) = -85.3\text{mm}$$

The normal caustic is:

$$\delta_{CN} = \frac{1}{2}\delta_C = 42.65\text{mm}$$

35.6.2 Generator Power

As an example, let this spacing be $t_{GT} = 360$ mm. The radius of the generator lens is then given by:

Section 35.6: The Offner Null Lens 407

$$y_G = 360 \tan 3.576^\circ = 22.5 \text{ mm} \quad (35.25)$$

The test point is an object for the generator. It is a distance l_G away. We already know the image distance since $l'_G = t_{GR}$. Let the magnification for this lens be set at $m_G = -0.6147$. The object distance is then found by:

$$l_G = \frac{l'_G}{m_G} = -585.68 \text{ mm} \quad (35.26)$$

Consequently, the power of the generator is:

$$\frac{-1}{l_G} + \frac{1}{l'_G} = \phi_G = 0.004485 \text{ mm}^{-1} \quad (35.27)$$

or

$$f_G = 222.96 \text{ mm}$$

From Table 10.1 we know that:

$$W_{040G} = \frac{1}{32} y_G^4 \phi_G^3 \sigma_t \quad (35.28)$$

We already have values for y_G and ϕ_G . Now we must determine the value of the structural aberration coefficient σ_t . The lens will be plano-convex and the material BK7 glass. The refractive index at HeNe is 1.51509. Therefore:

$$\sigma_t = 8.7444X^2 - 12.8912XY + 4.32Y^2 + 8.6519 \quad (35.29)$$

Since the lens is plano-convex (flat side facing test point), the shape factor $X = -1$. So:

$$\sigma_t = 8.7444 + 12.8912Y + 4.32Y^2 + 8.6519 \quad (35.30)$$

Y is the magnification factor:

$$Y = \frac{1+m}{1-m} \quad (35.31)$$

But $m_G = -0.6147$, therefore, $Y = 0.2386$. Inserting this value into Equation 35.30:

$$\sigma_t = 20.718$$

So:

$$W_{040G} = \left(\frac{1}{32} \right) (22.5)^4 (0.004485)^3 (20.718) = 0.01494 \text{ mm} = 14.94 \mu\text{m} = 23.61 \lambda$$

Since the thin lens tuner is at the center of curvature, it will not introduce any

Table 35.2
Alternate solutions for generator lens where SPHA = 21.93 λ .

EFFL	R _G	l _G	l' _G	PMAG	y _G
135	-69.538	-294.249	249.447	-0.8477	15.59
195	-100.442	-497.32	320.778	-0.645	20.05
225	-115.895	-619.106	353.455	-0.5709	22.09
300	-154.527	-998.287	428.886	-0.4296	26.81

significant spherical aberration of its own. So we would like the generator to introduce the same amount of spherical aberration as the value computed earlier for W_{040N} , i.e., 13.88 μm or 21.93 λ . We can use ZEMAX to help us. Place a variable on the convex surface and on the object distance. In Gen, set the paraxial working $f/\# = 8$. In the MFE, turn on EFFL and SPHA (Weight 1). Target values are 223 and 21.93 respectively. PMAG is left off. After the optimization is run, EFFL = 223, SPHA = 21.93, PMAG = -0.5754, object thickness = -610.525, and the back image distance = 351.325.

Actually, there is a whole range of lens focal lengths and object-image conjugates that can accomplish the same task. Some results from ZEMAX are shown in Table 35.2.

35.6.3 Power of Tuning Lens

Next we need a starting power (Φ_T) and radius (R_T) for the tuner (which is also going to be a BK7 plano-convex lens). As indicated in Figure 35.7, the tuner is set up to image the generator onto the parabola. The object distance for the tuner is -351.325 mm (as found by the ZEMAX optimization). The image distance is the radius of the mirror, i.e., 7280 mm.

$$\Phi_T = \frac{-1}{l_T} + \frac{1}{l'_T} = \frac{1}{351.325} + \frac{1}{7280} = 0.002984 \quad (35.32)$$

Therefore:

$$f_T = 335.151 \text{ mm}$$

and:

$$R_T = -0.51509f_T = -172.633 \text{ mm}. \quad (35.33)$$

35.7 Null Lens in ZEMAX

Now we combine the generator, tuner (with a 10-mm thickness), and the parabolic mirror. We will reflect off the mirror and use the M-solve. At this point, however, we will *not* ray trace back through the null lens. In the MFE we have the operands EFFL, SPHA, and PMAG, all of which will be turned off. But we now add the operand RAID at the mirror surface and use it four times for pupil p_y values of

Section 35.7: Null Lens in ZEMAX 409

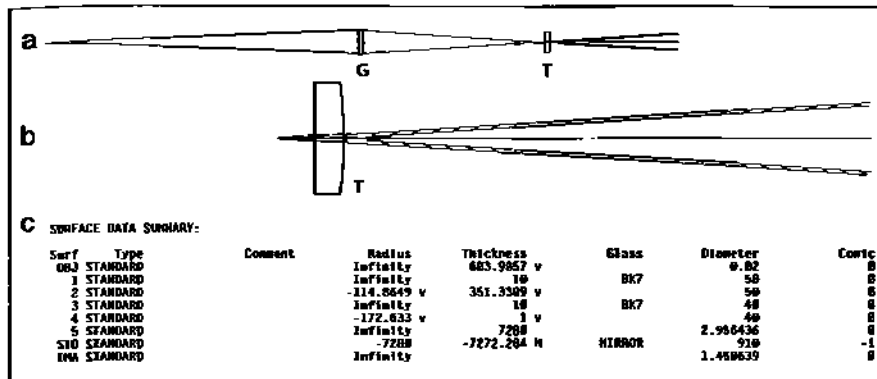


Fig. 35.8 Partial layout of system showing: (a) null lens; (b) a blowup detail around tuner; (c) prescription.

0.25, 0.50, 0.75, and 1. RAID gives us the real ray angle of incidence (in degrees) at the surface. After inserting RAID hit update and look at the numbers in the value column. What we want to do in this optimization is drive these values down to much smaller numbers, i.e., we want to drive the rays toward normal incidence. (Remember that the purpose of the null lens is to make the rays coincident with the surface normals.) Leave the RAID weights at 1. Figure 35.8a shows the initial layout of the null lens, and Figure 35.8b shows further detail around the tuner. Note the separation between the outgoing and returning marginal ray. This separation is due to the fact that the outgoing ray is not coincident with the marginal surface normal of the mirror. In other words the angle of incidence for this ray is not 0°. The prescription with assigned variables is shown in Figure 35.8c.

The MFE is presented in Figure 35.9a for the pre-optimization case, and the post-optimization case is shown in Figure 35.9b. Note that the RAID values for the latter are much smaller than the former.

The next step is to assemble the full double-pass system and couple the back half to the front using pickup. The layout is shown in Figure 35.10 along with the pre-optimized prescription (and assigned variables). The OPD plot and spot diagram are shown in Figure 35.11. Note that the use of RAID has already gotten us to a diffraction-limited condition.

Although the pre-optimized null lens is good, further optimization can make it even better. Go to Field and get rid of the 0.01° field angle. Go to the MFE and insert TRAC after the RAID lines. This will give you 3 lines of TRAC operands. Now go back and reinsert your 0.01° so that PMAG will work. Set the PMAG target to -1 and Weight 1. Active operands will now be PMAG, RAID and TRAC. Run the optimization. The post-optimized OPD and spot diagram are shown in Figure 35.12. The null lens is now extremely good.

The 91-cm f/4 parabola represents a fairly benign case for a null lens design. When spherical aberration values in the hundreds or thousands of waves, the

410 Chapter 35 Null Lens Design

Merit Function Value: 3.6947468E-903									
Num	Type	Int1	Int2	Hx	Hy	Px	Py	Target	Weight
1	EFPL	1				2.23000E-002		-3.51383E+002	6.000
2	SPRA	#	1			2.19300E-001		-2.62512E+001	6.000
3	PMAG					0.00000E+000		5.85791E-001	6.000
4	RAID	6	1	0.0000	0.0000	0.0000	0.2500	0.00000E+000	5.58179E-004
5	RAID	6	1	0.0000	0.0000	0.5000	0.5000	0.00000E+000	1.97069E-003
6	RAID	6	1	0.0000	0.0000	0.7500	0.7500	0.00000E+000	3.18392E-003
7	RAID	6	1	0.0000	0.0000	1.0000	0.0000	0.00000E+000	4.83131E-003

b. Merit Function Value: 1.41582346E-906									
Num	Type	Int1	Int2	Hx	Hy	Px	Py	Target	Weight
1	EFPL	1				2.23000E-002		-2.57681E+002	6.000
2	SPRA	#	1			2.19300E-001		-2.18000E+001	6.000
3	PMAG					0.00000E+000		5.85791E-001	6.000
4	RAID	6	1	0.0000	0.0000	0.0000	0.2500	0.00000E+000	1.78750E-006
5	RAID	6	1	0.0000	0.0000	0.5000	0.5000	0.00000E+000	5.68434E-014
6	RAID	6	1	0.0000	0.0000	0.7500	0.7500	0.00000E+000	2.25887E-006
7	RAID	6	1	0.0000	0.0000	1.0000	0.0000	0.00000E+000	5.68434E-014

Fig. 35.9 MFE before (a) and after (b) the optimization.

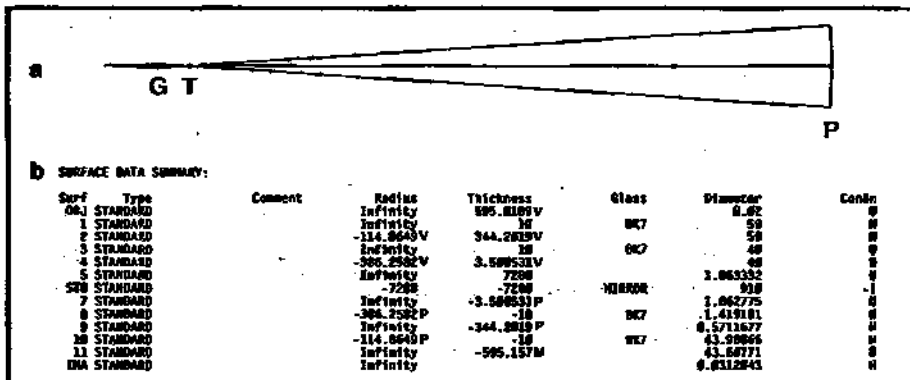


Fig. 35.10 Layout of double-pass system and prescription prior to optimization.

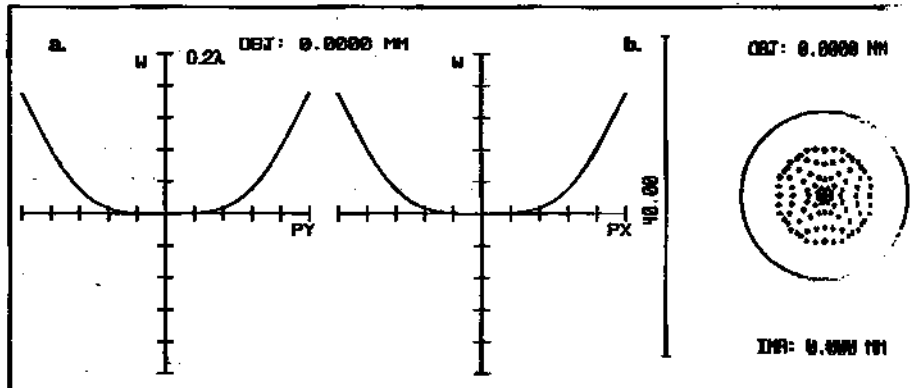


Fig. 35.11 Pre-optimized OPD (a) and spot diagram (b).

design is more challenging. For example, consider the null lens design for a 10" diameter $f/0.6$ parabola. This becomes $f/1.2$ at the radius of curvature. Here the parabola has over 3600λ (HeNe) of spherical aberration. This means that the

Section 35.7: Null Lens In ZEMAX 411

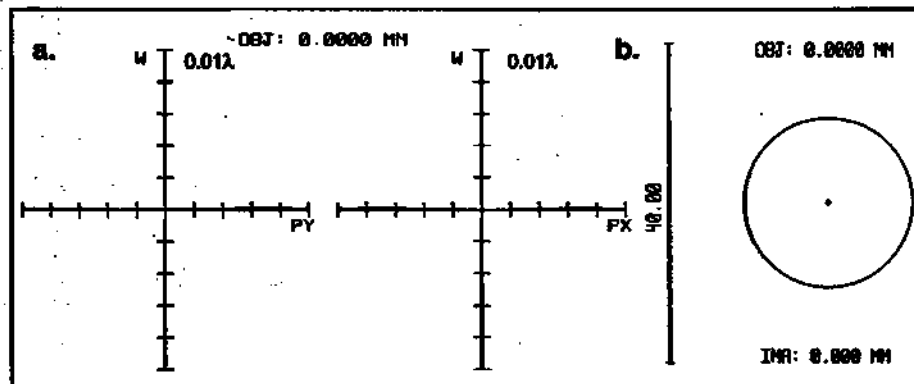


Fig. 35.12 Post-optimized OPD (a) and spot diagram (b).

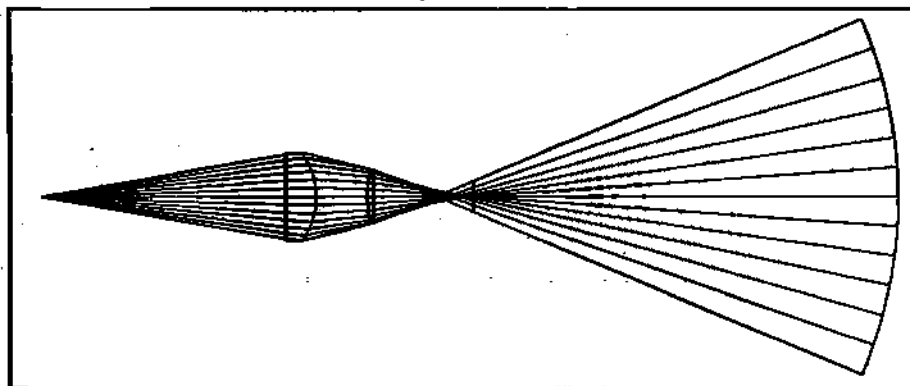


Fig. 35.13 Post-optimized layout for fast parabola-null lens system.

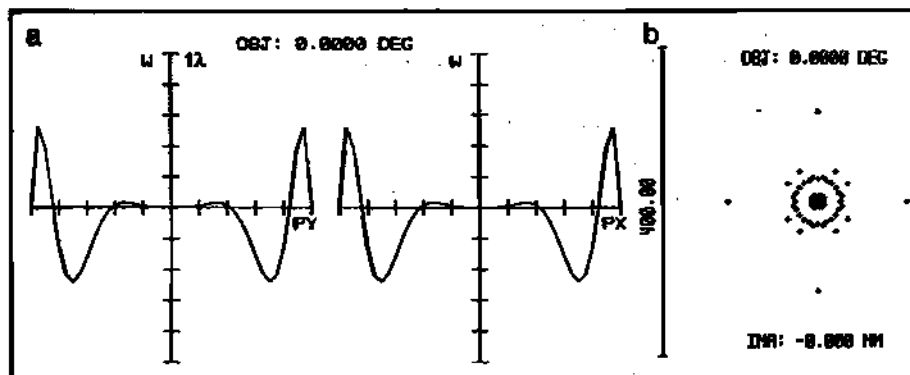


Fig. 35.14 OPD plot (a) and spot diagram (b) for system shown in Figure 35.13.

surface normal spherical, W_{non} , is over -1800λ . However, the basic procedure outlined here can still be successfully implemented. Figure 35.13 shows an Offner design using a pair of plano-convex BK7 lenses. The OPD plot and spot diagram are shown in Figure 35.14. This design is not diffraction-limited, but does allow the possibility of using commercial off-the shelf photo convex lenses. The design

412 Chapter 35 Null Lens Design

can be further improved by allowing all four surface radii to vary.

Chapter 36

Final Exam

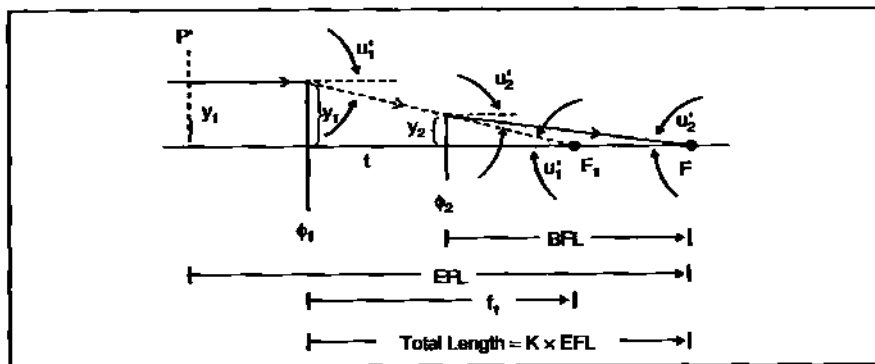


Fig. 36.1 First order layout of the telephoto lens.

36.1 Introduction

Except for a few remaining tidbits, this course is essentially over. The final exam will involve the design of a telephoto lens. The telephoto lens is one in which the rear principal plane (from which the EFL is measured) sits way out in front of the lens. This results in a long focal length lens in a short overall package. Another way of putting it is that the total track of the lens (first surface to image surface) is shorter than the EFL. You will do all the manual pre-design first, followed by the ZEMAX optimization. The background design philosophy of the telephoto will be provided in this chapter.

36.2 First Order Telephoto

The telephoto consists of two major lens components: a positive lens followed at some distance by a negative lens. The first order layout is shown in Figure 36.1 with all the pertinent parameters indicated.

Our goal in this section is to determine the powers (focal lengths) of the front and back components of the telephoto. We'll do this using the PRTE.

36.2.1 Focal Length of Positive Component

From the bending equation we know that the marginal ray angle after the first component is given by:

$$u'_1 = -y_1 \phi_1 = \frac{-y_1}{f_1} \quad (36.1)$$

Next, using the transfer equation, we find the marginal ray height on the second component.

$$y_2 = y_1 + u'_1 t_{12} \quad (36.2)$$

Substituting in Equation 36.1:

$$y_2 = y_1 + \left(\frac{-y_1}{f_1} \right) t_{12} \quad (36.3)$$

$$y_2 = y_1 \left(1 - \frac{t_{12}}{f_1} \right) \quad (36.4)$$

Now obtain the ratio of marginal ray heights at the two component surfaces:

$$\frac{y_2}{y_1} = \frac{f_1 - t_{12}}{f_1} \quad (36.5)$$

From the transfer equation applied at the second component:

$$y_3 = 0 = y_2 + u'_2 t_{23} \quad (36.6)$$

But t_{23} is the back focal length:

$$t_{23} = \text{BFL} \quad (36.7)$$

Substituting Equation 36.7 into Equation 36.6 and solving for u'_2 :

$$u'_2 = \frac{-y_2}{\text{BFL}} \quad (36.8)$$

However, if you examine Figure 36.1 closely you will also see that:

$$u'_2 = \frac{-y_1}{\text{EFL}} \quad (36.9)$$

Equating Equations 36.8 and 36.9:

$$\frac{y_2}{\text{BFL}} = \frac{y_1}{\text{EFL}} \quad (36.10)$$

or

$$\frac{y_2}{y_1} = \frac{\text{BFL}}{\text{EFL}} \quad (36.11)$$

Section 36.2: First Order Telephoto 415

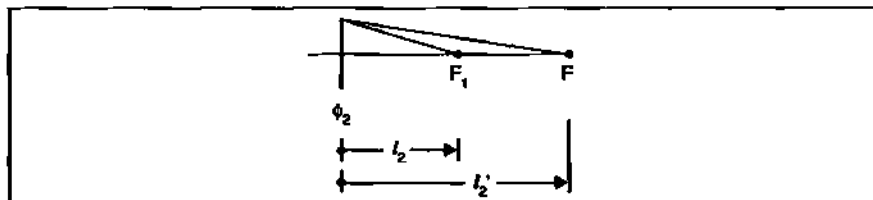


Fig. 36.2 Object-image conjugates for negative component.

Again, looking at Figure 36.1 we see that:

$$BFL = \kappa \cdot EFL - t_{12} \quad (36.12)$$

where κ is a fraction called the *telephoto ratio*.

From now on we will let $f = EFL$ and $t = t_{12}$. Equation 36.12 becomes:

$$BFL = \kappa f - t \quad (36.13)$$

Substitute Equation 36.13 into Equation 36.11:

$$\frac{y_2}{y_1} = \frac{\kappa f - t}{f} \quad (36.14)$$

Now combine Equations 36.14 and 36.5:

$$\frac{f_1 - t}{f_1} = \frac{\kappa f - t}{f} \quad (36.15)$$

Solve for f_1 :

$$(f + t - \kappa f)f_1 = tf$$

$$f_1 = \frac{tf}{f + t - \kappa f} \quad (36.16)$$

36.2.2 Focal Length of Negative Component

The focal length of the negative component can be found with the help of the Gaussian lens formula as illustrated in Figure 36.2. Here we see the second component, the focal point F_1 due to the first component, and the system focal point F due to both components.

The distance between the vertex of the second component and F_1 is the object distance l_2 . The separation between the vertex and F is the corresponding image distance l_2' .

$$\frac{-1}{l_2} + \frac{1}{l_2'} = \frac{1}{f_2} \quad (36.17)$$

From Figure 36.1 we see that:

$$l_2 = f_1 - t \quad (36.18)$$

and that:

$$l'_2 = BFL = kf - t \quad (36.19)$$

Substitute Equations 36.18 and 36.19 into Equation 36.17:

$$\frac{1}{f_2} = \frac{-1}{f_1 - t} + \frac{1}{kf - t} \quad (36.20)$$

Getting the righthand-side under a common denominator:

$$\begin{aligned} \frac{1}{f_2} &= \frac{-(kf - t) + (f_1 - t)}{(f_1 - t)(kf - t)} \\ \frac{1}{f_2} &= \frac{-kf + f_1}{(f_1 - t)(kf - t)} \end{aligned} \quad (36.21)$$

Solving for f_2 :

$$f_2 = \frac{(f_1 - t)(kf - t)}{(f_1 - kf)} \quad (36.22)$$

36.2.3 Example

Let the system focal length be 10", and the telephoto ratio be 0.8. There is a whole family of positive-negative lens pairs that will satisfy these conditions as a function of t .

From Equation 36.16:

$$\left. \begin{array}{l} f_1 = \frac{10t}{2+t} \\ \text{From Eq. 36.22} \\ f_2 = \frac{(f_1 - t)(8 - t)}{f_1 - 8} \end{array} \right\} \quad (36.23)$$

Suppose we let $t = 3"$, then $f_1 = 6"$ and $f_2 = -7.5"$. A plot of $f_1(t)$ and $f_2(t)$ is shown in Figure 36.3.

36.2.4 Preparation For ZEMAX Telephoto Optimization

Once the lens powers for the front and back components of the telephoto are obtained, you must achromatize each separately using the thin lens power formulas from Chapter 16. So now you will have two powers for the front telephoto component and two powers for the rear telephoto component. Each of these achromats will be contact (or cemented) achromats.

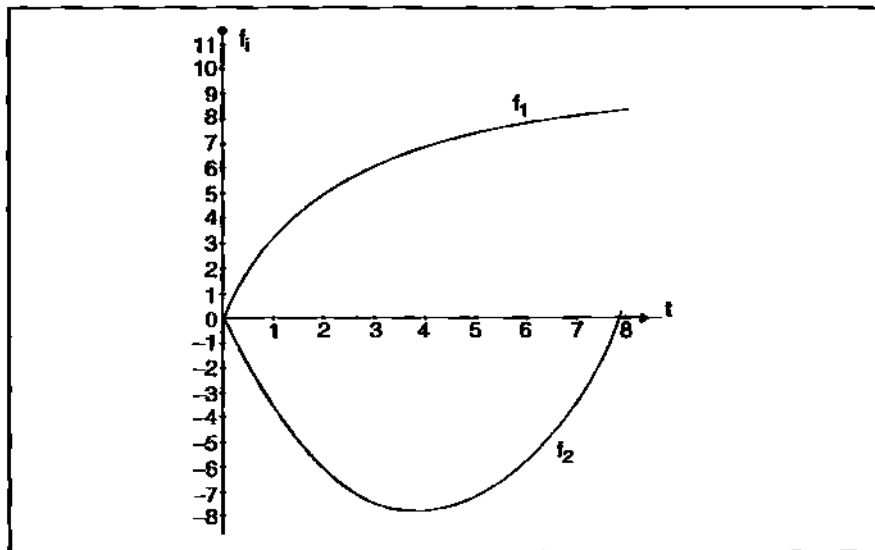


Fig. 36.3 Plots of telephoto lens pairs as a function of t for $f = 10"$ and $k = 0.8$.

The next step is finding (using Equation 4.22 on page 40) the starting radii that can be inserted into ZEMAX. You can initially assume that the front achromat crown is equi-convex, and that the rear half crown is equiconcave. Altogether you need to find six radii. Insert each achromat into ZEMAX separately. Assign real thicknesses to each. Optimize both to regain the proper EFL and color correction.

Assemble the front and rear halves with the initial t value stated in the example. Place the stop midway between the lenses. Tweak the assembled system to restore *all* the first order properties of the system. This includes the system EFL and $f/\#$, the focal lengths of the front and rear halves, the desired total track, and axial color. Allow the front inter-lens airspace to float, and slave the rear airspace to the front.

36.3 Telephoto in ZEMAX

Now that all the first order properties are where they should be, it's time to start working on the aberrations. Look at SPHA. It is going to be a huge number. You need to knock this down using lens bending. As the lenses bend, their respective principal planes will shift around to insure the proper separation between P'_1 and P'_2 so that the first order properties of the system will be maintained. Keep this flexibility as you add field. When you add field, it is suggested that you do so in several stages. The apertures of the lenses will increase in diameter with increasing field so keep an eye on the layout to make sure that lens thicknesses are sufficient to prevent premature surface crossings. After you have optimized for full field (still keeping all first order conditions) look at the *Layout* (and use about 7

418 Chapter 36 Final Exam

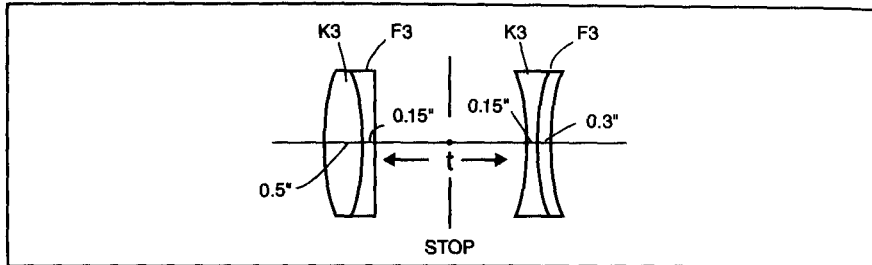


Fig. 36.4 Starting telephoto configuration.

rays under Layout's *Settings*). Note that the meridional ray distribution at the paraxial image plane for the 10° field is terrible; RMS spot sizes at the three field positions are in the mid-hundreds, and axial color is off quite a bit, but there is room for some significant improvement even under the strict conditions imposed. To improve things somewhat, let the stop position float *within* the inter-lens airspace while holding the thickness of that airspace at its current value. Also hold the current radii values.

More dramatic improvements can be realized by *relaxing* the strict telephoto constraints. You must maintain the first order properties of the system (EFL and f/#), and keep the total track within 3% of its pre-design value. You can let the stop position float *within* the inter-lens airspace (while holding the thickness of that airspace constant). Lateral color is going to be troublesome, and you will likely have to accept a compromise. Axial color, on the other hand, should be well controlled.

From this point on you are on your own. Good luck!

36.4 Final Exam

Design a 10" EFL f/5.5 achromatic telephoto lens with a telephoto ratio of 0.8 (which can be controled using the TOTR operand). The lens should be designed for the F, e, C spectrum using Schott K3 and F3 glasses. The field is $\bar{U} = 10^\circ$. Let $t = 3"$ in the pre-design (and for the initial separation in ZEMAX). The stop can be *initially* placed midway between the front and back components. Initial lens thicknesses are indicated in Figure 36.4. Table 36.1 provides data on the glass for the manual calculation.

Table 36.1		
Glass	Crown	Flint
Schott	K3	F3
n_e	1.52031	1.6168
v_e	59.15	37.18

Section 36.4: Final Exam 419

Meet or beat the following RMS spot sizes (using square; centroid):

Table 36.2		
	Strict	Relaxed
\bar{U}	RMS	RMS
0°	236 μm	34 μm
7°	245	77
10°	283	114

For the strict case, maintain the powers of the front and rear components to those calculated manually, and keep the Stop midway between those components. For the relaxed case, the total track must be within 3% of its specified value.

You should have excellent color correction, and the sagittal and tangential fields should appear reasonably flat.

Suggested folder name: Telephot and file name: Telf1o1b, etc

Chapter 37

The Attic

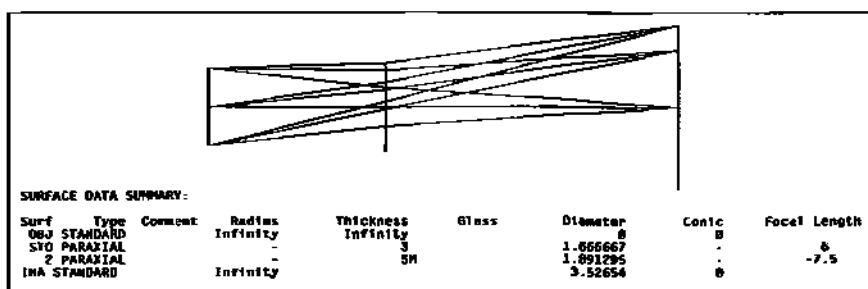


Fig. 37.1 A paraxial telephoto lens.

37.1 Introduction

You can think of this chapter as the course's attic. It contains a hodgepodge of useful information that did not quite fit in anywhere "downstairs," but we did not want to throw-away.

37.2 Paraxial Lenses

There is a useful feature in ZEMAX under *Surface Type* called *Paraxial*. We saw it employed briefly in Chapter 22 where it was used to represent the eye's lens. But ZEMAX's paraxial lenses can be used to model all the thin lens pre-designs discussed in the course. Perhaps another example will best illustrate this point. Since you are in the middle of your telephoto take-home exam, let's use paraxial lenses to model a telephoto. We'll use the example from Section 36.2.4. There the front positive element had a 6" focal length, the rear negative element focal length was -7.5", and the separation between the two was 3 inches. When inserting these lenses into ZEMAX you bypass the *Radius* column and insert data under the *Focal Length* header (located to the right of the *Conic* header). No data is entered under the *Glass* header. However, aperture sizes must be included (which can be done by specifying an *Aper Type* under *General Systems Data*). Figure 37.1 shows the paraxial layout (along with the prescription) of your exam problem. If you check the *Sys* data, you'll see that this is indeed a 10" EFL f/6 system. Paraxial lenses, being ideal, do not introduce any aberration. Call up the spot diagram. You'll see

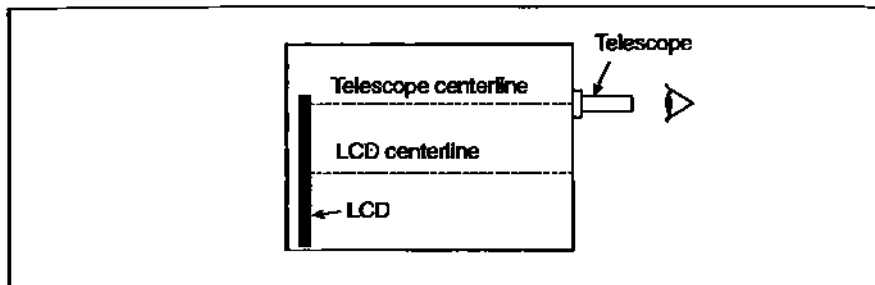


Fig. 37.2 Customer's box showing location of LCD and telescope.

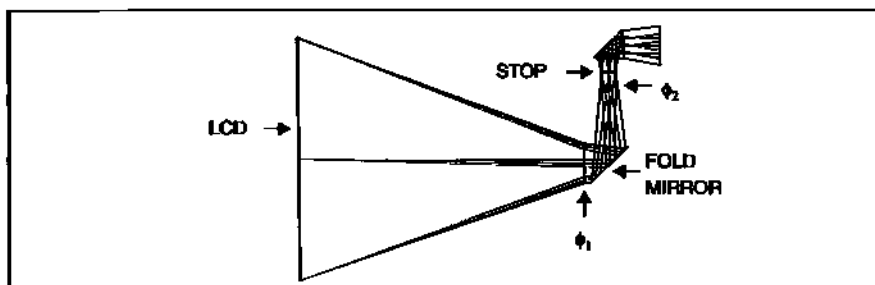


Fig. 37.3 Inverted telephoto with two 90° folds.

SURFACE DATA SUMMARY:

Surf	Type	Comment	Radius	Thickness	Glass	Diameter	Conic	Tilt About X
06J STAND			Infinity	11		9.2	B	
1 PARAXIAL			-	1		1.5	-	
2 COORDBRK			-	8		-	-	45
3 STANDARD			Infinity	8	MIRROR	2.052988	B	
4 COORDBRK			-	.3		-	-	45
5 PARAXIAL			-	-0.5		0.7533527	-	
STO STANDARD			Infinity	-1		0.6	B	

Fig. 37.4 Prescription (Lines 1- 6) for layout shown in Figure 37.3.

a dot in the center of the Airy disk. The system is diffraction limited out to 10° (and beyond). If only the real lens design was this simple, but then lens design would not offer much by way of employment opportunities.

37.3 Tilting a Flat Mirror

If fold mirrors are needed in a system, you will usually find them either before or after the photographic objective. However, situations can arise in which overall system geometry and space constraints force locating a fold flat *within* the objective. The following is a real case. The customer wanted to observe a large liquid crystal display (LCD) through a telescope that was displaced laterally several inches away from the center of the display. Furthermore, the box in which all the components were to be placed was cramped. The geometry is illustrated in Figure 37.2.

Section 37.4: Right Angle Prism 423

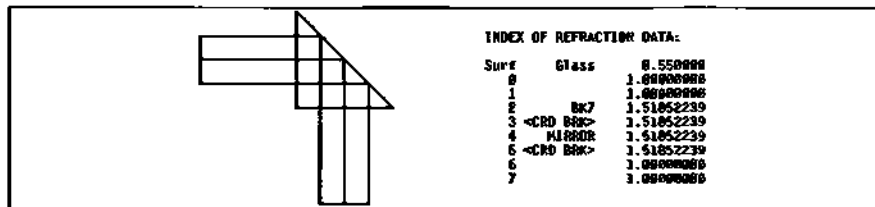


Fig. 37.5 Layout for right angle prism.

SURFACE DATA SUMMARY:

Surf	Type	Comment	Radius	Thickness	Glass	Diameter	Conic	Tilt About X
OBJ STANDARD			Infinity	Infinity		0	0	
STO STANDARD			Infinity	1		0.5	0	
2 STANDARD			Infinity	0.5	BK7	1	0	
3 COORDBK			-	0		-	-	-45
4 STANDARD			Infinity	0	MIRROR	1.4142	0	
5 COORDBK			-	-0.5		-	-	-45
6 STANDARD			Infinity	-1		1	0	
IMA STANDARD			Infinity			0.5	0	

Fig. 37.6 Prescription for right angle prism.

The solution called for a telephoto lens because we needed a long EFL compared to the tight space available. The telephoto would also be used backwards. The separation required between the positive and negative components forced locating a 90° fold flat between them. Another 90° fold was needed exterior to the telephoto to complete the connection between the LCD and the observer's telescope. The layout (using paraxial lenses) is illustrated in Figure 37.3.

Let's look at the prescription shown in Figure 37.4. The internal mirror is shown on Line 3. It is *sandwiched* between two *Coordinate Breaks* which are obtained from the *Surface Type* menu.

For a fold mirror, the *Coordinate Break* requires angle information (in degrees) which is located under the *Tilt About X* header lying three spaces to the right of the *Conic* header. For the internal 90° fold, +45° is inserted for the *Coordinate Break* ahead of, and also behind, the mirror surface.

37.4 Right Angle Prism

You'll notice that the exterior 90° fold in Figure 37.3 is accomplished using a right angle prism. The layout of a stand-alone right angle prism is illustrated in Figure 37.5 along with the corresponding prescription in Figure 37.6. The orthogonal faces of the prism are 1" wide. The collimated incident beam is a half inch in diameter as set by the stop. (This allows you to see the prism clearly.) The glass is BK7. The incident face of the prism is on Line 2, and the thickness to the hypotenuse is 0.5". There is a *Coordinate Break* on Line 3 with a *Tilt About X* of -45°. Although there is no radius or diameter specified for this *Coordinate Break*, the medium is still assumed to be glass. If you look up the *Index of Refraction Data* after clicking on *Pre* you'll see that Lines 3, 4, and 5 have the BK7 index associated with it. There is a thickness given on this Line 5 as well that takes us from the mirror surface to the exit face of the prism (a distance of 0.5"). The index on Line 6 is air.

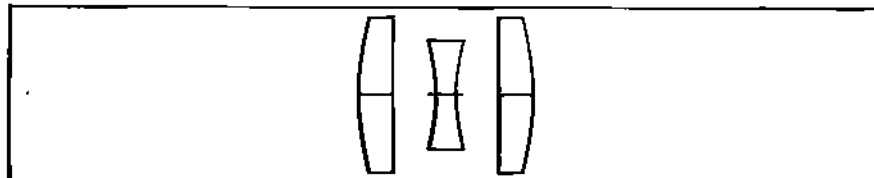


Fig. 37.7 An aligned optical system.

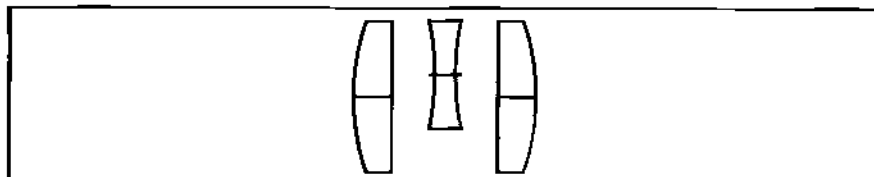


Fig. 37.8 Example of lens decentration.

SURFACE DATA SUMMARY:								
Surf	Type	Comment	Radius	Thickness	Glass	Diameter	Conic	Decenter Y
OBJ	STANDARD		Infinity	Infinity		8	0	
1	STANDARD		2.894199	0.3	SK16	1.28	0	
2	STANDARD		-15.79423	0.3446022		1.28	0	
3	COORDBK		-	0		-	-	
STB	STANDARD		-2.41665	0.2	F4	0.92	0	0.2
5	STANDARD		2.41665	0		0.92	0	
6	COORDBK		-	0.3446022		-	-	-0.2
7	STANDARD		15.79423	0.3	SK16	1.28	0	
8	STANDARD		-2.894199	4.274346		1.28	0	
IMA	STANDARD		Infinity			1.050652	0	

Fig. 37.9 Prescription for decentered system shown in Figure 37.8.

37.5 Lens Alignment

Throughout this course all components of a multi-element optical system had their respective optical axes aligned as illustrated by the triplet in Figure 37.7. It is essential that the real manufactured lens also have its components properly aligned. If this alignment is not achieved, aberrations are introduced, that will degrade image quality. Lens decentration and tilt are two culprits which will cause problems. The effects these have on image quality can be modeled in ZEMAX. Lenses can be decentered and tilted relative to one another. This would be part of what's called a *tolerance analysis*. Here we are going to see how you introduce decentration and tilt on a lens using ZEMAX.

37.5.1 Lens Decentration

We are going to illustrate lens decentration by shifting the negative element in the triplet laterally as shown in Figure 37.8. In the prescription shown in Figure 37.9, the entire negative element (Lines 4 and 5) is sandwiched between two *Coordinate Breaks* (Lines 3 and 6). The only entry needed for the first *Coordinate Break* is under the header *Decenter Y*. The number entered here is the amount of vertical offset in lens units. In this example, we use +0.2 which shifts the attached local coordinate system upwards by two tenths of an inch. Note that the thickness on Line 5, the second surface of the negative element, is zero. This is normally where

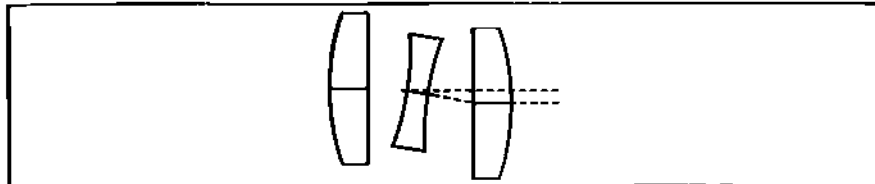


Fig. 37.10 Improperly executed tilt of center lens.

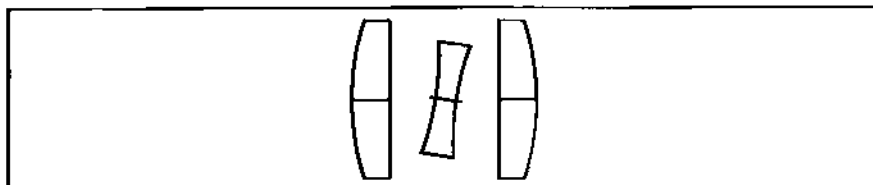


Fig. 37.11 Properly executed tilt of center lens.

the distance to the next optical surface would be placed. However, this thickness will now be attached to the second *Coordinate Break* on Line 6. Under the *Decenter Y* header we insert -0.2 to restore the local coordinate system to its original condition.

37.5.2 Lens Tilt

To tilt the center lens we maintain the *Coordinate Breaks* on the same two lines (3 and 6). This time we will insert angles (in degrees) under the *Tilt About X* header. On Line 3 we insert $+20^\circ$, and on Line 6, -20° . Left alone, our layout would look strange as shown in Figure 37.10. Note that the rear positive lens is decentered with respect to the front positive lens.

To fix this we work with the values under the *Thickness* header. On Line 5, the last surface of the negative lens, we insert a thickness of $-0.2''$. This relocates the second *Coordinate Break* back to the front surface of this lens (where the first *Coordinate Break* was placed). In essence, both *Coordinate Breaks* are now coincident. So the tilt restoration takes place at the same location where it was disturbed to begin with. The thickness assigned to the second *Coordinate Break*, Line 6, (which will take us to front surface of the rear positive lens) includes the thickness of the negative element ($0.2''$) as well as the rear interlens airspace (0.3447). So this thickness becomes $0.5447''$. With these modifications the layout now appears as shown in Figure 37.11.

37.6 Off-Axis Parabola

There is one significant application of decentration that we must talk about. Off-axis parabolas (OAP) are very important in modern optical systems. Their particular attraction is the lack of a central obscuration. OAPs are often found in test sys-

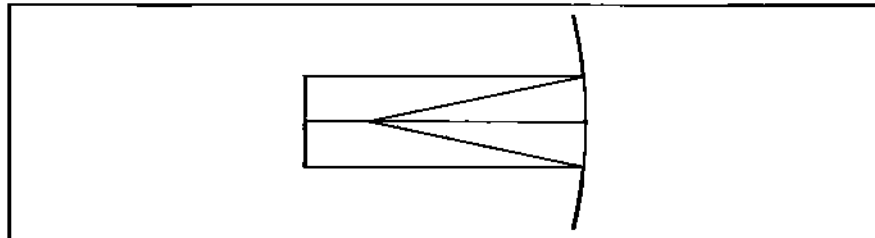


Fig. 37.12 On-axis parabolic mirror with stop in front.

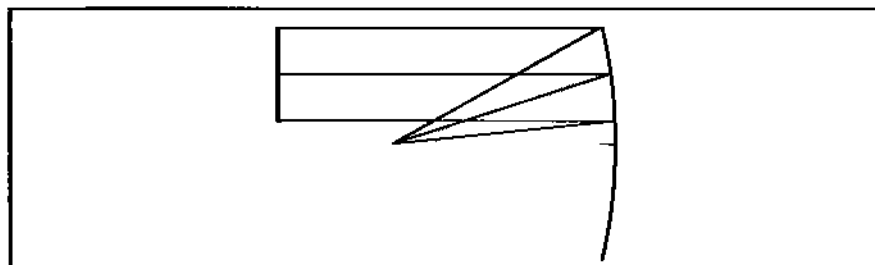


Fig. 37.13 Stop with decentered full parabola.

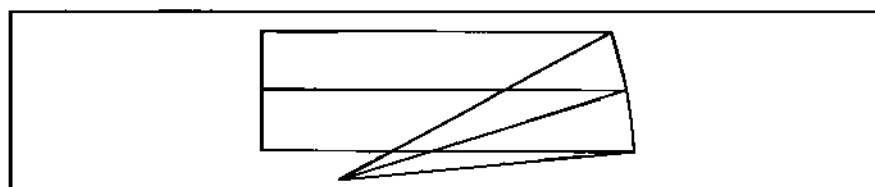


Fig. 37.14 Off-axis parabola.

tems such as collimators. What we'll do now is show you how to model an OAP in ZEMAX. We start with a rotationally symmetric 100-mm/f2.5 parabolic mirror as shown in Figure 37.12. We have placed a stop in front of the mirror at an arbitrary distance of 125 mm. The stop is 40 mm in diameter. Now insert a new surface between the stop and the parabola. Make it a *Coordinate Break*. Go out to the header *Decenter Y* and insert a value of -30. The result is shown in Figure 37.13. We still see the full parabola, but we are only using the upper portion of it. To restrict the layout to show only the working portion, we impose a hard aperture on the mirror surface itself. Go to the mirror line and double click on the *Standard* box. Select *Aperture Type* → *Circular Aperture* → *Max Radius = 20* → *Aper Y Decenter = 30* → *OK*. The result is the OAP shown in Figure 37.14.

37.7 Aberrations Induced by Decentration

The following is a true story. It took place not so long ago in geological time and in this very galaxy. The name has been changed to protect the author. Arthur, a young optical engineer, wanted to see, empirically, how the Airy pattern evolved

Section 37.7: Aberrations Induced by Decentration 427

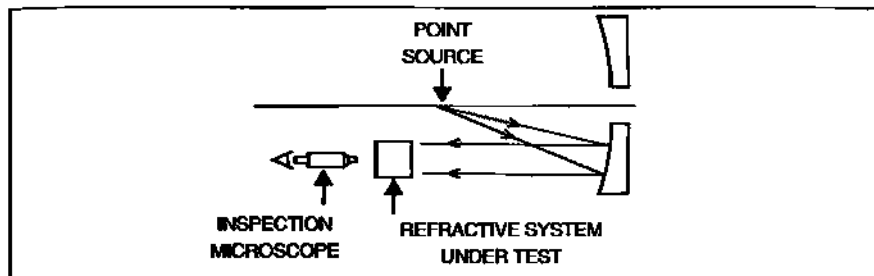


Fig. 37.15 Arthur's experiment to view the Airy pattern.



Fig. 37.16 Paraxial lens intercepting the full mirror beam.

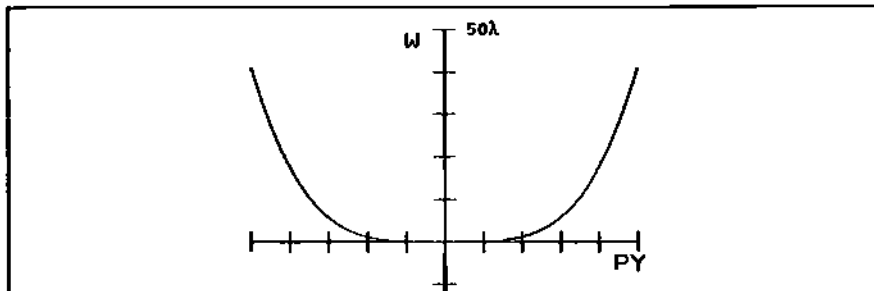


Fig. 37.17 OPD profile across beam from the mirror.

with defocus. He set up an experiment using available equipment. He placed a spatially filtered HeNe point source at the focal point of a high-quality *spherical mirror*. This became his collimator. He also had a very good photographic lens which he carefully aligned to the collimator. But since the mirror had a central hole in it, he had to laterally offset his lens so that its aperture would be fully illuminated. He then set up a microscope to examine the image formed by the lens. His experimental setup is illustrated in Figure 37.15.

Arthur peered into the microscope utterly confident that he would see a defocused Airy pattern. What he actually saw stunned him. He saw lots of off-axis aberrations. He double checked his alignment (and even pulled out the performance records on both the mirror and the lens). He could find nothing wrong. Arthur had a perfect mirror and lens perfectly aligned, but a lousy image. Can you guess what happened?

Let's use ZEMAX to model Arthur's experiment. We'll place a point source

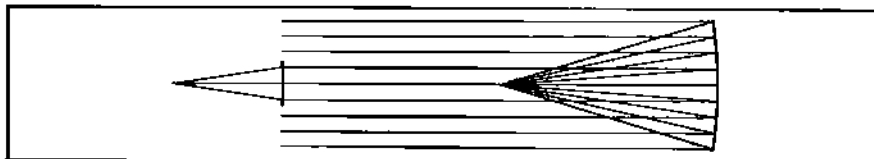


Fig. 37.18 Small paraxial lens intercepting the mirror beam.

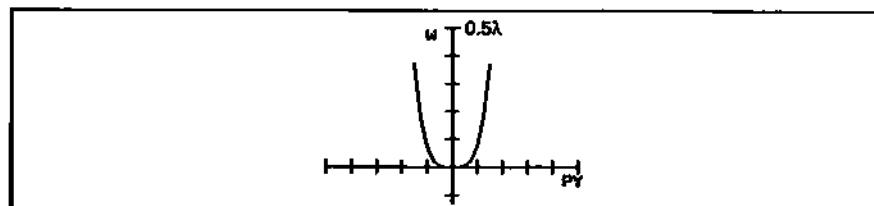


Fig. 37.19 OPD profile across mirror beam defined by smaller lens aperture.

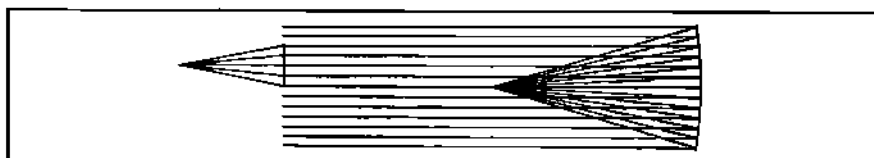


Fig. 37.20 Decentered paraxial lens intercepting the mirror beam.

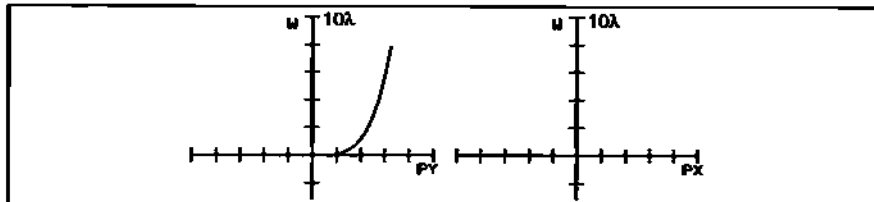


Fig. 37.21 OPD profiles across mirror beam defined by decentered lens aperture.

at the focal point of a 100-mm $f/1.67$ spherical mirror. The resulting “collimated” beam will have spherical aberration imposed on it after the reflection. A certain distance away we place a *paraxial* lens ($EFL = 50$ mm) having the same diameter as the mirror. It catches the beam and brings it to a focus. The layout is shown in Figure 37.16. The amount of spherical aberration is shown by the OPD profile in Figure 37.17. There’s about 40 waves of it.

If we make the paraxial lens 20 mm in diameter as indicated in Figure 37.18, the amount of spherical aberration in the imaging beam will be dramatically reduced as can be seen in Figure 37.19. Now we are down to less than 0.4 waves.

Now let’s shift the smaller diameter paraxial lens upward from the mirror axis by 10 mm as shown in Figure 37.20. The OPD plots along the Y and X pupil axes are no longer the same as can be seen in Figure 37.21. In fact along the Y-

Section 37.7: Aberrations Induced by Decentration 429

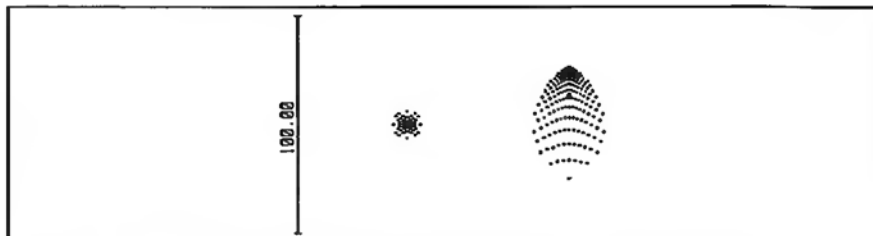


Fig. 37.22 Comparing spot diagrams for centered and decentered lens positions.

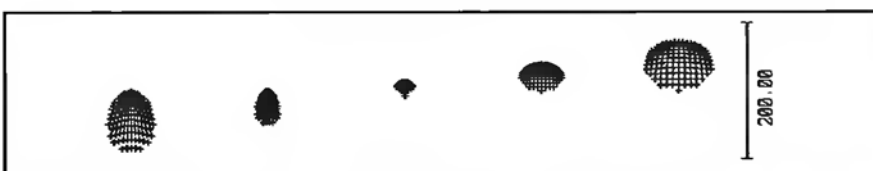


Fig. 37.23 Astigmatism detected via a through focus spot diagram.

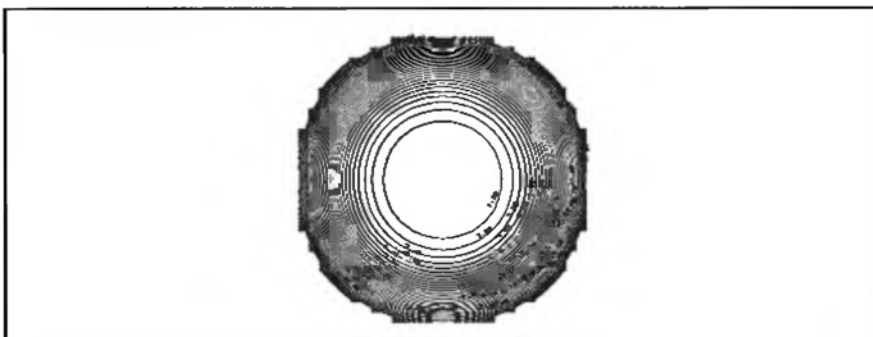


Fig. 37.24 OPD contour (fringe) map of full mirror beam.

axis the profile is highly asymmetric. Also note that the scale is 10 waves, not the previous 0.5 waves (even though the lens aperture size is the same).

Next, compare the spot diagrams for the on-axis and decentered cases as shown in Figure 37.22. The former is symmetric, but the latter shows a lot of coma. In fact, if we run a through focus spot diagram (Figure 37.23), we can see that astigmatism is also present.

How can coma and astigmatism pop up in a beam that originally had only spherical aberration? Look at Figure 37.24. This is an OPD contour map of the full beam from the mirror. Each circular line is a contour of constant OPD, and each line is 1 wave different from its nearest neighbors. (A profile across a diameter is what was plotted back in Figure 37.17.) Now superimpose on this map the lens diameter for both on-axis and decentered cases as illustrated in Figure 37.25. The wavefront for the on-axis case is rotationally symmetric and only spherical aber-

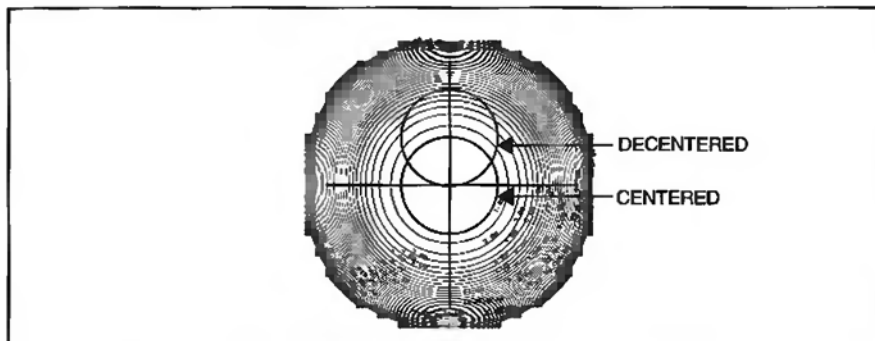


Fig. 37.25 The lens aperture superimposed on the contour map: a) centered; b) decentered. From Linear Systems, Fourier Transforms, and Optics by J. D. Gaskill, © John Wiley and Sons, 1978. Reprinted by permission of John Wiley and Sons, Inc.

wave to Fig 37.26

ration is present. But for the decentered case, there is no rotational symmetry of the contour lines within the lens aperture footprint. This lack of rotational symmetry *is the reason* why Arthur saw coma and astigmatism in the image.

37.8 Zernike Polynomials

Throughout this course we have worked with rotationally symmetric imaging systems. As a consequence, we were able to *calculate* aberration contributions surface by surface based upon a *paraxial* ray trace through the system, and employing the Seidel summations formulated in Table 10.1 on page 111. Using this method, the *Seidel* aberrations were determined. However, as soon as the system becomes non-rotationally symmetric, this technique can no longer be utilized. This occurs when a component is tilted or decentered relative to the rest of the system. To determine aberration content, a great many *real* rays have to be traced (usually on a uniform grid) through the system to establish an OPD map in the exit pupil. You can think of this as a circular piece of graph paper with a rectilinear grid on it. At each point defined by the crossing of orthogonal grid lines, there's a thin vertical stick representing the OPD. If all the sticks are of the same height then there is no aberration. But if the sticks vary in height across this representation of the exit pupil, then there is aberration. But what kind of aberration is it? To find out, we must employ a *wavefront fitting* technique.

This is akin to “fitting” a square profile with sine waves of different spatial frequencies and amplitudes as in done in Fourier analysis. This is illustrated in Figure 37.26.

Our situation is more complicated because it is 2-dimensional with circular geometry and no repetition of the pattern. But there is a (infinite) series of terms called the Zernike polynomial that does the trick. Each term of the Zernike polynomial is defined over the *unit* circle (normalized pupil), and represents a specific

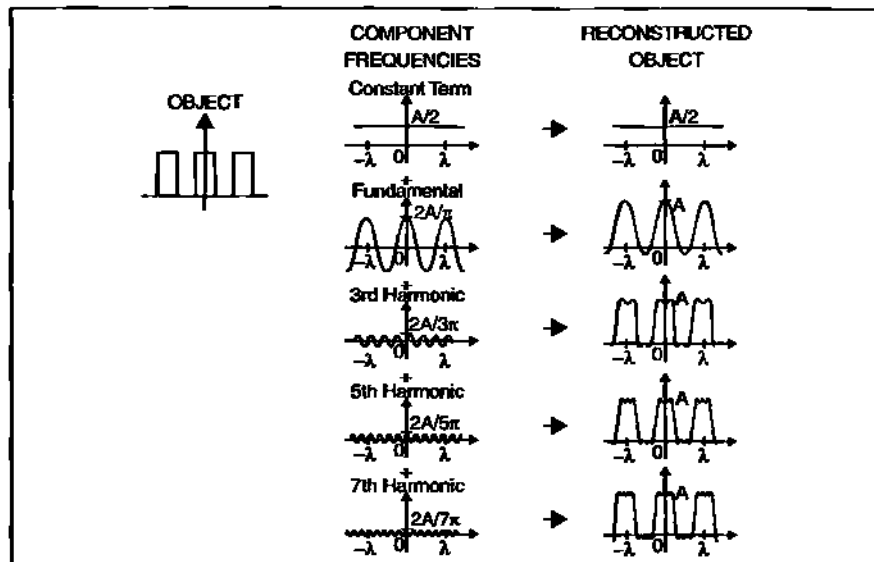


Fig. 37.26 In Fourier analysis, a square wave is approximated using different sine wave components.

3-dimensional surface (x, y pupil locations and OPD heights). Each term contains a coefficient, Z_i , which determines the maximum height at the rim. The coefficients Z_i are independent of each other as a result of an orthogonality condition between terms similar to that found between terms of a Fourier decomposition. If I have an aberrated wavefront in the pupil, I can approximate that wavefront by a properly weighted mixture of Zernike terms. And just like the example shown in Figure 37.26, the approximation gets better and better as more Zernike terms are utilized. The user can select the number of terms employed. (Typically 36 terms are available in most design codes for fitting the OPD map, which is usually sufficient.)

The fitting process works as follows. In the code we have two OPD surfaces. The first is defined by the real ray trace which gives OPD values only at *discrete* points in the pupil. The second surface is that defined by the ensemble of Zernike terms (that has OPD values at *all* points in the pupil). Once the user has selected the number of Zernike terms to use, the software concentrates on the finding the Z_i values that will yield the "best fit" to the discrete OPD data. The best fit is that which minimizes the RMS error between the two surface representations.

For more information on Zernike polynomials, see Chapter 1 in *Applied Optics and Optical Engineering*, Volume XI (Academic Press, 1992). This chapter was authored by Jim Wyant and Kathy Creath. The discussion on Zernike's starts on page 28.

Chapter 38

Fini

38.1 Introduction

We are almost done. This chapter will summarize the things we have learned, introduce the subject of tolerancing, and then (to put things in perspective) point out some of the topics not covered here, but which are suitable for a more advanced course.

38.2 What Has Been Accomplished

This course has been a mixture of both design and analysis. On the design side you learned how to start from scratch using paraxial analysis to come up with a thin lens pre-design. The outputs of pre-design were element powers, surface radii, and element spacings. You then transferred that data to a contemporary design code, ZEMAX. But never lose sight of the fact that the ZEMAX optimization process was built upon your pre-design foundation. Analysis tells us how good (or bad) the design is. Analysis provides enlightenment on the current design, and tells us which areas need improvement.

You learned how to use ZEMAX in this course. You know how to set up a prescription, assign variables, design a merit function, and the order in which things are done. You also learned the importance of bookkeeping (or keeping track of your design) through the use of scripts and filename protocols. (Would it not be embarrassing to end up with a good design and not know how you got there?) You also learned how to use ZEMAX's extensive analysis capability to determine the quality of your design and whether it met specifications.

You also learned where the analysis numbers and plots in ZEMAX come from, and how to compute them with pencil and paper for simple systems. This includes paraxial ray tracing and the use of that data to determine the Seidel aberrations. Refer back to Figure 1.1 (on page 2) to see all the things you learned how to do without a computer.

You gained a lot of practice using ZEMAX through the homework exercises assigned. Starting from a simple singlet, the complexity of the problems gradually increased. This complexity roughly followed the historical progression of photographic lenses. Although photographic lenses formed the backbone of the course, some other imaging systems were incorporated; e.g., designing transmission

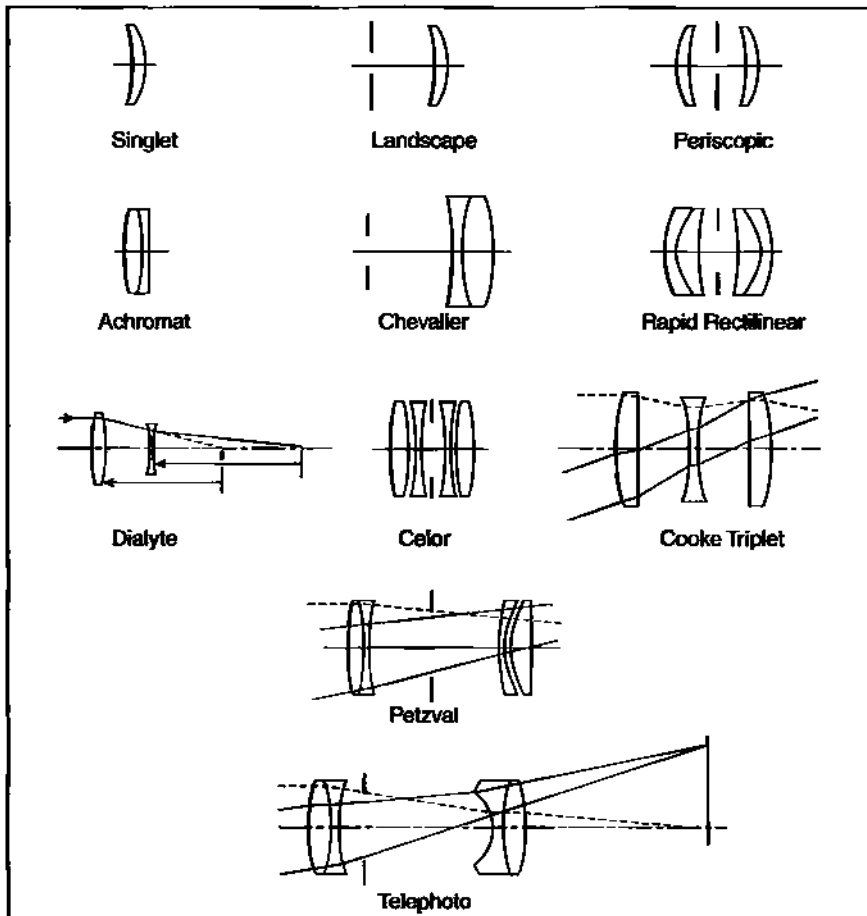


Fig. 38.1 ZEMAX design problems.

spheres for Fizeau interferometers. Figure 38.1 illustrates and summarizes most of the ZEMAX-based problems you confronted in this course.

While wrestling with the various designs shown in Figure 38.1, you learned some of the traditional design techniques which guided your work. These principles are listed below.

1. Restoring first order properties (account for glass thickness)
2. Lens bending (control aberrations)
3. Stop size (control light level, spherical aberration, and f-number)
4. Stop location (control coma, astigmatism, and field curvature)
5. Lens splitting (control spherical aberration)
6. Design from long to short conjugate

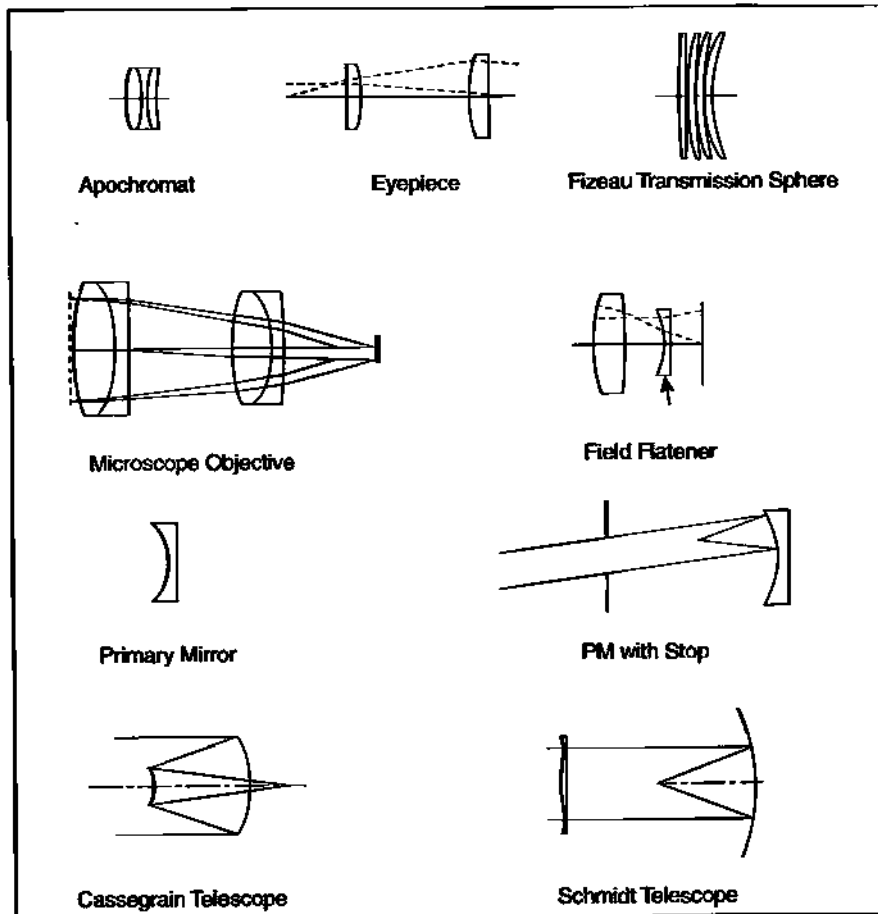


Fig. 38.1 (continued) ZEMAX design problems.

7. Distributing the bending workload
8. Symmetry (control coma, distortion, and lateral color)
9. Design rear half of symmetric system first
10. Allowing symmetric design to go asymmetric
11. Balancing aberrations
12. Petzval sum and field flattening
13. Color correction (achromatic and apochromatic)
14. Use of field lenses
15. Use of aspheric surfaces
16. Degrees of freedom and system parameters (first and third) to be controlled.

38.3 Tolerancing

Suppose that you have a design that meets the specifications required by the customer. Are you done? Absolutely not! Now comes the tedious part. A design is not really complete until you do a *tolerance* analysis to see how sensitive your design is to small variations in index, dispersion, element thickness and spacing, curvatures, element decentration and tilt. These variations come about because of the practical limitations imposed by the manufacturing and assembly process, and by the boundaries set by metrology. You will also have to use melt data, spherometer, thickness and spacing measurements (and perhaps profilometer and/or interferometer data for aspheres) to tweak the design so that the “as built” lens will still meet the specifications. A sensitive design means more care needs to be taken during fabrication and optical testing.

To give you an idea what tolerancing is all about, we’ll do a simple example. Consider a singlet. The specification on the focal length is $f \pm \Delta f$. We’ll work the problem using powers. From Section 4.6.2 we know that:

$$\varphi = \varphi_1 + \varphi_2 - \left(\frac{t}{n} \right) \varphi_1 \varphi_2 \quad (38.1)$$

From Section 4.5 on page 36 we know the power of single refracting surface:

$$\varphi_1 = (n - 1)C_1 \quad (38.2)$$

$$\varphi_2 = -(n - 1)C_2 \quad (38.3)$$

Insert Equations 38.2 and 38.3 into Equation 38.1:

$$\varphi = (n - 1)C_1 - (n - 1)C_2 + \left(\frac{t}{n} \right) (n - 1)^2 C_1 C_2$$

or:

$$\varphi = (n - 1)(C_1 - C_2) + \left(\frac{(n - 1)^2}{n} \right) t C_1 C_2 \quad (38.4)$$

Equation 38.4 is the thick lens version of the lens maker equation (Section 4.6.3). It tells us that $\varphi(n, t, C_1, C_2)$ is a function of four independent variables: refractive index, lens thickness, and two lens curvatures. The question we want to address is the following: How does φ change for small changes in each of the respective variables? The change $d\varphi$ is given by:

$$d\varphi = \left(\frac{\partial \varphi}{\partial n} \right) dn + \left(\frac{\partial \varphi}{\partial t} \right) dt + \left(\frac{\partial \varphi}{\partial C_1} \right) dC_1 + \left(\frac{\partial \varphi}{\partial C_2} \right) dC_2 \quad (38.5)$$

where:

$$\left(\frac{\partial \varphi}{\partial n} \right) = (C_1 - C_2) + tC_1C_2 - \frac{(tC_1C_2)}{n^2} \quad (38.6)$$

$$\left(\frac{\partial \varphi}{\partial t} \right) + \left[\frac{(n-1)^2}{n} \right] C_1C_2 \quad (38.7)$$

$$\left(\frac{\partial \varphi}{\partial C_1} \right) = (n-1) + \left[\frac{(n-1)^2}{n} \right] tC_2 \quad (38.8)$$

$$\left(\frac{\partial \varphi}{\partial C_2} \right) = -(n-1) + \left[\frac{(n-1)^2}{n} \right] tC_1 \quad (38.9)$$

Let's assume that our lens is equiconvex and made of BK7 glass. The operating wavelength is $\lambda = 0.55 \mu\text{m}$ and the focal length is 100 mm. Our independent parameters have the following values:

$$n = 1.518522$$

$$t = 5 \text{mm}$$

$$C_1 = 0.009723 \text{mm}^{-1}$$

$$C_2 = -0.009723 \text{mm}^{-1}$$

Now insert these values into Equations 38.6 through 38.9:

$$\left(\frac{\partial \varphi}{\partial n} \right) = 0.019178 \text{mm}^{-1}$$

$$\left(\frac{\partial \varphi}{\partial t} \right) = -0.000017 \text{mm}^{-2}$$

$$\left(\frac{\partial \varphi}{\partial C_1} \right) = 0.509914$$

$$\left(\frac{\partial \varphi}{\partial C_2} \right) = -0.509914$$

Substituting these into Equation 38.5:

$$d\varphi = \left(0.019178 \text{mm}^{-1} \right) dn + \left(-0.000017 \text{mm}^{-2} \right) dt + (0.509914) dC_1 + (-0.509914) dC_2 \quad (38.10)$$

By just looking at Equation 38.10, one can see from the coefficients that the lens is more sensitive to curvature changes than either index or thickness changes. Let's see how much change is needed in each parameter to cause a focal length change from 100 mm to 101 mm. (That's a power change where $d\phi = -0.000099 \text{ mm}^{-1}$.) The results for each parameter are shown in Table 38.1.

Table 38.1

Parameter	Computation	Value
index change	$dn = \frac{-0.000099 \text{ mm}^{-1}}{0.019178 \text{ mm}} = -0.005163$	
thickness change	$dt = \frac{-0.000099 \text{ mm}^{-1}}{-0.000017 \text{ mm}} = 5.824 \text{ mm}$	
C_1 change:	$dC_1 = \frac{-0.000099 \text{ mm}^{-1}}{0.509914} = -0.000194 \text{ mm}^{-1}$	
C_2 change:	$dC_2 = \frac{-0.000099 \text{ mm}^{-1}}{-0.509914} = 0.000194 \text{ mm}^{-1}$	

As you can see, it does not take much change in curvature to change the focal length by 1 mm. But it takes a big change in thickness to get the same effect. To get the radius of curvature change using the first surface as an example:

$$dR_1 = \frac{1}{C_1} + \left[\frac{1}{C_1 + dC_1} \right]$$

$$dR_1 = \frac{1}{0.009723} + \frac{1}{0.009723 - 0.000194} = 2.094 \text{ mm}$$

Next, let's check things out in ZEMAX. We insert our lens prescription into the code. The radii values are ± 102.8489 . (With these you'll note that the EFL = 100.005.) We'll do the tolerance check in two different ways: manually and automatically. In the manual method we'll go into the LDE and change the numbers for the radii and thickness by hand. The index change is not as easy since this must be done by going to the ZEMAX glass catalog (via the Gla button) and adding a new glass to the catalog under the file name misc.agf. Table 38.2 tabulates the results, and shows that the change in parameter values computed above do result in a millimeter focal length change.

Now for the automatic method: First remove the M-solve on the second lens surface thickness if present. Next select Editors → Merit Function. Insert EFL with weight '1'. The current 'value' should be 100.005, but leave the 'target' value blank. Next, select Editors → Merit Function → Tolerance Data → Tools → Default Tolerances. This will get you to the Default Tolerances menu. We are interested only in the column under 'Surface Tolerances'. Put a checkmark in the square box

Section 38.3: Tolerancing 439

Table 38.2

Parameter	Initial Value	Delta	New Value	Focal Length
n	1.5185224	- 0.005163	1.5133594	101.0002 mm
t	5 mm	5.824 mm	10.824 mm	100.9845 mm
R ₁	102.8489 mm	2.094 mm	104.9428 mm	101.0043 mm
R ₂	-102.8489 mm	-2.094 mm	-104.9428 mm	101.0043 mm

to the left of radius, thickness, and (further down) index. (These are the only checks that should be seen over the entire menu.) Just to the right of 'radius' make sure 'millimeters' is active (not fringes). In the right column under 'Surface Tolerances', start filling in the data boxes with the change values previously computed for the radius (2.094), thickness (5.824), and index (0.005163). (Do not worry about signs since the code will compute both positive and negative changes.) Now click on Save and then OK. This gets you back to the Tolerance Editor menu. Change the value of TWAV tolerance operand from 0.6328 to 0.55. Delete the second TTHI operand between surfaces 2 and 3 because we're not doing anything with the image airspace. For the TTHI between surfaces 1 and 2 make sure there is a 1 under both Int1 and Int2 headers. The lens prescription, merit function and tolerance editor listings should look as shown in Figure 38.2.

To run the tolerance analysis, go to the tool-bar row atop the main menu. Select Tools → Tolerancing. The tolerancing menu will be displayed. If there is a checkmark beside 'Fast Tolerance Mode', turn it off. Underneath, for the box labeled Merit: select 'Merit Function'; for Mode: select 'Sensitivity'; Fields: leave blank; Opt. Cycles: select 'Auto'. The 'Perform Sensitivity' box should have a checkmark. The entries on the righthand side under Monte Carlo are defaults and can be left as is. Now click OK and the tolerance analysis will run. The results are displayed upon completion. The results for our example are shown in Figure 38.3. For our purposes we are interested in the 'Sensitivity Analysis' (particularly those values we have boxed). These are in basic agreement with the manual analysis in Table 38.2.

This completes our foray into tolerancing. It was limited to a very simple case which examined just one lens specification, i.e., focal length. But the tolerance analysis turned out to be not so simple. A multi-element photographic lens would have a dozen or more specifications each of which will be affected by small changes in the basic prescription parameters. In addition to focal length, there would be specifications on f-number, field coverage, color correction, the Seidel aberrations, RMS spot size, Strehl ratio, wavefront variance, resolution and/or MTF, etc. In a multi-element lens, we also have to put tolerances on element decentration, despace, and tilt. A full-blown tolerance analysis is a major undertaking, and takes up a lot of designer time to complete.

a)

SURFACE DATA SUMMARY:

Surf	Type	Comment	Radius	Thickness	Glass	Diameter	Conic
06J STANDARD			Infinity	Infinity		0	0
STO STANDARD			102.8489	5	BK7	20	0
2 STANDARD			-102.8489	98.33988		19.73885	0
IMA STANDARD			Infinity			0.3226957	0

b)

Merit Function Value: 1.00005043E+002

Num	Type	Int1	Int2	Hx	Hy	Px	Py	Target	Weight	Value	% Cont
1	EFFL		1					0.00000E+000	1	1.00005E+002	100.000

c)

Num	Type	Int1	Int2	Min	Max
1	(TWAV)			5.50000E-001	0.00000E+000
2	(TRAD)	1		-2.09400E+000	2.09400E+000
3	(TRAD)	2		-2.09400E+000	2.09400E+000
4	(TTHI)	1	1	-5.82400E+000	5.82400E+000
5	(TIND)	1		-5.16300E-003	5.16300E-003

Fig. 38.2 a) Starting lens prescription; b) merit function; c) tolerance list.

Sensitivity Analysis:

Type	Sf1	Sf2	Minimum			Maximum		
			Value	MF	Change	Value	MF	Change
TRAD	1	-2.094000	98.985844	-1.019999	2.094000	101.004314	0.999271	
TRAD	2	-2.094000	101.004314	0.999271	2.094000	98.985844	-1.019999	
TTHI	1	1	-5.824000	99.439512	-0.965531	5.824000	100.989586	0.984542
TIND	1	0.005163	101.008631	1.003588	0.005163	99.821272	-0.983771	

Fig. 38.3 Tolerance analysis listing for sample case.

38.4 Things Not Covered

This has been an introductory level course. As such it has covered the basics. But that alone was sufficient to fill a semester. However, it is important to put things in perspective. The list below covers important design topics that would be appropriate for a follow-up course.

Things not covered:

1. Tolerancing in depth
2. Fabrication and mechanical design issues
3. Environmental issues
4. Metrology issues
5. Wide-angle and low f-number systems
6. IR and UV systems
7. Improvements due to glass choice
8. Zoom lenses
9. Index differences between object and image space
10. MTF optimization

Section 38.4: Things Not Covered 441

- 11. Non-rotationally symmetric designs**
- 12. Non-traditional optics (diffractive and micro optics)**
- 13. Non-image forming optics**
- 14. Coatings**
- 15. Ghost images**
- 16. Polarization effects**

As a designer you should have a good understanding of fabrication and metrology techniques being used in the shops. If your ground-breaking design cannot be built and/or measured because the surfaces or tolerances exceed the current state-of-the-art, then you have wasted the customer's time and money. You should also be aware of the environment in which the lens will be used. For instance, if you're designing a reconnaissance lens to be used aboard carrier-based aircraft, you need to worry about the damaging effects of humidity, salt air, and mold. Some glasses are more susceptible than others.

In this course you had no freedom to choose different glasses for a particular design problem. The problems were further restricted to the visible spectrum, to relatively benign fields and f-numbers, and to air as the object-space medium. Glass choice is an obvious area where design improvements could be found. But if designs are needed in the IR and UV regions of the spectrum, one finds that there is a relative dearth of glass types available. Often a trade-off must be made between axial color, field, and f-number, which may also involve refractive vs. reflective or catadioptric (which has some of both) systems. Back in the visible, wide-angle fast objectives (lenses) can involve very complicated design issues (particularly the effects of higher-order aberrations) which were not touched upon in this course. Zoom lenses and anamorphic lenses (as used in wide-screen cinematography) present their own unique design challenges. For underwater cameras, the object-space medium is water, which opens up a whole new batch of design considerations.

Very few of the designs you worked on here were capable of achieving diffraction-limited performance. Hence, the use of the TRAC operand to reduce RMS spot size was an acceptable tool. When peak-to-valley wavefront errors are a wave or so, the use of other operands involving OPD or MTF are appropriate. In some designs, the use of the MTF operand is essential, particularly if you are trying to optimize performance within a certain spatial frequency bandwidth.

Anamorphic lenses mentioned above are but one example of non-rotationally symmetric designs. Others include the use of off-axis segments such as the OAP (illustrated in the last chapter), and off-axis Cassegrains. The latter are used to provide a broadband, compact system without paying the attenuation penalty associated with a central obscuration.

A whole new cast of characters is introduced with holographic (analog or digital) optical elements (as used, for example, in optical testing to replace the glass null lens), diffractive optical elements as used in MEMS devices, and large

Fresnel lenses for light collection applications. They all present new and often difficult design challenges.

38.5 Optical Design Codes

I do not think you can teach a lens design course today without thoroughly incorporating a specific lens design code. It should be one that is widely used in the industry. To do otherwise is a disservice to students. The code should also be easy for students to learn so that they gain enough versatility to do the design exercises assigned. My choice for this course was ZEMAX. It has proven itself effective and popular with students. However, this should in no way be construed as denigrating the merits or capabilities of other fine codes. As the student moves from the classroom into professional life, he or she will likely need to become conversant with one or more of these other important codes. Those currently being used in the industry are: Code-V (Optical Research Associates); SYNOPSYS (Optical Systems Design, Inc.); OSLO (Sinclair Optics). Each code has its strong points, neat features, and little quirks.

Appendix A

Bibliography

Lens Design

- Kingslake, Rudolph, *Lens Design Fundamentals*. New York: Academic Press, 1978.
- Kingslake, Rudolph, *A History of the Photographic Lens*. Boston: Academic Press, 1989.
- Malacara, Daniels and Malacara, Zacarias, *Handbook of Lens Design*. New York, Marcel Dekker, 1994.
- Rutten, Harry G.J., and Martin A.M. van Venrooij, *Telescope Optics*. Richmond, VA: Willmann-Bell, Inc., 1988.
- Smith, Gregory H., *Practical Computer Aided Lens Design*. Richmond, VA: Willmann-Bell, Inc., 1998.
- Shannon, Robert R., *The Art and Science of Lens Design*. Cambridge and New York: Cambridge University Press, 1997.
- Smith, Warren, *Modern Lens Design*. New York: McGraw-Hill, 1992.

Aberration Theory

- Welford, W.T., *Aberrations of the Symmetrical Optical System* (First edition). Boston: Academic Press, 1974.
- Mahajan, V., *Aberration Theory Made Simple*. (TT-6). Bellingham: SPIE Press, 1991.

Linear Systems and Fourier Optics

- Gaskill, J., *Linear Systems, Fourier Transforms, and Optics*. New York: John Wiley and Sons, 1978.
- Goodman, J., *Introduction to Fourier Optics*. New York: McGraw-Hill, 1969.

Geometric Optics

- Hecht, E. and Zajac, A., *Optics* (First edition). Boston: Addison-Wesley, 1974.
- Pedrotti, F. and Pedrotti, L., *Introduction to Optics* (Second edition). New Jersey: Prentice Hall, 1993.
- Sears, F., *Optics* (Third edition). Boston: Addison-Wesley, 1958.

Optical Systems

Kingslake, R., *Optical Systems Design*. New York: Academic Press 1983.

Smith, W., *Modern Optical Engineering*. New York: McGraw-Hill, 1966.

Historical

Kingslake, R., *A History of the Photographic Lens*. New York: Academic Press, 1989.

King, H.C., *The History of the Telescope*. Cambridge: Sky Publishing Corporation, 1955.

Optical Testing

Malacara, Daniel, *Optical Shop Testing*. New York: John Wiley and Sons, 1978.

Suiter, H.R., *Star Testing Astronomical Telescopes*. Richmond, VA: Willmann-Bell, Inc., 1994.

Appendix B

Answers to *Manual Calculation Assignments*

- Section 1.3** a) $EFL = 400 \text{ mm}$;
 b) $\phi = 0.0025 \text{ mm}^{-1}$;
 c) $C = 0.002419 \text{ mm}^{-1}$;
 d) $R = 413.459 \text{ mm}$;
 e) $y_i = 35 \text{ mm}$;
 f) $D_{\text{airy}} = 14.32 \mu\text{m}$
- Section 4.9** a) $\phi_1 = 0.00125 \text{ mm}^{-1}$ and $\phi_2 = 0.00125 \text{ mm}^{-1}$;
 b) marginal and chief ray heights and angles *after*
 refraction at second surface: $y_2 = 19.934073$;
 $u_2 = -0.049918$; $y_2 = 0.230716$; $u_2 = 0.087201$;
 c) $BFL = 399.3364$;
 d) $y_3 = 35.05320$
- Section 5.7** a) EP axial location = 3.919 ; EP diameter = 26.56 ;
 b) $y_1 = 13.28$; $u_1 = 0$; $\bar{y}_1 = -7.103$; $\bar{u}_1 = 14^\circ$
- Section 10.8** 1) $S_{11} = 0.000508 \text{ mm}$ & $S_{12} = 0.007498 \text{ mm}$;
 2) $S_1 = 0.008006 \text{ mm}$;
 3) $W_{040} = 1.705\lambda$;
 4) $S_1 = 0.008043 \text{ mm}$ & $W_{040} = 1.712\lambda$
- Section 11.11** $\delta_{MB} = -1.201 \text{ mm}$; $D_{MB} = 40.04 \mu\text{m}$
- Section 14.8** 1. $W_{220P} = 2.15\lambda$ and $R_P = -606 \text{ mm}$
 2a. $R_F = -206.7$

Section 16.6	$\phi_a = 0.2116 \text{ in}^{-1}$	$\phi_b = 0.1116 \text{ in}^{-1}$
	$f_a = 4.725 \text{ in}$	$f_b = -8.957 \text{ in}$
	$R_1 = 4.885 \text{ in}$	$R_4 = -30.866 \text{ in}$
Section 17.9	Aberration	C_1
	SPHA (RHS)	0.1927
	SPHA (LHS)	0.1279
	COMA	0.1644
Section 18.7	a) $\Delta f_{ss} = -129 \mu\text{m}$	
Section 23.7	b) $S_1 = 0.000059 \text{ mm}$	
Section 24.9	a) $\kappa = -6.9316$	
Section 26.7	Primary... $\kappa = -1.0127717$	
	Secondary... $\kappa = -2.1711596$	
Section 29.12	a) $l_s' = -10.03819''$ and $l_t' = -0.88694''$	
	b) $\Delta l' = 0.15135$	
	c) Aperture independent	
Section 30.9	1) $C = (2/3)(R/r)^2 W_{131}^2$ where $\bar{H} = 1$	
Section 31.5	2) For coma: $S = 0.00719$	
	3) For astigmatism: $S = 0.08480$	

Appendix C

Final Prescriptions for ZEMAX Design Assignments

Section 6.6 (See page 62)

SURFACE DATA SUMMARY:

Surf	Type	Comment	Radius	Thickness	Glass	Diameter	Conic
OBJ	STANDARD		Infinity	Infinity		0	0
1	STANDARD		Infinity	30		31.99182	0
2	STANDARD		18.40123	4	BK7	15.05234	0
3	STANDARD		26.45887	10.89924		12.95934	0
STO	STANDARD		Infinity	51.69412		5.540256	0
5	STANDARD		Infinity	-1.885763		54.50754	0
IMA	STANDARD		Infinity			53.12145	0

Section 9.5 (See page 101)

SURFACE DATA SUMMARY:

Surf	Type	Comment	Radius	Thickness	Glass	Diameter	Conic
OBJ	STANDARD		Infinity	Infinity		0	0
1	STANDARD		Infinity	5		4	0
STO	STANDARD		-13.31641	0.5	BK7	4	0
3	STANDARD		-25.75452	0.2		4.056825	0
4	STANDARD		44.48081	0.5	BK7	4.083255	0
5	STANDARD		-26.55421	0.2		4.089992	0
6	STANDARD		14.76026	0.5	BK7	4.068018	0
7	STANDARD		31.19985	31.2		4.013391	0
IMA	STANDARD		Infinity			3.416314e-005	0

Section 12.9 (Symmetric, See page 145)

SURFACE DATA SUMMARY:

Surf	Type	Comment	Radius	Thickness	Glass	Diameter	Conic
OBJ	STANDARD		Infinity	Infinity		0	0
1	STANDARD		Infinity	50		98.93771	0
2	STANDARD		82.616	12	BK7	48.8611	0
3	STANDARD		100.0834	16.90413		40.34937	0
STO	STANDARD		Infinity	16.90413		24.77193	0
5	STANDARD		-100.0834	12	BK7	39.25713	0
6	STANDARD		-82.616	372.507		47.33132	0
7	STANDARD		Infinity	-12.23369		373.6826	0
IMA	STANDARD		Infinity			361.6317	0

448 Appendix C Final Prescriptions for ZEMAX Design Assignments

Section 12.9 (Unsymmetric, See page 145)

SURFACE DATA SUMMARY:

Surf	Type	Comment	Radius	Thickness	Glass	Diameter	Conic
OBJ STANDARD		Infinity	Infinity	0		0	0
1 STANDARD		Infinity	50		BK7	118.9529	0
2 STANDARD		38.8435	12			59.42808	0
3 STANDARD		31.36844	33.85738			47.39647	0
STO STANDARD		Infinity	44.74381			25.8074	0
5 STANDARD		-104.644	12		BK7	66.95441	0
6 STANDARD		-61.37046	423.3487			72.21751	0
IMA STANDARD		Infinity				363.4662	0

Section 19.6 (Number 1, See page 218)

SURFACE DATA SUMMARY:

Surf	Type	Comment	Radius	Thickness	Glass	Diameter	Conic
OBJ STANDARD		Infinity	Infinity	0		0	0
STO STANDARD		Infinity	2.003568			1	0
2 STANDARD		-17.3405	0.7		BK7	2.81519	0
3 STANDARD		-2.137334	0.001			2.929369	0
4 STANDARD		-2.137334	0.2		SF2	2.929465	0
5 STANDARD		-3.459902	10.24684			3.211373	0
6 STANDARD		Infinity	-0.1991257			8.957686	0
IMA STANDARD		Infinity				8.831642	0

Section 19.6 (Number 2, See page 219)

SURFACE DATA SUMMARY:

Surf	Type	Comment	Radius	Thickness	Glass	Diameter	Conic
OBJ STANDARD		Infinity	Infinity	0		0	0
STO STANDARD		143.8682	5		BK7	40.24748	0
2 STANDARD		-198.4018	17.47783			40.29472	0
3 STANDARD		-168.6382	3		SF2	38.95245	0
4 STANDARD		1990.355	350.1269			39.13623	0
5 STANDARD		Infinity	-4.123524			71.09631	0
IMA STANDARD		Infinity				69.89796	0

Section 20.4 (Mid-Term, See page 225)

SURFACE DATA SUMMARY:

Surf	Type	Comment	Radius	Thickness	Glass	Diameter	Conic
OBJ STANDARD		Infinity	170			5.934	0
STO STANDARD		15.90826	1.5		BK7	8.808594	0
2 STANDARD		-15.17339	0.5		SF2	8.77689	0
3 STANDARD		-118.6775	18.39008			8.694167	0
4 STANDARD		6.302020	1		BK7	5.320453	0
5 STANDARD		-9.904115	0.5		SF2	5.299111	0
6 STANDARD		163.0552	8.008825			5.002325	0
7 STANDARD		Infinity	-0.01431904			0.6024879	0
IMA STANDARD		Infinity				0.6037096	0

Section : 449

Section 25.10 (Symmetric, See page 284)

SURFACE DATA SUMMARY:

Surf	Type	Comment	Radius	Thickness	Glass	Diameter	Conic
OBJ STANDARD		Infinity	Infinity	Infinity		0	0
1 STANDARD		2.144466	0.2	F1	1.66	0	0
2 STANDARD		0.9832692	0.33	LFI	1.66	0	0
3 STANDARD		2.840316	0.2999835		1.66	0	0
STO STANDARD		Infinity	0.2999835		1.129656	0	0
5 STANDARD		-2.840316	0.33	LFI	1.58	0	0
6 STANDARD		-0.9832692	0.2	F1	1.58	0	0
7 STANDARD		-2.144466	9.268761		1.58	0	0
8 STANDARD		Infinity	-0.06169861		7.270405	0	0
IMA STANDARD		Infinity			7.219661	0	0

Section 25.10 (Unsymmetric, See page 284)

SURFACE DATA SUMMARY:

Surf	Type	Comment	Radius	Thickness	Glass	Diameter	Conic
OBJ STANDARD		Infinity	Infinity	Infinity		0	0
1 STANDARD		2.182134	0.2	F1	1.644311	0	0
2 STANDARD		0.9892601	0.3	LFI	1.39551	0	0
3 STANDARD		2.858363	0.2999835		1.329789	0	0
STO STANDARD		Infinity	0.2999835		1.137904	0	0
5 STANDARD		-2.634111	0.3	LFI	1.275392	0	0
6 STANDARD		-0.9554678	0.2	F1	1.342588	0	0
7 STANDARD		-2.007218	9.403327		1.561329	0	0
8 STANDARD		Infinity	-0.09703547		7.286912	0	0
IMA STANDARD		Infinity			7.204517	0	0

Section 26.7 (See page 299)

SURFACE DATA SUMMARY:

Surf	Type	Comment	Radius	Thickness	Glass	Diameter	Conic
OBJ STANDARD		Infinity	Infinity	Infinity		0	0
STO STANDARD		-120.5982	-50	MIRROR	30.03264	-1.012771	
2 STANDARD		-25	58.49368	MIRROR	6.904444	-2.171146	
IMA STANDARD		Infinity			12.15512	0	

Section 28.8 (Symmetric, See page 327)

SURFACE DATA SUMMARY:

Surf	Type	Comment	Radius	Thickness	Glass	Diameter	Conic
OBJ STANDARD		Infinity	Infinity	Infinity		0	0
1 STANDARD		Infinity	2		4.147395	0	0
2 STANDARD		3.756919	0.55	SK4	2.531612	0	0
3 STANDARD		-5.904957	0.1794750		2.380344	0	0
4 STANDARD		-4.179668	0.2	RAF4	2.018276	0	0
5 STANDARD		7.377284	0.5		1.764519	0	0
STO STANDARD		Infinity	0.5		1.444857	0	0
7 STANDARD		-7.377284	0.2	RAF4	1.735857	0	0
8 STANDARD		4.179668	0.1794750		1.936504	0	0
9 STANDARD		5.904957	0.55	SK4	2.192348	0	0
10 STANDARD		-3.756919	8.609543		2.347788	0	0
IMA STANDARD		Infinity			7.356567	0	0

450 Appendix C Final Prescriptions for ZEMAX Design Assignments

Section 28.8 (Unsymmetric, See page 327)

SURFACE DATA SUMMARY:

Surf	Type	Comment	Radius	Thickness	Glass	Diameter	Conic
OBJ STANDARD		Infinity	Infinity			0	0
1 STANDARD		Infinity		2		4.135963	0
2 STANDARD		4.082339		0.55	SK4	2.533406	0
3 STANDARD		-6.807277	0.1794758			2.361963	0
4 STANDARD		-5.004801		0.2	BAF4	2.043898	0
5 STANDARD		11.04463		0.5		1.815549	0
STO STANDARD		Infinity		0.5		1.442453	0
7 STANDARD		-4.344418		0.2	BAF4	1.696269	0
8 STANDARD		3.688759	0.1794758			1.941387	0
9 STANDARD		5.259271		0.55	SK4	2.257647	0
10 STANDARD		-3.112943	8.737022			2.38203	0
11 STANDARD		Infinity	-0.05002801			7.338427	0
IMA STANDARD		Infinity				7.294361	0

Section 30.9 (Symmetric, See page 353)

SURFACE DATA SUMMARY:

Surf	Type	Comment	Radius	Thickness	Glass	Diameter	Conic
OBJ STANDARD		Infinity	Infinity			0	0
1 STANDARD		3.826085	0.4		SK16	2.841025	0
2 STANDARD		-46.41105	0.8408516			2.760986	0
3 STANDARD		-4.428166		0.1	F4	1.679633	0
4 STANDARD		Infinity		0		1.655325	0
STO STANDARD		Infinity		0.1	F4	1.655325	0
6 STANDARD		4.428166	0.8408516			1.658926	0
7 STANDARD		46.41105		0.4	SK16	2.530075	0
8 STANDARD		-3.826085	8.571194			2.621718	0
9 STANDARD		Infinity	-0.02361118			7.294072	0
IMA STANDARD		Infinity				7.281434	0

Section 30.9 (Unsymmetric, See page 353)

SURFACE DATA SUMMARY:

Surf	Type	Comment	Radius	Thickness	Glass	Diameter	Conic
OBJ STANDARD		Infinity	Infinity			0	0
1 STANDARD		4.800023	0.4		SK16	3.289883	0
2 STANDARD		-84.39801	1.306519			3.221419	0
3 STANDARD		-3.551622		0.1	F4	1.624424	0
4 STANDARD		Infinity		0		1.616395	0
STO STANDARD		Infinity		0.1	F4	1.616395	0
6 STANDARD		4.404154	0.7439994			1.641767	0
7 STANDARD		16.15798		0.4	SK16	2.653362	0
8 STANDARD		-3.111851	8.921046			2.681313	0
9 STANDARD		Infinity	-0.05730429			7.285874	0
IMA STANDARD		Infinity				7.25719	0

Section : 451

Section 33.6 (Strict, See page 387)

SURFACE DATA SUMMARY:

Surf	Type	Comment	Radius	Thickness	Glass	Diameter	Conic
OBJ STANDARD		Infinity	Infinity	0		0	0
1 STANDARD		2.971001	0.5	K7	2.3	0	0
2 STANDARD		-2.971001	0.12	LP7	2.3	0	0
3 STANDARD		10.34909	1.913613		2.3	0	0
STO STANDARD		Infinity	1.913613		0.7851245	0	0
5 STANDARD		9.514931	0.1	LP7	1.74	0	0
6 STANDARD		1.479832	0.1686		1.74	0	0
7 STANDARD		1.628767	0.4	K7	1.736354	0	0
8 STANDARD		-5.179081	2.500203		1.745438	0	0
IMA STANDARD		Infinity			1.686738	0	0

Section 33.6 (Relaxed, See page 387)

SURFACE DATA SUMMARY:

Surf	Type	Comment	Radius	Thickness	Glass	Diameter	Conic
OBJ STANDARD		Infinity	Infinity	0		0	0
1 STANDARD		2.971001	0.5	K7	2.3	0	0
2 STANDARD		-2.971001	0.12	LP7	2.3	0	0
3 STANDARD		10.34909	1.021635		2.3	0	0
STO STANDARD		Infinity	1.021635		0.8427219	0	0
5 STANDARD		9.372499	0.1	LP7	1.160364	0	0
6 STANDARD		1.502658	0.1686		1.192706	0	0
7 STANDARD		1.731683	0.4	K7	1.358014	0	0
8 STANDARD		-3.277882	3.582934		1.396679	0	0
9 STANDARD		Infinity	-0.03115152		1.759643	0	0
IMA STANDARD		Infinity			1.743759	0	0

Section 36.4 (Final Exam, Strict, See page 418)

SURFACE DATA SUMMARY:

Surf	Type	Comment	Radius	Thickness	Glass	Diameter	Conic
OBJ STANDARD		Infinity	Infinity	0		0	0
1 STANDARD		1.886333	1.1	K3	2.795979	0	0
2 STANDARD		-3.337525	0.15	F3	2.604389	0	0
3 STANDARD		5.571421	1.084116		2.21167	0	0
STO STANDARD		Infinity	1.084116		1.256477	0	0
5 STANDARD		-1.411945	0.15	K3	1.319968	0	0
6 STANDARD		-1.004813	0.25	F3	1.346521	0	0
7 STANDARD		-2.043152	4.163051		1.55971	0	0
8 STANDARD		Infinity	-0.3358958		3.609511	0	0
IMA STANDARD		Infinity			3.421312	0	0

Section 36.4 (Final Exam, Relaxed, See page 418)

SURFACE DATA SUMMARY:

Surf	Type	Comment	Radius	Thickness	Glass	Diameter	Conic
OBJ STANDARD		Infinity	Infinity	0		0	0
1 STANDARD		1.666188	0.6	K3	2.171862	0	0
2 STANDARD		-5.283875	0.0001		2.10121	0	0
3 STANDARD		-5.283875	0.15	F3	2.10098	0	0
4 STANDARD		4.62753	0.5304812		1.861025	0	0
STO STANDARD		Infinity	1.346948		1.482866	0	0
6 STANDARD		-1.06272	0.15	K3	1.427499	0	0
7 STANDARD		-0.9241599	0.0001		1.466375	0	0
8 STANDARD		-0.9241599	0.2	F3	1.466334	0	0
9 STANDARD		-1.490674	5.260377		1.678154	0	0
10 STANDARD		Infinity	-0.08550042		3.582917	0	0
IMA STANDARD		Infinity			3.553355	0	0

Appendix D Glossary

Aberration: An ideal monochromatic point image is formed from a spherical converging wavefront. Wavefronts that are not spherical are considered aberrated as are the images they form. The common aberrations affecting the point image are spherical aberration, coma, and astigmatism. Aberrations that effect image point location axially and laterally also occur. These are field curvature and distortion.

Abbe number: A number which quantifies the dispersive nature of glass.

Achromat: A lens composed of two elements with different dispersive properties which correct primary axial color.

Airy Disk: In geometric optics, an ideal lens forms a point image of a point object. When physical optics is taken into account, the point object is imaged by an ideal lens as a finite-sized circular disk (assuming a circular aperture).

Aplanat: An optical imaging system that has no spherical aberration or coma.

Aspheric: An optical surface that is not spherical in shape.

Axial Color: The refractive index of glass is wavelength dependent so glass lenses form images of different colors at different points along the optical axis.

Back Image Distance: The separation between the last optical surface in an imaging system and the paraxial image plane.

Chief Ray: The ray from the maximum field position that passes through the center of the stop.

Conic Constant: A number that defines an optical surface's departure from a spherical surface.

Corrector Plate: A refractive optical element that eliminates spherical aberration in an imaging system.

Curvature: The reciprocal of the radius of curvature for an optical surface.

Defocus: The axial separation between the paraxial image plane and a different plane of observation.

Depth of Focus: Roughly the axial range over which the image appears unchanged to an observer.

Dispersion: Variation of the refractive index with wavelength.

Diffraction Limited: The performance of the imaging system is limited not by geometric aberrations, but by the physical optics phenomenon of diffraction.

454 Appendix D Glossary

Effective Focal Length: The separation between the rear principal plane and the paraxial image plane.

Entrance Pupil: Image of stop formed by optics to the left of stop.

Exit Pupil: Image of stop formed by optics to the right of stop.

Field Angle: The angle an object point makes with respect to the optical axis as determined from the vertex of the entrance pupil.

Field Flattener: Usually a negative element close to the image plane that reduces or eliminates Petzval field curvature.

Field of View: Object scene that fits within defined image plane format.

Format: That which physically limits the image scene extent in the image plane, e.g., the size of a CCD chip.

f-number: The ratio of the effective focal length to the entrance pupil diameter for an object at infinity.

Lateral Color: Chromatic aberration associated with the chief ray.

Magnification: Ratio of image height to object height.

Marginal Ray: Ray from the axial object point to the rim of the entrance pupil.

Merit Function: A number that summarizes the state of optimization of an imaging system. The lower the number, the better the optimization.

Modulation Transfer Function (MTF): A measure of image contrast as a function of spatial frequency.

Null Lens: A refractive or reflective optical system interposed between a test point and an aspheric mirror in a radius of curvature test configuration. Compensates for the spherical aberration associated with the normals to the mirror surface.

Numerical Aperture: Defines the light collection capability of an optical system in object space for a finite object distance.

Optical Path Length: The actual path length multiplied by the refractive index within that path.

Optical Path Difference: The separation between an aberrated wavefront and a reference sphere at some point in the exit pupil.

Optical Power: The reciprocal of focal length.

Principal Plane(s): An optical imaging system has a pair of principal planes (front and rear). These planes, along with a knowledge of focal point locations, can represent the first order imaging properties of the system (no matter how complicated that system may be). The image point location of any object point can be determined via simple graphical ray tracing techniques.

Paraxial Plane: For an optical imaging system, trace rays which lie close to the optical axis through the system for a given axial object point. The convergence point of such rays in image space defines the location of the paraxial

Section : 455

image plane.

Point Spread Function: A profile or three-dimensional plot of the image of a point object.

Ray Fan Plot: A representation of optical imaging system performance. Ray pierces in the image plane are plotted against corresponding pierces across both vertical (tangential) and horizontal (sagittal) diameters in the entrance pupil.

Refractive Index: The ratio of the speed of light in vacuum to its speed in optical medium such as glass.

Relative Illumination: A measure of the variation in irradiance across an image plane format.

Resolution: A measure of the amount of detail that can be observed in an image.

RMS: Acronym for root mean square.

Secondary Spectrum: The residual axial color after achromatic correction.

Seidel Aberrations: Conventional designation for the common aberrations that include spherical aberration, coma, astigmatism, field curvature and distortion.

Spherochromatism: The variation of spherical aberration with color (wavelength).

Spot Diagram: A representation of optical imaging system performance. Ray pierces in the image plane are plotted for a uniform grid of rays piercing the entrance pupil.

Stop: The limiting aperture of an imaging system.

Star Image: The finite-sized image of a point object due to the presence of aberration and/or diffraction.

Strehl Ratio: The ratio of the central intensity (or irradiance) of an aberrated star image to the corresponding intensity (or irradiance) in an unaberrated star image.

Thin Lens: A mathematical construct for a lens that has no thickness.

Transverse Ray Aberration: A measure of aberration in the image plane.

Vignetting: Rays from an object that do not make it to the image plane due to blockage by some aperture in the imaging system.

Wavefront: A surface that has the same optical path length from an object point. It is also a surface having the same phase.

Wavelength: Light is an electromagnetic wave. The length of one complete sinusoidal cycle is called the wavelength. Wavelength determines the color of light.

Appendix E

Description of ZEMAX Merit Function Operands Utilized in this Book

- ASTI:** Astigmatism wavefront aberration coefficient in waves for the surface(s)/system designated.
- AXCL:** The axial separation (in lens units) between the wavelength extremes selected.
- COMA:** Coma wavefront aberration coefficient in waves for the surface(s)/system designated.
- DIFF:** Difference between two operands.
- DIST:** System distortion in percent.
- DIVI:** Division of two operands.
- EFLL:** System focal length in lens units at the primary wavelength.
- EFLY:** Focal length of subsystem between designated surfaces in lens units at the primary wavelength.
- FCGS:** Sagittal field curvature in waves for a specified field position.
- FCGT:** Tangential field curvature in waves for a specified field position.
- FCUR:** Field curvature wavefront aberration coefficient in waves for the surface(s)/system designated.
- LACL:** Lateral color which provides the Δy height difference in the paraxial plane for chief rays at the extreme wavelengths.
- MNCA:** Used to set a minimum axial air thickness between designated surfaces.
- MNCG:** Used to set a minimum axial glass thickness between designated surfaces.
- MXCA:** Used to set a maximum axial air thickness between designated surfaces.
- MXCG:** Used to set a maximum axial glass thickness between designated surfaces.
- OPTH:** The optical path length in lens units from the first optical surface (object at infinity) to the designated surface.
- PARR:** Paraxial radial distance (in lens units) from the axis at a specified surface for a specified ray (field location and pupil coordinate).

PETC: Petzval curvature in inverse lens units.

PETZ: Petzval radius of curvature in lens units.

PMAG: Paraxial magnification.

RAID: Real ray angle of incidence (in degrees) at a specified surface.

SPHA: Spherical aberration wavefront aberration coefficient in waves for the surface(s)/system designated.

TOTR: Total track (in lens units) from first optical surface to image plane.

TRAC: The radial transverse aberration measured in the image plane for a specified ray (field location, pupil coordinate, and color) with respect to the centroid. Multiple TRACs are inserted into the merit function via the default merit function. TRAC is used to minimize the RMS spot radius.

TTHI: Cumulative axial thickness from first designated surface to the second designated surface (which includes the thickness following this second surface).

Index

A

Abbe
number 54
sine condition 83
aberrations
astigmatism 73–75, 303
balancing 123
coefficient 103
coma 71–73
decentration 424
defocus 68, 303
distortion 75–77
exit pupil 82
field curvature 75–77
generator 338
image plane 4, 82
spherical 68–71
Table of 111
wavefront 77–82, 301
description 77
diffraction 82
gradients 302
windows 253
achromat
bending 185, 187
constraints 180
example 181
flat field 205
one-glass 211
powers 181
secondary spectrum 198
symmetric 271
thin lens 207
ZEMAX 187, 202
aerial resolution 7
Airy disk 204
analysis options in ZEMAX 15
aplanat 192
apoachromat 229
apoachromatic
constraint 212, 229
power solution 230
area weighted RMS 277
aspheric surfaces 23

astigmatism 73, 147, 152, 153
axial color 175, 195, 213, 259
axial intensity 365

B

back focal length 85
back image distance 85
baffles 298
bending
achromat 191
coma 154
coma and astigmatism 191
Seidel spherical aberration 187
thin lens 119
BK7 information 57
breaking symmetry 143, 277
broad sources 374
buried stop 46

C

Carl Steinheil 143
caustic 71, 124
Celor lens 315
central obscuration 296
Chevalier lens 217
Chevalier, Charles 217
chief ray 46
defined by stop 43
Chrétien, Henri J. 299
Coddington's equations 329, 331
mirrors 334
coma 71, 147
lens bending 154
Seidel contributions 151
thin lens formulation 152
conic constant 24, 261
feature in ZEMAX 261
of a parabola 262
convex-plano lens 21
convolution 390
Cooke triplet 35, 343
coordinate breaks 423
corrector plate 264
curvature 36

- D**
 Dall-Kirkham 287
 Dallmeyer, John Henry 283
 decentration (lens) 424
 defocus 68
 departure from sphere 27
 depth of focus
 diffractive 375
 geometric 371
 Rayleigh 371
 design type map 6
 diagnostic plots 65
 dialog boxes 12
 dialyte lens 207, 219, 227, 315
 front-end 346
 inverted 377
 diffractive depth of focus 370
 dispersion 51, 52, 207
 distortion 75, 169
- E**
 effective f-number 19
 effective focal length (EFL) 6, 38
 entrance pupil 45
 equi-biconvex lens 21
 exit pupil 45
 eye model 245
 eyepiece 239
 field lens 242
 first-order layout 239
 Kellner 245
 Ramsden 245–247
 Ramsden design example 246
- F**
 field
 curvature 75
 flattener 163
 flattening 140
 lens 242
 vs. f-number 154
 first order properties 17
 Fizeau interferometer 98
 f-number 19
 focal length (EFL) 6
 focus shift 120, 253, 370, 371
 format size 6
 Fourier transform 390
 front landscape lens 62
 F-Solve 86
- G**
 Galilean telescope 49
 Gaussian 34
- H**
 lens formula 34
 generalized power 315
 geometric depth of focus 371
 glass
 catalog 18
 chart 54–58
 properties 57
- I**
 half-field angle 7
 higher order spherical 189
- L**
 image compactness 347
 image space f-number 19
 initial prescription 11
- K**
 Kellner eyepieces 245
- L**
 Lagrange 48
 invariant 49
 landscape lens 51
 lateral color 193, 350
 layout drawing 13
 lens 117
 aspheric correction 263
 bending 117, 154
 decentration 424
 maker's equation 40
 splitting 95
 tilt 425
 lens data editor 11
 LF1 information 285
 limiting aperture 43
 longitudinal spherical aberration 68
 plot 321
- M**
 magnification 41
 marginal ray (defined by stop) 43
 maximum field angle 46
 medial focus 75
 melt data 55
 merit function 88
 micro-lithography 98
 microscope 221
 minimum blur 71
 mirrors 261, 290, 334
 modulation 389
 transfer function
 and symmetry 396
 in ZEMAX 396

- transfer function (MTF) 389
monochromatic designs 8
M-solve 85
MTF (modulation transfer function) 389–398
- N**
null lens 399, 408
numerical aperture 222
- O**
oblique power 330
obscuration ratio 297
off-axis
 aberration coefficients 110
 calculations 150
 parabola 425
Offner null lens 405
optical
 path length 77
 transfer function 392
optical power 33
- P**
parabolic mirror 261
paraxial
 lenses 421
 ray trace equations 33
paraxial working f-number 19
partial
 primary axial color 213–214
partial dispersion 55, 195
periscopic lens 135
Petzval
 aberration coefficient 159
 curvature 157
 design procedure 380
 lens 377
 radius 161
 sum 159
 wavefront 159
Petzval, Joseph M. 381
phase transfer function 395
polychromatic designs 8
power expressions
 single reflecting surface 37
 thin lens 39
 two element system 37
power of a surface 36
primary axial color 175
principal
 plane 40
PRTE (paraxial ray trace equations) 33
pupil 43
- entrance 46
exit 45
function 82
pupils 43
- R**
Ramsden eyepiece 245–247
Rapid Rectilinear 283
ray fan plot 65, 65–66
Rayleigh Rules 375
 quarter-wave criteria 375
 resolution criteria 375
Rayleigh, Lord 370
rear landscape lens 61
refractive index 51
relative illumination 282–283
relay systems 249
resolution 7, 373
right angle prism 423
rings and arms 87
Ritchey, George W. 298
Ritchey-Chrétien system 287
RMS
 spot plots 93
 spot size 90
- S**
sag 22
sagittal focus 73
Schmidt plate 266
Schmidt, Bernhard 270
secondary
 color 195
 mirror 290
 spectrum 186, 202
Seidel Coefficient 107, 111, 116, 161, 255, 257
 for spherical aberration 265
thin lens 118
window 257
Seidel polynomials 80
SF2 information 183
shape factor 21
sign conventions 21
sine condition 83
single reflecting surface 37
sixth-order aberrations 173
Snell's Law 4, 37
specifications, design 5
spherical aberration 68
 balancing 123
 bending 119
 coefficient 103
 coefficient derivation 110

- higher order 189
- parabolic mirror 399
- parabolic mirror 399
- Seidel Coefficient**
 - thin lens 109, 117
 - transverse 148
 - window 255
- spherical mirror 264
- spherochromatism 190
- spot diagram 67
- star images 374
- stop 43
 - defined 43
 - shifting 58
- stray light 298
- Strehl Ratio 355, 365
 - in ZEMAX 375
- surface
 - normals 402
 - power 36
- symmetric achromatic 271
- symmetry 135, 396
- system resolution 7

- T**
- tangential focus 73, 307
- Taylor, H. Dennis 345
- telephoto 413, 416
- telescope
 - Cassegrain 287, 290
 - Dall-Kirkham 287
 - Gregorian 289
 - Newtonian 287
 - Ritchey-Chrétien 287
 - Schmidt 289
- Tessar lens 346
- thin len
 - astigmatism 153
 - coma 154
 - spherical aberration 109, 117, 128
 - tilting (lens) 425
- thin-lens** 39, 109, 110, 111, 119, 128, 207, 332
 - aberration table 111
 - achromat 207

- bending 119
- Coddington's equations 332
- pre-design 33
- tilted window 258
- tilting
 - flat mirror 422
 - lens 425
- toric surfaces 336
- TRAC 30, 60, 85
- transmission sphere 101
- Transverse 148
- transverse ray aberration 82
- transverse spherical aberration 148
- triplet 343
- two element system 37

- V**
- vignetting 280
- von Hoegh, Emil 326

- W**
- wavefront 77
- aberration
 - coefficient 80, 107, 111
 - aberrations 77
 - color aberration 178
 - description 77
 - diffraction 82
 - gradients 302
 - tilt 167
 - variance 357
 - asymmetric aberrations 363
 - in ZEMAX 361
 - numerical example 360
- windows 251
 - in ZEMAX 258
 - Seidel coefficients 257
- Wollaston rear landscape lens 61
- Wollaston, William 62
- working f-number 19

- Z**
- Zemax® 11
- Zernike polynomials 80, 430

Errata.
Introduction to Lens Design

with Practical Zemax® Examples as of February 28, 2005

Note: Any additional errata should be reported to LensDesign@willbell.com. Both the author and publisher will see all e-mail sent to this address.

1. **Page 82**, Equations 7.6 and 7.7 did not print. They are as follows:

$$\text{PSF} = P(\xi, n) \bullet P^*(\xi, n) \quad (7.6)$$

$$T = -\left(\frac{R}{nr}\right)\left(\frac{dW}{dy}\right) \quad (7.7)$$

2. **Page 109**, first sentence: replace Buchdahl with Seidel.
3. **Page 146**, delete point 2 in the 4 point list: 2. Try dummy image surface. Any improvement?
4. **Page 152**, equation in mid-page should read:

$$S_{II} = \frac{1}{2}(0.349955)4^2(0.020383)^2(0.99507)$$

5. **Page 170** Eq. 15.10 should read

$$W_D = \left[W_{311} \bar{H}^3 \right] \rho \cos \phi$$

6. **Page 200**, Eq. 18.16 should read

$$\Delta\phi_{dC} = [(n_{da} - 1) - (n_{Ca} - 1)](C_1 - C_2) + [(n_{db} - 1) - (n_{Cb} - 1)](C_3 - C_4)$$

7. **Page 282**, Equation in Figure 25.19 point 4 should read: $P_\theta = RA_L \ell A_0^{-2} \times \cos^4 \theta$ where R is Radiance. .

8. **Page 291**, Third equation down from top of the page should read (no “cm”):

$$u'_P = -0.24876 = u_S$$

9. **Page 319**, mid page equation, value within parenthesis should read 0.1:

$$c = 43.93(0.1)^2 = 0.4393$$

10. **Page 335** Second sentence after Section 29.8 should read: This is the same form as Equation 29.29

11. **Page 336**, Figure 29.7 centimeters should read millimeters

12. **Page 351**, in Equation 30.23 the term dy_{CF} should read $d\bar{y}_{CF}$

13. **Page 353**, in first line, second paragraph the term dy_{CF} should read $d\bar{y}_{CF}$

14. **Page 357**, Table 31.1 replace Greek letter lambda (λ) with symbol for microns (μm). Second line above Section 31.2.2 (Wavefront Variance) should be changed from $\sigma = 0.05 \lambda$ to $\sigma = 0.05 \mu\text{m}$

15. **Page 363**, reference to Figure 31.6 in last line should be Figure 31.7

16. **Page 366**, just before Equation 32.5, change Equation 32.23 to 32.4

17. **Page 419**, and additional column titled “Strict no DIS” should be added to Table 36.2:

Table 36.2			
	Strict	Strict no DIS	Relaxed
\bar{U}	RMS	RMS	RMS
0°	$236\mu\text{m}$	$100\mu\text{m}$	$34\mu\text{m}$
7°	245	128	77
10°	283	173	114

18. **Page 430**, caption crediting Gaskill under Fig. 37.25 should be moved to Fig. 37.26

19. **Page 446**, Section 29.12 part a) should read . . . and $l_t' = -9.88694''$

20. **Page 446**, Section 30.9 part 1) the 2/3 fraction should read 3/2:

$$C = (3/2)(R/r)^2 W_{131}^2 \text{ where } \bar{H} = 1$$

21. **Page 460**, add index entries under D as follows: degrees of freedom 315, 343